Universidade de São Paulo
Instituto de Física

Understanding strongly coupled non-Abelian plasmas using the gauge/gravity duality

Stefano Ivo Finazzo

Thesis presented to the Instituto de Física da Universidade de São Paulo as a requisite to the title of Doctor of Science

Adviser: Prof. Dr. Jorge Noronha
Examining committee:

Prof. Dr. Jorge Noronha - IFUSP (adviser)
Prof. Dr. Diego Trancanelli - IFUSP
Prof. Dr. Fernando Tadeu Caldeira Brandt - IFUSP
Prof. Dr. Giorgio Donato Torrieri - UNICAMP
Prof. Dr. Nelson Ricardo de Freitas Braga - UFRJ

São Paulo
2015

Universidade de São Paulo
Instituto de Física

Estudando plasmas não-Abelianos fortemente acoplados usando a dualidade *gauge/gravity*

Stefano Ivo Finazzo

Tese apresentada ao Instituto de Física da Universidade de São Paulo como requisito para o titulo de Doutor em Ciências

Orientador: Prof. Dr. Jorge Noronha
Comissão examinadora:

Prof. Dr. Jorge José Leite Noronha Junior - IFUSP (orientador)
Prof. Dr. Diego Trancanelli - IFUSP
Prof. Dr. Fernando Tadeu Caldeira Brandt - IFUSP
Prof. Dr. Giorgio Donato Torrieri - UNICAMP
Prof. Dr. Nelson Ricardo de Freitas Braga - UFRJ

São Paulo
2015

FICHA CATALOGRÁFICA
Preparada pelo Serviço de Biblioteca e Informação
do Instituto de Física da Universidade de São Paulo

Finazzo, Stefano Ivo

"Estudando plasmas não-Abelianos fortemente acoplados usando a dualidade gauge/gravity" – "Understanding strongly coupled non-Abelian plasmas using the gauge/gravity". São Paulo, 2015.

Tese (Doutorado) – Universidade de São Paulo. Instituto de Física. Depto. de Física Experimental

Orientador: Prof. Dr. Jorge José Leite Noronha Junior

Área de Concentração: Física

Unitermos: 1.Colisões de íons pesados relativísticos; 2. Teoria quântica de campo; 3. Física teórica; 4. Física de alta energia; 5. Física nuclear.

USP/IF/SBI-019/2015

Agradecimentos

Embora uma tese seja um empreendimento solitário, por natureza, isso não significa que o autor tenha de encarar este desafio sozinho.

De fato, essa tese simplesmente não existiria sem a ajuda dessas pessoas, e de muitas outras. Eu escrevi a tese sozinho, mas não poderia escrever uma palavra se não fosse por elas. Para elas, todos meus agradecimentos.

Agradeço à minha mãe, pois sem ela não estaria (literalmente) escrevendo essas palavras. E por tudo mais.

Agradeço ao meu orientador, Jorge Noronha, por me orientar, acompanhar e participar deste trabalho. E também o agradeço pela amizade nesses anos.

Agradeço à minha avó, pelos pratos de lasanha e talharim, pelos bifes empanados e pelo divino frango com batatas - todos feitos com muito carinho.

Agradeço a Duda, Eva, Francesca, Laila, Nicole, Nina e Serena, pelo apoio canino.

Agradeço ao pessoal do GHRAFITE: Jorgivan, Hugo, Luiz, Romulo, Samuel, Renato e Maicon; à Marina e ao Fernando; e também ao pessoal do anexo LAPISEIRA, Camila, Raphael e Ricardo. E também à Nayara, GRHAFITEira honorária.

Ao Romulo e Hugo, agradecimentos mais que especiais pela colaboração no capítulo 8.

Agradeço aos *brothers* do Clube do Café, pela amizade e conversas jogadas fora: Viktor, Lelas e LM. E a garota do tempo do IAG, a Livia.

Agradeço à Ana, pela amizade. Juizo, amigona!

A todos demais que minha cabeça mole esqueceu no momento: obrigado!

Por último em ordem alfabética, mas em primeirissimo lugar no meu coração: agradeço ao meu favo de mel, Yasmin... pelo carinho, pelo amor, por tudo... Te amo.

A FAPESP, pelo apoio financeiro (projeto 2011/21691-6).

Resumo

Finazzo, S. I. **Estudando plasmas não-Abelianos fortemente acoplados usando a dualidade *gauge/gravity*.** 2014. Tese (Doutorado) - Instituto de Física, Universidade de São Paulo, São Paulo, 2015.

O estudo de teorias de calibre não-Abelianas fortemente acopladas, em especial de aspectos térmicos e fora do equilíbrio, é um problema central para a compreensão da Cromodinâmica Quântica (*Quantum Chromodynamics* - QCD) - em particular, para entender a evolução do Plasma de Quarks e Glúons (*Quark-Gluon Plasma*- QGP). A técnica mais promissora, QCD na rede, obteve sucesso ao tratar de fenômenos no vácuo e em equilíbrio térmico, como espectros e termodinâmica, mas enfrenta desafios consideráveis ao lidar com fenômenos fora do equilíbrio. Uma ferramenta adaptada para lidar com problemas envolvendo plasmas fortemente acoplados em tempo real é a dualidade *gauge/gravity*, que mapeia uma Teoria Quântica de Campos (*Quantum Field Theory* - QFT) fortemente acoplada em d dimensões em uma teoria de gravitação em $d+1$ dimensões, a qual, de modo geral, é mais fácil de ser resolvida. Nesta tese, estudamos diversas aplicações da dualidade *gauge/gravity* em teorias não-Abelianas fortemente acopladas que modelam qualitativamente o QGP. Nós estudamos o cálculo holográfico do potencial entre um par quark-antiquark pesado ($Q\bar{Q}$) para dipolos $Q\bar{Q}$ estáticos e se movendo com relação ao plasma, apresentando um formalismo geral para o cálculo da parte real e imaginária para uma grande classe de teorias gravitacionais duais. Um estudo da massa de Debye holográfica, baseado no maior comprimento de correlação de operadores ímpares por transformações de CT, foi empreendido, com aplicações em modelos *bottom-up* que reproduzem a termodinâmica da teoria de Yang-Mills SU(N_c) pura e da QCD. Para estes modelos, também calculamos vários coeficientes de transporte associados com o transporte de cargas no plasma, como a condutitividade elétrica, a constante de difusão de carga e coeficientes de transporte associados a uma teoria de hidrodinâmica relativística de segunda ordem.

Palavras-chave: dualidade *gauge-gravity*, plasmas não-Abelianos, fenômenos de transporte.

Abstract

Finazzo, S. I. **Understanding strongly coupled non-Abelian plasmas using the gauge/gravity duality**. 2014. Thesis (PhD) - Instituto de Física, Universidade de São Paulo, São Paulo, 2015.

The study of strongly coupled non-Abelian gauge theories, especially concerning their thermal and non-equilibrium aspects, is a central problem for understanding Quantum Chromodynamics (QCD) - in particular, to understand the evolution of the Quark-Gluon Plasma (QGP). The most successful approach, lattice QCD, succeeds in dealing with vacuum and equilibrium phenomena, such as spectra and thermodynamics, but faces a considerable challenge when it comes to with non-equilibrium phenomena. A tool adapted to deal with real time problems in strongly coupled plasmas is the gauge/gravity, which maps a strongly coupled d dimensional Quantum Field Theory (QFT) to a $d+1$ dimensional theory of gravity, which, in general, is easier to solve. In this thesis, we study several applications of the gauge/gravity duality to strongly coupled non-Abelian theories which model qualitatively the QGP. We deal with the holographic evaluation of the heavy quark-antiquark ($Q\bar{Q}$) potential for static and moving $Q\bar{Q}$ dipoles, presenting a general formalism for the computation of the real and imaginary parts for a large class of dual theories of gravity. A study of the holographic Debye mass, based on the largest screening length of CT-odd operators, is pursued, with applications on bottom-up holographic models that reproduce the thermodynamics of pure SU(N_c) Yang-Mills theory and QCD. For these models, we also compute several transport coefficients associated with charge transport in the plasma, such as the electric conductivity, the charge diffusion constant, and transport coefficients associated with a theory of second order relativistic hydrodynamics.

Keywords: gauge-gravity duality, non-Abelian plasmas, transport phenomena.

List of Publications

Main papers

These papers constitute the backbone of the thesis.

1. S. I. Finazzo, R. Rougemont, H. Marrochio and J. Noronha, *Hydrodynamic transport coefficients for the non-conformal quark-gluon plasma from holography*. JHEP 1502 (2015) 051. arXiv:1412.2968 [hep-ph].

2. S. I. Finazzo and J. Noronha, *Debye screening mass near deconfinement from holography*, Phys. Rev. D **90**, 115028 (2014). arXiv:1411.4330 [hep-th].

3. S. I. Finazzo and J. Noronha, *Thermal suppression of moving heavy quark pairs in strongly coupled plasma*. JHEP 1501 (2015) 051. arXiv:1406.2683 [hep-th].

4. S. I. Finazzo and J. Noronha, *Holographic calculation of the electric conductivity of the strongly coupled quark-gluon plasma near the deconfinement transition*, Phys. Rev. D **89**, no. 10, 106008 (2014). arXiv:1311.6675 [hep-th].

5. S. I. Finazzo and J. Noronha, *Estimates for the Thermal Width of Heavy Quarkonia in Strongly Coupled Plasmas from Holography,* JHEP **1311**, 042 (2013). arXiv:1306.2613 [hep-ph].

Related papers

These papers, while not covered in the thesis, deal with related topics and were published during the PhD of the candidate.

1. R. Critelli, S. I. Finazzo, M. Zaniboni and J. Noronha, *Anisotropic shear viscosity of a strongly coupled non-Abelian plasma from magnetic branes*, Phys. Rev. D **90**, 066006 (2014). arXiv:1406.6019 [hep-th].

2. C. S. Machado, S. I. Finazzo, R. D. Matheus and J. Noronha, *Modification of the B Meson Mass in a Magnetic Field from QCD Sum Rules*, Phys. Rev. D **89**, 074027 (2014). arXiv:1307.1797 [hep-ph].

Contents

List of Figures

List of Tables

Chapter 1

Introduction

One of the outstanding open problems in physics is the confinement problem. How are quarks bound inside hadrons (such as the protons and neutrons)? This problem is the essence of the structure of nuclear matter, addressing an age old question - "what is the structure of matter?". The current theory of strong interactions, *Quantum Chromodynamics* (QCD) is a non-Abelian gauge theory (Yang-Mills theory) with gauge group SU(3), describing the interaction of the quarks (fermionic fields in the fundamental representation of SU(3)) with the gluons (gauge fields in the adjoint representation of SU(3)), which are the mediators particles of the strong interaction. Hadrons, then, are described as composed of quarks bound together by the gluons. QCD, while extremely successful for the description of phenomena at high energies, where the effective coupling constant between the quarks and gluons is weak (due to the property of asymptotic freedom [1–3], which says that the effective coupling constant of the quarks and gluons becomes weaker as one increases the typical energy scale of the process in question[1]) and usual perturbative methods are appplicable, presents a formidable challenge to deal with at low energies, where perturbation theory breaks down and other methods, appropriate in the non-perturbative regime, must be sought of.

One of the ways to approach the question of confinement and structure of matter is to consider its behavior at finite temperature and/or density. For instance, at zero baryonic chemical potential, $\mu_B = 0$ and at zero temperature, $T = 0$, QCD matter is confined inside the hadrons, due to the confinement property of QCD. However, as one increases the temperature of the system, the asymptotic freedom property of QCD kicks in - the quark-gluon interaction becomes progressively weaker and quarks become loosely bound inside the hadrons. Eventually, one would expect that at extremely high temperatures (for instance, for $T \gg\sim m_\pi$, where $m_\pi \sim 140\,\mathrm{MeV}$ is the pion mass which sets the scale

[1]For a complete list of original references on QCD, including textbooks and historical references, we refer the reader to [4].

for typical low energy phenomena of hadronic physics), the hadrons "melt", releasing the quarks and gluons previously bound inside into a large "soup" of interacting quarks and gluons. The resulting system is called the *Quark-Gluon Plasma* (QGP) [5, 6]. Thus, the study of the transition of nuclear matter from the confined state at $T = 0$ to the deconfined QGP at high temperatures is a guide to further understanding of QCD. Also, the QGP could furnish clues to the early stages of the universe - as the early universe cools from its expansion, the hot soup quarks and gluons cools and coalesces into a hadron gas.

The experimental way to probe the existence and the properties of the QGP is through ultrarelativistic heavy-ion collisions. Initial experiments at the Super Proton Collider (SPS) at CERN provided initial clues towards establishing the QGP [2]. The existence of the QGP, signaling the existence of a new state of matter, was latter confirmed at the Relativistic Heavy Ion Collider (RHIC) at the Brookhaven National Laboratory (BNL) [6, 8–11]. As of the date of this thesis, the QGP was being explored both at RHIC and at the Large Hadron Collider (LHC) at CERN. The collision of heavy ions (Au-Au collisions at RHIC and Pb-Pb collisions at LHC) at very high energies (as high as 200 GeV per nuclei at RHIC and 2.76 TeV at LHC) are sufficiently energetic to generate, in the collision region, the QGP. [6]

However, contrary to initial theoretical expectations, the QGP produced at RHIC and at LHC behaves as a nearly perfect fluid which indicates that in these experimental conditions, the QGP does not have high enough temperature so as to be a weakly-coupled plasma, but rather it behaves as a strongly coupled plasma[3]. This means that perturbation theory methods to study the QGP are, once again, not generally applicable. This motivates once again the search for non-perturbative methods to study non-Abelian theories, now at finite temperature.

The most successful non-perturbative method applied to QCD is, arguably, lattice gauge theory [12], which has been successfully applied to a wide range of non-perturbative phenonemena, both at zero and at finite temperature. However, lattice methods are naturally formulated in Euclidean time, which at finite temperature corresponds to Matsubara's formalism, suited for computation of observables in interesting properties, such as transport phenomena (which characterize the hydrodynamical behaviour of the system) and the movement of heavy probes through the plasma, are characterized by non-equilibrium properties, and as such must be computed necessarily in a real-time formalism. Thus, the need arises for effective non-perturbative methods that can be applied to strongly coupled non-Abelian plasmas which also can be used at real-time.

[2] A post-mortem review of the heavy-ion experiments in the SPS can be found in Ref. [7]

[3] Contrary to a naive expectation, the deconfined phase not necessarily is a weakly-coupled plasma. For example, the $\mathcal{N} = 4$ super Yang-Mills theory to be studied in later chapters describes a deconfined plasma, but can be strongly coupled at all scales.

One such method is a surprising result coming from string theory [4], the AdS/CFT correspondence [14], also known as the gauge/gravity duality. This conjecture describes an equivalence between Quantum Field Theories (QFT) in d flat dimensions to quantum theories of gravity in $(d+1)$ (or more) dimensions, giving a precise dictionary of how to relate observables in one theory to the other. The main appeal of this conjecture, from the point view of phenomenology of the QGP, is that it consists of a strong/weak duality - that is, when one side of the duality is at strong coupling, the other side is weakly coupled, and vice-versa. In this case, a strongly coupled QFT means that its dual theory of gravity is a classical theory of gravity. Thus, we can map, using the gauge/gravity duality, strongly coupled problems in QFT to classical gravity problems, in a higher dimensional gravitational theory. One can then hope that the corresponding problem in the dual theory of gravity is more tractable than that in the original field theory. As we will explore in this thesis, for several observables, this is the case. Though the quantum field theories for which the corresponding dual theory of gravity is known are not QCD, these QFTs are similar to QCD in many ways, which means that they can be used as proxy theories or as qualitative or semi-quantitative approximations to "real-world" QCD.

In this thesis, we will use the gauge/gravity duality as a tool to explore the dynamics of strongly coupled non-Abelian plasmas which can serve as proxies to pure Yang-Mills theories and QCD. The focus will be on real-time processes, specially the movement of heavy probes through the plasma and transport phenomena, albeit we will also work with equilibrium phenomena. The gauge theories we will consider include $\mathcal{N}=4$ Super Yang-Mills (SYM) (via the original AdS/CFT correspondence), the gauge theory dual to Gauss-Bonnet gravity (a gravity theory with higher order derivatives), and a class holographic bottom-up models that reproduce the thermodynamics of QCD at zero baryonic chemical potential, $\mu_B = 0$. [15–17]

This thesis is organized as it follows: after a brief review of non-Abelian gauge theories, QCD and an overview of the dynamics of the QGP (Chapter 2), we discuss the basics of the gauge/gravity duality and the main computational tools of the holographic dictionary used in this work (Chapter 3). The next chapters contain the original thesis work. The observables we will consider in this thesis include the imaginary part of the heavy quark-antiquark $Q\bar{Q}$ potential both in static (Chapter 4) and moving (Chapter 5) $Q\bar{Q}$ dipoles, which is associated with the thermal width of heavy quarkonia (such as J/ψ and $\Upsilon(1S)$). Associated with this study, we explore the Debye screening mass (Chapter 6), which sets the typical thermal screening length between two external probes in the plasma, studying its evaluation using the gauge/gravity duality. Transport coefficients associated

[4] A useful, but somewhat outdated, reference letter on string theory and related topics can be found on [13].

with the charge transport in the plasma, such as the charge conductivity and the diffusion constant, are relevant observables to understand the effect of strong external electric and magnetic in the QGP - we deal with the holographic evaluation of these coefficients in Chapter 7. Complementing and extending the analysis of Chapter 7, in Chapter 8 we consider a second order theory of hydrodynamics, focusing on the holographic evaluation of its transport coefficients. The resulting theory can then be used in numerical codes of hydrodynamics, in order to understand the effect of higher order corrections on the Knudsen number. In Chapter 9 we present our conclusions.[5]

The results concerning Chapters 4 and 5 have been published in JHEP [18, 19]. The results of Chapters 6 and 7 were published in PRD [20, 21], respectively. The results of Chapter 8 have been published in JHEP [22]. Other research papers, about related topics and done during the period that the thesis refer to but not covered in this thesis, can be found in Refs. [23, 24] (both published in PRD).

[5]This thesis is supplemented by several appendices, which present basic material with more detail than in the main body of the text or deal with technical aspects of the calculations performed in the main body of the thesis. Appendix A shows that a traceless stress-energy tensor is equivalent to conformal invariance of the theory, at the classical level. Appendix B shows the equivalence between requiring infalling boundary conditions in a black hole horizon and horizon regularity. Appendix C we present with more detail the relation between Wilson loops and the static energy of a heavy quark-antiquark pair. Appendix D presents several complementary results on holographic Wilson loops, complementing the analysis of Chapters 4 and 5. Appendix E serves a prelude to Chapter 6, showing the perturbative computation of the Debye screening mass in QED and QCD. Appendix F presents some technical details to complement the holographic computation of the Debye screening mass in Chapter 6. Finally, Appendix G complements the discussion on second order transport coefficients in Chapter 8.

Chapter 2

The Structure of QCD Matter under Extreme Conditions

2.1 The structure of QCD matter under extreme conditions

The structure of matter under extreme conditions is one of the outstanding problems in physics. In particular, one is interested in the structure of hadrons under extreme conditions - that is, what happens to baryons (bound states of three quarks, $q_1 q_2 q_3$) and mesons (bound states of a quark and an antiquark, $q_1 \bar{q}_2$) at high temperatures, high densities or strong external fields (for example, strong external magnetic fields). The theory of strong interactions, namely, Quantum Chromodynamics (QCD) [1–3] is the correct description of the inner constituents of hadrons in the limit of short distances and high energies, due to the fact that QCD is an asymptotically free quantum field theory (QFT) - i.e., at short distances, the interaction between quarks is weak and usual perturbation theory techniques can be successfully applied. However, at long distances and low energies, perturbation theory breaks down and other approaches must sought off.

In this Chapter we will review some basic results about Yang-Mills theories and QCD, with a special view to finite temperature results. Section 2.2 begins with a presentation of the basics of Yang-Mills theory and QCD. Section 2.3 is dedicated to the most salient features of QCD - the properties of confinement and asymptotic freedom, described within the unified language of the renormalization group. In Section 2.4 we present the basics about finite temperature field theories, and an overview of the current status of the QCD phase diagram. Section 2.5 finishes this chapter describing the experimental results that supports the view that the QGP formed in ultrarelativistic heavy-ion collisions is a strongly coupled plasma.

2.2 Quantum Chromodynamics

2.2.1 Definition and action

QCD is defined as a Lorentz invariant and gauge invariant quantum field theory in (3+1) dimensions with gauge group $\mathrm{SU}(N_c)$[1], the special unitary group (the group of unitary matrices with determinant +1) of rank N_c (N_c is called the number of colors) and N_f Dirac fermions (the quarks) which transform in the fundamental representation of the gauge group[2]. The action of QCD can be written as

$$S = \int d^4x \, (\mathcal{L}_{YM} + \mathcal{L}_f) \,, \tag{2.1}$$

where $\mathcal{L}_{YM}$ is the Yang-Mills Lagrangean density and $\mathcal{L}_f$ is the Lagrangean density for the Dirac fermions.

The Yang-Mills Lagrangean density $\mathcal{L}_{YM}$, which describes the interaction of the gauge fields A^a_μ (the gluons), where $a = 1, 2, \ldots, N_c^2 - 1$ is a $SU(N_c)$ index in the adjoint representation, can be written as

$$\mathcal{L}_{YM} = -\frac{1}{4} \mathrm{Tr}\, F_{\mu\nu} F^{\mu\nu} = -\frac{1}{4} F^a_{\mu\nu} F^{a,\mu\nu} \tag{2.2}$$

where F is the Yang-Mills field strength, defined by

$$F^a_{\mu\nu} = \partial_\mu A^a_\nu - \partial_\nu A^a_\mu + g f_{abc} A^b_\mu A^c_\nu, \tag{2.3}$$

where g is the gauge coupling constant and f_{abc} are the group structure constants. The trace in Eq. (2.2) is over the color indices: $\mathrm{Tr}\, F_{\mu\nu} F^{\mu\nu} = F^a_{\mu\nu} F^{\mu\nu}_a$. Due to the last term in Eq. (2.3), the Yang-Mills Lagrangean (2.2) has cubic and quartic terms in A which implies that the gluons are self-interacting - in terms of Feynman diagrams, the gauge fields have cubic and quartic vertices. Thus, even without fermions, Yang-Mills theory defined by

$$S_{YM} = \int d^4x \, \mathcal{L}_{YM} \tag{2.4}$$

is a non-trivial interacting theory on its own.

[1] Let us fix our metric conventions here: the Minkowski metric in d dimensions is denoted $\eta_{\mu\nu}$, with signature $(-, +, \ldots, +)$. Also, throughout this work, we work with a natural system of units and set $\hbar = c = k_B = 1$. Thus, in the unit system used in this thesis, G_4, Newton's constant in four dimensions is not set to 1. Unless explicitly stated, Einstein's summation convention is assumed throughout.

[2] Textbooks and reviews of QFT and QCD can be found on Refs. [25–27]. A guide to the original references is Ref. [4], as already remarked.

The Lagrangean density of the quarks, $\mathcal{L}_f$, is given by

$$\mathcal{L}_f = \sum_{n=1}^{N_f} \bar{\psi}_n^i \left(i \not{D}_{ij} + m_n \right) \psi_n^j, \tag{2.5}$$

where ψ_n^i is the Dirac spinor for the the n-th quark, m_n is its corresponding mass and $\not{D}_{ij} = \gamma_\mu D_{ij}^\mu$, where $i, j = 1, 2, \cdots, N_c$ are gauge group indices for the fundamental representation and D_{ij}^μ is the covariant derivative for the Dirac fermions in fundamental representation of $SU(N_c)$ associated with the gauge connection A:

$$D_{ij}^\mu = \delta_{ij} \partial^\mu + i g T_{ij}^a A_a^\mu, \tag{2.6}$$

where T^a are a set of generators for SU(N_c). In Eq. (2.6), the last term gives rise, when substistuted Eq. (2.5), to a quark-quark-gluon vertex, giving the interaction between the quark sector and the Yang-Mills sector. For QCD, $N_c = 3$ and $N_f = 6$. The six flavors of quarks, in increasing mass order, are the up quark (with a current mass of $m_u \sim 3\,\text{MeV}$), the down quark ($m_d \sim 6\,\text{MeV}$), the strange quark ($m_s \sim 130\,\text{MeV}$), the charm quark ($m_c \sim 1.3\,\text{GeV}$), the bottom quark ($m_b \sim 4.5\,\text{GeV}$) and the top quark ($m_t \sim 174\,\text{GeV}$). However, it is useful to consider N_c other than 3, even $N_c \to \infty$ - this may be a reasonable approximation even for QCD phenomenology, sucessfully describing qualitative features of finite N_c QCD [29–31]. Also, for reasons to be explained in Chapter 3, the large N_c limit is the most convenient limit of the gauge/gravity duality. As a final remark, depending of the energy scale of the phenomenon in question, N_f can be taken to effectively smaller than 6. For the range of energies we will mostly work with (few hundreds of MeV), only the up, down and strange quarks are dynamical, with the heavier quarks, such as the charm or the bottom quarks being too heavy - these quarks can be considered as external, non-dynamical, probes in plasma[3]. Finally, one should note that the Yang-Mills action (with or without fermions) is renormalizable in 4 or less spacetime dimensions [28].

2.2.2 Symmetries of QCD - Gauge and conformal invariances

When dealing with a physical system, one of the most important steps is to identify all the symmetries of the system, whether they are exact or approximate symmetries, and whether they survive or are broken by quantization of the theory. Symmetries lead to conservation laws (by Nöether's Theorem) and strongly constrain the behavior of physical

[3]The top quark is too massive ($m_t = 174\,\text{GeV}$). In heavy ion collisions the top quarks produced decay almost immediately, when compared to the typical time-scale of the evolution of the system ($\sim$ fm/c). Thus, they are not expected to play any relevant role in the dynamics of heavy ion collisions and of the quark gluon plasma.

observables, playing a central role in determining the possible dynamics of the theory.

Gauge invariance

The symmetries of the pure Yang-Mills action (2.4) include, apart from Poincaré symmetry as a global symmetry, a SU(N_c) local gauge symmetry. Let $U(x)$ be a element of the fundamental representation of SU(N_c), that is, a $N_c \times N_c$ unitary matrix with positive unit determinant whose entries are local functions of the space-time coordinates x. Then, as A^a_μ are fields on the adjoint representation, they transform as

$$T^a A^a_\mu \to T^a A'^a_\mu = U \left(T^a A^a_\mu - \frac{i}{g} U^{-1} \partial_\mu U \right) U^{-1}. \tag{2.7}$$

The action (2.4) is built to be explicitly invariant under SU(N_c) gauge transformations. This gauge symmetry implies that two sets of gauge fields A^a_μ and A'^a_μ describe the same physics, as long they are connected by a gauge transformation (in the jargon, the fields A^a_μ and A'^a_μ are in the same orbit). This indicates that the A_μ gauge fields furnish a redundant description of the system. This leads to two novel features of Yang-Mills theories. The first one is that quantization of Yang-Mills theories must deal with a way of eliminating the extra degrees of freedom of the theory - either by choosing an explicit gauge or by introducing unphysical fields (the Faddeev-Popov ghosts) [32, 33]. The second one, more important to the question at hand, is that the field A^a_μ do not, by themselves, constitute observables - their vacuum expectation values depend on the gauge choice. Physical observables must arise from gauge invariant operators, such as the the Lagrangean density (2.2). This point is a key observation that will arise frequently throughout this thesis.

Conformal invariance

The symmetries discussed so far are symmetries that survive after quantization of the theory. There is one more symmetry of Yang-Mills theory, which will also play a fundamental role throughtout this work - conformal symmetry [34], which holds only, in the case of Yang-Mills theories, in four dimensions. However, in contradiction to the previous symmetries, this symmetry is broken after quantization. A general conformal transformation is defined by

$$x_\mu \to x'_\mu = \Lambda(x) x_\mu, \tag{2.8}$$

where $\Lambda(x)$ is a smooth function of the space-time coordinate x. That is, a conformal transformation is a local scale transformation. The conformal group in d dimensions is given by SO(d,2); it is composed of Poincaré transformations (the Poincaré group is a

subgroup of the conformal group) together with glocal scale transformations, defined by

$$x_\mu \to x'_\mu = \lambda x_\mu, \tag{2.9}$$

and special conformal transformations,

$$x_\mu \to x'_\mu = \frac{x_\mu - a_\mu}{1 - 2a \cdot x + a^2 x^2}, \tag{2.10}$$

where $\lambda > 0$ and a^μ are the transformation parameters. Let us count the number of generators of the conformal group SO(d,2): Lorentz transformations are generated by anti-symmetric $d \times d$ matrices (describing both boosts and rotations) which contributes with $d(d-1)/2$ generators; together with d parameters to describe translations, we get $d(d+1)/2$ generators for the Poincaré group. Scale transformations contribute with one generator, as described by Eq. (2.9), and special conformal transformations with d generators. Summing everything up, we get $(d+1)(d+2)/2$ generators for the conformal group. For $d = 4$, we have 15 generators.

Conformal invariance implies that the theory is invariant under transformations that preserve angles between curves in space-time. Scale invariance, which is a more restricted symmetry, implies that the theory has no dimensionful scales - there is no natural "ruler" in the theory with which one can compare quantities. A sign that Yang-Mills is (classically) conformal invariant in four dimensions comes from the fact that its action does not possess dimensionful parameters - in $d = 4$ the coupling constant g is dimensionless.

To verify conformal invariance, it is sufficient to verify that the symmetric energy-momentum tensor $T_{\mu\nu}$ of the theory is traceless[4]. For pure Yang-Mills, the symmetrized energy-momentum tensor is given by

$$T^{YM}_{\mu\nu} = -F^a_{\mu\rho} F^{\rho}_{\nu\ a} + \frac{1}{4} F^a_{\rho\lambda} F^{\rho\lambda} \eta_{\mu\nu}. \tag{2.11}$$

Thus,

$$T^{YM,\mu}_{\ \ \ \mu} = \frac{1}{4}(d-4) F^a_{\mu\nu} F^{a,\mu\nu} \tag{2.12}$$

It follows that, for $d = 4$, $T^{YM,\mu}_{\ \ \ \mu} = 0$. This establishes the classical scale invariance of Yang-Mills. Now, this symmetry does not survive at the quantum level. A formal way of seeing this is to note that measure of the path integral for the generating functional of the Yang-Mills theory is not invariant under scale transformations. A more intuitive way of seeing this is to note that the quantization of Yang-Mills generates, dynamically, a mass scale for the theory, Λ_{YM}. We will explore this point further in Section 2.3.

[4]See Appendix A for a proof of this statement

Symmetries of QCD at the classical level

The full QCD action (2.1) is also Poincaré invariant. Also, it is still gauge invariant, as the quarks ψ_i transform as a vector in the fundamental representation of the gauge group, that is, as

$$\psi_i(x) \to \psi_i'(x) = U_{ij}(x)\psi_j(x). \tag{2.13}$$

Using the transformations (2.7) and (2.13), it is possible to check that the covariant derivative defined in Eq. (2.6) transforms as a vector:

$$D_\mu\psi \to (D_\mu\psi)' = UD_\mu\psi. \tag{2.14}$$

Thus, the fermionic part (2.5) of the action (2.1) is also invariant by gauge transformations, as promised. The fate of conformal symmetry is more subtle. The fermionic part of the stress energy tensor is

$$T^f_{\mu\nu} = \frac{i}{4}\sum_{n=1}^{N_f}\bar{\psi}_n\left(\gamma_\mu\overrightarrow{D}_\nu + \gamma_\nu\overrightarrow{D}_\mu - \gamma_\mu\overleftarrow{D}_\nu - \gamma_\nu\overleftarrow{D}_\mu\right)\psi_n \tag{2.15}$$

where $\overrightarrow{D}_\nu$ ($\overleftarrow{D}_\nu$) indicates a right (left derivative, respectively) - we also note that we suppressed color indices. It follows that, using Dirac equation, $(iD_\mu\gamma^\mu - m)\psi = 0$, that

$$T^{f,\mu}{}_\mu = \sum_{n=1}^{N_f} m_n\bar{\psi}_n\psi_n. \tag{2.16}$$

Thus, if all quarks are massless, $m_n = 0$ for $n = 1, \ldots, N_f$, then $T^{f,\mu}{}_\mu = 0$ and the theory is still conformally invariant. Note that this argument independs of color structure. This result, in hindsight, is evident since a quark mass introduces a dimensionful scale in the theory.

Let us discuss briefly the remaining symmetries of QCD, for the sake of completeness. The QCD action also possess a U(1) global vector symmetry, $\psi \to \psi' = e^{i\theta}\psi$, where θ is a phase. The conserved charge associated with this symmetry is the baryonic number. Also, if all quarks are massless, the theory possesses a U(1) axial symmetry, where the quark fields transform as $\psi \to e^{i\gamma_5\theta}\psi$. The vector U(1) symmetry survives quantization, but the axial U(1) is broken, resulting in a chiral anomaly [35, 36]. A final symmetry, valid in the limit of zero quark masses, is a $\mathrm{SU}(N_f)_L \times \mathrm{SU}(N_f)_R$ global symmetry, where the subscript L (R) indicates that the group acts on left (right, respectively) handed quark fields. However, when QCD is quantized, a mechanism of spontaneous symmetry breaking breaks $\mathrm{SU}(N_f)_L \times \mathrm{SU}(N_f)_R$ to a vector $\mathrm{SU}(N_f)$. In the case of $N_f = 2$ (which is

equivalent to setting the up and down quark masses to zero), the three Goldstone bosons corresponding to the three broken generators are the pions, and the remaining vector SU(N_f) symmetry group turns out to be the isospin group. [37]

2.3 Renormalization group flow, asymptotic freedom and confinement

2.3.1 Renormalization group flow and asymptotic freedom

One of the most remarkable features of QCD comes from the perturbative computation of the renormalization group [38–41]. The renormalization group allows us to understand how the couplings of the theory change as one looks at the theory from different scales - it is a key tool for making sense of the renormalization procedure and for understanding second order phase transitions, especially for computing the scaling behavior at the critical point. A more complete discussion of the intuitive picture of the renormalization picture will be presented in the next Chapter. In this section, we will analyze only the renormalization group equation for the gauge coupling g in QCD.

The main result of the renormalization group are the renormalization group equations, a set of differential equations for the evolution of the couplings as a function of the scale. The renormalization group equation for the effective gauge coupling $\bar{g}$ is

$$\mu \frac{d\bar{g}}{d\mu} = \beta(\bar{g}), \tag{2.17}$$

where μ is the renormalization scale and the β function depends on the dynamics of theory. In QFTs, the most common procedure is to compute β perturbatively, from the Callan-Symanzik equation. In QCD, at 1 loop in perturbation theory[5],

$$\beta(\bar{g}) = -\beta_0 \bar{g}^3 + O(\bar{g}^5) \tag{2.18}$$

where

$$\beta_0 = \frac{1}{(4\pi)^2}\left(\frac{11}{3}N_c - 2\frac{N_f}{3}\right). \tag{2.19}$$

For a sufficiently small number of quark flavors, such that $\beta_0 > 0$ (for instance, for QCD with $N_c = 3$, this means that $N_f < 33/2.$), the renormalization group equation (2.17) has a stable fixed point at $\bar{g} = 0$ with $\mu \to \infty$ - a stable trivial ultraviolet (UV) fixed point.

[5]For a review of the Callan-Symanizik equation and of this computation, see Refs. [25] or [26]. In the next chapter a more complete discussion of the renormalization group is going to be given. For reference, the beta function in QCD has been calculated to 4-loops in perturbation theory, in the minimal subtraction scheme [42].

Put in other words, the renormalization group flow is such that the effective coupling goes to 0 as the typical energy scale at which we analyze the theory grows. That is, the theory becomes free at sufficiently high energies or short enough distances - this the content of asymptotic freedom.

The breaking of conformal invariance can be seen as the consequence of the necessity of the introduction of a scale for quantization. At a fixed point of the renormalization group equations conformal invariance is restored. In the case of QCD, conformal invariance is approximately restored at high energies. The fact that away from the UV fixed point the theory does not retain its classical conformal symmetry implies that $\langle T^{\mu}_{\mu} \rangle \neq 0$. The consequence for Yang-Mills theory is that the theory develops a non-trivial gluon condensate $\langle \mathrm{Tr} F^2 \rangle \neq 0$.

Let us now explore the infrared behavior of the theory. The solution of the renormalization group equation (2.17), using the 1-loop beta function of Eq. (2.18), is

$$g(\mu) = \frac{4\pi}{\beta_0} \frac{1}{\log \frac{\mu^2}{\Lambda^2}} \tag{2.20}$$

where Λ, which comes about as an integration constant while solving Eq. (2.17), sets the typical energy scale for strong interactions. For QCD, $\Lambda \sim 200\,\mathrm{MeV}$, of the order of the mass of the pion. For $\mu \sim \Lambda$, $g(\mu) \gg 1$, which indicates that the theory becomes strongly coupled - this signals, naively, the breakdown of the perturbative expansion.

2.3.2 Confinement

This breakdown of perturbation theory is expected to be associated with the fact that, at low energies, the degrees of freedom present in the Lagrangean (2.1), quarks and gluons, are not the physical degrees of freedom of the strong interactions. Indeed, one can only observe colorless degrees of freedom: the hadrons, such as baryons, mesons and glueballs. Quarks and gluons are then confined to the interior of hadrons. This is the intuitive description of the property of confinement.

A useful picture of confinement arises when one thinks of mesons, that is, hadrons composed of a quark and an antiquark. When one draws, in the static limit, the eletric field lines for an electron-positron pair, interacting by the electromagnetic interaction described by QED, the field lines joining the pair are spreaded out (Figure 2.1(a)). However, the chromo-electromagnetic fields which bounds a meson are organized in such a way that they concentrate mainly into a small region of space joining the quark and the antiquark, forming a flux tube (Figure 2.1(b)) - the energy contained in the flux tube increases linearly with the separating distance between the quarks: the potential energy of the static quark-antiquark pair $V_{q\bar{q}}$ for a large separation distance L is expected to be of the

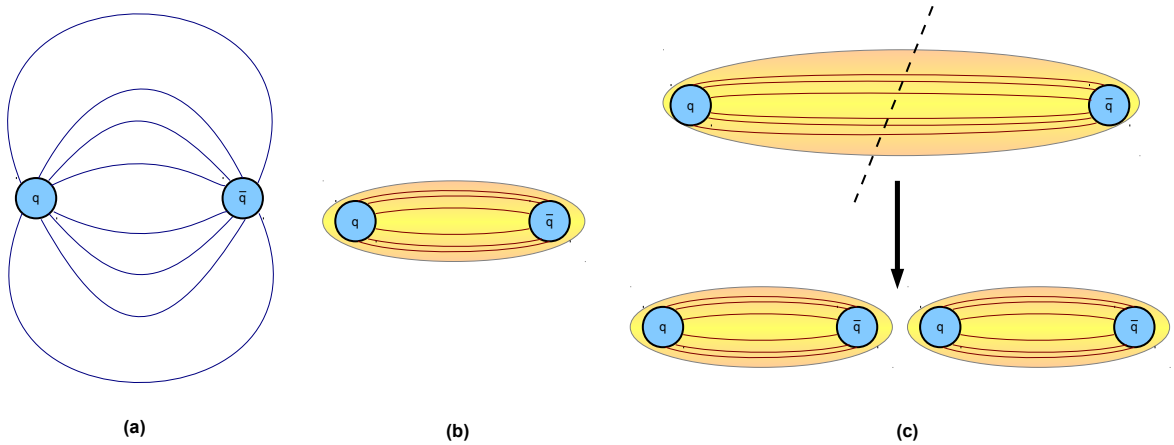

Figure 2.1: *Pictoric description of confinament using flux tubes. (a) Field lines between a static quark and an antiquark pair in the case of an electromagnetic interaction. (b) Field lines between a quark and an antiquark in the case of the strong interaction. The lines bunch up and are confined to a narrow tube of flux lines joining the quark and the antiquark. (c) For light dynamical quarks, stretching the flux tube can lead to a situation where it is energetically more stable to break the tube into two mesons, by creating another quark-antiquark pair from the vacuum.*

form

$$V_{q\bar{q}}(L \to \infty) \approx \sigma L, \tag{2.21}$$

where σ is called the string tension of the flux tube. In a theory with light quarks, at large separations, the energy of the tube can be great enough that the most stable configuration of the system is the flux tube breaking creation of a quark and an antiquark pair from the vacuum, resulting in two mesons (Figure 2.1(c)). In this case, one eventually expects that $V_{q\bar{q}} \to 0$ for $L \gtrsim m_{\text{meson}}^{-1}$, where m_{meson} is the mass of the lightest meson that can be created with the adequate quantum numbers of the system. Conversely, as $L \to 0$ the mesons become weakly interacting and the theory approaches its conformal regime. Thus, since the meson separation L is the only dimensionful scale in the conformal regime, we must have $V_{q\bar{q}} \propto -1/L$ (the minus sign is to give the interaction its attractive character). A perturbative calculation at tree level (the one gluon exchange) yields

$$V_{q\bar{q}}(L \to 0) \approx -\frac{\alpha_s}{L}, \tag{2.22}$$

where $\alpha_s = g^2/(4\pi)$. In passing, we mention that a successful phenomenolgical parametrization that interpolates between the expected behavior for a confining theory in the IR and the conformal behavior in the UV is the Cornell potential [43], given by

$$V_{q\bar{q}}(L) = -\frac{\alpha_s}{L} + \sigma L. \tag{2.23}$$

A precise definition of what is meant by confinement is an open question in the literature [44]. For pure Yang-Mills theories, without fermions, the presence of an area law for large spatial Wilson loops [45] can be taken as a signal for confinement (we will explore this point further in Chapter 4). Alternatively, at finite temperature, a null expectation value of the Polyakov loop is a good order parameter for characterizing a confined phase [46, 47]. However, when the theory has light dynamical quarks, both definitions of confinement turn out not to be precise and we lack a precise test for confinement in this case. [44]

2.3.3 Non-perturbative methods

From the study of the renormalization group flow, we see that the coupling constant becomes large as one goes to the infrared (IR) of the theory, as indicated by Eq. (2.20). Therefore, to study pure Yang-Mills theories and QCD at low energies, it is then necessary to go beyond perturbation theory and use non-perturbative methods. Quite a few non-perturbative methods have been developed during the last decades to deal with this problem. In this section, we will list some of these techniques, calling attention to some of the advantages and drawbacks of each approach.

Some of these methods exploit the low-energy symmetries of QCD to write an effective action for the hadronic interaction - this is the basic premise of chiral perturbation theory, which exploits the pattern of $\mathrm{SU}(N_f) \times \mathrm{SU}(N_f)$ chiral symmetry breaking of QCD [48]. The effective theory possesses a few universal parameters that can, at least on principle, be computed directly from QCD (or fitted from data). However, the resulting effective theory is non-renormalizable and thus lack predictive power beyond the first few orders in perturbation theory.

An alternative approach is to start from high energies, exploiting asymptotic freedom and the reliability of perturbative techniques in the UV. The idea is then to extend the perturbative calculation close to the non-perturbative regime, parametrizing non-perturbative effects in the vacuum condensates using Wilson's Operator Product Expansion (OPE) [49] and matching the results to phenomenological expressions that come about from the assumption that the low-energy effective degrees of freedom are given by hadronic degrees of freedom. This is, roughly, the procedure pursued by the QCD Sum Rules (QCDSR) [50] (for a review, see Ref. [51]; a pedagogical introduction can be found in [52]). The QCDSR are fairly successful in explaining semi-quantitatively the hadronic spectrum. However, the QCDSR approach suffers from a lack of precision, dictated mainly by the extrapolation of a perturbative series to the non-perturbative regime.

Arguably the main technique for exploring non-perturbative QCD is to use lattice gauge theory [45] (for an introduction and reviews of lattice QCD, see Refs. [53, 54]). In-

stead of maintaining explicit Poincaré invariance and hiding explicit gauge invariance by choosing a fixed gauge, as in ordinary perturbative calculations, lattice QCD is based on maintaining explicit gauge invariance and sacrificing Poincaré invariance, by discretizing space-time on a hyper-cubic lattice. The infinite dimensional path-integrals that give expectation values of observables of the continuum theory then become, after discretization, high dimensional integrals which can then be solved numerically using Monte Carlo and importance sampling methods. The continuum observables are determined by extrapolating the discretized results computed using the finite lattice gauge theories.

Lattice QCD, albeit being a powerful tool, has three main drawbacks to the type of problems considered in this thesis. The first one is the numerical power required to compute observables with accuracy. In the past decades, lattice calculations were mainly restricted to pure gauge theories, as calculations with dynamical fermions were prohibitive in terms of computational power due to the extremely costly procedure of evaluating the fermionic determinant. Nowadays, however, with the available computational power of modern computers, it is possible to realize reliable computations in QCD with (2+1) light flavors accurately. For example, the light hadronic spectrum has been computed in lattice QCD with remarkable accuracy [55] (for a review, see Ref. [56]).

The second drawback is of a more serious nature. Lattice QCD computations start from the partition function Z for the field theory. In Minkowski space-time, in a path-integral formulation, the partition function is given by

$$Z = \int D\phi \, e^{iS[\phi]}, \tag{2.24}$$

where ϕ is the set of all basic fields of the theory, described by the action $S[\phi]$. To use importance sampling, lattice methods require the passage from real time t to imaginary time τ, by the transformation $t \to i\tau$. In this case, the partition function becomes

$$Z = \int D\phi \, e^{-S_E[\phi]}, \tag{2.25}$$

where the metric is now Euclidean and S_E is the Euclidean action. Importance sampling uses e^{-S_E} as a Boltzmann weighting factor in a Monte Carlo calculation, to be able to select the most representative contributions to Z. The problem is that not all physical observables can be computed at imaginary time; for example, spectral functions or transport properties require computations at real time. Correlations functions, the main object computed in lattice QCD calculations, can, in principle, be analytically continued from imaginary time to real time. However, numerical analytic continuation is a delicate subject and such computations require extremely precise computations and large statistics. Recent progress in perfoming this analytic continuation on the lattice is based on the

Maximum Entropy Method, as implemented in Ref. [57]. A review of the progress of the computation transport properties on the lattice can be found on Ref. [58].

The third problem is the sign problem [58]. When including a chemical potential μ for the quarks, for example, in the action in Eq. (2.25) receives a new term to take into account μ. However, this new term is not hermitean, which means that the weight e^{-S_E} may be complex. Again, in such a case importance sampling cannot be used straightforwardly.

The last method to be considered, and the method to be used throughout this work, is the gauge/gravity duality [14]. A more complete description of this method will be the main subject of the next chapter. However, an heuristic way of thinking of the physical basis of the gauge/gravity duality, to be developed further in the next chapter, is thinking of it as a geometrization of the renormalization group [59], with the energy scale parameter taking the role of an extra dimension. Then one maps problems of a strongly coupled quantum field theory to a problem of a classical gravity theory. It is not a method without drawbacks: the calculations are done in gauge theories which model many of the properties of QCD - such as confinement, its hadronic spectra or its thermodynamics - but these theories are not QCD; moreover, albeit the IR properties of these models are well defined, in the UV all these models are not asymptotically free, being, instead, strongly coupled. However, even with these problems, the gauge/gravity duality is still a powerful tool, providing analytical or semi-analytical solutions for many quantum field theory problems that would be hard to solve otherwise in a strongly coupled theory. Moreover, all computations can be done in real-time, which allows for the extraction of transport coefficients, for example.

2.4 QCD at Finite Temperature

So far, we have focused on the limit of Yang-Mills theory and QCD at zero temperature. However, the question we posed at the beginning of this chapter, "What is the behavior of matter under extreme conditions of temperature and pressure?", require finite temperature calculations of equilibrium and non-equilibrium quantities. In this section we explore how we can formulate this question.

2.4.1 Finite Temperature Field Theory

The first step is to formulate quantum field theory at finite temperature. In this subsection we will briefly review the imaginary time (Matsubara) formalism; results from the real time, closed time path, formalism will be introduced in this thesis as needed. For a more complete discussion and an overview of thermal field theory, see Refs. [60, 61].

First, let us remember how a transition amplitude is computed in quantum field theory at zero temperature in the path integral formulation. Let $\phi(t, x^i)$ be a (set of) bosonic fields in d dimensions, with $i = 1, 2, \cdots, d-1$. Then,

$$\langle \phi(t_1, x_1^i) | \phi(t_2, x_2^i) \rangle = \langle \phi_1 | e^{-i\hat{H}(t_1 - t_2)} | \phi_2 \rangle = \int D\phi \, e^{iS[\phi]}, \tag{2.26}$$

where the action $S[\phi]$ is written in terms of the Lagrangian density $\mathcal{L}$ as

$$S = \int_{t_1}^{t_2} dt \int d^3x \, \mathcal{L}[\phi]. \tag{2.27}$$

In Eq. (2.26), the boundary conditions on the fields are

$$\begin{aligned} \phi(t_1, x_1^i) &= \phi_1, \\ \phi(t_2, x_1^i) &= \phi_2. \end{aligned} \tag{2.28}$$

In quantum mechanics, the expectation value of the observable $\hat{O}$ in a state described by the density matrix $\hat{\rho}$ is given by

$$\langle \hat{O} \rangle = \mathrm{Tr} \left(\hat{\rho} \hat{O} \right). \tag{2.29}$$

If the Hamiltonian of the system is given by $\hat{H}$ and the system is in thermal equilibrium with a thermal bath at temperature T, then the density matrix is given by[6]

$$\rho = \frac{e^{-\beta \hat{H}} \hat{O}}{Z}, \tag{2.30}$$

where $\beta = 1/T$ and Z is the partition function,

$$Z = \mathrm{Tr}\, e^{-\beta \hat{H}}, \tag{2.31}$$

which gives the correct normalization for the density matrix $\hat{\rho}$.

Now, introducing the complete basis $|\phi\rangle$, the trace in (2.31) can be written as

$$Z = \int d\phi_1 \langle \phi_1 | e^{-\beta \hat{H}} | \phi_1 \rangle. \tag{2.32}$$

The matrix element in Eq. (2.32) can written using the path-integral formulation for the amplitude in Eq. (2.26). First, we note that $\phi_1 = \phi_2$ in (2.32). Then we identify

[6] We are discussing the formulation in the canonical ensemble; the grand canonical ensemble is obtained by changing $\hat{H}$ to $\hat{H} - \mu \hat{N}$, where $\hat{N}$ is the conserved number operator associated with the chemical potential μ.

$\beta = i(t_1 - t_2)$. Thus, the partition function Z can be written as

$$Z = \int D\phi \, e^{-S_E[\phi]} \tag{2.33}$$

where $S_E[\phi]$ is the Euclidean action, obtained from the Minkowski action S by passing to imaginary time τ, $t \to -i\tau$. The boundary conditions in (2.33) are $\phi(0, x^i) = +\phi(\beta, x^i)$; that is, ϕ obeys periodic boundary conditions[7]. The expectation value (2.34) can be written as

$$\langle \hat{O} \rangle = \int D\phi \, O[\phi] e^{-S_E[\phi]}. \tag{2.34}$$

In the imaginary time formalism presented above, the periodic boundary conditions, written with an Euclidean signature, correspond to compactification in a circle in the imaginary time direction - the length of the circle is $\beta = 1/T$. This means that at high temperatures, $\beta \to 0$, a thermal field theory is effectively described by a lower dimensional Euclidean field theory. Also, perturbation theory in this formalism is, at least in principle, analogous to perturbation theory in the $T = 0$ case. The main difference is that, since all fields are (anti)-periodic in time, Fourier transforms of the temporal dependence of the fields reduce to Fourier series, where the discrete frequencies, given by $\omega_n = 2\pi n/\beta$ ($\omega_n = (2n + 1)\pi/\beta$ if the fields are fermionic) are known as the Matsubara frequencies. The main problem is that, beyond one loop in perturbation theory, different scales come into play - for instance, one has to consider expansions not only on the coupling constant g, but also on gT and gT^2. The disentanglement of this multitude of scales is a complex problem that has to be solved in order to improve perturbative computations (see, for instance, Ref. [62]).

2.4.2 The Phase Diagram of QCD

Equipped with a formalism to deal with quantum field theories in thermal equilibrium, one can start searching for answers to the question posed in the beginning of the section. In this subsection, we will describe the phase diagram of QCD, as it is currently understood, focusing on the region of the diagram with zero baryonic chemical potential, $\mu_B = 0$. As already noted, perturbative QCD cannot be applied safely at strong coupling. This, together with the many new challenges that perturbation theory at finite temperature present, means that perturbation theory cannot be used to reliably explore the entire phase diagram of QCD.

Some qualitative information can be inferred from the two main characteristics of

[7] We assumed that ϕ is a set of bosonic fields. The boundary conditions for a fermion ψ are anti-periodic ones, $\psi(0, x^i) = -\psi(\beta, x^i)$. This difference in the boundary conditions takes into account the different statistics of fermions and bosons. [60, 61]

QCD. The two main parameters that characterize the phase diagram are the temperature T of the thermal medium and the baryonic chemical potential μ_B associated with the conserved baryonic number.[8] We know that in the conditions that we live in, $T \ll m_\pi$ and $\mu_B \approx 1\,\text{GeV}$ quarks and gluons are confined inside the hadrons. Also, due to asymptotic freedom, when $T \gg m_\pi$, with $T \gg \mu_B$, since the typical interaction energy between quarks and gluons in the thermal bath is of order T, which implies in this case that quarks and gluons are weakly interacting and become the physical degrees of freedom. This means that one should expect that, as $T \to \infty$, the quarks and gluons inside the hadrons become deconfined - that is, the hadrons "melt" into the quark-gluon plasma (QGP) [5, 65, 66, 68, 69]. This argument indicates that QCD must possess a non-trivial phase diagram, with at least one kind of phase transition, a confinement-deconfinement phase transition at high temperatures.

Gleaning from a variety of approaches, using effective theories such as Nambu-Jona Lasinio models (see Ref. [70] for a review), general arguments from large-N_c Yang-Mills theories and, more recently, lattice QCD calculations [9] we have tentative descriptions of a number of patches of the phase diagram, which can then be collated to sketch what the phase diagram of QCD should look like.

The free quark-gluon plasma

The simplest example of relevance to heavy-ion collisions which one can study is the free QGP, so we pause to briefly consider its thermodyanmics. In the UV, we have a free gas of non-interacting $N_c^2 - 1$ gluons and N_f quarks with N_c colors. For simplicity, we will deal with massless fermions. Setting the chemical potential for all quark flavors to zero, we have that, since a bosonic degree of freedom contributes to $T^4/90\pi^2$ to the Helmholtz free energy density f and a fermionic degree of freedom contributes with 7/8-ths of the bosonic value. Then, the free energy f of the free QGP is given by

$$\begin{aligned} f &= -\underset{\text{(gluons)}}{(N_c^2-1)} \times \frac{\pi^2}{90}T^4 - \underset{\text{(flavors)}}{N_f} \times \underset{\text{(colors)}}{N_c} \times \frac{7}{8}\frac{\pi^2}{90}T^4 = \\ &= -\left[(N_c^2-1) + N_f N_c \frac{7}{8}\right]\frac{\pi^2}{90}T^4 \end{aligned} \tag{2.35}$$

The pressure p and entropy density s of the free QGP follow from standard thermodynamical relations. The pressure is given by $p = -f$, whereas the entropy density is given

[8] Given the large external electric and magnetic fields that may be present in the QGP created in heavy ion collisions at RHIC and the LHC [63] (for a review, see Ref. [64]), one may include, for example, the external magnetic field B as a new parameter to characterize the thermodynamics of the plasma. This is a recent topic of interest in lattice calculations [67], and we will have more to say about this in Chapter 7

[9] See Refs. [71, 72] for reviews of the state of art on the thermodynamics computed using lattice QCD.

by

$$s = -\frac{\partial f}{\partial T} = \left[(N_c^2 - 1) + N_f N_c \frac{7}{8}\right] \frac{2\pi^2}{45} T^3. \tag{2.36}$$

Finally, the energy density ϵ is given by

$$\epsilon = -T^2 \frac{\partial (f/T)}{\partial T} = \left[(N_c^2 - 1) + N_f N_c \frac{7}{8}\right] \frac{\pi^2}{30} T^4. \tag{2.37}$$

Zero baryonic chemical potential

Let us focus our attention first in the case of vanishing chemical potential, $\mu_B = 0$. In the limit of infinitely heavy quarks, we have a pure $SU(N_c)$ gauge theory to study. Since a lattice calculation with no dynamical quarks requires far less computational resources and thus can be done in larger lattices, it is well known that $SU(3)$ Yang-Mills has a first order phase transition [74]: for $T < T_c$, we have a confined gas of glueballs and for $T > T_c$ we have a plasma of deconfined gluons. The transition is of first order since the entropy density s is discontinuous at T_c: $s(T < T_c) \ll s(T > T_c)$, jumping to a finite value at $T = T_c$.

For $SU(3)$ theories with (2+1) dynamical quarks, the situation is much more intricate, as shown in the so-called "Columbia" plot, in Figure 2.2. From chiral symmetry, in the limit of small quark masses, the phase transition is expected to be of first order [75]. For increasing quark masses, we pass by a line of second order confinement-deconfinement phase transitions and then to a region where, although there is a sudden increase of the entropy of the system with increasing temperature characterizing a rapid increase of the number of degrees of the system, all thermodynamic functions and their derivatives to all orders are continuous. This sudden, but continuous to all orders, increase of the entropy, therefore, does not qualify as a true phase transition, being called a crossover. However, for simplicity, in this work we will refer to a crossover as a phase transition, keeping in mind the above remark. For heavy quarks, we pass through another line of second order phase transitions, then going back to a first order phase transition as the quarks become heavy and non-dynamical.

The point P in Figure 2.2 represents the point with physical quark masses. The thermodynamics of this point has been extensively studied on the lattice as computing the fermionic determinant has become feasible in the last few years. The seminal calculation perfomed in [73] and confirmed by further studies[10] show that, with physical quarks, the phase transition is of the crossover type. In Figure 2.3 we present the equation of state (presented as the entropy density s as a function of the temperature T) from recent lattice

[10] See Refs. [71, 72] for a full list of references; the most recent equations of state as computed on the lattice can be found in Refs. [76, 77].

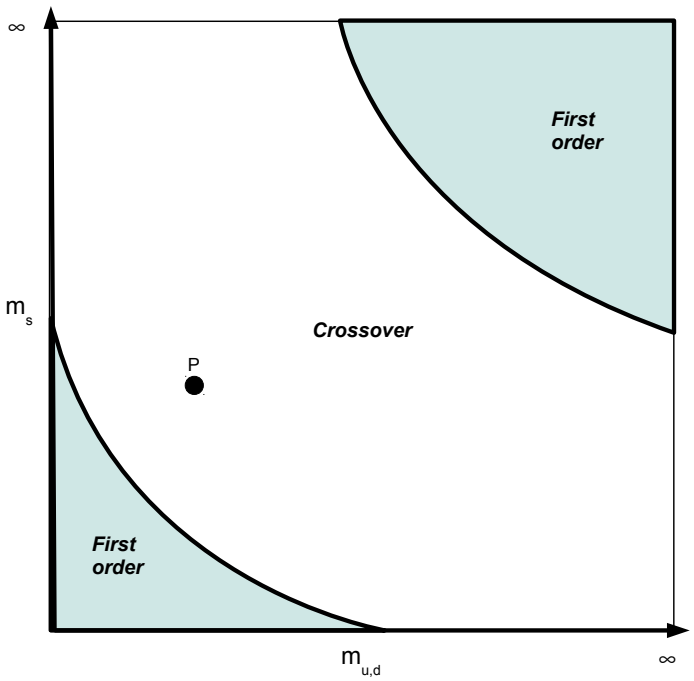

Figure 2.2: *The Columbia plot for QCD with (2+1) dynamical flavors, showing the type of phase transition for each choice of quark masses. The point P is the point with the physical quark masses.*

results [78]. Around $T = T_c = 150\,\mathrm{MeV}$, the entropy density increases rapidly, characterizing the crossover. For T a few times T_c, the entropy density is about 80% of the entropy density of the free QGP with $N_c^2 - 1 = 8$ gluons and $N_f = 3$ fermions (Eq. (2.36)). The approach to the Stefan-Boltzmann limit is slow - this is not surprising, since $\alpha(Q^2)$ decreases logarithmically with Q^2.

Non-zero baryonic chemical potential

For $\mu_B \neq 0$ the situation is more challenging to lattice calculations, due to the sign problem, and one must resort to effective theories (such as Nambu-Jona-Lasinio models) and qualitative arguments (see Refs. [79, 80] for reviews; for recent progress in lattice calculations at $\mu_B \neq 0$, see Ref. [81]). Figure 2.4 shows what is believed to be the current picture for the phase diagram of QCD. For low temperatures and chemical potentials, QCD matter is expected to behave as a hadronic gas, as expected from confinement. There is a line of first order phase transitions as one increases T and μ_B, which characterizes a transition from the hadronic phase to the quark-gluon plasma. The line of first order phase transitions ends at a second order critical point, $(\bar{\mu}, \bar{T})$. For $\mu < \bar{\mu}$, there is no true phase transition, only a crossover connecting the hadronic phase to the QGP phase. At low temperatures, but increasing μ_B, it is expected that there is another phase

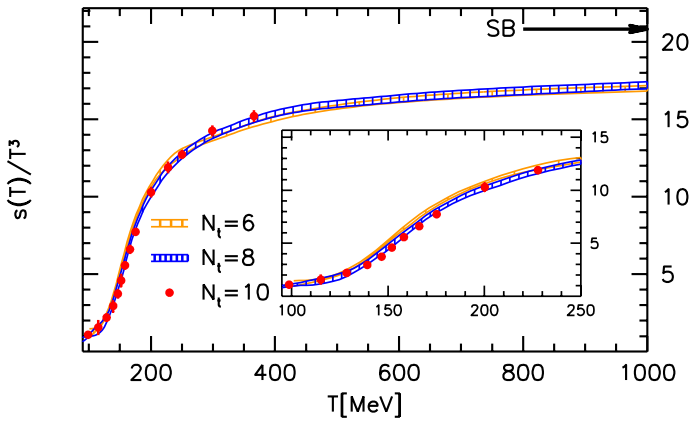

Figure 2.3: *The entropy density s as a function of T for (2+1) QCD, as computed from lattice QCD (figure reproduced from Ref. [78]).*

transition, to a color superconductor (CSC) phase. The reason is an analogy to a normal conductor/superconductor phase transition in condensed matter systems - a weakly coupled gas of fermions (described by the Fermi liquid theory) has a spontaneously broken U(1) gauge symmetry at low temperatures, generating effective atractive interactions among the fermions mediated by the photons, now massive after the symmetry breaking. The same mechanism at high density is expected to work in the case of QCD, with the photons replaced by the gluons. However, due to the non-trivial structure of SU(3), the pattern of symmetry breaking is richer. The exact structure of the phase diagram for $T \ll \mu_B$ is unknown (much more so then in the case $T \gg \mu_B$) - the position and character of the Fermi liquid/CSC phase transition and the number and characteristics of each of the CSC phases are unknown.

2.5 Heavy Ion Collisions, QGP, and strongly coupled plasmas

Since the existence of the quark-gluon plasma in QCD was proposed, it was argued that it could be produced through sufficiently high energy heavy ion collisions [5, 65, 66, 68, 69]. However, it was first thought that the plasma would be produced at such

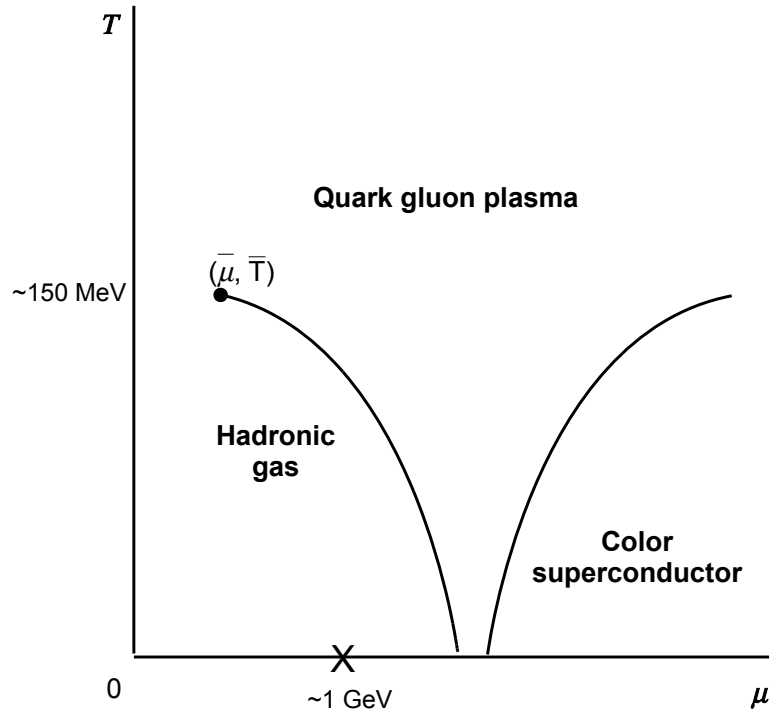

Figure 2.4: *The (expected) phase diagram for QCD. The solid lines are expected to be lines of first order phase transitions. For the hadron gas/quark-gluon plasma phase transition, the line of first order phase transitions are expected to end in a second order critical point. The cross marks the ground state of infinite nuclear matter. The hadron liquid/gas phase transition is not shown in this simplified picture.*

high temperatures that it would behave, due to asymptotic freedom, as a weakly coupled plasma such that perturbative calculations would be applicable to study its properties. However, as heavy ion collider experiments began to access experimental conditions where the plasma was expected to be produced, it became clear that the plasma was, instead, strongly coupled [8–11]. In this section we briefly describe the basic time evolution of the QGP produced in heavy ion collision and the main arguments as to why it should be a strongly coupled plasma.

The evolution of the QGP produced in heavy-ion collisions can be summarized as follows (Figure 2.5): first, both nuclei collide. Since both ions are close to the light speed c, in the center of mass frame both are contracted, being described effectively as two hadronic "pancakes". Immediately after collision, the resulting medium in the collision region is out of equilibrium, the so called the pre-thermalization phase. After $\sim$ 1 fm/c, the medium thermalizes sufficiently so that a hydrodynamic description of the QGP, corresponding to a close-to-equilibrium description, can be applied. The QGP fireball then expands, cooling off in the process. After $\sim$ 10-15 fm/c, the QGP is sufficiently cool so that its temperature T is below to the critical temperature T_c; at this stage, the quarks and gluons coalesce into hadrons (hadronization) - this is the so-called chemical freeze-out. The hadron gas produced still interacts, due to the residual strong interaction. As the nuclear interaction is of short range, after some time the hadrons cannot interact with other anymore (kinetic freezeout). Thus, we have a free gas of hadrons, whose decay products then reach the detectors.

As already mentioned, the first theoretical expectations were for a weakly coupled QGP. However, the experimental results from RHIC (Relativistic Heavy Ion Collider) [6, 8–11] indicate that the plasma produced in heavy-ion collisions is strongly coupled. Evidence for this comes from several arguments. The main argument is that the observed behavior is characterized by a strong elliptic flow (Figure 2.6). Non-central collisions result in an almond shaped collision region. The pressure and energy density distribution of this almond-shaped plasma is correspondingly anisotropic - the pressure gradient along the major axis is lower than the pressure gradient along the minor axis. The posterior hydrodynamical evolution of the fluid depends then on its shear viscosity η (among other transport coefficients for thermodynamics), which is a measure of the momentum diffusion in the plasma. A dimensionless measure of the fluidity of the plasma at zero μ_B can be estimated by the ratio of the shear viscosity η by the entropy density s, η/s. If the plasma is weakly (strongly) coupled, $\eta/s \gtrsim 1$ ($\eta/s \ll 1$, respectively) - we will justify this affirmation below. Thus, a weakly coupled plasma is a viscous plasma, and momentum transport is efficient - the initial pressure anistropy is quickly diffused and the resulting flow is isotropic. In a strongly coupled plasma, we have an almost perfect fluid, with little

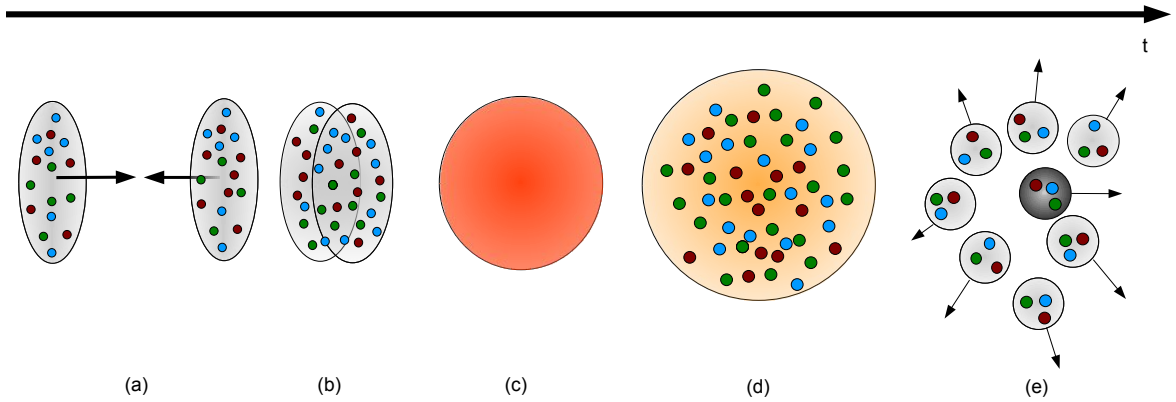

Figure 2.5: *A cartoon picture of the evolution of the QGP produced in heavy ion collisions. Two heavy ions collide at relativistic speed in the center of mass frame (a); during a short phase (∼ 1 fm/c) the collision region is in a state outside thermal equilibrium ((b), pre-thermalization); then the resulting QGP is sufficiently close to equilibrium so that an hydrodynamical description is valid (c); the QGP expands and, in the process, cools off (d); as the QGP cools off below the critical temperature T_c, the quarks and gluons coalesce into hadrons ((e), hadronization and freeze-out), interact with another hadrons, decay and finally can be measured by the detectors. The figure pictures a central collision.*

momentum diffusion: the initial pressure anisotropy survives hydrodynamical evolution. Thus, after the cooling of the QGP, a weakly coupled plasma will result in an isotropic distribution of particles in the detector, whereas the strongly coupled plasma will be characterized by an anisotropic distribution - the so called elliptic flow. The results of RHIC indicated a strong elliptic flow, is qualitatively with that of a perfect relativistic fluid. A hydrodynamical analysis of the QGP with first order transport coefficients [83] indicated that values of η/s of the order 0.1-0.3 furnished a good description of elliptic flow. The picture of strongly coupled QGP is further supported by the measurement of jet quenching - hard partons plowing through the plasma interact with the medium, losing energy and momentum. Thus, the jets produced by these partons in the plasma are quenched, having less particles with hard momenta. (See [82] for more details on the time evolution of the QGP and its hydrodynamical description.)

Now, let us briefly justify the connection between the shear viscosity and the gauge coupling. From kinetic theory [84][11] it is known that

$$\eta \sim n\langle p\rangle l_{mfp}, \tag{2.38}$$

[11]We should note that one of the main hypothesis of kinetic theory assumes the existence of quasi-particle excitations in the plasma, which are free-streaming between collisions. However, a strongly coupled fluid does not have a quasi-particle description. An example is the strongly coupled $\mathcal{N} = 4$ plasma [85, 86], for which no quasi-particle description is possible. It is an open question if the same happens for QCD in the context of heavy ion collisions.

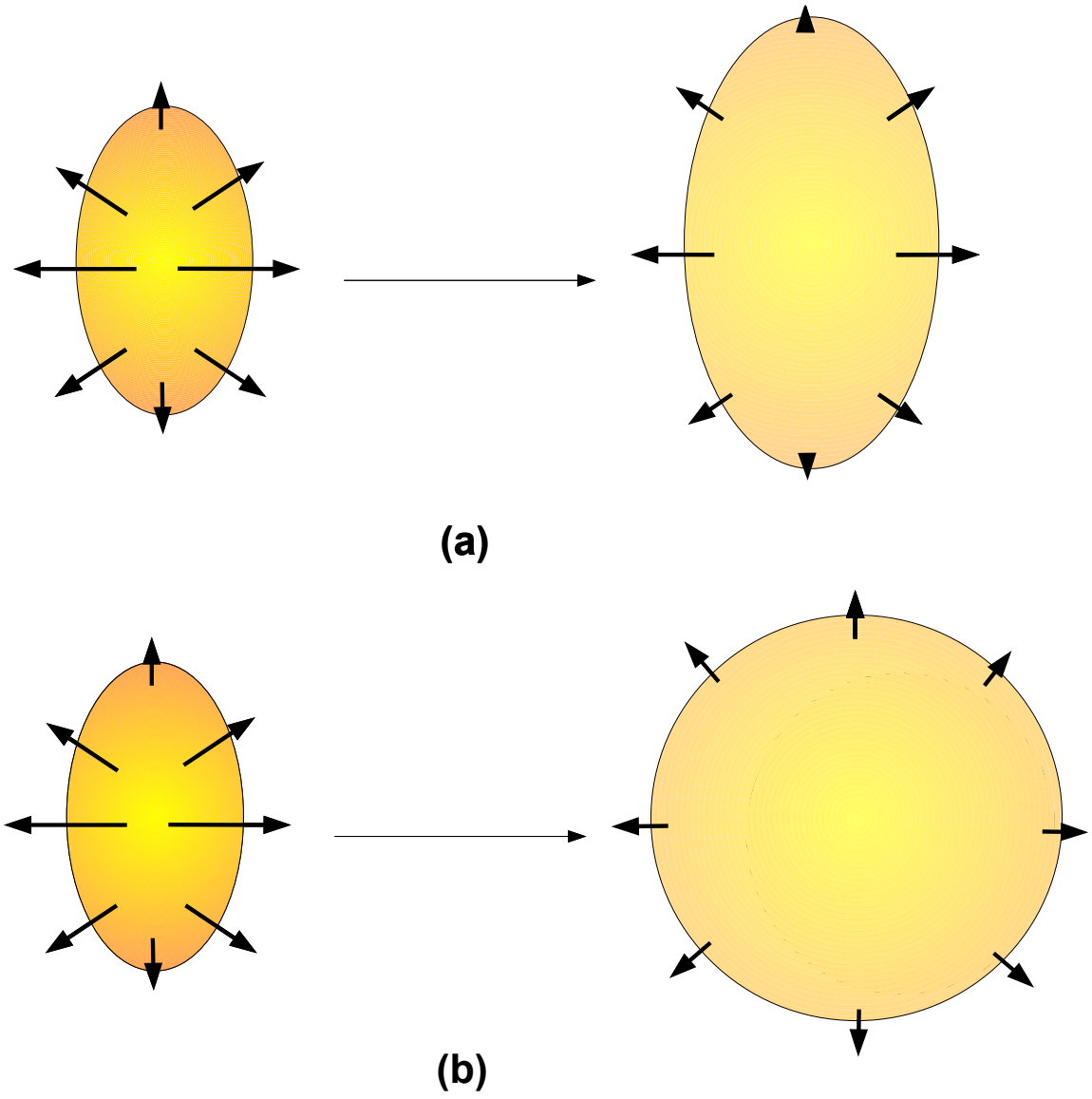

Figure 2.6: *A cartoon picture of the elliptic flow of the QGP. A strongly coupled plasma (a) does not exhibit good momentum transport(because $l_{mfp} \ll 1/T$, so that an initial spatial (and thus momentum) anisotropy is propagated to late times in its evolution. Contrast this with a weakly coupled plasma (b), which can diffuse momentum efficiently and thus diffuse the initial momentum anistropy.*

where n is the (quasi)particle density, $\langle p \rangle$ is the average momentum of the particles and l_{mfp} is the mean free path. The entropy density s proportional to n. Then,

$$\frac{\eta}{s} \sim \langle p \rangle l_{mfp}. \tag{2.39}$$

Now, a small (large) mean free path compared to $\langle p \rangle$ corresponds to a strongly (weakly) interacting plasma. A simple consequence of Eq. (2.39) [87] can be inferred using the uncertainty principle. A particle with momentum $\langle p \rangle$ cannot be localized with a precision greater than $1/\langle p \rangle$. Thus, the mean free path is bounded below by $1/\langle p \rangle$. Therefore, $\langle p \rangle l_{mfp} \gtrsim 1$, and

$$\frac{\eta}{s} \gtrsim 1. \tag{2.40}$$

Restoring units,

$$\frac{\eta}{s} \gtrsim \frac{\hbar}{k_B}. \tag{2.41}$$

This is a simple estimate of a quantum mechanical lower bound for η/s for a system with a hydrodynamical description (assuming the validity of a quasi-particle picture and of kinetic theory, see footnote 11). The results extracted from a comparison of hydrodynamic calculations to the QGP data, $\eta/s \sim 0.1 - 0.3$, indicate that the the QGP is close to the lower bound of Eq. (2.41). Moreover, no other system known in nature seems to have a shear viscosity/entropy density ratio lower that the QGP, as indicated in Figure 2.7.

Before the near-perfect hydrodynamic behavior and the shear viscosity of the QGP were estimated, computations using the gauge/gravity duality provided the first hints of a fluid that came close to the limitations imposed by Eq. (2.41). Specifically, as we will explore later in the next chapter, for a large class of gauge theories which accept a description at strongly coupling by a dual gravitational theory [90],

$$\frac{\eta}{s} = \frac{1}{4\pi} \sim 0.08, \tag{2.42}$$

close to the estimates of η/s for the QGP of Ref. [83]. A perturbative description of η in gauge theories in the netx-to- leading log calculation yields [88, 89]

$$\eta = \kappa \frac{T^3}{g^4 \ln g^{-1}}, \tag{2.43}$$

with $\kappa \sim 100$, which yields values of $\eta/s \gg 1/(4\pi)$, for all reasonable choices of T and g compatible with the experimental conditions of the QGP. This indicates one of the virtues of the gauge-gravity framework to study strongly coupled non-Abelian plasmas. In the next chapter we will outline the basics of the gauge/gravity duality, including the calculation of Eq. (2.42).

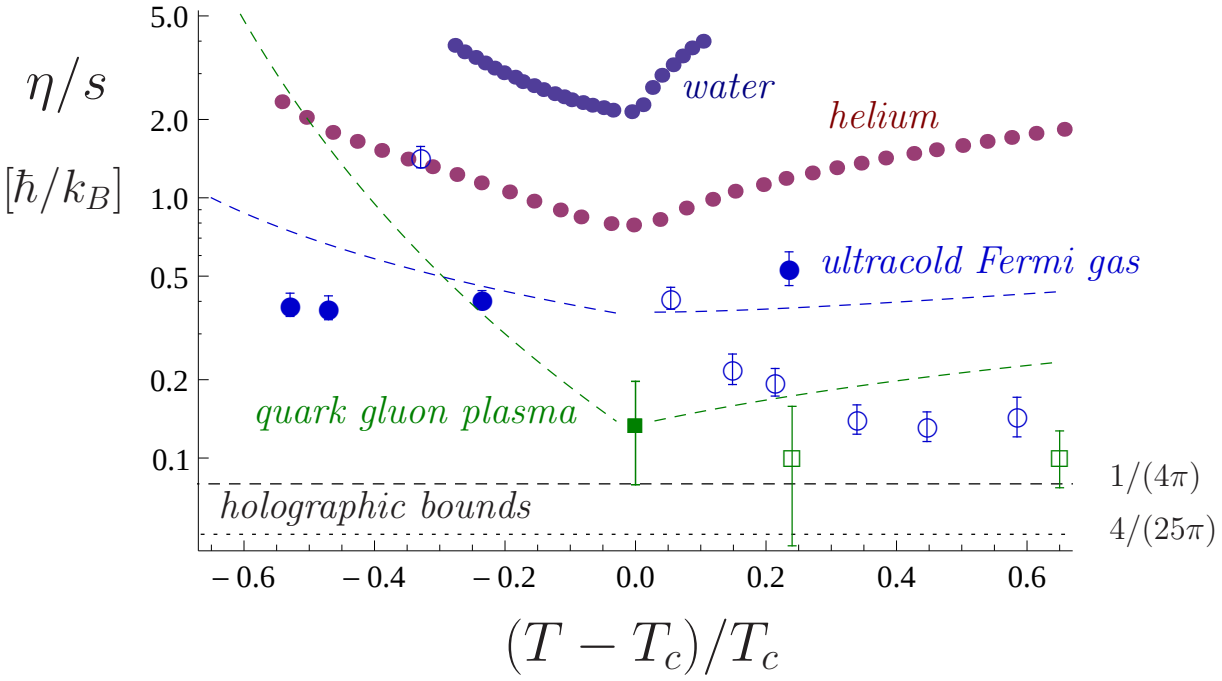

Figure 2.7: *A comparison of the shear viscosity/entropy density ratio η/s for temperatures near the phase transition for some systems which admit a hydrodynamic description. T_c is the corresponding critical temperature for each system (temperature of the endpoint of the liquid-gas transition line for water and helium, superfluid phase transition for ultracold Fermi fluids and confinement/deconfinement temperature of the QGP). The top dashed horizontal line refer to the holographic result for a large class of strongly coupled gauge theories with gravity duals [90]; the lower dashed horizontal line refer to the theory dual to Gauss-Bonnet gravity [91, 92] . This figure was extracted from Ref. [59], wherein the original references for data can be found.*

Chapter 3

Gauge/gravity duality

In this chapter, we present a self-contained review of some of the fundamental aspects of the gauge/gravity duality necessary for this work. We will start from a intuitive, heuristic point of view (Sections 3.1 and 3.2), based on a geometrical interpretation of the renormalization group flow. The most well-known and studied case of the gauge/gravity duality, the AdS/CFT correspondence, is treated in Section 3.3. The main computational tool of the duality is presented in Section 3.4, which is applied to relate scaling dimensions on the gauge theory with the masses of fields in the dual theory of gravity in Section 3.5. Aspects of the duality at finite temperature are treated in Section 3.6. Section 3.7 presents the prescriptions for computing correlation functions from holography. A phenomelogical application is in Section 3.8, which reviews the computation of transport coefficients using the membrane paradigm.

3.1 Bird's eye overview

The gauge/gravity duality, essentially, is the statement of an equivalence between theories of quantum gravity in $(d+1)$ dimensions and quantum field theories in d dimensions [14,93,94]. It can be seen as a concrete example of the holographic principle [95,96]. It is also an example of a weak/strong coupling duality. When the quantum field theory is strongly coupled, the corresponding quantum gravity dual is weakly coupled, that is, a classical theory of gravity; in the other hand, when the the gravity theory is in the full quantum regime, the dual QFT is weakly coupled, amenable to treatment by perturbative methods. Thus, the gauge/gravity duality may be used to probe quantum theories of gravity or, alternatively, to probe strongly coupled QFTs - the latter being our application of interest.

The original review of the gauge/gravity duality can be found in Ref. [97]. Pedagogical introductions are given in Refs. [98–100] or in textbooks [101,102]. For applications of the

gauge/gravity duality in heavy ion physics, see Refs. [59, 103].

3.2 Heuristic arguments

In this section we will present some heuristic arguments to motivate the validity of the duality gauge/gravity. These arguments, while physically intrusctive, are informal - many are based on the arguments presented in Ref. [59]. These arguments are even more heuristic than the arguments used to establish specific cases of the duality, using explicit constructions from string theory. In this section, we will try to avoid using string theory, instead arguing directly from quantum field theory and general relativity that the gauge/-gravity duality duality should be expected to hold in some special cases. Specifically, the main view point taken in this section is that the gauge/gravity duality is a geometrization of the renormalization group. This point of view is also useful to justify the use of bottom-up gauge/gravity constructions as means of developing effective theories that are close to QCD in the infrared (IR). For completeness, and since it will play an important role in this thesis, we present in the next section the AdS/CFT correspondence, using the standard string theory arguments as a paradigmatic example of a well established example of the gauge/gravity duality.

3.2.1 From gravity to a field theory

Let us consider probing the event horizon of a black hole in a $d+1$ dimensional spacetime as an observer in the asymptotically flat geometry far from the event horizon. We send to the horizon a robot which emits light signals at a given wavelength. As the robot approaches the horizon, the wavelength of the emitted signals by the robot gets redshifted, as observed by the distant observer. The robot takes infinite time, as measured by the distant observer, to approach the horizon - the distant observer sees the robot ultimately being frozen near the horizon, sending low frequency redshifted signals.

Now, consider a swarm of these robots, sent isotropically from the asymptotic spatial infinity to the black hole horizon. The asymptotic observer at infinity sees the swarm of robots being frozen the horizon, sending all low frequency signals. Thus, the robots effectively constitute a membrane covering the event horizon, called the membrane horizon [104]. If another robot is sent afterwards towards the membrane horizon, it will perturb the membrane horizon as a low frequency fluctuation. Thus, the perturbation will propagate as a hydrodynamical low-frequency fluctuation on the horizon. This suggests that the membrane horizon behaves as a hydrodynamical theory - that is, as a d dimensional field theory. Incidentally, we should note that the low-frequency fluctuations of the membrane horizon can be characterized by means of corresponding membrane transport coefficients

- this fact will be exploited in Section 3.8 to evaluate transport coefficients of strongly coupled non-Abelian plasmas.

3.2.2 From a field theory to a theory of gravity - Renormalization group *redux*

Now, let us consider the renormalization group flow of a d dimensional field theory defined on a lattice with spacing a. Let the dynamics of the theory be described by the hamiltonian

$$\hat{H} = \sum_{x,i} J_i(x)\hat{O}_i(x), \tag{3.1}$$

where $\hat{O}_i(x)$ are local operators with couplings $J_i(x)$, with x labelling the lattice sites and $i = 1, 2, \ldots$ label the combinations of operators that enter into the hamiltonian.

The renormalization group (RG) [38–41], already briefly discussed in Chapter 2 in connection with the asymptotic freedom of QCD, is a tool to analyze the dependence of observables as a function of the lattice spacing a. We consider a series of coarse-grained lattices with spacing u, and corresponding coarse grained couplings $J_i(x, u)$, chosen in such a way that the ground state and low energy excitations of the theory are left invariant. The scale dependence of the couplings obey flow equations, the renormalization group equations (of which Eq. (2.17) was a special case)

$$u\frac{\partial}{\partial u}J_i(x, u) = \beta_i, \tag{3.2}$$

where the beta functions β_i encode the flow of the coupling $J_i(x, u)$, and may depend on the couplings $J_j(x, u)$ and the scale u.

Now, we can recast the RG flow by stacking the coarse grained theories with lattice spacing u on top of each other (see Figure 3.1). In this point of view, the dependence on the scale u can be seen by recasting the original d dimensional theory described in Eq. (3.1) by a $d + 1$ dimensional framework, where the scale u takes the place of the extra dimension. The scale dependent couplings $J_i(u, x)$ must then be local fields in this $d + 1$ dimensional space-time. The coordinate u runs from the original ultraviolet (UV) theory with $u = a$ to the deep infrared (IR) with $u \to \infty$. Thus, we have that the RG flow of the original d-dimensional theory is related to a $d + 1$ dimensional field theory. Let us now argue that this dimension must be a curved dimension and that the $d + 1$ dimensional field theory must be a theory of gravity, whose low-energy effective action is given by Einstein-Hilbert action coupled to matter fields.

To do so, we ask what must be the field content (the bulk fields) and the (bulk) Lagrangian of the $d+1$ field theory. Generalizing the argument in the previous paragraph,

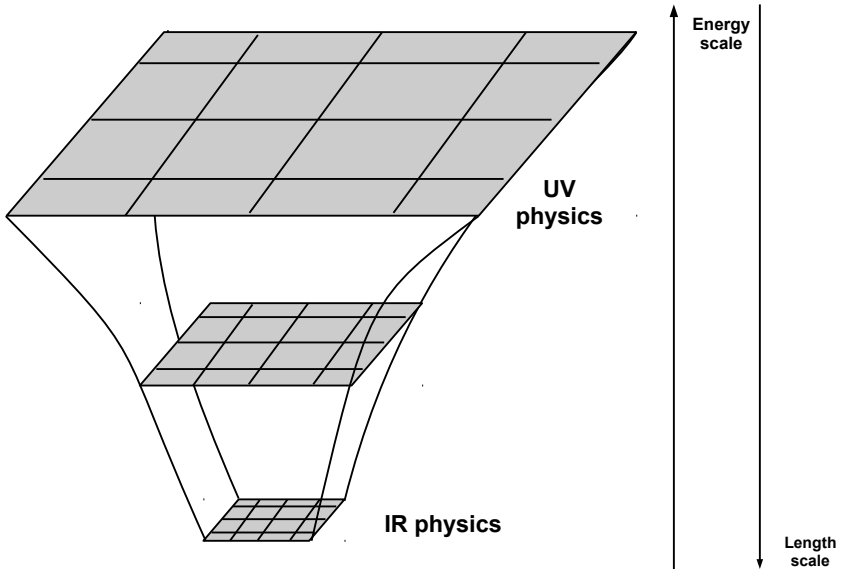

Figure 3.1: *Stacking the coarse grained lattices with scale u on top of each other, and the resulting curved space description.*

to each operator $\hat{O}_i(x)$ in the d dimensional field theory there must be corresponding bulk fields $\phi_i(x,u)$. We impose as boundary conditions on these fields $\phi_i(x,u)$ that they give the UV couplings of the operators, that is,

$$\phi_i(x,u=a) = J_i(x). \tag{3.3}$$

This boundary condition implies that the spin, charges and quantum numbers of the bulk fields $\phi_i(x,u)$ must be equal to the spin, charges and quantum numbers of the operators $\hat{O}_i(x)$. The combination $\phi_i(x,a)\hat{O}_i(x)$ must be a scalar and part of the Hamiltonian of the theory - that is, $\phi_i(x,a)$ are the sources of the operators $\hat{O}_i(x)$.

In particular, we consider d dimensional QFTs where there is a well-defined energy-momentum tensor operator $\hat{T}_{\mu\nu}$. Thus, there must be a corresponding spin-2 bulk field $g_{\mu\nu}$ which sources $\hat{T}_{\mu\nu}$ by Eq. (3.3). Now, assuming that the $a \to 0$ limit of the d dimensional QFT is Lorentz invariant, we can use the Weinberg's theorem [105], which states that any spin 2 field must respect the equivalence principle and couple universally to all fields or else decouple in the low energy limit. The latter means that $g_{\mu\nu}(x, u \to \infty) \to 0$ - that is, according to Eq. (3.3), that no sources of the energy-momentum tensor can affect the dynamics of the theory; in other words, that we have a topological field theory. Discarding this hypothesis, we then conclude that $g_{\mu\nu}$ obeys the equivalence principle. Applying now the Weinberg-Witten theorem [106], which says that spin 2 fields in Poincaré invariant theories (with conserved energy-momentum tensors) must be massless, we see that $g_{\mu\nu}$ can be identified with the graviton field, and that its low-energy dynamics must be dictated

by the Einstein-Hilbert action.

As a last remark, the dynamics of the d dimensional *local* QFT must correspond to the dynamics of $d+1$ dimensional local theory of gravity. This means that the dynamics of the theory of gravity must be enconded in a non-local way in the dynamics of the dual QFT. Thus, the gauge/gravity description is also called a holographic correspondence.[1]

3.2.3 A geometrical description of a CFT - Anti de-Sitter space

The dual geometry for a CFT

Recapping the content of the previous two sections, we argued, first starting from a gravitational theory and then starting from a QFT, that there must be a duality between d dimensional field theories and theories of gravitation in $d+1$ dimensions.

Now, we present an argument that leads to a metric describing a d dimensional conformal field theory - for a review of conformal symmetry, recall Sub-Section 2.2.2 and Section 2.3.

A theory which is conformally invariant possess no intrisic scales. However, a classically field theory which is conformally invariant may develop a scale anomaly when quantized which then breaks conformal invariance. This happens whenever $\beta_i \neq 0$, for then, from the RG flow equations (2.17), the couplings are scale dependent. This, in fact, is the fate of an $SU(N_c)$ Yang-Mills theory (and thus of QCD), which is conformally invariant in the classical regime but acquires a scale Λ_{QCD} from dimensional transmutation, because, as seen in Eq. (2.18), $\beta_g \neq 0$.

However, there can exist values of the couplings in other gauge theories such that $\beta_i = 0$. In this case, we have a fixed point of the RG flow equations - if this happens as $a \to 0$ then we have an UV fixed point; if this happens as $a \to \infty$, then we have an IR fixed point[2]. At the fixed point, the field theory behaves as a conformal theory. Thus, understanding the dynamics of a CFT is useful for understading the dynamics of a QFT on the vicinity of a fixed point.

Consider then a Lorentz invariant d-dimensional CFT, which we suppose that has a gravitational dual description in $d+1$ dimensions. Let us take the emergent dimension (whose associated coordinate we label z and take it to be associated with the scale with we probe the field theory). We require that the conformal group SO(d,2) is mapped to

[1] The gauge/gravity correspondence, in its best known examples, such as the AdS/$\mathcal{N}=4$ Super Yang-Mills (SYM) correspondence to be described below, furnish explicit examples of quantum gravity theories which respect the holographic principle [95, 96], by virtue of its construction. However, it must be noted that the holographic principle is not equivalent to its realization by gauge/gravity duality - the holographic principle is a feature that may expected be respected by any theory of quantum gravity [108].

[2] If, moreover, the couplings themselves are zero at the fixed point, $J_i \to 0$, the fixed point is called a trivial fixed point; therefore, QCD has a UV trivial fixed point.

the group of isometries of the $d+1$ dimensional space-time. However, as already shown in Sub-Section 2.2.2, SO(d,2) has $d(d+1)/2$ generators. As a group of isometries of $d+1$ dimensional space-time, this corresponds to a maximally symmetric space-time [107]; thus, it must correspond to a space with a constant curvature scalar: either de Sitter (dS), Minkowski or Anti-de Sitter (AdS) spacetimes in $d+1$ dimensions. However, only AdS_{d+1} has the correct isometry group SO(d,2). Thus, the theory dual of gravity for a CFT takes place in a AdS_{d+1} space-time, which we now proceed to briefly discuss some of its most important properties.

Brief review of the properties of Anti de-Sitter space

The metric of an AdS_{d+1} space-time is, in the so called Poincaré coordinates,

$$ds^2 = \frac{L^2}{z^2}\left(-dt^2 + d\vec{x}^2 + dz^2\right), \tag{3.4}$$

where $(t, \vec{x})$ are coordinates for copies of d dimensional Minkowski spacetimes at each fixed z, the emergent coordinate of the fifth dimension, and L is called the radius of AdS_{d+1}. The coordinate z is interpreted as the length scale of the RG group flow - $z \to 0$ is the UV of the theory and $z \to \infty$ is the IR limit of the theory. Another useful parametrization of AdS space used in this thesis is given by the coordinate transformation $z \to L/U$, which yields[3]

$$ds^2 = \frac{U^2}{L^2}\left(-dt^2 + d\vec{x}^2\right) + \frac{L^2}{U^2}dU^2, \tag{3.5}$$

In this coordinate system, U is interpreted as the energy scale in the RG flow. The curvature scalar $\mathcal{R}$ of the geometry is

$$\mathcal{R} = -\frac{d(d+1)}{L^2}. \tag{3.6}$$

Since $\mathcal{R} < 0$, the curvature of AdS space is negative - AdS is an example of hyperbolic geometry[4]. As a maximally symmetric space, the Riemann curvature tensor $\mathcal{R}_{\mu\nu\alpha\beta}$ of AdS space-time is given by

$$\mathcal{R}_{\mu\nu\alpha\beta} = \frac{\mathcal{R}}{d(d+1)}(g_{\mu\alpha}g_{\nu\beta} - g_{\nu\alpha}g_{\mu\beta}), \tag{3.7}$$

[3]It should be noted that the metric in Eqs. (3.4) or (3.5) coordinatizes only a patch of AdS space; global coordinates (accompanied with the correspoding causal structure described by means of a Penrose diagram) can be found, for instance, in [107].

[4]Indeed, one extrinsic definition of AdS_{d+1} is via the embedding of a $d+1$ hyperboloid in a $d+2$ dimensional Minkowski space.

From Eqs. (3.6) and (3.7) it is easy to check that the AdS geometry is a solution for Einstein's equation in vacuum with a cosmological constant Λ,

$$\mathcal{R}_{\mu\nu} - \frac{1}{2}\mathcal{R}g_{\mu\nu} + \Lambda g_{\mu\nu} = 0, \tag{3.8}$$

as long as $\Lambda = -d(d-2)/(2L^2)$, that is, with a negative cosmological constant.

The main feature of AdS space is that it serves as a "box" for gravity. For $z \to 0$ AdS space has an asymptotic Minkowski boundary. Material particles and light signals sent from the interior of AdS space to the boundary return to the boundary in finite time for an observer inside AdS space. This can be seen from the geodesic equation, for material particles; for light signals, this follows more simply from taking $ds^2 = 0$ and solving for t in Eq. (3.5).

3.3 The AdS/CFT correspondence

The main example of a gauge/gravity duality is the $\mathrm{AdS}_5 \otimes S^5/\mathcal{N} = 4$ Super Yang-Mills (SYM) correspondence, for which we have both a heuristic argument from string theory and extensive checks perfomed by exploiting the symmetries of the theories involved. Since we will use this correspondence as a check and as a useful example for many applications of the gauge/gravity duality, and also since it provides an explicit example of a top-down gravity dual, we will review the arguments for its construction here.

The main point is to consider a stack of coincident D3-Branes in type IIB string theory and look at the resulting theory from two complementary points of view [14]. First, I will present the necessary facts needed on Dp-branes to present the argument.

3.3.1 Dp-branes

Dp-Branes [109] arise in string theory, perturbatively, when considering possible boundary conditions for open strings. Open strings which obey Dirichlet conditions have their ends fixed in p dimensional hypersurfaces, which are called Dp-Branes. The fields describing the open string can inject fluxes in the ending surface. Thus, the Dp-branes are charged with respect to the fields of the theory. In particular, they are charged with respect to the antisymmetric p forms of string theory. Thus, low-energy fluctuations of the end points of the string, represented by the Dp-brane can be described by a generic action of the form

$$S = -T_p \int d^{p+1}x \ [\ldots], \tag{3.9}$$

where the coupling T_p is given by

$$T_p = \frac{1}{(2\pi)^p g_s l_s^{p+1}}, \tag{3.10}$$

where l_s is the string length and g_s is the string coupling constant. From T_p we see that as $g_s \to \infty$, $T_p \to 0$ - this means that Dp-brane is an intrisically non-perturbative object, since its contribution to the partition function is most important when the coupling constant is large. Therefore, Dp-branes are dynamical, non-perturbative, objects in string theory, with their own dynamics. Since they are extended objects, T_p is called the Dp-brane tension and it is the mass source for the brane. In this non-perturbative point of view, the open strings are considered as fluctuations of the fields in the brane worldvolume.

If the open strings in the theory carry Chan-Paton charges on their endpoints, then these fields source gauge field on the Dp-brane worldvolume. In the case of an isolated Dp-brane, the gauge field on the worldvolume has gauge group U(1). If we have a stack N of coincident Dp branes, massless (since they have zero length) open strings can connect any pair of branes - this is the basis of an argument showing that the gauge fields on the brane worldvolume transform under the gauge group U(N) (for a nice presentation of this argument, see, for instance, [109, 110].

3.3.2 The decoupling argument - The stringy point of view

Let us then consider, in type IIB string theory, a stack of N coincident Dp-branes and look at the low-energy limit of the theory. That is, we take the string tension $\alpha' \to 0$, where we defined $\alpha' = l_s^2$.

The four dimensional gauge theory in the worldvolume of the brane is given by the low energy open-string fluctuations of the Dp-branes and is described by $\mathcal{N} = 4$ SYM theory with gauge group SU(N_c). $\mathcal{N} = 4$ SYM is a conformal theory with $\mathcal{N} = 4$ copies of the supersymmetry algebra; its most remarkable feature is that it is a superconformal theory - it is invariant by transformations of the super conformal group PSU(2,2|4), which includes the conformal group in four dimensions SU(4,2). Moreover, it remains conformal even after quantization: it has been proven that the beta function vanishes at all orders in perturbation theory (see Ref. [111] for a review of the proofs of this statement) and it has been argued that this result holds non-perturbatively [112]. Its field content includes, along with the gauge fields, eight fermionic fields and six scalars, all transforming in the adjoint representation of SU(N). Alongside the open string fluctuations which give $\mathcal{N} = 4$ SYM on the worldvolume, we have closed strings propagating in the spacetime (whose low energy limit is type IIB supergravity), which interact with the open strings of the

Dp-branes. Thus, we can write the action of the theory as

$$S = S_{\text{branes}} + S_{\text{bulk}} + S_{\text{int}}, \tag{3.11}$$

where S_{branes} is the action for the fields in the brane worldvolume, S_{bulk} the action for the closed strings in the 10 dimensional spacetime, and S_{int} is an interaction term between the brane fields and the space-time fields. However, since $S_{\text{int}} \propto G_{10}$, where G_{10} is the ten dimensional Newton's constant, and since $G_{10} \propto g_s\alpha^2$, in the low energy limit $\alpha' \to 0$, $S_{\text{int}} \to 0$. Thus, in the low energy limit, the theory is described by $\mathcal{N} = 4$ SYM in the worldvolume of the branes and free supergravity in the bulk of the ten dimensional spacetime, with the worldvolume and bulk sectors being non-interacting.

3.3.3 Decoupling argument - Supergravity point of view

Now, let us look at the low energy limit from a second point of view, taking, along with $\alpha' \to 0$, the string coupling constant $g_s \to 0$. In this limit, type IIB string theory reduces to type IIB supergravity. However, as $g_s \to 0$, the mass of the Dp branes must be large, according to (3.10). Thus, the stack of Dp-branes must deform the space-time. Type IIB supergravity solutions corresponding to the space-time deformed by the stack of D3-branes have been found [113]. The metric of this solution is given by

$$ds^2 = H(r)^{1/2}(-dt^2 + dx_1^2 + dx_2^2 + dx_3^2) + \frac{1}{H(r)^{1/2}}(dr^2 + r^2 d\Omega_5^2) \tag{3.12}$$

where (t, x_1, x_2, x_3) are coordinates parametrizing the world volume of the D3-branes, r is a coordinate perpendicular to the world-volume of the brane and $d\Omega_5^2$ is the metric for a unit five sphere S^5. The warping factor $H(r)$ is given by

$$H(r) = 1 + \frac{L^4}{r^4}, \tag{3.13}$$

where the constant L is given by

$$L^4 = \alpha'^2 N g_s. \tag{3.14}$$

Type IIB supergravity also has an antisymmetric 4-form A_4, whose self-dual field strength 5-form $F_5 = dA_4$, in this solution, is given by

$$F_5 = (1 + *)dt \wedge dx_1 \wedge dx_2 \wedge dx_3 \wedge (dH^{-1}). \tag{3.15}$$

The charge of the black brane in this solution is $Q = g_s N$. This solution corresponds to an extremal black hole extended along the (t, x_i) directions, thus being called a black $p = 3$-brane. This solution is extremal in the sense that it saturates the bound $|Q| \leq M$ between the charge Q and mass M - in this case, the event horizon coincides with the singularity at $r = 0$.

Now, consider field fluctuations near the horizon at $r = 0$, with arbitrary energy E_{hor}. By the gravitational redshift, the corresponding energy of the fluctuation as seen to a distant observer far from the horizon is $E \sim (-g_{00})^{-1/2} E_{\text{hor}} \sim r E_{\text{hor}} \to 0$. Thus, every fluctuation near the horizon is a low-energy fluctuation as seen by the distant observer. Moreover, low energy gravitational fluctuations distant from the horizon are non-interacting - this comes from the fact that effective gravitational coupling is proportional to E^2. Thus, we have two sectors of low-energy fluctuations in the geometry: near horizon fluctuations, which are seen as low-energy fluctuations by a distant observer, and low energy gravitational fluctuations far from the horizon. Both sectors do not interact with each other.

Considering only the near horizon geometry, at $r \sim 0$, then $H(r) \sim L^4/r^4$. Thus, the near horizon metric is $ds^2 = ds^2_{\text{AdS}_5} + ds^2_{S^5}$, where $ds^2_{\text{AdS}_5}$ is the metric of a AdS_5 space and $ds^2_{S^5}$ the metric of a five sphere, both sharing the common radius L. Thus, the near horizon geometry is $\text{AdS}_5 \otimes S^5$. Thus, near horizon fluctuations are described by type IIB supergravity on a $\text{AdS}_5 \otimes S^5$ background.

3.3.4 The AdS/CFT correspondence

Let's summarize the results of the previous paragraphs. From the stringy point of view, we found out that we have, at low energies, $\mathcal{N} = 4$ SYM in the worldvolume of the D3-branes plus free supergravity in the bulk of the 10 dimensional space time. From the supergravity extremal black $p = 3$-brane point of view, we found out that we have, at low energies, fluctuations near the horizon at $r = 0$ and free supergravity fluctuations far from the horizon.

Assuming that it is reasonable to identify the dynamics of free supergravity theories from both point of views, we can then argue that, somehow, $\mathcal{N} = 4$ SYM in the worldvolume of the D3-branes is equivalent to a type IIB supergravity on a $\text{AdS}_5 \times S^5$ background - this is the basic statement of the AdS/CFT correspondence. [14]

3.3.5 Regimes of validity and versions of the correspondence

Now, let's examine when the above correspondence is valid. For supergravity to be a valid approximation, the typical length scale of the geometry, here given by the radius

L, must large compared to typical string scale, here given by the string length $l_s = \sqrt{\alpha'}$. Also, loop corrections of string theory must be negligible, that is, $g_s \to 0$. In summary, we must have

$$\frac{l_s}{L} \ll 1 \qquad \text{and} \qquad g_s \to 0. \tag{3.16}$$

By Eq. (3.14), and as $g_s = g_{YM}^2$, supergravity is valid when

$$\lambda \equiv N_c g_{YM}^2 \gg 1 \qquad \text{and} \qquad g_{YM} \to 0, \tag{3.17}$$

where λ is the 't Hooft coupling. Thus, supergravity is valid when $\mathcal{N} = 4$ SYM theory is in the large N_c limit and with large 't Hooft coupling. This justifies the name *duality* given to the gauge/gravity duality: as the gravity theory is weakly coupled, the dual gauge theory is strongly coupled.

As stated, the duality is valid only in the 't Hooft limit with λ large, but fixed, and with $g_{YM} \to 0$. Maldacena's conjecture is that the duality is valid for arbitrary λ and g_{YM} in the gauge theory side - that is, when we consider the full string theory (with finite α') in the quantum regime (with finite g_s). However, due to the dual character of the conjecture - when the gauge theory is strongly coupled and hard to deal with, the gravity theory is in the classical regime, and when the gauge theory is weakly coupled and amenable to perturbative methods, the gravity theory is in the full quantum regime - it is not easy to prove the validity of the AdS/CFT correspondence. However, many checks, exploiting the fact that $\mathcal{N} = 4$ SYM has a large number of symmetries and thus many quantities protected by these symmetries can be evaluated at the perturbative level and then extrapolated safely to the non-perturbative region, where then they can be compared with the corresponding computations at strong coupling using the correspondence. For instance, the triangle anomaly in the SO(6) R-current three point function has been checked [94]. Also, another non-trivial check is the computation of anomalous dimension of operators in $\mathcal{N} = 4$ SYM and the comparison with the results obtained from AdS/CFT correspondence [94, 114]. See Ref. [97] for more tests of the correspondence.

As a useful result that will be employed later, we relate Newton's constant with the number of branes N_c (equivalently, the rank N_c of SU(N_c)) and the AdS_5 radius L. Ten dimensional Newton's constant G_{10} is related to the string length $l_s = \alpha'$ and the string coupling constant g_s by

$$32\pi^2 G_{10} = (2\pi l_s)^8 g_s^2. \tag{3.18}$$

By using Eq. (3.14) and remembering that $g_s = g_{YM}^2$, we see that

$$G_{10} = \frac{\pi^4 L^8}{2N_c^2}. \tag{3.19}$$

Since S^5 is compact, we may consider the dimensional reduction of the theory on AdS_5 only. The effective five dimensional Newton's constant is given by $G_5 = G_{10}/V_{S^5}$, where $V_{S^5} = \pi^3 L^5$ is the volume of S^5. Then,

$$G_5 = \frac{\pi L^3}{2N_c^2}. \tag{3.20}$$

3.3.6 Top-down and bottom-up constructions

We presented the most well-known and established example of the gauge/gravity duality, namely the $AdS_5 \otimes S^5/\mathcal{N} = 4$ SYM duality. However, as argued in Section 3.2, the gauge/gravity duality is expected to be valid in more general setups. For phenomenological applications, one is interested in finding gravity theories which more closely model the physical system at hand. For instance, to pursue a realistic model for QCD, one may want to break conformal invariance and supersymmetry, introduce fermions in the fundamental representation, and include confinement and chiral symmetry breaking in the gauge theory.

There have been two main paths in the literature pursued in order to build theories of gravity with more realistic dual QFT's. The first one is to start from other string theory based constructions and then build the corresponding gauge theories and gravity theories pairs, in a manner analogous to the one performed above for type IIB superstring theory/$\mathcal{N} = 4$ SYM. This is the so-called top-down approach. Examples are the Klebanov/Strassler cascading $\mathcal{N} = 1$ SYM, [115], which is a confining gauge theory, and the Sakai-Sugimoto model [116], which presents chiral symmetry breaking and includes fermions in the fundamental representation.

An alternative choice is to start from the phenomenology of the desired gauge theory, and then build an effective gravity theory whose associated dual gauge theory possesses the desired phenomelogical characteristics. One does not have a well known string theory construction, and thus the specific gravity/gauge theory pair is not known - if such pair exists. On the other hand, the resulting gravity theories possess few bulk fields as parameters, providing useful and simple models for some aspects of QCD. This is the bottom-up approach. Examples of this approach are given by the hard-wall [117] and soft-wall [118] models, models which present the pattern of chiral symmetry breaking of QCD [119] and the Einstein + scalar confining models of Gubser and Nellore [15] and Gursoy, Kiritsis et al. [16, 17], both of which will play a role in this work.

3.4 The duality at work - Extracting observables of the QFT

After arguing for the validity of the gauge/gravity duality, let us now discuss more practical aspects of the correspondence. Namely, how to extract non-perturbative information of a gauge theory from its dual theory of gravity. In the process, we will also formulate more precisely the mathematical content of the duality.

3.4.1 The fundamental equality

In the "strong" version of the gauge/gravity duality, we have an equivalence between two quantum theories - a theory of quantum gravity gravity in $(d+1)$ dimensions and a gauge theory in d dimensions. The description of a quantum theory is by means of the its generating functional Z, from which all correlation functions can be obtained. This lead the authors of Refs. [93] and [94] to conjecture that the quantitative expression of the duality is obtained by means of the equality of the partitions function of the gravity theory and of its dual gauge theory. Thus, the computation of the partition function of one of the theories of the pair is enough to compute the partition function and all observables in its corresponding dual.

Let us explain these afirmations. Let $\hat{O}(x)$ be an operator in the d dimensional quantum field theory, with $\phi(x,z)$ being its associated bulk field in the dual $(d+1)$ dimensional theory of gravity. As discussed above, $\phi_0(x) = \phi(x, z \to 0)$ is a field in the d dimensional QFT that sources the operator $\hat{O}(x)$. The main statement of the gauge/gravity duality is that the following relation between the generating functionals of both theories must hold

$$Z_{\text{QFT}}[\phi_0] = Z_{\text{gravity}}[\phi \to \phi_0]. \tag{3.21}$$

In the QFT side, the partition function Z_{QFT} is given by

$$Z_{\text{QFT}}[\phi_0] = \int \prod_i D\phi_i \, e^{-S_{\text{QFT}} + \int d^d x \, \phi_0 O} = \left\langle e^{\int d^d x \, \phi_0 \hat{O}} \right\rangle, \tag{3.22}$$

where ϕ_i is the collection of fields in the theory and S_{QFT} the action of the QFT. On the gravity side, the partition function Z_{gravity} is not known in the full quantum regime. However, in the case we are interested in, i.e. the strong 't Hooft coupling limit of the QFT, the dual theory of gravity becomes classical - and then we may use a semi-classical approximation for Z_{gravity},

$$Z_{\text{gravity}} \approx e^{-S_{\text{gravity}}[\phi \to \phi_0]}, \tag{3.23}$$

where S_{gravity} is the classical action for a theory of gravity corresponding to the classical limit of the $d+1$ dimensional quantum gravity theory. The action S_{gravity} is evaluated at a saddle-point, subjected to the boundary condition that the bulk field ϕ goes to ϕ_0 at the boundary of the space-time. If there is more than one saddle-point, a summation over all saddle-points is implied. Combining Eqs. (3.21), (3.22) and (3.23) we get an approximation for the d dimensional QFT partition function in the strong 't Hooft coupling limit,

$$Z_{\text{QFT}}[\phi_0] \approx e^{-S_{\text{gravity}}[\phi \to \phi_0]}. \tag{3.24}$$

With the QFT partition function (3.24) written in terms of the gravity theory at hand, we may proceed to extract the (Euclidean) n-point correlation functions $\langle \hat{O}(x_1) \dots \hat{O}(x_n) \rangle$. From standard QFT lore [25], n-point connected correlation functions $\langle \hat{O}(x_1) \dots \hat{O}(x_n) \rangle_{\text{connected}}$ are given by the nth functional derivative of $\log Z_{\text{QFT}}[\phi_0]$ with respect to the source $\phi_0(x)$, after taking the sources to zero

$$\langle \hat{O}(x_1) \dots \hat{O}(x_n) \rangle_{\text{connected}} = (-1)^n \frac{\delta^n}{\delta\phi_0(x_1) \dots \delta\phi_0(x_n)} \log Z_{\text{QFT}}[\phi_0] \Big|_{\phi_0=0}. \tag{3.25}$$

Using Eq. (3.24), the n-point correlation functions can be computed holographically by

$$\langle \hat{O}(x_1) \dots \hat{O}(x_n) \rangle_{\text{connected}} = \frac{\delta^n}{\delta\phi_0(x_1) \dots \delta\phi_0(x_n)} S_{\text{gravity}} \Big|_{\phi_0=0}. \tag{3.26}$$

In general, the on-shell action S_{gravity} is divergent - it picks up a infinite contribution from the near-boundary region. In terms of the dual QFT, this corresponds to a UV divergence. This constitutes an example of the UV/IR-correspondence - the asymptotic boundary defines the long distance, IR, regime of the gravitational theory. On the other hand, the near boundary contribution to S_{gravity} generates the usual UV divergences of the dual QFT. A process, called holographic renormalization [120–122], that regularizes and renormalizes the on-shell action S_{gravity} must be applied in order to compute physical correlation functions. The holographic renormalization procedure also leads to a formal way of understanding the gauge/gravity duality as a holographic version of the renormalization group [123].

3.5 Scaling dimensions

A simple way to see the renormalization group interpretation of the gauge/gravity duality at work is to look at how massive fields in the bulk gravity theory are related to scaling dimensions of the dual quantum field theory. Let us analyze a simple example, of

a scalar field $\phi(x,z)$ on an asymptotically AdS_{d+1} space-time. The bulk action is given by

$$S = -\frac{1}{2}\int d^d x\sqrt{-g}\left[(\partial\phi)^2 - m^2\phi^2\right], \tag{3.27}$$

The classical equation of motion that follows from $\delta S = 0$ is a wave equation on AdS_{d+1}, that is

$$(\Box - m^2)\phi(x,z) = 0, \tag{3.28}$$

where $\Box$ is the Laplacian operator on a scalar field,

$$\Box\phi = D_\mu D^\mu\phi = \frac{1}{\sqrt{-g}}\partial_\mu(\sqrt{-g}g^{\mu\nu}\partial_\nu\phi). \tag{3.29}$$

Writing Eq. (3.28) in the background given by the asymptotic AdS metric in Eq. (3.4), then passing to momentum space in the transverse directions by

$$\phi(k,z) = \int \frac{d^d x}{(2\pi)^d} e^{ik\cdot x}\phi(x,z), \tag{3.30}$$

we arrive at (after taking $z \to 0$)

$$\left[z^2\partial_z^2 + (d-1)Lz\partial_z + L^2m^2\right]\phi(k,z) = 0. \tag{3.31}$$

This differential equation has two linearly independent solutions, given by $\phi_1(z) \propto z^{d-\Delta}$ and $\phi_2(z) \propto z^\Delta$, where Δ is given by

$$\Delta = \frac{d}{2} + \sqrt{\frac{d^2}{4} + m^2L^2}. \tag{3.32}$$

Since ϕ_1 and ϕ_2 are linearly independent solutions, the general near boundary solution is

$$\phi(k, z\to 0) \approx A(k)\phi_1 + B(k)\phi_2, \tag{3.33}$$

where $A(k)$, $B(k)$ are constants with respect to z. Back to coordinate space, the asymptotic solution is given by Eq. (3.33) but with $A = A(x)$ and $B = B(x)$. Requiring that Δ is real means that

$$m^2 \geq -\frac{d^2}{4L^2}. \tag{3.34}$$

That is, in AdS space a scalar field ϕ can have a negative mass squared m^2, as long as m^2 satisfies Eq. (3.34), known as the Breitenlohner-Freedman bound [124]. If this bound is satisfied, then $\Delta > d - \Delta$; thus ϕ_1 dominates over ϕ_2 for $z \to 0$. Also, if $m^2 < 0$ then $d - \Delta < 0$ (as $\Delta > 0$ always) - thus, the solution ϕ_1 is non-normalizable and ϕ_2 is normalizable. The non-normalizable solution ϕ_2, as it blows up on the boundary, must

deform the dual gauge theory. This suggests the interpretation ϕ_2 as a source in the gauge field. The normalizable solution ϕ_1 is interpreted to give the vacuum expectation value of the operator sourced by ϕ_2. [125]

Now, to apply Eq. (3.24) we need to consider the on-shell action of the scalar field. Thus, we need to put Eq. (3.33) back into the action (3.27). However, the UV divergences mentioned in Section 3.4 mean that $S \to \infty$, as $\phi \to \infty$ due to the non-normalizable solution. In this Section, we will adopt a very simple regularizing procedure and impose an IR cutoff on the geometry at $z = \epsilon$, where $\epsilon \ll 1$. Then, we introduce a boundary regularized field $\phi_{reg}(x)$ at the cutoff plane $z = \epsilon$ by

$$\phi_{reg}(x) = \epsilon^{d-\Delta}\phi(x, \epsilon), \tag{3.35}$$

which is finite as $\epsilon \to 0$. Now, integrating the action (3.27) by parts, the bulk term is zero by the equations of motion and we are left with the boundary term evaluated at the UV cutoff

$$S \sim \left(\frac{L}{\epsilon}\right)^{2d} \int d^d x\, \phi(x, \epsilon) O(x, \epsilon), \tag{3.36}$$

where we identified $O(x, z)$ as a the dual z dependent operator, where z gives the renormalization group flow, as discussed in Section 3.2. Introducing the regularized field $\phi_{reg}(x)$ of Eq. (3.35) we get

$$S \sim L^{2d}\epsilon^{-\Delta} \int d^d x\, \phi_{reg}(x)\; O(x, \epsilon). \tag{3.37}$$

Requiring that S is finite for all ϵ implies that the boundary operator $O(x)$ should satisfy

$$O(x) = \epsilon^{\Delta} O(x, \epsilon), \tag{3.38}$$

so that

$$S \sim L^{2d} \int d^d x\, \phi_{reg}(x)\; O(x), \tag{3.39}$$

which is now finite for all ϵ. From Eq. (3.38), we see that Δ gives the scaling dimension of the operator associated with O. From the gravity theory side, (3.35), we may associate $d - \Delta$ with scaling dimension of the bulk field $\phi(x, z)$. Thus, we see that the mass and scaling behavior of a bulk scalar field determines the scaling behavior of the correspondent operator in the dual gauge theory.

Consider a deformation of the field theory in order to include the operator $\hat{O}(x)$ in the action. Then, as discussed in Section 3.4, $\phi_{reg}(x)$ is associated with the UV coupling of the field theory. In fact, we see that if

1. $m^2 > 0$, then $d - \Delta > 0$ and the coupling $\phi(x) \to 0$ as $\epsilon \to \infty$, by (3.35). That is, $O(x)$ is an irrelevant operator, since its effective coupling at the IR is vanishingly

small. On the other hand, $\phi(x) \to \infty$ as $\epsilon \to 0$ and the UV behavior of the theory is changed by the deformation. As mentioned above, ϕ_2 is then identified with a source in the QFT.

2. $m^2 < 0$, then $\Delta - d > 0$, and $\phi(x) \to \infty$ as $\epsilon \to 0$. Thus $O(x)$ is called a relevant operator, since its effective coupling in the IR is large. On the other hand, $\phi \to 0$ as $\epsilon \to \infty$ - the operator does not change the UV behavior of the theory.

3. $m^2 = 0$, then $\Delta = d$ and the scaling behavior of $\hat{O}(x)$ cannot be understood only from the analysis above. Since this case lies on the boundary of the foregoing cases, the operator O is marginal.

3.6 The duality at finite temperature

So far, we have analyzed the gauge/gravity duality at zero temperature. Our main interest in this thesis is the finite temperature aspects of strongly coupled gauge theories from the gauge/gravity standpoint. So, it is necessary to understand how the duality works a finite temperature [126].

Also, this leads to one of the main virtues of the gauge/gravity duality - it can - and has been - used to study strongly coupled field theories at finite temperature in real time [127, 128]. As already mentioned in the last chapter, the main non-perturbative method to study strongly coupled gauge theories, lattice gauge theory, is formulated in Euclidean time and is ill-suited to compute quantities in real time, such as transport coefficients. The gauge/gravity duality provides a powerful method of extracting real time information at finite temperature, which is the origin of its main appplications.

3.6.1 Heuristic argument

The main idea to formulate the duality at finite temperature is to consider a black hole in the interior of the bulk geometry. The key argument is that, semi-classically, a black hole emits Hawking radiation with a thermal spectrum at temperature T [129,130]; a black hole inside an asymptotically AdS_5 space then emits thermal radiation in the direction of the boundary. However, as discussed in Subsection 3.2.3, all radiation incoming at the boundary is radiated back to the black hole. Thus, we conclude that the black hole acts as a perfect absorver - a perfect black body, and that the boundary is in thermal equilibrium with the black hole in the bulk. Thus, the gauge theory at the boundary of the geometry is also in thermal equilibrium at temperature T. In summary, a black hole emitting Hawking radiation at temperature Tin the bulk of the geometry is correspondent to a non-Abelian

gauge theory in thermal equilibrium at the same temperature T - that is, a non-Abelian plasma.

3.6.2 AdS_5/Schwarzschild black hole

The simplest example of the gauge/gravity duality at finite temperature is to consider $\mathcal{N} = 4$ SYM at finite temperature. In Section 3.3, we started from a extremal black 3-brane - therefore, we started with $T = 0$. To consider a finite temperature black hole, we move away from extremality. The corresponding near extremal, near horizon geometry is given by the Schwarzschild/AdS_5 geometry, whose metric is

$$ds^2 = \frac{L^2}{z^2}\left(-h(z)dt^2 + d\vec{x}^2 + \frac{dz^2}{h(z)}\right) \tag{3.40}$$

where $h(z) \equiv 1 - z^4/z_h^4$ is the blackening factor of the black hole. The event horizon of this black brane is at $z = z_h$.

3.6.3 Temperature

Let's study the thermodynamics of this black hole. Since the same procedure will be used to study the thermodynamics of all models in this work, we will work out the thermodynamics of the AdS_5 /Schwarzschild black hole in more detail.

The simplest way to extract the temperature of the black brane with metric (3.40) is to consider the Euclidean version of the black hole [132]. First, we analytically continue the metric (3.40) to imaginary time $\tau = it$, obtaining

$$ds^2 = \frac{L^2}{z^2}\left(h(z)d\tau^2 + d\vec{x}^2 + \frac{dz^2}{h(z)}\right), \tag{3.41}$$

Now, the Euclidean version of the AdS_5 /Schwarzschild black brane must end smoothly at the event horizon. An indication that this is so stems from the signature of the metric (3.40) changes from $(+,+,+,+,+)$ to $(-,+,+,+,-)$ if one could go from $z > z_h$ to $z < z_h$. On the other hand, a theorem in linear algebra states that a real symmetric bilinear form must have the number of positive and negative signs in any diagonal basis. Since the metric defines a symmetric bilinear form, the signature must be a topological invariant [131].[5] Thus, the Euclidean version of the geometry is cigar-shaped, with the

[5]This argument, however, is faulty since the real-time metric (3.40) does not describe global Schwarzschild/AdS_5 (Kruskal-like global coordinates for Schwarzschild/AdS can be found, for instance, in [128]). However, note that, if one insists in using the local patch (3.40), the signature of the metric changes from $(-,+,+,+,+)$ to $(+,+,+,+,+)$ at the event horizon, which leads to no contradiction with the theorem used in the main text.

event horizon being the tip of the cigar where the geometry ends smoothly.

Therefore, the Euclidean geometry must be completely regular and smooth at the event horizon. However, let's us study the geometry near the horizon. Change coordinates from z to $r = z - z_h$ and consider the metric at the vicinity of the horizon at $r \sim 0$. The metric becomes

$$ds^2 \approx \left(\frac{L^2 r}{4z_h^3}d\tau^2 + \frac{4L^2}{r z_h}dr^2\right) + \frac{L^2}{z_h^2}d\vec{x}^2. \tag{3.42}$$

We then consider the coordinate $\rho = \sqrt{16L^2 r/z_h}$:

$$ds^2 \approx \left(\frac{2\rho^2}{L^4 z_h^2}d\tau^2 + d\rho^2\right) + \frac{1}{z_h^2}d\vec{x}^2. \tag{3.43}$$

The expression in brackets is the metric of a plane in polar coordinates, if we identify as the polar angle the coordinate $\theta = 2\tau/(z_h)$. If the period of θ is less than 2π, then we we have a a conical singularity at $\rho = 0$. Since we require smoothness of the metric for all ρ, this implies that the period of coordinate θ must 2π. That is, τ must be periodic with period β given by $2\beta/(z_h) = 2\pi$ or $\beta = \pi z_h$. However, if the coordinate τ is periodic with period β, then we are considering a thermal field theory with temperature given by $\beta = 1/T$. Thus, the black hole temperature is

$$T = \frac{1}{\pi z_h}, \tag{3.44}$$

which is also the corresponding temperature of the dual gauge theory.

3.6.4 Entropy density

The entropy S of a black hole described by Einstein's equations in the semi-classical regime is given by the Bekenstein-Hawking formula [133, 134],

$$S = \frac{A}{4G_d} \tag{3.45}$$

where A is the area of the hypersurface defined by the event horizon and G_d is Newton's constant in d dimensions. For the geometry described by the metric (3.40), we evaluate the 4-dimensional area of the hypersurface $z = z_h$, which yields

$$S = \left(\frac{1}{z_h}\right)^3 V_3, \tag{3.46}$$

where V_3 is the volume of the Minkowski slice at $z = z_h$. Since $V_3 \to \infty$, $S \to \infty$. However, the entropy density $s \equiv= S/V_3$ is well-defined and given by

$$s = \left(\frac{1}{z_h}\right)^3. \tag{3.47}$$

Eliminating z_h by using (3.44), we obtain

$$s = \frac{\pi^3}{4G_5}T^3. \tag{3.48}$$

Using Eq. (3.20) to eliminate G_5 and L^3 in favor of N_c, we get

$$s = \frac{\pi^2 N_c^2}{2}T^3. \tag{3.49}$$

A basic requirement of the gauge/gravity duality is that the number of degrees of freedom in both sides of the duality be equal. Since the entropy is a measure of the number of degrees of freedom, the entropy density of the gravity theory and of the dual quantum field theory must be the same. Thus, s must be the entropy density $s_{\mathcal{N}=4\ \mathrm{SYM},\lambda\to\infty}$ of $\mathcal{N} = 4$ SYM in the 't Hooft limit $\lambda \gg 1$ with $N_c \to \infty$.

A first check of this result is that in a conformal field theory at finite temperature, the only scale present in the theory is the temperature T. Thus, by dimensional analysis, $s \propto T^3$. Also, in the large N_c limit, s scales as N_c^2 since the number of gluons scales as N^2. Thus, $s = cN_c^2T^3$ - the only thing remaining is to determine the constant, which may depend on the 't Hooft coupling λ. The entropy density of free $\mathcal{N} = 4$ SYM in the large N_c limit is given by the entropy density of a free gas of $(N_c^2 - 1) \approx N_c^2$ gluons (2 with two polarization each), 4 N_c^2 fermions and 6 N_c^2 scalars. That is, we have $8N_c^2$ bosonic degrees of freedom and $8N_c^2$ fermionic degrees of freedom with spin 1/2. Each bosonic degree of freedom contribute with $(2\pi^2/45)T^3$ to the entropy density, while the contribution of each fermionic degree of freedom is 7/8-ths (see Section 2.4) of the bosonic contribution. That is

$$s_{\mathcal{N}=4\ \mathrm{SYM},\lambda=0} = \left(8 + \frac{7}{8} \times 8\right)\frac{2\pi^2}{45}N_c^2T^3 = \frac{2\pi^2}{3}N_c^2T^3. \tag{3.50}$$

Note that $s_{\mathcal{N}=4\ \mathrm{SYM},\lambda\to\infty} = 3/4 s_{\mathcal{N}=4\ \mathrm{SYM},\lambda=0}$ - the number of degrees of freedom do not change radically as one goes from weak coupling to strong coupling. This matches qualitatively the observed lattice result for pure SU(3) Yang-Mills [74], that for $T \gtrsim 2T_c$, the entropy density is about 80% of the free result, as remarked in Section 2.4.

The remainder of the thermodynamics of the strongly coupled $\mathcal{N} = 4$ SYM plasma follows from the equation of state (3.49). The pressure follows from $s = (dp/dT)$, and the

energy density from $p = -\epsilon + Ts$; we then have[6]

$$\epsilon_{\mathcal{N}=4,\lambda\to\infty} = \frac{3\pi^2}{8} N_c^2 T^4 = \frac{3}{4}\epsilon_{\mathcal{N}=,\lambda=0} \tag{3.51}$$

and

$$p_{\mathcal{N}=4,\lambda\to\infty} = \frac{\pi^2}{8} N_c^2 T^4 = \frac{3}{4} p_{\mathcal{N}=4,\lambda=0}. \tag{3.52}$$

3.6.5 General expressions for the thermodynamics from holography

Let us consider fairly general dual theories of gravity, described by effective actions (containing up to two derivative terms in a derivative expansion) which are given by the usual Einstein-Hilbert action coupled to matter fields, so as Bekenstein-Hawking formula can still be applied - the derivation of the Bekenstein-Hawking formula and the usual thermodynamics of black holes depend upon the fact that Einstein's gravity is a two derivative action. Methods for computing the entropy in higher curvature gravity have been developed - reviews can be found in [135] and [136].

We will assume that we have a gauge theory whose $d+1$ dimensional dual theory of gravity has a background metric gravity dual that is diagonal and is of the form

$$ds^2 = e^{2A(z)} \left(-h(z) dt^2 + dx_1^2 + \ldots + dx_{d-1}^2 + \frac{1}{h(z)} dz^2 \right), \tag{3.53}$$

where $A(z)$ and $h(z)$ describe the geometry. This action has SO(3) rotation symmetry in the x_i spatial sections at each fixed z. We will assume, so as to the geometry describe a black brane, that $h(z)$ has a simple zero at $z = z_h$, so that for $z \sim z_h$, $h(z) \approx h'(z_h)(z - z_h)$. The hypersurface $z = z_h$ defines the event horizon of the black brane. We will assume that the asymptotically AdS_{d+1} boundary is at $z \to 0$. The Euclidean version of the metric is

$$ds_E^2 = e^{2A(z)} \left(h(z) d\tau^2 + dx_1^2 + \ldots + dx_{d-1}^2 + \frac{1}{h(z)} dz^2 \right), \tag{3.54}$$

Following the same argument of the previous paragraphs, we derive the temperature T of the black brane as a function of the horizon position z_h

$$T = \frac{|h'(z_h)|}{4\pi}. \tag{3.55}$$

[6]Note that the specific heat of AdS/Scharzschild black hole, given by $c = (d\epsilon/dT)$, is positive: $c > 0$. This implies that the AdS/Scharzschild black is thermodynamically *stable*. This is a more formal way of checking the thermodynamical stability mentioned in Subsection 3.2. It should be also be mentioned that is in opposition to a asymptotically flat black hole, for instance, the black hole described by the Scharzschild solution has $c < 0$ and thus is inherently unstable.

The black brane entropy density follows the Bekenstein-Hawking formula (3.45), which results in

$$s = \frac{e^{3dA(z_h)}}{4G_5}. \tag{3.56}$$

3.7 Euclidean and real time correlation functions

The prescription presented in Section 3.4 permits the evaluation of Euclidean correlators. However, for studying real time phenomena in a finite temperature field theory one needs to examine Green's functions with different boundary conditions, such as the retarted and advanced Green's functions. In principle, one could, from the Euclidean correlators, obtain the real-time Green's functions by analytical continuation. However, in practice this is often a prohibitive task, since it requires knowledge of the Euclidean correlator at all frequencies (and not only on the Matsubara frequencies) - in most practical cases the Euclidean correlator is only known at the Matsubara frequencies or in some part of the frequency space by some high or low temperature expansion. Hence, a practical mean to extract real time correlation functions it is needed. This practical recipe was proposed in Ref. [127] and later justified in Ref. [128]. In this subsection, we will largely follow the discussion in the Appendix C of Ref. [137], where it was presented an alternative, simpler, justification for the procedure presented in Ref. [127].

3.7.1 Euclidean correlation functions

We start by considering the Euclidean 2-point correlation function of the bosonic operator $\hat{O}$ in momentum space, $G_E(\omega_n, \vec{k})$, where ω_n are the Matsubara frequencies in 4 dimensions. The Euclidean correlator $G_E(\omega_n, \vec{k})$ is defined by the Fourier transform of the 2-point correlation function in coordinate space, that is

$$G_E(\omega_n, \vec{k}) = \frac{1}{\beta}\int_0^\beta d\tau \int d^3x e^{-i(\vec{k}\cdot\vec{x}-\omega_n\tau)} \left\langle \hat{O}(x)\hat{O}(0)\right\rangle \tag{3.57}$$

To compute it, we use the Euclidean prescription (3.26), derived from the the fundamental equation (3.24). The difference is that at finite temperature, apart from requiring that the bulk field $\phi(x, z)$ dual to the operator $\hat{O}$ satisfies $\phi(z \to 0) \to \phi_0$, we require also regularity at the horizon.

The Euclidean version of the action is given by

$$S_E = \int d^5x\sqrt{g_E}\left[\frac{1}{2q(z)}(\partial\phi_E)^2 + \frac{1}{2}m^2\phi_E^2\right], \tag{3.58}$$

where the Euclidean metric $g_{E,\mu\nu}$ is defined in (3.54) and $\phi_E(\tau, \vec{x}, z)$ is the Euclidean

version of the bulk field $\phi(t, \vec{x}, z)$. Here, $q(z)$ is a z-dependent bulk coupling constant; we will assume that $q(z)$ is smooth and finite at the boundary and at the horizon. We also introduce the momentum space version of $\phi_E(\tau, \vec{x}, z)$ by

$$\phi_E(\omega_n, \vec{k}, z) = \frac{1}{\beta} \int_0^\beta d\tau \int d^3x \, e^{-i(\vec{k}\cdot\vec{x} - \omega_n \tau)} \phi_E(\tau, \vec{x}, z). \tag{3.59}$$

The equation of motion one derives from Eq. (3.58) is, in coordinate space,

$$\partial_\mu \left[\sqrt{g_E} \, g_E^{\mu\nu} \, \partial_\nu \left(\frac{\phi_E}{q} \right) \right] + m^2 \frac{1}{q} \phi_E = 0. \tag{3.60}$$

In momentum space, using the specific form of the background (3.54) for $d = 4$, one finds that

$$\left[\partial_z^2 + \left(3A' + \frac{h'}{h} \right) \partial_z - \frac{1}{h} \left(\frac{\omega_n^2}{h} + \vec{k}^2 + e^{2A} m^2 \right) \right] \frac{\phi_E(\omega, \vec{k}, z)}{q(z)} = 0. \tag{3.61}$$

Let us analyze each of the boundary conditions on ϕ separately:

(a) *Near boundary, $z \to 0$*

For $z \to 0$, since the geometry is asymptotically Euclidean AdS, $h \to 1$ and $e^A \to L/z$. The equation of motion (3.61) becomes the equation of motion for a scalar field in AdS_5 space at zero momentum, that is, Eq. . Thus, near the boundary, the solution $\phi_1 \sim z^{d-\Delta}$ is the leading solution, where Δ is given by Eq. (3.32).

(b) *Near horizon, $z \to z_h$*

For $z \to z_h$, $h(z) \approx h'(z_h)(z - z_h)$ and $q(z) \approx q(z_h)$. The, the equation of motion becomes, near horizon

$$\partial_z^2 \phi_E + \frac{1}{z - z_h} \partial_z \phi_E - \frac{\omega_n^2}{h'(z_h)^2} \frac{1}{(z - z_h)^2} \phi_E = 0, \tag{3.62}$$

whose linearly independent solutions are

$$\phi_{E,1} \sim |z - z_h|^{\omega_n/(4\pi T)} \tag{3.63}$$

$$\phi_{E,2} \sim |z - z_h|^{-\omega_n/(4\pi T)} \tag{3.64}$$

The regular solution at the horizon is $\phi_{E,1}$, while $\phi_{E,2}$ is divergent at $z \to z_h$.

With the regular and normalizable solution ϕ_E^{reg} determined, we may proceed to input the on-shell ϕ_E back into the action (3.58). After integrating by parts and using the

equation of motion to eliminate the bulk term, we arrive at

$$S_E = \int d^4x \; g_E^{\mu\nu} \phi_E^{reg} \partial_\mu \left(\frac{\phi_E^{reg}}{q(z)} \right) \Bigg|_{z=\epsilon}^{z=z_h}, \tag{3.65}$$

where we introduced, as in Section , an UV cutoff at $z = \epsilon$. Then, introducing the momentum space ϕ_E by Eq. (3.59)

$$S_E = \beta \sum_n \int \frac{d^3k}{(2\pi)^3} \; J_E[\phi_E^{reg}](\omega_n, \vec{k}, z) \Big|_{z=\epsilon}^{z=z_h}, \tag{3.66}$$

where J_E is a functional of ϕ_E given by

$$J_E[\phi_E](\omega_n, \vec{k}, z) = \phi_E(-\omega_n, -\vec{k}, z) \frac{h(z)}{q(z)} e^{2A(z)} \phi_E(\omega_n, \vec{k}, z). \tag{3.67}$$

The Euclidean correlation function G_E defined by (3.57) in is then given by the prescription (3.26), that is,

$$G_E(\omega_n, \vec{k}) = -\frac{\delta^2}{\delta\phi(\omega_n, \vec{k}) \delta\phi(\omega_n, \vec{k})} S_E, \tag{3.68}$$

which yields

$$G_E(\omega_n, \vec{k}) = -\left(J_E[\phi_E^{reg}](\omega_n, \vec{k}, z) \right) \Big|_{z=\epsilon}^{z=z_h}. \tag{3.69}$$

Now, since the equation of motion for ϕ_E depends on ω_n and $\vec{k}$ only upon their squares ω_n^2 and $\vec{k}^2$, and since the boundary conditions are invariant under the transformation $\omega_n \to -\omega_n$ and $\vec{k} \to -\vec{k}$, it follows that the functional (3.67) satisfies

$$J_E[\phi_E](\omega_n, \vec{k}, z) = J_E[\phi_E](-\omega_n, -\vec{k}, z). \tag{3.70}$$

Thus, in Eq. (3.69), we have two pairs of terms that are equal to each other. We remark, in passing, that Eq. (3.70) will play an important role when we discuss the justification for the real-time prescription.

To complete the discussion of the Euclidean correlator, let's simplify Eq. (3.69) a bit further. Suppose that $\omega_n \neq 0$, then as $\phi_E^{reg} \sim |z - z_h|^{\omega_n/(4\pi T)}$ near the horizon, $J_E[\phi_E^{reg}] \to 0$ as $z \to z_h$. Then, the horizon contributions to Eq. (3.69) vanish and we have, finally,

$$G_E(\omega_n, \vec{k}) = \lim_{z \to 0} J_E[\phi_E^{reg}](\omega_n, \vec{k}, z). \tag{3.71}$$

3.7.2 The real-time prescription

We first note that, at finite temperature, we must include, besides the boundary condition $\phi \to \phi_0$ used in Eq. (3.24) at the boundary of the bulk theory, the regularity condition of ϕ at the horizon of the black brane. However, in real time, more boundary conditions at the horizon become possible, such as incoming or outgoing boundary conditions. This reflects the fact that, in real time, one has many more possible choices of Green's functions (such as retarted, advanced, etc.) than in imaginary time. With this in mind, the proposal of Ref. [127] to compute retarted Green's functions from gauge-gravity consists in associating with retarted Green's function the infalling boundary conditions on the horizon.

Let us summarize the prescription to compute a retarted correlator from the gauge/-gravity duality. For simplicity, we consider a bulk scalar field $\phi(x,z)$ dual to the gauge theory operator $\hat{O}$ in the general background (3.53). Let the bulk action for scalar field ϕ be given by

$$S = -\frac{1}{2}\int d^5x\sqrt{-g}\left[\frac{1}{q(z)}(\partial\phi)^2 + m^2\phi^2\right] \tag{3.72}$$

One wants to evaluate the retarted correlation function in the gauge theory given by

$$G^R(\omega,\vec{k}) = -i\int d^3x dt\, e^{i\omega t - i\vec{k}\cdot\vec{x}}\theta(t)\left\langle\left[\hat{O}(t,\vec{x}),\hat{O}(0,\vec{0})\right]\right\rangle. \tag{3.73}$$

The procedure is then the following:

1. One solves the classical bulk equations of motion, subjected to in-falling boundary conditions at the horizon and also imposes that $\phi \to \phi_0$ at the boundary at $z \to \infty$. Call ϕ^{in} the solution subjected to these conditions.

2. Plug the solution found in the first step into the action. Integrating by parts and passing to momentum space, the action can be generally written in the form

$$S = \int \frac{d\omega d^3k}{(2\pi)^4}\, J[\phi^{in}](r,\omega,\vec{k})\Big|\, z = z_{hz\to 0}, \tag{3.74}$$

   where $J[\phi]$ is a functional quadratic on ϕ.

3. The retarted Green's function is then given by

$$G^R(\omega,\vec{k}) = \lim_{z\to 0} J[\phi^{in}](\omega,\vec{k}). \tag{3.75}$$

3.7.3 Justifying the real-time procedure

Let us now justify the procedure described in the previous section. The goal is to prove that one can perform an analytical continuation of the bulk fields which give the Euclidean correlator in Eq. (3.71), and that this analytical continuation, supplemented with adequate boundary conditions on the horizon, gives the retarted correlator. The main message is that ingoing (outgoing) boundary conditions on the bulk fields at the horizon corresponde to the retarted (advanced) real-time correlation function.

Let's repeat the steps performed for the bulk field $\phi_E(\tau, \vec{x}, z)$ in an Euclidean gravity theory for the bulk field $\phi(x, z)$ in a gravity theory with Lorentzian signature. The metric is now given by the Lorentzian signature ansatz Eq. (3.53) and the corresponding action is given by Eq. (3.72), both of which are analytical continuations of the Euclidean space-time (3.54) and the Euclidean action (3.58). The Fourier transform of $\phi(\omega, \vec{k}, z)$ is now given by

$$\phi(\omega, \vec{k}, z) = \int d^4x\, e^{-i(\vec{k}\cdot\vec{x}-\omega t)}\phi(t, \vec{x}, z). \tag{3.76}$$

The bulk equation of motion for $\phi(\omega, \vec{k}, z)$ is given by

$$\left[\partial_z^2 + \left(3A' + \frac{h'}{h}\right)\partial_z - \frac{1}{h}\left(-\frac{\omega^2}{h} + \vec{k}^2 + e^{2A}m^2\right)\right]\frac{\phi(\omega, \vec{k}, z)}{q(z)} = 0, \tag{3.77}$$

which is the same as the equation of motion for ϕ_E, but with the change $\omega_n^2 \to -\omega^2$. The near boundary solution is unchanged from the Euclidean case. The near horizon solution, on the other hand, is slightly changed due to the sign change in Eq. (3.77). The asymptotic solutions are now

$$\phi_{in} \sim |z_h - z|^{-\frac{i\omega}{4\pi T}} \qquad \text{(in-falling solution)} \tag{3.78}$$

$$\phi_{out} \sim |z_h - z|^{\frac{i\omega}{4\pi T}} \qquad \text{(out-going solution)}. \tag{3.79}$$

The solution ϕ_{in} represents an in-going wave into the horizon and ϕ_{out} an out-going wave. Contrary to the Euclidean case, both near horizon solutions in real time are now acceptable, at least in principle. Before discussing this point, let's write down the on-shell action, which is now given by

$$S = \int \frac{d\omega d^3k}{(2\pi)^4}\, J[\phi](\omega, \vec{k}, z)\Big|_{z=\epsilon}^{z=z_h}, \tag{3.80}$$

where the functional $J[\phi]$ is the real version of the functional $J_E[\phi_E]$:

$$J[\phi](\omega, \vec{k}, z) = -\phi(-\omega, -\vec{k}, z)h(z)e^{3A(z)}\frac{1}{q(z)}\partial_z\left(\phi(\omega, \vec{k}, z)\right). \tag{3.81}$$

Now, let us return to the question of in-falling and outgoing boundary conditions. Comparing the equations of motion for the Euclidean bulk field ϕ_E (Eq. (6.20)) and for the real time bulk field ϕ, we see that

$$\phi_E(\omega_n) = \begin{cases} \phi_{in}(i\omega_n) & \text{for} \quad \omega_n > 0 \\ \phi_{out}(i\omega_n) & \text{for} \quad \omega_n < 0 \end{cases} \tag{3.82}$$

This implies that the functionals J and J_E satisfy the relation

$$\lim_{z\to 0} J_E[\phi_E](\omega_n, \vec{k}, z) = \begin{cases} -\lim_{z\to 0} J[\phi_{in}](i\omega_n, \vec{k}, z) \\ -\lim_{z\to 0} J[\phi_{out}](i\omega_n, \vec{k}, z) \end{cases} \tag{3.83}$$

Since the retarted correlator is given by analytic continuation of the Euclidean correlator, [60]

$$G^R(i\omega_n, \vec{k}) = -G^E(\omega_n, \vec{k}) \qquad \text{for} \quad \omega_n > 0, \tag{3.84}$$

it follows from Eqs. (3.71),(3.83) and (3.84) that

$$G^R(\omega, \vec{k}) = \lim_{z\to 0} J[\phi^{in}](\omega, \vec{k}), \tag{3.85}$$

as promised.

We now only need to consider the zero frequency case $\omega = \omega_n = 0$ to complete the argument. The first fact to notice is that in this limit, the equations of motion for ϕ and ϕ_E are identical. The near-horizon solutions are given by

$$\begin{aligned} &\phi \sim \text{const} \qquad \text{(regular)} \\ &\phi \sim \log(z - z_h) \qquad \text{(divergent)} \end{aligned} \tag{3.86}$$

The divergent solution at the horizon could generate extra terms on Eq. (3.80), but must be discarded imposing horizon regularity.

In passing, we note that the outgoing boundary condition involving ϕ^{out} yields, by the same argument, the advanced correlator G^A:

$$G^A(\omega, \vec{k}) = -i \int d^3x dt\, e^{i\omega t - i\vec{k}\cdot\vec{x}} \theta(t) \left\langle \left[\hat{O}(0, \vec{0}), \hat{O}(t, \vec{x})\right] \right\rangle = \frac{1}{16\pi G_5} \lim_{z\to 0} J[\phi^{out}](\omega, \vec{k}), \tag{3.87}$$

We also note that this argument can be generalized to higher spin operators and in the case where there is mixing of fluctuations from different channels - see Ref. [137] for details.

3.8 Transport coefficients

Many of the applications of the gauge/gravity duality involve the calculation of transport coefficients for strongly coupled plasmas. In this section, we will present an useful and practical way to evaluate transport coefficients using holography, the membrane paradigm [104] as applied to the gauge/gravity duality [138].[7]

3.8.1 Brief review of the literature

The computation of transport coefficients is, in a way, at the heart of gauge/gravity duality. The seminal work regarding the computation of the shear viscosity in the strongly coupled $\mathcal{N} = 4$ SYM plasma was done in Ref. [143]; the computation essentially consisted in studying metric fluctuations in the xy channel, which as we will explain below, couple with the shear viscosity η. The authors of Ref. [143] have used the fact that the low energy cross section graviton scattering from an AdS/Scharzschild solution is given by the area of the horizon to deduce that, for $\mathcal{N} = 4$ SYM at strong coupling, the shear viscosity is given by

$$\eta = \frac{\pi}{8} N^2 T^3. \tag{3.88}$$

In Ref. [144], which studied transport coefficients in the membrane horizon, the shear viscosity and the diffusion constant were computed in other gauge/gravity pairs of theories. The authors of Ref. [144] noticed that in all backgrounds analyzed in their work, the following relation held

$$\frac{\eta}{s} = \frac{1}{4\pi} \tag{3.89}$$

This lead to a general holographic computation [90] (see also Ref. [145]) that proved that, for all gauge theories with dual theories of gravity with isotropic backgrounds and effective actions with a maximum of two derivatives, the result in Eq. (3.89) holds at strong 't Hooft coupling.[8] A further alternative way of compute transport coefficients is

[7] We note that this procedure relies crucially on the existence of the stretched membrane horizon, which relies itself on the validity of the black hole complementarity conjecture [139, 140] - that is, the argument that while distant observers see the membrane horizon infinitesimally near the black hole horizon, an infalling observer sees nothing special while crossing the black hole horizon; in particular, they see no membrane horizon. However, the validity of the black hole complemntarity is a thorny question of black hole physics and quantum gravity. Recently, for instance, the validity of black hole complementarity has been put in check by the so-called AMPS solution to the problem of the black hole information paradox [141]. See, for instance, Ref. [142] for a counterargument to the AMPS firewall solution.

[8] In Refs. [144] and [90], it was also conjectured that the result (3.89) provided an absolute lower bound for the shear viscosity/entropy ratio in quantum fields theories - that is, in all QFTs, either at strong or weak coupling, $\eta/s \geq 1/(4\pi)$. However, it was shown, in gauge theories dual to theories of gravity which do not satisfy the conditions used in Ref. [90], namely, having an isotropic background and a two derivative effective action, that it is possible that $\eta/s \leq 1/(4\pi)$. For example, Gauss-Bonnet gravity, a higher derivative theory of gravity of gravity, in an asymptotically AdS_5 background [146], can lead to $\eta/s \leq 1/(4\pi)$ in the dual gauge theory [91,92] (see also Ref. [147]). It is possible to have components of the

to focus on quasinormal modes of black branes [152], which can be put in correspondence with hydrodynamical poles of the relevant Green's functions.

3.8.2 Kubo formulas

The main tool to compute transport coefficients from microscopic quantum field theories are the Kubo formulas, one of the main results of the linear response theory [61]. In this section I will present the derivation of Kubo formulas for the shear viscosity and electric conductivity, which will be discussed in a later chapter.

Linear response theory

Consider a quantum system at finite temperature described by the Hamiltonian

$$\hat{H} = \hat{H}_0 + \hat{H}', \tag{3.90}$$

where $\hat{H}_0$ is the original Hamiltonian of the system and H' is a small perturbation of $\hat{H}_0$ described by

$$\hat{H}' = -\lambda \hat{O} \delta(t), \tag{3.91}$$

where $\lambda \ll 1$ is a small coupling constant and $\hat{O}$ is a time-independent operator. This fluctuation represents a small external "kick" to the system at $t = 0$. The objective of linear response theory is to characterize the response of the system to this fluctuation.

The equation of motion for the density matrix $\hat{\rho}(t)$ of the complete system is

$$i\frac{\partial \hat{\rho}}{\partial t} = [\hat{H}, \hat{\rho}], \tag{3.92}$$

Since $\lambda \ll 1$, using time-dependent perturbation theory to linear order in the perturbation,

$$\hat{\rho}(t) = e^{-i\hat{H}_0 t}\hat{\rho}_0 e^{i\hat{H}_0 t} + \delta\hat{\rho}(t), \tag{3.93}$$

where

$$\delta\hat{\rho}(t) = ie^{-i\hat{H}_0 t}[\lambda\hat{O}, \hat{\rho}_0]e^{i\hat{H}_0 t}\theta(t), \tag{3.94}$$

where $\hat{\rho}_0$ is the density matrix of unperturbed Hamiltonian $\hat{H}_0$.

Now, let $\hat{P}(t)$ be an operator whose expectation value we are interested in computing

shear viscosity tensor η_{ijkl} satisfying $\eta_{ijkl}/s < 1/(4\pi)$ in anisotropic backgrounds, such as deformations of $\mathcal{N} = 4$ SYM by an axion field [148,149] or by including external magnetic fields, such as in Refs. [150,151] and [24].

in the perturbed system. Then, its expectation value is given by

$$\langle \hat{P}(t) \rangle = \mathrm{Tr}\left(\hat{\rho}(t)\hat{P}\right). \tag{3.95}$$

Inserting Eq. (3.94) in Eq. (3.95),

$$\langle \hat{P}(t) \rangle = \mathrm{Tr}\left\{\hat{P}e^{-i\hat{H}_0 t}\hat{\rho}e^{i\hat{H}_0 t}\right\} + \delta\langle \hat{P}(t) \rangle, \tag{3.96}$$

where

$$\delta\langle \hat{P}(t) \rangle = i\mathrm{Tr}\left\{e^{-i\hat{H}_0 t}\left[\lambda\hat{O}, \hat{\rho}_0\right] e^{i\hat{H}_0 t}\hat{P}\right\}\theta(t). \tag{3.97}$$

Since $\hat{P}(t)$ is a Heisenberg picture operator, the corresponding Schrodinger picture operator $\hat{P}$ is

$$\hat{P}(t) = e^{-i\hat{H}_0 t}\hat{P}e^{i\hat{H}_0 t}. \tag{3.98}$$

Using Eq. (3.98) and the invariance of the trace by cyclic permutations, we arrive at

$$\delta\langle \hat{P}(t) \rangle = i\theta(t)\langle\left[\hat{P}(t), \lambda\hat{O}(0)\right]\rangle. \tag{3.99}$$

The main result of linear response theory is Eq. (3.99), which relates the fluctuations of the expectation value of an operator with a time-ordered expectation value of the operator in the equilibrium state.

Scalar field

The simplest example is to consider the response of an operator $\hat{O}$ which is coupled to fluctuations of the field $\phi_0(\vec{x}, t)$. The perturbation hamiltonian is given by

$$\hat{H}' = -\phi_0\hat{O}. \tag{3.100}$$

We start by considering a small localized kick given by an external field,

$$\phi_0(t, \vec{x}) = \delta\phi_0\, \delta^{(3)}(\vec{x})\, \delta(t). \tag{3.101}$$

Identifying in Eq. (3.99) $\hat{P}$ with $\hat{O}$ and $\phi_0\hat{O}$ with $\lambda\hat{O}$, we arrive at

$$\delta\langle\phi_0\rangle(t, \vec{x}) = \phi_0 i\theta(t)\langle\left[\hat{O}(t, \vec{x}), \hat{O}(0, \vec{0})\right]\rangle. \tag{3.102}$$

Now, integrating over an arbitrary distribution of "kicks" over space-time,

$$\delta\langle\phi_0\rangle(t, \vec{x}) = i\int dt' d^3x' \theta(t - t')\phi_0(t', \vec{x}')\langle\left[\hat{O}(t, \vec{x}), \hat{O}(t', \vec{x}')\right]\rangle, \tag{3.103}$$

Considering the Fourier transform of Eq. (3.103),

$$\delta\langle\hat{O}\rangle(\omega) = \phi_0(\omega)G^R_{\mu\nu}(\omega, \vec{k} = \vec{0}), \tag{3.104}$$

where G^R is retarted correlator of $\hat{O}$

$$G^R(\omega, \vec{k}) = -i\int d^3x dt\, e^{i\omega t - i\vec{k}\cdot\vec{x}}\theta(t)\langle\Big[\hat{O}(t,\vec{x}), \hat{O}(0,\vec{0})\Big]\rangle. \tag{3.105}$$

We will assume that the the low frequency response of the system to the external perturbation is given by a Ohm's law of the form,

$$\delta\langle\hat{O}\rangle = \chi\partial_t\phi_0, \tag{3.106}$$

where χ is the transport coefficient associated with the low frequency regime. Comparing the Fourier transform of Eq. (3.106) with the result of linear response theory Eq. (3.104) we derive

$$\chi(\omega) = -\frac{G^R(\omega, \vec{k} = 0)}{i\omega} = -\frac{\mathrm{Im}\, G^R(\omega, \vec{k} = 0)}{\omega}. \tag{3.107}$$

Eq. (3.107) is called Kubo's formula, which permits us to evaluate the transport coefficient χ, which determines the low momentum, low frequency response of the system to external fluctuations in terms of the underlying microscopic theory here represented by the retarted correlator G^R.

Conductivity

Let us now apply Eq. (3.99) to the response of a system due to an external electromagnetic field perturbation. In this case, the perturbation hamiltonian density is given by

$$\hat{H}' = -A^\mu J_\mu, \tag{3.108}$$

where A^μ is the vector potential of the external electromagnetic field and J_μ is the electromagnetic current. Again starting from a small localized kick of the field of the form

$$A_\mu(t, \vec{x}) = A_\mu\delta^{(3)}(\vec{x})\delta(t), \tag{3.109}$$

and identifying A_μ with $\lambda\hat{O}$ and J_μ with $\hat{P}$, we see that, in Eq. (3.99),

$$\delta\langle J_\mu\rangle(t, \vec{x}) = A^\nu i\theta(t)\langle\Big[J_\mu(t,\vec{x}), J_\nu(0,\vec{0})\Big]\rangle \tag{3.110}$$

Integrating over a distribution of "kicks",

$$\delta\langle J_\mu\rangle(t,\vec{x}) = i\int dt'd^3x'\theta(t-t')A^\nu(t',\vec{x}')\langle[J_\mu(t,\vec{x}),J_\nu(t',\vec{x}')]\rangle, \tag{3.111}$$

Passing to momentum space, using the convolution theorem, we arrive at

$$\delta\langle J_\mu(\omega)\rangle = A^\nu(\omega)G^R_{\mu\nu}(\omega,\vec{k}=\vec{0}), \tag{3.112}$$

where $G^R_{\mu\nu}(\omega,\vec{k})$ is the retarted current-current correlator:

$$G^R_{\mu\nu}(\omega,\vec{k}) = -i\int d^3xdt\, e^{i\omega t-i\vec{k}\cdot\vec{x}}\theta(t)\langle\Big[J_\mu(t,\vec{x}),J_\nu(0,\vec{0})\Big]\rangle. \tag{3.113}$$

Now, the space-space part of Eq. (3.112) is equivalent to Ohm's law. In time domain, Ohm's law can be written as

$$\delta\langle J_i\rangle = \sigma_{ij}\partial_t A^j, \tag{3.114}$$

where σ_{ij} is the conductivity tensor. Passing to the frequency domain,

$$\delta\langle J_i\rangle = -i\omega\sigma_{ij}(\omega)A^j(\omega). \tag{3.115}$$

Comparing Eqs. (3.115) and (3.112), we see that the conductivity tensor can be calculated in terms of the microscopic theory by

$$\sigma_{ij}(\omega) = -\frac{G^R_{ij}(\omega,\vec{k}=0)}{i\omega} = -\frac{\mathrm{Im}\,G^R_{ij}(\omega,\vec{k}=0)}{\omega}. \tag{3.116}$$

Eq. (3.116) is the Kubo's formula for the electric conductivity.

Shear viscosity

For a last example of a Kubo formula for a transport coefficient, we consider the shear viscosity η of a relativistic fluid. More details on hydrodynamics, we refer the reader to Chapter 8, where higher order theories and theories with bulk dissipation coefficients are taken into account. In this section we work only with the simple example of relativistic Navier-Stokes - the objective here will be to show one can derive Kubo formula for transport coefficients in theories of hydrodynamics from the knowledge of the retarted energy-momentum tensor correlator.

Hydrodynamics is an effective theory, valid in the long wavelength and low frequency limit. In hydrodynamics, we relinquish knowledge of the microscopic theory, considering only a coarse grained, macroscopic, version of the microscopic theory where the main

degree of freedom is taken to be four-velocity vector field u_α of the fluid. The stress energy tensor $T^{(0)}_{\mu\nu}$ of a perfect relativistic fluid is uniquely fixed considering homogeneity and isotropy of the fluid in its rest frame, where $u_\alpha = (-1, 0, 0, 0)$ being given by [153]

$$T^{(0)}_{\mu\nu} = (\epsilon + p)u_\mu u_\nu + p g_{\mu\nu}, \tag{3.117}$$

where ϵ is the energy density of the fluid and p its pressure. Now, a non-perfect fluid includes an extra term, which depends upon the gradients of u_μ,

$$T_{\mu\nu} = T^{(0)}_{\mu\nu} + \Pi_{\mu\nu}. \tag{3.118}$$

where $\Pi_{\mu\nu}$ is called the dissipative tensor. In the case of relativistic Navier-Stokes theory, the dissipative tensor is given by

$$\Pi_{\mu\nu} = -\Delta_{\mu\alpha}\Delta_{\nu\beta}\left[\eta\nabla^{\langle\alpha}u^{\beta\rangle} + \zeta g^{\alpha\beta}\nabla_\lambda u^\lambda\right], \tag{3.119}$$

where ∇ is the covariant derivative and $\Delta_{\mu\alpha}$ is a projector orthogonal to the four velocity, given by

$$\Delta_{\mu\alpha} \equiv g_{\mu\alpha} + u_\mu u_\alpha. \tag{3.120}$$

Also, in Eq. (3.119), the brackets indicate symmetrization with null trace

$$\nabla_{\langle\alpha}u_{\beta\rangle} \equiv \nabla_\alpha u_\beta + \nabla_\alpha u_\beta - \frac{1}{3}g_{\alpha\beta}\nabla_\lambda u^\lambda. \tag{3.121}$$

In Eq. (3.119), η is the shear viscosity and ζ is the bulk viscosity.

The goal now is to relate the shear viscosity η with a microcospic theory. We will, once again, use linear response theory. The stress-energy tensor is sourced by fluctuations of the metric (see Appendix A). Let us consider a fluctuation of the spatial part of the metric around flat space, $g_{ij} = \delta_{ij} \to g'_{ij} = \delta_{ij} + h_{ij}$. Expanding $T_{\mu\nu}$ to first order in h, we get

$$\delta T_{ij} = p h_{ij} - \frac{1}{2}\kappa h^k_k \delta_{ij} + \eta\left(-\partial_t h_{ij} + \frac{1}{3}\delta_{ij}\delta^{kl}\partial_t h_{kl}\right) - \frac{1}{2}\zeta\delta_{ij}\delta^{kl}\partial_t h_{kl}, \tag{3.122}$$

where $\kappa = -V\partial p/\partial V$ is the bulk modulus. The Fourier transform of Eq. (3.122) is given by

$$\begin{aligned}\delta T_{ij}(\omega) = h_{kl}(\omega)&\left(p\delta^k_i\delta^l_j - \frac{1}{2}k\delta_{ij}\delta^{kl}\right) + \\ &+ \frac{i\omega}{2}\left[\eta\left(\delta^k_i\delta^l_j + \delta^l_i\delta^k_j - \frac{2}{3}\delta_{ij}\delta^{kl}\right) + \zeta\delta_{ij}\delta^{kl}\right]h_{kl}(\omega)\end{aligned} \tag{3.123}$$

In special, the xy channel yields

$$\delta T_{xy} = (p + i\omega\eta)h_{xy}. \tag{3.124}$$

Now, on the other hand, consider the microscopic theory whose low momentum expansion is the hydrodynamical classical theory. Then, the perturbation hamiltonian density is given by

$$\hat{H}' = -\frac{1}{2}h_{ij}\hat{T}^{ij}, \tag{3.125}$$

since metric fluctuations source the energy momentum tensor. As in the case of the electric conductivity, we consider a small localized kick, $h_{kl}(t,\vec{x}) = h_{kl}\delta^{(3)}(\vec{x})\delta(t)$, and identify $\lambda\hat{O} = h_{kl}\delta^{(3)}(\vec{x})/2$ and $\hat{P}(t) = T_{ij}(t,\vec{x})$. Proceeding as in that case we arrive, after passing to the frequency domain,

$$\delta\langle\hat{T}_{ij}(\omega)\rangle = -\frac{1}{2}h_{kl}G^R_{ijkl}(\omega), \tag{3.126}$$

where $G^R_{ijkl}(\omega)$ is the retarted Green's function of the stress energy-momentum tensor,

$$G^R_{\mu\nu\rho\lambda}(\omega) = -i\int dtd^3x e^{i\omega t - i\vec{k}\cdot\vec{x}}\theta(t)\left\langle\left[T_{\mu\nu}(t,\vec{0}), T_{\rho\lambda}(0,\vec{0})\right]\right\rangle. \tag{3.127}$$

Now, in the hydrodynamic regime we identify $\langle\hat{T}_{ij}\rangle$ with the classical stress-energy tensor T_{ij} of the fluid. Then, comparing Eq. (3.124) with Eq. (3.126) we see that,

$$\eta = -\lim_{\omega\to 0}\frac{1}{\omega}\mathrm{Im}\, G^R_{xyxy}(\omega, \vec{k} = 0), \tag{3.128}$$

which is Kubo formula for the shear viscosity. A Kubo formula for the bulk viscosity ζ follows from comparing the traces on the ij and kl indices of Eq. (3.124) and Eq. (3.126):

$$\zeta = -\frac{4}{9}\frac{1}{\omega}\mathrm{Im}\, G^{R,ij}_{ijij}(\omega, \vec{k} = 0). \tag{3.129}$$

3.8.3 Membrane transport coefficients

In this work, we will mainly work with the membrane paradigm as applied to the gauge/gravity duality [138]. In this section we will prove the result Eq. (3.89) in this way, as an illustration of the technique. In this work, the membrane paradigm will be used primarily to compute the electric charge susceptibility and the electric conductivity of the plasma in Chapter 7.

The main idea is to consider the transport coefficients of the membrane horizon. For a fairly general class of bulk fields, it will be shown that the transport coefficients for the membrane horizon are exactly the same transport coefficients of the dual non-Abelian

plasma. The formalism of the membrane paradigm excels when treating with bulk fluctuations given by massless scalar fields and vector fields.

Throughout this section, I will assume that the background has the form given by Eq. (3.53).

Scalar fields

Let us present first the formalism for massless scalar fields. Consider an operator $\hat{O}$ whose associated bulk field has its fluctuations around the background described by a massless scalar field ϕ with action

$$S_{\text{bulk}} = -\frac{1}{2}\int d^{d+1}x\,\sqrt{-g}\frac{1}{q(z)}(\partial\phi)^2, \tag{3.130}$$

where $q(z)$ is a z-dependent bulk coupling. To have a well-posed variational problem in the bulk, one must adjoin to S_{bulk} a term defined in the membrane horizon at $z_0 = z_h - \epsilon$, where $\epsilon \ll 1$, whose action is given by

$$S_{\text{surf}} = \int_{z=z_0} d^d x\,\sqrt{-\gamma}\,\Pi_{mb}(z_0,x)\phi(z_0,x), \tag{3.131}$$

where Π_{mb} is a "membrane ϕ-charge" given by

$$\Pi_{mb}(z_0,x) = -\frac{h(z_0)}{q(z_0)}e^{-A(z_0)}\partial_z\phi(z_0,x), \tag{3.132}$$

and $\gamma = \det(-\gamma_{\mu\nu})$, with $\gamma_{\mu\nu}$ being the induced metric on the membrane horizon.

The membrane horizon term cancels the contribution from the bulk that comes about when we integrate by parts when considering $\delta S = \delta S_{\text{bulk}} + \delta S_{\text{surf}}$. Now, as proven in Appendix B, the requirement of infalling boundary conditions at the membrane horizon is equivalent to requiring that the bulk fields depend near z_0 only upon the Eddington-Finkelstein coordinate v defined implicitly by

$$dv = dz + \sqrt{\frac{g_{zz}}{g_{tt}}}dt = dz + \frac{1}{h(z)}dt. \tag{3.133}$$

Then, applying the chain-rule to $\phi(t,\vec{x},r) = \tilde{\phi}(v,\vec{x})$, we see that

$$\partial_z\phi = \sqrt{\frac{g_{zz}}{g_{tt}}}\partial_t\phi = \frac{1}{h(z)}\partial_t\phi, \tag{3.134}$$

so that

$$\Pi_{mb} = -\frac{1}{q(z_0)}\frac{e^{-A(z_0)}}{\sqrt{h(z_0)}}\partial_t\phi. \tag{3.135}$$

Now, $e^{-A(z_0)}/\sqrt{h(z_0)} = \sqrt{g_{tt}}$ is the rescaling factor for the distant observer examining the dynamics of the membrane horizon. Then, Eq. (3.135) gives a relation between the current of the membrane paradigm and the time response of the fluctuation,

$$\Pi_{mb} = -\chi \partial_{\hat{t}} \phi, \tag{3.136}$$

where $\hat{t}$ is the rescaled time coordinate. Eq. (3.136) is a Ohm's law for the membrane scalar current, defining its associated membrane transport coefficient χ_{mb} by

$$\chi_{mb} = \frac{1}{q(r_0)} e^{3A(z_0)}. \tag{3.137}$$

Abelian gauge fields

Let us now extend the membrane paradigm formalism to a U(1) gauge field $A_\mu(x, z)$ in the bulk, dual to the electric current operator J^μ. The bulk action is given by

$$S_{\text{bulk}} = -\frac{1}{4} \int d^{d+1}x \, \sqrt{-g} \frac{1}{f(z)} F_{\mu\nu} F^{\mu\nu}, \tag{3.138}$$

where $F_{\mu\nu} = \partial_\mu A_\nu - \partial_\nu A_\mu$ is the electromagnetic field strength tensor and $f(z)$ is a possible z-dependent coupling. A well-posed variational problem requires, alongisde S_{bulk}, a membrane horizon term given by

$$S_{\text{surf}} = \int_{z=z_0} d^d x \, \sqrt{-\gamma} \, j^\mu_{mb}(z_0, x) A_\mu(z_0, x), \tag{3.139}$$

where the membrane current j^μ_{mb} is given by

$$j^\mu_{mb}(z_0, x) = -\frac{e^{A(z_0)}}{h(z_0) f(z_0)} \partial_z F^{r\mu}(z_0, x). \tag{3.140}$$

The argument applied for scalar fields that near the membrane horizon the bulk fields can only depend upon the Eddington-Finkelstein still holds; this requirement leads to the constraint

$$\partial_z A_i = \sqrt{\frac{g_{zz}}{g_{tt}}} \partial_t A_i = \frac{1}{h(z)} \partial_t A_i \qquad \text{as} \quad z \to z_0. \tag{3.141}$$

Then, fixing the $A_r = 0$ gauge, $F_{ri} = F_{ti}/h(z)$ and, thus,

$$j^i_{mb}(z_0, x) = -\frac{1}{h(z_0) f(z_0)} e^{-A(z_0)} F^i_t. \tag{3.142}$$

By the same rescaling argument, the membrane's Ohm's law in the rescaled orthonormal time can be written as, assuming isotropy,

$$\delta\langle j^i_{mb}\rangle = \sigma_{mb}\partial_{\hat{t}} A_j, \tag{3.143}$$

where σ_{mb} is the membrane conductivity. Comparing Eqs. (3.142) and (3.143) we obtain

$$\sigma_{mb} = \frac{1}{f(z_0)}. \tag{3.144}$$

3.8.4 Flow equations

Now that we know the transport coefficients on the membrane horizon, we have to discuss how to relate the membrane transport coefficient with the transport coefficients of the boundary gauge theory. This connection is described by the bulk flow equations.

Scalar fields

Let us start again with the bulk scalar field. We start by observing that, at the linear response level, we may write, using Eq. (3.104), the real-time prescription (3.75) as

$$G^R(\omega,\vec{k}) = \lim_{z\to 0}\frac{\Pi(\omega,\vec{k},z)}{\phi(\omega,\vec{k},z)}. \tag{3.145}$$

where

$$\Pi(\omega,\vec{k},z) = \frac{1}{q(z)}e^{3A(z)}h(z)\partial_z\phi(\omega,\vec{k},z) \tag{3.146}$$

can be identified as the conjugate momentum to $\phi(\omega,\vec{k},z)$ in a z-slice. Using Eq. (3.145) into Eq. (3.107), we see that the transport coefficient χ can be written in terms of the bulk fields as

$$\chi = \lim_{z\to 0}\frac{\Pi(\omega,\vec{k}=0,z)}{i\omega\phi(\omega,\vec{k}=0,z)}. \tag{3.147}$$

This motivates to define a bulk z-dependent transport coefficient $\bar{\chi}(\omega,\vec{k},z)$ by

$$\bar{\chi}(\omega,\vec{k},z) = \frac{\Pi(\omega,\vec{k},z)}{i\omega\phi(\omega,\vec{k},z)}. \tag{3.148}$$

Then the boundary transport coefficient $\chi(\omega)$ is given by following the flow of the bulk transport coefficient to the boundary

$$\chi(\omega) = \lim_{z\to 0}\bar{\chi}(\omega,\vec{k}=0,z). \tag{3.149}$$

Thus, our objective is now to follow the flow of the bulk transport coefficient $\bar{\chi}$ from the membrane horizon to the boundary. From the definition of the conjugate momentum (3.146) and the equation of motion for the scalar field (3.77), we derive an equation for the flow of the bulk transport coefficient $\bar{\chi}$

$$\partial_z \bar{\chi} = \frac{i\omega}{h(z)} \left[\frac{\bar{\chi}^2}{\Sigma(z)} - \Sigma(z) \left(1 - \frac{\vec{k}^2}{\omega^2} h(z) \right) \right], \tag{3.150}$$

where $\Sigma(z)$ is given by

$$\Sigma(z) = \frac{1}{q(z)} e^{3A(z)}. \tag{3.151}$$

Now, at the horizon we impose that $\bar{\chi}$ is regular. Since $h(z) \to 0$ as $z \to z_h$, this means that the expression in brackets in Eq. (3.150) must vanish at the horizon. In the zero momentum limit, $\vec{k} = 0$ (which is the only limit we will be interested in), this implies that

$$\bar{\chi}(\omega, \vec{k} = 0, z_0) = \Sigma(z_0) = \frac{1}{q(z_0)} e^{3A(z_0)} = \frac{s}{q(z_0)}. \tag{3.152}$$

Comparing with Eq. (3.137), we see that

$$\bar{\chi}(\omega, \vec{k} = 0, z_0) = \chi_{mb}(\omega), \tag{3.153}$$

that is, at the membrane horizon the bulk transport coefficient is given by the membrane transport coefficient. Thus, the transport coefficient at the boundary is given by following the flow from the membrane transport coefficient to the boundary.[9]

Now, consider the low-frequency limit, $\omega \to 0$. Then, the flow equation (3.150) becomes trivial, $\partial_z \bar{\chi} = 0$. Therefore, the flow from the horizon to the boundary and the DC transport coefficient $\chi(\omega = 0)$ is given by

$$\chi = \lim_{\omega \to 0} \lim_{z \to 0} \bar{\chi} = \chi_{mb}, \tag{3.154}$$

that is, at zero frequency, the membrane transport coefficient is equal to the boundary theory transport coefficient.

[9] We note that (3.150) is a Riccati equation. The Riccati equation, a first order non-linear equation, is equivalent to a second order linear equation - in this case, the equation of motion for ϕ, Eq. (3.75). A first order equation has one boundary condition, while a second order equation must have two boundary conditions. The flow equation (3.150) is subjected only to a boundary condition at the horizon. The equation of motion for ϕ is subjected to a boundary condition at the horizon and another at the asymptotic AdS boundary.

Universality of the shear viscosity in holography

An appplication of membrane paradigm is to prove the universality of the shear viscosity/entropy density ratio η/s in holographic theories. To compute the shear viscosity, we can use Kubo formula (3.128) and compute the retarted correlation function of $\hat{T}_{xy}$. As discussed in Section 3.2, the bulk field that couples with the energy-momentum tensor is the metric $g_{\mu\nu}$. Thus, to compute the retarted correlator using the real-time prescription, we should have to compute the on-shell action of the theory under fluctuations of the metric, $g_{\mu\nu} \to g_{\mu\nu} + h_{\mu\nu}$. However, as shown in [90], for strongly coupled field theories dual to theories of gravity with up to two derivatives in the effective gravitational action, the fluctuations $h_{\mu\nu}$ of the metric over an isotropic background in the transverse x direction are such that $g^{yy}h_{xy} = h^y_x$ decouple from the remaining metric fluctuations. The action for fluctuations of h^y_x fluctuations is given by

$$S = \frac{1}{16\pi G_5}\int d^5x\sqrt{-g}\frac{1}{2}(\partial h^y_x)^2. \tag{3.155}$$

That is, h^y_x behaves a massless scalar field with constant coupling $q(z) = 1/16\pi G_5$. We can then immediately apply Eq. (3.152) and compute the shear viscosity:

$$\frac{\eta}{s} = \frac{1}{4\pi}, \tag{3.156}$$

a result that is valid for all strongly coupled field theories dual to theories of gravity with up to two derivatives in the effective gravitational action. [138]

Abelian gauge field

Let us now turn our attention to the case of an Abelian gauge field and focus on the computation of transport coefficients linked to the charge transport in the plasma.

Eq. (3.145) now reads

$$\lim_{z\to 0} A^i(\omega,\vec{k}) = \lim_{z\to 0} G^{R,ij}(\omega,\vec{k})j_j(\omega,\vec{k},z), \tag{3.157}$$

where j_μ is the conjugate momentum to the bulk field A_μ in the z-constant slices

$$j^\mu = -\frac{1}{f(z)}\sqrt{-g}F^{r\mu} = -\frac{1}{f(z)}e^{5A(z)}F^{r\mu}. \tag{3.158}$$

Now, consider a fluctuation of A_μ along the x_3-axis. Then, as we will show, the effect of theses fluctuations on the gauge invariant fields $F^{\mu\nu}$ and j^μ separate cleanly in two different channels - one corresponding to effects on the components transverse to the fluctuation,

that is, the components x_1 and x_2, and one corresponding to the components parallel to the fluctuation, x_3. This motivates us to write two z-dependent electric conductivities, the longitudinal channel conductivity $\bar{\sigma}_L$

$$\bar{\sigma}_L(\omega, \vec{k}, z) = \frac{j^3(\omega, \vec{k}, z)}{F_{3t}(\omega, \vec{k}, z)} \tag{3.159}$$

and the transverse channel conductivity σ_T

$$\bar{\sigma}_T(\omega, \vec{k}, z) = \frac{j^1(\omega, \vec{k}, z)}{F_{1t}(\omega, \vec{k}, z)} = \frac{j^2(\omega, \vec{k}, z)}{F_{2t}(\omega, \vec{k}, z)}. \tag{3.160}$$

Our objective is now to write equations for the flow of $\bar{\sigma}_L$ and $\bar{\sigma}_T$. From the flow equations, we will be able to extract the two independent components of the conductivity tensor σ_{ij} by following the flow of the z-dependent conductivities from the membrane horizon to the boundary

$$\sigma_L \equiv \sigma^{11} = \lim_{z\to 0} \bar{\sigma}_L(\omega, \vec{k} = 0, z) \tag{3.161}$$

$$\sigma_T \equiv \sigma^{33} = \lim_{z\to 0} \bar{\sigma}_T(\omega, \vec{k} = 0, z) \tag{3.162}$$

The first step is to write the Maxwell equations that follow from the bulk action (3.138), that is,

$$\partial^\mu \left(\frac{\sqrt{-g}}{f} F_{\mu\nu} \right) = 0. \tag{3.163}$$

The goal is first to write all equations in terms of gauge invariant quantities. Using Eq. (3.158), the z component equation can be writen as

$$\partial_3 j^3 + \partial_t j^t = 0 \qquad (z), \tag{3.164}$$

which expresses charge conservation along the x_3 axis. By the same token, the remaining equations yield

$$-\partial_z j^t + \frac{\sqrt{-g}}{f(z)} g^{tt} g^{33} \partial_3 F_{3t} = 0 \qquad (t) \tag{3.165}$$

$$-\partial_z j^1 - \frac{\sqrt{-g}}{f(z)} g^{00} g^{11} \partial_t F_{t1} + \frac{\sqrt{-g}}{f(z)} g^{33} g^{11} \partial_3 F_{31} = 0 \qquad (x_1) \tag{3.166}$$

$$-\partial_z j^3 + \frac{\sqrt{-g}}{f(z)} g^{tt} g^{33} \partial_t F_{3t} = 0 \qquad (x_3). \tag{3.167}$$

The Maxwell equation that comes from the (x_2) component is the same as Eq. (3.164) to

(3.167) with $(x \to y)$. We also must impose the validity of Bianchi's identity,

$$D_\mu F_{\nu\rho} + D_\rho F_{\mu\nu} + D_\nu F_{\rho\mu} = 0. \tag{3.168}$$

The independent equations that follow from Eq. (3.168) are, in terms of F and j,

$$\partial_z F_{3t} - \frac{\sqrt{-g}}{f(z)} g_{33} g_{zz} \partial_t j^z - \frac{\sqrt{-g}}{f(z)} g_{33} g_{tt} \partial_3 j^t = 0 \tag{3.169}$$

$$\partial_z F_{1t} - \frac{\sqrt{-g}}{f(z)} g_{zz} g_{11} \partial_t j^2 = 0 \tag{3.170}$$

$$\partial_3 F_{t1} + \partial_t F_{13} = 0 \tag{3.171}$$

The equations of motion can be divided in two groups. One group that involves only j^t, j^z and F_{3t}, Eqs. (3.164), (3.165), (3.167) and (3.169), which will be used to derive the flow equation for $\bar{\sigma}_L$, and a second group that involves only j^1, F_{1t} and F_{13}, Eqs. (3.166), (3.170) and (3.171), which will lead to the flow equation for $\bar{\sigma}_T$.

Let's study the first group and derive the flow equation for $\bar{\sigma}_L$ first. From the defition of $\bar{\sigma}_L$, Eq. (3.159),

$$\partial_z \bar{\sigma}_L = \frac{\partial_z j^3}{F_{3t}} - \frac{j^3}{F_{3t}^2} \partial_z F_{3t}. \tag{3.172}$$

Using Eq. (3.166) to eliminate $\partial_z j^3$ and Eq. (3.169) to eliminate $\partial_z F_{3t}$, and passing to momentum space, considering a plane wave with momentum $q = (\omega, 0, 0, k)$,

$$\partial_z \bar{\sigma}_L = -\frac{\sqrt{-g}}{f(z)} g^{tt} g^{33} (i\omega) + \frac{i j^3 g_{zz}}{F_{3t}^2} \frac{f(z)}{\sqrt{-g}} \left(\omega g_{33} j^3 + g_{zz} + k g_{zz} j^t \right). \tag{3.173}$$

The final step is to use Eq. (3.164) in momentum space to eliminate j^t. We then arrive at the flow equation for $\bar{\sigma}_L$,

$$\partial_z \bar{\sigma}_L = \frac{i\omega}{h(z)} \left[\frac{\bar{\sigma}_L^2}{\Sigma_A(z)} \left(1 - \frac{\vec{k}^2}{\omega^2} h(z) \right) - \Sigma_A(z) \right] \tag{3.174}$$

The same procedure using the second group of equations lead to the second flow equation,

$$\partial_z \bar{\sigma}_T = \frac{i\omega}{h(z)} \left[\frac{\bar{\sigma}_T^2}{\Sigma_A(z)} - \Sigma_A(z) \left(1 - \frac{\vec{k}^2}{\omega^2} h(z) \right) \right], \tag{3.175}$$

where $\Sigma_A(z)$ is defined by

$$\Sigma_A(z) = \frac{1}{f(z)} e^{A(z)}. \tag{3.176}$$

With the flow equations in hand, we may proceed to follow the flow from membrane

horizon to boundary, as in the case of the scalar field. The first remark is that in the zero momentum limit $\vec{k} \to 0$, both flow equations collapse: $\bar{\sigma}_L = \bar{\sigma}_T = \bar{\sigma}$ with

$$\partial_z \bar{\sigma} = \frac{i\omega}{h(z)} \left[\frac{\bar{\sigma}^2}{\Sigma_A(z)} - \Sigma_A(z) h(z) \right]. \tag{3.177}$$

In the zero frequency limit, the term in brackets must vanish near the horizon so that

$$\bar{\sigma}(\omega, \vec{k} = 0, z_0) = \Sigma_A(z_0) = \frac{e^{A(z_0)}}{f(z_0)} = \sigma_{mb}, \tag{3.178}$$

after comparing with Eq. (3.144) The flow, once again, is trivial when $\omega \to 0$, and thus the conductivity is given by

$$\sigma = \lim_{\omega \to 0} \lim_{z \to 0} \bar{\sigma} = \chi_{mb}. \tag{3.179}$$

Diffusion coefficient

Another application of the membrane paradigm formalism for gauge fields that will be useful in applications will be the calculation of the charge susceptibility and the diffusion constant of the plasma [144,154,155], which characterizes the diffusion of the small charge perturbation induced by an external electric field. As we show below, to first order in a derivative expansion, D is related to a pole of retarted correlator (see also [58,336]).

Let us consider that the current J_μ correspond to a conserved current. Then, it satisfies the current conservation equation,

$$\partial_t n + \partial_i J^i = 0, \tag{3.180}$$

where $n = J^0$ is the electric charge density. For low momentum and frequencies, we may suppose that, in a gradient expansion, Fick's law holds,

$$J_i = -D \partial_i n, \tag{3.181}$$

where D is the *diffusion constant*. Therefore, $n(x)$ satisfies the diffusion equation,

$$\partial_t n = D \partial_i \partial^i n. \tag{3.182}$$

Passing to momentum space, we obtain the propagator G^R_{00},

$$G^R_{00}(\omega, \vec{k}) = \frac{G^R(0, \vec{k})}{-i\omega + D\vec{k}^2}. \tag{3.183}$$

Therefore, D is a pole in the 00 component of the Green's function. By Eq. (3.180), D

will also be a pole of G^R_{33}.

Let's study the diffusion constant first. We consider, in the flow equation for $\bar{\sigma}_L$, the low frequency and low momentum limit, but with $\omega \sim \vec{k}^2$. The flow equation then simplifies to

$$\frac{\partial_z \bar{\sigma}_L}{\bar{\sigma}_L^2} = -\frac{i\vec{k}^2}{\omega}\frac{1}{\Sigma_A}. \tag{3.184}$$

This equation is a first order separable ordinary differential equation, which can be solved using the boundary condition (3.152), resulting in

$$\frac{1}{\bar{\sigma}_L(r)} = \frac{1}{\sigma} + i\frac{\vec{k}^2}{\omega}\int_{z_0}^{z} dz' \frac{1}{\Sigma_A}. \tag{3.185}$$

Since $G^R_{33}(k_\mu) = \sigma_L(k\mu) = \bar{\sigma}_L(z \to 0)$, we find that

$$G^R_{33}(k_\mu) = \frac{\omega^2 \sigma}{i\omega - D\vec{k}^2}, \tag{3.186}$$

where D is given by the formula [138]

$$D = \sigma \int_{z_0}^{0} dz' \frac{1}{\Sigma_A} = \sigma \int_{z_0}^{0} dz' f(z) e^{-A(z)}. \tag{3.187}$$

Charge susceptibility and Einstein's relation

As a final application, we will study the charge susceptibility χ_2. The charge susceptibility is defined by

$$\chi_2 = \frac{\partial n}{\partial \mu}. \tag{3.188}$$

That is, at the linear level on the chemical potential μ,

$$n = \chi_2 \mu + O(\mu^2). \tag{3.189}$$

The bulk field that couples to the chemical potential μ is the zeroth component of the gauge field A^0. In special, $\mu = A_t(z \to 0)$. Also, $n = j_0(z \to 0)$. Let us choose a static bulk configuration, which corresponds to a zero momentum limit. Then, from the bulk field equations (3.164) to (3.167),

$$\partial_z j_t = 0 \tag{3.190}$$

and

$$\partial_z A_t = \frac{f(z)}{\sqrt{-g}} g_{zz} g_{tt} j^t, \tag{3.191}$$

which can be integrated to

$$j_t(z) = \text{constant} = n \tag{3.192}$$

and to

$$A_t(z) = A_t(z_0) + n \int_{z_0}^{z} dz'\ e^{-A(z)} h(z). \tag{3.193}$$

Imposing horizon regularity, $A_t(z_0) = 0$, Then, taking $z \to 0$, $\mu = A_t(z \to 0)$, using (3.189) we see that χ_2 is given by

$$\chi_2 = \frac{1}{\int_{z_0}^{0} dz' f(z) e^{-A(z)}}. \tag{3.194}$$

We note, in passing, that Eqs. (3.194) and (3.187) imply that

$$D\chi_2 = \sigma. \tag{3.195}$$

That is, Einstein's relation involving the conductivity σ, the diffusion constant D and the charge susceptibility χ_2 holds for this class of gauge theories dual to theories of gravity.

Application: $\mathcal{N} = 4$ SYM at finite temperature.

To exemplify the use of the formulas resulting from the membrane paradigm, let's compute some of the transport coefficients for a strongly coupled $\mathcal{N} = 4$ SYM plasma. The metric of the gravity dual is given by the AdS_5/Schwarzshild backgound of Eq. (3.40). The shear viscosity is given by Eq. (3.156), since the background is isotropic. In this case, $f(z) = g^2$ is a constant bulk coupling constant. Then, applying Eq. (3.178), we find that

$$\sigma_{\mathcal{N}=4SYM} = \frac{1}{f(z_h)} \left(\frac{1}{z_h L} \right) = \frac{\pi T}{g^2}, \tag{3.196}$$

as $z_h = 1/(\pi L T)$. We see that $\sigma_{\mathcal{N}=4SYM} \propto T$, as required by dimensional analysis, since T is the only scale of the theory. Now, Eq. (3.187) yields

$$D_{\mathcal{N}=4SYM} = \frac{1}{2\pi T}. \tag{3.197}$$

Finally, using either (3.194), we have that

$$\chi_{2,\mathcal{N}=4SYM} = \frac{2\pi^2 T^2}{g^2}. \tag{3.198}$$

These results were obtained first in Ref. [157] and later checked using the membrane paradigm in Ref. [138]. In Chapter 7 we will apply the membrane paradigm formalism to

compute the electrical conductivity, the diffusion coefficient and the charge susceptibility of a bottom-up model that more closely resembles (2+1) flavor QCD.

3.9 $\mathcal{N} = 4$ SYM plasma at large N as a reasonable proxy of the QCD plasma

As a final point in this brief introduction to the gauge/gravity duality, we give a brief argument to why the $\mathcal{N} = 4$ SYM plasma should be taken as a reasonable proxy to the strongly coupled QGP. The main idea is that while $\mathcal{N} = 4$ SYM and QCD are wildly different theories in vacuum, QCD at temperatures of a few T_c becomes qualitatively similar (at least in some aspects) to the $\mathcal{N} = 4$ SYM plasma. This partially justifies considering $\mathcal{N} = 4$ SYM as a reasonable starting point for building holographic models relevant for the phenomenology of the QGP.

At a first glance, $\mathcal{N} = 4$ SYM and "real-world" QCD are two very different beasts at zero temperature. $\mathcal{N} = 4$ SYM is a (super)conformal field theory, possessing no scales; the gauge coupling constant does not run and can be set to any value - as a dial. Pure Yang-Mills theory is classically conformally invariant; however, as discussed in Chapter 2, quantization breaks conformal invariance and a scale is dynamically generated in the theory by dimensional transmutation. Moreover, strongly coupled $\mathcal{N} = 4$ SYM is strongly coupled at all scales; pure SU(N_c) Yang-Mills theory is asymptotically free, becoming weakly coupled in the UV. Also, $\mathcal{N} = 4$ SYM has no confinement, whereas pure Yang-Mills is (as far as we know) a confining gauge theory. Moreover, $\mathcal{N} =$ SYM is supersymmetric, with scalars and fermions in the adjoint representation of gauge group. Pure Yang-Mills is not supersymmetric. QCD introduces massive fermionic degrees of freedom, but in the fundamental representation of the gauge group. Also, QCD at low energies has an additional (approximate) symmetry, namely $\mathrm{U}(3)_L \times \mathrm{U}_R(3)$ chiral symmetry which is believed to be spontaneously broken in the $T = 0$ regime, resulting in a non-vanishing chiral condensate.

However, the introduction of temperature breaks conformal symmetry and supersymmetry in $\mathcal{N} = 4$ SYM. Conformal symmetry is broken due to the introduction of a dimensionful scale, the temperature T. The adjoint fermions in $\mathcal{N} = 4$ SYM acquire a mass due to the imposition of anti-periodic boundary conditions. The adjoint bosons, in turn, acquire a mass at the one-loop level in perturbation theory. The gauge vector fields remain massless, due to gauge invariance. Thus, we have a theory of massless gauge bosons and massive fermions and scalars in the adjoint representation.

In turn, as discussed in the previous Chapter, pure Yang-Mills has a first order confinement/deconfiment transition. With (2+1) flavors with physical masses, lattice gauge

theory indicates that QCD has has a crossover phase transition [73,76,78,158]. For $T \gg T_c$, asymptotic freedom is restored and the theory is weakly coupled. However, for $T \sim T_c$, the theory is still strongly coupled.

Thus, at $T \sim T_c$, QCD and strongly coupled $\mathcal{N} = 4$ both possess a similar set of features: both are deconfined gauge theories, at strong coupling, with no conformal or supersymmetry. This means that as a proxy model for "real-world" QCD near T_c, $\mathcal{N} = 4$ may be qualitatively similar to each other. Also, we may use $\mathcal{N} = 4$ as a springboard for model building, either in a top-down or in a bottom-up approach, incorporating more features of QCD to build more realistic models. Thus, using the gauge/gravity duality, we may probe the strong coupling limit of $\mathcal{N} = 4$ SYM and others holographic models for QCD - we may understand strong coupling phenomena in theories that are QCD-like, but not exactly QCD. This is the main motivation for using the gauge-gravity as a tool to probe strong coupling phenomena.

Chapter 4

Holographic Wilson Loops - Real and Imaginary Parts

4.1 Introduction

One of the most important gauge invariant quantities defined in non-Abelian $SU(N_c)$ gauge theories [12, 159] is the Wilson loop

$$W(C) = \frac{1}{N_c}\mathrm{tr}\, P \exp\left[ig \oint_C \hat{A}_\mu dx^\mu\right], \tag{4.1}$$

where C is a closed loop embedded in a 4-dimensional spacetime, P indicates path-ordering, g is the coupling, $\hat{A}_\mu$ is the non-Abelian gauge field potential operator while the trace is performed over the fundamental representation of $SU(N_c)$ (other representations can also be used but we will use the fundamental representation in this Chapter). In particular, the case where C is a rectangular loop of spatial length L and extended over $\mathcal{T}$ in the time direction, as depicted in Figure 4.1, has been extensively studied over the years. With this contour, the limit $\mathcal{T} \to \infty$ of the vacuum expectation value of (4.1) gives

$$\lim_{\mathcal{T}\to\infty} \langle W(C)\rangle_0 \sim e^{i\mathcal{T}V_{Q\bar{Q}}(L)}, \tag{4.2}$$

where $V_{Q\bar{Q}}(L)$ is known as the heavy quark potential (the vacuum interaction energy between two infinitely massive probes in the fundamental representation).[1]. In the vacuum of a confining gauge theory $\langle W(C)\rangle$ should obey an area law defined by $\lim_{L\to\infty} V_{Q\bar{Q}}(L)/L = \sigma$, with σ being the string tension [12].

In the imaginary time formulation of thermal gauge theories [61], all bosonic fields

[1] In Appendix C we review the argument that leads to the relation (4.2)

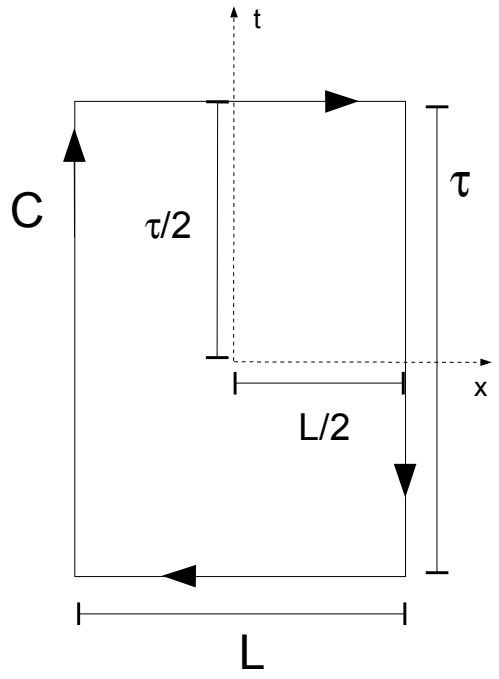

Figure 4.1: *The rectangular Wilson loop, along with the choice of the coordinate system used.*

are required to be periodic (or anti-periodic in the case of fermionic fields) in the Euclidean time τ with period $\beta = 1/T$ and the order parameter for the deconfinement phase transition in an $SU(N_c)$ theory without dynamical fermions is characterized by the path ordered Polyakov loop [160–162]

$$\mathbf{L}(\vec{x}) = \frac{1}{N_c} P\, e^{i\, g \int_0^{1/T} \hat{A}_0(\vec{x},\tau) d\tau} \,. \tag{4.3}$$

This operator becomes gauge invariant (up to a phase) after performing the trace. In a pure gauge theory there are also global gauge transformations that are only periodic up to an element of $Z(N_c)$, which is the center of $SU(N_c)$. In this case, $\mathrm{tr}\,\mathbf{L}$ transforms as a field of charge one under the global $Z(N_c)$ symmetry, i.e., $\mathrm{tr}\,\mathbf{L} \to e^{i2\pi a/N_c}\mathrm{tr}\,\mathbf{L}$ where $a = 0, \ldots, N_c - 1$. Below T_c the system is $Z(N_c)$ symmetric, which implies that $\langle \mathrm{tr}\,\mathbf{L} \rangle = 0$. Above T_c this global symmetry is spontaneously broken, $\langle \mathrm{tr}\,\mathbf{L} \rangle \neq 0$, and the system lands in one of the possible $Z(N_c)$ vacua. The thermal average of the Polyakov loop correlator $\mathcal{C}(r,T) \equiv \langle \mathrm{tr}\,\mathbf{L}^\dagger(r)\,\mathrm{tr}\,\mathbf{L}(0) \rangle$ is associated with the difference in the free energy of the system due to the inclusion of an infinitely heavy $Q\bar{Q}$ pair separated by a distance r in the medium [163]. Such a formulation has been used to define a heavy quark potential at finite temperature on the lattice [164–166].

However, the rectangular Wilson loop can also be computed in gauge theories at

finite temperature. In this case, the expectation value of the Wilson loop operator for the same rectangular contour can be evaluated in a thermal state of the gauge theory with temperature T (in Minkowski spacetime) and the $\mathcal{T} \to \infty$ limit

$$\lim_{\mathcal{T}\to\infty} \langle W(C) \rangle \sim e^{i\mathcal{T}V_{Q\bar{Q}}(L,T)} \tag{4.4}$$

defines a quantity $V_{Q\bar{Q}}(L,T)$ which we call here the "heavy quark potential at finite temperature". In general, this heavy quark potential in QCD can have an imaginary part, as shown in [167–175, 178] (for recent studies about quantum decoherence effects in quarkonia see [176, 177]), while the quantity defined using the Polyakov loop correlator is necessarily real. The imaginary part of the potential defines a thermal decay width which, at weak coupling, is related to the imaginary part of the gluon self energy induced by Landau damping and the $Q\bar{Q}$ color singlet to color octet thermal break up.

In this Chapter we shall elaborate on the method proposed in [179] to estimate the thermal width of heavy quarkonia at strong coupling using worldsheet fluctuations of the Nambu-Goto action associated with the heavy quark pair in the gauge/gravity duality [14, 93, 94]. In this approach, the thermal width of heavy quarkonium states stems from the effect of thermal fluctuations due to the interactions between the heavy quarks and the strongly coupled medium. This is described holographically by integrating out thermal long wavelength fluctuations in the path integral of the Nambu-Goto action in the curved background spacetime. At sufficiently strong coupling, this calculation can be done analytically and a simple formula for the imaginary part of the Wilson loop can be found in this approach that is valid for any gauge theory that is holographically dual to classical gravity[2]. The formula is used to revisit the calculation of the thermal width in strongly coupled $\mathcal{N} = 4$ SYM theory done in [179]. Moreover, we compute the imaginary part of the potential for a strongly-coupled conformal field theory dual to Gauss-Bonnet (GB) gravity. We also prove a general result that establishes the connection between the thermal width and the presence of an area law for the Wilson loop at zero temperature in gauge theories with gravity duals, which may be useful for the study of the imaginary part of the heavy quark potential in confining gauge theories dual to gravity.

This Chapter is organized as follows. In the next section we will revisit the general setup concerning the holographic calculation of Wilson loops. In section 4.3 we discuss the holographic calculation of $\mathrm{Re}\, V_{Q\bar{Q}}$, which is necessary to derive our main formula for the imaginary part of the potential in Section 4.4. In Section 4.5 we apply the formula to compute the imaginary part in two different strongly coupled gauge theories with gravity

[2]The background metric has to fulfill certain conditions for the method to be applicable. This is shown in Section 4.2.

duals. Final comments on this Chapter are given in Section 4.6[3].

4.2 Holographic setup

After the original calculation of the rectangular Wilson loop in the vacuum of strongly coupled $\mathcal{N} = 4$ SYM theory [4] [180, 181] and its generalization to finite temperature in [182, 183], rectangular Wilson loops have been extensively studied in strongly coupled gauge theories using the gauge/gravity duality.

According to the gauge/gravity prescription [180], the expectation value of $W(C)$ in a strongly coupled gauge theory dual to a theory of gravity is

$$\langle W(C) \rangle \sim Z_{str}, \tag{4.5}$$

where Z_{str} is the generating functional of the string in the bulk which has the loop C at the boundary. In the classical gravity approximation

$$Z_{str} \sim e^{iS_{str}}, \tag{4.6}$$

where S_{str} is the classical string action propagating in the bulk evaluated at an extremum, $\delta S_{str} = 0$. In the case of a rectangular Wilson loop at nonzero T other extrema can become relevant as one increases the value of LT [184]. In this thesis we are only interested in deeply bound states where $LT < 1$ and this question becomes less important[5]. In the classical approximation the worldsheet action S_{str} may be taken as the Nambu-Goto action[6]

$$S_{str} = S_{NG} = \frac{1}{2\pi\alpha'} \int d\sigma d\tau \sqrt{-det(G_{\mu\nu}\partial_a X^\mu \partial_b X^\nu)}, \tag{4.7}$$

where $X^\mu(\tau, \sigma)$ are the worldsheet embedding coordinates, $\mu, \nu = 0, 1, \ldots, 4$, $a, b = \sigma, \tau$, and $\alpha' = l_s^2$, where l_s is the string length.

Its worth noticing that this problem is analogous to the problem of the catenary dealt in the elementary variational calculus. There, we want to discover the form that a string assumes when held fixed at the two extremes, when acted only by the force of gravity. Here, we want to discover the form that the string worldsheet assumes when its extremes are held fixed in the form of the curve C at the 4d boundary of a 5d spacetime. The

[3] Other aspects of the calculations are presented in Appendix D.

[4] Note that in $\mathcal{N} = 4$ SYM the Wilson loop operator also contains the 6 adjoint scalars.

[5] We shall come back to this point when discussing the calculation of the imaginary part later in Section 4.5 and also in Appendix D.

[6] For gravity duals derived within string theory, supersymmetry requires the presence of fermions on the worldsheet but those only enter as an $\hbar$ correction to the action and can be neglected in the supergravity limit in which $\alpha' \to 0$.

gravitational force is given by the deformation of the spacetime, which "pushes" down the worldsheet into the bulk.

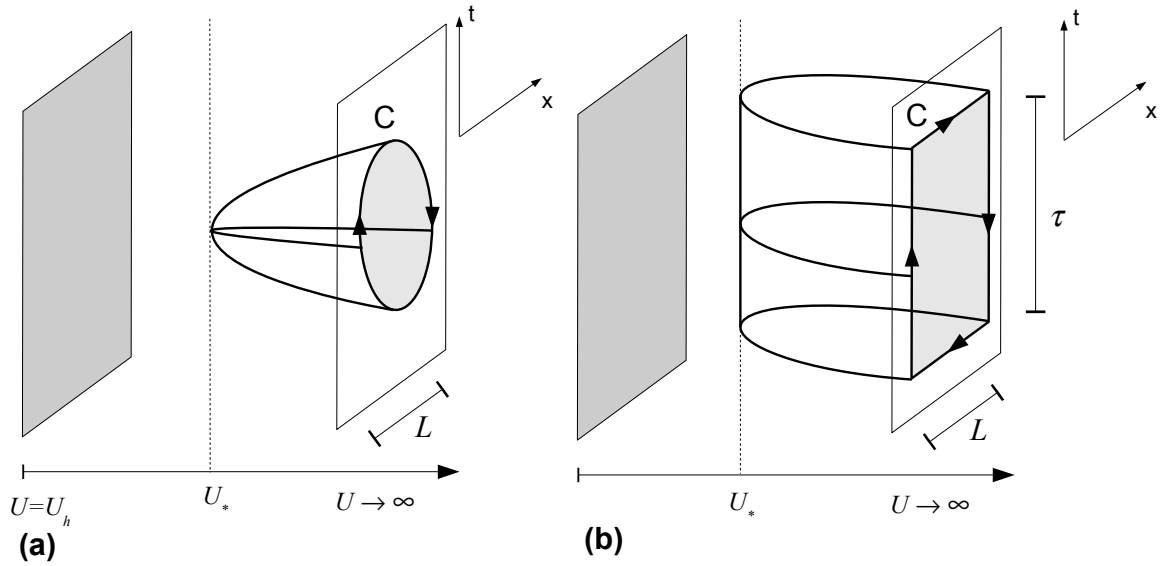

Figure 4.2: *The Maldacena prescription for the calculation of Wilson loops via the gauge/gravity duality. In (a) we present the situation for an arbitrary loop C. In (b) we consider rectangular Wilson loops with $\mathcal{T} \to \infty$. In both cases U_h is the position of the horizon of the black brane and U_* denotes the bottom of the sagging string in the bulk.*

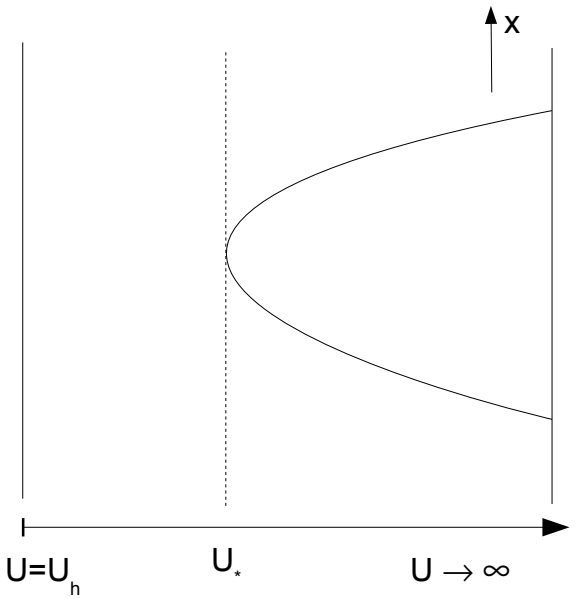

Figure 4.3: *A slice of the string worldsheet for the rectangular Wilson loop at fixed time t.*

Therefore, the Wilson loop in the strongly coupled gauge theory can be determined using the classical solution of (4.7) which has the loop C as the boundary of the clas-

sical string worldsheet. For the case of rectangular Wilson loops one can then calculate $V_{Q\bar{Q}}(L,T)$ (see Figure 4.2). We will consider an effective 5-dimensional curved spacetime, which will describe the gravity model dual to the gauge theory[7]. Finite temperature effects are taken into account by introducing a near-extremal black brane in the gravity dual and we assume, in this Chapter, that the metric of the gravity dual has the following general form[8]

$$ds^2 = -G_{00}(U)dt^2 + G_{xx}(U)d\vec{x}^2 + G_{UU}(U)dU^2, \tag{4.8}$$

where $\vec{x} = (x, y, z)$ denotes the usual spatial coordinates while U is the radial direction. The metric (4.8) is assumed to have an asymptotic boundary at $U \to \infty$. The position of the horizon of the black brane, U_h, is given by the (first simple) root of $G_{00}(U) = 0$ starting from the boundary and we will also assume here that $G_{UU}(U_h) \to \infty$, with $G_{00}(U_h)G_{UU}(U_h)$ finite. The black brane temperature T (which is a function of the position of the horizon, $T = T(U_h)$) corresponds to the temperature of the thermal bath in the gauge theory. Also, note that the thermal state of the gauge theory considered here is assumed to be invariant under spatial $SO(3)$ rotations and the $Q\bar{Q}$ pair is at rest in the local rest frame of the plasma - in the next Chapter we will consider examples of anisotropic situations

4.3 Real part of the heavy quark potential

We start by establishing the holographic formalism for the computation of the real part of the heavy quark potential. The calculation of the real part of the potential within the gauge/gravity duality is well-known and can now be found in textbooks [102], for instance. For the sake of completeness, we provide a review of those results in this Section.

4.3.1 The general formalism

For the rectangular Wilson loop, we choose the coordinate system shown in Figure 4.1 in which the string worldsheet coordinates are written in static gauge, $X^\mu = (t, x, 0, 0, U(x,t))$, $\tau = t$ and $\sigma = x$. Furthermore, since $\mathcal{T} \to \infty$, any slice of the worldsheet with constant t has the same form (as shown in Figure 4.2(b)) - this means that we can take $U(x,t) = U(x)$. We present a sketch of a fixed t slice of the string worldsheet in Figure 4.3. With these choices and the general metric (4.8), the action (4.7) takes the

[7] In the case of $AdS \times S_5$ we choose a fixed configuration in S_5 for the compact string coordinates.
[8] The metric (4.8) is assumed to be given in the string frame.

form

$$S_{NG} = \frac{\mathcal{T}}{2\pi\alpha'} \int_{-L/2}^{L/2} dx \sqrt{M(U(x))(U')^2 + V(U(x))}, \tag{4.9}$$

where $U' \equiv dU/dx$, $M(U) \equiv G_{00}G_{UU}$ and $V(U) \equiv G_{00}G_{xx}$. For the models considered in this work, we will always have $M(U) > 0$. The action (4.3.1) is only implicitly dependent on x and, thus, the associated Hamiltonian is a constant of motion

$$\mathcal{H}_{NG} = \frac{V(U)}{\sqrt{M(U)(U')^2 + V(U)}} = \text{const.} = \sqrt{V(U_*)}, \tag{4.10}$$

where $U_* \equiv U(x = 0)$ and also $U'(0) = 0$ (since the string has its minimum at $x = 0$). We can solve (4.10) for U' and obtain

$$\frac{dU}{dx} = \left[\frac{V(U)}{M(U)}\left(\frac{V(U)}{V(U_*)} - 1\right)\right]^{1/2}. \tag{4.11}$$

Since the endpoints of the string are located at $x = -L/2$ and $x = L/2$, we integrate (4.11) to obtain a relation between U_* and L,

$$\frac{L}{2} = \int_{U_*}^{\infty} dU \, \sqrt{M(U)} \left[V(U)\left(\frac{V(U)}{V(U_*)} - 1\right)\right]^{-1/2}. \tag{4.12}$$

We may deduce another consequence of (4.11) which will be useful later. In fact, differentiating (4.11) with respect to x and then setting $x = 0$ and $U = U_*$ one finds

$$U''(0) = \frac{1}{2}\frac{V'(U_*)}{M(U_*)}, \tag{4.13}$$

where $V'(U) = dV(U)/dU$. Since $x = 0$ is a minimum, $U''(0) > 0$, and one can see that $V'(U_*) > 0$.

Finally, we use (4.11) to obtain an expression for the action evaluated at the classical solution of the equations of motion

$$S_{str} = \frac{\mathcal{T}}{\pi\alpha'} \int_{U_*}^{\infty} dU \, \sqrt{M(U)} \sqrt{\frac{V(U)}{V(U_*)}} \left(\frac{V(U)}{V(U_*)} - 1\right)^{-1/2}. \tag{4.14}$$

The (yet to be regularized) real part of the heavy quark potential is simply given by $\lim_{\mathcal{T}\to\infty} S_{str}/\mathcal{T}$. The equations (4.12) and (4.14) (minus the regularization) solve the problem. To obtain $\mathrm{Re}\, V_{Q\bar{Q}}$ as a function of L and T we either eliminate U_* from both equations or, when this is not possible, parametrize both L and $\mathrm{Re}\, V_{Q\bar{Q}}$ as functions of U_*.

Note that (4.14) is UV divergent. This UV divergence, which is characteristic of Wilson loops, appears in the holographic approach from the fact that the string must stretch from the bulk to the boundary. Note that this is the same type of UV divergence found in $\mathcal{N}=4$ SYM at $T=0$ [180], which is to be expected since in thermal gauge theories all UV divergences must come from the vacuum contribution [61]. This implies that the same regularization chosen for the vacuum can be used to render the $T\neq 0$ potential finite. The regularized real part of the potential at nonzero temperature can be written as

$$\begin{aligned}\mathrm{Re}\, V^{reg}_{Q\bar{Q}}(L,T) &= \frac{1}{\pi\alpha'}\int_{U_*}^{\infty} dU\left[\sqrt{M(U)}\sqrt{\frac{V(U)}{V(U_*)}}\left(\frac{V(U)}{V(U_*)}-1\right)^{-1/2}-\sqrt{M_0(U)}\right]\\ &- \frac{1}{\pi\alpha'}\int_{0}^{U_*} dU\,\sqrt{M_0(U)}. \end{aligned} \tag{4.15}$$

where $M_0(U)=\lim_{U\to\infty} M(U)$. This temperature independent regularization scheme for the real part of the potential is well defined for any asymptotically AdS_5 geometry, even in the case in which the dual gauge theory displays confinement at $T=0$ (in the sense of an area law for the rectangular Wilson loop in the vacuum)[9]. See also [164,165] for further arguments for using temperature independent subtractions in the Wilson and Polyakov loops.

The expectation value of the Polyakov loop $|\langle \mathrm{tr}\,\mathbf{L}\rangle|$ can be easily extracted from Eq. (4.15) by assuming that when $L\to\infty$, $U_*\to U_h$ and $\mathrm{Re}\, V^{reg}_{Q\bar{Q}}\to 2F^{reg}_Q$. This gives the (regularized) heavy quark free energy

$$F^{reg}_Q(T) = \frac{1}{2\pi\alpha'}\int_{U_h}^{\infty} dU\left[\sqrt{M(U)}-\sqrt{M_0(U)}\right]-\frac{1}{2\pi\alpha'}\int_0^{U_h} dU\,\sqrt{M_0(U)} \tag{4.16}$$

and the Polyakov loop $|\langle \mathrm{tr}\,\mathbf{L}(T)\rangle| = \exp\{-F^{reg}_Q(T)/T\}$. While this simple procedure gives the correct expression for $F^{reg}_Q(T)$ [185,186] in this type of gravity duals, we note that other configurations for the string worldsheet besides the U-shaped one must be taken into account when $LT>1$ [184,187]. In the following we will always consider the regularized expressions for the quantities discussed above and, thus, the superscript "reg" will be omitted from the formulas in the rest of the Chapter.

[9] As explained in [184], the regularization scheme involving the subtraction of the contribution coming from two "straight" strings running from U_h to $U\to\infty$ is temperature dependent. Moreover, since the connected U-shaped contribution to the potential is of order N_c^0 and this kind of disconnected contribution involving the two straight strings is of order N_c^2 [184], it becomes problematic to use the latter to regularize the heavy quark potential in the large N_c limit where these classical gravity calculations are performed. Therefore, in this work we opted to use the expression in Eq. (4.15), which is well defined in the large N_c limit.

4.3.2 Confinement from the holographic Wilson loop

Before finishing this section, let us analyse the connection between confinement (defined, for the purposes of this Chapter, as the area law in the Wilson loop, as given by the relation $\lim_{L\to\infty} V_{Q\bar{Q}}(L)/L = \sigma$ - see Chapter 2 and Ref. [44] for a discussion of the definition of confinement). For the general metric in Eq. (4.8), it was shown in Refs. [188,189], that if there is a U_0 such that $V(U)$ has a minimum or $M(U)$ diverges, then the theory linearly confines with string tension

$$\sigma = \frac{1}{2\pi\alpha'}\sqrt{V(U_0)}. \tag{4.17}$$

Let us prove this theorem. Assume that $V(U)$ has a minimum at $U = U_0$, where $M(U)$ is regular. Starting from Eq. (4.15), using Eq. (4.12), it is possible to rewrite this equation as

$$F_Q^{reg}(T) = \frac{\sqrt{V(U_*)}}{2\pi\alpha'}L - \frac{1}{\pi\alpha'}\int_{U_h}^{\infty} dU\,\left(\sqrt{\frac{M(U)}{V(U)}}\sqrt{V(U)^2 - V(U_*)^2} - \sqrt{M_0(U)}\right) + \\ - \frac{1}{\pi\alpha'}\int_0^{U_*} dU\,\sqrt{M_0(U)}. \tag{4.18}$$

If we prove that the second term is subleading for $L \to \infty$, then Eq. (4.17) follows. Then $V'(U_0) = 0$. Writing $V(U)$ as $V(U) = e^{-2A(U)}$, then L given by (4.12) in Eq. (4.18) can be written as

$$\frac{L}{2} = \int_{U_*}^{\infty} dU\,\frac{\sqrt{M(U_*)}}{e^{2A(U)}}\frac{1}{\sqrt{e^{4(A(U)-A(U_*))}-1}}. \tag{4.19}$$

Now, suppose that the string drops in the bulk down to $U \sim U_*$. Then, $U_0 \sim U_*$ and we may expand the exponential inside the square root in Eq. (4.19) to yield, near the lower limit of the integral,

$$\int_{U_0} dU\,\frac{\sqrt{M(U_0)}}{e^{2A(U)}}\frac{1}{\sqrt{4A'(U_0)(U-U_0) + 8A''(U_0)(U-U_0)^2}}. \tag{4.20}$$

As $V(U)$ is a minimum at $U = U_0$, by hypothesis, $V'(U_0) = 0$ and $V''(U_0) > 0$, then $A'(U_0) = 0$ and $A''(U_0) > 0$. Then, the square root in (4.20) is real and we can write (as $U < U_0$)

$$L \sim 2\int_{U_0} \frac{1}{\sqrt{8A''(U_0)}(U_0 - U)} \propto -\lim_{U\to U_0^-} \ln(U_0 - U) \to \infty. \tag{4.21}$$

Thus, as the second term in (4.18) is finite, the first term dominates and (4.17) holds. Thus, if $V(U)$ has a minimum at $U = U_0$, with $M(U)$ regular, Eq. (4.17) holds. To

complete the proof, assume that $M(U)$ diverges at U_0. Then Eq. (4.19) implies $L \to \infty$ at $U = U_0$, and Eq. (4.17) also holds.

We can build an intuitive picture for this result: as one pulls the quarks apart and $L \to \infty$, the bottom of the classical string becomes flat at U_0 and cannot penetrate any further into the geometry. In the deconfined phase of a ($T = 0$ confining) gauge theory, however, U_0 is hidden by the horizon and $\sigma = 0$.

4.4 Thermal worldsheet fluctuations and the imaginary part of the heavy quark potential in strongly coupled plasmas

We now generalize the procedure proposed in Ref. [179] to extract the imaginary part of heavy quark potential, $\mathrm{Im}\, V_{Q\bar{Q}}$, using the gauge/gravity duality. After deriving a formula for $\mathrm{Im}\, V_{Q\bar{Q}}$ using the saddle point approximation, we discuss its limitations and present some general conditions for the existence of such an imaginary part in this setup. We remark that other approaches have been proposed to extract the imaginary part of the potential using holography in [190–192]. These different methods give results that are qualitatively equivalent in the case of $\mathcal{N} = 4$ SYM theory. The method discussed in detail in this section has the advantage of being of easy implementation in comparison to the other schemes since $\mathrm{Im}\, V_{Q\bar{Q}}$ for a generic gravity dual (4.8) can be directly computed using the formula in Eq. (4.36) derived below.

4.4.1 The saddle point approximation

In the previous section, we saw that the classical solution to the Nambu-Goto action (4.7) can be used to compute the real part of the heavy quark potential. To extract $\mathrm{Im}\, V_{Q\bar{Q}}(L, T)$ we have to consider the effect of thermal worldsheet fluctuations about the classical configuration $U = U_c(x)$. Such fluctuations, although taken here to be small, may turn the integrand of (4.3.1) negative near $x = 0$ and generate an imaginary part for the effective string action. The corresponding physical picture is that some part of the string, through thermal fluctuations, may reach the horizon (see Figure 4.4).

Therefore, we shall consider the effect of worldsheet fluctuations $\delta U(x)$ ($\delta U(\pm L/2) = 0$) around the classical configuration $U_c(x)$

$$U(x) = U_c(x) \to U(x) = U_c(x) + \delta U(x). \tag{4.22}$$

The classical configuration $U_c(x)$ solves $\delta S_{NG} = 0$. For simplicity, the fluctuations $\delta U(x)$

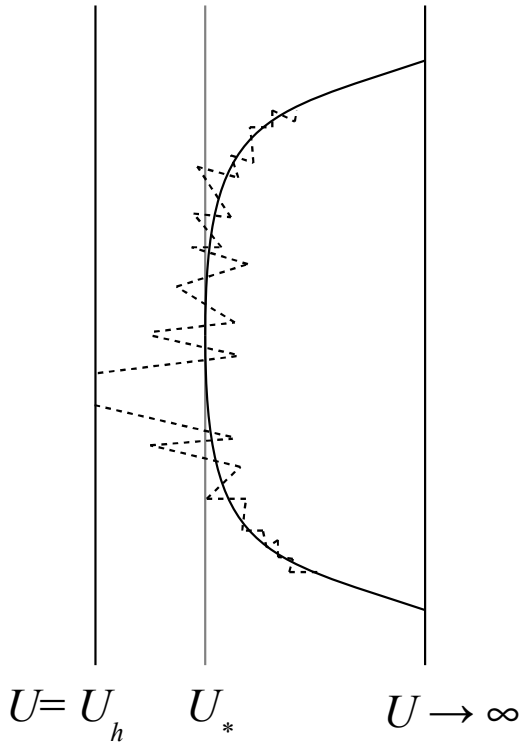

Figure 4.4: *An illustration of the effect of thermal fluctuations (dashed line) around the classical string configuration (solid line). If the bottom of the classical string solution is close enough to the horizon, thermal worldsheet fluctuations of very long wavelength may be able to reach the black brane horizon at U_h.*

are taken to be of arbitrarily long wavelength, i.e., $\frac{d\,\delta U(x)}{dx} \to 0$. The string partition function that takes into account the fluctuations is then

$$Z_{str} \sim \int \mathcal{D}\delta U(x) e^{iS_{NG}(U_c(x)+\delta U(x))}. \tag{4.23}$$

If $\delta U(x)$ is such that the integrand in S_{NG} acquires an imaginary part then, by considering Eq. (4.4) through Eq. (4.6), $\mathrm{Im}\, V_{Q\bar{Q}}(L,T) \neq 0$. Note that we are assuming that the fluctuations are not strong enough to allow for transitions to different classical extrema of Z_{str}.

We proceed by dividing the interval $-L/2 < x < L/2$ into $2N$ points $x_j = j\Delta x$ $(j = -N, -N+1, \ldots, N)$ with $\Delta x \equiv L/(2N)$ and then take the $N \to \infty$ limit in the end of the calculation. Then, Z_{str} becomes

$$Z_{str} \sim \lim_{N\to\infty} \int d[\delta U(x_{-N})] \ldots d[\delta U(x_N)] \exp\left[i \frac{\mathcal{T}\Delta x}{2\pi\alpha'} \sum_j \sqrt{M(U_j)(U_j')^2 + V(U_j)} \right], \tag{4.24}$$

where $U_j \equiv U(x_j)$ and $U'_j \equiv U'(x_j)$. The thermal fluctuations are most important around $x = 0$ where $U = U_*$, which means that it is reasonable to expand $U_c(x_j)$ around $x = 0$ and keep only terms up to second order in x_j. Given that $U'_c(0) = 0$ we obtain

$$U_c(x_j) \approx U_* + \frac{x_j^2}{2} U''_c(0). \tag{4.25}$$

Since the string worldsheet fluctuations which will be more important in generating an imaginary part are those near the black brane horizon (as will be discussed in more detail in Subsection 4.4.2), we can consider only small fluctuations around the bottom of the string. Taking this into account, we expand the classical solution around $x_j = 0$, the bottom of the classical solution, and consider small fluctuations around it. The inclusion of these small higher order corrections to the imaginary part, which are associated with the small fluctuations away from the bottom of the string, could in principle be considered, although the calculations become considerably more involved. As we are considering only small fluctuations around the classical configuration, we expand $V(U(x_j)) = V(U_c(x_j)+\delta U(x_j))$ in x_j and δU, keeping only the terms up to second order in the monomial $x_j^m \delta U^n$

$$V(U_j) \approx V_* + \delta U V'_* + U''_c(0) V'_* \frac{x_j^2}{2} + \frac{\delta U^2}{2} V''_*, \tag{4.26}$$

where $V_* \equiv V(U_*)$, $V'_* \equiv V'(U_*)$, and etc. The function $M(U)$ admits the same expansion as $V(U)$ but, in the action (3.1), $M(U)$ appears only via $M(U)(U'(x))^2$. Using Eq. (4.25) we see that $U'(x) \approx x_j U''_c(0)$ and, therefore, $U'(x)^2$ is already a term of second order in $x_j^m \delta U^n$. Then, we consider only the zeroth order term in the expansion of $M(U)$, i.e., $M(U) \approx M(U_*)$. Combining this with Eqs. (4.25) and (4.26) we can approximate the exponent in Eq. (4.24) as

$$S_j^{NG} = \frac{\mathcal{T} \Delta x}{2\pi\alpha'} \sqrt{C_1 x_j^2 + C_2} \tag{4.27}$$

where

$$C_1 = \frac{U''_c(0)}{2} \left[2 M_* U''_c(0) + V'_*\right] \tag{4.28}$$

and

$$C_2 = V_* + \delta U V'_* + \frac{\delta U^2}{2} V''_*, \tag{4.29}$$

where we defined $M_* \equiv M(U_*)$. Since $U''_c(0) > 0$ and $M, V'_* > 0$, one sees that $C_1 > 0$.

If the function in the square root of Eq. (4.27) is negative then S_j^{NG} contributes to $\mathrm{Im}\, V_{Q\bar{Q}}(L,T) \neq 0$. The next step consists in determining when this happens and what the corresponding contribution to Z_{str} is. In order to do that, let us isolate the j-th such

contribution to Z_{str}

$$I_j \equiv \int_{\delta U_{jmin}}^{\delta U_{jmax}} d(\delta U_j)\, \exp\left[i\frac{\mathcal{T}\Delta x}{2\pi\alpha'}\sqrt{C_1 x_j^2 + C_2}\right], \tag{4.30}$$

where δU_{jmin}, δU_{jmax} are the roots of $C_1 x_j^2 + C_2$ in δU. For $\delta U_{jmin} < \delta U < \delta U_{jmax}$ we have $C_1 x_j^2 + C_2 < 0$, which means that Eq. (4.30) is exactly the contribution to $\mathrm{Im}\, V_{Q\bar{Q}}(L,T) \neq 0$ we were looking for - the total contribution for all x_j is $\prod_j I_j$.

The integral in Eq. (4.30) can be evaluated using the saddle point method in the classical gravity approximation where $\alpha' \ll 1$. The exponent has a stationary point when the function

$$D(\delta U_j) \equiv C_1 x_j^2 + C_2(\delta U_j) \tag{4.31}$$

assumes an extremal value. This happens for

$$\delta U = -\frac{V_*'}{V_*''}. \tag{4.32}$$

Requiring that the square root has an imaginary part implies that $D(\delta U_j) < 0 \to -x_c < x_j < x_c$ where

$$x_c = \sqrt{\frac{1}{C_1}\left[\frac{V_*'^2}{2V_*''} - V_*\right]}. \tag{4.33}$$

We take $x_c = 0$ if the square root in Eq. (4.33) is not real. Under these conditions, we can approximate $D(\delta U)$ by $D(-V_*'/V_*'')$ in Eq. (4.30)

$$I_j \sim \exp\left[i\frac{\mathcal{T}\Delta x}{2\pi\alpha'}\sqrt{C_1 x_j^2 + V_* - \frac{V_*'^2}{2V_*''}}\right]. \tag{4.34}$$

Since the total contribution to the imaginary part is given by $\prod_j I_j$, returning to the continuum limit and invoking the prescription (4.5), we find

$$\mathrm{Im}\, V_{Q\bar{Q}} = -\frac{1}{2\pi\alpha'}\int_{|x|<x_c} dx \sqrt{-x^2 C_1 - V_* + \frac{V_*'^2}{2V_*''}}\,. \tag{4.35}$$

Evaluating the integral in Eq. (4.35) [193] and using Eq. (4.13) and Eq. (4.28) we finally find a closed expression for $\mathrm{Im}\, V_{Q\bar{Q}}$

$$\mathrm{Im}\, V_{Q\bar{Q}} = -\frac{1}{2\sqrt{2}\alpha'}\sqrt{M_*}\left[\frac{V_*'}{2V_*''} - \frac{V_*}{V_*'}\right]. \tag{4.36}$$

Eq. (4.36) reduces to the result derived in Ref. [179] where it was assumed that the background metric was such that $M(U) = 1$. The only difference between the general formula in Eq. (4.36) and the previous one found in Ref. [179] is the presence of the factor $\sqrt{M_*}$ (M gives an idea of how much warped the space-time is in the bulk). Also, note that $\mathrm{Im}\, V_{Q\bar{Q}}$ is UV finite. Moreover, the fluctuations also change the real part of the potential. This is discussed in Appendix D, Section D.1.

An important condition that must be satisfied in order for the saddle point calculation shown here to be applicable is $V_*'' \neq 0$. If $V_*'' = 0$ then Eq. (4.31) does not have extrema and higher orders terms in δU must be kept in the expansion Eq. (4.26) for V, which signals the breakdown of the saddle point approximation.

Finally, an equivalent derivation of the imaginary part of $V_{Q\bar{Q}}$ using a covariant background expansion of the Nambu-Goto action is given in Appendix D, Section D.1.

4.4.2 The relationship between $\mathrm{Im}\, V_{Q\bar{Q}}$, confinement, and the black brane

A first glance into the derivation of Eq. (4.36) may give the misleading idea that the presence of a black brane is not necessary in order to have $\mathrm{Im}\, V_{Q\bar{Q}} \neq 0$. However, the absence of a black brane implies that $\mathrm{Im}\, V_{Q\bar{Q}} = 0$, as we shall explain below. Moreover, when the metric satisfies the conditions for the presence of an area law for the rectangular Wilson loop mentioned in Section 4.3 one can show that $\mathrm{Im}\, V_{Q\bar{Q}}(L \to \infty) = 0$. These results are exact within the semiclassical approximation used for the string partition function in Eq. (4.23).

The existence of a black brane is necessary for $\mathrm{Im}\, V_{Q\bar{Q}} \neq 0$

As mentioned in Section 4.2, for the general metric in Eq. (4.8) $G_{00}(U_h) = 0$ and $G_{UU}(U_h) \to \infty$, with $G_{00}(U_h)G_{UU}(U_h)$ being finite. Therefore, $M(U)$ is finite and positive for every U and $V(U) > 0$ if $U > U_h$, but $V(U_h) = 0$. The important point here is that for $U < U_h$ it is possible that $V(U) < 0$.

In Eq. (4.23), requiring that the square root possesses an imaginary part means that $K(U) \equiv M(U)(U')^2 + V(U) < 0$ for some U. Since $M(U), V(U) > 0$ for $U > U_h$, for any worldsheet fluctuation δU such that $U(x) = U_c(x) + \delta U(x) > U_h$ one has $K > 0$ for every $x \in [-L/2, L/2]$. However, if the fluctuation is such that $U < U_h$, $V(U)$ may be negative and $K(U(x)) < 0$ for some interval in x even though $M(U) > 0$. In other words, if the worldsheet fluctuations are such that a portion of the string reaches the horizon and probes the black brane, then an imaginary part for the heavy quark potential may be generated. This is illustrated in Figure 4.4. Therefore, in this approach an imaginary

part for $V_{Q\bar{Q}}$ appears when we consider worldsheet fluctuations in which $\delta U < 0$.

On the other hand, if a black brane horizon is not present and the metric (4.8) is regular everywhere we have that G_{00}, G_{UU} is positive for every $U > 0$. Then, we have $M(U), V(U) > 0$ and, thus, $K(U) > 0$ for every $U > 0$. This implies that $\mathrm{Im}\, V_{Q\bar{Q}} = 0$, exactly. Therefore, in our approach the heavy quark potential can develop an imaginary part due to the thermal worldsheet fluctuations induced by the presence of a black brane.

If the rectangular Wilson loop displays an area law then $\mathrm{Im}\, V_{Q\bar{Q}}(L \to \infty) = 0$

Suppose that $M(U)$ diverges at the confinement scale U_0 (with $V(U_0) \neq 0$). In this case, for large L we have $U_* \sim U_0$. Moreover, in this case when $L \to \infty$ the string worldsheet lays nearly flat at U_0. We may write $U_c(x) \sim U_0 - \epsilon$, where $\epsilon \ll U_0$. Finally, since $M(U_0)$ is large we may neglect the second term in the expression of $K(U)$. Therefore, for long wavelength fluctuations $\delta U' = 0$ the Nambu-Goto action in Eq. (4.23) takes the form

$$S_{NG} \approx \frac{\mathcal{T}}{2\pi\alpha'} \int_{-L/2}^{L/2} dx\, U_0 \sqrt{M(U_0 - \epsilon + \delta U)}. \tag{4.37}$$

Note that now we cannot consider fluctuations such that $\delta U > \epsilon$ since then we would be taking M past its divergence. Therefore, only fluctuations with $\delta U < \epsilon$ are allowed in this case. However, note that this implies that $M > 0$ and, thus, the square root that appears in the evaluation of the potential is always real. Therefore, in this situation $\mathrm{Im}\, V_{Q\bar{Q}} = 0$.

Alternatively, suppose now that M does not diverge at U_0 but rather that $V(U)$ has a minimum at U_0. For small fluctuations about $U_c(x) = U_0$ where $U_c'(0) = U_c''(0) = \ldots = 0$ (since the string lays nearly flat at U_0) one finds

$$V(U_0 + \delta U) \approx V(U_0) + \frac{1}{2} V''(U_0) \delta U^2, \tag{4.38}$$

where $V''(U_0) > 0$. Thus, $V(U) > 0$ in the neighborhood of $U = U_0$, $x = 0$ and $K(U) > 0$. Therefore, S_{NG} is real and $\mathrm{Im}\, V_{Q\bar{Q}} = 0$. We then conclude that $\mathrm{Im}\, V_{Q\bar{Q}}(L \to \infty) = 0$ if the background metric is such that the rectangular Wilson loop displays an area law.

We may summarize these results as follows. Suppose that U_0 is the value of the U coordinate at which the metric satisfies the conditions for confinement and that U_h is the position of the black brane horizon. If $U_0 > U_h$ then the classical string cannot go past U_0. As discussed above, we cannot consider fluctuations beyond U_0. Effectively, U_0 acts as a "barrier" for the classical string. However, if $U_h > U_0$, the horizon hides this barrier and we may have fluctuations that reach U_h. Both cases are sketched in Figure 4.5.

4.4.3 Using $\mathrm{Im}\, V_{Q\bar{Q}}$ to estimate the thermal width of heavy quarkonia at strong coupling

In the next section we will compute $\mathrm{Im}\, V_{Q\bar{Q}}$ in two different conformal plasmas using the prescription derived above. To estimate the thermal width $\Gamma_{Q\bar{Q}}$ of the heavy $Q\bar{Q}$ pair we will use a first-order non-relativistic expansion

$$\Gamma_{Q\bar{Q}} = -\langle\psi|\mathrm{Im}\, V_{Q\bar{Q}}(L,T)|\psi\rangle, \tag{4.39}$$

where

$$\langle\vec{r}|\psi\rangle = \frac{1}{\sqrt{\pi}a_0^{3/2}}e^{-r/a_0} \tag{4.40}$$

is the ground-state wave function of a particle in a Coulomb-like potential of the form $V(L) = -K/L$ and $a_0 = 2/(m_Q K)$ is the Bohr radius (m_Q is the mass of the heavy quark Q such that $m_Q/T \gg 1$). Even though the real part of the potential at finite temperature for the cases studied here is not given by just the $\sim 1/L$ term, this provides the leading contribution for the potential between deeply bound $Q\bar{Q}$ states in a conformal plasma, which justifies the use of Coulomb-like wave functions to determine the width. Moreover, in potential models of the bottomonium spectrum, the $\Upsilon(1S)$ state is mostly bound due to the Coulomb part of the Cornell potential. The thermal width is then given by

$$\Gamma_{Q\bar{Q}} = -\frac{4}{a_0^3}\int_0^\infty dL\, L^2 e^{-2L/a_0}\,\mathrm{Im}\, V_{Q\bar{Q}}(L,T)\,. \tag{4.41}$$

Actually, as it will be discussed shortly, we should take Eq. (4.41) as representing a lower bound for the heavy quarkonia thermal width computed within the thermal worldsheet fluctuation method presented here. We emphasize that this approximation to the thermal width of heavy quarkonia is made using the imaginary part of the heavy quark potential as an input for a potential model in QCD, in a phenomenological approach. Also, for very heavy states, the distance between the quarks in the meson can be so small that perturbative QCD effects are not negligible.

4.5 Calculation of $\mathrm{Im}\, V_{Q\bar{Q}}$ in some gravity duals

4.5.1 An overview of the models

Using the general framework described in the previous section, we shall now study the imaginary part of the heavy quark potential and the corresponding heavy quarkonia thermal width in two different strongly coupled plasmas dual to theories of classical gravity. In particular, we will consider the following models:

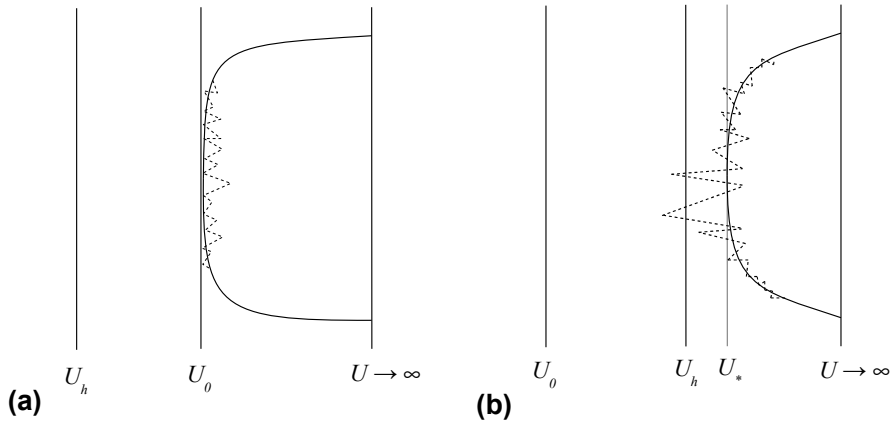

Figure 4.5: *An illustration of the relationship between thermal worldsheet fluctuations and confinement. Figure 4.5(a) shows that when $U_0 > U_h$ the classical string worldsheet, even with the inclusion of thermal fluctuations, cannot go beyond U_0. On the other hand, Figure 4.5(b) shows that when $U_0 < U_h$ the horizon hides the "barrier" at U_0 and the thermal fluctuations can reach the horizon.*

1. Strongly coupled, thermal $\mathcal{N} = 4$ SYM at large N_c. This case was already studied in Ref. [179] but here we shall perform a more complete study of the imaginary part of the potential and revisit the estimate for the thermal width of heavy quarkonia at strong coupling done in Ref. [179].

2. A simple model for QCD_3. Based on the observation that taking $T \to \infty$ in $\mathcal{N} = 4$ SYM reduces the theory to a non-supersymmetric Yang-Mills-like theory in 3 dimensions at $T = 0$. This is the simplest modification of thermal $\mathcal{N} = 4$ SYM that results in a confining theory, although in 3 spatial dimensions.

3. Gauss-Bonnet gravity [194–196]. This model includes $\mathcal{R}^2_{\mu\nu\lambda\rho}$ terms in the gravity dual action corresponding to higher order derivative corrections to the supergravity action.

In Appendix D, Section D.3 we discuss some other results involving Wilson loops and compute Im $V_{Q\bar{Q}}$ for some other simple top-down models of non-conformal strongly plasmas.

4.5.2 $\mathcal{N} = 4$ SYM

The metric for a near-extremal black-brane in $AdS_5 \times S_5$ is given by,

$$ds^2 = -\frac{U^2}{R^2} f(U) dt^2 + \frac{U^2}{R^2} d\vec{x}^2 + \frac{R^2}{U^2} \frac{1}{f(U)} dU^2 + R^2 d\Omega_5^2, \tag{4.42}$$

where R is the common radius of S_5 and AdS_5, $f(U) \equiv 1 - U_h^4/U^4$, $d\Omega_5^2$ corresponds to the S_5 part of metric and, as before, U_h is the position of the black brane horizon[10]. The boundary gauge theory is $\mathcal{N} = 4$ SYM with $N_c \to \infty$. The 't Hooft coupling in this strongly coupled gauge theory is given by $\lambda = R^4/\alpha'^2 \gg 1$. The temperature of the black brane (and of the dual gauge theory) is given by

$$T = \frac{U_h}{\pi R^2}. \tag{4.43}$$

In the following we always choose a fixed configuration for the string coordinates in S_5 and, thus, all the calculations are effectively done only using the AdS_5 piece. For this metric $M(U) = 1$ and $V(U) = (U^4 - U_h^4)/R^4$.

Heavy quark potential in the vacuum

The expressions for L, Eq. (4.12), and S^{nreg}, Eq. (4.14), turn, in this case, into

$$\frac{L}{2} = \frac{R^2}{U_*}\int_1^\infty dy\, \frac{1}{y^2\sqrt{y^4-1}} \quad \text{and} \tag{4.44}$$

$$S^{nreg} = \frac{\mathcal{T}}{\pi\alpha'}U_*\int_1^\infty dy\, \frac{y^2}{\sqrt{y^4-1}}. \tag{4.45}$$

where we made the change of variables $U \to y = U/U_*$. Note that the integral (4.45) diverges linearly when $y \to \infty$ and this is the UV divergence we already expected. The regularized potential is

$$V_{Q\bar{Q}} = \frac{U_*}{\pi\alpha'}\left[\int_1^\infty dy\, \left(\frac{y^2}{\sqrt{y^4-1}} - 1\right) - 1\right]. \tag{4.46}$$

The integrals in Eqs. (4.44) and (4.46) can be done in terms of the beta function, as described in Appendix D, Section D.2. After integration, one obtains

$$L = \frac{R^2}{U_*}\frac{2\sqrt{2\pi}\pi}{\Gamma(1/4)^2} \tag{4.47}$$

[10]The AdS_5 metric of (3.40) is related to Eq. (4.42) by the coordinate transformation $U \to R/z$, so that $f(U) = h(R/U)$. The remaining expressions follow from those given in Section 3.6. Whereas z takes the interpretation of a length scale in the renormalization group interpretation of the gauge/gravity duality, U is an energy scale in this coordinate system.

and

$$V_{Q\bar{Q}} = -U_* \frac{\sqrt{2\pi}}{\alpha' \Gamma(1/4)^2}. \tag{4.48}$$

In this particular case, it is possible to eliminate the parameter U_* from Eqs. (4.47) and (4.48) to obtain the potential as an explicit function of L [180]

$$V_{Q\bar{Q}} = -\frac{4\pi^2}{\Gamma(1/4)^4} \frac{R^2}{\alpha'} \frac{1}{L}. \tag{4.49}$$

From Eq. (4.49) we obtain an estimate for the Bohr radius that will be used throughout this work, $a_0 = \Gamma(1/4)^4/(m_Q 2\pi^2\sqrt{\lambda})$. For the case of a bottom quark $m_b \sim 4.7$ GeV and, using $\lambda = 9$ [197, 198], one finds $a_0 \sim 0.6\,\mathrm{GeV}^{-1}$.

Thermal $\mathcal{N} = 4$ SYM

We start by computing the heavy quark free energy from Eq. (4.16). For its regularization we use half of the regularization term used for the potential at $T = 0$, which gives

$$F_Q = -\frac{U_h}{2\pi\alpha'}. \tag{4.50}$$

Using Eq. (4.43) we can write Eq. (4.51) as

$$\frac{F_Q}{T} = -\frac{\sqrt{\lambda}}{2}. \tag{4.51}$$

This result [182, 183] is consistent with the fact that the only scale available in the calculation of the Polyakov loop in a thermal $\mathcal{N} = 4$ SYM theory is the temperature T.

For the rectangular Wilson loop at finite T we use the same regularization employed for the $T = 0$ case. The resulting expressions for L and $\mathrm{Re}\, V_{Q\bar{Q}}$ may be written as [182, 183]

$$LT(y_h) = \frac{2}{\pi} y_h \sqrt{1 - y_h^4} \int_1^\infty \frac{dy}{\sqrt{(y^4 - y_h^4)(y^4 - 1)}} \tag{4.52}$$

$$\frac{\mathrm{Re}\, V_{Q\bar{Q}}(y_h)}{T} = \frac{R^2}{\alpha'} \frac{1}{y_h} \left[\int_1^\infty dy \left(\sqrt{\frac{y^4 - y_h^4}{y^4 - 1}} - 1 \right) - 1 \right] \tag{4.53}$$

where $y_h \equiv U_h/U_*$ and $0 < y_h < 1$.

These integrals can be calculated in terms of hypergeometric functions [102, 190] as shown in Appendix D, Section D.2. One finds that

$$LT(y_h) = \frac{2\sqrt{2\pi}}{\Gamma(1/4)^2} y_h \sqrt{1 - y_h^4}\, {}_2F_1\left[\frac{1}{2}, \frac{3}{4}; \frac{5}{4}; y_h^4\right] \quad \text{and} \tag{4.54}$$

$$\frac{\mathrm{Re}\, V_{Q\bar{Q}}}{T} = -\frac{R^2}{\alpha'}\frac{\sqrt{2\pi^3}}{\Gamma(1/4)^2}\frac{1}{y_h}\,{}_2F_1\left[-\frac{1}{2}, -\frac{1}{4}; \frac{1}{4}; y_h^4\right]. \tag{4.55}$$

These equations cannot be solved exactly and must be analyzed as a function of y_h. However, when $LT \ll 1$ it is possible to expand both expressions in powers of $(LT)^4$, obtaining, at first order (Appendix D, Section D.2)

$$\frac{\mathrm{Re}\, V_{Q\bar{Q}}}{T} = -\frac{4\pi^2\sqrt{\lambda}}{\Gamma(1/4)^4 LT}\left[1 + c(LT)^4\right], \tag{4.56}$$

where

$$c = \frac{3}{5\cdot 2^7\pi^2}\Gamma(1/4)^8. \tag{4.57}$$

The fact that the potential only depends on the combination LT is expected since $\mathcal{N} = 4$ SYM is a conformal plasma.

Let us examine Eq. (4.54). In Figure 4.6 we plot LT as a function of y_h. One sees that there is a maximum value of y_h, $y_{h,max} = 0.85$, and that LT is a decreasing function of y_h for $y_h > y_{h,max}$. Physically, this means that for $y_h > y_{h,max}$, one has to take into account highly curved configurations for the string worldsheet which are not solutions of the Nambu-Goto action but are important for $y_h > y_{h,max}$ [184]. In fact, a calculation of the curvature scalar associated with the worldsheet metric in Appendix D, Section D.4 shows that it diverges for $y_h \to 1$. Therefore, we can only trust this U-shaped classical solution up to $y_{h,max}$. For further reference, the corresponding value of LT is $LT_{max} = LT(y_{h,max}) \sim 0.28$. From Figure 4.6 we also see that for $y_h \sim 0$, $LT \approx by_h$, where $b = 2\sqrt{2\pi}/\Gamma(1/4)^2 \sim 0.38$.

We show in Figure 4.7 the real part of the potential $\mathrm{Re}\, V_{Q\bar{Q}}/T$ computed in an analogous fashion (using only the allowed interval $0 < y_h < y_{h,max}$), along with the vacuum result (4.49) and the $LT \ll 1$ approximation (4.56). One can see that the vacuum contribution is very close to the thermal one. Also, the $LT \ll 1$ approximation is excellent for all values of LT in the allowed interval.

Estimating the Debye mass

We now shall describe a way to estimate the Debye screening mass m_D directly from the real part of the heavy quark potential. This approach is simple and driven primarily by phenomenological reasons. Yet, it provides results qualitatively similar to more refined estimates involving, for example, the lightest CT-odd supergravity mode [184], as we will explore with more detail in Chapter 6.

One may define the Debye mass $m_D(T)$ as the screening mass in the $Q\bar{Q}$ potential of

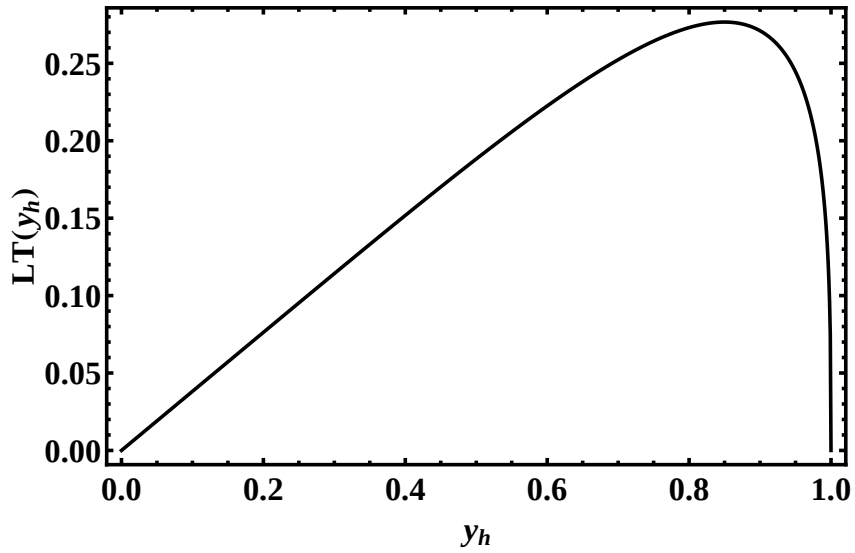

Figure 4.6: *LT as a function of y_h for the case of $\mathcal{N} = 4$ SYM at strong coupling. For $y_h > y_{h,max} \sim 0.85$ the solution of the classical Nambu-Goto action is not the dominant configuration and other connected configurations must also be taken into account [184].*

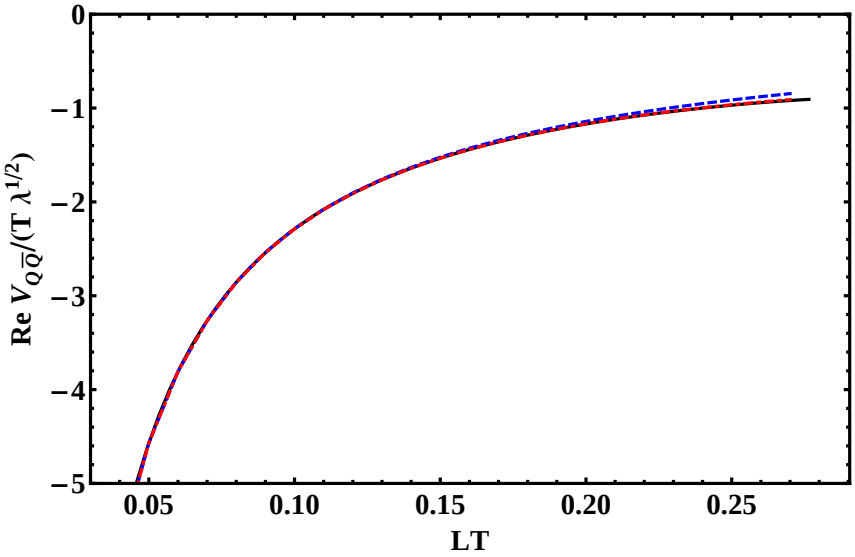

Figure 4.7: *The potential $\mathrm{Re}\, V_{Q\bar{Q}}/T$ for strongly coupled $\mathcal{N} = 4$ SYM (normalized by the 't Hooft coupling $\sqrt{\lambda}$) as a function of LT, considering the exact solution given by (4.54) and (4.55) (solid black curve), the approximation (4.56) valid for $LT \ll 1$ (dotted-dashed red curve), and the vacuum limit given by Eq. (4.49) (dashed blue curve).*

the Karsch-Merh-Satz (KMS) model [199]

$$\frac{\mathrm{Re}\, V_{Q\bar{Q}}(L,T)}{\sqrt{\lambda}} = -\tilde{C}_1 \frac{e^{-m_D(T)L}}{L} + \frac{\sigma}{m_D}\left(1 - e^{-m_D(T)L}\right) + \tilde{C}_2, \tag{4.58}$$

where $\tilde{C}_1$ is a Coulomb coupling constant, $\tilde{C}_2$ is a constant that appears due to the regularization procedure, and σ is the string tension (normalized by $\sqrt{\lambda}$). The model (4.58) describes, for $m_D \sim 0$, a Cornell-like potential and, for $\sigma \to 0$ but $m_D \neq 0$, a Debye screened Coulomb potential. For nonzero m_D and σ the result interpolates between both limits. For a conformal field theory, such as $\mathcal{N} = 4$ SYM, we must take $\sigma = 0$. Also, we know that in such theories $\mathrm{Re}\, V_{Q\bar{Q}}/T$ can only depend on LT. With this in mind, we write Eq. (4.58) in the form

$$\frac{\mathrm{Re}\, V_{Q\bar{Q}}}{\sqrt{\lambda}T} = -\tilde{C}_1 \frac{e^{-\frac{m_D}{T}(LT)}}{(LT)^{\delta}} + \tilde{C}_2, \tag{4.59}$$

where m_D/T must be a temperature independent constant in a conformal plasma and δ is an adjustable parameter. A similar function has been used to fit lattice data for the potential (see the review in [166]).

In the following we will use Eq. (4.59) to obtain an estimate for m_D through a fit to the numerical results for $\mathrm{Re}\, V_{Q\bar{Q}}/T$ as a function LT. However, we must stress that this is only a very rough estimate. First, Eq. (4.58) is only a phenomenological model for the effect of Debye screening in non-Abelian gauge theories. Second, and most importantly, the solution (4.54) and (4.55) imply that $\mathrm{Re}\, V_{Q\bar{Q}}/T$ computed using the classical string does not show exponential screening. This can be easily seen using a property of the derivative of the hypergeometric function (as discussed in Appendix D, Section D.2). Nevertheless, this is a very simple way to estimate m_D and moreover Eq. (4.59) provides a reasonable description of $\mathrm{Re}\, V_{Q\bar{Q}}/T$.

The numerical procedure is to fit Eq. (4.59) to the exact result given by Eqs. (4.54) and (4.55) using $\tilde{C}_1$, δ, and m_D as fitting parameters ($\tilde{C}_2 = -1$ is fixed by our regularization procedure). We obtain

$$m_D/T = 11.92 \qquad \tilde{C}_1 = 0.72\,, \qquad \delta = 0.74\,. \tag{4.60}$$

The exact result and the fitted function are shown in Figure 4.8. As a comparison, the calculation of the screening mass using the lightest CT-odd mode of type IIB supergravity gives $m_D/T = 10.694$ [184].

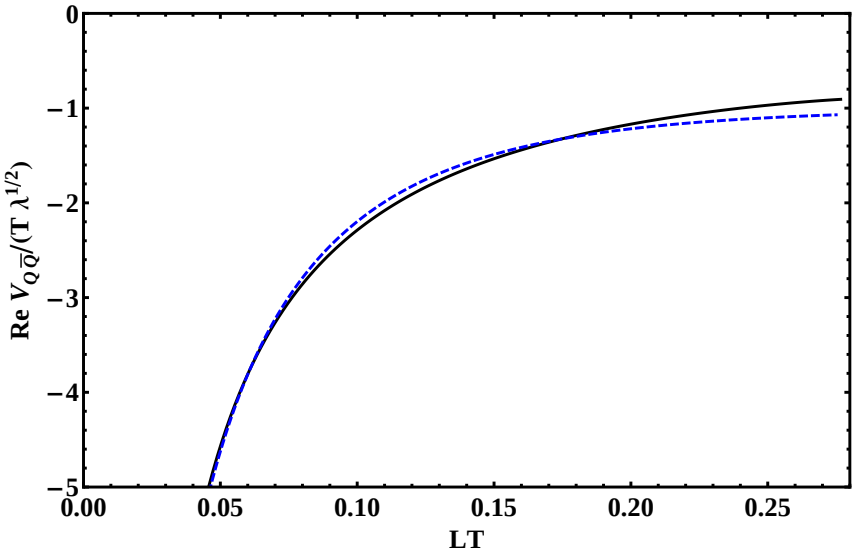

Figure 4.8: *A comparison of the exact result for* $\mathrm{Re}\, V_{Q\bar{Q}}/T$ *(solid black curve) and the fitted function* (6.134) *(dashed blue curve) for strongly coupled* $\mathcal{N} = 4$ *SYM.*

Imaginary part of the heavy quark potential in $\mathcal{N} = 4$ SYM

From the general formula in Eq. (4.36) we obtain

$$\frac{\mathrm{Im}\, V_{Q\bar{Q}}}{T} = -\frac{\pi\sqrt{\lambda}}{24\sqrt{2}}\frac{3y_h^4 - 1}{y_h}. \tag{4.61}$$

The condition $\mathrm{Im}\, V_{Q\bar{Q}} < 0$ implies $y_h > y_{h,min} = 3^{-1/4} \approx 0.760$. This translates into $LT > LT_{min} = 0.266$. For $LT < LT_{min}$, $\mathrm{Im}\, V_{Q\bar{Q}} = 0$. As before, we can trust this solution only if $y_h < y_{h,max}$. For $y_h > y_{h,max}$ we should consider other connected contributions and the formalism developed above to determine $\mathrm{Im}\, V_{Q\bar{Q}}$ is not valid. It should also be noted that $\mathrm{Im}\, V_{Q\bar{Q}}/T$ depends only on LT (via y_h), as expected to occur in a conformal plasma.

One can now use Eqs. (4.52) and (4.61) to determine the behavior of $\mathrm{Im}\, V_{Q\bar{Q}}/T$ as a function of LT. This is shown in Figure 4.9 considering only $LT < LT_{max}$. We also show the result obtained using the approximation $LT \approx by_h$, which ignores the fact that we should trust Eq. (4.61) only for $y_h < y_{h,max}$ (in this case the root of Eq. (4.61) is shifted to the right).

From Figure 4.9 we conclude that we are only able to reliably calculate $\mathrm{Im}\, V_{Q\bar{Q}}$ using Eq. (4.61) in a small range of LT. The approximation $by_h \sim LT$ is poor for two reasons. First, it is being used in a region of y_h near $y_{h,max}$. Second, the extrapolation performed in the region $y_h > y_{h,max}$ is done beyond the trusted region for y_h. Nevertheless, the linear behavior of $\mathrm{Im}\, V_{Q\bar{Q}}$ seen in Figure 4.9 agrees, qualitatively, with other calculations for $\mathrm{Im}\, V_{Q\bar{Q}}$ [190–192].

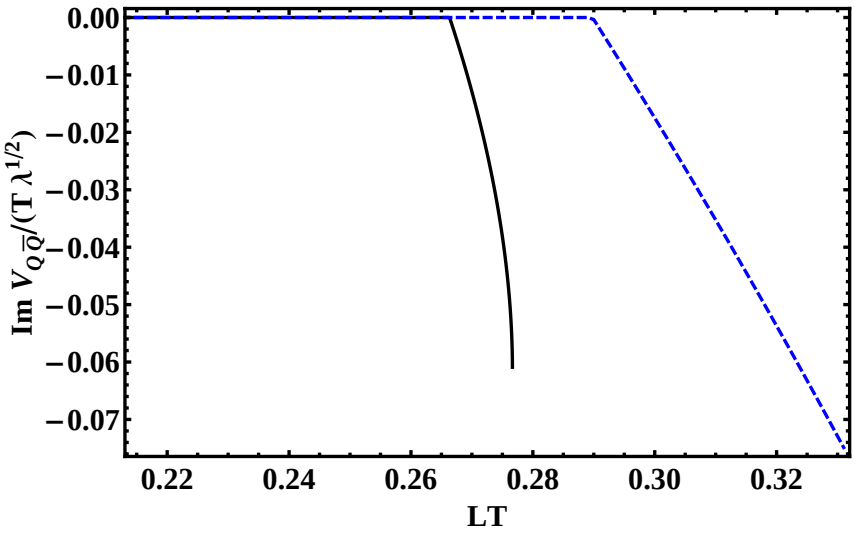

Figure 4.9: *The imaginary part of* $\mathrm{Im}\, V_{Q\bar{Q}}/T$ *as a function of* LT*. The solid black curve is the result using Eq. (4.52) to eliminate* y_h*, considering only* $LT < LT_{max}$*. The dashed blue curve is obtained using the approximation by* $y_h \sim LT$*, which ignores the fact that one should not trust Eq. (4.61) when* $LT > LT_{max}$*. Using this approximation, the root of Eq. (4.61) is shifted to the right.*

Estimating $\Gamma_{Q\bar{Q}}$ for the $\Upsilon(1S)$ state in a strongly coupled $\mathcal{N} = 4$ SYM plasma

We may rewrite the estimate (4.41) in a dimensionless form

$$\frac{\Gamma_{Q\bar{Q}}}{T} = -\frac{4}{(Ta_0)^3}\int_0^\infty dw\, e^{-\frac{2w}{Ta_0}} w^2 \frac{\mathrm{Im}\, V_{Q\bar{Q}}}{T}(w), \tag{4.62}$$

where $w = LT$. In the case of $\mathcal{N} = 4$ SYM, since $\mathrm{Im}\, V_{Q\bar{Q}}/T$ is only a function of $w = LT$ the only dependence of $\Gamma_{Q\bar{Q}}/T$ on the temperature is via the weight factor $\rho(w) = \exp(-2w/Ta_0)w^2$. The position of the "strip" in Figure 4.9 is independent of Ta_0. Note that as we increase (decrease) T, $\rho(w)$ shifts to the right (left, respectively) (see Figure 4.10).

We will adopt two approaches to estimate the thermal width. The first one consists of using only the "strip" in Figure 4.9 - this means that we will neglect the region $LT > LT_{\max}$ where our framework does not provide $\mathrm{Im}\, V_{Q\bar{Q}}$. We call this the "conservative" approach. The second one consists in using the approximation $LT \sim by_h$ in Eq. (4.61), ignoring the fact that for $LT \sim LT_{max}$ this approximation ceases to be valid - this will be called the "extrapolation".[11]

[11] The authors of [179] used this second approximation. However, the fact that we must impose $\mathrm{Im}\, V_{Q\bar{Q}} < 0$ was not considered - the expression (4.61) was used (for a fixed T) from $L = 0$ to $L \to \infty$ instead from L_{min} to L_{max}. Excluding from the integration the region $0 < L < L_{min}$ we obtain that the estimate of $\Gamma_{\Upsilon(1S)}$ in [179] is increased from 48 MeV to 165 MeV.

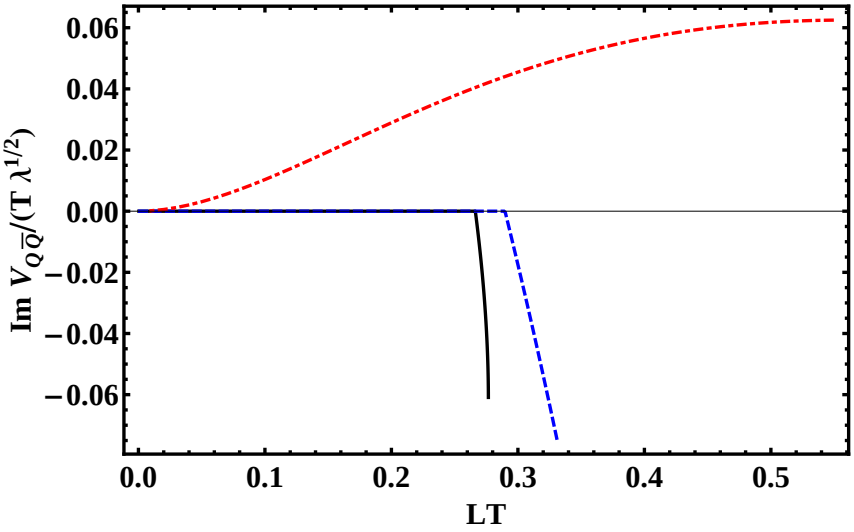

Figure 4.10: *As in Figure 4.9 but plotted against the Coulomb ground-state wavefunction (dash-dotted curve) for $T = 0.3$ GeV. The wave function has no particular scale on the vertical axis - it was conveniently normalized to fit the plot.*

In Figure 4.11 we show $\Gamma_{Q\bar{Q}}/T$ for the $\Upsilon(1S)$ state as a function of Ta_0 for $\lambda = 9$. We see that the conservative approach gives a thermal width that can be three orders of magnitude smaller than that computed using the extrapolation. For $a_0 \sim 0.6\,\mathrm{GeV}^{-1}$, $T \sim 0.5\,\mathrm{GeV}$, the thermal width varies from 0.5 MeV to 1.5 GeV between the conservative approach and the extrapolation. Therefore, the extrapolation considerably overestimates the thermal width while the conservative approach only gives a lower bound for this quantity.

The result for the conservative approach, shown in more detail in Figure 4.12, can be understood qualitatively as follows: the weight factor $\rho(w)$ samples only the small region of LT in which $\mathrm{Im}\,V_{Q\bar{Q}} \neq 0$. As one increases the temperature, $\rho(w)$ shifts to the right. For $LT_{min,max} \sim Ta_0$ the overlap between $\rho(w)$ and $\mathrm{Im}\,V_{Q\bar{Q}} \neq 0$ happens at the maximum of $\rho(w)$ at $w = Ta_0$ - this corresponds to the maximum in Figure 4.11. By increasing T even further, the overlap occurs before the maximum of $\rho(w)$ and $\Gamma_{Q\bar{Q}}$ decreases. The temperature dependence of $\Gamma_{Q\bar{Q}}/T$ found in this case is qualitatively similar to that found in recent lattice calculations [200].

4.5.3 A model for QCD_3

If we start from $\mathcal{N} = 4$ SYM and take $T \to \infty$, then the compactification radius $\beta = 1/T$ of the Euclidean time coordinate goes to 0. As already remarked in Section 3.9, the fermionic degrees of freedom of $\mathcal{N} = 4$ SYM become massive in the limit $\beta \to 0$, because of the anti-periodic boundary conditions in the compactified time. Moreover, the

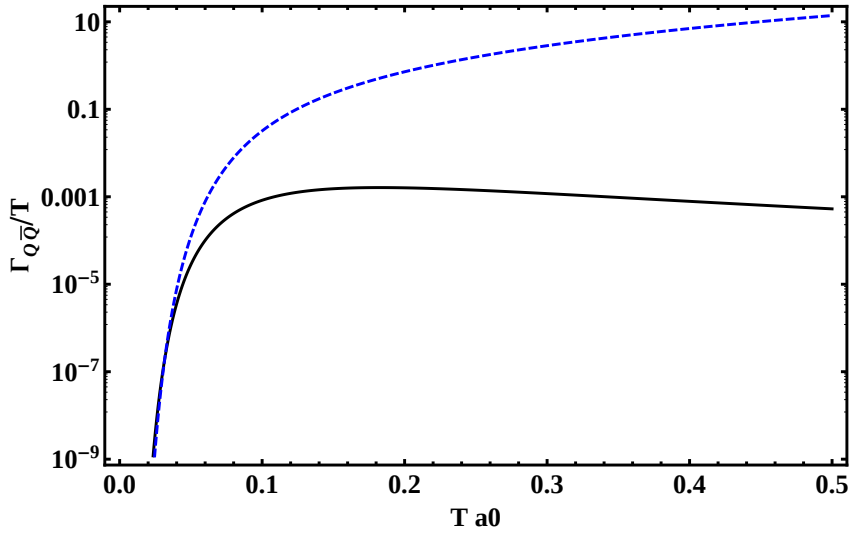

Figure 4.11: *The thermal width $\Gamma_{Q\bar{Q}}$ of the $\Upsilon(1S)$ state in $\mathcal{N}=4$ SYM divided by the temperature T as a function of Ta_0 in a logarithmic scale (the t'Hooft coupling is $\lambda = 9$). The solid black curve corresponds to the conservative approach and the dashed blue curve is the extrapolation explained in the text.*

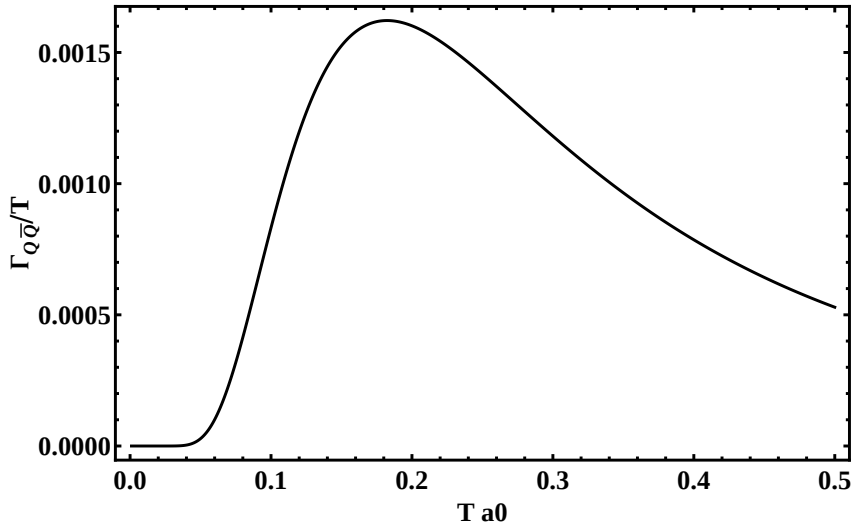

Figure 4.12: *The same as in Figure 4.11 but this time the result for the conservative approach is shown in detail.*

scalar fields decouple at one-loop. Therefore, all supersymmetry is broken and only the gauge fields remain - in the end we go from thermal $\mathcal{N}=4$ SYM with SU(N) gauge group in (3+1) dimensions to a SU(N) gauge theory in 3 dimensions at zero temperature.[12]

The calculation of $V_{Q\bar{Q}}$ for this model proceeds as before. In the metric (4.42) we drop the first Euclidean time coordinate; one of the remaining spatial coordinates is then assigned to be the Euclidean time. We have then $V(U)=U^4/R^4$ and $M(U)=1/f(U)$. The function M diverges at U_h - this means that the dual gauge theory confines. The string tension is then

$$\sigma=\frac{U_h^2}{2\pi\alpha' R^2}=\frac{\pi\sqrt{\lambda}T^2}{2}, \tag{4.63}$$

where λ is the 4 dimensional 't Hooft coupling constant.

The exact formulas for L and $V_{Q\bar{Q}}$ are evaluated following the procedure of the previous sections. One obtains

$$\frac{L}{2}=\frac{2\sqrt{2\pi}\pi}{\Gamma(1/4)^2}\frac{R^2}{U_*}\,{}_2F_1\left[\frac{1}{2},\frac{3}{4};\frac{5}{4};y_h^4\right] \quad \text{and} \tag{4.64}$$

$$F_{Q\bar{Q}}=-\frac{U_*}{\alpha'}\frac{\sqrt{2\pi}}{\Gamma(1/4)^2}\,{}_2F_1\left[\frac{1}{2},-\frac{1}{4};\frac{1}{4};y_h^4\right]. \tag{4.65}$$

The expression (4.64) for L has the same functional form of Eq. (4.54), minus the factor $\sqrt{1-y_h^4}$. This factor is responsible for deconfinement - it controls the divergence of the hypergeometric function at $y_h=1$ ($U_*=U_h$) and gives the mountain shaped form of Figure 4.6. Without it, L diverges for $y_h\to 1$, as expected from a confining gravity dual. A second consequence of Eqs.(4.64) and (4.65) is that the short-range behavior is the same of $\mathcal{N}=4$ SYM.

This example also gives a (very) tentative argument that $\mathrm{Im}\,F_{Q\bar{Q}}(LT\to\infty)\to 0$ for $\mathcal{N}=4$ SYM. Since this is a vaccuum gauge theory, V cannot have an imaginary part. This can be checked explicitly using Eq.(4.36). Since this is the high temperature limit of thermal $\mathcal{N}=4$ SYM, then we must have $\mathrm{Im}\,F_{Q\bar{Q}}(LT\to\infty)\to 0$.

4.5.4 Gauss-Bonnet gravity

Action and metric

We now consider a class of bulk theories that includes curvature squared corrections to the supergravity action for which the conjectured viscosity bound $\eta/s\geq 1/4\pi$ [90] can

[12] In Chapter 6 we will analyze this dimensional reduction of a (3+1) gauge theory at finite temperature to a 3 dimensional gauge theory at zero temperature in more detail.

be violated. The action for these models, called Gauss-Bonnet gravity [194–196], is

$$S = \frac{1}{16\pi G_5}\int d^5x\sqrt{-g}\left[\left(\mathcal{R}+\frac{12}{R^2}\right)+ \right. \\ \left. +\frac{\lambda_{GB}}{2}R^2\left(\mathcal{R}^2-4\mathcal{R}_{\mu\nu}\mathcal{R}^{\mu\nu}+\mathcal{R}_{\mu\nu\rho\sigma}\mathcal{R}^{\mu\nu\rho\sigma}\right)\right], \tag{4.66}$$

where G_5 is the five dimensional Newton constant, $\mathcal{R}_{\mu\nu\rho\sigma}$ is the Riemann tensor, $\mathcal{R}_{\mu\nu}$ is the Ricci tensor, $\mathcal{R}$ is the Ricci scalar, and λ_{GB} is a constant. The first parenthesis is the usual Einstein-Hilbert + cosmological constant action. The second parenthesis gives the curvature squared corrections. For this particular choice of curvature squared corrections, metric fluctuations in a given background have the same quadratic terms as Einstein gravity. The action (4.66) has an exact black-brane solution [146] given by

$$ds^2 = -a^2 f_{GB}(U)dt^2 + \frac{U^2}{R^2}d\vec{x}^2 + \frac{dU^2}{f_{GB}(U)}, \tag{4.67}$$

where

$$a^2 = \frac{1}{2}\left(1+\sqrt{1-4\lambda_{GB}}\right) \quad \text{and} \tag{4.68}$$

$$f_{GB}(U) = \frac{U^2}{R^2}\frac{1}{2\lambda_{GB}}\left[1-\sqrt{1-4\lambda_{GB}\left(1-\frac{U_h^4}{U^4}\right)}\right]. \tag{4.69}$$

The black brane horizon is the simple root of $f_{GB}(U)$, U_h. The plasma temperature is $T = aU_h/(\pi R^2)$. From Eq. (4.67) we see that the AdS radius is given by aR instead of just R. In particular, the 't Hooft coupling of the dual strongly coupled CFT is given by $\lambda = a^4R^4/\alpha'$. The functional form of a and f_{GB} implies that $\lambda_{GB} < 1/4$. However, in practice $\lambda_{GB} \leq 9/100$ to avoid causality violation at the boundary [91, 92].

The constant λ_{GB} is related to the ratio of the shear viscosity η and the entropy density s by [91, 92, 147]

$$\frac{\eta}{s} = \frac{1}{4\pi}(1-4\lambda_{GB}). \tag{4.70}$$

For $\lambda_{GB} > 0$ the viscosity bound for gauge theories with gravity duals, $\eta/s > 1/4\pi$, is violated. The constraint $\lambda_{GB} \leq 9/100$ implies that $\frac{4\pi\eta}{s} \geq 16/25$.

The evaluation of the real part of the heavy quark potential in the strongly coupled plasma dual to Gauss-Bonnet gravity (4.67) was already performed in [201] (see also [202, 203]). In this Section we extend the analysis of [201] to include the numerical evaluation of $\mathrm{Re}\, V_{Q\bar{Q}}$ and also the calculation of the imaginary part of the potential using the worldsheet fluctuation method. Moreover, we give an estimate of the dependence of the Debye screening mass in this theory as a function of η/s.

Polyakov loop and the real part of the heavy quark potential

Using Eqs. (4.12), (4.15), and (4.16) one obtains for the regularized heavy quark free energy

$$\frac{F_Q}{T} = -\frac{R^2}{2\alpha'} = -\frac{\sqrt{\lambda}}{2a^2} \tag{4.71}$$

while

$$LT(y_h) = \frac{2a}{\pi} y_h \sqrt{2\bar{f}_{GB}(1,y_h)\lambda_{GB}} \int_1^\infty \left[y^8 \bar{f}_{GB}(1,y_h)^2 - y^4 \bar{f}_{GB}(y,y_h)\bar{f}_{GB}(1,y_h)\right]^{-1/2} \tag{4.72}$$

and the real part of the heavy quark potential is given by

$$\frac{\mathrm{Re}\, V_{Q\bar{Q}}}{T} = \frac{R^2}{\alpha'}\frac{1}{y_h}\left\{\int_1^\infty dy \left[\left(1 + \frac{1}{\frac{y^4 \bar{f}_{GB}(y,y_h)}{\bar{f}_{GB}(1,y_h)}}\right)^{1/2} - 1\right] - 1\right\} \tag{4.73}$$

where $\bar{f}_{GB}(y,y_h)$ is a reduced form of $f_{GB}(U)$ defined by

$$\bar{f}_{GB}(y,y_h) = 1 - \sqrt{1 - 4\lambda_{GB}\left(1 - \frac{y_h^4}{y^4}\right)}. \tag{4.74}$$

For $\lambda_{GB} \neq 0$, both Eqs. (4.72) and (4.73) cannot be evaluated in terms of hypergeometric functions. In the limit $LT \ll 1$ one can show [201] that

$$\frac{\mathrm{Re}\, V_{Q\bar{Q}}}{T} = -\frac{4\pi^2\sqrt{\lambda}}{\Gamma(1/4)^4 LT}\left(1 + \frac{c}{a^6\sqrt{1-4\lambda_{GB}}}(LT)^4\right), \tag{4.75}$$

where c is the constant given by Eq. (4.57)[13].

We can also evaluate Eqs. (4.72) and (4.73) numerically by fixing λ_{GB} and using y_h as a parameter. In Figure 4.13 we show LT as a function of y_h for $\lambda_{GB} = 0$ ($4\pi\eta/s = 1$) and $\lambda_{GB} = -0.25$ ($4\pi\eta/s = 2$). We see that increasing λ_{GB} (decreasing η/s) lowers $y_{h,max}$ and LT_{max}. However, as shown in Figure 4.14, the behavior of $\mathrm{Re}\, V_{Q\bar{Q}}$ as a function of LT does not change significantly with λ_{GB}. Moreover, one sees that the approximation in Eq. (4.75) is excellent for the values of λ_{GB} considered here. In the end, the main effect of increasing λ_{GB} is to reduce the allowed interval for LT.

[13] In Ref. [201] this corresponds to Eq. (34), which can be obtained after some manipulations involving gamma functions. Here we have not performed the entropy subtraction done in Ref. [201] to obtain their Eq. (35).

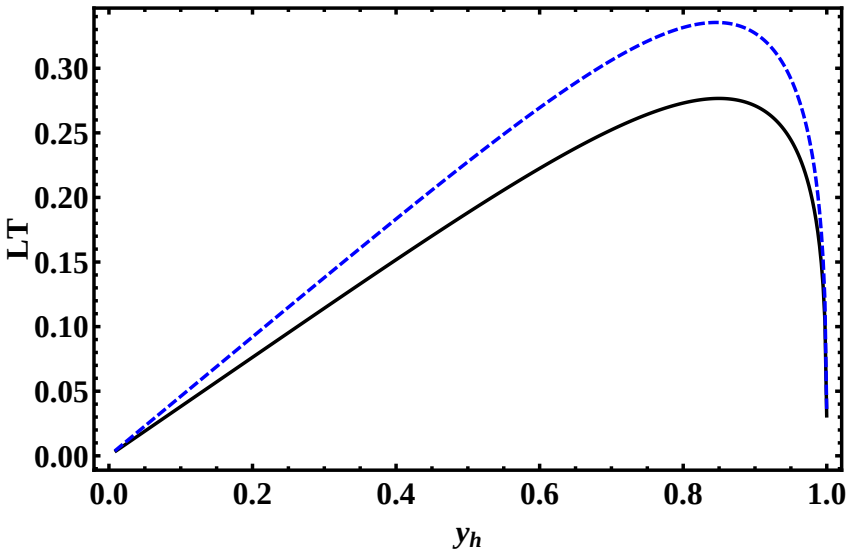

Figure 4.13: *LT as a function of y_h in the CFT dual to Gauss-Bonnet gravity. The solid black curve is the result for $\lambda_{GB} = 0$ ($4\pi\eta/s = 1$); the dashed blue curve is the result for $\lambda_{GB} = -0.25$ ($4\pi\eta/s = 2$).*

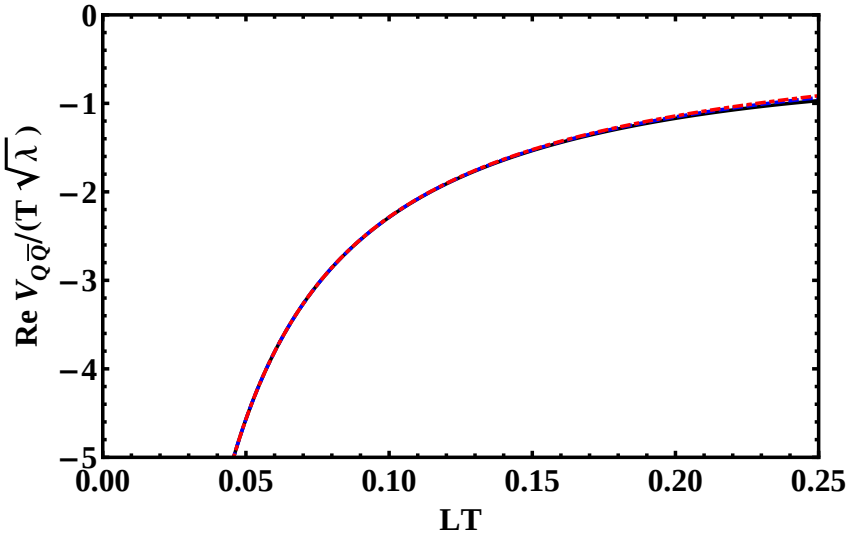

Figure 4.14: $\mathrm{Re}\, V_{Q\bar{Q}}/T$ *as a function of LT in the CFT dual to Gauss-Bonnet gravity. The solid black curve is the result for $\lambda_{GB} = 0$ ($4\pi\eta/s = 1$); the dotted-dashed red curve is the result for $\lambda_{GB} = -0.25$ ($4\pi\eta/s = 2$); the dotted blue curve corresponds to the approximation in Eq.* (4.75).

Estimate of the Debye mass and its dependence on η/s

Using the simple fitting procedure described in section 4.5.2 we can obtain a simple estimate for the Debye screening mass in GB gravity and its dependence with η/s. We use, as before, the model (4.59) (with $\sigma = 0$). Since we do not have exact expressions for LT and $\mathrm{Re}\, V_{Q\bar{Q}}/T$ in this case, we cannot prove whether the real part of the potential computed using the classical string shows exponential Debye screening or not. In any case, the cautionary remarks previously made for $\mathcal{N} = 4$ SYM are still applicable here and must be kept in mind.

The fitting procedure is done as before for the case of SYM. Varying the values of λ_{GB} (therefore, η/s) we obtain the results for m_D shown in Figure 4.15 (the parameters δ and $\tilde{C}_1$ do not vary appreciably with respect to those found in the SYM calculation). Here we consider both positive λ_{GB} (corresponding to $4\pi\eta/s < 1$) and negative λ_{GB} ($4\pi\eta/s > 1$). In Figure 4.15, the shaded region denotes the result for m_D computed using values of λ_{GB} that lead to problems with causality. One can see that m_D decreases with increasing η/s for the allowed values of λ_{GB}. This result is reasonable since larger η/s in general means weaker coupling, which in turns implies that heavy quark pairs are less screened by the medium.

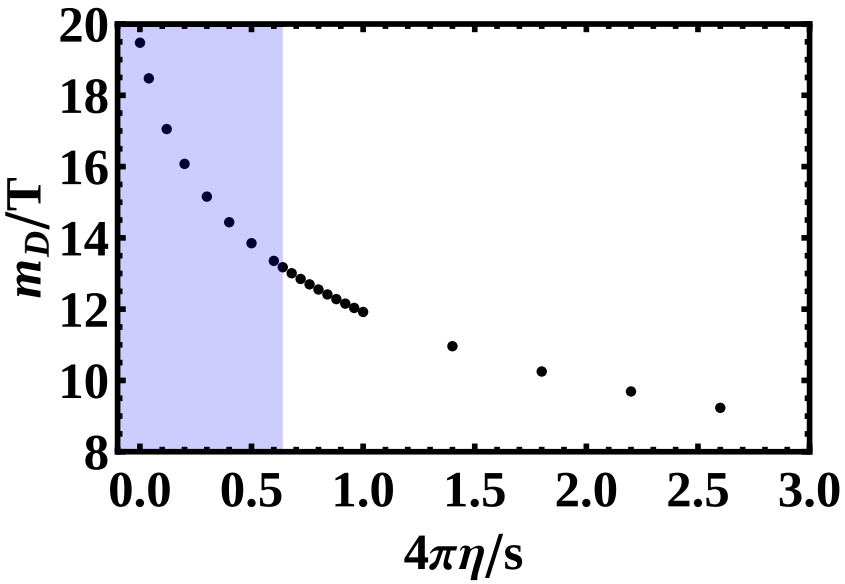

Figure 4.15: *An estimate for the Debye screening mass m_D as a function of $4\pi\eta/s$ in the strongly coupled conformal plasma dual to Gauss-Bonnet gravity. The shaded blue region can be excluded since m_D in this region was determined using values of λ_{GB} that lead to problems with causality.*

Imaginary part of the heavy quark potential in GB gravity

Using Eq. (4.36) we can calculate $\mathrm{Im}\, V_{Q\bar{Q}}$ in this theory and study its dependence on η/s. The full expression, while easy to derive, is rather cumbersome and therefore omitted in the text. However, a simple expansion for $\lambda_{GB} \ll 1$ results in a more useful expression

$$\frac{\mathrm{Im}\, V_{Q\bar{Q}}}{T} = -\frac{\pi\sqrt{\lambda}}{24\sqrt{2}}\frac{1}{y_h}\left[(3y_h^4-1)+\frac{\lambda_{GB}}{3}(9y_h^4-34y_h^8+9y_h^{12})\right]+O(\lambda_{GB}^2). \tag{4.76}$$

For $\lambda_{GB}=0$ we recover the $\mathcal{N}=4$ SYM result (4.61). As before, enforcing $\mathrm{Im}\, V_{Q\bar{Q}}<0$ gives a lower limit for y_h while the condition regarding the validity of the classical string calculations gives a maximum value of y_h (Figure 4.13). In Figure 4.16 we show the numerical results for $\mathrm{Im}\, V_{Q\bar{Q}}/T$ for $\lambda_{GB}=-0.25$. Only a small interval of LT is allowed in the conservative approach and increasing λ_{GB} shifts this interval to the left. We also see that Eq. (4.76) is a satisfactory approximation to the numerical result for $\lambda_{GB}=-0.25$.

4.5.5 Thermal width of $\Upsilon(1S)$ and its dependence on η/s

In Figure 4.17 we present a lower bound for the thermal width $\Gamma_{Q\bar{Q}}$ of the $\Upsilon(1S)$ state as a function of η/s for $\lambda=9$ and $T\sim 300\,\mathrm{MeV}$. Since changing η/s changes the sampling region for L, we have again that the shape of Figure 4.17 reproduces the shape of the associated ground-state Coulomb wave function. The shaded blue region denotes the values of the width computed using values of λ_{GB} that lead to causality violations in the gauge theory. Note that the thermal width, normalized by the value found in strongly coupled SYM, decreases with increasing η/s.

4.6 Discussion and Conclusions of This Chapter

In this Chapter we used the gauge/gravity duality to study the imaginary part of the heavy quark potential in strongly coupled plasmas. This imaginary part can be used to estimate the thermal width of heavy quarkonia in strongly coupled plasmas, which may be seen as the strongly coupled analog of the Landau damping induced thermal width found in perturbative QCD calculations [167–169]. The thermal worldsheet fluctuation method, originally developed in Ref. [179], was used here to obtain a lower bound for the thermal width of heavy quarkonium states, such as the $\Upsilon(1S)$, in 2 different holographic toy models of the strongly coupled quark-gluon plasma (QGP): strongly coupled $\mathcal{N}=4$ SYM at large N_c and the strongly coupled CFT dual to GB gravity. Moreover, we proved a general result using the thermal worldsheet fluctuation approach that establishes the connection between the imaginary part of the heavy quark potential at nonzero temperature and the

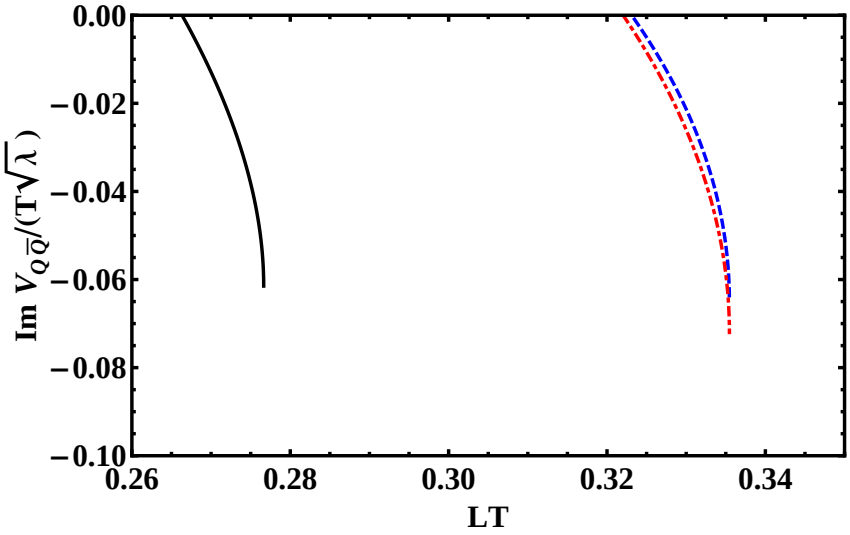

Figure 4.16: $\mathrm{Im}\, V_{Q\bar{Q}}/T$ *as a function of* LT *in the CFT dual to Gauss-Bonnet gravity. The full black curve is the result for* $\lambda_{GB} = 0$*; the dashed blue curve is the result for* $\lambda_{GB} = -0.25$*; and the dashed-dotted red curve corresponds to the approximation in Eq.* (4.76).

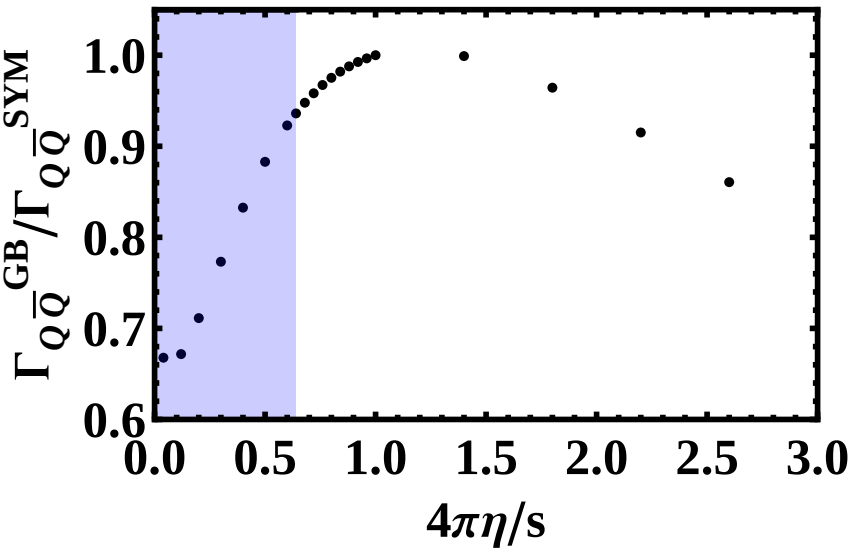

Figure 4.17: *Lower bound for* $\Upsilon(1S)$ *thermal width* $\Gamma_{Q\bar{Q}}$ *computed via Gauss-Bonnet gravity, normalized by the* $\mathcal{N} = 4$ *SYM result. We used the gauge theory coupling* $\lambda = 9$ *and* $T = 300\,\mathrm{MeV}$*. The shaded blue region denotes the values of the width computed using values of* λ_{GB} *that lead to causality violations in the gauge theory.*

area law of the Wilson loop at zero temperature.

In the case of strongly coupled SYM we found that the thermal width of $\Upsilon(1S)$ is actually very small in comparison to the plasma temperature for reasonable (and large) values of the t'Hooft coupling. The estimates previously made for this quantity in Ref. [179] have been improved in the calculations done in this Chapter and the nontrivial consistency conditions, discussed at length in this manuscript, have conspired to bring down the previous value of the thermal width to values that may be consistent with recent phenomenological models for the quenching of heavy quarkonia in the QGP [212, 213]. It would be interesting to use the imaginary contribution to the heavy quark potential found here to study other quarkonium states [214].

Moreover, even though the real part of the heavy quark potential (computed with the classical string approximation) does not show explicit exponential screening in a strongly coupled $\mathcal{N} = 4$ SYM plasma, a simple phenomenological estimate for the Debye screening mass can still be extracted via a fit to the real part of the heavy quark potential. Surprisingly enough, this rough estimate for the Debye screening mass is still in fair agreement (within $\sim 11\%$) with the result obtained using the lightest CT-odd supergravity mode [184] (see also Chapter 6, where we present a more careful definition of the Debye mass and present details of these holographic calculations).

We remark that in our estimate for the imaginary part of the heavy quark potential in $\mathcal{N} = 4$ SYM is proportional to T^2, which was also obtained in other non-perturbative calculations such as the holographic computations based on complexified worldsheet coordinates [190] or the calculation performed using particular choices of worldsheet configurations in Ref. [192]. This behavior is in stark contrast with the T scaling of the imaginary part found in pQCD calculations [167–169]. In Ref. [207], the thermal width of mesons in $\mathcal{N} = 4$ SYM was computed within the D7 flavor brane setup and, in this calculation, a nonzero thermal width for mesons arises from worldsheet instantons being exchanged between the tip of the D7-brane and the black hole horizon. This method can be used to understand the momentum dependence of this instanton-induced thermal width of a meson that is moving relative to the thermal bath. In our method, the nontrivial D-brane dynamics associated with the inclusion of fundamental flavor is not included. Therefore, the $1/\sqrt{\lambda}$ effects found in Ref. [207] cannot appear in our approach. Rather, our calculation of the width is to be interpreted as an estimate for this quantity in the limit where the mass of the quarks is very large (static meson approximation), in the same spirit of Refs. [190–192].

We also computed the thermal width of heavy quarkonia in the CFT dual to GB gravity to study its dependence with η/s. For a fixed temperature of $T = 0.3$ GeV the width has a maximum around $\eta/s = 1/4\pi$ and decreases for larger values of η/s. Following the

phenomenological procedure to extract the Debye mass from the real part of the potential described above, we obtained an estimate for the dependence of m_D with η/s in this gravity model. Our results suggest that Debye screening effects decrease with increasing η/s in a strongly coupled plasma.

In this Chapter we assumed that the plasma is isotropic and conformal[14] and that the $Q\bar{Q}$ pair is at rest with respect to the thermal bath. It would be interesting to generalize the calculations for the imaginary part of the heavy quark potential performed here by considering gravity models dual to plasmas where these conditions are dropped. For instance, one could compute the thermal width in an anisotropic strongly coupled plasma [148,208] or in non-conformal gravity models of the QGP such as of Refs. [15,209].

The results of this Chapter were published in Ref. [18]. For more examples of the computation using this method, see Refs. [210, 211] where the imaginary part of the heavy quark potential was computed in a strongly coupled anisotropic plasma using the method described here.

[14]Simple non-conformal models and the respective results for the imaginary part of the potential can be found in Appendix D, Section D.3.

Chapter 5

Thermal suppression of moving heavy quark pairs in strongly coupled plasma

5.1 Introduction

In heavy ion collisions, useful probes to studying the formation and evolution of the QGP [5] are the heavy quarkonia (J/ψ and Υ mainly) formed in hard processes before the thermalization of the plasma. The seminal work of Matsui and Satz [199] argued that, in a thermal bath, the binding interaction of the heavy quark-antiquark ($Q\bar{Q}$)pair is screened by the medium, resulting in the melting of the heavy quarkonia. However, the $Q\bar{Q}$ pair is not necessarily produced at rest in the QGP and the effects of its motion through the plasma must taken into account when considering the effects of the medium in the $Q\bar{Q}$ interaction.

As shown in the previous Chapter, the interaction energy $V_{Q\bar{Q}}(L,T)$ may possess, at finite temperature, a nonzero imaginary part, which can be used to estimate a thermal width of the quarkonium. Calculations of $\mathrm{Im}V_{Q\bar{Q}}(L,T)$ relevant to QCD and heavy ion collisions were performed for static $Q\bar{Q}$ pairs using, for instance, perturbative QCD (pQCD) [167, 168], lattice QCD [178, 200, 216] and using the gauge/gravity duality [18, 179, 191, 192, 211, 217] (for recent studies about quantum decoherence effects in quarkonia see [176, 177]). However, all of these calculations of $\mathrm{Im}V_{Q\bar{Q}}(L,T)$ in the literature were performed considering static $Q\bar{Q}$ pairs. To accurately determine the suppression of quarkonia formed in heavy ion collisions it is necessary to evaluate $\mathrm{Im}V_{Q\bar{Q}}(L,T)$ for moving quarkonia in the QGP [212–215]. In Ref. [218], it was shown using effective theory techniques that in a weakly coupled QGP the heavy quarkonia decay width is a nontrivial function of the temperature and velocity. However, for the two different scenarios considered in Ref. [218] involving the different scales in the problem, it was found that the decay width of very rapidly moving quarkonia decreases with the pair's velocity.

From the viewpoint of holography and the gauge/gravity duality [14,94,126], the evaluation of $\langle W(C)\rangle$ (and thus of $V_{Q\bar{Q}}(L,T)$) in the large N_c strongly coupled 4-dimensional gauge theory corresponds to, in the 5-dimensional bulk geometry perspective of the gravity dual, the problem of finding a classical string configuration that has the closed loop C as the boundary of the string worldsheet in the bulk [180, 181], as shown in Chapter 4. Holographic calculations of the real part of $V_{Q\bar{Q}}(L,T)$ in strongly coupled plasmas, for moving $Q\bar{Q}$ pairs, were already considered by Liu et al. [219,220] in the case of a strongly coupled $\mathcal{N}=4$ SYM plasma. The computation of $\mathrm{Re}\, V_{Q\bar{Q}}(L,T)$ for moving $Q\bar{Q}$ in more general backgrounds dual to strongly coupled QFTs were studied in Ref. [221].

In Ref. [207], the momentum dependence of meson widths was computed within the gauge/gravity duality and it was shown that this quantity receives nontrivial contributions from instantons on the string worldsheet. An interesting feature of their approach is that the thermal width becomes very large for rapidly moving mesons. Thus, while the general arguments from Refs. [219,220,222] indicate that the dissociation temperature of mesons decreases with the pair's rapidity, the results of Ref. [207] show that even before complete dissociation the imaginary part of rapidly moving mesons may be already large enough to cause suppression of these states in a strongly coupled plasma.

A general approach to determine the imaginary part of the static heavy quark potential using string worldsheet fluctuations was developed in the last Chapter. In this Chapter, we generalize this method to estimate the imaginary part of $V_{Q\bar{Q}}(L,T)$ for moving quarkonia, starting from the evaluation of the real part as done in [219, 220]. The main idea is, following [219, 220], to consider a boost from the frame where the plasma is at rest and the $Q\bar{Q}$ dipole is moving to a frame where the $Q\bar{Q}$ dipole is at rest, while the plasma is moving. The procedure presented in this work can be used for a large class of strongly coupled theories dual to gravity though in this work we focus on its application to strongly coupled $\mathcal{N}=4$ SYM plasma. The method pursued here, however, has limitations. In the static case these limitations (that stem from the saddle point approximation used in the calculation of the imaginary part of the potential) were discussed in detail in the last Chapter and we shall see in this Chapter that similar limitations restrict our discussion here to the case of slowly moving quarkonia (therefore, our results are much more relevant to RHIC collisions than those at the LHC). We note, however, that the overall qualitative behavior found here, i.e., slowly moving quarkonia are less stable than the static case and that $Q\bar{Q}$ pairs are more stable when they are aligned with their velocity axis, is consistent with the findings of [207, 219, 220, 222].

This Chapter is organized as follows: in Section 5.2, we discuss the case where the $Q\bar{Q}$ dipole is moving perpendicularly to the axis that joins the $Q\bar{Q}$ pair - this presents a simpler problem where, in the case of strongly coupled $\mathcal{N}=4$ SYM, some simple analytical

results can be obtained. The case of a general orientation of the $Q\bar{Q}$ pair is a more complex problem that is dealt with in Section 5.3, together with numerical calculations for this quantity in an $\mathcal{N} = 4$ SYM plasma. In Section 5.4 we present our conclusions and outlook.

5.2 Dipole Perpendicular To The Hot Wind

5.2.1 General results - Real part

In this section we evaluate general expressions for the real and imaginary part of potential energy $V_{Q\bar{Q}}$ of quark-antiquark $Q\bar{Q}$ pair moving with the $Q\bar{Q}$ dipole axis oriented perpendicularly to a strongly coupled non-Abelian plasma, using holographic methods. This case is computationally simpler than the case of a dipole with an arbitrary orientation with respect to the wind. In fact, this case can be solved analytically in the case of strongly coupled $\mathcal{N} = 4$ SYM and it represents an extreme case (and check) of the calculations of $V_{Q\bar{Q}}$ for arbitrary orientations of the dipole with respect to the wind. Our calculations for the real part follow the analysis done in [219, 220].

As in the last Chapter, we start by assuming that our $d+1$-dimensional gauge theory in Minkowski space has a gravity dual with the following metric,

$$ds^2 = -G_{00}(U)dt^2 + G_{xx}(U)dx_i^2 + G_{UU}(U)dU^2, \tag{5.1}$$

where $i = 1, 2, ..., d$, x_i are orthornormal spatial coordinates for the boundary and U is the radial coordinate. We will assume that our gravity dual has an asymptotically AdS_5 boundary at $U \to \infty$ and a black brane horizon at $U = U_h$, where we will assume that $G_{UU}(U_h) \to \infty$, with $G_{00}(U_h)G_{UU}(U_h)$ finite. The presence of a black brane (which implies $G_{00} \neq G_{xx}$) breaks the original $SO(d, 1)$ Lorentz isometry of the metric in the transverse spacetime coordinates (t, x_i) to only a rotational $SO(d)$ isometry in the spatial coordinates x_i.

The fact that we do not have the full $SO(d, 1)$ isometry group means that the metric (5.1) is not invariant under rigid Lorentz boosts of the Minkowski spacetime slices we have at each fixed U. This is expected, since the presence of a black brane in the gravity dual is associated with a thermal boundary field theory, and in this case there is a preferred reference frame (namely, the frame where the thermal medium is at rest). Boosting this frame with a velocity $\vec{v}$ means that the an observer in this frame sees the medium moving past him with velocity $-\vec{v}$.

We can exploit this fact to study the effect of the plasma on a $Q\bar{Q}$ pair in the thermal medium. Starting from a reference frame where the plasma is at rest and the $Q\bar{Q}$ dipole is moving with a constant velocity - we can boost to a reference frame where the dipole

is at rest but the plasma is moving past it. This is the main idea used in this calculation. When interpreting the results of our calculations, we will interchange frequently between both points of view.

With these considerations in mind, let us consider a $Q\bar{Q}$ pair moving with rapidity η along the x_d direction with the plasma at rest in this reference frame. Let us then boost our reference frame in the x_d direction with rapidity η, so that the $Q\bar{Q}$ is now at rest and the plasma moves with rapidity $-\eta$ in the x_d direction (the $Q\bar{Q}$ now feels a hot wind):

$$\begin{aligned} dt' &= dt' \cosh\eta - dx'_d \sinh\eta \\ dx_d &= -dt' \sinh\eta + dx'_d \cosh\eta. \end{aligned} \tag{5.2}$$

Applying this boost to the transverse coordinates of the metric (5.1), the geometry now becomes (after dropping the primes):

$$\begin{aligned} ds^2 = &- (G_{00}\cosh^2\eta - G_{xx}\sinh^2\eta)dt^2 + (G_{xx}\cosh^2\eta - G_{00}\sinh^2\eta)dx_d^2 + \\ &- 2(G_{xx} - G_{00})\sinh\eta\,\cosh\eta\, dt\, dx_d + G_{xx}dx_j^2 + G_{rr}dr^2, \end{aligned} \tag{5.3}$$

where $j = 1, 2, .., d-1$.

Now, consider a $Q\bar{Q}$ dipole oriented perpendicularly to the wind in the gauge theory. Let x_1 be the direction to which the dipole is aligned and let L be the length of the line joining both quarks. The quarks are located at $x_1 = L/2$ and $x_1 = -L/2$. As discussed in Section 5.1, the heavy quark-antiquark potential energy $V_{Q\bar{Q}}$ of this system is related to the expectation value of a rectangular Wilson loop by Eq. (4.2). Holographically, in the supergravity limit (corresponding to a strongly coupled plasma) we can evaluate $\langle W(C)\rangle$ by the prescription of the last Chapter,

$$\langle W(C)\rangle \sim e^{-iS_{str}} \tag{5.4}$$

where S_{str} is the classical Nambu-Goto action of a string in the bulk,

$$S_{str} = -\frac{1}{2\pi\alpha'}\int d\sigma d\tau \sqrt{-det(G_{MN}\partial_\alpha X^M \partial_\beta X^N)}, \tag{5.5}$$

evaluated at an extremum of the action, $\delta S_{str} = 0$. The resulting equations of motion must be solved with the boundary condition that the worldsheet of the string, parametrized by spacetime target functions $X^M(\sigma,\tau)$ ($M = 0, 1, \ldots, d-1$ are the target spacetime indices, $\alpha, \beta = \sigma, \tau$ are the worldsheet coordinates), must describe the curve C, in the boundary of the bulk geometry. Plugging back S_{str} in Eq. (5.4) we extract the real part of $V_{Q\bar{Q}}$. Once we include thermal fluctuations of the string in Eq. (5.4), we will be able to evaluate the

imaginary part of $V_{Q\bar{Q}}$ in this case.

Since the dipole is perpendicular to the wind, x_{d-1} is constant along the line joining the endpoints of the string - this means that we can take X^{d-1} to be constant. We use the remaining symmetry of Eq. (5.5) to completely fix the static gauge given by $(X^0 = \tau = t, X^1 = \sigma = x, X^i = \text{const}, X^{d-1} = \text{const}, U = U(\sigma))$, where $i = 1, ..., d-2$. With this gauge choice, Eq. (5.5) becomes, after inserting the background metric (5.3),

$$S_{str} = -\frac{\mathcal{T}}{2\pi\alpha'}\int_{-L/2}^{L/2} d\sigma\sqrt{\tilde{M}(U)U'(\sigma)^2 + \tilde{V}(U)}, \tag{5.6}$$

where we defined

$$\tilde{M}(U) \equiv M(U)\cosh^2\eta - N(U)\sinh^2\eta \tag{5.7a}$$

$$\tilde{V}(U) \equiv V(U)\cosh^2\eta - P(U)\sinh^2\eta \tag{5.7b}$$

and

$$M(U) \equiv G_{00}G_{UU} \tag{5.8a}$$

$$V(U) \equiv G_{00}G_{xx} \tag{5.8b}$$

$$P(U) \equiv G_{xx}^2 \tag{5.8c}$$

$$N(U) \equiv G_{xx}G_{rr} \tag{5.8d}$$

Also, $U' \equiv dU/d\sigma$. We see that Eq. (5.6) has formally the same form found in the case of a plasma at rest - we only need to replace $\tilde{M}$ and $\tilde{V}$ by M,V, respectively [18]. We also see that taking $\eta \to 0$ takes Eq. (5.6) back to the case in which the plasma is at rest. However, an important difference between Eq. (5.6) and the corresponding action in the case where the plasma is at rest is that in the latter the function M is always positive whereas here $\tilde{M}$ can be negative, depending on the bulk geometry and η.

Let us proceed to solve the variational problem $\delta S = 0$. Since the calculation is very similar to the $\eta = 0$ case presented in the last Chapter, here we will only sketch the basic steps. First we write down the Hamiltonian associated with Eq. (5.6), which is a constant of motion. Then, since the string is symmetric with respect to $X_1 = \sigma = 0$, we have $U'(0) = 0$, with the corresponding position of the deepest position in the bulk being $U(0) = U_c$. From the Hamiltonian, we can write the equation of motion for $U(\sigma)$,

$$\frac{dU}{d\sigma} = H(U(\sigma)) \tag{5.9}$$

with $H(U)$ defined by

$$H(U) \equiv \sqrt{\frac{\tilde{V}(U)}{\tilde{V}_c}\frac{\tilde{V}(U)-\tilde{V}_c}{\tilde{M}(U)}}\,. \tag{5.10}$$

The subscript c in $\tilde{V}_c$ and $\tilde{M}_c$ means that we evaluate these functions at $U = U_c$, i.e., $F_c \equiv F(U_c)$. It follows by the chain rule that

$$\frac{d^2U}{d\sigma^2} = \frac{1}{2}\frac{dH}{dU}(U(\sigma)) \tag{5.11}$$

and in particular

$$\frac{d^2U}{d\sigma^2}(\sigma = 0) = \frac{1}{2}\frac{\tilde{V}_c'}{\tilde{M}_c}, \tag{5.12}$$

where $\tilde{V}' \equiv d\tilde{V}/dU$. This equation will be useful later in the calculation of $\mathrm{Im}\, V_{Q\bar{Q}}$. From Eq. (5.11), using the boundary condition that at the boundary of the bulk geometry the string has to reach the Wilson loop contour - or more precisely, $U(\sigma \to L/2) = \Lambda$, where Λ is an UV cutoff, we can relate L with U_c as follows

$$\frac{L}{2} = \int_{U_c}^{\Lambda} dr \frac{1}{\sqrt{H(U)}}\,. \tag{5.13}$$

Plugging Eq. (5.11) back in Eq. (5.6) we can relate S_{str} and U_c

$$S_{str} = \frac{\mathcal{T}}{\pi\alpha'}\int_{U_c}^{\Lambda} dU\, \sqrt{\tilde{M}(U)}\sqrt{\frac{\tilde{V}(U)}{\tilde{V}(U_*)}}\left[\frac{\tilde{V}(U)}{\tilde{V}(U_*)} - 1\right]^{-1/2}. \tag{5.14}$$

This action is formally infinite when we remove the cutoff UV Λ, since this means that the string worldsheet stretches from $U = U_c$ to the conformal boundary at $U \to \infty$ and thus has infinite area. To regularize S_{str}, we subtract the $T \to 0$ divergence in S_{str}. This comes from the fact that in a thermal field theory all UV divergences should come from the vacuum, as discussed in the last Chapter. The regularized Wilson loop is, therefore,

$$\begin{aligned} S_{str}^{reg} = \frac{\mathcal{T}}{\pi\alpha'}&\left\{\int_{U_c}^{\infty} dU\, \sqrt{\tilde{M}(U)}\sqrt{\frac{\tilde{V}(U)}{\tilde{V}(U_*)}}\left[\frac{\tilde{V}(U)}{\tilde{V}(U_*)} - 1\right]^{-1/2} - \sqrt{M_0(U)}\right\} \\ &- \frac{\mathcal{T}}{\pi\alpha'}\int_{U_h}^{U_c}\sqrt{M_0(U)}, \end{aligned} \tag{5.15}$$

where $M_0(U) \equiv G^0_{00}(U)G^0_{UU}(U)$, with $G^0_{\mu\nu}$ being the metric in the absence of the black brane. Using Eqs. (5.15) and (5.4) we have, finally, $\mathrm{Re}\, V_{Q\bar{Q}} = S_{str}^{reg}/\mathcal{T}$ as a function of U_c.

Together with Eq. (5.13) we can find $L(U_c)$ and $\mathrm{Re}\, V_{Q\bar{Q}}(U_c)$.

5.2.2 General results - Imaginary part

The main idea to evaluate $\mathrm{Im}\, V_{Q\bar{Q}}$, as before, is to consider thermal fluctuations of the string worldsheet. The action (5.6) is exactly of the form already considered in the last Chapter. However, now the function $\tilde{M}(U)$ is not strictly positive. When $\tilde{M}(U) > 0$ the argument used in the calculation of the imaginary part from [18, 179] is left unchanged. However, when $\tilde{M}(U)$ is negative, the thermal fluctuations that may generate an imaginary part must take place away from $x_1 = 0$ and, thus, must have large amplitudes. Fluctuations of this kind cannot be considered using the current approximations employed in our approach, as we discuss below.

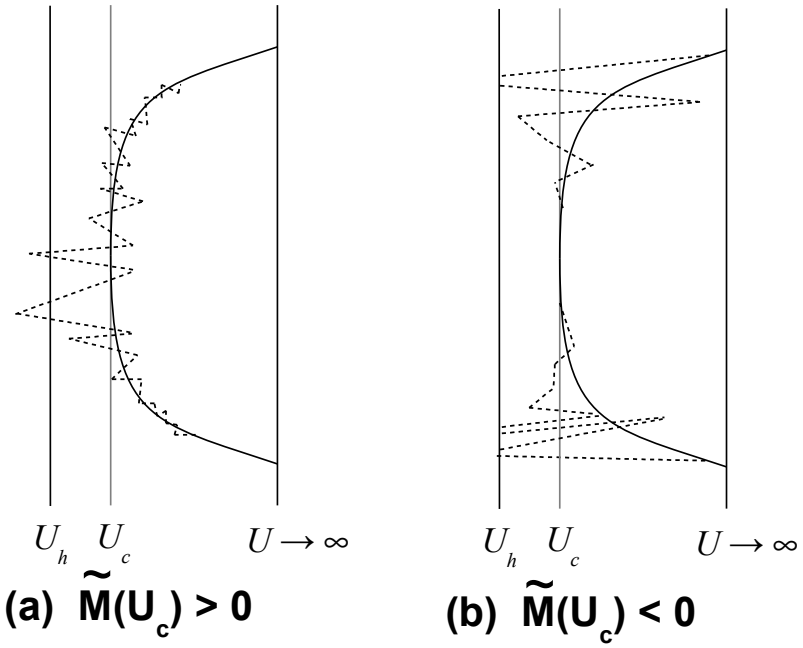

Figure 5.1: *Thermal fluctuations of the string worldsheet responsible for* $\mathrm{Im}\, V_{Q\bar{Q}} \neq 0$ *when (a)* $\tilde{M}(U) > 0$ *and (b)* $\tilde{M}(U) < 0$*. Fluctuations of the second type, large and distant from* $U = U_c$ *cannot be considered in our current approach since they require corrections that go beyond the saddle point approximation.*

If $\tilde{M}(U_c) > 0$, the argument in Section 4.4 can be readily used. In the end, one concludes that in this case

$$\mathrm{Im}\, V_{Q\bar{Q}} = -\frac{1}{2\sqrt{2}\alpha'}\sqrt{\tilde{M}_c}\left[\frac{\tilde{V}_c'}{2\tilde{V}_c''} - \frac{\tilde{V}_c}{\tilde{V}_c'}\right], \tag{5.16}$$

if $\mathrm{Im}\, V_{Q\bar{Q}} < 0$.

If, instead, $\tilde{M}(U_c) < 0$, the argument is the same up to the point where we write Eq. (4.27) in the last Chapter,

$$\mathcal{L}_j = \sqrt{C_1 x_j^2 + C_2} \tag{5.17}$$

with C_1 and C_2 given by Eqs. (4.28) and (4.29), with the substitutions $M, V \to \tilde{M}, \tilde{V}$. The argument of the square root in Eq. (5.17) is, now, positive for a small interval of x_j and negative outside of this interval. This means that the square root is purely real inside this interval and negative outside this interval. Thus, $\mathcal{L}_j$ has an imaginary part only outside of the interval centered in $x_1 = 0$. However, our calculation is only valid for $x_1 \sim 0$, near the bottom of the string - we do not have access to the fluctuations that may occur far from $x_1 = 0$ since they would require to go beyond the saddle point approximation. Thus, there is still an imaginary part for the potential in this case but, due to the saddle point approximation, we cannot compute it with this formalism derived. This interesting case, which corresponds to the case of large $Q\bar{Q}$ rapidities, is beyond the range of applicability of the approximations employed in our method and a more general construction involving the explicit D-branes degrees of freedom [223] corresponding to fundamental quarks used in [207] may be required[1].

5.2.3 An explicit example - Thermal $\mathcal{N} = 4$ SYM

Let us apply the results of the foregoing subsection for the case of $\mathcal{N} = 4$ SYM plasma. The gravity dual to thermal $\mathcal{N} = 4$ SYM is type IIB superstring theory on $AdS_5 \times S^5$ with a black brane. The metric of the gravity dual is given by Eq. (4.42). It follows that the functions in Eqs. (5.8) are

$$M(U) = 1 \tag{5.18a}$$

$$V(U) = \frac{U^4}{R^4}\left(1 - \frac{U_h^4}{U^4}\right) \tag{5.18b}$$

$$P(U) = \frac{U^4}{R^4} \tag{5.18c}$$

$$N(U) = \left(1 - \frac{U_h^4}{U^4}\right)^{-1}. \tag{5.18d}$$

After some algebra, one obtains from Eqs. (5.13) and (5.15)

$$LT = \frac{2y_c}{\pi}\sqrt{1 - y_c^4 \cosh^2\eta}\int_1^\infty \frac{dy}{\sqrt{(y^4-1)(y^4-y_c^4)}}, \tag{5.19}$$

[1] We note that even though the worldsheet fluctuation method is formally applicable in general, at the moment we have not worked out the technically nontrivial issues needed to go beyond the saddle point approximation.

$$\frac{\mathrm{Re}\, V_{Q\bar{Q}}}{T} = \frac{\sqrt{\lambda}}{y_c}\left\{\int_1^\infty dy\, \left[\frac{y^4}{\sqrt{(y^4-1)(y^4-y_c^4)}} - 1\right] - \frac{1}{y_h}\right\}, \tag{5.20}$$

where $y_h \equiv U_h/U_c$, $y_c \equiv 1/y_h$ and $\lambda = R^4/\alpha'^2$ is the 't Hooft coupling of the gauge theory. Note that since $U_c > U_h$ one has $0 < y_c < 1$. It is possible to integrate Eqs. (5.21) and (5.22) analytically (see the Appendix D for details; the main idea is to use integral representations of the hypergeometric function [193])

$$LT = \frac{2\sqrt{2\pi}y_c}{\Gamma(1/4)^2}\sqrt{1 - y_c^4\cosh^2\eta}\,{}_2F_1\left(\frac{1}{2},\frac{3}{4},\frac{5}{4},y_c^4\right), \tag{5.21}$$

$$\frac{\mathrm{Re}\, V_{Q\bar{Q}}}{T} = -\frac{\sqrt{\lambda}}{y_c}\frac{\sqrt{2\pi^3}}{\Gamma(1/4)^2}\left[{}_2F_1\left(\frac{1}{2},-\frac{1}{4},\frac{1}{4},y_c\right) + y_c^4\cosh^2\eta\,{}_2F_1\left(\frac{1}{2},\frac{3}{4},\frac{5}{4},y_c^4\right)\right]. \tag{5.22}$$

where ${}_2F_1(a,b,c,d)$ is the Gauss hypergeometric function. The limit $\eta \to 0$ yields the expressions shown in the previous Chapter, Eqs. (4.54) and (4.55); for Eq. (5.21) this is immediate, whereas for Eq. (5.22) it requires some use of the properties of hypergeometric functions (namely, Gauss recursion formulas) [193].

In Fig. 5.2 we show the behavior of LT for this perpendicular case as a function of y_c for several choices of η. The maximum of the $LT(y_c)$, LT_{max} indicates the limit of validity of the saddle point approximation - to go to higher LT it is necessary to include further connected contributions past the saddle point approximation [184]. We see from Fig. 5.3 that increasing η reduces LT_{max}. A systematic study of LT_{max} as a function of η is presented in Fig. 5.3. In the literature [219, 220], LT_{max} has been used to define a dissociation length for the moving $Q\bar{Q}$ pair - the dominant configuration for S_{str} in this case would be two straight strings (two heavy quarks) running from the boundary to the horizon. In this Chapter, based on the discussion in Ref. [184] (see also the last Chapter), we choose to use this quantity to define the region of applicability of the U-shaped string configuration (which is dependent on the pair's rapidity). Moreover, the dissociation properties of heavy quarkonia should be sensitive to the imaginary part of the potential and that will be estimated later in this section using the expression for $\mathrm{Im}\, V_{Q\bar{Q}}$ computed above.

We proceed to show, in Fig. 5.4, $\mathrm{Re}\, V_{Q\bar{Q}}/(T\sqrt{\lambda})$ as a function of LT for some choices of η. We see that for short distances the $Q\bar{Q}$ pair does not feel the moving plasma, as expected. For each η the upper branch corresponds to another saddle point of the string action (which is associated to the curve to the right of LT_{max} in Fig. 5.2), which is suppressed with respect to the lower branch.

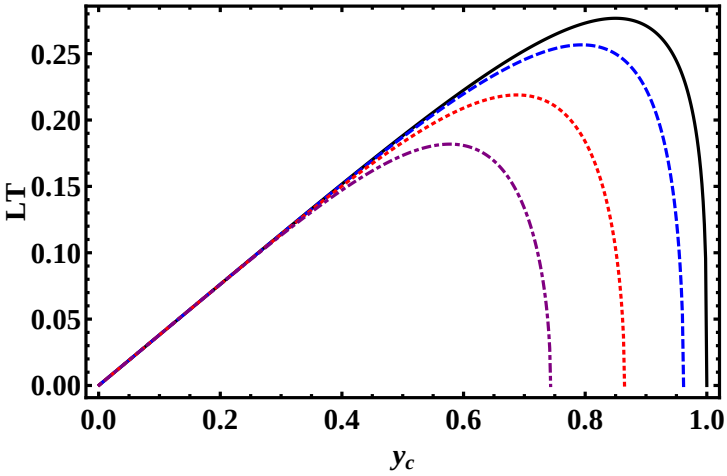

Figure 5.2: *LT as a function of y_c for a $Q\bar{Q}$ pair oriented perpendicularly to the hot wind in an $\mathcal{N} = 4$ SYM plasma. Different rapidities are considered: the solid black curve corresponds to $\eta = 0$, the dashed blue curve to $\eta = 0.4$, the dotted red curve to $\eta = 0.8$, and the dashed-dotted purple curve to $\eta = 1.2$.*

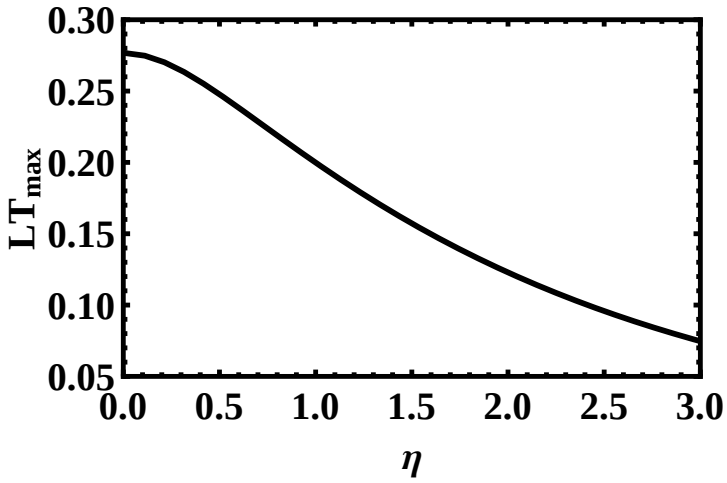

Figure 5.3: *LT_{max} as a function of rapidity η for a $Q\bar{Q}$ pair oriented perpendicularly to the hot wind in an $\mathcal{N} = 4$ SYM plasma.*

Now, let us proceed to the evaluation of the imaginary part in this case. First, the condition $\tilde{M}(U_c) > 0$ leads to

$$y_c < y_{max,1} = (1 - \tanh^2 \eta)^{1/4} \,. \tag{5.23}$$

When this is valid, use of Eq. (5.16) yields, after some algebra,

$$\frac{\mathrm{Im}\, V_{Q\bar{Q}}}{T} = -\frac{\pi}{24\sqrt{2}} \frac{\sqrt{\lambda}}{y_c} \sqrt{\frac{1 - y_c^4 \cosh^2 \eta}{1 - y_c^4}} (3 y_c^4 \cosh^2 \eta - 1) \,. \tag{5.24}$$

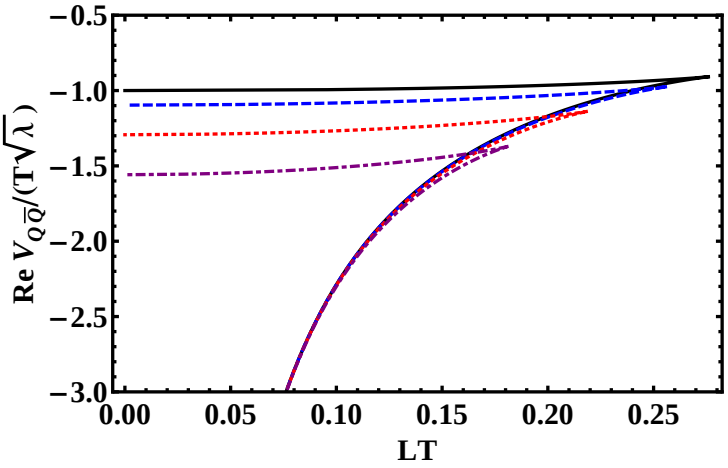

Figure 5.4: $\mathrm{Re}\, V_{Q\bar{Q}}/(T\sqrt{\lambda})$ *as a function of* LT *for a* $Q\bar{Q}$ *pair oriented perpendicularly to the hot wind in an* $\mathcal{N} = 4$ *SYM plasma. Different rapidities are considered: the solid black curve corresponds to* $\eta = 0$*, the dashed blue curve to* $\eta = 0.4$*, the dotted red curve to* $\eta = 0.8$ *and the dashed-dotted purple curve to* $\eta = 1.2$*.*

Imposing that $\mathrm{Im}\, V_{Q\bar{Q}} < 0$ leads to

$$y_c > y_{min} = \frac{1}{3^{1/4}\sqrt{\cosh^2 \eta}}\,. \tag{5.25}$$

Also, we must take $y_c < y_{max,2}$, where $y_{max,2}$ is the maximum value of y_c for which the connected contribution we consider is valid (see Fig. 5.2). These conditions lead to a narrow window where our method is applicable, shown in Fig. 5.5. One sees that $y_{max,2} < y_{max,1}$ so the case $\tilde{M}(U_c) < 0$ does not need to be considered in our case. For $y < y_{min}$, $\mathrm{Im}\, V_{Q\bar{Q}} = 0$. For $y_{max,2} < y < y_{max,1}$, our method is not applicable and the imaginary part of the potential has to be computed using other methods.

Taking into account these intervals of applicability, we show the result of Eq. (5.24) for $\mathrm{Im}\, V_{Q\bar{Q}}$ as a function of LT in Fig. 5.6 for some choices of the rapidity η. One can see, from Eq. (5.24), that $\mathrm{Im}\, V_{Q\bar{Q}}$ roughly scales as T^2 (since $y_c = U_h/U_c \propto T$). This scaling was seen in a calculation of $\mathrm{Im}\, V_{Q\bar{Q}}$ using complex world-sheet coordinates [191] and in lattice calculations [178], opposed to the T scaling predicted by pQCD [167]. Also, for increasing rapidity, the onset of the imaginary part happens for smaller LT which indicates that the suppression becomes stronger. However, the actual magnitude of the imaginary part computed in this case must be interpreted with caution. The apparent smaller magnitude observed at larger rapidities happens not because the imaginary part (or, equivalently, the thermal width) really decreases but simply because we chose to plot only the values that are consistent with the very stringent requirements used in the last Chapter. One could have used the linear extrapolation employed in the original study [179] and that

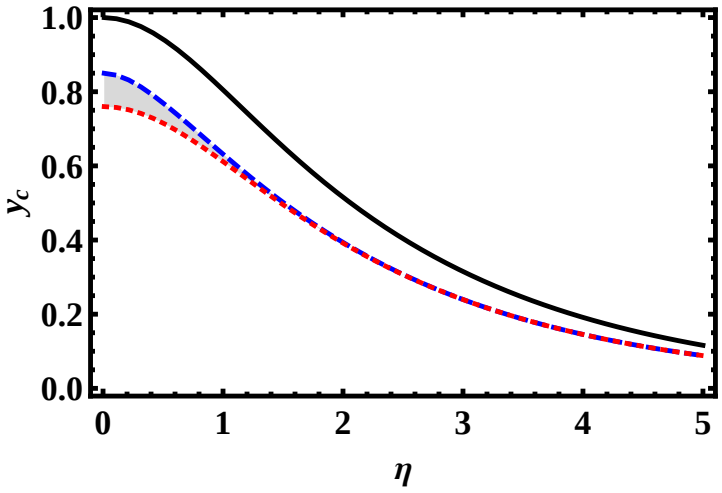

Figure 5.5: *From top to bottom, the limiting curves $y_{max,1}$ (solid black line), $y_{max,2}$ (dashed blue line) and y_{min} (dotted red curve) as a function of the rapidity η for a $Q\bar{Q}$ pair oriented perpendicularly to the hot wind in an $\mathcal{N}=4$ SYM plasma. The filled area represents the region where our method can be reliably used to estimate* $\mathrm{Im}\, V_{Q\bar{Q}}$.

would give the correct qualitative result that at large rapidity $Q\bar{Q}$ pairs are less stable. However, in the last Chapter this extrapolation was shown to largely overestimate the thermal width and, thus, in this thesis we chose to be very "conservative" and plot in Fig. 5.6 only the region consistent with the approximations used in our method. However, we stress that the correct way to interpret our findings is that the heavy quark potential of moving quarkonia should have, in general, larger imaginary parts than the corresponding static case.

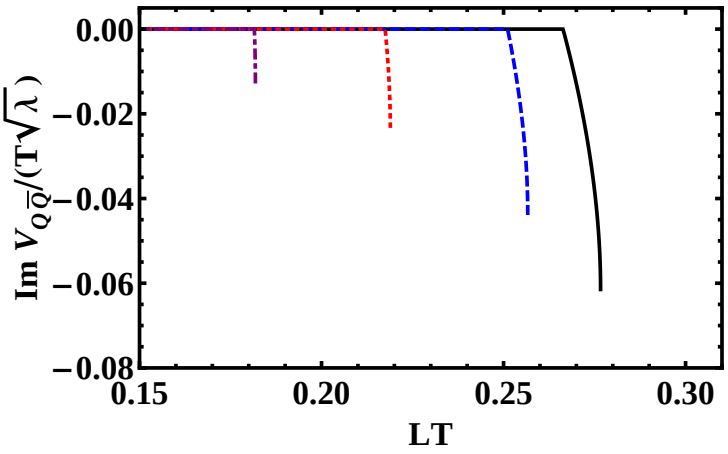

Figure 5.6: $\mathrm{Im}\, V_{Q\bar{Q}}/(\sqrt{\lambda}T)$ *as a function of LT for a $Q\bar{Q}$ pair oriented perpendicularly to the hot wind in an $\mathcal{N}=4$ SYM plasma. The solid black curve corresponds to $\eta=0$, the dashed blue curve to $\eta=0.4$, the dotted red curve to $\eta=0.8$, and the dashed-dotted purple curve to $\eta=1.2$.*

5.3 Dipole at Arbitrary Angles

The next step is to generalize the previous calculations for a dipole oriented at an arbitrary angle with respected to its velocity vector. The main difference, in the gravity dual calculation of the Wilson loop, is that we cannot take $X_{d-1} = const$ anymore. As emphasized in Refs. [219, 220], the system has now two effective degrees of freedom. The calculation of the imaginary part, though it follows the same general lines as before, now needs two pieces of information that can be extracted from the classical solution.

5.3.1 General Results - Real Part

Let us proceed to orient the $\bar{Q}Q$ dipole at an arbitrary angle with respect to the hot wind in the X_{d-1} direction. Our objective will be, as before, to extract the real and imaginary parts of the heavy quark-antiquark potential energy $V_{\bar{Q}Q}$ holographically. We will take the dipole to be in the (X_1, X_{d-1}) plane. Let θ be the angle of the dipole with respect to the X_{d-1} axis (see Fig. 5.7). If $\theta = \pi/2$ the dipole is oriented along X_1 and we return to the case of the previous section.

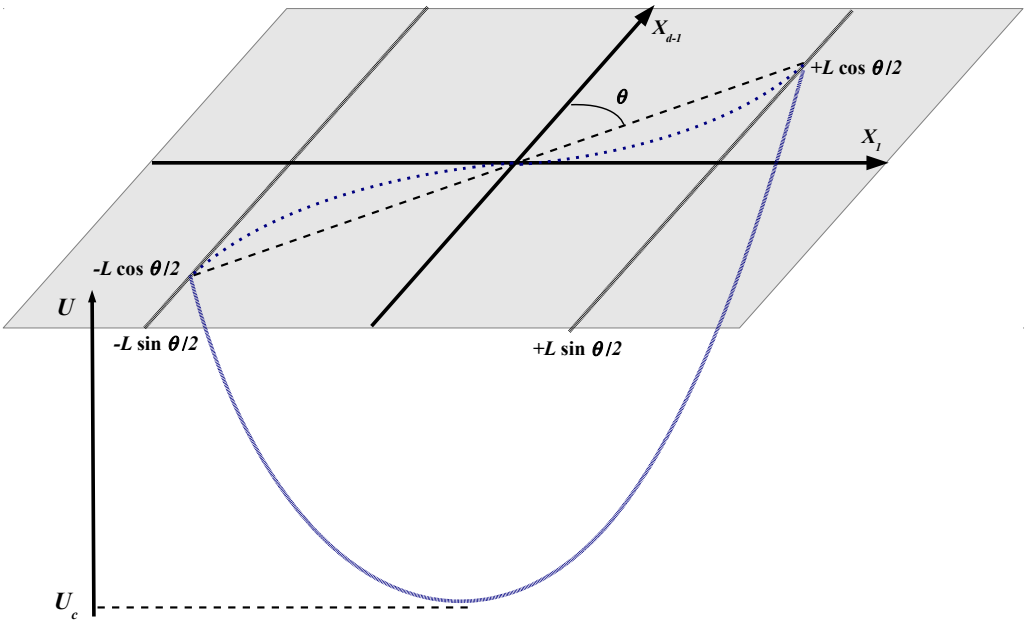

Figure 5.7: *The geometry of the $\bar{Q}Q$ dipole, as described in the text, along with the string in the bulk joining the ends of the heavy quark pair. Note that the projection of this string on (X_1, X_{d-1}) at the boundary is not a straight line joining the $\bar{Q}Q$ quarks but a curved line.*

Using the holographic prescription, in order to evaluate $V_{Q\bar{Q}}$ we should evaluate S_{str} given by Eq. (5.5) with the boundary condition that the string described by S_{str} joins the endpoints of the dipole. However, now we have two fixed parameters (aside from η,

which tells us how to rotate the Minkowski slices): the length of the dipole L and the angle θ. If we followed the calculations of the previous section of this thesis, we would have only one constant of motion, given by the Hamiltonian of the problem, to relate to both L and θ. Indeed, as discussed in Refs. [219,220], one has to consider also a "sagging" of the string along the line segment joining the quark-antiquark pair, as described in Fig. 5.7. In terms of the string worldsheet, this means that have to consider the behavior of the embedding function $X_{d-1}(\sigma)$. We cannot, as in the previous section, take $X_{d-1}(\sigma)$ as given. Rather, $X_{d-1}(\sigma)$ must be taken as the second degree of freedom of the string worldsheet and that makes a difference both in the computation of the real and imaginary parts of the potential.

This implies that we must slightly modify the static gauge used in the previous section. A possible choice of the string worldsheet coordinates, which will be used in this work, is $(X^0 = \tau = t, X^1 = \sigma = x, X^i = \text{const}, X^{d-1} = X^{d-1}(\sigma), U = U(\sigma))$, where $i = 1, ..., d-2$. Now we have two degrees of freedom, $X_{d-1}(\sigma)$ and $U(\sigma)$. We note that if the projection of the string on the (X_1, X_{d-1}) plane was a straight line, then $X_{d-1}(\sigma)$ would be given by $\sigma/\tan\theta$. The boundary conditions to be imposed here are

$$\begin{aligned} U\left(\pm\frac{L}{2}\sin\theta\right) &= \Lambda \\ X_d\left(\pm\frac{L}{2}\sin\theta\right) &= \pm\frac{L}{2}\cos\theta \end{aligned} \tag{5.26}$$

which, taken together, imply that the string has as its endpoints the heavy quarks. As in Section 5.2, Λ is an UV cutoff. The background metric is still given by the generic boosted metric in Eq. (5.3).

With these modifications, the action (5.5) now becomes

$$S_{str} = -\frac{\mathcal{T}}{2\pi\alpha'}\int d\sigma\mathcal{L}, \tag{5.27}$$

where we defined the Lagrangian

$$\mathcal{L} \equiv \sqrt{\left[M(U)\cosh^2\eta - N(U)\sinh^2\eta\right]U'(\sigma)^2 + V(U)X_d'(\sigma)^2 + \left[V(U)\cosh^2\eta - P(U)\sinh^2\eta\right]} \tag{5.28}$$

with the functions M, N, V and P defined as in Eq. (5.8). This action does not depend on σ explicitly, so the associated Hamiltonian

$$\mathcal{H} \equiv Q \equiv \mathcal{L} - \frac{dU}{d\sigma}\frac{\partial\mathcal{L}}{\partial U'} - \frac{dX_d}{d\sigma}\frac{\partial\mathcal{L}}{\partial X_d'} \tag{5.29}$$

is a constant of motion. Another constant of motion is

$$K \equiv \frac{\partial \mathcal{L}}{\partial X_d'}, \tag{5.30}$$

since $\mathcal{L}$ does not depend on X_d explicitly. Inserting the Lagrangian (5.28) in the first integrals (5.30) and (5.29) we obtain, after some algebra,

$$\begin{aligned} Q^2 \left[M(U)\cosh^2\eta - N(U)\sinh^2\eta\right] U'(\sigma)^2 + Q^2 V(U) X_{d-1}'(\sigma)^2 + \\ + \left[V(U)\cosh^2\eta - P(U)\sinh^2\eta\right]\left\{Q^2 - \left[V(U)\cosh^2\eta - P(U)\sinh^2\eta\right]\right\} = 0 \end{aligned} \tag{5.31}$$

and

$$\begin{aligned} K^2 \left[M(U)\cosh^2\eta - N(U)\sinh^2\eta\right] U'(\sigma)^2 + V(U)(K^2 - V(U))\, X_{d-1}'^2(\sigma) + \\ + K^2 \left[V(U)\cosh^2\eta - P(U)\sinh^2\eta\right] = 0\,. \end{aligned} \tag{5.32}$$

Eqs. (5.31) and (5.32) can be recast in a more convenient form; first we solve Eq. (5.31) for $X_d'^2$, then we substitute the resulting expression in Eq. (5.32) to obtain an equation involving only $U'(\sigma)$. Then one can use the common term $\left[M(U)\cosh^2\eta - N(U)\sinh^2\eta\right] U'(\sigma)^2$ to obtain a simplified equation for X_d'. After these manipulations, one ends up with the final form for the equations of motion, namely

$$\begin{aligned} Q^2 V(U)\left[M(U)\cosh^2\eta - N(U)\sinh^2\eta\right] U'(\sigma)^2 = \\ = (V(U) - K^2)\left[V(U)\cosh^2\eta - P(U)\sinh^2\eta\right]^2 - V(U)\left[V(U)\cosh^2\eta - P(U)\sinh^2\eta\right] Q^2 \end{aligned} \tag{5.33}$$

and

$$Q^2 V^2 (X_{d-1}')^2 = K^2 \left[V(U)\cosh^2\eta - P(U)\sinh^2\eta\right]^2 . \tag{5.34}$$

Referring back to the Fig. 5.7, we define U_c as the minimum value of U that the string reaches in the bulk. By the symmetry of the string worldsheet, we must have $U(\sigma = 0) = U_c$, $U'(\sigma = 0) = 0$ and $X_d(\sigma = 0) = 0$. Using these conditions in Eq. (5.33) we obtain an equation relating U_c with Q and K

$$(V_c - K^2)(V_c \cosh^2\eta - P_c \sinh^2\eta) - V_c Q^2 = 0, \tag{5.35}$$

where we used, as before, $F_c \equiv F(U_c)$.

From the equations of motion (5.33) and (5.34), and taking into account the boundary

conditions (5.51), we are lead to two relations between L, θ and Q,K and U_c

$$\frac{L}{2}\sin\theta = Q\int_{U_c}^{\Lambda} dU \left\{ \frac{V(U)}{V(U)\cosh^2\eta - P(U)\sinh^2\eta} \times \right. \\ \left. \times \frac{M(U)\cosh^2\eta - N(U)\sinh^2\eta}{\left[(V(U)-K^2)\left[V(U)\cosh^2\eta - P(U)\sinh^2\eta\right] - V(U)Q^2\right]} \right\}^{-1/2} \tag{5.36}$$

and

$$\frac{L}{2}\cos\theta = K\int_{U_c}^{\Lambda} dU \sqrt{\frac{\left[M(U)\cosh^2\eta - N(U)\sinh^2\eta\right]\left[V(U)\cosh^2\eta - P(U)\sinh^2\eta\right]}{V(U)\left\{(V(U)-K^2)\left[V(U)\cosh^2\eta - P(U)\sinh^2\eta\right] - V(U)Q^2\right\}}}. \tag{5.37}$$

In these equations, if the metric is asymptotically AdS, the integrals converge and we can formally take $\Lambda \to \infty$. The general procedure, to be described in more details when we treat the explicit example of $\mathcal{N} = 4$ SYM, is to specify a value for the constant Q and solve Eq. (5.35) to obtain U_c as a function of Q and K. Then, plugging $U_c = U_c(Q, K)$, we may solve Eqs. (5.36) and (5.37) to relate the set of integration constants (Q, P) with the geometrical parameters (L, θ).

With the problem of the integration constants taken care of, we can evaluate the action in the saddle-point approximation and obtain

$$S = \frac{\mathcal{T}}{\pi\alpha'}\int_{U_c}^{\Lambda} dU \sqrt{\frac{V(U)\left[M(U)\cosh^2\eta - N(U)\sinh^2\eta\right]\left[V(U)\cosh^2\eta - P(U)\sinh^2\eta\right]}{\left\{(V(U)-K^2)\left[V(U)\cosh^2\eta - P(U)\sinh^2\eta\right] - V(U)Q^2\right\}}}. \tag{5.38}$$

We regularize this action as before (the process of reorienting the string clearly cannot introduce new UV divergences). The regularized action is thus

$$S_{reg} = \frac{\mathcal{T}}{\pi\alpha'}\int_{U_c}^{\Lambda} dU \left\{ \sqrt{\frac{V(U)\left[M(U)\cosh^2\eta - N(U)\sinh^2\eta\right]\left[V(U)\cosh^2\eta - P(U)\sinh^2\eta\right]}{\left\{(V(U)-K^2)\left[V(U)\cosh^2\eta - P(U)\sinh^2\eta\right] - V(U)Q^2\right\}}} + \right. \\ \left. - \sqrt{M_0(U)} \right\} - \frac{\mathcal{T}}{\pi\alpha'}\int_0^{U_c} dU \sqrt{M_0(U)}, \tag{5.39}$$

with M_0 being, as before, the function $M(U)$ defined for $T = 0$, in the absence of the black brane. The real part of the heavy quark potential of the $Q\bar{Q}$ pair is $\mathrm{Re}\, V_{Q\bar{Q}} = S_{reg}/\mathcal{T}$.

5.3.2 Imaginary part - General results

Let us proceed to discuss the imaginary part. As before, we consider thermal fluctuations in the string worldsheet, following the ideas exposed on the previous Chapter. The

main difference is that now we have two degrees of freedom, $U(\sigma)$ and $X_{d-1}(\sigma)$. Thus, in principle, we have to consider fluctuations $\delta U(\sigma)$ and $\delta X_{d-1}(\sigma)$, with $\partial U/\partial\sigma \to 0$ and $\partial X_{d-1}/\partial\sigma \to 0$. Including these fluctuations, the stringy partition function takes the form

$$Z_{str} \sim \int D(\delta U)\, D(\delta X_{d-1}) e^{iS_{str}(\bar{U}+\delta U, \bar{X}_{d-1}+\delta X_d)} \tag{5.40}$$

where $\bar{U}$ and $\bar{X}_{d-1}$ are the classical solutions of $\delta S_{str} = 0$ described in the previous section. Partitioning the interval $[-L/2\sin\theta, L/2\sin\theta]$ in $2N$ subintervals and using the action (5.27), we can write

$$Z_{str} \sim \left(\int_{-\infty}^{\infty} d(\delta U_{-N})\, d(\delta X_{d-1,-N})\right) \cdots \left(\int_{-\infty}^{\infty} d(\delta U_N)\, d(\delta X_{d-1,N})\right) e^{i\frac{\mathcal{T}\Delta_\pi}{2\pi\alpha'}\mathcal{L}_j}, \tag{5.41}$$

where $\Delta x = (L/2\sin\theta)/2N$ and

$$\mathcal{L}_j = \sqrt{\tilde{M}(U(x_j))(U'(x_j))^2 + V(U(x_j))(X'_{d-1}(x_j))^2 + \tilde{V}(x_j)}, \tag{5.42}$$

with $\tilde{M}$ and $\tilde{V}$ given in Eq. (5.7). Only considering fluctuations near the bottom of the string, i.e., at $\sigma = 0$ with $U = U_c$, we can expand the classical solution $\bar{U}(\sigma)$ around $\sigma = 0$ to quadratic order on σ, and the functions $\tilde{M}$ and $\tilde{V}$ around $\bar{U}$ - the calculations are the same as for the static or perpendicular cases, noting that we keep only terms up to quadratic order in the monomial $\delta U^m\, \delta X_{d-1}^n \sigma^p$. As for $X_{d-1}(x_j)$, if the string did not sag, then we would have $X_{d-1}(\sigma) = \sigma/\tan\theta$. With the sagging, X_{d-1} does not assume such a simple form. However, around $\sigma = 0$ one must be able to expand $X_{d-1}(\sigma)$ as

$$X_{d-1}(\sigma) = \frac{\sigma}{\tan\tilde{\theta}} + b\sigma^3 + O(\sigma^5), \tag{5.43}$$

where $\tilde{\theta}$ would be equal to θ if the string did not sag and b was a constant. Even terms do not participate in this expansion because the problem is evidently symmetric under reflections with respect to the origin of the (X_1, X_d) plane (see Fig. 5.7 where the projection of the string was drawn taking this into account) and $X_d(\sigma)$ must be an odd function of σ. Therefore, up to $\mathcal{O}(\sigma^2)$,

$$X'_{d-1}(\sigma)^2 = \frac{1}{\tan^2\tilde{\theta}} + \frac{6b}{\tan\tilde{\theta}}\sigma^2. \tag{5.44}$$

Inserting Eq. (5.44) into Eq. (5.42) we arrive, after some algebra, at

$$\mathcal{L}_j = \sqrt{\tilde{C}_1 x_j^2 + \tilde{C}_2}, \tag{5.45}$$

where we defined

$$\tilde{C}_1 \equiv \tilde{M}_c \bar{U}''(0)^2 + \frac{1}{2}\left(\frac{V_c'}{\tan^2\tilde{\theta}} + \tilde{V}_c'\right)\bar{U}''(0) + \frac{6b}{\tan\tilde{\theta}}V_c \tag{5.46}$$

and

$$\tilde{C}_2 \equiv \left(\frac{V_c}{\tan^2\tilde{\theta}} + \tilde{V}_c\right) + \left(\frac{V_c'}{\tan^2\tilde{\theta}} + \tilde{V'}_c\right)\delta U + \left(\frac{V_c''}{\tan^2\tilde{\theta}} + \tilde{V''}_c\right)\frac{(\delta U)^2}{2}. \tag{5.47}$$

Following the same argument presented in the previous section, we must have $\tilde{C}_1 > 0$. If this is the case, then imposing that Eq. (5.45) has an imaginary part, summing all such contributions of $\mathcal{L}_j$ in Eq. (5.41) and finally taking the continuum limit we arrive at a new and explicit analytical expression for $\mathrm{Im}V_{Q\bar{Q}}$ valid for a large class of gravity duals

$$\mathrm{Im}\, V_{Q\bar{Q}} = -\frac{1}{4\alpha'}\frac{1}{\sqrt{\tilde{C}_1}}\left[\frac{\left(\frac{V_c'}{\tan^2\tilde{\theta}} + \tilde{V}_c'\right)^2}{2\left(\frac{V_c''}{\tan^2\tilde{\theta}} + \tilde{V}_c''\right)} - \left(\frac{V_c}{\tan^2\tilde{\theta}} + \tilde{V}_c\right)\right]. \tag{5.48}$$

For this expression to be valid, we must impose $\mathrm{Im}V_{Q\bar{Q}} < 0$. Also, note that to compute $\tilde{C}_1$ using Eq. (5.47) we need to use two pieces of information concerning the shape of $\bar{U}(\sigma)$ at $\sigma \sim 0$, $\bar{U}''(0)$ and b.

5.3.3 An explicit example - Thermal $\mathcal{N} = 4$ SYM

Let us apply the results of the foregoing sections to strongly coupled thermal $\mathcal{N} = 4$ SYM. The metric is given by equation (4.42), and the M, N, P, V functions are the same as in Eq. (5.18a). Evaluation of the equations of motion (5.33) and (5.34) lead to

$$q^2\left(\frac{dy}{d\tilde{\sigma}}\right)^2 = (y^4 - \cosh^2\eta)(y^4 - 1 - p^2) - q^2(y^4 - 1) \qquad \text{and} \tag{5.49}$$

$$\left(\frac{dz}{d\tilde{\sigma}}\right)^2 = \frac{p^2}{q^2}\left(\frac{y^4 - \cosh^2\eta}{y^4 - 1}\right)^2, \tag{5.50}$$

where we defined the dimensionless variables $y \equiv U/U_h$, $z \equiv X_d U_h/R^2$ and $\tilde{\sigma} \equiv \sigma U_h/R^2$ as well as the dimensionless integration constants $q^2 \equiv R^4Q^2/U_h^4$ and $p^2 = R^4K^2/U_h^4$.

With these variables, the boundary conditions (5.51) become

$$\begin{aligned} y\left(\pm\pi\frac{LT}{2}\sin\theta\right) &= \tilde{\Lambda} \\ z\left(\pm\pi\frac{LT}{2}\sin\theta\right) &= \pm\pi\frac{LT}{2}\cos\theta \end{aligned} \tag{5.51}$$

where we substituted L for the dimensionless variable $LT = LU_h/(\pi R^2)$ to explicit show the conformal character of the gauge theory and $\tilde{\Lambda}$ is the dimensionless UV cutoff. Using the equations above we arrive at expressions relating the integration constants q, p with the physical parameters LT, θ:

$$\frac{LT}{2}\pi\sin\theta = q\int_{y_c}^{\tilde{\Lambda}}\frac{dy}{\sqrt{(y^4-1-p^2)(y^4-\cosh^2\eta)-q^2(y^4-1)}} \qquad \text{and} \tag{5.52}$$

$$\frac{LT}{2}\pi\cos\theta = p\int_{y_c}^{\tilde{\Lambda}}dy\,\frac{y^4-\cosh^2\eta}{y^4-1}\frac{1}{\sqrt{(y^4-1-p^2)(y^4-\cosh^2\eta)-q^2(y^4-1)}}\,. \tag{5.53}$$

The condition (5.35) reduces to

$$(y_c^4-1-p^2)(y_c^4-\cosh^2\eta)-q^2(y_c^4-1)=0\,. \tag{5.54}$$

The real part of the heavy quark potential, after regularization, is given by Eq. (5.39). This yields

$$\frac{\mathrm{Re}\,V_{Q\bar{Q}}}{T} = \sqrt{\lambda}\int_{y_c}^{\infty}dy\left[\frac{y^4-\cosh^2\eta}{\sqrt{(y^4-\cosh^2\eta)(y^4-1-p^2)-q^2(y^4-1)}}-1\right]-\sqrt{\lambda}(y_c-1)\,. \tag{5.55}$$

These results agree with those in Ref. [220]. As for the imaginary part, we use Eq. (5.48)

$$\frac{\mathrm{Im}\,V_{Q\bar{Q}}}{T} = -\frac{\pi\sqrt{\lambda}}{12}\frac{[3(\cos^2\tilde{\theta}+\cosh^2\eta\sin^2\tilde{\theta})-y_c^4]}{\sqrt{y''(0)^2\left(\frac{y_c^4-\cosh^2\eta}{y_c^4-1}\right)+\frac{2y_c^3y''(0)}{\sin\tilde{\theta}}+\frac{6\tilde{b}}{\tan\tilde{\theta}}(y_c^4-1)}}, \tag{5.56}$$

where we defined $\tilde{b} = U_h^2 b/R^4$. For this formula to be valid, we must guarantee that $\mathrm{Im}\,V_{Q\bar{Q}} < 0$. In terms of $\tilde{\sigma}$, the expansion (5.57) takes the form

$$z(\tilde{\sigma}) = \frac{\tilde{\sigma}}{\tan\tilde{\theta}} + \tilde{b}\tilde{\sigma}^3 + O(\tilde{\sigma}^5)\,. \tag{5.57}$$

With these expressions, we can proceed to solve the equations numerically. We consider η and θ as given and fixed. The first step is to relate (q,p) with (LT,θ). First, we solve Eq. (5.54) for y_c as a function of q and p

$$y_c(q,p) = \left[\frac{1}{2}\sqrt{\left(-\cosh^2(\eta) - p^2 - q^2 - 1\right)^2 - 4\left(p^2\cosh^2(\eta) + \cosh^2(\eta) + q^2\right)} + \right.$$
$$\left. + \frac{\cosh^2(\eta)}{2} + \frac{p^2}{2} + \frac{q^2}{2} + \frac{1}{2}\right]^{1/4} . \tag{5.58}$$

Then, we substitute Eq. (5.58) into equations (5.52) and (5.53). This results in two equations relating (q,p) to (L,θ). However, the ratio of these equations involves only (q,p) and θ. Thus, for fixed θ, we can solve this equation numerically for p as a function of q, $p(q)$. Therefore, y_c is now a function only of p, $y_c = y_c(q,p(q))$. We can insert $p(q)$ and $y_c(q,p(q))$ into any of the equations (5.52) or (5.53) to solve for LT as a function of q. Finally, we can obtain $\mathrm{Re}\, V_{Q\bar{Q}}$ as a function of LT by considering the parametric curve $(LT(q), \mathrm{Re}\, V_{Q\bar{Q}}(q))$.

In Fig. 5.8 we present the numerical results for p as a function of q, for a fixed angle and some choices of the rapidity η and for fixed η and some choices of θ, reproducing (and extending) the results in Refs. [219,220]. We see that p is a monotonically increasing function of q, as it should be for the problem to be well-posed.

In Fig. 5.9 we show LT as a function of q. We see that LT assumes a maximum value, LT_{max} which depends strongly on the rapidity η, for a fixed orientation of the dipole, but only slightly on the angle θ, with η fixed. As discussed in the perpendicular case, we will not take LT_{max} to define the dissociation length, but only as an indicative of the limit of validity of our classical gravity calculation.

In Fig. 5.10 we present $\mathrm{Re}\, V_{Q\bar{Q}}$ as a function of LT. The region of small LT does not change appreciably with either the rapidity η or the angle θ, as it should be expected, since for small temperatures or short distances the interaction of the $Q\bar{Q}$ pair with the plasma should not be relevant. Near LT_{max}, $\mathrm{Re}\, V_{Q\bar{Q}}$ varies slightly with η and almost nothing at all with θ (note that in Fig. 5.10 (right plot) we are considering only a small region of LT to zoom in the effect of varying θ). The upper, unphysical, branch in the Fig. 5.10 represents the region $0 < q < q_{max}$, where q_{max} is the value of q which gives LT_{max}: $LT_{max} = q_{max}$. The lower branch, which is the dominant contribution to the action, is given by the region with $q > q_{max}$.

With the real part under control, let us move on to compute $\mathrm{Im}\, V_{Q\bar{Q}}$ for this case. Before using Eq. (5.56) to calculate $\mathrm{Im}\, V_{Q\bar{Q}}$, we must obtain $\tilde{\theta}$, $y''(0)$ and $\tilde{b}$ for the LT in consideration, for fixed θ and η. The effective angle $\tilde{\theta}$ is obtained directly from Eq. (5.50) evaluated at $\tilde{\sigma} = 0$, $y = y_c$ (noting that $z'(0) = 1/\tilde{\theta}$, from Eq. (5.57)). To evaluate

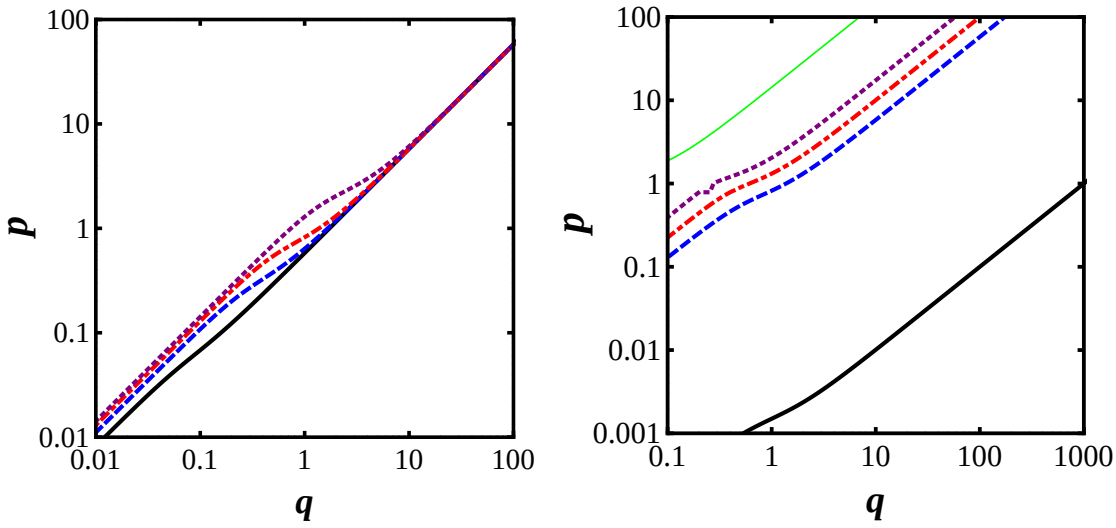

Figure 5.8: *The constant p as a function of q, (left plot) for $\theta = \pi/3$ and $\eta = 0.1$ (thick black curve), $\eta = 0.5$ (dashed blue curve), $\eta = 1.0$ (dashed-dotted red curve) and $\eta = 2.0$ (dotted purple curve) and (right plot) for $\eta = 1.0$ and $\theta = \pi/2$ (thick black curve), $\theta = \pi/3$ (dashed blue curve), $\theta = \pi/4$ (dashed-dotted red curve), $\theta = \pi/6$ (dotted purple curve) and $\theta = \pi/45$ (thin green curve). The calculations are done for the case of a strongly coupled $\mathcal{N} = 4$ SYM plasma.*

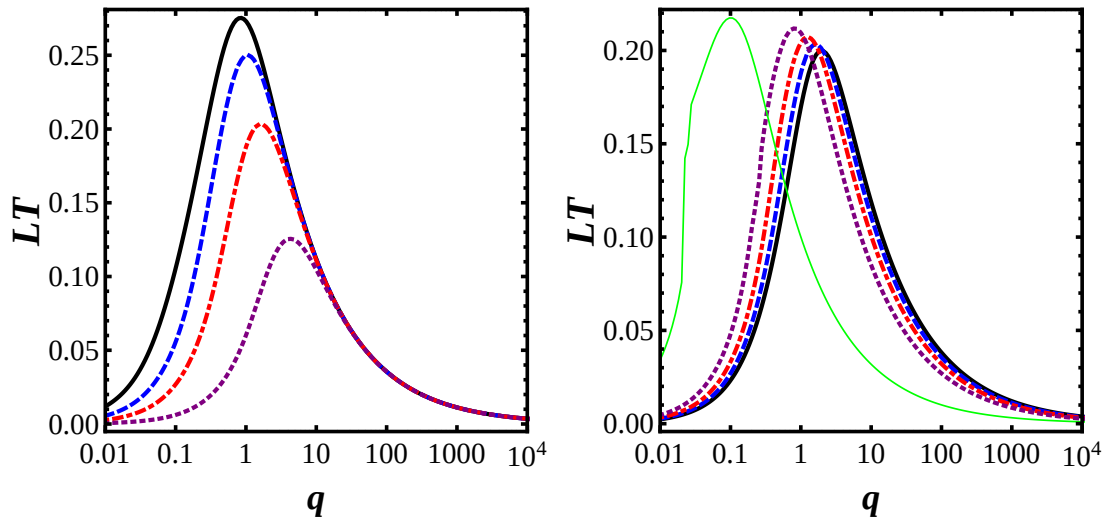

Figure 5.9: *LT as a function of q, (left plot) for $\theta = \pi/3$ and $\eta = 0.1$ (thick black curve), $\eta = 0.5$ (dashed blue curve), $\eta = 1.0$ (dash-dotted red curve) and $\eta = 2.0$ (dotted purple curve); and (right plot) for $\eta = 1.0$ and $\theta = \pi/2$ (thick black curve), $\theta = \pi/3$ (dashed blue curve), $\theta = \pi/4$ (dashed-dotted red curve), $\theta = \pi/6$ (dotted purple curve) and $\theta = \pi/45$ (thin green curve). The calculations are done for the case of a strongly coupled $\mathcal{N} = 4$ SYM plasma.*

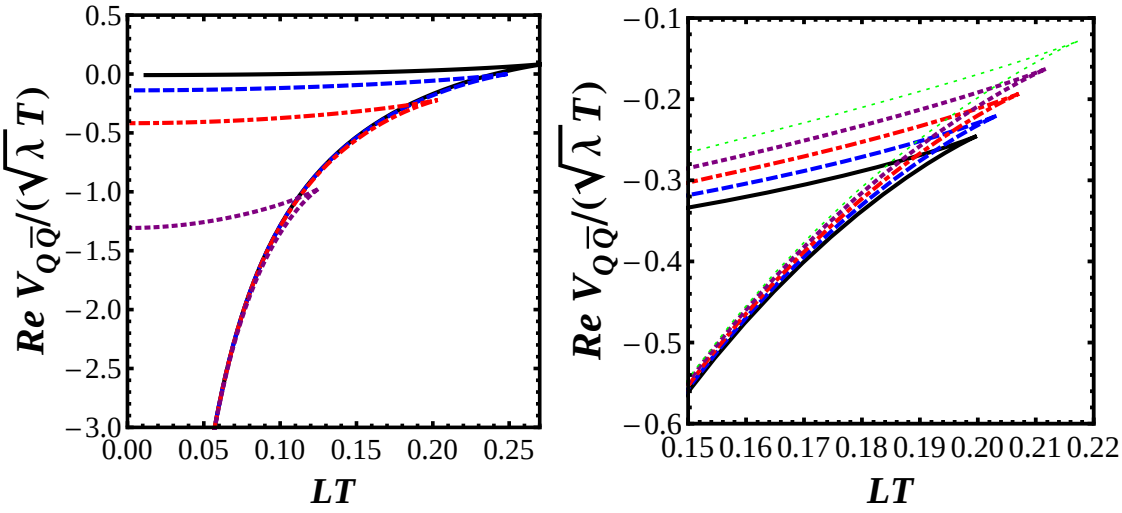

Figure 5.10: $\mathrm{Re}\, V_{Q\bar{Q}}$ *as a function of* q*, (left plot) for* $\theta = \pi/3$ *and* $\eta = 0.1$ *(thick black curve),* $\eta = 0.5$ *(dashed blue curve),* $\eta = 1.0$ *(dashed-dotted red curve) and* $\eta = 2.0$ *(dotted purple curve); and for* $\eta = 1.0$ *and* $\theta = \pi/2$ *(thick black curve),* $\theta = \pi/3$ *(dashed blue curve),* $\theta = \pi/4$ *(dashed-dotted red curve),* $\theta = \pi/6$ *(dotted purple curve) and* $\theta = \pi/45$ *(thin green curve). In (right plot) we show only the detail of* $\mathrm{Re}\, V_{Q\bar{Q}}$ *around* LT_{max}*. The calculations are done for the case of a strongly coupled* $\mathcal{N} = 4$ *SYM plasma.*

$y''(0)$ and $\tilde{b}$ we solve the equations of motion (5.49) and (5.50) subject to the boundary conditions $y(0) = y_c$ and $z(0) = 0$. In principle we could use the set (5.51) of boundary conditions, but since these conditions refer to the string far from $\tilde{\sigma} = 0$, exactly the region of interest for the evaluation of $y''(0) = 0$ and $z'''(0) = 0$, they are not very useful. An example of the shape of the string when we solve these equations numerically is given in Fig. (5.11) - we note in this figure we subtracted the contribution that would appear if the projection of the string on (X_1, X_D) were a straight line joining the endpoints of the $\bar{Q}Q$ dipole. After figuring out the shape of the string, we may evaluate $y''(0)$ and $\tilde{b}$.

With $y''(0)$ and $\tilde{b}$ known, considering only $LT < LT_{max}$ and ensuring that Eq. (5.56) is negative, we can calculate $\mathrm{Im}\, V_{Q\bar{Q}}$ as a function of q. As we know $LT(q)$, we can plot $\mathrm{Im}\, V_{Q\bar{Q}}/T$ as a function of LT. In Fig. 5.12 we show the results of these calculations. We see that, for a fixed $\theta \neq \pi/2$, increasing η decreases the interval of LT allowed for the calculation. Such a behavior is also confirmed when we investigate the LT_{min} for the onset of the imaginary part, as shown in Fig. 5.13. We see that LT_{min} decreases strongly with η; there is also a slight increase for decreasing θ. When we fix η and vary θ (Fig. 5.12 - right panel), we see that the region where the calculation is valid decreases and $\mathrm{Im}\, V_{Q\bar{Q}}/T$ is smaller as θ decreases from the perpendicular case $\theta = \pi/2$ to $\theta \to 0$. This suggests that a dipole oriented parallel to the wind should have a smaller thermal width and the interactions between the heavy quark-antiquark pair are less screened by the plasma in comparison to the perpendicular case.

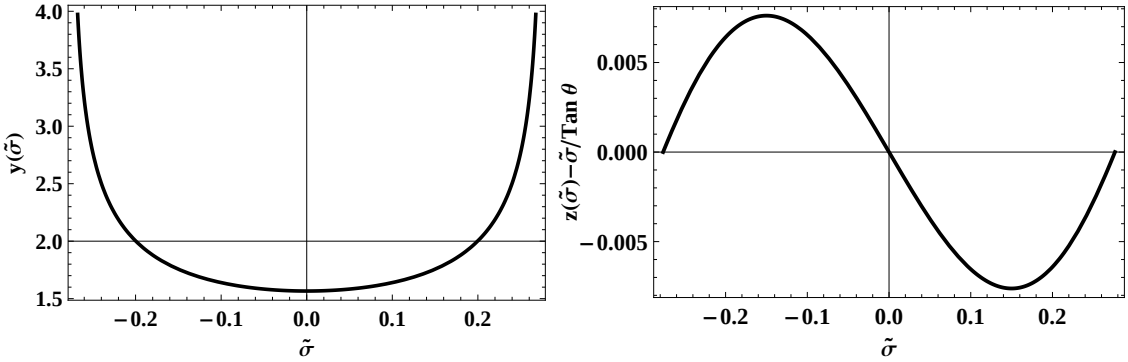

Figure 5.11: *The profile of the string for an $\mathcal{N} = 4$ SYM plasma. (left plot) y as a function of $\tilde{\sigma}$. (right plot) $z - \tilde{\sigma}/\tan\theta$ as a function of $\tilde{\sigma}$ - the subtraction of $\tilde{\sigma}/\tan\theta$ is to remove the trivial shape the string would assume if its projection on the (X_1, X_{d-1}) plane were a straight line segment joining the endpoints of the dipole. These figures refer to a situation with $\theta = \pi/3$, $\eta = 1.0$, and $LT = 0.203$.*

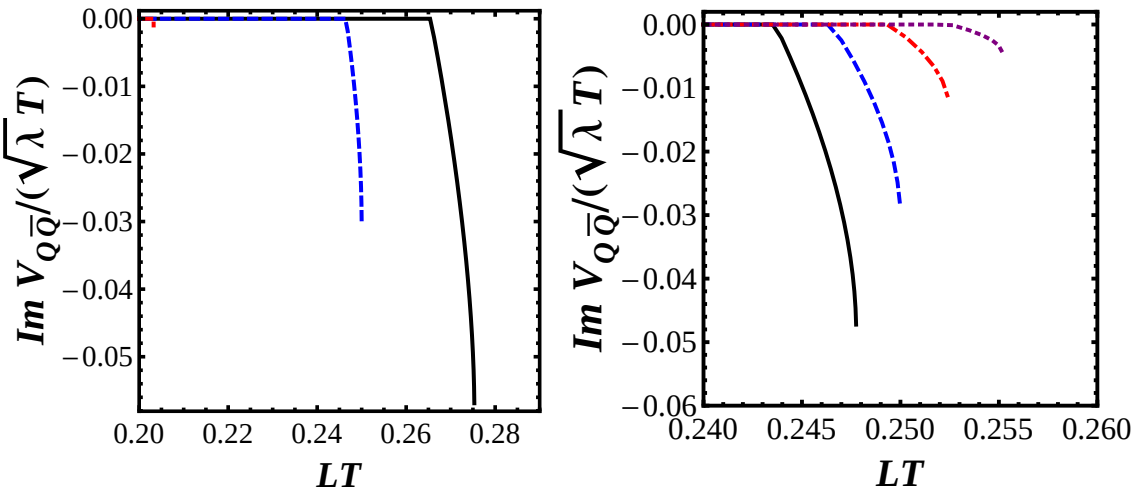

Figure 5.12: $\mathrm{Im}\, V_{Q\bar{Q}}/(\sqrt{\lambda}T)$ *as a function of q, (left panel) for $\theta = \pi/3$ and $\eta = 0.1$ (solid black curve), $\eta = 0.5$ (dashed blue curve) and $\eta = 1.0$ (dotted-dashed red curve) and (right panel) for $\eta = 0.5$ and $\theta = \pi/2$ (solid black curve), $\theta = \pi/3$ (dashed blue curve), $\theta = \pi/4$ (dotted-dashed red curve) and $\theta = \pi/6$ (dotted purple curve).*

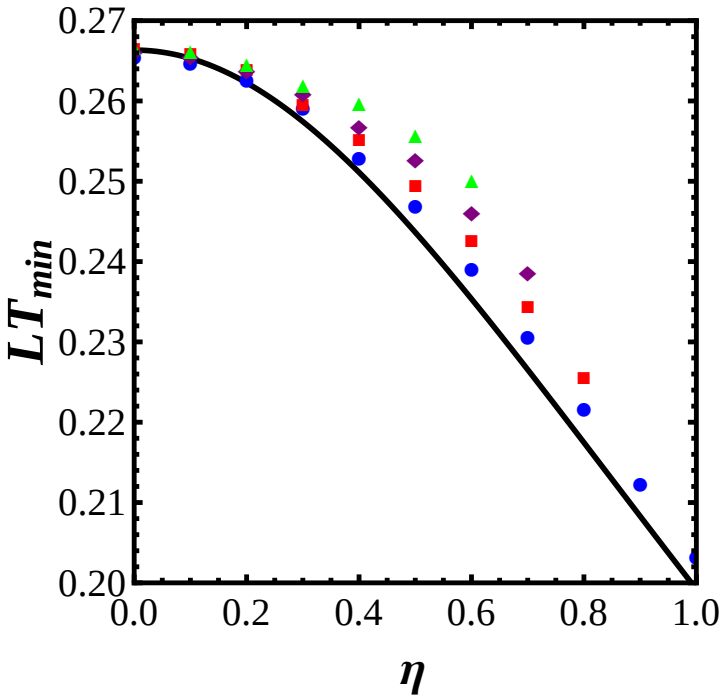

Figure 5.13: *LT_{min} for various angles θ, as a function of the rapidity η, for a $Q\bar{Q}$ pair moving through an $\mathcal{N} = 4$ SYM plasma. The solid black curve corresponds to $\theta = \pi/2$, $\theta = \pi/3$ (blue circles), $\theta = \pi/4$ (red squares), $\theta = \pi/6$ (purple diamonds), and $\theta = \pi/45$ (green triangles).*

5.4 Discussion and Conclusions

In this Chapter, we have used the thermal worldsheet fluctuation method presented in the last chapter to investigate the imaginary part $\mathrm{Im}\, V_{Q\bar{Q}}$ of moving heavy quarkonia in strongly coupled plasmas with gravity duals. We have developed a general formalism to holographically compute $\mathrm{Im}\, V_{Q\bar{Q}}$ in the case where the heavy quark dipole has an arbitrary orientation with respect to the plasma velocity of the underlying strongly coupled plasma. The general formula for this quantity is shown in Eq. (5.48). Also, we have discussed in detail the regime of validity of the method in this case with nonzero rapidity, expanding the discussion of the last Chapter. In fact, we found that the requirement for small thermal fluctuations around the classical worldsheet solution imposes severe constraints in the calculation of $\mathrm{Im}\, V_{Q\bar{Q}}$. The most important constraint in this case is that only slowly moving quarkonia can be considered. In fact, for large rapidities the range of applicability of the saddle point approximation used in the calculation of the imaginary part of the potential decreases significantly. Therefore, the case corresponding to moderately large quarkonia rapidities would require to go beyond the saddle point approximation in the calculation of the string path integral for the worldsheet fluctuations. This challenging task is beyond the scope of the present study and we hope to address this problem in a

future work. It would be interesting to see if the other holographic methods to determine $\mathrm{Im}\, V_{Q\bar{Q}}$ [191, 192] are better suited to tackle the problem of rapidly moving quarkonia (this is the case of the method used in Ref. [207]).

We have applied the worldsheet fluctuation method to evaluate $\mathrm{Im}\, V_{Q\bar{Q}}$ for heavy quarkonia moving through a strongly coupled $\mathcal{N} = 4$ SYM plasma. When the velocity becomes parallel ($\theta \to 0$) to the heavy quark dipole, we find that the imaginary part of the potential becomes smaller than that in the perpendicular case ($\theta = \pi/2$). This shows that at strong coupling the anisotropy induced by the nonzero rapidity of the heavy quark pair becomes a relevant factor in the calculation of the associated thermal width in the plasma, which is suppressed for small angles.

We found a strong dependence of $\mathrm{Im}\, V_{Q\bar{Q}}$ on the rapidity and, taking into account the strict consistency constraints imposed in our holographic setup, for increasing η the onset of the imaginary part of the potential occurs at smaller values of LT, though the precise magnitude of this quantity cannot be reliably determined at the moment with our approximations. Our results indicate that moving quarkonia are indeed less stable in a strongly coupled plasma, which is consistent with previous findings using other approaches [207, 219, 220, 222].

It would be interesting to extend the calculations performed here to other gravity backgrounds, such as those that display a confinement-deconfinement transition described by bottom-up Einstein + Scalar models [15–17, 185, 224].

The results of this Chapter were accepted for publication in JHEP [19]. [2]

[2] We should also mention Ref. [225] which also discussed the effects of nonzero rapidity on the imaginary part of the heavy quark potential. In their work, they computed $\mathrm{Im}\, V_{Q\bar{Q}}$ only for parallel and perpendicular configurations. In our work we not only considered arbitrary orientations of the dipole with respect to the hot plasma wind but also discussed in detail the regime of applicability of the calculations done using the saddle point approximation (this critical analysis was not performed in Ref. [225]).

Chapter 6

Debye Screening Mass at Strong Coupling from Holography

6.1 Introduction

In the deconfined phase of non-Abelian gauge theories, the inverse of the Debye screening mass, m_D^{-1}, can be used to define a screening length of the thermal medium that roughly signals the effective maximum interaction distance between two colored heavy probes. Debye screening is the mechanism behind Matsui and Satz's well known proposal [226] that the "melting" (dissociation) of heavy quarkonia states in the QGP is a signature of deconfinement.

Although in weakly coupled Abelian and non-Abelian plasmas the Debye screening mass has been calculated long ago at one loop in perturbation theory [5, 61, 227], higher order perturbative calculations [228–231] indicate the breakdown of the perturbation series expansion for this quantity. Thus, a non-perturbative, gauge invariant definition of the Debye screening mass is needed. A definition that is inherently non-perturbative and gauge invariant was proposed by Arnold and Yaffe in Ref. [232] where m_D was defined as the largest inverse screening length among all the possible Euclidean correlation functions involving pairs of CT-odd operators in the thermal gauge field theory. Previous studies concerning thermal screening lengths in non-Abelian plasmas include lattice calculations [233–239], non-perturbative analyses of the gluon propagator at finite temperature [240–243], other analytical approaches [244, 245], and holographic calculations [184, 246, 247].

In this Chapter we use the gauge/gravity duality [14, 93, 94, 126] to understand the general properties of the smallest thermal screening mass associated with the CT-odd operator, $\sim \mathrm{Tr} F_{\mu\nu}\tilde{F}^{\mu\nu}$, in non-conformal strongly coupled plasmas described by Einstein gravity plus a scalar field. We shall follow Ref. [184] and *identify* this thermal screening mass as the Debye mass m_D in the strongly-coupled plasma. After associating this Debye

screening mass in the field theory with the lowest lying mass in the spectrum [249,250] of axion fluctuations in the bulk [184], we show (given some reasonable conditions regarding the axion effective action) that the bulk axion spectrum is gapped, positive, and discrete in the deconfined phase of these theories. This shows that this thermal screening radius, which may be relevant for the melting of heavy quarkonia in this class of strongly-coupled large N_c plasmas, is necessarily finite (even in the case of a second order deconfining transition). Also, we find that m_D/T generally follows the behavior of the expectation value of the Polyakov loop operator near the phase transition. In fact, for a first order deconfinement phase transition m_D/T jumps from zero below the critical temperature T_c to a finite value immediately above it.

To estimate the behavior of this screening mass in a non-conformal strongly coupled plasma with similar properties to the QCD plasma, we consider a variety of holographic bottom-up models constructed using 5 dimensional Einstein + scalar effective bulk actions. The first model, which we call Model A, is built in the context of Improved Holographic QCD (IHQCD) [16,17,209,224,252], being a simple analytical model [253] involving an Einstein+scalar gravity bulk action dual to a strongly coupled non-Abelian which possesses a first order confinement/deconfinement phase transition. The second class of models (Model B) [15, 137, 254] are also based on Einstein+scalar bulk actions but now the scalar potentials are chosen in order to reproduce some lattice QCD thermodynamical results. The model that reproduces lattice data for pure SU(3) Yang-Mills, which possesses a first order deconfinement transition [74,255,256], is called Model B1, whereas the model that matches lattice data for QCD with (2+1) light flavors of quarks [78] is called Model B2. For all models, A, B1, and B2, we obtain, numerically, the screening mass m_D as a function of the temperature T. For models A and B1, both of which present a first order phase transition, we explicitly verify the existence of a discontinuity in m_D/T at the critical temperature T_c, where m_D/T jumps discontinuously from 0 to a finite value above T_c. For the model B2, which displays a crossover phase transition, m_D/T increases with T smoothly from 0 and has a local minimum at a given temperature (following a behavior similar to that shown by the speed of sound), after which it then continuously rises to its conformal limit.

As a final application, we consider the screening mass in a strongly coupled conformal plasma dual to Gauss-Bonnet gravity [146, 194]. In this theory the shear viscosity to entropy density ratio, η/s, is different than $1/(4\pi)$ [90,143,145] for a range of values of the controlling parameter of the theory, λ_{GB}, associated with the higher order derivatives in the action as shown in [91,92]. Thus, in this case one can see how m_D/T depends upon η/s in this strongly coupled plasma and compare with the results of the phenomenological approach based on fits to the heavy quark potential at strong coupling pursued in Chapter

4. We find the intriguing result that m_D/T decreases with increasing η/s.

This Chapter is organized as follows: in Section 6.2 we motivate the non-perturbative definition of thermal screening lengths in non-Abelian gauge theories and present the holographic prescription for evaluating these quantities in strongly coupled plasmas dual to bottom-up theories of gravity involving the metric and a scalar field. In this section we also present some general results for the thermal screening mass associated with $\mathrm{Tr}F_{\mu\nu}\tilde{F}^{\mu\nu}$ which are valid in this holographic framework. In Section 6.3 we briefly review the results and techniques of Refs. [184, 249, 250] for evaluating this thermal screening mass in a strongly coupled $\mathcal{N}=4$ SYM plasma. Section 6.4 is dedicated to the evaluation of m_D and the Polyakov loop in Model A. In Section 6.5 we review some general results for the B class of models pertinent to our purposes. Section 6.6 (Section 6.7) is reserved for the evaluation of m_D in the B1 Model (B2 Model, respectively). We show that the heavy quark free energy (extracted from the expectation value of the Polyakov loop) in these holographic models for $SU(N_c)$ Yang-Mills theory nicely describes recent lattice data [257]. In Section 6.8 we analyze $m_D \times \eta/s$ in Gauss-Bonnet gravity. Section 6.9 contains our conclusions and outlook[1].

6.2 General Results For The Holographic Debye Screening Mass

In this section, after some preliminary results on screening lengths in thermal gauge theories, we will review the non-perturbative definition of the Debye screening mass. Then, we will motivate the holographic prescription for the evaluation of the Debye mass and explore some general properties of the Debye screening mass extracted holographically.

6.2.1 Screening lengths in thermal gauge theories

Let $\hat{O}$ be a gauge invariant operator and consider the (equal-time) Euclidean 2-point correlation function

$$G_E(\vec{x}) \equiv \langle 0|\hat{O}^\dagger(\vec{x})\hat{O}(\vec{0})|0\rangle. \tag{6.1}$$

A QFT in thermal equilibrium can, as usual, be studied using the Matsubara (or imaginary time) formalism [61] (as discussed in Section 2.4), where we consider the compactification

[1]Supporting this Chapter, we have two Appendices. In Appendix E we review the perturbative compuation in QED and QCD of the Debye screening mass at one loop in perturbation theory, also pausing to present some more aspects of the physical significance of the Debye screening mass. Appendix F is reserved to supporting results for our holographic computations. Appendix F.1 shows the relationship between Einstein and string frame, necessary to properly compute Polyakov loops. In Appendix F.2 we present the technical details of a coordinate change used in the study of the B models. We also present the evaluation of the glueball spectrum at $T=0$ in Model B1 in Appendix F.3.

of the imaginary time $\tau = it$ direction in a circle of radius $\beta = 1/T$, where T is the temperature of the thermal bath. A key insight to this discussion [184, 232] is that the resulting Euclidean symmetry allows us, instead of compactifying along the time direction, to compactify along any of the spatial directions; for instance, we may compactify along the x spatial direction. Let $\{|n\rangle\}$ be a complete set of eigenstates of the translation operator H_E along the x direction, with corresponding eigenvalues E_n. Then, inserting the completeness relation for the basis $\{|n\rangle\}$ one finds

$$G_E(x) = \sum_{n=0}^{\infty} \langle 0|\hat{O}^\dagger(x)|n\rangle\langle n|\hat{O}(0)|0\rangle. \tag{6.2}$$

Since H_E is an Euclidean translation operator

$$\hat{O}(x) = e^{H_E|x|}\hat{O}(0)e^{-H_E|x|} \tag{6.3}$$

and, thus,

$$G_E(x) = \sum_{n=0}^{\infty} e^{-E_n|x|}|c_n|^2, \tag{6.4}$$

where

$$c_n \equiv \langle n|\hat{O}(0)|0\rangle. \tag{6.5}$$

For large spatial separations, the ground state contribution to Eq. (6.4) dominates and

$$G_E(x) \sim e^{-E_0|x|}|c_0|^2. \tag{6.6}$$

Thus, E_0^{-1} may be taken as the screening length of $G_E(x)$ - for distances $|x|$ greater than E_0^{-1} the fluctuations of $\hat{O}$ are effectively not correlated.

6.2.2 Non-perturbative definition of the Debye screening mass

In this section we briefly review the non-perturbative definition of the Debye screening mass proposed in [232].

In quantum electrodynamics (QED), perturbatively, the Debye screening mass m_D is defined as the pole in 00 component of the photon propagator at zero frequency, $\Pi_{00}(0, \vec{p}^2)$ (Figure 6.1) - i.e., the solution of

$$\Pi_{00}(0, \vec{p}^2 = -m_D^2) + m_D^2 = 0. \tag{6.7}$$

The screening length of the static potential of two static test charges is given by the inverse Debye mass m_D^{-1}. Magnetic fields are unscreened in perturbation theory so that $\Pi_{ij} \to 0$ as

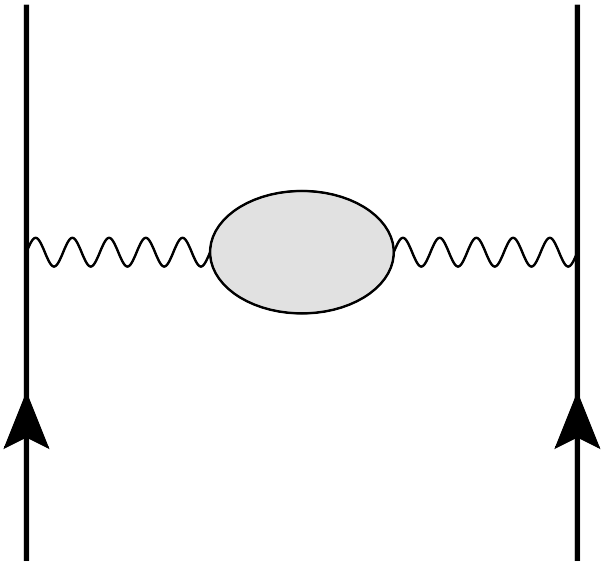

Figure 6.1: *Perturbative definition of the Debye mass. A single photon (gluon) is exchanged between two static test charges. The pole of the photon (gluon) propagator at zero frequency gives the Debye screening mass m_D, the inverse screening length of the static potential.*

$\vec{p} \to 0$ - the Debye screening mass captures the physics of electric screening. This definition can be applied perturbatively to non-Abelian gauge theories, yielding the lowest order, one-loop, perturbative result in the ultrarelativistic approximation (neglecting particle masses and chemical potentials) [5, 61, 227]

$$m_D = \sqrt{\frac{N_c}{3} + \frac{N_f}{6}} gT + O(g^2 T), \tag{6.8}$$

for an $SU(N_c)$ gauge theory with N_f minimally coupled fermions, where g is the gauge theory coupling constant. In Appendix E we review the details of this computation, which serves as a contrapoint to the non-perturbative, geometric, approach pursued by the gauge/gravity duality.

This definition is not valid non-perturbatively, for it suffers from two basic problems beyond the lowest, one-loop, order: (a) the order g^2T correction already receives contributions beyond perturbation theory [228–231] and (b) it is not gauge-invariant in non-Abelian theories. Point (b) can be illustrated by considering that, in QED, an equivalent definition of m_D is

$$\langle \vec{E}(\vec{x}) \rangle \cdot \vec{E}(\vec{0}) \rangle \sim \frac{e^{-m_D |\vec{x}|}}{|\vec{x}|^3} \qquad \text{for } |\vec{x}| \to \infty, \tag{6.9}$$

where the correlation function is defined at equal times. However, although $\vec{E}$ is gauge invariant in QED, the chromo-electric field $\vec{E}_a$ in a non-Abelian gauge theory is clearly not

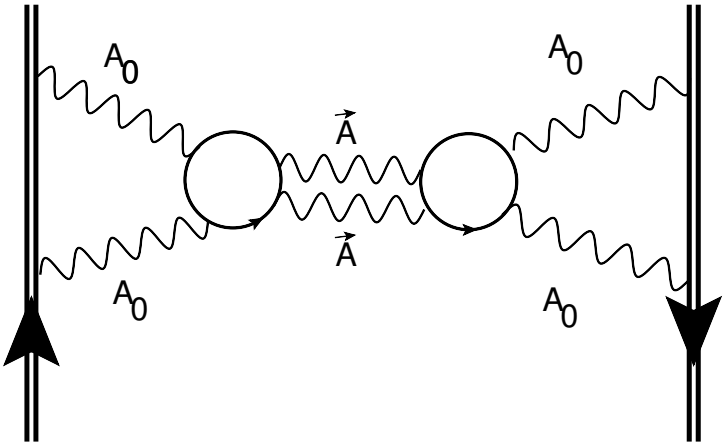

Figure 6.2: *Two Polyakov loops directly coupled to electric photons but indirectly to magnetic photons.*

gauge-invariant. Thus, definition (6.9) does not yield a gauge invariant screening length in a non-Abelian gauge theory.

A tentative gauge-invariant, non-perturbative, definition of the Debye screening mass used sometimes in the literature is achieved through of the correlator of two Polyakov loops. Let $L(\vec{x})$ be the Polyakov loop operator,

$$L(\vec{x}) = \frac{1}{N_c}\mathrm{Tr}\, P \exp\left(i\int_0^\beta A_0(\tau,\vec{x})d\tau\right), \tag{6.10}$$

where P indicates path-ordering, N_c is the number of colors and the trace is in the fundamental representation. Then, the Debye mass would be defined by

$$\langle L(\vec{x})L^\dagger(0)\rangle \sim e^{-m_D|\vec{x}|} \qquad \text{as } |\vec{x}| \to \infty. \tag{6.11}$$

However, this definition does not capture the nature of the electric screening, even in QED; although the Polyakov loop operator couples directly only to electric (A_0) photons, the electric photons can, in turn, couple to unscreened magnetic photons ($\vec{A}$), as indicated in Figure 6.2. In a non-Abelian gauge theory, such coupling to magnetic gluons can be achieved even more directly by exchaging the fermion loops in Figure 6.2 by two four-gluon vertices.

Ref. [232] proposed a way to define the Debye screening mass in an explicit gauge invariant (and non-perturbative) manner using Euclidean time reflection symmetry that is useful in the context of strongly-coupled plasmas. Consider the CT (the composite of time reversal T and charge conjugation C) transformation in real time. The corresponding symmetry in Euclidean time is R_τ, where R_τ is the imaginary (Euclidean) time reflection. To see this, note that any Lorentz invariant theory must have CPT symmetry, where

P stands for spatial inversion. Correspondingly, any Euclidean invariant theory must be rotation invariant. Since PR_τ is a pure rotation in an Euclidean theory, CPT must correspond to PR_τ. Also given that P is time independent, R_τ must correspond to CT. Since A_0 is even under R_τ and $\vec{A}$ is odd under R_τ, the authors of Ref. [232] defined the Debye screening mass m_D as the inverse of the largest correlation length (or, equivalently, the smallest screening mass) of all correlation functions $\langle \hat{A}(\vec{x})\hat{B}(\vec{0})\rangle$ involving two local, gauge invariant operators $\hat{A}$, $\hat{B}$, both odd under Euclidean time reflection R_τ (CT in real time). This construction explicitly removes the magnetic gluon exchange and takes into account only the chromo-electric gluons. Thus, according to [232], the Debye screening mass may be defined as the largest inverse screening length in this channel

$$G_E(\vec{x}) = \langle \hat{A}(\vec{x})\hat{B}(\vec{0})\rangle \sim e^{-m_D|\vec{x}|} \quad \text{as } |\vec{x}| \to \infty\,. \tag{6.12}$$

In our study, we will consider the CT odd operator $\mathrm{Tr}\, F^a_{\mu\nu}\tilde{F}^{b,\mu\nu}$, where $\tilde{F}$ is the dual field strength to F and assume that it sources the Debye mass. Thus, our problem is then to find the largest screening length of the correlation function $\langle \mathrm{Tr}\, F^a_{\mu\nu}\tilde{F}^{b,\mu\nu}(\vec{x})\mathrm{Tr}\, F^a_{\mu\nu}\tilde{F}^{b,\mu\nu}(\vec{0})\rangle$.

6.2.3 An alternative definition of the Debye screening mass

Consider a (3+1) dimensional thermal non-Abelian plasma (with some fermionic degrees of freedom coupled to the gauge fields) in the Matsubara formalism. The partition function of the theory is

$$Z = \int \left[D\bar{\psi}\right]\left[D\psi\right]\left[DA\right]\exp\left[-\frac{1}{g^2}\int_0^\beta d\tau \int d^3x \mathcal{L}_E\right], \tag{6.13}$$

where $\mathcal{L}_E$ is the Euclidean lagrangean density and g is the coupling constant. As usual, all bosonic (fermionic) fields satisfy periodic (anti-perodic, respectively) boundary conditions. Let L be a typical length scale of the theory. For example, it may be the confinement length scale Λ^{-1} or the inverse of the confinement/deconfinement transition temperature, T_c^{-1}. Suppose that the temperature is high enough, or $\beta L \ll 1$ - effectively, the limit of small compactification radius in the time direction. Then we may integrate Eq. (6.13) in the imaginary time arriving at

$$Z \sim \int \left[DA\right]\exp\left[-\frac{1}{g^2 T}\int d^3x \mathcal{L}_{eff}\right]. \tag{6.14}$$

The fermions, since they obey anti-periodic boundary conditions, become infinitely massive in this limit and decouple from the theory - the effective Lagrangean density $\mathcal{L}_{eff}$ contains only bosonic degrees of freedom. The partition function (6.14) represents the

partition function of a 3 dimensional Euclidean gauge theory at $T = 0$. The degrees of freedom of this theory are the gauge field $\vec{A}_a$ (the spatial components of the original gauge field) and a scalar field in the adjoint representation of the gauge group, A_a^0. However, as A_a^0 gets a mass of order gT, it also decouples from the theory. The resulting effective theory is a 3 dimensional pure Yang-Mills theory. Thus, the physical states of the effective theory are glueballs.

Instead of performing the compactification along the (imaginary) time, we can, as indicated previously, compactify along any spatial direction - say z. The resulting effective theory is unchanged. The R_τ transformation becomes a reflection along the z axis. Thus, we may take the Debye mass of the thermal plasma as the z-reflection odd glueball in the 3 dimensional effective gauge theory.

6.2.4 Holographic prescription for the evaluation of the Debye mass

From the preceding discussion, we see that to evaluate the Debye screening mass we have to evaluate correlation lengths of two point functions in a non-Abelian plasma - or, equivalently, evaluate the R_τ odd glueball spectra in a 3 dimensional Yang-Mills theory at zero temperature. From the holographic standpoint, the extraction of the glueball masses in the large N_c and strong coupling limit was first done in Refs. [249,250]. The holographic prescription for evaluating the glueball masses is to analyze in the theory of gravity dual to the QFT in question the fluctuations of the bulk fields that source, in the corresponding gauge theory, the gauge invariant operators that couple to the glueballs which have the same quantum numbers of the dual bulk field. In the case of the $J^{PC} = 0^{-+}$ glueballs, one must analyze the operator $\mathrm{Tr}\, F^a_{\mu\nu}\tilde{F}^{b,\mu\nu}$ which is sourced by an axion field $a(x)$ in the bulk. The mass spectrum of the glueballs is given by the eigenvalues of the equations of motion of the fluctuations in the bulk.

In this subsection, we will present a justification for this procedure, based directly on the holographic procedure for computing correlation functions [93, 94] (based on the formalism discussed in Ref. [137] and already discussed, in connection with real time correlation functions, in Chapter 3).

Let our gravity dual be described by the background metric (with Euclidean signature)

$$ds^2 = g_{\tau\tau}d\tau^2 + g_{xx}d\vec{x}^2 + g_{rr}dr^2 = e^{2\mathcal{A}(r)}\left[h(r)d\tau^2 + d\vec{x}^2 + e^{2\mathcal{D}(r)}\frac{dr^2}{h(r)}\right]. \tag{6.15}$$

where $\mathcal{A}$,$\mathcal{D}$ and h are functions only of the radial coordinate r. We will suppose that, in this coordinate system, the asymptotically AdS_5 boundary is at $r = 0$ (where $e^{2\mathcal{A}} \sim e^{2B} \sim R^2/r^2$, where R is the asymptotic AdS radius, and also $h \to 1$), and that we have a

black brane horizon at $r = r_H > 0$ (this will be taken to mean that $h(r)$ has a simple zero at $r = r_H$, so that $h \sim h'(r_H)(r - r_H)$). Suppose that the bulk action for the fluctuations of a massless scalar field ϕ_E, associated in the boundary gauge theory with the gauge invariant operator $\hat{O}_\phi$, about this background is given by

$$S = \frac{1}{2}\int d^4x dr \sqrt{g}\left[\frac{1}{2} g^{\mu\nu}\partial_\mu\phi_E\partial_\nu\phi_E\right]. \tag{6.16}$$

Then, as shown in Section 3.7, Eqs. (3.70) and (3.71), (with $q(r) = 1$ and the notation change $z \to r$), we have that the Euclidean correlator in momentum space $G_E(\omega_n, \vec{k})$ is given holographically by

$$G_E(\omega_n, \vec{k}) = \frac{1}{2}\lim_{r\to 0} J_E[\phi](\omega_n, \vec{k}, r), \tag{6.17}$$

where

$$J_E[\phi_E](\omega_n, \vec{k}, r) = \phi_E(-\omega_n, -\vec{k}, r)h(r)e^{2A(r)}\phi_E(\omega_n, \vec{k}, r). \tag{6.18}$$

Let us remember also that the equations of motion are, in coordinate space, given by Eq. (3.58)

$$\partial_\mu\left[\sqrt{g_E}\; g_E^{\mu\nu}\; \partial_\nu\left(\phi_E(\tau, \vec{x}, r)\right)\right] = 0. \tag{6.19}$$

In momentum space, using the specific form of the background (3.54), we obtain (6.20)

$$\left[\partial_r^2 + \left(3\mathcal{A}' + \frac{h'}{h}\right)\partial_r - \frac{1}{h}\left(\frac{\omega_n^2}{h} + \vec{k}^2\right)\right]\phi_E(\omega, \vec{k}, r) = 0. \tag{6.20}$$

Now, the ground state has $\omega_n \to 0$ - we will assume this to simplify the discussion. The near horizon ($r \sim r_H$) behavior of the regular solution is then $\tilde{\phi} \sim const.$ Suppose that $M^2 = -\vec{k}^2$ is an eigenvalue of the equation of motion (6.20). Integrating both sides in r, we get

$$\sqrt{g}g^{rr}\partial_r\phi_E = M^2\int_{r_H}^{r} \phi_E\; dr' \tag{6.21}$$

Thus,

$$G_E(0, \vec{k}) = \frac{M^2}{2}\left[\lim_{r\to 0}\phi_E(\omega_n = 0)\right]\int_{r_H}^{0} dr'\phi_E(\omega_n = 0) \tag{6.22}$$

As the solution is regular, the integral is finite. However, since the geometry is asymptotically AdS_5, the remaining limit in the previous equation is divergent. This means that G_E has a pole at $\vec{k}^2 = -M^2$, corresponding to a state with mass M^2.

6.2.5 General properties of the holographic axion spectrum

Armed with the holographic prescription for extracting the Debye screening mass by means of the bulk axion spectrum, we now examine some general properties of the axion spectrum in a large class of gravity duals. For the remainder of this Chapter, we will write the metric using the notation below

$$ds^2 = e^{2\mathcal{A}(z)}\left(f(z)d\tau^2 + d\vec{x}^2 + \frac{dz^2}{f(z)}\right) \tag{6.23}$$

where $\mathcal{A}(z)$ and $f(z)$ are functions of the conformal radial coordinate z. The horizon is at $z = z_h$ (z_h is a simple zero of $f(z)$), and the asymptotically AdS_5 ($e^{2\mathcal{A}} \sim R^2/z^2$) boundary is at $z = 0$. The action for the fluctuations of the massless axion in these backgrounds is assumed to be of the form[2]

$$S = \frac{1}{32\pi G_5}\int d^5x\,\sqrt{g}\,\left(\mathcal{Z}(z)\,g^{\mu\nu}\partial_\mu a\,\partial_\nu a\right)\,, \tag{6.24}$$

where $G_5 \sim 1/N_c^2$ is the 5-dimensional gravitational constant and $\mathcal{Z}(z)$ is a given function of the holographic coordinate z - the reason for including this axion coupling function is that in certain classes of backgrounds, as in those of Improved Holographic QCD [16, 17, 209, 224, 252], a resummation of the contributions originating from string theory should result in an effective action for the axion that involves this multiplicative factor. The specific form for this function will be defined later in the Chapter.

The equation of motion for the axion is

$$\partial_\mu(\mathcal{Z}(z)e^{5\mathcal{A}}g^{\mu\nu}\partial_\nu a) = 0 \tag{6.25}$$

and, in momentum space (taking the Matsubara frequency to zero since we want the largest inverse correlation length) with the plane wave Ansatz $a(\vec{x}, z) \to e^{i\vec{k}\cdot\vec{x}}a(z)$, one finds the equation of motion (with $M^2 = -\vec{k}^2$)

$$\partial_z(e^{2\mathcal{B}}f(z)a') + M^2e^{2\mathcal{B}}a = 0, \tag{6.26}$$

where $a'(z) = da(z)/dz$ and we have defined the function

$$\mathcal{B}(z) \equiv \frac{3}{2}\mathcal{A}(z) + \frac{1}{2}\log\mathcal{Z}(z)\,. \tag{6.27}$$

An alternative, but useful, form of the equation of motion is obtained by introducing

[2]Note that since in IHQCD the bulk axion is trivial in the background, the action for its fluctuations is easily determined to be the one in (6.24) [258].

$\psi = e^{\mathcal{B}} a$, which leads to

$$-\psi'' - \frac{f'}{f}\psi' + \frac{1}{f}\left[f(\mathcal{B}'^2 + \mathcal{B}'') + f'\mathcal{B}'\right]\psi = \frac{M^2}{f}\psi\,. \tag{6.28}$$

This form of the equation of motion is especially useful at zero temperature where $f = 1$. In this case, we have the Schrödinger-like equation

$$-\psi'' + \mathcal{V}(z)\psi = M^2\psi, \tag{6.29}$$

where the potential $\mathcal{V}$ is defined as

$$\mathcal{V}(z) = \mathcal{B}'(z)^2 + \mathcal{B}''(z)\,. \tag{6.30}$$

The pole of the corresponding Euclidean Green's function is obtained by imposing a Dirichlet condition for the fluctuation at the boundary while at the horizon z_h the axion fluctuation must be finite. This completely specifies the eigenvalue problem to find M^2.

Let us now state some basic facts about the bulk axion spectrum in these theories. First, M^2 is real. Second, the spectrum is gapped ($M^2 > 0$) if there is a black brane horizon in the bulk. Third, the spectrum is discrete.

That the spectrum is purely real follows simply from the fact that Eq. (6.26) and its boundary conditions are posed as a Sturm-Liouville problem.

Now, let us analyze the mass gap. It is easy to see $M = 0$ is not in the spectrum. If $M = 0$, then the equation of motion (6.26) can be easily integrated yielding two linearly independent solutions, $a \propto$ const and $a \propto \int dz\, e^{-2\mathcal{B}} f^{-1}$. The solution $a \propto$ constant $\neq 0$ is not normalizable in the UV and must be discarded. The other solution is normalizable; however, near the horizon, as $f(z) \sim -|f'(z_h)|(z_h - z)$ and $\mathcal{B} \sim \mathcal{B}(z_h)$, $a \propto \log(z - z_h) \to \infty$. Thus, the normalizable solution in the UV is not finite on the horizon. Thus, $M = 0$ does not satisfy the boundary conditions and is not in spectrum if there is a horizon.

To prove that $M^2 < 0$ is not allowed we employ an argument used by Witten [126]. The equation of motion (6.26) can be obtained from the on shell action

$$\frac{1}{32\pi G_5\, T}\int_0^{z_h} dz\, \mathcal{Z}(z) e^{3\mathcal{A}}\left[f(\partial_z a)^2 - M^2 a^2\right]\,. \tag{6.31}$$

If a is a normalizable solution of the equations of motion, then after integrating Eq. (6.31) by parts one sees that it must vanish. Now, suppose that $M^2 < 0$. Then in Eq. (6.31) both terms are strictly positive. Thus, we must have $da/dz = 0$ and $a = 0$, since the solution is normalizable. This is just the trivial solution and, thus, $M^2 < 0$ cannot be an eigenvalue of the equation of motion. Therefore, as we have already shown that $M \neq 0$, we see that

$M^2 > 0$. This shows the existence of the mass gap.

Finally, intuitively, the spectrum must be discrete - the axion is confined into an asymptotically AdS_5 spacetime with a black brane deep in the bulk. The Dirichlet asymptotic boundary and the horizon work as two "walls" that confine the axion into an infinite well, hence the discrete spectrum.

6.3 Debye screening mass in $\mathcal{N} = 4$ SYM

6.3.1 The axion spectrum

In this section we review the holographic evaluation of the Debye mass (i.e., the smallest thermal mass associated with axion fluctuations in the bulk) in a strongly coupled $\mathcal{N} = 4$ SYM plasma by means of the gauge/gravity duality [184]. Since the dilaton is constant in this case the equations of motion for the dilaton and the axion fluctuations are degenerate. Also, the $\mathcal{Z}$ function is constant and one can set it to unity since one can consistently set the other bulk fields in type IIB supergravity, apart from the metric and the five-form F_5, to be trivial. Thus, one can simply retrieve the result from Ref. [249] for the spectrum of a massless scalar field in a Schwarzschild AdS_5 background. The final result for the ground state is given by Ref. [184]

$$m_D = c\,\pi\,T \tag{6.32}$$

where $c = 3.4041$. Since the analytical and numerical procedures used in this case will be applied with minimal changes in the next two sections, it will be useful to review here the numerical procedure used to determine the constant c defined above in some detail.

The Schwarzschild AdS_5 metric is written in the Poincaré patch as (recall Eq. (3.40))

$$ds^2 = \frac{R^2}{z^2}\left(f(z)d\tau^2 + d\vec{x}^2 + \frac{dz^2}{f(z)}\right) \tag{6.33}$$

where $f(z) = 1 - z^4/z_h^4$, and where z_h is the z-coordinate of the black brane horizon. The black hole temperature is $T = \pi R^2 z_h$. The equation of motion is given by Eq. (6.29); it is useful to write it in terms of the normalized variable $u = z/z_h = \pi R^2 T z$ and the dimensionless mass $\tilde{M} = M/(\pi T)$. We need to match the solution of equation of motion Eq. (6.29) with the asymptotic equation of motion near the boundary, $z \to 0$,

$$-\frac{d^2\psi}{du^2} + \mathcal{V}_{\rm asy}\psi = \tilde{M}^2\psi, \tag{6.34}$$

with the asymptotic potential $\mathcal{V}_{\rm asy}(u) = \mathcal{V}(u \to 0) = 15/(4u^2)$ (see Eq. (6.30)). The

general solution of the asymptotic equation (6.34) is

$$\psi(u) = C_1\sqrt{u}[J_2(\tilde{M}u) + C_2 Y_2(\tilde{M}u)], \tag{6.35}$$

where J_n and Y_n are Bessel functions of the first and second kind, respectively, and C_1, C_2 are integration constants. Since Y_2 does not vanish at the boundary, we pick J_2 as the asymptotic solution setting $C_2 = 0$. The coefficient C_1 is chosen to fix the leading coefficient of the series expansion of the Bessel function to 1; then $C_1 = M^2/8$. Thus, at the boundary, the full solution ψ must match the asymptotic solution

$$\psi_{asy}(u) = \frac{8\sqrt{u}}{\tilde{M}^2} J_2(\tilde{M}u) = u^{5/2} - \frac{1}{12}\tilde{M}^2 u^{9/2} + \frac{1}{384}\tilde{M}^4 u^{13/2} + \mathcal{O}(\tilde{M}^6 u^{17/2}). \tag{6.36}$$

To obtain the axion spectrum numerically we use a shooting procedure. One starts with an initial value for $\tilde{M}^2$ and numerically solve the equation of motion (6.28) imposing as boundary conditions that the solution $\psi(u)$ matches the asymptotic solution (6.36) and its first derivative for some $u_0 \ll 1$. One then integrates the initial value problem up to near the horizon. When $\tilde{M}^2$ is not an exact eigenvalue $\psi(u)$ diverges at the horizon. However, $\psi(u \to 1)$ changes sign when one passes by an exact eigenvalue and, thus, one can bracket it by scanning when such sign change happens. Care must be taken to certify that one has not missed the ground state (or an excited state) by starting with values of $\tilde{M}^2$ only slightly above zero. Proceeding this way, one obtains for the ground state of the axion spectrum $\tilde{M} = m_D/(\pi T)$ the result (6.32).

6.4 Debye screening mass in Model A

6.4.1 A simple model of IHQCD

General IHQCD backgrounds

For an interesting, slightly more realistic, toy model for a pure Yang-Mills plasma at strong coupling, we will explore a simple, analytic, Improved Holographic QCD (IHQCD) model which presents a first order confinement/deconfinement transition, which we will name in this thesis Model A. This model is based on the Einstein+dilaton models studied by Gursoy et al. [16, 17, 209, 224, 252, 253], where the dilaton ϕ in the bulk is chosen as to correspond to the gauge coupling the dual gauge theory. The effective five dimensional action, in the Einstein frame, for the metric and the dilaton in IHQCD is

$$S = \frac{1}{16\pi G_5}\int g^5 x\sqrt{g}\left[R - \frac{4}{3}(\partial\phi)^2 + V(\phi)\right], \tag{6.37}$$

plus a Gibbons-Hawking boundary term, necessary to give a well posed variational problem (this term and other contributions needed in the process of holographic renormalization [121, 122] do not affect our discussion and are, thus, dropped altogether). The action (6.37) also picks a UV divergence from its asymptotic AdS_5 boundary - this means that one has include counterterms in order to render the action finite. However, for our discussion, it is not necessary to perform the full holographic renormalization procedure. The potential $V(\phi)$ is assumed to contain part of the sub-critical 5d string theory contributions to the effective action. The metric background (in the Einstein frame) is written in the conformal gauge in the usual form

$$ds^2 = b(z)^2\left[f(z)d\tau^2 + d\vec{x}^2 + \frac{dz^2}{f(z)}\right], \tag{6.38}$$

while the dilaton will be assumed to depend only upon the radial coordinate z, $\phi = \phi(z)$. The boundary is at $z \to 0$. Comparing with Eq. (**??**), we see that $b(z) = e^{A(z)}$. The Einstein's and scalar equations of motion that follow from extremizing Eq. (6.37) are

$$\begin{aligned} \frac{f''}{f'} + 3\frac{b'}{b} &= 0, \\ 6\frac{b'^2}{b^2} - 3\frac{b''}{b} &= \frac{4}{3}\phi'^2 \qquad \text{and} \\ 6\frac{b'^2}{b^2} + 3\frac{b''}{b} + 3\frac{b'}{b}\frac{f'}{f} &= \frac{b^2}{f}V, \end{aligned} \tag{6.39}$$

where the prime indicates differentiation with respect to z. The equation of motion for ϕ is a combination of the previous equations - as usual for Einstein's equations there is some redundancy in the equations of motion (due to Bianchi's identity). It is convenient to recast the equations of motion in an alternative form; define $W \equiv -b'/b^2$. Also, introduce $\lambda = e^{\phi}$, the boundary gauge theory coupling [16]. Then,

$$\begin{aligned} f'' &= 3Wbf', \\ W' &= 4W^2 b - \frac{1}{f}\left(Wf' + \frac{1}{3}bV\right) \qquad \text{and} \\ \frac{\lambda'}{\lambda} &= \frac{3}{2}\sqrt{bW'}. \end{aligned} \tag{6.40}$$

The beta function of the theory is given by [16]

$$\beta = \frac{\lambda'}{b'/b}. \tag{6.41}$$

The geometry must be asymptotically anti de-Sitter so that we have an UV fixed point: as $z \to 0$, $b \to R/z$. The gravity dual correspond to a confining gauge theory as long as, in the IR, $z \to \infty$, [17, 253]

$$\beta(\lambda) = -\frac{3}{2}\lambda\left[1 + \frac{3(\alpha-1)}{4\alpha}\frac{1}{\log\lambda} + O\left(\frac{1}{\log^2\lambda}\right)\right], \tag{6.42}$$

with $\alpha > 1$. The corresponding IR geometry is

$$b(z) \to e^{(pz)^\alpha}(pz)^p, \tag{6.43}$$

where q and p are constants.

An exact solution - Model A

An analytic solution of the equations of motion (6.40) is given by trying the following ansatz for b, [17, 253]

$$b(z) = \frac{R}{z}e^{-\frac{1}{3}\Lambda^2 z^2}, \tag{6.44}$$

where Λ is an infrared scale, of the order of Λ_{QCD}. All other bulk fields can be found from the equations of motion (6.40). To do so, it is useful to define the dimensionless variable $Z \equiv \Lambda^2 z^2$. Another useful dimensionless variable will be $y = \Lambda z = \sqrt{Z}$. First, we evaluate W

$$\frac{dW}{dz} = 2e^{\frac{\Lambda z^2}{3}}\frac{z\Lambda^2}{R}\left(1 + \frac{2}{9}\Lambda^2\right). \tag{6.45}$$

Then, we solve the last of the equations of motion (6.40) for $d\phi/dZ = (d\lambda/dZ)/\lambda$

$$\frac{d\phi}{dZ} = \frac{1}{2}\sqrt{1 + \frac{9}{4Z}}, \tag{6.46}$$

whose solution leads to (with $\Lambda(Z=0) = \Lambda_0$ being the UV coupling)

$$\frac{\Lambda(Z)}{\Lambda_0} = e^{\frac{1}{2}\sqrt{Z(Z+\frac{9}{2})}}\left[\sqrt{Z} + \sqrt{Z + \frac{9}{2}}\right]^{9/4}. \tag{6.47}$$

The beta function that follows is

$$\beta = -\frac{3}{2}\Lambda\frac{\sqrt{1 + \frac{9}{2Z}}}{1 + \frac{3}{2Z}}. \tag{6.48}$$

In the IR, $Z \to \infty$, as $\Lambda \sim 2 \log Z$,

$$\beta = -\frac{3\Lambda}{2}\left(1 + \frac{3}{8\log\Lambda} + \cdots\right). \tag{6.49}$$

Thus, for this solution, $\alpha = 2$ and we have a confining gauge theory dual. On the other hand, the UV ($Z \to 0$) behavior is

$$\beta = -3\Lambda\sqrt{\frac{y}{2}} + \frac{5\Lambda y^{3/2}}{3\sqrt{2}} + \cdots \tag{6.50}$$

This does not vanish in the UV - this means that the UV fixed point is not trivial and the theory is not asymptotically free. Finally, we can derive the horizon function by integrating the first of the equations of motion (6.40), imposing the boundary conditions $f(0) = 1$ (the geometry is asymptotically AdS), and $f(z_h) = 0$ ($z = z_h$ defines the black brane horizon),

$$f(y, y_h) = 1 - \frac{(y^2-1)e^{y^2}+1}{1 + e^{y_h^2}(y_h^2 - 1)}. \tag{6.51}$$

where $Z_h = \lambda^2 z_h^2$. Finally, the dilaton potential for this solution is given by the second equation in Eq. (6.40),

$$V(y, y_h) = \frac{12}{R^2} e^{\frac{2y^2}{3}} \left[\left(\frac{1}{3}y^4 + \frac{5}{6}y^2 + 1\right) f(y, y_h) - \left(\frac{1}{2} + \frac{1}{3}y^2\right)\frac{y}{2}\frac{\partial f}{\partial y}(y, y_h)\right]. \tag{6.52}$$

Note that the potential depends explicitly on the temperature via the position of the horizon y_h. This is not going to be the case in the other type of models considered in Section6.5.

6.4.2 Thermodynamics

Let us now review the thermodynamics of this solution [17, 253]. The temperature T of the thermal bath is given by the black brane temperature (see Eq. (3.55)):

$$T = \frac{|f'(z_h)|}{4\pi} = \frac{\Lambda}{2\pi}\frac{y_h^3}{y_h^2 - 1 + e^{-y_h^2}}. \tag{6.53}$$

where $y_h \equiv \lambda z_h$. The entropy density is given by the Bekenstein-Hawking formula (3.45), which yields

$$s = \frac{b(z_h)^3}{4G_5} = \frac{R^3\Lambda^3}{4G_5}\frac{e^{-y_h^2}}{y_h^3}. \tag{6.54}$$

Moreover, the pressure follows from $s = \partial p/\partial T$

$$p(y_h) = -\int_{y_h}^{\infty} s(T(x))\frac{dT(x)}{dx} \tag{6.55}$$

and the energy density is given by $\epsilon = sT - p$.

The temperature function $T(y_h)$ has a minimum for $T_{\rm min} = 0.396\Lambda$, $y_h^{\rm min} = 1.466$. For $T < T_{min}$, there is no possible black brane solution and the system is in a thermal gas phase. However, for $T_{\rm min} < T < T_c$, where $T_c = 0.400\Lambda$ is reached at $y_h^c = 1.299$, albeit there is a black brane solution, the pressure is negative - this signs that the thermal plasma is in a metastable phase. For $T > T_c$ (thus, $y_h < y_h^c$), we have a deconfined thermal plasma state. Since the entropy density has a discontinuity at $T = T_c$, the transition is of first order. It is possible to explicitly write the equation of state of the system in terms of the speed of sound squared

$$c_s^2 = \frac{d\log T}{d\log s} = \frac{1}{3+y_h^2}\frac{3 - y_h^2 - (3+2y_h^2)e^{-y_h^2}}{y_h^2 - 1 + e^{-y_h^2}}. \tag{6.56}$$

In Fig. 6.3 we compare the equation of state of this model, given by Eqs. (6.53) and (6.56), with lattice results for a pure glue SU(3) Yang-Mills plasma [255]. We see that this gravity dual provides a reasonable qualitative description of the equation of state of a pure glue plasma, more so considering its relative simplicity and the fact that it is an analytical solution of the Einstein+scalar equations of motion. However, it must be noted that this simple realization of IHQCD does not describe lattice data quantitatively between $T/T_c = 1.1 - 2.5$[3].

6.4.3 Polyakov loop

An interesting observable to compute in this model is the vacuum expectation value of the Polyakov loop operator [160–163] (see also Chapter 4 and Appendix C). Holographically, the evaluation of the Polyakov loop in a thermal gauge theory in the imaginary time formalism corresponds to calculating the classical worldsheet action for a *straight* string in the bulk stretching from the conformal boundary to the horizon. This string worldsheet wraps the imaginary time circle S^1, as discussed in Chapter 4. At strong coupling and large N_c, the norm of the expectation value of the Polyakov loop operator (6.10) is given by

$$|\langle \hat{L} \rangle| \sim e^{-F_Q/T} \sim e^{-S_{NG}}, \tag{6.57}$$

[3]This can be remedied by choosing an appropriate dilaton potential and, as shown in [16, 17, 209, 224, 252], a good quantitative agreement with pure glue lattice QCD thermodynamics in this temperature range can be achieved.

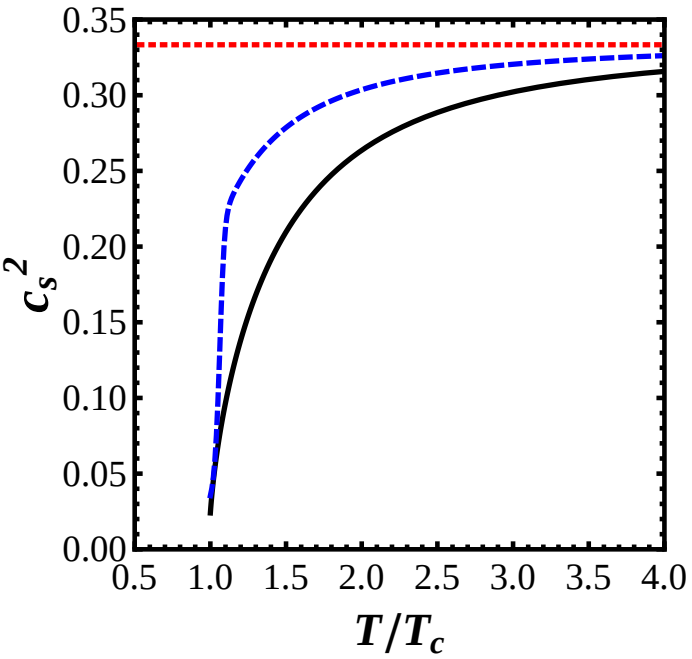

Figure 6.3: *Speed of sound squared c_s^2 of the plasma as a function of T/T_c, where T_c denotes the critical temperature for a deconfining first order transition. The solid black line is the result for the particular IHQCD model studied (see Eq.* **??***), the dashed blue line corresponds to lattice results from [255] for an SU(3) Yang-Mills plasma while the horizontal red line gives the result for a conformal plasma, $c_s^2 = 1/3$.*

Using expression (4.16) with the background (6.38), one can see that

$$\frac{F_Q^{reg} T_c}{\sigma} = -\frac{T_c}{\Lambda b_s^2 y_{min}} \int_{y_h}^{y_h^c} dy b_s(y)^2, \tag{6.58}$$

where $b^{(0)}(y)$ is the vacuum form of $b_s(y)$ and where $b_s \equiv \lambda^{2/3} b$ is the b function in the Einstein frame - since our background comes from a 5 dimensional non-critical string theory, $g^s_{\mu\nu} = \lambda^{4/3} g_{\mu\nu}$, where $g_{\mu\nu}$ is the metric in the Einstein frame [17,253]. In the particular case of Model A, $b_s^{(0)} = b_s$. Also, for comparison with lattice results, we normalized F_Q^{reg} by the string tension σ and by the critical temperature T_c. The holographic string tension in IHQCD is given by [16, 17] $\sigma = L^2 \Lambda^2 b_s^2(y_{min})/(2\pi\alpha')$. The evaluation must be performed at $y = y_{min}$ instead of y_c since at the temperature T_{min} we are still in the thermal glueball gas phase, where the theory is confining and has a string tension.

Note that the Polyakov loop computed on the lattice depends on the choice of renormalization scheme since the heavy quark bare free energy is divergent in the continuum limit (one needs to subtract the divergent part and fix the renormalization constant). In the calculations of Ref. [257] this constant term was set to zero. Clearly, any other value for the constant would be fine and the scheme dependence just corresponds to adding an

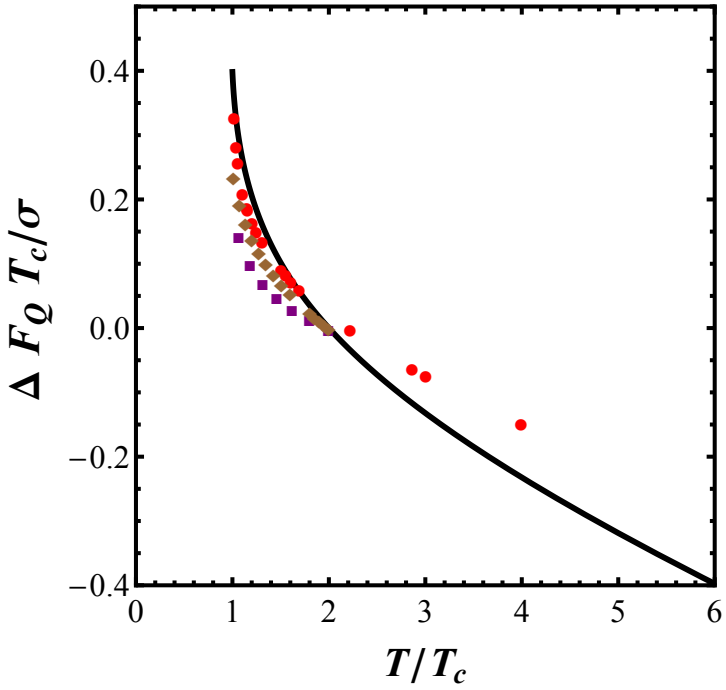

Figure 6.4: $\Delta F_Q T_c/\sigma = (F_Q(T) - F_Q(2T_c))T_c/\sigma$ *as a function of* T/T_c *for model A (solid black line) defined in* **??** *and for* $SU(N_c)$ *Yang-Mills [257] with* $N_c = 3$ *(red circles),* 4 *(purple squares), and* 5 *(brown diamonds).*

additive constant in the free energy of the renormalized Polyakov loop [4]. In this Chapter we chose to compare the free energy difference $\Delta F_Q T_c/\sigma = (F_Q(T) - F_Q(2T_c))T_c/\sigma$ as a function of T/T_c computed in the model with the one found on the lattice (note that this still corresponds to choosing a scheme in which the free energy difference vanishes at $2T_c$).

We compare in Fig. 6.4 the holographic result (6.58) with the lattice results for the $SU(N_c)$ Yang-Mills lattice data with different number of colors from [257]. One can see that even though the thermodynamics of the simple IHQCD model only reproduces qualitatively the lattice data, the holographic result for F_Q gives a reasonable description of the lattice data for $T_c < T < 2T_c$. Moreover, even though holographic models ought to be valid only for large N_c, reasonable agreement is seen even for $N_c = 3$.

6.4.4 Debye screening mass

Axion spectrum in the vacuum

Let us begin by studying the bulk axion spectrum at $T = 0$ (i.e., we set $f = 1$). The first step is to discuss the function $\mathcal{Z}$ in the action for the axion fluctuations (6.24), which represents a partial resummation of higher order forms coming from 5-dimensional

[4] We thank M. Panero for discussions about this point.

c_4	m_{axion}/Λ
0.1	3.0433
1.0	2.996
10.0	2.986

Table 6.1: *Glueball mass $m_{J^{PC}=0^{-+}}$ associated with the bulk axion at $T = 0$ for some choices of c_4 computed using Model A.*

sub-critical string theory [16, 17]. In the UV, $Z(\lambda) \sim$ const while in the IR $(\lambda) \propto \lambda^4$ to ensure glueball universality. We will use the following standard IHQCD parametrization that interpolates between these two cases [258]

$$Z(\lambda) = c_0 + c_4\lambda^4, \tag{6.59}$$

where c_0 and c_4 are constants. By a suitable normalization of the action one can set $c_0 = 1$. To study the dependence of the results with c_4, we choose three values for it spanning a large range of values for this coefficient: 0.1, 1, and 10.

The numerical procedure to find the spectrum is the same as the one described in 6.3. For the vacuum case we consider the Schrödinger equation (6.29) and the asymptotic potential in the UV, including the first subleading correction in $1/y$, which gives

$$\mathcal{V}(y) = \frac{15}{4y^2} - \frac{9\sqrt{2}c_4}{(1+c_4)y} + \mathcal{O}(1)\,. \tag{6.60}$$

The asymptotic equation (including the subleading term) can be solved analytically and the linearly independent solutions are Whittaker functions $M_{\kappa,\mu}$ and $W_{\kappa,\mu}$ [193]. If we consider only the leading term in $1/y$, these solutions reduce to the Bessel functions found in 6.3. The normalized near boundary series expansion, including the subleading term in Eq. (6.60), is given by

$$\psi(y) = y^{1/2}\left(y - \frac{9\sqrt{2}c_4}{5}\frac{y^2}{1+c_4} + \cdots\right)\,. \tag{6.61}$$

Using the shooting method to solve the eigenvalue problem, we obtain the results shown in Table 6.1. One can see that glueball mass associated with the bulk axion in the vacuum is quite insensitive to the choice of c_4 and $m_{J^{PC}=0^{-+}} \sim 3\Lambda$. This value is also comparable with the corresponding results for the lightest $J^{PC} = 0^{++}$ and $J^{PC} = 2^{++}$ glueballs in this model, $m_{J^{PC}=0^{++}} \approx 2.5\Lambda$ and $m_{J^{PC}=2^{++}} = \sqrt{8}\Lambda \sim 2.2\Lambda$ [253].

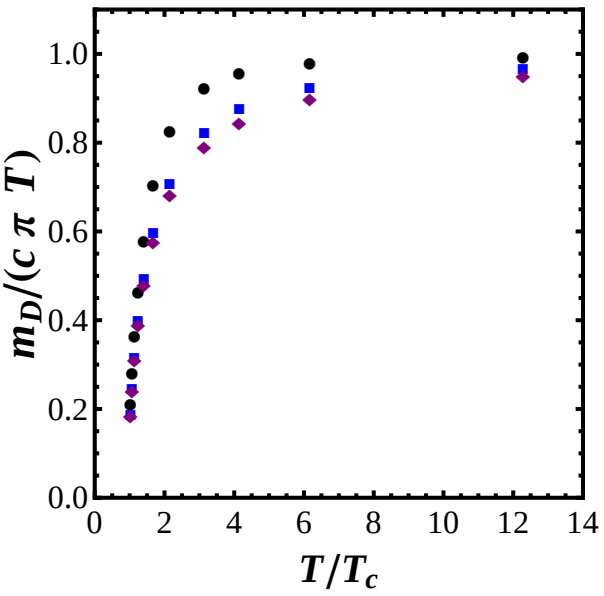

Figure 6.5: *Debye screening mass m_D for the simplified IHQCD model A discussed in Eq.* **??**, *normalized by the $\mathcal{N} = 4$ SYM Debye mass at strong coupling $c\pi T$ with $c = 3.4041$. We present the results for $c_4 = 0.1$ (black circles), 1 (blue squares) and 10 (purple diamonds).*

Debye screening mass

Let us now proceed to extract the Debye screening mass in this model. Consider now the background at nonzero temperature. The equation of motion to solve is now of the form (6.28). The asymptotic solution is the same as in the $T = 0$ case since $f \to 1$ for $y \to 0$. We use the same choices for c_4 employed in the preceding calculation. Our results can be found in Fig. 6.5. Since at high temperatures $T \gg \Lambda$ the geometry of the gravity dual simplifies to AdS_5, one must have $m_D(T \gg \lambda) \to c\,\pi T$ with $c = 3.4041$ as shown in Section 6.3. Thus, our results for m_D are normalized by $c\,\pi T$.

One can see that the results are somewhat insensitive to the choice of c_4 as long as $c_4 \gtrsim 1$. Also, we note that for $T \to T_c^+$, $m_D/(c\pi T) \sim 0.18$, which is nearly independent of c_4 - the Debye mass has a discontinuity at $T = T_c$. As expected, for increasing temperature, the plasma becomes more and more screened - m_D is monotonically increasing with T until it reaches its conformal value.

Ref. [246] computed the thermal screening lengths for an $\mathcal{N} = 2^*$ plasma, which is non-conformal deformation of the $\mathcal{N} = 4$ SYM plasma obtained by giving a mass μ to the adjoint scalars and fermions [259–261]. Using this top-down non-conformal construction [246] also obtained that m_D/T (computed from the axion fluctuations) becomes smaller than its conformal value at low temperatures when $\mu/T > 1$. However, this theory does not possess a finite temperature phase transition and, thus, the discontinuity in m_D/T at T_c found here is a new feature brought in by the non-conformal plasmas constructed within IHQCD.

6.5 B class of models - Overview

In this section we shall describe a second class (Model B) of strongly coupled non-Abelian plasmas with gravity duals described by Einsten+scalar actions [15,137,254] (see also [185,186]) built in order to reproduce some of the thermodynamic results obtained on the lattice at zero baryon chemical potential. Even though the bulk fields are the same as in the previous section, in these models the scalar field corresponds to a relevant operator in the UV.

The interpretation put forward in Ref. [254] is that since these gravity models cannot truly describe perturbative QCD physics in the UV, one must choose an intermediate semi-hard scale at which asymptotic freedom is replaced by conformal invariance. In fact, given that the scaling dimension Δ of the glueball operator $\mathrm{Tr}\, F^2$ is not a protected quantity in QCD and it becomes smaller than 4 towards the IR, this semi-hard scale may be used to define the range of applicability of this effective holographic model in this context. This implies that, in general, these models should not be used at high temperatures where asymptotic freedom becomes dominant. However, as will be shown in Chapters 7 and 8, these non-conformal bottom-up models are able to describe not only the equilibrium quantities found on the lattice but also the temperature dependence of some nontrivial transport coefficients such as the electrical conductivity recently computed on the lattice [262] and transport coefficients associated with second order hydrodynamics. Moreover, these models also give valuable insight into the energy loss experienced by heavy (and also light quarks) in the QGP near the crossover phase transition [263–265]. Therefore, we believe that it is relevant to consider these constructions here as well and investigate the temperature dependence of m_D/T in these models. We shall see that by carefully choosing the scalar potential one can obtain a much better quantitative description of the thermodynamics of pure glue as well as that of QCD with light dynamical flavors found on the lattice[5].

6.5.1 Bulk action

Even though the bulk action that defines these models is the same as that studied in Section 6.4, we find it convenient to follow the convention of Ref. [15] (compare the dilaton normalization in Eq. (6.37) with the one below) where the Einstein+scalar action is

$$S = \frac{1}{2\kappa_5^2}\int d^5x\,\sqrt{g}\left[\mathcal{R} - \frac{1}{2}(\partial_\mu\phi)(\partial^\mu\phi) - V(\phi)\right], \tag{6.62}$$

[5] We note that the models considered here do not have the correct bulk degrees of freedom to fully describe the physics associated with chiral symmetry breaking. See Refs. [266, 267] for a model which describes chiral symmetry breaking in this class of Einstein + scalar models by including a second scalar field, following the spirit of the KKSS model [268].

where $k_5^2 = 8\pi G_5$. The scalar field in this action is related to the dilaton in Model A (6.37) by a factor of $\sqrt{3/8}$. The potential $V(\phi)$ is chosen in such a way that the thermodynamic properties of the model (6.62) mimic the ones desired from the gauge theory - in the next subsections we will describe simple choices of $V(\phi)$ which achieve this task. The desired solutions of Eq. (6.62) must be asymptotically AdS_5 for the boundary gauge theory to have a UV fixed point. The potential $V(\phi)$ is chosen in order to interpolate between a free massive scalar field (plus cosmological constant term) near the boundary, $V(\phi) \sim -12/R^2 + m^2\phi^2/2$, and a potential which yields the Chamblin-Reall solution [269] deep in the bulk, $V(\phi) = V_0 e^{\gamma\phi}$, with $\gamma < 0$.

6.5.2 Metric ansatz

As we wish to study the gauge theory at finite temperature, the solution also must contain a black brane in the bulk. We also want translation symmetry in the gauge theory and rotational SO(3) symmetry in the spatial directions but not the full Lorentz SO(3,1) symmetry since the at nonzero temperature the thermal gauge theory is not invariant by Lorentz boosts. An Ansatz which is able to satisfy these requirements, called here the Gubser gauge [15], is

$$ds^2 = e^{2A}(h\, d\tau^2 + d\vec{x}^2) + e^{2B}\frac{d\phi^2}{h}, \tag{6.63}$$

where the holographic radial coordinate is given by the scalar field ϕ itself. We require that A, B, and h are only functions of ϕ, i.e., $A(\phi)$, $B(\phi)$, and $h(\phi)$. The asymptotically AdS_5 boundary is recovered when $\phi \to 0$. This choice, as shown in Ref. [15], is convenient to solve the equations of motion for the action (6.62). However, this gauge choice is not very useful for analyzing the glueball spectra or studying Wilson and Polyakov loops. For these purposes, it is convenient to go back to conformal gauge. We discuss this point in more detail in Appendix F.2.

6.5.3 The equations of motion

It is possible to write a "master" equation that yields all the metric functions in the Ansatz (6.63) in terms of a single ordinary first order differential equation [15]. The equations of motion derived from the action (6.62) are the Einstein's equations

$$\mathcal{R}_{\mu\nu} - \frac{g_{\mu\nu}}{2}\mathcal{R} = 8\pi G_5 T_{\mu\nu}, \tag{6.64}$$

where $T_{\mu\nu}$ is the stress-energy tensor for the scalar field. The equation of motion for the scalar field ϕ is

$$\nabla_\mu \nabla^\mu \phi - V' = 0, \tag{6.65}$$

where ∇ indicates the covariant derivative and $V' = dV/d\phi$ (in this section, primes will always indicate derivatives with respect to ϕ). With the Ansatz (6.63), one can see that the equation of motion for the $\tau\tau$ component is

$$2e^{2B}V + 6A'h' + h(24A'^2 - 12B'A' + 12A'' + 1) = 0 \tag{6.66}$$

while for the xx the equation of motion is

$$2e^{2B}V + 14A'h' - 2B'h' + 2h'' + h(24A'^2 - 12B'A' + 12A'' + 1) = 0\,. \tag{6.67}$$

The common term in parenthesis can be eliminated from both equations, which yields

$$h'' + (4A' - B')h' = 0\,. \tag{6.68}$$

The $G_{\phi\phi}$ equation of motion is

$$6A'h' + h(24A'^2 - 1) + 2Ve^{2B} = 0\,. \tag{6.69}$$

Using the $G_{\tau\tau}$ equation of motion (6.66) to eliminate $24A'^2$ from Eq. (6.66) we obtain

$$A'' - A'B' + \frac{1}{6} = 0\,. \tag{6.70}$$

The last equation of motion is given by the scalar equation (6.65),

$$(4A' - B') + \frac{h'}{h} - \frac{e^{2B}}{h}V' = 0. \tag{6.71}$$

We use the set consisting of Eqs. (6.68) to (6.71) as our equations of motion. These equations are not completely independent due to Bianchi's identity. In this case, the derivative of Eq. (6.70) follows from the derivative of the other equations of motion and one can use any subset of three equations among these to obtain the full geometry.

6.5.4 Zero temperature master equation

We start by describing zero temperature solutions. With a vacuum solution at hand, one can proceed to explore the properties of the $T = 0$ strongly coupled non-Abelian gauge theory with gravity dual given by Eq. (6.62). Although this class of models was built primarily in order to reproduce the thermodynamics of QCD near the crossover phase transition [73], in Appendix F.3 we show that the glueball spectra is reasonably described by a confining, zero temperature version of these models.

When $T = 0$, the boundary gauge theory has full Lorentz invariance and, thus, we set

$h = 1$ in (6.63)

$$ds^2 = e^{2A}(d\tau^2 + d\vec{x}^2) + e^{2B}d\phi^2 \tag{6.72}$$

where τ is the Euclidean time. The equation of motion (6.68) is identically satisfied when $h = 1$. The remaining equations of motion (6.69), (6.70), and (6.71) simplify to

$$A'' - A'B' + \frac{1}{6} = 0, \tag{6.73}$$

$$24(A')^2 - 1 + 2e^{2B}V = 0 \qquad \text{and} \tag{6.74}$$

$$4A' - B' - e^{2B}V' = 0\,. \tag{6.75}$$

Now, following the procedure used in Ref. [15] for the $T \neq 0$ case, our goal here is to obtain a first order master equation for $G(\phi) \equiv A'(\phi)$. Then, one can integrate G to obtain A and the remaining metric function B. Combining Eqs. (6.74) and (6.75), we arrive at

$$\frac{V}{V'} = \frac{-8G + 2B'}{24G^2 - 1}\,. \tag{6.76}$$

We can now use Eq. (6.73) to eliminate B' from this equation and find the master equation at $T = 0$

$$G + \frac{V}{3V'} = -\frac{6G'G}{24G^2 - 6G' - 1}\,. \tag{6.77}$$

This is a first order ordinary differential equation for $G = A'$ for a given potential $V(\phi)$. To solve it, we have to specify a boundary condition for $G(\phi)$. Since all the potentials we shall consider have the IR ($\phi \to \infty$) asymptotic $V(\phi) \propto e^{\gamma\phi}$, we see that for $\phi \to \infty$, $V/3V' = 1/(3\gamma)$. Thus, Eq. (6.77) implies that when $\phi \to \infty$ one must have

$$G(\phi \to \infty) = -\frac{1}{3\gamma}\,. \tag{6.78}$$

6.5.5 Finite temperature master equation

The procedure for extracting a master equation for the finite temperature case is very similar to the zero temperature case [15]. Let us summarize the necessary steps. From Eqs. (6.69) and (6.71), one can obtain

$$\frac{V}{V'} = \frac{-6G\tilde{h} - 24G^2 + 1}{8G - 24B' + 2\tilde{h}} \tag{6.79}$$

where $\tilde{h} \equiv h'/h$. Now, using Eq. (6.68) to eliminate B' from this equation,

$$\frac{V}{3V'} = \frac{-6G^2\tilde{h} - 24G^3 + G}{24G^2 - 6G' - 1 + 6\tilde{h}G}. \tag{6.80}$$

To remove $\tilde{h}$ from the numerator in Eq. (6.80), we sum G on both sides. Then, manipulating a bit further the resulting expression, we get

$$\frac{G'}{G + \frac{V}{3V'}} = -4G + \frac{G'}{G} + \frac{1}{6G} - \tilde{h}. \tag{6.81}$$

Now, solving Eq. (6.68) for h''/h' and then using Eq. (6.70) to eliminate B' from the resulting expression, one can see that

$$\frac{h''}{h'} = -4G + \frac{G'}{G} + \frac{1}{6G}. \tag{6.82}$$

Thus, using Eq. (6.82) into Eq. (6.81),

$$\frac{G'}{G + \frac{V}{3V'}} = \frac{h''}{h'} - \frac{h'}{h} = \frac{d}{d\phi}\left[\log h' - \log h\right] = \frac{d}{d\phi}\log\tilde{h}. \tag{6.83}$$

Finally, using Eq. (6.81), we derive the final form of the master equation for a finite temperature geometry

$$\frac{G'}{G + \frac{V}{3V'}} = \frac{d}{d\phi}\log\left[\frac{G'}{G} + \frac{1}{6G} - 4G - \frac{G'}{G + \frac{V}{3V'}}\right]. \tag{6.84}$$

Let us now discuss the boundary conditions for the master equation (6.84). First, we require that $h(\phi)$ has a simple zero at $\phi = \phi_h$, which is the radial position of the event horizon. Thus, $h(\phi_h) = 0$ but $h'(\phi_0) \neq 0$ so that for $\phi \lesssim \phi_h$, $h(\phi) \approx -h'(\phi_h)(\phi - \phi_h)$. Therefore, from Eqs. (6.69) and (6.70) one obtains the constraints

$$V(\phi_h) = -3e^{-2B(\phi_h)}G(\phi_h)h'(\phi_h) \qquad \text{and} \tag{6.85}$$

$$V'(\phi_h) = e^{-2B(\phi_h)}h'(\phi_h). \tag{6.86}$$

Thus, from Eqs. (6.85) and (6.86) we conclude that

$$\left(G + \frac{V}{3V'}\right)\Big|_{\phi=\phi_h} = 0. \tag{6.87}$$

Moreover, we can also show that

$$\frac{d}{d\phi}\left(G+\frac{V}{3V'}\right)_{\phi=\phi_h}=G'(\phi_h)+\frac{1}{3}-\frac{V(\phi_h)V''(\phi_h)}{3(V'(\phi_h))^2}. \tag{6.88}$$

Thus, near the horizon one may expand $G+V/(3V')$ in a series around $\phi=\phi_h$,

$$G(\phi)=-\frac{1}{3}\frac{V(\phi_h}{V'(\phi_h)}+\frac{1}{6}\left(\frac{V(\phi_h)V'(\phi_h)}{V'(\phi_h)^2}-1\right)(\phi-\phi_h)+O[(\phi-\phi_h)^2]. \tag{6.89}$$

Thus, by fixing the position of the horizon ϕ_h we may use the series solution (6.89) to obtain $G(\phi)$ near the horizon, at $\tilde{\phi}=\phi_h-\delta\phi$, for $\delta\phi\ll\phi_h$, and then integrate numerically out from $\phi=\tilde{\phi}$ out to $\phi=0$, using the series values for $G(\tilde{\phi})$ and $G'(\tilde{\phi})$ as boundary conditions.

6.5.6 Geometry asymptotics

As mentioned above, the potential near the boundary ($\phi\to 0$) is given by

$$V(\phi)\sim-\frac{12}{R^2}+\frac{m^2}{2}\phi^2\,. \tag{6.90}$$

The UV scaling dimension Δ of the gauge theory operator associated with ϕ is determined by the larger root of

$$\Delta(\Delta-4)=m^2R^2\,. \tag{6.91}$$

In the coordinate system (6.63), the asymptotic AdS_5 geometry ($\phi\to 0$) is given by

$$A(\phi)=\frac{\log\phi}{\Delta-4}+O(1)\qquad\text{and} \tag{6.92}$$

$$B(\phi)=-\log\phi+O(1), \tag{6.93}$$

with $h(\phi\to 0)\to 1$. This also fixes the asymptotic behavior $G(\phi\to 0)\sim 1/(\phi(\Delta-4))$.

6.5.7 Obtaining the geometry and the thermodynamics

With the boundary conditions fixed and with the asymptotic behavior defined above one can obtain the full metric from $G(\phi)$. First, one can see that

$$A(\phi)=A_h+\int_{\phi_h}^{\phi}d\tilde{\phi}\,G(\tilde{\phi}), \tag{6.94}$$

where $A_h = A(\phi_h)$ is the integration constant. Since near the boundary A behaves as in Eq. (6.92), one can obtain the integration constant A_h

$$A_h = \frac{\log \phi_h}{\Delta - 4} + \int_0^{\phi_h} d\phi \left[G(\phi) - \frac{1}{(\Delta - 4)\phi} \right]. \tag{6.95}$$

Now, let us also evaluate $B(\phi)$ and $h(\phi)$. One can solve Eq. (6.70) for B' in terms of G to obtain

$$B(\phi) = B_h + \int_0^{\phi_h} d\phi \left[\frac{G'(\phi)}{G(\phi)} + \frac{1}{6G(\phi)} \right]. \tag{6.96}$$

with $B_h = B(\phi_h)$ being an integration constant, which we will determine in the end of this subsection. Also, given that A and B are known, one can integrate Eq. (6.68) to obtain

$$h(\phi) = h_0 + h_1 \int_{\phi_h}^{\phi} d\tilde{\phi}\, e^{-4A(\tilde{\phi}) + B(\tilde{\phi})}, \tag{6.97}$$

where h_0 and h_1 are integration constants. To determine them, remember that $h(\phi \to 0) = 1$ and $h(\phi_h) = 0$ so that

$$h_0 = 0 \qquad \text{and} \qquad h_1 = \frac{1}{\int_{\phi_h}^{0} d\phi\, e^{-4A(\phi) + B(\phi)}}. \tag{6.98}$$

Let us obtain the thermodynamics. First, the temperature is given by the Hawking temperature of the black hole in the bulk, which for the coordinate system in Eq. (6.63) by following the argument in Section 3.2 is given by

$$T = \frac{e^{A_h - B_h} |h_h'|}{4\pi}. \tag{6.99}$$

Let us also obtain an alternative expression for Eq. (6.99). We first suppose that we have rewritten the metric in the domain-wall gauge, given by

$$ds^2 = e^{2\tilde{A}}(-\tilde{h}dt^2 + d\vec{x}^2) + \frac{dr^2}{\tilde{h}}, \tag{6.100}$$

where $\tilde{h} = \tilde{h}(r)$ and $\tilde{A} = \tilde{A}(r)$, where r is the holographic coordinate. Comparing with the coordinate system (6.63), we see that we must require

$$\left| \frac{dr}{d\phi} \right| = e^{B}. \tag{6.101}$$

Now, in the domain-wall gauge, as the ϕ coordinate goes from $\phi \to 0$ (boundary) to $\phi = \phi_h$ (horizon), the r coordinate goes from $r \to \infty$ to $r = \phi_h$. Thus, in Eq. (6.101), we

must choose the minus sign

$$\frac{dr}{d\phi} = -e^B. \tag{6.102}$$

In the domain wall gauge, $\tilde{A}(r) \sim r/L$ for $r \to \infty$. Therefore, by a simple application of the chain rule,

$$G(\phi) = \frac{dA}{d\phi} = \frac{dr}{d\phi}\frac{dA}{dr} \approx -\frac{e^B}{L} \tag{6.103}$$

as $\phi \to 0$. Thus,

$$1 \approx -LG(\phi)e^{-B(\phi)} \qquad \text{as} \qquad \phi \to 0. \tag{6.104}$$

Inserting 1 in the form (6.104) into Eq. (6.99) we get

$$T \approx \frac{L}{4\pi} e^{-2B_h} G(\phi_h) h'(\phi_h) \exp\left[A_h + B_h - B(\phi) - \log\frac{G(\phi_h)}{G(\phi)}\right] \qquad \text{as} \qquad \phi \to 0. \tag{6.105}$$

Now, using the first constraint (6.85) and the B function in the form (6.96) into Eq. (6.105) we can eliminate both h' and B_h from the latter, obtaining

$$T \approx -\frac{LV(\phi_h)}{12\pi} \exp\left[A_h + \int_\phi^{\phi_h} \frac{d\tilde{\phi}}{6G(\tilde{\phi})}\right]. \tag{6.106}$$

Finally, pluggings A_h from Eq. (6.95) into Eq. (6.106), and then taking $\phi \to 0$ so that we can exchange the $\approx$ sign for an equality, we obtain

$$T = \frac{\phi_h^{1/(\Delta-4)}}{\pi L} \frac{V(\phi_h)}{V(0)} \exp\left\{\int_0^{\phi_h} \left[G(\phi) - \frac{1}{(\Delta-4)\phi} + \frac{1}{6G(\phi)}\right]\right\}. \tag{6.107}$$

To arrive at Eq. (6.107) we also have used the fact that $V(\phi \to 0) \to -12/L^2$, to leading order in ϕ.

From Eqs. (6.99) and (6.107) we can also evaluate B_h explicitly. Using the second constraint (6.86) to remove h' from Eq. (6.99), we obtain

$$T = \frac{e^{A_h + B_h}|V_h'|}{4\pi}. \tag{6.108}$$

Comparing Eqs. (6.107) and (6.108), we arrive at an expression for B_h

$$B_h = \log\left[\frac{4V(\phi_h)}{V(0)V'(\phi_h)L}\right] + \int_0^{\phi_h} \frac{d\phi}{6G(\phi)}. \tag{6.109}$$

Let us continue with the thermodynamics. As Eq. (6.62) is just the Einstein-Hilbert action coupled with some matter fields, the entropy of the black hole (and, thus, of the plasma) is given by the Bekenstein-Hawking formula (3.45). Thus, the entropy density of

the plasma is given by

$$s = \frac{2\pi}{k_5^2} e^{3A(\phi_h)} = \frac{2\pi}{k_5^2} e^{3\int_0^{\phi_h}\left[G(\phi) - \frac{1}{(\Delta-4)\phi}\right]}. \tag{6.110}$$

Therefore Eqs. (6.107) and (6.110) give a thermodynamical equation of state parametrized by ϕ_h: $(T(\phi_h), s(\phi_h))$. In particular, we can write a more convenient equation of state in terms the sound speed c_s^2:

$$c_s^2 = \frac{d\log T}{d\log s} = \frac{d\log T/d\phi_h}{d\log s/d\phi_h}. \tag{6.111}$$

6.5.8 The scaling dimension of $\mathrm{Tr}\, F^2$ and the trace anomaly.

In this subsection, we will discuss the relation between the trace anomaly and the scaling dimension [254], expanding the discussion in Ref. 2.2. This will allow us to understand the meaning of Δ in our holographic models and the limit of validity of our calculations. In this section, we will expand further the discussion of conformal and scale symmetry started in Chapter 2 with the aim of understanding how the breaking of scale dimension is related, at the quantum level, with the trace anomaly. This will be useful to set the limit of validity of Model B, already hinted in the first paragraphs of this Section.

We start by looking more closely to scale transformations. Let $\mathcal{L}$ be the lagrangian density for a classical field theory for a (representative) field $\phi(x)$. Suppose that $\mathcal{L}$ is invariant under the scale transformation

$$\begin{aligned} x^\mu &\to e^\sigma x^\mu \qquad \text{and} \\ \phi(x) &\to e^{-D\sigma}\phi(xe^\sigma), \end{aligned} \tag{6.112}$$

The associated conserved current this symmetry using from Noether's theorem is given by

$$\partial_\mu D^\mu = 0, \tag{6.113}$$

where

$$D^\mu = T^{\mu\nu} x_\nu, \tag{6.114}$$

with $T^{\mu\nu}$ being the stress-energy tensor. If the lagrangian is not invariant by scale transformations, then it follows that

$$\partial_\mu D^\mu = T^\mu_\mu. \tag{6.115}$$

Thus, if $T^\mu_\mu = 0$, the theory is scale invariant. In particular, pure $SU(N_c)$ Yang-Mills

theory in four dimensions, with lagrangian density $\mathcal{L}$

$$\mathcal{L} = -\frac{1}{4g^2}\mathrm{Tr}F_{\mu\nu}F^{\mu\nu}, \tag{6.116}$$

satisfies $T^{\mu\nu} = 0$ and thus is classicaly scale invariant.

Quantization may break the scale invariance present in a classical theory, as already remarked in Chapter 2. If the beta function β of the theory is not zero, $\beta \neq 0$, then the coupling constant g runs with the energy scale E as described by the renormalization group equation (recall Eq. (2.17))

$$\beta(g(E)) = \frac{\partial g}{\partial \log \frac{E}{\mu}}. \tag{6.117}$$

where μ is some reference energy scale. For an infinitesimal scale variation, with $E = e^{\sigma}\mu$, with $\sigma \ll 1$, one sees that g runs as

$$g \to g' = g + \sigma\beta(g). \tag{6.118}$$

The lagrangian density $\mathcal{L}$ transforms as

$$\mathcal{L}(g) \to \mathcal{L}'(g') = \mathcal{L}(g + \sigma\beta(g)) \approx \mathcal{L}(g) + \beta\sigma\frac{\partial \mathcal{L}}{\partial g}. \tag{6.119}$$

Under a scale transformation $\mathcal{L}$ transforms as $\delta\mathcal{L} = \sigma\partial_\mu D^\mu$ and we conclude that (using also Eq. (6.115))

$$\partial_\mu D^\mu = T^\mu_\mu \beta(g)\frac{\partial \mathcal{L}}{\partial g}. \tag{6.120}$$

For pure $SU(N_c)$ Yang-Mills, with lagrangian density (6.116), this yields, in particular

$$T^\mu_\mu = \frac{\beta(\alpha)}{8\pi\alpha^2}\mathrm{Tr}\, F^2_{\mu\nu}, \tag{6.121}$$

where we redefined the coupling constant as $\alpha(\mu) = g(\mu)/4\pi$, as usual. Thus, the trace of the energy momentum tensor is proportional to $\mathrm{Tr}\, F^2_{\mu\nu}$.

Now we come to the main point of this subsection. As $\langle T^\mu_\mu \rangle = \epsilon - 3p$, T^μ_μ is a physical observable and thus invariant under the renormalization group. Thus, the scaling dimension of T^μ_μ is given by its canonical dimension, $d_c = 4$. This remark will allow us to evaluate the scaling dimension of $\mathrm{Tr}\, F^2_{\mu\nu}$. First, let us remember that, for a generic operator $\hat{O}$, its renormalization group equation is given by

$$\frac{d\hat{O}}{d\log\mu} = -\Delta\hat{O}, \tag{6.122}$$

where Δ is the scaling dimension of $\hat{O}$, the sum of its canonical dimension d_c and its anomalous dimension γ, $\Delta = d_c + \gamma$. Thus, applying this relation to T^μ_μ we find

$$\frac{dT^\mu_\mu}{d\log\mu} = -4T^\mu_\mu. \tag{6.123}$$

Inserting Eq. (6.121) in both sides of Eq. (6.123) and using the chain rule in the form $d\beta(\alpha(\mu))/d\log\mu = (d\beta/d\alpha)(d\alpha/d\log\mu)$, we finally derive, for pure $SU(N_c)$ Yang-Mills,

$$\Delta = 4 + \beta'(\alpha) - \frac{2\beta(\alpha)}{\alpha}. \tag{6.124}$$

Thus, the perturbative scaling dimension Δ of $\mathrm{Tr}\,\mathrm{F}^2_{\mu\nu}$ is connected to the beta function β in pure Yang-Mills theory by Eq. (6.124). Using the pQCD beta function at 3 loops [270], one can find that, with the scale set at $\mu = 3\,\mathrm{GeV}$, $\alpha = 0.253$ and $\Delta = 3.93$ [254].

In this class of models, the scaling dimension of $\mathrm{Tr}\,\mathrm{F}^2_{\mu\nu}$ in the UV is fixed and it does run to the conformal fixed point result $\Delta = 4$ as one takes $\mu \to \infty$. Thus, one way of estimating the range of validity of this class of models is to evaluate Δ for the chosen potential $V(\phi)$ and see to which scale μ this Δ corresponds to - the model is valid up to $T < \mu$. This implies, in general, that we can trust these models up to $T \sim 1 - 4\,\mathrm{GeV}$, or, optimistically, at least up to $\sim 4T_c$. At higher temperatures, $T \gtrsim 4T_c$, asymptotic freedom becomes relevant and these bottom up models, whose UV fixed point is not trivial, are not useful anymore for phenomenonological applications in QGP physics.

6.5.9 Choice of potential

In this framework, the potential $V(\phi)$ is chosen to match the QCD plasma thermodynamics at zero chemical potential. As mentioned above, the main restrictions on $V(\phi)$ are that near the boundary $\phi \to 0$, $V(\phi) \sim -12/R^2 + m^2\phi^2/2$ while near the black brane horizon, $V(\phi) \sim V_0 e^{\gamma\phi}$. A simple, fairly featureless, potential that satisfies both conditions is

$$V(\phi) = -\frac{12}{R^2}(1 + a\phi^4)^{1/4}\cosh(\gamma\phi) + b_2\phi^2 + b_4\phi^4 + b_6\phi^6, \tag{6.125}$$

where γ, b_2, b_4 and b_6 are the free parameters of the potential[6].

The parameter a controls the nature of the thermodynamical phase transition; as we shall see, $a = 1$ implies that the bulk theory has a Hawking-Page transition and thus the dual gauge theory has a first order phase transition - this class of models can

[6] Ref. [271] obtained an important constraint that must be obeyed in order to avoid naked singularities that cannot be covered by a black brane horizon at finite temperature: $V(0) \geq V(\phi)$ for $\phi \neq 0$. For the choices of scalar potentials used in Chapters 6 and 7, within the range in temperature we were interested in, we did not find any naked singularities that could not be covered by a horizon. The potential choice used in Chapter 8 does not suffer from this issue.

	a	γ	b_2	b_4	b_6	Δ
Model B1	1	$\sqrt{2/3}$	5.5	0.3957	0.0135	3.0
Model B2	0	0.606	0.703	-0.12	0.0044	3.0

Table 6.2: *Parameters for the B1 (first order phase transition) and B2 (crossover phase transition) models. The last column shows the corresponding scaling dimension Δ of each model.*

be used to mimic the properties of the deconfinement transition in $SU(N_c)$ Yang-Mills theory [74, 255]. On the other hand, $a = 0$ implies that the dual gauge theory has a crossover phase transition and the model can be used to describe the thermodynamics of QCD with (2+1) light quark flavors [78]. The models with $a = 1$ and $a = 0$ will be called here B1 models and B2 models, respectively.

The near-UV ($\phi \to 0$) mass m^2 of the bulk effective action can be extracted from Eq. (6.125)

$$m^2 = -\frac{12\gamma^2}{R^2} + 2b_2\,. \tag{6.126}$$

On the other hand, as in the UV Eq. (6.91) holds, one obtains that b_2, Δ, and γ are not independent

$$b = \frac{6\gamma^2}{R^2} + \frac{\Delta(\Delta-4)}{2R^2}\,. \tag{6.127}$$

In Table 6.2 we show the parameters for both models we consider in this Chapter. We remark that in both models $\Delta = 3$, as used before in [263–265]. These two sets of parameters were chosen in order to fit lattice data for pure $SU(3)$ Yang-Mills theory and QCD, respectively - we shall display the numerical results for the thermodynamics in the corresponding sections for each model.

In Table 6.2 we show the parameters for both models we will consider in this work, B1 and B2. We remark that in both models, $\Delta = 3$. These parameters were chosen in order to fit lattice data for pure $SU(3)$ Yang-Mills and QCD, respectively - we will display the numerical results for the thermodynamics in the corresponding sections for each model.

6.6 Debye screening mass and Polyakov loop in the B1 model

Let us start by the B1 model which possesses a first order deconfining phase transition and models the thermodynamics of pure $SU(N_c)$ Yang-Mills theory.

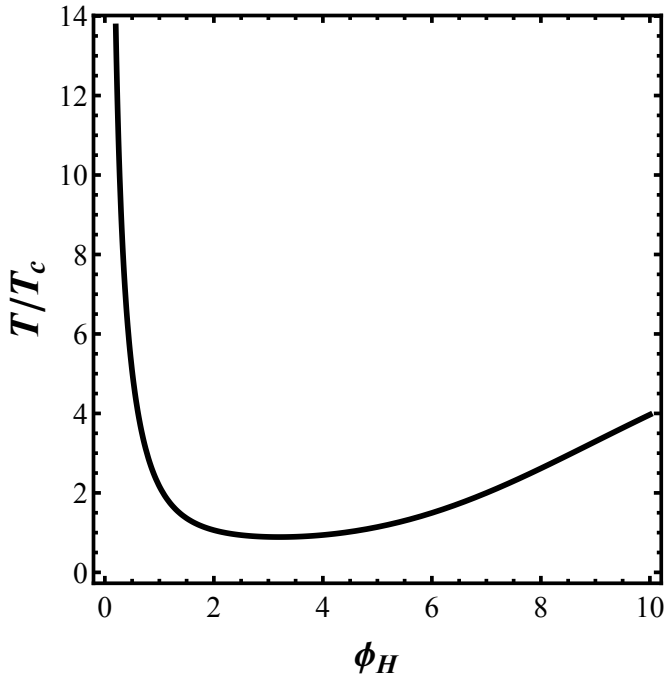

Figure 6.6: *Temperature T (normalized by the critical temperature T_c) as a function of the horizon position in the holographic coordinate ϕ_h for the B1 model.*

6.6.1 Thermodynamics

To obtain the thermodynamics of this model we use Eqs. (6.107) and (6.110). We start by presenting, in Fig. 6.6, the temperature T (normalized by the critical temperature T_c for the first order transition) as a function of ϕ_h. As in Model A, we have two characteristic temperatures. First, we have a minimum temperature T_{min} (given by the minimum of T in Fig. 6.6) below which the black hole solution does not exist and the dominating bulk geometry corresponds to a thermal gas. The second distinctive temperature is the critical temperature, T_c, at which the pressure of the black brane solution vanishes. For temperatures T such that $T_{min} < T < T_c$, the thermal plasma is in a (superheated) metastable phase. For the parameters we used, given in Table 6.2, $T_{min} = 0.89T_c$, with $\phi_{h,min} = 3.20$ and $\phi_{h,c} = 2.20$.

From Eq. (6.110) we evaluate the entropy density s as a function of ϕ_h. Using the results shown in Fig. 6.6, one can eliminate ϕ_h and obtain s as a function of T. With $s(T)$, one may proceed to evaluate all the thermodynamic functions. For instance, the pressure p is given by

$$p = -\int_{\infty}^{\phi_h} s(x)T'(x)dx, \tag{6.128}$$

while c_s^2 is given by Eq. (6.111). In Fig. 6.7 we show the pressure p (normalized by the $\mathcal{N} = 4$ SYM result) as a function of T/T_c. In Fig. 6.8, we compare the model results for the equation of state written in terms of c_s^2 with the corresponding lattice results for

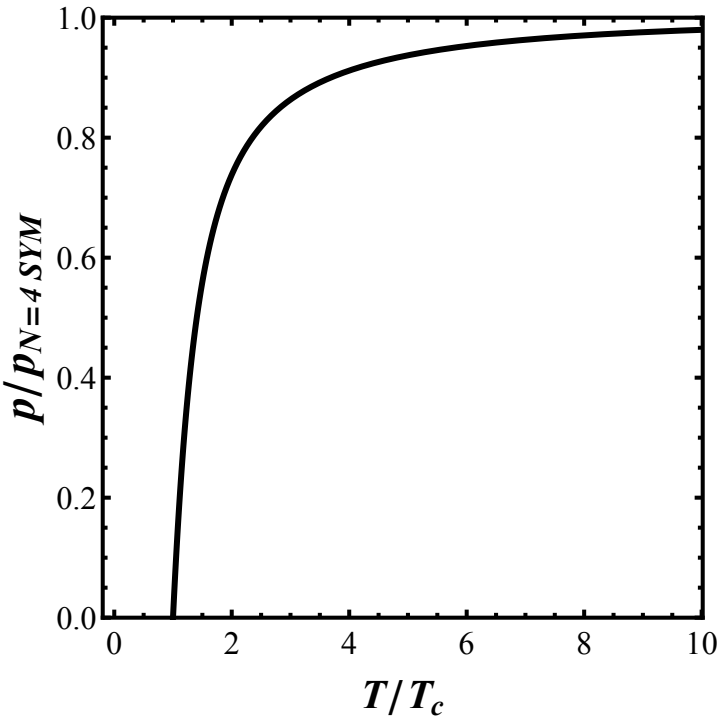

Figure 6.7: *The pressure p of the plasma for model B1, normalized by the $\mathcal{N}=4$ SYM result, as a function of the normalized temperature T/T_c.*

pure $SU(3)$ Yang-Mills [74]. We see that the B1 model is in fair agreement with $SU(3)$ thermodynamics representing a quantitative improvement with respect to model A.

6.6.2 Polyakov loop

The computation of the expectation value of the Polyakov loop proceeds as in Subsection 6.4.3 using Eq. (6.58). This equation assumes that the geometry is in the conformal gauge; however, our numerical solution is obtained in the $\phi = z$ gauge. Thus, we need to perform a coordinate system change - the details of this gauge change can be found in Appendix F.2. Also, our geometry is given in the Einstein frame; to evaluate the Polyakov loop we have use the string frame. As in Model A, we assume that our geometry is related to some 5 dimensional subcritical string theory and the string frame metric is related to the Einstein frame metric by $g^s_{\mu\nu} = \lambda^{4/3} g_{\mu\nu}$, where $\lambda = e^{\phi}$. A final remark is that in this model $b(y) \neq b_{(0)}(y)$ so that the cancelation that took place in Model A does not happen in this case. The regularized expression for the heavy quark free energy is

$$\frac{F_Q^{reg} T_c}{\sigma} = \frac{T_c}{\Lambda b_s^2(y_{min})} \int_0^{y_h^c} dy \, \left(b_s^2(y) - b_{(0),s}^2(y)\right) - \frac{T_c}{\Lambda b_s^2(y_{min})} \int_{y_h}^{y_h^c} dy \, b_s^2(y), \tag{6.129}$$

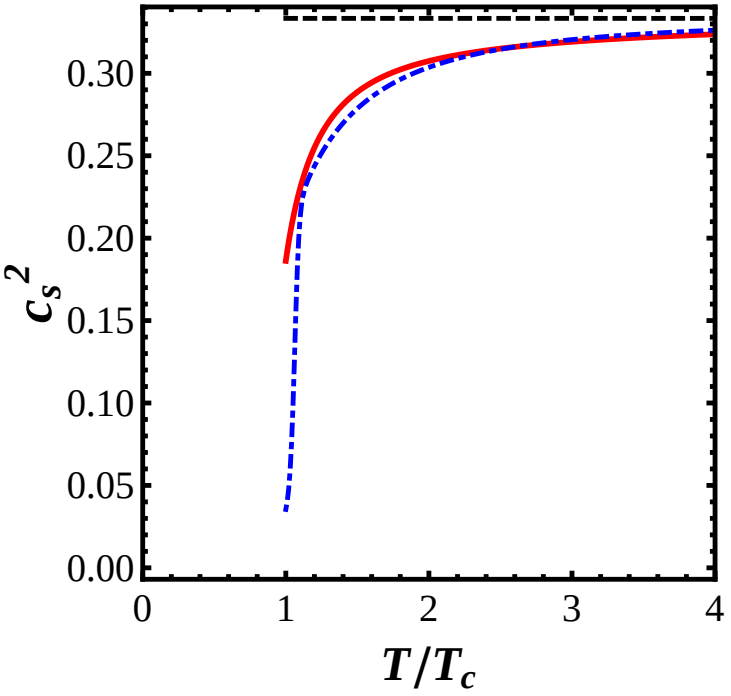

Figure 6.8: *The speed of sound squared of the plasma c_s^2 for model B1 as a function of the normalized temperature T/T_c (solid red curve), compared with $SU(3)$ Yang-Mills lattice results (dot-dashed blue curve) [74]. The black dashed line is the CFT result, $c_s^2 = 1/3$.*

where $y = \phi$ in order to mantain the same notation used in (6.58).In Fig. 6.9 we show our numerical results for $\Delta F_Q \equiv F_Q(T) - F_Q(2T_c)$, comparing with lattice results for $SU(N_c)$ [257]. One can see that model B1 follows more closely the lattice data in comparison that found for Model A.[7]

6.6.3 Debye screening mass

We may now proceed to evaluate the Debye screening mass in the model B1. To obtain the Debye mass, we have to obtain the lowest eigenvalue M^2 of the corresponding Eq. (6.28). As in the preceding subsection, this equation was written in the conformal gauge whereas our numerical solution for the metric is obtained in the Gubser gauge. The numerical procedure to find m_D is exactly the same as described in 6.4.4. As in model A, we assume that the axion action is given by Eq. (6.24), with the $\mathcal{Z}$ function given by the parametrization (6.59). We use the same values of c_4 as in the study of model A, $c_4 = 0.1, 1$, and 10.

The numerical results for the Debye screening mass in this model are presented in Fig.

[7]It should be noted that our models are built to study phenomena near the confinement/deconfinement transition from $T \sim T_c = 150$MeV to $T \sim 3 - 4\,T_c \sim 450 - 600\,$MeV. By construction, these models are strongly coupled in the UV. A reflection of this fact is that one cannot describe adequately both the Polyakov loop and the thermodynamics simultaneously at high temperatures, near the conformal regime, as argued in Ref. [272].

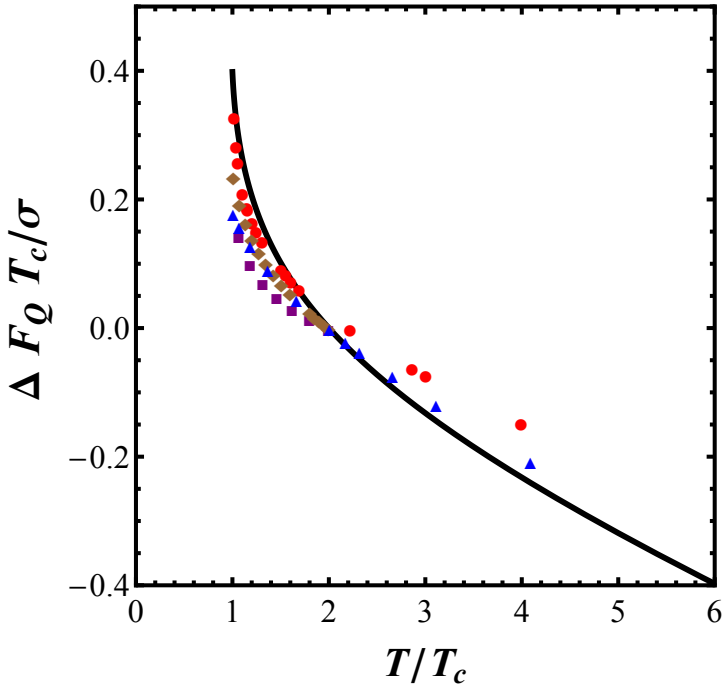

Figure 6.9: $\Delta F_Q T_c/\sigma = (F_Q(T) - F_Q(2T_c))T_c/\sigma$ *as a function of* T/T_c *for the model A (solid black line), model B1 (blue triangles), and for* $SU(N_c)$ *Yang-Mills [257] with* $N_c = 3$ *(red circles), 4 (purple squares), and 5 (brown diamonds).*

6.10. As in the case of model A, m_D/T has a discontinuity at $T = T_c$ where it jumps from 0 to a finite value $m_D/(c\pi T) \sim 0.35$ (somewhat higher than the jump in model A to $m_D/(c\pi T) \sim 0.2$). The value of the jump is not sensitive to the choice of c_4 and the overall behavior of m_D/T as a function of T saturates for large c_4. Note that we vary c_4 by two orders of magnitude and m_D/T varies only by $\sim 20\%$ at high temperatures.

6.7 Debye screening mass in the B2 model

6.7.1 Thermodynamics

In this section we describe a choice of scalar potential that yields an equation of state for the holographic strongly coupled plasma that closely matches the lattice results for (2+1) QCD [78]. The parameters for this potential can be found in Table 6.2. For this model, the black brane solution always dominates over the thermal gas solution; thus, there is no metastable phase and no T_{min}. Also, there is no confinement at $T = 0$. Moreover, the temperature T as a function of ϕ_h is monotonically decreasing, as it can be seen in Fig. 6.11. The pressure of the black brane phase is always positive and, thus, one cannot define a critical temperature T_c as in Models A or B1. The phase transition in Model B2 is of crossover type; the thermodynamic quantities and their derivatives

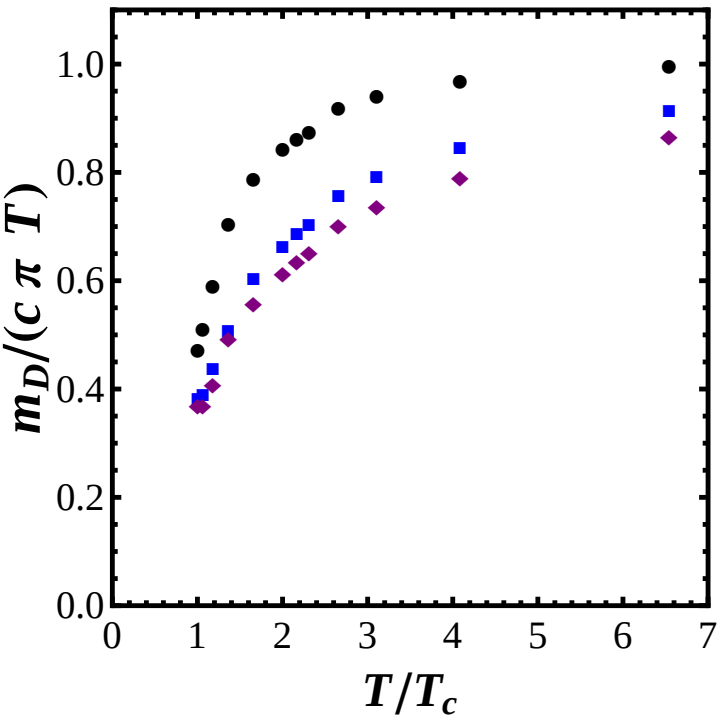

Figure 6.10: *Debye screening mass for the model B1, normalized by the $\mathcal{N}=4$ SYM result $c\,\pi T$ (with $c = 3.4041$) as a function of T/T_c for $c_4 = 0.1$ (black circles), 1 (blue squares), and 10 (purple diamonds).*

of all orders are continuous across the "phase transition". In fact, the phase transition is characterized only by a sudden, but continuous, change of the thermodynamics properties.

Model B2 gives a reasonable description of (2+1) QCD thermodynamics, as it can be seen in Fig. 6.13 (pressure p as a function of the temperature T) and in Fig. 6.12 (equation of state in terms of c_s^2)[8]. We also display the trace anomaly in Fig. 6.13. The 5-dimensional Einstein's constant $G_5 = 0.501$ is chosen to reproduce lattice data for the pressure in Fig. 6.13. We also note that this model provides a quantitative description of the norm of the expectation value of the Polyakov loop found on the lattice [263].

6.7.2 Debye screening mass

Following the same procedure employed in previous sections, we may now evaluate the Debye screening mass as a function of the temperature in this model. The results are shown in Fig. 6.15. The Debye screening mass m_D/T has a local minimum around $T \sim 150$ MeV showing a similar temperature dependence found for c_s^2 (Fig. 6.11). This minimum means, intuitively, that the plasma gets less screened (more transparent) to the strong interaction between colored heavy probes near the phase transition. Once again, larger values of c_4 show convergence and imply a faster rising to the conformal result (in

[8] We use the position of the minimum of c_s^2 to set the scale of the temperature and express T in MeV.

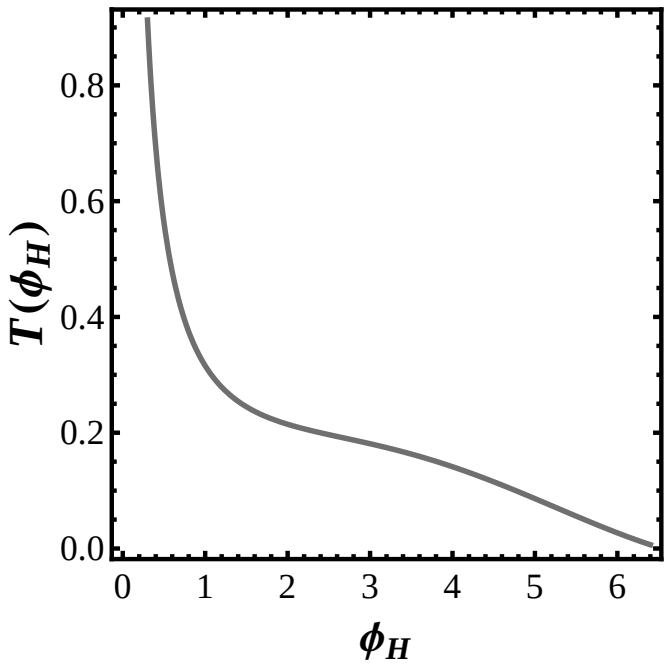

Figure 6.11: *Temperature T as a function of the horizon position in the holographic coordinate ϕ_h for the model B2.*

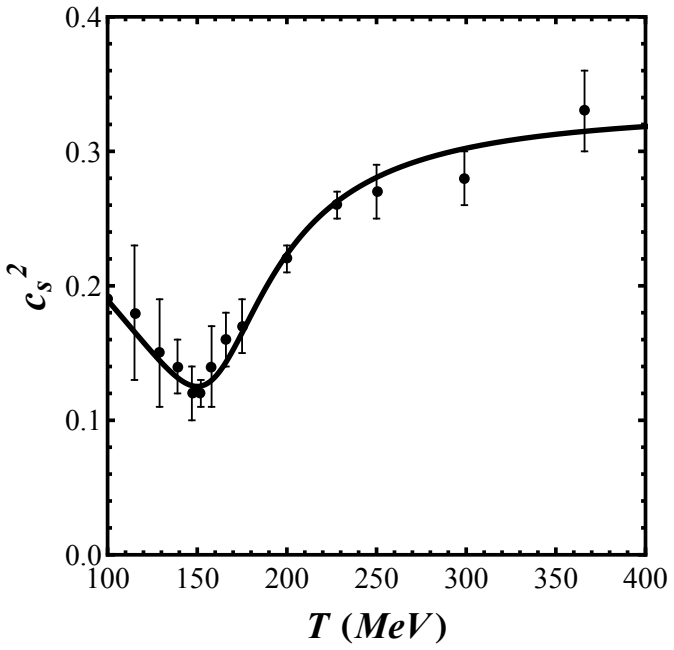

Figure 6.12: *The speed of sound squared of the plasma c_s^2 as a function of temperature T, for the B2 model (solid curve), compared with (2+1) flavors $SU(3)$ QCD lattice results (data points) [78].*

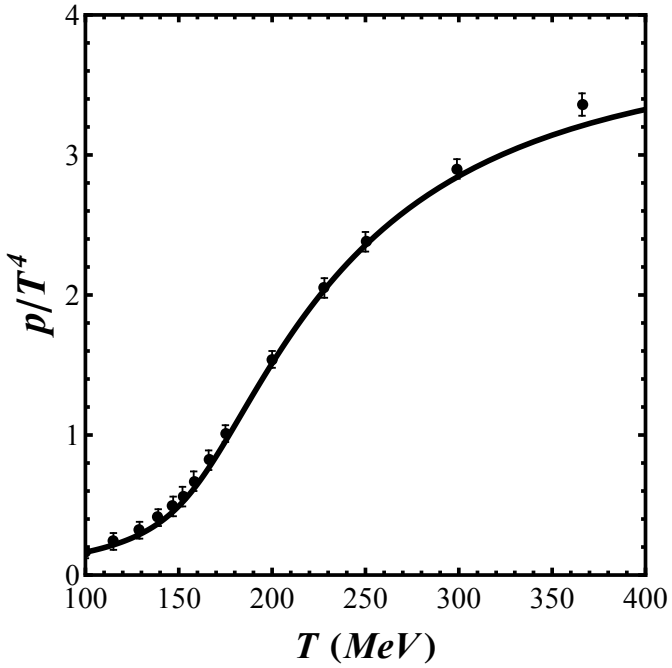

Figure 6.13: *The pressure of the plasma p/T^4 as a function of the normalized temperature T, for the B2 model (solid curve), compared with (2+1) flavors $SU(3)$ QCD lattice results (data points) [78].*

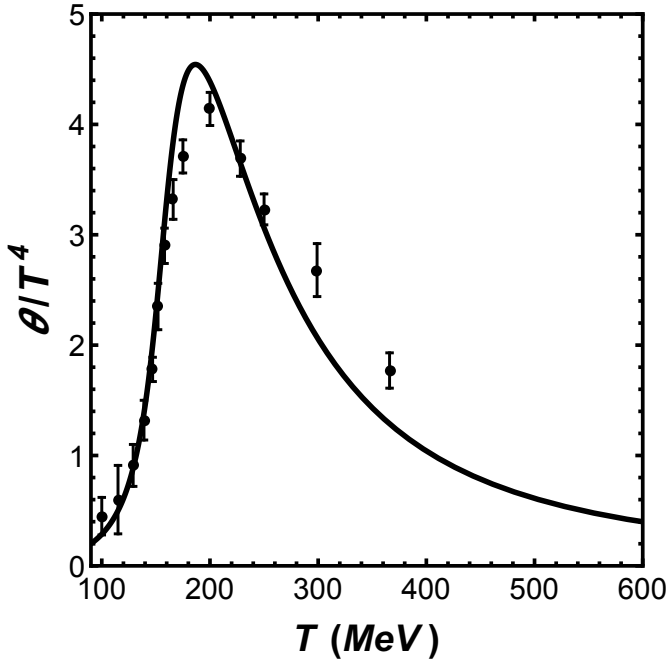

Figure 6.14: *The trace anomaly of the plasma θ/T^4 as a function of the normalized temperature T, for the B2 model (solid curve), compared with (2+1) flavors $SU(3)$ QCD lattice results (data points) [78].*

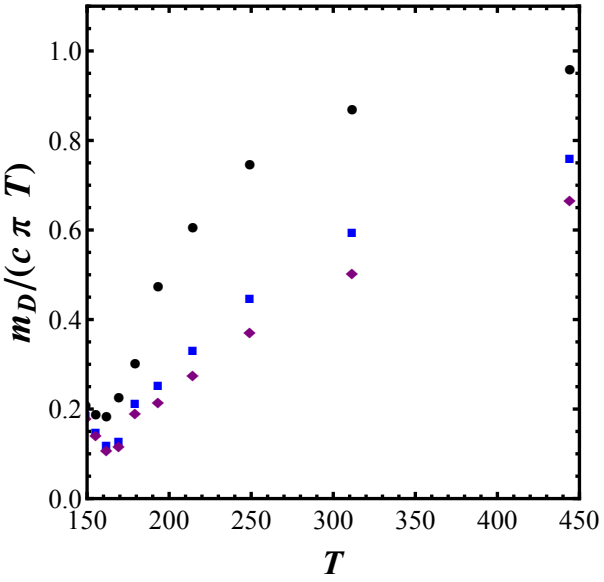

Figure 6.15: *Debye screening mass m_D for the model B2 with a crossover transition, normalized by the $\mathcal{N} = 4$ SYM result $c\,\pi T$ (with $c = 3.4041$) as a function of the temperature T for $c_4 = 0.1$ (black circles), 1 (blue squares) and 10 (purple diamonds).*

this case by varying c_4 by two orders of magnitude the high T values of m_D/T vary by $\sim 30\%$).

6.8 Debye mass dependence with η/s - Gauss-Bonnet gravity

6.8.1 Action and Background Geometry

As a final application of the holographic evaluation of the Debye screening mass, we consider a class of bulk actions that include curvature squared corrections to the supergravity action of type IIB superstrings and that violate the holographic viscosity limit $\eta/s \geq 1/4\pi$ [90], described by Gauss-Bonnet gravity. The action for these models, called Gauss-Bonnet gravity [194], is given by Eq. (4.66) of Chapter 4. For this particular choice of curvature squared corrections, the metric fluctuations in a given background have the same quadratic terms of Einstein gravity. The exact black-brane solution given by Eq. (4.67) is rewritten in the conformal gauge, using $z = R/U$

$$ds^2 = \frac{R^2}{z^2} a^2 \left(f_{GB}(z) d\tau^2 + d\vec{x}^2 + \frac{dz^2}{f_{GB}(z)} \right), \tag{6.130}$$

where

$$a^2 = \frac{1}{2}\left(1 + \sqrt{1 - 4\lambda_{GB}}\right) \quad \text{and} \tag{6.131}$$

$$f_{GB}(z) = \frac{1}{2\lambda_{GB}}\left[1 - \sqrt{1 - 4\lambda_{GB}\left(1 - \frac{z^4}{z_h^4}\right)}\right]. \tag{6.132}$$

The z coordinate black brane horizon at the simple root of $f_{GB}(z)$, z_h. The common temperature of the black brane and of the thermal bath is $T = a/(\pi R^2 z_h)$.

6.8.2 The Debye screening mass

We have not specified the string theory construction that leads to Gauss-Bonnet gravity but such a discussion can be found in [195]. The only field that can contribute to the channel used to define the Debye mass is the axion, which is once again trivial in this background. The action for the axion fluctuations (6.24) including only two derivatives is (this is still a conformal system and, thus, $\mathcal{Z} = 1$)

$$S = \frac{\alpha}{32\pi G_5}\int d^5x\, e^{5\mathcal{A}}(\partial a)^2, \tag{6.133}$$

where $\mathcal{A}(z) = \log(R/z)$. Apart from the constant factor of proportionality α in the action, this is the same action that would be obtained with a background of the form (6.23). So our equation of motion is still Eq. (6.28), with $\mathcal{B} = 3/2\log(z/R)$. As in Section 6.3 we use the dimensionless variable $y = z/z_h$, which yields the dimensionless mass $\tilde{M} = M/(\pi T)$.

Also, one can check that in this case the potential $\mathcal{V}(y)$ in Eq. (6.28) has the same asymptotic form near the boundary, namely $\mathcal{V}(y \to 0) = 15/(4y^2)$ - the leading term in $1/y$ is not changed. So, the asymptotic solutions are the same and all the tools used in 6.3 can be applied in this case without modifications. To obtain the Debye screening mass as a function of η/s, we analyze several values of λ_{GB} and then use Eq. (4.70) to obtain the corresponding values of η/s.

We also compare our numerical results with the phenomenological procedure pursued in Chapter 4. In that Chapter, we have evaluated in the strongly coupled plasma dual to Gauss-Bonnet gravity the expectation value of the rectangular Wilson loop operator at finite temperature, which yields the potential energy $V_{Q\bar{Q}}$ of a heavy quark-antiquark pair that depends on η/s [201]. Using fits for the real part of the potential of the form

$$\frac{\mathrm{Re}\, V_{Q\bar{Q}}}{\sqrt{\lambda}T} = -\tilde{C}_1\frac{e^{-\frac{\tilde{m}_D}{T}(LT)}}{(LT)^\delta} + \tilde{C}_2, \tag{6.134}$$

where L is the interquark distance while $\tilde{C}_1$, δ, and $\tilde{m}_D$ were taken as fit parameters (we note that $\tilde{C}_2 = -1/\alpha^2$ by our regularization procedure) we found an estimate for the Debye screening mass $\tilde{m}_D$. For $\lambda_{GB} = 0$ we found $\tilde{m}_D = 3.79\pi T$, in reasonable agreement

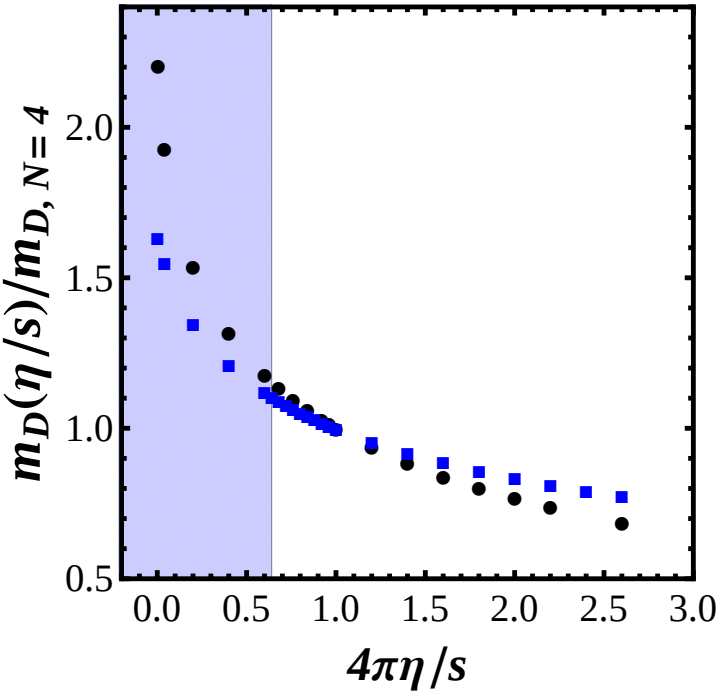

Figure 6.16: *Debye mass m_D for the Gauss-Bonnet gravity dual, as a function of η/s, normalized by the $\mathcal{N} = 4$ SYM value. The black circles correspond to the results obtained by computing the lightest CT odd mode; the blue squares are the results obtained by fits to the heavy quark-antiquark potential evaluated holographically [18]. The shaded region corresponds to values of η/s which violate the causality bound [91, 92].*

with the result of Eq. (6.32).

We present the results for the Debye mass m_D (normalized by the SYM value) as a function of the η/s in Fig. 6.16. We note that we have not restricted our calculations to the interval $\frac{4\pi\eta}{s} \geq 16/25$ as required by causality but considered, for completeness, $\eta/s \geq 0$. One can see that for increasing η/s the interaction between colored external probes in the plasma is less screened. This is reasonable, at least from the point of view of a weakly coupled plasma since η/s is roughly proportional to the mean free path of momentum isotropization of the plasma and changing η/s does not change the number of degrees of freedom of the system. Thus, less screening should correspond to a larger mean free path and, thus, to a larger η/s. We also note the unexpected coincidence between the results obtained by finding the lightest CT odd mode and those obtained following the simple phenomenological procedure using the heavy quark potential described in the previous paragraph.

6.9 Discussion and Conclusions of This Chapter

In this Chapter we have identified the Debye screening mass m_D in non-Abelian gauge theories at strong coupling with the lightest CT-odd mode in the spectrum (associated with the operator $\mathrm{Tr}F_{\mu\nu}\tilde{F}^{\mu\nu}$), following Ref. [184,232]. We used this prescription to holographically evaluate the Debye screening mass for a class of gravity duals involving the metric and a scalar field. Besides the conformal cases of $\mathcal{N}=4$ SYM at strong coupling and the gauge theory dual to Gauss-Bonnet gravity (where the scalar field in the bulk vanishes), we investigated in detail an analytic bottom-up model with a first order confinement/deconfinement transition (Model A), and two bottom-up holographic models that describe the thermodynamics of QCD as seen on the lattice - Models B1 (pure glue, first order phase transition) and B2 (QCD, crossover transition).

The calculation of m_D/T in both models for a pure Yang-Mills plasma with a first order phase transition at T_c, models A and B1, revealed some interesting features. Both models approach the conformal limit for $T \gg T_c$ and exhibit relatively little sensitivity to the axion coupling prefactor $\mathcal{Z}$. The most remarkable feature of both models is the discontinuity of m_D/T at the critical temperature T_c - m_D jumps from 0 in the thermal gas phase ($T < T_c$) to a nonzero value at $T = T_c$. This behavior for m_D/T in a pure SU(N_c) Yang-Mills plasma is consistent with previous lattice studies [239].

We also computed the expectation value of the Polyakov loop in these models finding an impressive agreement with lattice results [257] even for $N_c = 3$. Moreover, even Model A, which does not provide an adequate quantitative description of SU(3) thermodynamics, yields a reasonable description for the Polyakov loop. This suggests that the Polyakov loop is largely insensitive to a variation in the number of colors N_c in a pure glue plasma and that even $N_c = 3$ may be reasonably described by a large-N_c expansion [257]. Moreover, it would be interesting to identify more clearly what is the specific nonperturbative mechanism present in these holographic models that is responsible for this simultaneous description of lattice QCD thermodynamics and the expectation value of the polyakov loop.

Model B2 provides a reasonable description of the thermodynamics of (2+1) QCD[9]. The Debye screening mass, correspondingly, satisfies $m_D(T) > 0$ strictly and is always continuous. Near the crossover phase transition region at $T \sim 150\,\mathrm{MeV}$, we see a minimum of m_D/T (Fig. 6.15). This minimum resembles, qualitatively, that found for the speed of sound squared $c_s^2(T)$, as shown in Fig. 6.12. For all the models, A, B1, and B2 the

[9]We should, however, emphasize that the gauge theory described by this gravity dual does not strictly possesses fermions in the fundamental representation. Those can be included using D-branes in the bulk geometry [223, 273]. See Ref. [274] for a general review and [275] for a study of the Veneziano limit in bottom-up constructions.

conformal regime is reached from below; that is, $m_D(T) < c\pi T$. The minimum of m_D/T near the phase transition may have consequences for the energy loss of colored probes in the plasma [276]. Also, such a minimum implies that correlations in the medium are less screened, which effectively increases the range of interactions and this may be responsible for the (expected) small value of η/s around $T \sim 150$ MeV [277–280]. Equivalently, in this temperature range the expectation value of the Polyakov loop becomes small and, within the framework of the semi-QGP model [281, 282], such a reduction may also lead to a suppression of η/s [283, 284].

The Debye screening mass of $\mathcal{N} = 4$ SYM at strong coupling, $m_D = 3.4041\,\pi T$, extracted using the procedure of Ref. [232], yields a result that is remarkably close to the crude estimate used in Ref. [18] where fits to the heavy quark-antiquark potential gave $m_D = 3.79\pi T$. However, this coincidence should be interpreted with caution since, as discussed in Ref. [18], the heavy quark-antiquark potential in $\mathcal{N} = 4$ SYM at strong coupling is not exponentially screened (for small values of LT) as required to obtain the Debye screening mass from $V_{Q\bar{Q}}$.

By considering a gravity theory with higher order derivatives such that the gauge plasma does not satisfy $\eta/s = 1/(4\pi)$, namely Gauss-Bonnet gravity, we have evaluated the dependence of m_D/T with η/s, as shown in Fig. 6.16. We found that in this case less screening is seen as η/s is increased. It would be interesting to check this result in other strongly coupled gauge theories. In particular, one could consider gravity duals that correspond to gauge theories in which $\eta/s < 1/(4\pi)$ still in the context of applications to the quark-gluon plasma. For example, axion-induced anisotropic deformations of $\mathcal{N} = 4$ SYM [148, 149] or strongly coupled $\mathcal{N} = 4$ SYM subjected to an external magnetic field [24, 285, 286]. However, the prescription of Ref. [232] cannot be straightforwardly applied to these theories because they are not invariant by CP - P invariance is explicitly broken by the inclusion of the axion field in Ref. [148] and by the presence of an external magnetic field in Ref. [24].

The results of this Chapter where published in PRD [20].

Chapter 7

A holographic calculation of the electric conductivity of the strongly coupled quark-gluon plasma near the deconfinement transition

7.1 Introduction

As mentioned in Chapter 3, the gauge/gravity duality [14, 93, 94] is a powerful non-perturbative tool that can be used to investigate the transport properties of strongly coupled gauge theories with large number of colors N_c [103]. In particular, after the seminal calculation of the shear viscosity to entropy density ratio, η/s, performed in [90, 143, 145], a lot of effort has been put towards the determination of other transport coefficients that can be used to fully characterize the non-equilibrium dynamics of strongly coupled plasmas, such as the QGP formed in ultrarelativistic heavy ion collisions [6].

While much attention has been given to the holographic calculation of transport coefficients associated with the diffusion of energy and momentum in the hydrodynamic expansion, such as η and also the bulk viscosity [137, 287], much less is known about transport coefficients associated with other conserved currents such as the electric conductivity σ and the charge diffusion coefficient D (in the context of heavy ion collisions) (see Section 3.8 to see how these coefficients are computed using the gauge/gravity duality). The electric conductivity, in particular, may be relevant [64, 288] for the time evolution of the strong electromagnetic fields present in non-central ultrarelativistic heavy ion collisions at RHIC and the LHC [63] while Ref. [289] claimed that the directed flow in asymmetric heavy ion collisions may be used to estimate the value of this coefficient in the QGP.

A recent lattice QCD calculation [262] performed using 2 + 1 dynamical flavors

found that σ_{DC}/T is enhanced near the deconfinement transition[1]. A similar behavior has been found using a parton-hadron non-perturbative approach [292] (other recent non-perturbative calculations include [293]). Given the usual difficulties encountered in computing spectral functions from Euclidean correlators determined on the lattice, further independent confirmation of such an enhancement computed using other non-perturbative approaches, such as the gauge/gravity duality, are certainly welcome.

The conductivity in strongly coupled plasmas has been studied before using holography (see, for instance, [86,157,290,294–303]). However, in order to understand how the strong violation of conformal invariance at temperatures $T \sim 150 - 400$ MeV found in current lattice QCD calculations [76, 78] affects the electric conductivity, it is necessary to drop the assumption of a conformal plasma. While top-down string theory constructions of non-conformal plasmas[2]are known (see Refs. in [103]), these models cannot yet describe the specific temperature dependence of the equilibrium quantities of finite temperature QCD found on the lattice. On the other hand, bottom up holographic models in 5 dimensions involving the metric and a bulk scalar field are able to adequately describe the violation of conformal invariance seen in the thermodynamical properties of QCD at vanishing chemical potentials [15, 185, 209, 224, 252, 254, 304]. One should keep in mind that such phenomenological models for the strongly coupled QGP may be only useful when $T \sim 150 - 300$ MeV. For lower temperatures an effective description involving explicit hadronic degrees of freedom should be used [279,280,305,306] while at sufficiently high temperatures a weak coupling description of the QGP is more appropriate[3] (note also that these non-conformal holographic models remain strongly coupled even in the UV, which is not the case of an asymptotically free theory such as QCD).

A few years ago it was shown in Ref. [311] that the effects of a nonzero baryon chemical potential can be nicely incorporated into this class of models by adding a $U(1)$ gauge field in the bulk that is dual to the conserved baryon current at the boundary[4]. This general strategy follows directly from the holographic dictionary which establishes that global symmetries at the boundary are dual to gauge symmetries in the bulk [94]. While it is possible to include D-branes into this type of bottom up model to describe its flavor content [275,312,313], the Einstein+Scalar+Maxwell model pursued in Ref. [311] contains

[1]See Refs. [88, 89, 290] and, more recently, [291] for studies about the electric conductivity in weakly coupled plasmas.

[2]By a non-conformal plasma we mean a plasma whose associated field theory is non-conformal even at $T = 0$.

[3]In fact, recent calculations [307–310] involving Hard Thermal Loop perturbation theory were shown to provide a good description of the high temperature QGP properties in equilibrium.

[4]For QCD with three dynamical quark flavors, the equilibrium pressure may depend on the baryon μ_B, electric charge μ_Q, and strangeness μ_S chemical potentials besides the temperature T, i.e., $p = p(T, \mu_B, \mu_Q, \mu_S)$. The case described in [311] corresponds to setting $\mu_Q = \mu_S = 0$ (i.e., all quark flavors have the same chemical potential equals $\mu_B/3$).

the minimum physics needed to study the effects of global conserved charges in a strongly coupled plasma. Similar models, usually defined in asymptotically AdS_4 spaces, have been used in condensed matter applications [314,315]. See also [316,317] for applications of the Einstein+Scalar+Maxwell model in the study of the QCD phase diagram.

Moreover, this type of model provides a straightforward way to compute the transport coefficients associated with the given conserved charges when their chemical potentials vanish. In fact, in this case the on-shell gauge field in the bulk vanishes and the Maxwell action enters only in the description of the small fluctuations needed in a linear response analysis. More specifically, the metric and the scalar field define the non-conformal background (taken at zero chemical potential) while the Maxwell action acts as a probe, entering only in the calculation of 2-point functions of the given channel evaluated on this background. Therefore, while the gauge field does not backreact on the background, it determines the calculation of susceptibilities and other transport coefficients such as the electric conductivity.

In this Chapter, we shall use this Einstein+Scalar+Maxwell model to compute the frequency dependent electric conductivity and the charge diffusion coefficient in a strongly coupled plasma with thermodynamic properties similar to those displayed by QCD with three dynamical flavors [78] at zero chemical potential. The non-conformal background described by the Einstein-Scalar sector has a few parameters that enter into the scalar potential and are fixed to match lattice QCD thermodynamics [78] at zero chemical potential. The gauge field couples with the metric in the usual way through the Maxwell action but it also couples to the background scalar field ϕ. This coupling is described by an a priori unknown scalar function, $f(\phi)$, which does not affect the system's pressure though it enters directly in the calculation of the electric charge susceptibility $\chi_2^Q(T)$, as we will show below. Thus, $f(\phi)$ can be fixed by imposing that the electric charge susceptibility of the model matches the corresponding lattice data for $\chi_2^Q(T)/T^2$ [318]. Once $f(\phi)$ is determined, one can use the holographic dictionary [127] and extract the retarded Green's function of the electric current, which is used to compute the frequency dependent susceptibility $\sigma(\omega)$. The DC conductivity is simply $\sigma_{DC} = \lim_{\omega\to 0}\sigma(\omega)$ and it may be computed directly using the membrane paradigm [138] (for a detailed discussion of the membrane paradigm, see Section 3.8). The charge diffusion coefficient D can be directly obtained using the Einstein relation involving the σ_{DC} and χ_2^Q, Eq. (3.195), which is valid for this class of theories [138]. Since all the parameters of the model are fixed to match known equilibrium quantities computed on the lattice, the transport properties obtained in the model can be interpreted as holographic predictions that may be compared with the results of other methods.

This Chapter is organized as follows. In Section 7.2 we present the details about the

holographic model used in this Chapter, which is an extension of the Einstein + scalar model B2 of the last Chapter (Section 6.7). Section 7.3 is reserved to the calculation of the electric charge susceptibility χ_2^Q and its comparison to lattice data. In Section 7.4, we present the study of the frequency dependence of the conductivity and also compute the charge diffusion constant. The spectral function that enters in the calculation of $\sigma(\omega)$ is then used in Section 7.5 to compute the Euclidean correlator. In Section 7.6 we present the conclusions and an outlook regarding this Chapter.

7.2 Non-conformal holographic model

The holographic model that defines the strongly coupled plasma studied in this thesis is based on the Eintein + scalar model B2 considered in Section 7.2, with its action being given by Eq. (6.62). The background geometry is given by the ansatz (6.63), with the potential given by Eq. (6.125) with the parameters of Table 6.2. The resulting thermodynamics can be seen in Figures 6.11, 6.12 and 6.13, and the model gives a good description when compared to lattice data [78].

To the action (6.62) we incorporate a U(1) Abelian field A_M with action given by

$$S_M = -\frac{1}{2\kappa^2}\int d^5x\sqrt{-g}\,\frac{f(\phi)}{4}F_{\mu\nu}F^{\mu\nu} \tag{7.1}$$

where the field tensor is $F_{\mu\nu} = \nabla_\mu A_\nu - \nabla_\nu A_\mu$ and $f(\phi)$ is an unknown function of the background scalar field. The gauge field in the background is set to zero, $A_\mu = 0$ (remember that μ_Q=0). Its fluctuations are needed to compute the retarded Green's function associated with the electric current. This function enters in the calculation of the electric charge susceptibility, $\chi_2^Q(T) = (\partial^2 p/\partial\mu_Q^2)_T$, which is defined at $\mu_Q = 0$.

7.3 Electric charge susceptibility

We now proceed to fix the form the bulk U(1) gauge coupling $f(\phi)$. The strategy is to compute, via holography, the electric charge susceptibility and then choose a simple form for $f(\phi)$ that reproduces the corresponding lattice data for the charge susceptibility $\chi_2^Q(T)$.

In the following, we will use the membrane paradigm to compute the electric charge susceptibility. The applicability of this method for this type of calculations was discussed in detail in Section 3.8 (see also Ref. [138]). The most convenient gauge to work out these

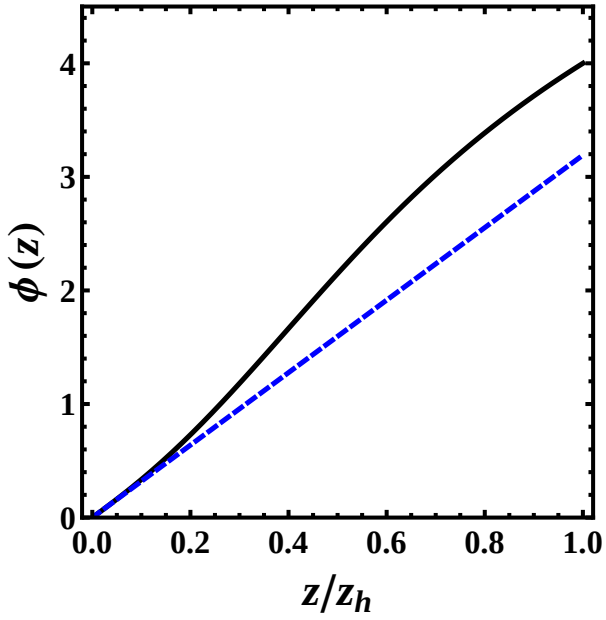

Figure 7.1: *A typical profile of the function $\phi(z)$, for $T/T_c = 0.74$. The solid line is the function $\phi(z)$ and the dashed curve is the AdS_5 result $\phi(z) = z$, which must be the boundary limit of $\phi(z)$.*

calculations is the conformal gauge (Appendix F.2), defined by

$$ds^2 = e^{2\tilde{A}(z)}\left(-\tilde{h}(z)dt^2 + d\vec{x}^2 + \frac{dz^2}{\tilde{h}(z)}\right), \tag{7.2}$$

where now the bulk scalar field is a function of z, i.e., $\phi = \phi(z)$, the horizon is at $z = z_h$ ($\phi(z \to z_h) = \phi_h$), and the asymptotically AdS_5 boundary is located at $z \to 0$ (where $\phi(z \to 0) \to 0$). The gauges (6.63) and (7.2) are related by the equation

$$z(\phi) = \int_0^{\phi} d\phi'\, e^{B(\phi')-A(\phi')}, \tag{7.3}$$

which can be inverted to yield $\phi(z)$. Moreover, we have that $\tilde{A}(z) = A(\phi(z))$ and $\tilde{h}(z) = h(\phi(z))$. We shall use the conformal gauge in all the calculations below. In Figure 7.1 we show a typical profile of the function $\phi(z)$ for a temperature near but below the phase transition.

From the membrane paradigm, the electric charge susceptibility $\chi_2^Q(T)$ in conformal gauge is simply given by Eq. (3.194), namely

$$\chi_2^Q = \frac{1}{\int_0^{z_h} dz\, [e^{\tilde{A}(z)} f(\phi(z))]^{-1}}\,. \tag{7.4}$$

We remark that the gauge field is zero for the $\mu_Q = 0$ calculations. In fact, $f(\phi)$ only enters in the calculation of χ_2^Q and $\tilde{A}(z)$, $\tilde{h}(z)$, and $\phi(z)$ are, of course, not influenced

by the gauge field at $\mu_Q = 0$, justifying our procedure for solving only the equations for the metric and the scalar field pursued in the previous section. We note that the proper dimensionless quantity to evaluate is χ_2^Q/T^2. For a conformal field theory, χ_2^Q/T^2 is a constant. For 3 flavor QCD in the Stefan-Boltzmann limit $\chi_2^{SB}/T^2 = 2/3$[5].

Let's investigate the minimum physical requirements that the gauge coupling $f(\phi)$ must satisfy. First, $f(\phi)$ must clearly be positive and smooth in the bulk. Second, in order to recover the correct UV fixed point behavior $\chi_2^Q/T^2 \to$ constant for $T \to \infty$, we must require, apart from the geometry being asymptotically AdS_5, that $f(\phi)$ goes to a finite constant as $z_h \to 0$ ($\phi(r_h) \to 0$), in order to render the integral in Eq. (7.4) proportional to T^2. Third, in order to have $\chi_2^Q \to 0$ as $T \to 0$, we must require that $f(\phi) \to 0$ as $\phi \to \infty$ so that the integral in Eq. (7.4) diverges.

With these requirements in mind, we have chosen three different simple parametrizations for the gauge coupling in order to check the sensitivity of the electric transport coefficients with the choice of $f(\phi)$. The parametrizations are:

$$f_1(\phi) = \frac{\mathrm{sech}(a_1\,\phi)}{g_{5,1}^2}, \tag{7.5}$$

$$f_2(\phi) = \frac{1}{g_{5,2}^2}\frac{1}{(\phi^2 + a_2^2)} \qquad \text{and} \tag{7.6}$$

$$f_3(\phi) = \frac{e^{-a_3^2\phi^2}}{g_{5,3}^2}, \tag{7.7}$$

where a_1, a_2, a_3, and $g_{5,i}$ are constants. In order to best fit the lattice results for χ_2^Q/T^2 of Ref. [318] (for another set of lattice data for χ_2^Q, which are however compatible with [318], see Ref. [319]), we have chosen $a_1 = 0.4$, $a_2 = 4.0$ and $a_3 = 0.23$. For comparison, we show the profiles of the resulting couplings $f(\phi(z))$ in Figure 7.2; we see that, although the functional forms of each parametrization in Eq. (7.5) are different, the choice of parameters lead to qualitatively similar profiles for $f(\phi(z))$. We have normalized the results for χ_2^Q computed holographically using the highest temperature we had available numerically ($T/T_c \sim 10$) and assumed that the conformal regime $\chi_{2\,CFT}^Q$ [290] has already been reached at this temperature - this is reasonable since the holographic results reach conformality already at $T \sim 500\,\mathrm{MeV}$. One can see in Figure 7.3 that the holographic model calculation for $\chi_2^Q/\chi_{2\,CFT}^Q$ is in good agreement with lattice results [318] (normalized by the Stefan-Boltzmann limit) for $T < 300\,\mathrm{MeV}$ for the three different parametrizations chosen in Eqs.(7.5)-(7.7). For $T > 300\,\mathrm{MeV}$ there is a sizeble discrepancy. However, this is not worrisome since these holographic models are not expected to model accurately QCD at high temperatures (i.e., the weakly coupled regime).

[5]For convenience, we have set the electric charge to 1 in this Chapter.

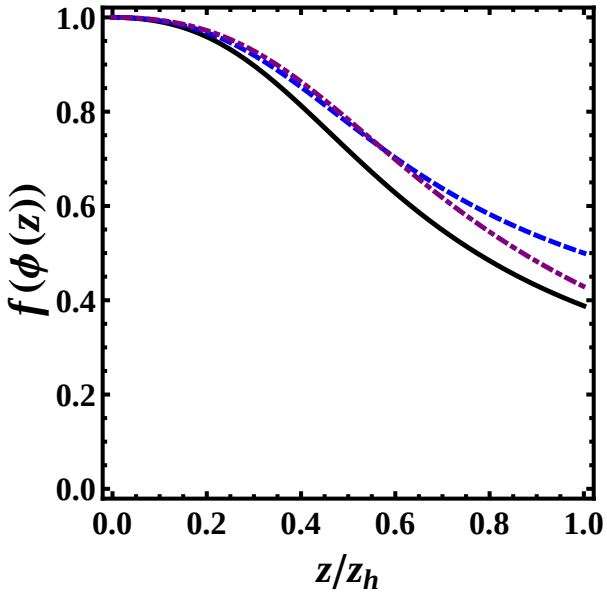

Figure 7.2: *Typical profiles of the $U(1)$ gauge coupling $f(\phi)$ in the z coordinate system, that is, the function $f(\phi(z))$. We display the profiles for the three parametrizations (7.5); the solid black curve is for $f_1(\phi(z))$ with $a_1 = 0.4$, the dashed red curve is for $f_2(\phi(z))$ with $a_2 = 4.0$ and the dot-dashed curve is for $f_3(\phi(z))$ with $a_3 = 0.23$. The constants $g_{5,i}$ were chosen in order to normalize $f(\phi(z))$ to 1 as $z \to 0$. These profiles where evaluated at $T/T_c = 0.74$.*

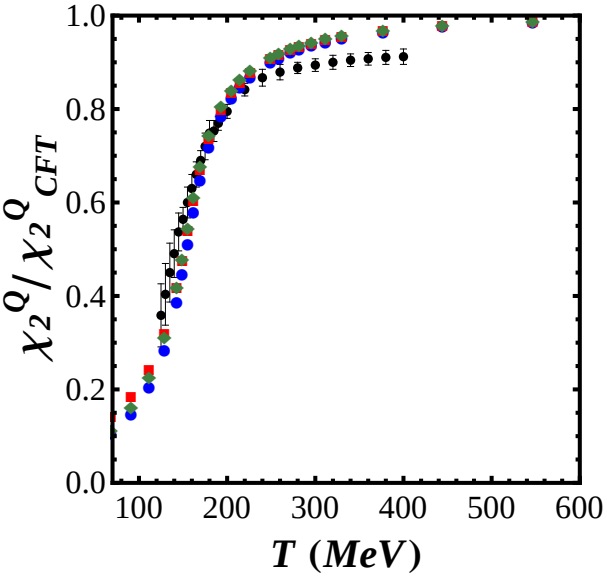

Figure 7.3: *The electric charge susceptibility χ_2^Q of the holographic model, normalized by its conformal limit, as a function of the temperature T of the plasma. The circles, squares, and diamonds correspond to the results found using the parametrizations in Eqs. (7.5), (7.6), and (7.7), respectively. The lattice data points for χ_2^Q/χ_2^{SB} [318] are in black.*

7.4 Holographic calculation of the electric conductivity and charge diffusion constant

The frequency dependent conductivity associated with the conserved current operator $\hat{J}^i$ ($\mathbf{x} = x_1, x_2, x_3$) is a 3 x 3 matrix, $\sigma^{ij}(\omega)$ in Fourier space and it is directly related to the retarded Green's function of $\hat{J}^i$ via Eq. 3.116, that is,

$$\sigma^{ij}(\omega) = -\frac{G_R^{ij}(\omega, \mathbf{k} = 0)}{i\omega}\,, \tag{7.8}$$

where $G_R^{ij}(k) = -i\int d^4x\, e^{-ik\cdot x}\theta(t)\left\langle\left[\hat{J}^i(t,\mathbf{x}), \hat{J}^j(0,\mathbf{0})\right]\right\rangle_T$ (with $k_\mu = (-\omega, \mathbf{k})$). The conductivity appears in Ohm's law as $\langle\hat{J}^i(\omega)\rangle = \sigma^{ij}(\omega)F_{jt}(\omega, z \to 0)$. Rotational invariance implies that $\sigma^{ij}(\omega) = \sigma(\omega)\delta^{ij}$ and, without any loss of generality, we shall assume here that the external electric field is in the x_1 direction.

7.4.1 DC conductivity

The DC electric conductivity is simply the limit $\sigma_{DC} = \lim_{\omega\to 0}\sigma(\omega)$. For the type of theory we consider in this thesis, σ_{DC} can be straightforwardly computed using the general formula (3.179) via the membrane paradigm, which gives (in conformal gauge)

$$\sigma_{DC} = f(\phi(z_h))e^{\tilde{A}(z_h)}. \tag{7.9}$$

It is now clear that if $f(\phi)$ satisfies the properties given in the foregoing section, then σ_{DC}/T goes to a constant when $T \to \infty$ (the expected conformal behavior found in [290]) and $\sigma_{DC}/T \to 0$ as $T \to 0$. Since $V(\phi)$ is completely fixed by the thermodynamics and $f(\phi)$ was fixed to reproduce the lattice data for the electric charge susceptibility, we have no more free parameters left to determine and $\sigma(\omega)$ can then be considered a prediction of the holographic model.

Using the parametrizations for $f(\phi)$ discussed above, we obtain the result shown in Figure 7.4 for σ_{DC}, where we again normalize by the conformal result. One can see that the DC conductivity varies rapidly in the crossover region, a feature also seen in recent lattice QCD calculations [262]. Note also that the results for $\sigma_{DC}/\sigma_{DC,CFT}$ are robust with respect to the specific form of the gauge coupling $f(\phi)$ (though note that ours choices for this function guarantee that the conformal limit is reached from below). Also, we remark that since our charge susceptibility in principle includes the strange quark contribution, our results may be taken as estimates for the DC conductivity in the QCD plasma near the deconfinement transition (in the case of QCD the result would be then normalized by its value in the Stefan-Boltzmann limit). In Figure 7.5 we compare the results for σ/T

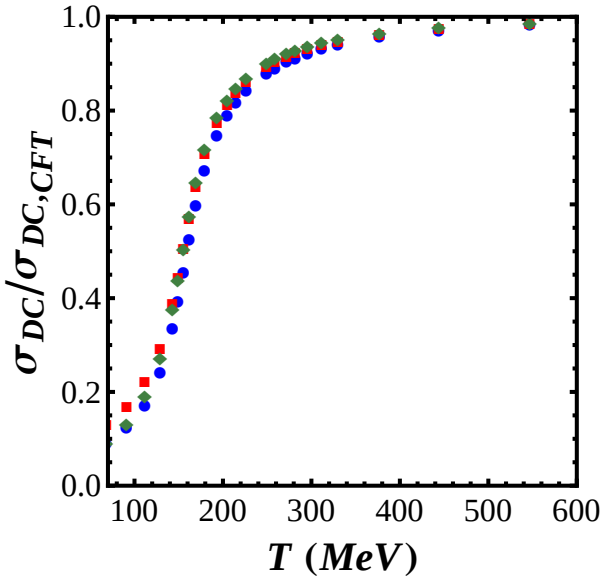

Figure 7.4: *The DC conductivity divided by its conformal value as a function of the temperature T of the plasma. The circles, squares, and diamonds correspond to the results found using the parametrizations in Eqs. (7.5), (7.6), and (7.7), respectively.*

from our model with several partonic transport models and lattice calculations. We see that impressive qualitative agreement is seen between our holographic setup and the most recent lattice computations.

7.4.2 Charge diffusion coefficient

The small charge disturbance created by the external electric field eventually diffuses back into thermal equilibrium and this diffusion process is controlled (to lowest order in a derivative expansion) by a single transport coefficient D called the charge diffusion constant (Subsection 3.8.4). This coefficient defines the hydrodynamic mode of the $G_R^{x_1x_1}$ correlator [336], which has been previously investigated in holography (see, for instance, Refs. [144, 154, 155]).

Within the membrane paradigm, Einstein's relation among the transport coefficients involved is valid and the charge diffusion constant can be directly obtained using our previous results for χ_2^Q and σ_{DC} using Eq. (3.187), that is,

$$D = \frac{\sigma_{DC}}{\chi_2^Q}\,. \tag{7.10}$$

Thus, we may compute directly this diffusion coefficient in the dimensionless form D/D_{CFT}, arriving at the results shown in Figure 7.6. Again, the results are not sensitive to the specific form of $f(\phi)$ at high temperatures $T > 150$ MeV. However, for $T < 150$ MeV, D/D_{CFT} becomes very sensitive to the choice of $f(\phi)$. The curve dispersion is due to the

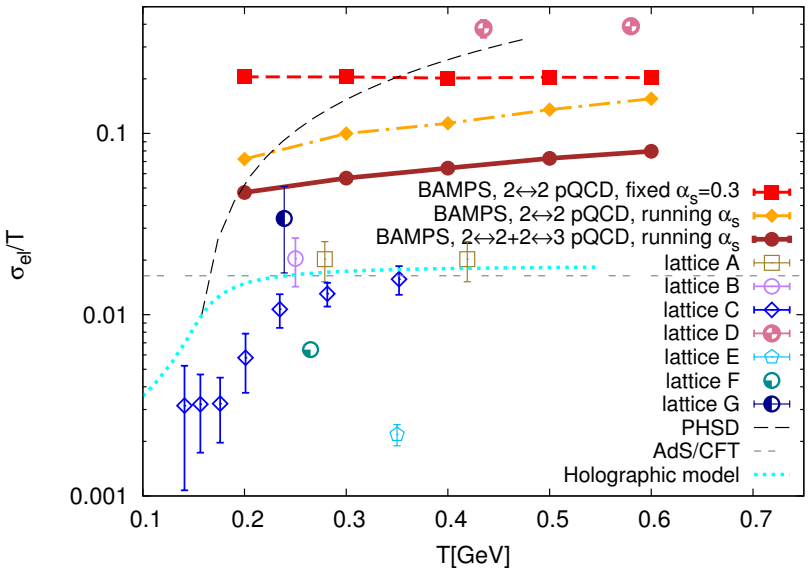

Figure 7.5: *The DC conductivity temperature ratio σ/T for several partonic transport models (Boltzmann Approach to Multi-Parton Scattering, BAMPS) and several lattice calculations, together with results for strongly coupled $\mathcal{N} = 4$ SYM and our holographic model. Figure reproduced from [321, 322] - see wherein for a complete list of references.*

fact that both σ_{DC} and χ_2^Q vary strongly as $T \sim T_c = 150\,\text{MeV}$ and, since $D = \sigma_{DC}/\chi_2^Q$, D becomes sensitive to the particular way that σ_{DC} and χ_2^Q vary near the phase transition. That is, D for $T < 150\,\text{MeV}$ is sensitive to the choice of $U(1)$ coupling. This does not constitute a problem per se because this holographic model certainly does not provide a good guide for the physics of the plasma at those low temperatures since the plasma is then in the hadron gas phase. However, the fact that $D/D_{CFT} < 1$ at low temperatures should be robust (for instance, this behavior has been seen in the non-conformal top-down model studied in Ref. [296]). Thus, the overall shape of the curve shown in Eq. (7.6) provides an estimate for the temperature dependence of the charge diffusion constant in the strongly coupled QGP, which may be checked by lattice calculations in the near future.

We compare, in Fig. 7.7, the results for DT with a recent lattice calculation [320]. We see that in the range of temperature between 150-300 MeV our holographic model furnishes a good description of the lattice results. For higher temperatures, however, the lattice data rises to about twice the expected asymptotic conformal result in holography, $D = 1/(2\pi T)$ - this is expected, since the conformal high temperature limit in these holographic models is strongly coupled.

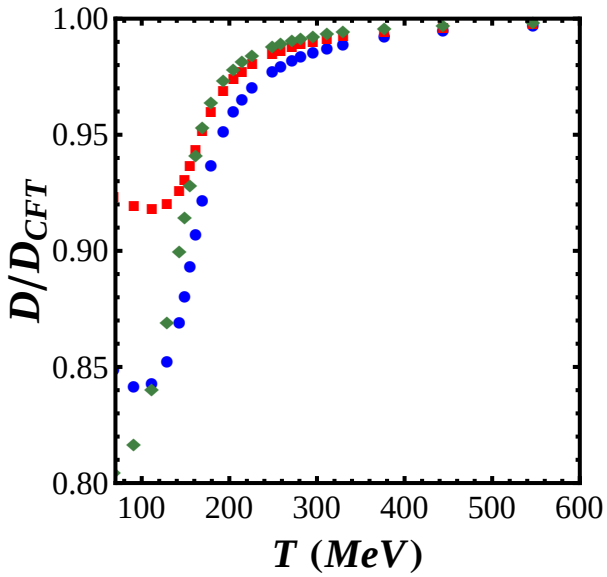

Figure 7.6: *The charge diffusion constant of the plasma normalized by the conformal result as a function of the temperature T of the plasma. The circles, squares, and diamonds correspond to the results found using the parametrizations in Eqs. (7.5), (7.6), and (7.7), respectively.*

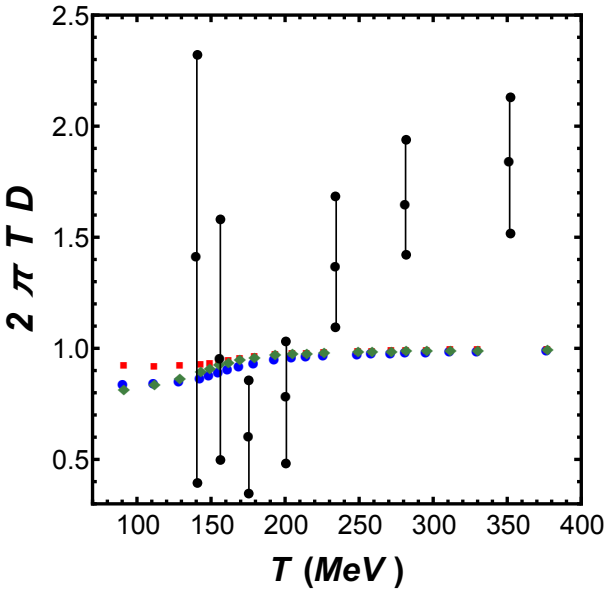

Figure 7.7: *Charge diffusion constant D, normalized by the conformal result $D = 1/(2\pi T)$. The black points are the lattice results from Ref. [320], with the associated error bars. The circles, squares, and diamonds correspond to the results found using the parametrizations in Eqs. (7.5), (7.6), and (7.7), respectively.*

7.4.3 AC electric conductivity

To obtain the AC conductivity $\sigma(\omega)$, we must compute $G_R^{x_1 x_1}(\omega)$. The equations of motion for the bulk fields in response to the fluctuations can be written in terms of gauge invariant quantities such as the bulk conserved current and the bulk field strength. Moreover, these equations of motion can be reduced to first order differential equations with respect to the z coordinate, which completely describe the flow of the fields from the black brane horizon to the boundary, as discussed in Section 3.8. For nonzero momentum there are two such flow equations, Eqs. (3.174) and (3.175): one for the longitudinal channel involving the x_1 direction and another equation for the transverse part. However, in our case when the momentum is taken to be zero these two equations converge (as required by rotation invariance) to the following expression

$$\partial_z \bar{\sigma}(\omega, z) = i\,\omega\,\frac{\Sigma(z)}{\tilde{h}(z)}\left[\frac{\bar{\sigma}(\omega, z)^2}{\Sigma(z)^2} - 1\right] \tag{7.11}$$

where

$$\Sigma(z) = f(\phi(z))\, e^{\tilde{A}(z)}. \tag{7.12}$$

Regularity at the horizon provides the initial condition

$$\bar{\sigma}(\omega, z_h) = \sigma_{DC} \tag{7.13}$$

and the AC conductivity is obtained by following the flow from the horizon to the boundary, as discussed in Section 3.8,

$$\sigma(\omega) = -\frac{\mathrm{Im}\, G_R(\omega)}{\omega} = \bar{\sigma}(\omega, z \to 0)\,. \tag{7.14}$$

In the limit of $\omega \to 0$, the flow equation is trivial: $\partial_z \bar{\sigma} = 0$. Thus, $\bar{\sigma}$ remains at its initial value set at the horizon, which is nothing but σ_{DC}. This is the basis for the formulas used in the DC calculations in the previous section. In this case, following Ref. [138], one only needs to evaluate $\bar{\sigma}$ at the horizon to determine σ_{DC}. Now, if $\omega \neq 0$, the full flow from horizon to the boundary must be considered to determine $\sigma(\omega)$.

The numerical procedure to evaluate $\sigma(\omega)$ is straightforward. With a fixed temperature (and thus a fixed background geometry), one has to integrate Eq. (7.11) for finite ω. We impose that the intercept of $\sigma(\omega)$ with the σ axis matches σ_{DC}. The units for ω are matched by imposing the correct conformal behavior for $\omega/T \gg 1$, that is, $\sigma(\omega)/T = \mathrm{C}_{AdS_5} \times \omega/T$, where C_{AdS_5} is a constant found by analyzing the strongly coupled conformal limit obtained using an AdS_5-Schwarzchild geometry with a constant $f(\phi)$.

Following this procedure we obtain for our three choices of $f(\phi)$ given in Eqs. (7.5),

(7.6), and (7.7) the results for $\mathrm{Re}\,\sigma(\omega)$ shown in Figure 7.8. First, we remark that we were able to reproduce the results obtained in [86] for strongly coupled $\mathcal{N}=4$ SYM (in that case, those were interpreted as R-current correlators). We see that for $T/T_c < 1$ one can find some nontrivial structure in $\mathrm{Re}\,\sigma(\omega)$ when compared to the conformal strongly coupled result[6]. Our holographic model is certainly not applicable in the thermal hadron gas phase which is present in QCD at low T. The lowest T chosen, $T \sim 0.5T_c$, is the absolute lowest temperature used in our model, that is, up to approximately 70 to 100 MeV. As T increases, these structures disappear. Already for $T \sim 2T_c$, the difference between the non-conformal and conformal results is negligible. This last remark can be seen more clearly in Figure 7.9, where the strongly coupled conformal result has been subtracted from the non-conformal results. Also, we see that all choices for $f(\phi)$ yield similar results for the AC conductivity, in agreement with the computation of susceptibility and DC conductivity shown before.

7.5 The Euclidean correlator

The AC conductivity $\sigma(\omega)$ is given by Eq. (7.8). However, note that $\mathrm{Re}\,\sigma(\omega) = \rho(\omega)/\omega$, where $\rho(\omega) \equiv -\mathrm{Im}\,G_R^{x_1x_1}(\omega)$ is the spectral density. The Euclidean correlator $G_E(T\tau)$ in the imaginary time formalism is related to the real time spectral density by the following relation [61]

$$G_E(T\tau) = \int_0^\infty d\omega\,\rho(\omega)\frac{\cosh\left[\omega\left(T\tau - \frac{1}{2}\right)/T\right]}{\sinh\left(\omega/2T\right)}. \tag{7.15}$$

It is interesting to check if the structures observed in $\mathrm{Re}\,\sigma(\omega)$ or, alternatively, in $\rho(\omega)$ due to the strong violation of conformal invariance experienced by the theory near the deconfinement transition are reflected at all in $G_E(T\tau)$. Using Eq. (7.15) with the results of the previous section, we evaluate $G_E(T\tau)$ for a range of temperatures and for all the three model choices of $f(\phi)$, obtaining the results shown in Figure 7.10. One can see that for all the different temperatures considered that the Euclidean correlator is basically featureless - the details present in $\rho(\omega)$ are smoothed out in the computation of the Euclidean correlator. The strongly coupled CFT limit is reached already in this case at fairly intermediate temperatures, $T \sim 2T_c$.

Also, all model choices of the gauge coupling yield similar results - displaying the consistency already seen in the calculations done in the previous sections. This suggests that in order to obtain the real time spectral density at strong coupling $\rho(\omega)$ from $G_E(T\tau)$ (reversing the direction of calculation) one needs to be able to evaluate the Euclidean correlator with extremely great precision, as already remarked in the previous analysis of

[6] We remind the reader that $T_c = 150$ MeV.

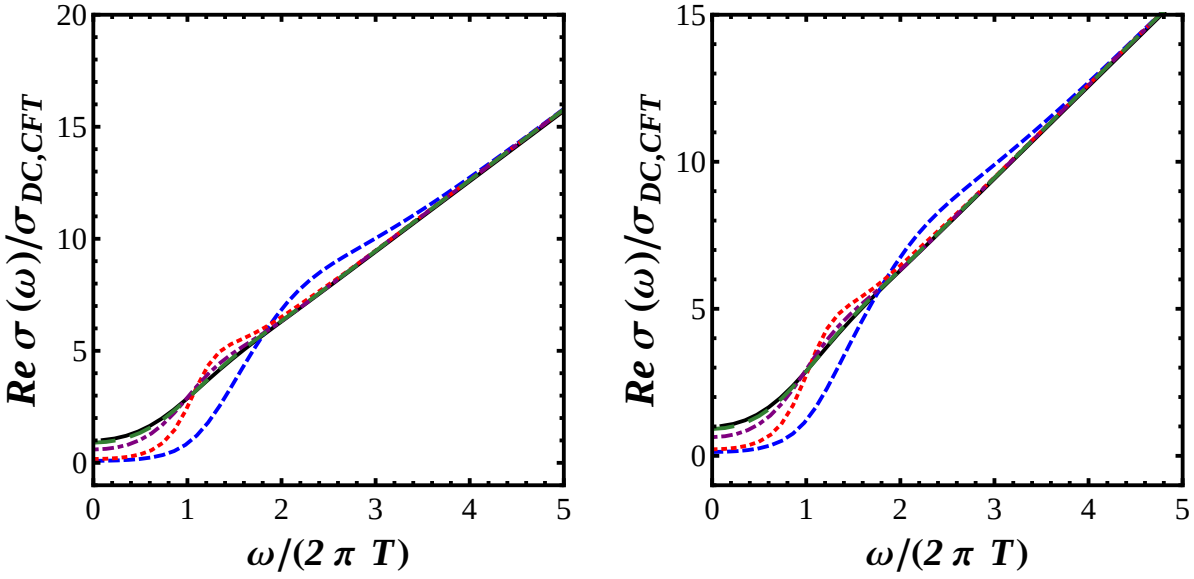

(a) *Model 1 - see* (7.5)

(b) *Model 2 - see* (7.6)

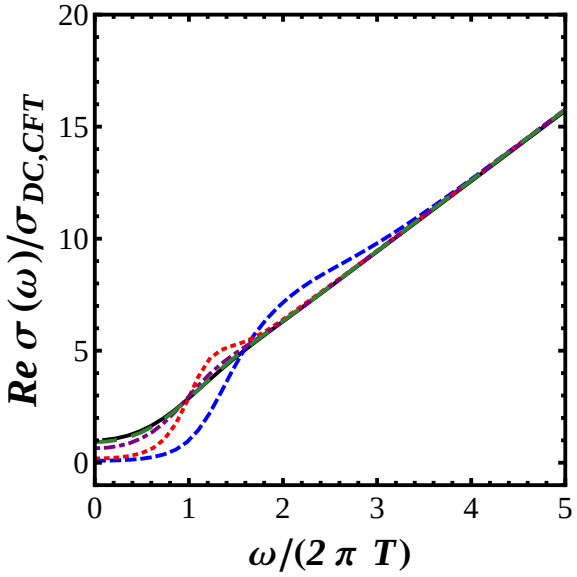

(c) *Model 3 - see* (7.7)

Figure 7.8: *The electric conductivity* $\mathrm{Re}\,\sigma(\omega)$ *(normalized by the DC conductivity in the CFT limit) as a function of* $\omega/(2\pi T)$ *for the different model choices of the gauge coupling in Eqs.* (7.5), (7.6), *and* (7.7). *The solid black curve is the conformal result at strong coupling, the short-dashed blue curve is for* $T/T_c = 0.45$, *the dotted red curve is for* $T/T_c = 0.74$, *the dash-dotted magenta curve is for* $T/T_c = 1.13$, *and the long dashed green curve is for* $T/T_c = 1.81$. *(Here,* $T_c \sim 150\,\mathrm{MeV}$*).*

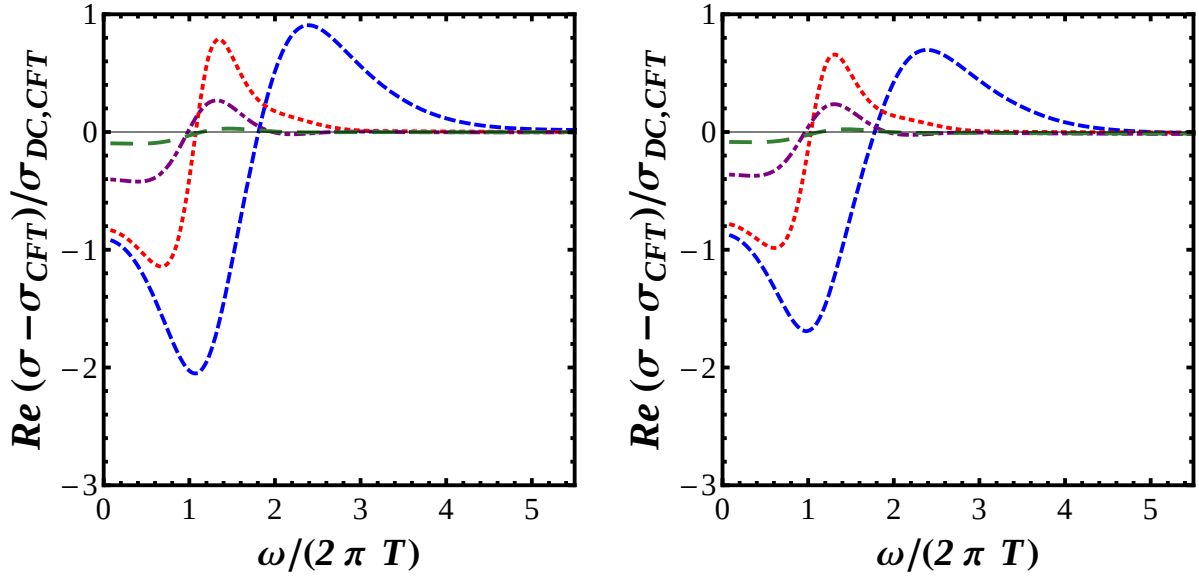

(a) *Model 1 - see* (7.5)

(b) *Model 2 - see* (7.6)

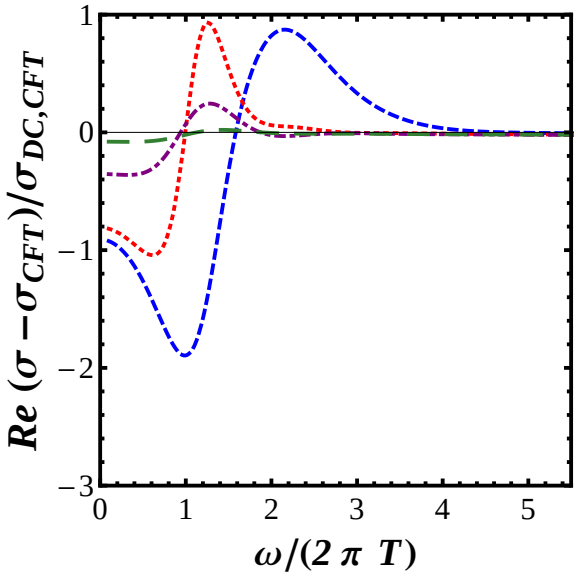

(c) *Model 3 - see* (7.7)

Figure 7.9: *The electric conductivity* $\mathrm{Re}\,\sigma(\omega)$ *subtracted from the corresponding strongly coupling CFT result (normalized by the DC conductivity in the CFT limit) as a function of* $\omega/(2\pi T)$ *for the different model choices of the gauge coupling in Eqs.* (7.5), (7.6), *and* (7.7). *The short-dashed blue curve is for* $T/T_c = 0.45$, *the dotted red curve is for* $T/T_c = 0.74$, *the dash-dotted magenta curve is for* $T/T_c = 1.13$, *and the long dashed green curve is for* $T/T_c = 1.81$. *(Here,* $T_c \sim 150\,\mathrm{MeV}$*).* *(Here,* $T_c \sim 150\,\mathrm{MeV}$*).*

Teaney in Ref. [86]. However, it is interesting to see that as the temperature is lowered towards the phase transition region the value of $G_E(T\tau)$ at the minimum (which must be at $\tau T = 1/2$) decreases. This is consistent with the behavior observed in Figure 7.9: for lower temperatures the region in ω for which $\rho(\omega) < \rho(\omega)_{CFT}$ becomes larger and, thus, for $T\tau = 1/2$ one should expect that the value of the integral performed with the conformal spectral density should be larger than the value found for the non-conformal theory. Also, this is consistent with the fact that $\sigma_{DC}/\sigma_{DC,CFT} < 1$ for those temperatures. Thus, at least within this model the downward shift of the minimum of the Euclidean correlator is a good indicator of the temperature dependence of the DC conductivity. This also seems to be the case in recent lattice calculations [323] (see also the general discussion in Ref. [324]).

7.6 Conclusions and Outlook for this Chapter

In this Chapter a non-conformal, bottom-up holographic model that is able to describe recent lattice QCD thermodynamics at zero chemical potential [78] was used to estimate the electric transport properties of the strongly coupled QGP near the deconfinement crossover phase transition. In order to access the electric properties of the plasma, the coupling between the bulk fields that define the background (the metric and a scalar field) and the bulk gauge field (which describes the conserved current in the gauge theory) was fixed by imposing that the charge susceptibility of the model agrees with recent lattice data [318] near the transition. All the parameters of the model were then fixed and the model was subsequently used to compute the frequency dependent electric conductivity (which has the DC conductivity as its $\omega \to 0$ limit) and the charge diffusion constant. We remark that in our phenomenological bottom up model, the coupling $f(\phi)$ between the scalar and gauge sectors is put in by hand and, clearly, its profile is not specified a priori in the model. However, some information about this function is obtained by imposing that the electric charge susceptibility of the model is similar to that found on the lattice. We have used three different parametrizations for this coupling, which give the same qualitative results for all the observables investigated in this thesis.

The ratio $\sigma_{DC}/\sigma_{DC,CFT}$ was found to vary very rapidly in the temperature range $T \sim 150 - 300$ MeV, which may have some interesting implications for heavy ion collision observables [63,64,288,289]. Also, we have shown that the charge diffusion constant of the plasma has a similar temperature dependence (when normalized by its conformal value) as $\sigma_{DC}/\sigma_{DC,CFT}$ when $T > 150$ MeV. Overall, we find that both the DC conductivity and the charge diffusion coefficient are suppressed with respect to their CFT values at low

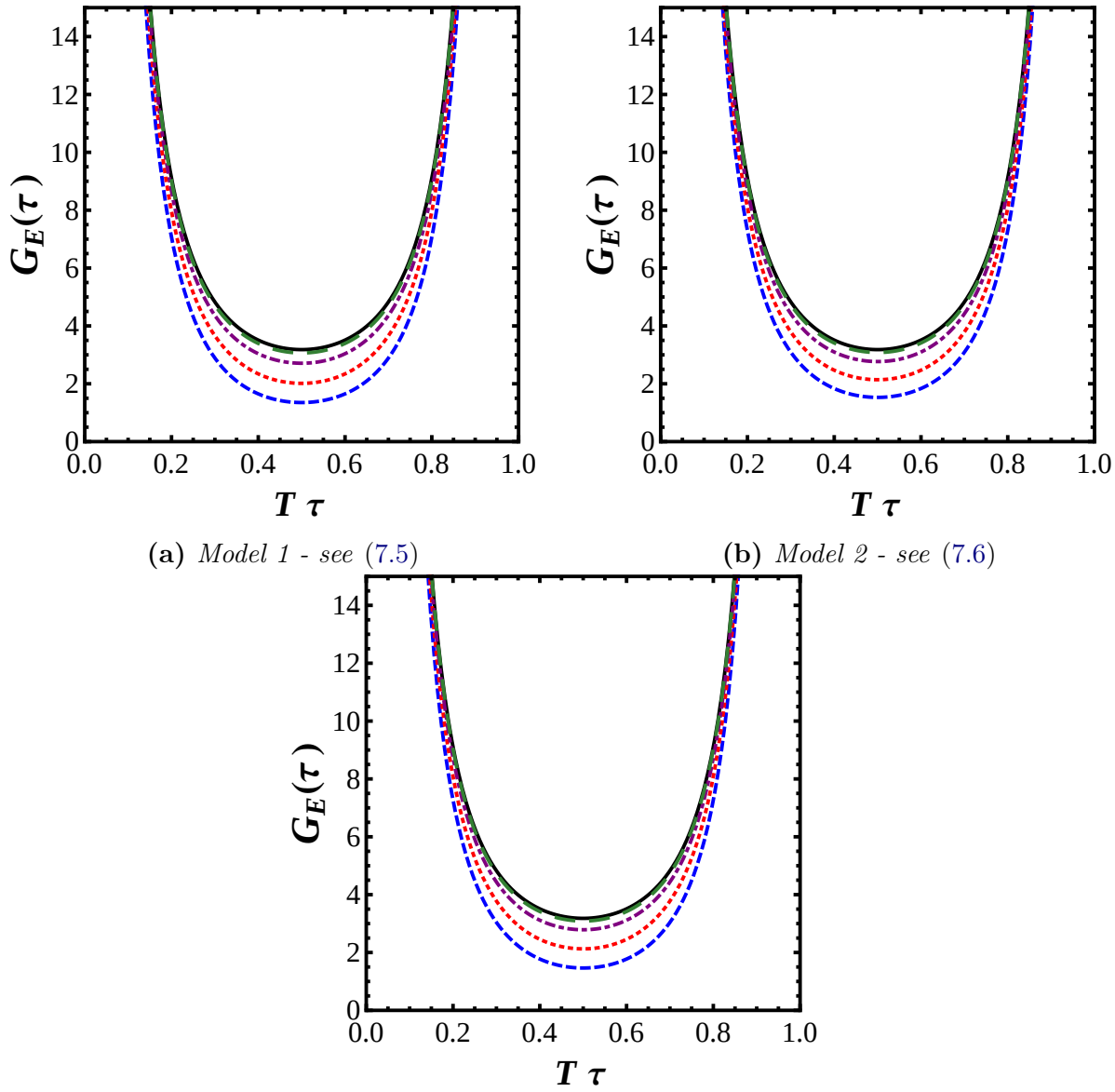

(a) *Model 1 - see* (7.5)

(b) *Model 2 - see* (7.6)

(c) *Model 3 - see* (7.7)

Figure 7.10: *The Euclidean correlator* $G_E(T\tau)$ *in Eq.* (7.15) *as a function of* $T\tau$*. The solid black curve is the conformal result at strong coupling, the short-dashed blue curve is for* $T/T_c = 0.45$*, the dotted red curve is for* $T/T_c = 0.74$*, the dash-dotted magenta curve is for* $T/T_c = 1.13$*, and the long dashed green curve is for* $T/T_c = 1.81$*.*

temperatures where the violation of conformal invariance is large[7]. It would be interesting to check if that is also going to be the case in lattice calculations (in this case the high T is a weakly interacting CFT). The results for $\mathrm{Re}\,\sigma(\omega)$ show distinct differences for temperatures below and above $T_c = 150$ MeV. Below T_c, the violation of conformal invariance makes $\mathrm{Re}\,\sigma(\omega)$ smaller than its CFT value for low ω (this is consistent with our findings that $\sigma_{DC}/\sigma_{DC,CFT} \leq 1$) while it approaches the CFT result from above at high frequencies.

We also computed the Euclidean correlator $G_E(T\tau)$ and its overall shape seems to be insensitive to the structure present in $\sigma(\omega)$. This means that, at least from the viewpoint of this holographic setup, the extraction of the spectral density from $G_E(T\tau)$ by analytic continuation may require very precise numerical results for the Euclidean correlator. However, within this model the downward shift of the minimum of the Euclidean correlator due to non-conformal effects seems to be a good indicator for the temperature dependence of the DC conductivity.

A generalization of the flow equation in Ref. (7.11) can be solved numerically for nonzero momenta yielding the complete spectral density $\rho(\omega, \mathbf{k})$, which can then be used to estimate holographically the photon and dilepton production rates in the QGP near the deconfinement transition. Such study was already done for $\mathcal{N} = 4$ SYM in Ref. [290] and it would be interesting to compute these observables with the model used in this thesis. We intend to pursue this study in the future.

The results of this Chapter were presented in Ref. [21].

[7] This infrared suppression was also observed in calculations performed within the soft-wall model [268] done in Ref. [325].

Chapter 8

Hydrodynamic transport coefficients for the non-conformal quark-gluon plasma from holography

8.1 Introduction

After the discovery of the quark-gluon plasma (QGP) in ultra-relativistic heavy ion collisions [8–11], a lot of effort has been put towards understanding how the spatial anisotropies present in the initial state are converted into the final flow of hadrons. Relativistic dissipative hydrodynamics has played an important role in our current view of the complicated spacetime evolution of the QGP formed in heavy ion collisions (for a recent review see [82]). The overall picture that is consistent with experimental data is that before hadronization the QGP evolves in time and space as a relativistic fluid with minimal dissipative effects. Indeed, current estimates [82] for the shear viscosity to entropy density ratio, η/s, of the QGP obtained by comparison to data are in the ballpark of the very small value $\eta/s = 1/(4\pi)$ [90] found in a broad class of strongly-coupled non-Abelian plasmas described by the gauge/gravity duality [14,93,94] (as discussed at length in Chapters 2 and 3). This suggests that the gauge/gravity duality may be useful for the study of the non-equilibrium properties of strongly interacting plasmas that are similar (if not quantitatively at least qualitatively so) to the QGP and, thus, several applications have been studied over the last years (see, for instance, the review [103]).

In fact, we shall show in this Chapter that a simple bottom-up holographic model that is able to describe (some of) the thermodynamic properties of the QGP near the crossover phase transition [73], namely Model B2 explored in Chapter 6, can be instrumental in providing estimates for the temperature dependence of a large number of second order transport coefficients that appear in consistent theories of (non-conformal) dissipative

relativistic hydrodynamics.

This Chapter is organized as follows. In the next section we shall review the dissipative hydrodynamic theory obtained at second-order in gradients in the case of a non-conformal, relativistic plasma (in the absence of conserved charges such as the baryon number) in a curved spacetime [326]. At this order in the gradient expansion, there are 17 coefficients (besides the speed of sound) that may possess some nontrivial temperature dependence (especially near the phase transition)[1]. In Section 8.3 we present our method to holographically compute the second order transport coefficients κ and τ_π in strongly-coupled plasmas that are described by a bulk action including the metric and a dynamical scalar field (see also Appendix G.1). In Section 8.4 we give the details of the parametrization of model B2 used in this Chapter. In Section 8.5 we compute the temperature dependence of several transport coefficients for this holographic bottom-up model. In Section 8.6 we use the 2nd-order gradient theory defined in Section 8.2 to write an Israel-Stewart-like hydrodynamic theory in flat spacetime with 13 transport coefficients that could be implemented in numerical hydrodynamics. Also, a guide to the temperature dependence of the several 2nd-order transport coefficients considered in this Chapter (given in terms of fitting functions that could be easily used in numerical hydrodynamics) can be found in Appendix G.2. Furthermore, in Appendix G.3 we perform a linear stability analysis around the static equilibrium for the non-conformal, 2nd order gradient expansion theory discussed in Section 8.2. Our conclusions and outlook for this Chapter can be found in Section 8.7.

The reader that is mostly interested in the hydrodynamic discussions and the specific temperature dependence of the transport coefficients (shown in Figs. 8.4 to 8.13) may want to focus on Sections 8.2, 8.6, and Appendices G.2 and G.3. The other sections are devoted to more detailed calculations involving the gauge/gravity duality.

8.2 Second-order non-conformal hydrodynamics via the gradient expansion

Relativistic dissipative hydrodynamics can be viewed as a type of effective theory for the long wavelength, low frequency behavior of an interacting system at finite temperature and/or chemical potential [335,336]. Such an effective theory may be constructed at weak coupling in the case of a dilute gas [337–343] whose microscopic behavior can be described by a Boltzmann-like equation for the system's effective quasi-particles [344,345]. On the

[1] We note that many more coefficients would be needed in the case where spatial isotropy in the equilibrium state is lost, as it occurs in anisotropic hydrodynamics [327–333] and in fluids in the presence of strong magnetic fields (see, for instance, [334]). However, these interesting generalizations will not be pursued here.

other hand, at strong coupling the fluid-gravity correspondence [346] provides an adequate framework to study the effects of spacetime gradients in a strongly coupled fluid.

In general, dissipation is included directly at the level of the equations of motion[2], which in the absence of conserved charges, correspond solely to the conservation of energy and momentum

$$\nabla_\mu T^{\mu\nu} = 0\,, \tag{8.1}$$

where ∇_μ is the covariant spacetime derivative in a curved 4-dimensional spacetime described by a metric $g_{\mu\nu}$, and $T^{\mu\nu}$ is the expectation value of the system's energy-momentum tensor operator (recall Section 3.8). We shall consider here matter described by a relativistic quantum field theory giving the equation of state, $P = P(\varepsilon)$, where ε and P are the local energy density and pressure of the fluid, respectively. The equation of state gives rise to the speed of sound in the fluid, $c_s = \sqrt{dP/d\varepsilon}$. The basic idea of the gradient expansion is that the macroscopic degrees of freedom in the long wavelength, low frequency limit are only the local energy density, ε, 4-velocity, u_μ, metric, $g_{\mu\nu}$ (in curved spacetime), and their gradients. In fact, the energy-momentum tensor can be generically decomposed as

$$T^{\mu\nu} = \varepsilon u^\mu u^\nu + P\Delta^{\mu\nu} + \pi^{\mu\nu} + \Delta^{\mu\nu}\Pi \tag{8.2}$$

where the flow obeys $u_\mu u^\mu = -1$, and $\Delta^{\mu\nu} = g^{\mu\nu} + u^\mu u^\nu$ is a local projection operator transverse to the flow. Note that such a decomposition inherently assumes that there is a well defined local rest frame (for examples of quantum field theories in far from equilibrium conditions without a local rest frame see Ref. [350]). Dissipation generally appears due to a nonzero shear stress tensor

$$\pi^{\mu\nu} = \Delta^{\mu\nu\alpha\beta} T_{\alpha\beta}\,, \tag{8.3}$$

which is transverse to the flow[3], symmetric, and traceless due to the definition of the tensor projector

$$\Delta^{\mu\nu\alpha\beta} = \frac{1}{2}\left(\Delta^{\mu\alpha}\Delta^{\nu\beta} + \Delta^{\mu\beta}\Delta^{\nu\alpha}\right) - \frac{1}{3}\Delta^{\mu\nu}\Delta^{\alpha\beta}\,. \tag{8.4}$$

The last term in Eq. (8.2) denotes the dissipative contribution to the energy-momentum tensor with non-vanishing trace, Π, called the bulk viscous pressure. In terms of Eq. (8.2), one can show that the conservation of energy and momentum become

$$\begin{aligned} D\varepsilon + (\varepsilon + P + \Pi)\theta + \frac{1}{2}\pi_{\mu\nu}\sigma^{\mu\nu} &= 0\,, \\ (\varepsilon + P + \Pi)Du^\mu + \nabla^\mu_\perp(P + \Pi) + \Delta^\mu_\nu \nabla_\alpha \pi^{\alpha\nu} &= 0\,, \end{aligned} \tag{8.5}$$

[2]For recent discussions including attempts to formulate dissipative hydrodynamics in terms of an effective action see, for instance, [347–349].

[3]Note in this Chapter we use the Landau frame, i.e., $u_\mu T^{\mu\nu} = -\varepsilon\, u^\nu$ [335].

where $D = u^\mu \nabla_\mu$ is the comoving derivative, $\nabla_\perp^\alpha = \Delta^{\alpha\beta}\nabla_\beta$ is the derivative transverse to the flow, $\theta = \nabla_\mu u^\mu$ is the scalar expansion rate, and $\sigma_{\mu\nu} = 2\Delta^{\alpha\beta}_{\mu\nu}\nabla_\alpha u_\beta$ is the shear tensor. The energy conservation equation can be written in terms of the equilibrium entropy density, $s = (\varepsilon + P)/T$, as follows

$$\nabla_\mu(su^\mu) = Ds + s\theta = -\frac{\pi_{\mu\nu}\sigma^{\mu\nu}}{2T} - \frac{\Pi\theta}{T}\,. \tag{8.6}$$

In the gradient expansion approach, since only ε and u_μ are the hydrodynamical variables, the dissipative components $\pi_{\mu\nu}$ and Π must be expressed solely in terms of derivatives of these quantities. To first order in gradients, this can be easily done and one finds

$$\pi^{\mu\nu} = -\eta\sigma^{\mu\nu}\,, \qquad \Pi = -\zeta\theta\,, \tag{8.7}$$

where η is the shear viscosity and ζ is the bulk viscosity, respectively. Note that in this case the second law of thermodynamics in (8.6) imposes that $\eta, \zeta \geq 0$. If one uses the expressions above for the dissipative contributions in $T^{\mu\nu}$, the conservation equations represent the relativistic extension of the well-known Navier-Stokes (NS) equations [335] [4] - which we have already analyzed in the context of Section 3.8.

In kinetic theory, the transport coefficients η and ζ are proportional to their corresponding mean free paths, ℓ [5]. One can now see how the power counting scheme adopted in the gradient expansion works. Since ℓ is a microscopic scale and ε and u_μ are taken to be slowly varying functions of time and space, one can associate with their gradients a characteristic (macroscopic) length scale $\sim 1/L_{macro}$ such that $\ell/L_{macro} \ll 1$. Therefore, terms such as those in (8.7) are taken to be of order 1 in the so-called Knudsen number $K_n \sim \ell/L_{macro}$ [6]. Clearly, the continuous description of the system as a fluid hinges on the assumption that K_n is sufficiently small. However, given that dissipation only appears at order 1 in this expansion, one may also entertain the case in which K_n is still sufficiently small to ensure a well-defined continuous description but the flow is such that higher order terms may be taken into account. Nevertheless, one should keep in mind that the radius of convergence of the gradient series is limited by the first nonzero non-hydrodynamical quasinormal mode, as recently shown in Ref. [355] in the context of strongly coupled gauge theories and discussed earlier in Ref. [356] in the context of kinetic theory.

[4] Another way to understand how dissipation appears is to notice that, for instance, in this NS fluid the inclusion of $\pi_{\mu\nu}$ breaks the time reversal invariance present in the ideal fluid equations of motion. However, it is possible to find nontrivial fluid patterns involving second order gradients where $\pi_{\mu\nu}$ is nonzero but time reversal is not broken - see [351, 352].

[5] Note that the mean free path for bulk viscosity is different than that for shear viscosity [353]. However, for simplicity, we shall denote any mean free path here by ℓ.

[6] We remark that the Knudsen "number" is actually a field since it depends on the spacetime coordinates. Moreover, in general one may consider several types of Knudsen numbers associated with different properties of the flow, see for instance [354].

For instance, in the early stages of a ultrarelativistic nucleus-nucleus collision [357], the local energy density and flow are expected to have sizable gradients and corrections of second order in K_n may be relevant at that stage of the QGP evolution. Also, as emphasized in [354], in collisions involving smaller systems such as proton-nucleus collisions at the LHC, the need for higher order Knudsen number corrections may be even more pressing. Therefore, it is reasonable to ask what are the expressions for $\pi_{\mu\nu}$ and Π including $\mathcal{O}(K_n^2)$ terms. Generalizing the previous analysis involving 2nd order terms in a conformal fluid done in [326], Romatschke proposed in [358] the following expansion for the dissipative parts of a non-conformal relativistic fluid in curved spacetime valid at $\mathcal{O}(K_n^2)$

$$\begin{aligned}
\pi^{\mu\nu} &= -\eta\sigma^{\mu\nu} + \eta\tau_\pi\left(D\sigma^{\langle\mu\nu\rangle} + \frac{\theta}{3}\sigma^{\mu\nu}\right) + \kappa\left(\mathcal{R}^{\langle\mu\nu\rangle} - 2u_\alpha u_\beta\mathcal{R}^{\alpha\langle\mu\nu\rangle\beta}\right) + s \\
&+ \lambda_1\sigma_\lambda^{\langle\mu}\sigma^{\nu\rangle\lambda} + \lambda_2\sigma_\lambda^{\langle\mu}\Omega^{\nu\rangle\lambda} - \lambda_3\Omega_\lambda^{\langle\mu}\Omega^{\nu\rangle\lambda} + \\
&+ 2\kappa^*\, u_\alpha u_\beta\mathcal{R}^{\alpha\langle\mu\nu\rangle\beta} + \eta\tau_\pi^*\,\sigma^{\mu\nu}\,\frac{\theta}{3} + \lambda_4\nabla^{\langle\mu}\ln s\,\nabla^{\nu\rangle}\ln s\,,
\end{aligned} \tag{8.8}$$

and

$$\begin{aligned}
\Pi &= -\zeta\theta + \zeta\tau_\Pi\, D\theta + \xi_1\sigma_{\mu\nu}\sigma^{\mu\nu} + \xi_2\,\theta^2 \\
&+ \xi_3\Omega_{\mu\nu}\Omega^{\mu\nu} + \xi_4\nabla_\mu^\perp\ln s\,\nabla_\perp^\mu\ln s + \xi_5\mathcal{R} + \xi_6 u^\mu u^\nu\mathcal{R}_{\mu\nu}\,,
\end{aligned} \tag{8.9}$$

where $\mathcal{R}^\lambda_{\mu\sigma\nu}$ is the Riemann tensor, $\mathcal{R}_{\mu\nu} = \mathcal{R}^\lambda_{\mu\nu\lambda}$ is the Ricci tensor, and $\mathcal{R} = g_{\mu\nu}\mathcal{R}^{\mu\nu}$ is the Ricci scalar [359]. Moreover, we have also defined the vorticity tensor $\Omega_{\mu\nu} = \frac{1}{2}\left(\nabla_\mu^\perp u_\nu - \nabla_\nu^\perp u_\mu\right)$ and the usual notation $B^{\langle\mu\nu\rangle} = \Delta^{\mu\nu}_{\alpha\beta}B^{\alpha\beta}$ for the traceless, symmetric, and transverse part of a second rank tensor $B^{\mu\nu}$. Eqs. (8.8) and (8.9) can then be used in the conservation equations (8.5) to define the equations of motion for a non-conformal fluid in a curved spacetime valid at second order in gradients[7].

One can see that besides the speed of sound squared $c_s^2 = dP/d\varepsilon$ that is already present in ideal hydrodynamics and the coefficients η and ζ that appeared at 1st order, there are now altogether 15 new transport coefficients that appear at second order in the gradient expansion. Following [360], one may distinguish these coefficients by separating out those that are of *thermodynamical* origin and those that are not. The set of coefficients κ, κ^*, λ_3, λ_4, ξ_3, ξ_4, ξ_5, ξ_6 can be determined via Kubo formulas involving only equilibrium quantities and Euclidean two- and three-point functions of the energy-momentum tensor components and, thus, they are of thermodynamical origin being suitable for lattice calculations [360]. However, the other coefficients η, ζ, τ_π, τ_π^*, τ_Π, λ_1, λ_2, ξ_1, and ξ_2 are as-

[7] Due to the fact that spacetime covariant derivatives generally do not commute in a curved spacetime, even when the metric is not dynamical (though still nontrivial) quantities such as $\mathcal{R}^\lambda_{\mu\nu\alpha}$, $\mathcal{R}_{\mu\nu}$, and $\mathcal{R}$ are expected to appear in the equations of motion for ε and u_μ. Also, we note that the expressions in (8.8) and (8.9) are in agreement with the corresponding terms (in flat spacetime) at $\mathcal{O}(K_n^2)$ found in [342].

sociated with quantities that define the dissipative properties of the theory (for instance, η is proportional to the imaginary part of a retarded Green's function) such as $\sigma_{\mu\nu}$ and are, thus, of dynamical origin [360].

There are several interesting points regarding these second order terms. First, as discussed in [358,360–363] not all of these coefficients are independent and we shall get back to this point in Section 8.5 where we compute several of these coefficients in the holographic model defined in Section 8.4. Second, for a conformal plasma only the terms that transform homogeneously under a Weyl transformation[8] are present [326] and this implies that κ^*, τ_{π^*}, λ_4, ζ, τ_Π, $\xi_{1,2,3,4,5,6}$ vanish in the conformal limit (therefore, in this case, $\Pi = 0$). Third, even though κ, κ^*, ξ_5, and ξ_6 do not contribute to the equations of motion in flat spacetime, they do contribute to the Kubo formulas for the other coefficients relevant to flat spacetime hydrodynamics and should then be taken into account, as discussed in [326,360]. Moreover, in a non-conformal fluid all of these coefficients may be nontrivial functions of the temperature, i.e., $\eta = \eta(T)$, especially near a phase transition (even if of the crossover type). This shows how challenging numerical 2nd order hydrodynamics can be if all of these temperature dependent transport coefficients are taken into account. Clearly, as long as these 2nd order gradient terms can be taken as small corrections, their effect should be under control. However, it is not clear at the moment if this is indeed the case for the type of event-by-event hydrodynamic simulations fed by the complicated initial conditions that describe the early stages of a heavy ion collision [357].

Furthermore, unfortunately the equations of motion defined by Eqs. (8.8) and (8.9) cannot be directly implemented in numerical hydrodynamic codes because, for instance, they are linearly unstable against small fluctuations around the static equilibrium (see Appendix G.3). In fact, in Section 8.6 we propose another second order theory that is more suitable for numerical investigations using the current relativistic hydrodynamic codes. This theory can be considered as a type of "UV completion" of the 2nd order theory in Eqs. (8.8) and (8.9) in the sense that it possesses a well defined (and causal) UV behavior (at least in the linear regime) but its long wavelength, low frequency asymptotic hydrodynamical solution is identical to the one obtained by Eqs. (8.8) and (8.9) with the same transport coefficients. We shall discuss these points in detail in Section 8.6.

[8] Under a Weyl transformation, $g_{\mu\nu} \to e^{-2\omega} g_{\mu\nu}$, where ω is an arbitrary (positive-definite) scalar function. In a conformal plasma, $T^{\mu\nu} \to e^{6\omega} T^{\mu\nu}$ while the temperature transforms as $T \to e^{\omega} T$, see [326].

8.3 Holographic calculation of the 2nd order coefficients κ and τ_π

In this section we discuss how we are going to evaluate the 2nd order hydrodynamic transport coefficients κ and τ_π, originally defined in [326], using the gauge/gravity duality [14, 93, 94]. First, we shall consider the case where the action in the bulk corresponds to 5-dimensional pure gravity (with a negative cosmological constant) and then later we will generalize this discussion for the case where the bulk action contains a dynamical scalar field.

8.3.1 Renormalized pure gravity action

In order to compute these transport coefficients, it is sufficient to consider only the small frequency ω, small momentum q limit of the (xy, xy)-component of the retarded propagator of the stress-energy tensor of the boundary quantum field theory, Eq. (8.10),

$$G^R_{\mu\nu\rho\lambda}(\omega) = -i \int dt d^3x e^{i\omega t - i\vec{k}\cdot\vec{x}} \theta(t) \left\langle \left[T_{\mu\nu}(t,\vec{0}), T_{\rho\lambda}(0,\vec{0}) \right] \right\rangle . \tag{8.10}$$

which can be written in momentum space as follows [358][9].

$$G^{xy,xy}_R(\omega, q) = P - i\eta\omega + \left(\eta\tau_\pi - \frac{\kappa}{2} + \kappa^* \right) \omega^2 - \frac{\kappa}{2} q^2 + \mathcal{O}(\omega q^2, \omega^3), \tag{8.11}$$

where κ^* is a second order hydrodynamic coefficient which is non-vanishing only for non-conformal fluids (see Eq. (8.8)), being related to κ by the following constraint [360–363]

$$\kappa^* = \kappa - \frac{T}{2} \frac{d\kappa}{dT} . \tag{8.12}$$

According to the gauge/gravity duality dictionary, discussed at length in Chapter 3, the stress-energy tensor of the plasma is sourced in the partition function of the boundary quantum field theory by the boundary value of a classical metric perturbation placed over an asymptotically AdS bulk. In Eq. (8.11), it was assumed that the xy-component of the metric perturbation has no dependence on the x- and y-directions, such that the 4-momentum of its Fourier mode is given by $k_\mu = (-\omega, q_x, q_y, q_z) = (-\omega, 0, 0, q)$. From Eqs. (8.11) and (8.12), one obtains the following Kubo formulas for κ and τ_π (valid for both

[9] This momentum expansion is analogous to the one performed in Section 3.8 for T_{xy}, Eq. (3.124).

conformal and non-conformal fluids)[10]

$$\kappa = -\lim_{q\to 0}\lim_{\omega\to 0}\frac{\partial^2 G_R^{xy,xy}(\omega,q)}{\partial q^2}, \tag{8.13}$$

$$\tau_\pi = \frac{1}{2\eta}\left(\lim_{q\to 0}\lim_{\omega\to 0}\frac{\partial^2 G_R^{xy,xy}(\omega,q)}{\partial \omega^2} - \kappa + T\frac{d\kappa}{dT}\right). \tag{8.14}$$

In order to compute κ and τ_π from Eqs. (8.13) and (8.14) via holography, we need to evaluate the renormalized on-shell bulk action and extract from it the retarded graviton propagator by following the prescription proposed in Ref. [127], which was later justified and generalized in Refs. [128,137,364]. Note that in this case one cannot use the membrane paradigm approach exposed in Chapters 3 and 7, since the Kubo formulas (8.14) require the real part of the retarted correlator.[11] In the case of pure gravity, the regularized action is defined by the sum of the Einstein-Hilbert (EH) action, the Gibbons-Hawking-York (GHY) action[12] [365,366] and the counterterm action[13] [154,326]

$$\begin{aligned} S_{\rm reg} &= S_{\rm EH} + S_{\rm GHY} + S_{\rm CT} \\ &= \frac{1}{16\pi G_5}\left\{\int_{\mathcal{M}_5} d^5x\sqrt{-g}\,[R(g)-2\Lambda] + 2\int_{\partial\mathcal{M}_5} d^4x\sqrt{-\gamma}K(\gamma) + \right. \\ &\qquad \left. -\frac{6}{L}\int_{\partial\mathcal{M}_5} d^4x\sqrt{-\gamma}\left[1+\frac{L^2}{2}\mathcal{P} - \frac{L^4}{12}\left(\mathcal{P}^{\mu\nu}\mathcal{P}_{\mu\nu}-\mathcal{P}^2\right)\ln(\epsilon)\right]\right\}, \end{aligned} \tag{8.15}$$

where G_5 is the five dimensional Newton's constant and the cosmological constant enforcing the existence of asymptotically AdS_5 geometries with radius L as solutions of Einstein's equations is given by $\Lambda = -6/L^2$. The metric induced at the boundary is given by $\gamma_{MN} = g_{MN} - \hat{n}_M\hat{n}_N$, where $\hat{n}_M$ is an outward directed unit vector orthogonal to the boundary. In a coordinate chart where the boundary of the asymptotically AdS space is at the value $u = 0$ of the radial coordinate, this is given by $\hat{n}_M = -\delta^u_M\sqrt{g_{uu}} \Rightarrow \hat{n}^M = -\delta^M_u/\sqrt{g_{uu}}$, and the metric induced at the regularizing boundary surface[14] $u = \epsilon$ can be

[10] We thank G. Moore and K. Sohrabi for discussions about these coefficients.

[11] In principle, one could compute the imaginary part of the the retarted correlator G_R and use the Kramers-Kronig relations to compute the real part from the imaginary part. However, this approach is plagued by numerical problems.

[12] The GHY action needs to be added to the EH action in order to properly define the variational problem with Dirichlet boundary conditions for the metric tensor when the spacetime manifold has a boundary.

[13] The counterterm action is obtained through the holographic renormalization procedure [120,122,368–370].

[14] Strictly speaking, this quantity diverges at $u = 0$. Therefore, in order to regularize quantities of interest, we introduce an ultraviolet cutoff $\epsilon \ll 1$ for the radial coordinate near the boundary, which must be taken to zero at the very end of the calculations after all the divergent terms in the on-shell gravity action have been canceled.

simply written as

$$\gamma_{\mu\nu} = g_{\mu\nu}\Big|_{u=\epsilon}. \tag{8.16}$$

The extrinsic curvature of the boundary of an asymptotically AdS space is given by (see [367] for a review)

$$K(\gamma) = \frac{\hat{n}^u}{2}\gamma^{\mu\nu}\partial_u\gamma_{\mu\nu} = -\frac{\sqrt{g^{uu}}}{2}\gamma^{\mu\nu}\gamma'_{\mu\nu}, \tag{8.17}$$

where the prime denotes a derivative in the radial direction. The boundary sectional curvature tensor and the boundary sectional curvature scalar are defined, respectively, by [368]

$$\mathcal{P}_{\mu\nu} = \frac{1}{2}\left(\mathcal{R}_{\mu\nu}(\gamma) - \frac{1}{6}\mathcal{R}(\gamma)\gamma_{\mu\nu}\right), \quad \mathcal{P} = \gamma^{\mu\nu}\mathcal{P}_{\mu\nu}, \tag{8.18}$$

where $\mathcal{R}_{\mu\nu}(\gamma)$ and $\mathcal{R}(\gamma)$ are the Ricci tensor and the Ricci scalar evaluated using the induced metric on the boundary surface.

Let us now consider a small perturbation in the metric, $h_{MN}(u,t,z)$, placed over a diagonal and isotropic gravitational background[15], $g^{(0)}_{MN}(u)$, which is assumed to be asymptotically AdS. Since we are only interested in the (xy,xy)-component of the retarded propagator of the boundary stress-energy tensor, as discussed in [154], if one fixes the gauge defined by the subsidiary condition $h_{Mu} = 0$, one only needs to consider $h_{xy}(u,t,z) \neq 0$ and set to zero all the other components of the metric perturbation since the linearized equation of motion for the xy-perturbation decouples from the other components of the metric perturbation in this gauge. Therefore, we consider the following disturbed line element

$$\begin{aligned} ds^2 &= g_{MN}(u,t,z)dx^M dx^N \\ &= g^{(0)}_{MN}(u)dx^M dx^N + 2h_{xy}(u,t,z)dxdy \\ &= g_{uu}(u)du^2 - g_{tt}(u)dt^2 + g_{xx}(u)(dx^2+dy^2+dz^2) + 2g_{xx}(u)\phi(u,t,z)dxdy, \end{aligned} \tag{8.19}$$

where we defined $\phi(u,t,z) = h^x_y(u,t,z)$ and, with the sign convention used in (8.19), we are considering the tt-component of the metric to be $-g_{tt}(u)$, with $g_{tt}(u) > 0$.

Let us now explicitly show that the EH action for the disturbed metric, up to second order in the metric perturbation ϕ, can be written as the action for a massless scalar field in the undisturbed background $g^{(0)}_{MN}$ plus total derivatives which shall contribute to the

[15]The index (0) refers to the undisturbed background.

final expression for the regularized on-shell boundary gravity action[16]. Up to $\mathcal{O}(\phi^2)$, we find

$$\sqrt{-g}R(g) \approx \left[\sqrt{-g^{(0)}}\left(1-\frac{\phi^2}{2}\right)\right]\left[R^{(0)}+\frac{3}{2}g^{MN}_{(0)}\partial_M\phi\partial_N\phi+2\phi\nabla^2_{(0)}\phi+\frac{g'_{xx}}{g_{uu}g_{xx}}\phi\phi'\right]. \tag{8.20}$$

Since we are assuming that the background metric is a solution of Einstein's equations, we can make use of these equations to write down two useful relations for our purposes. The first one comes from contracting the background metric with its equation of motion

$$g^{MN}_{(0)}\left[R^{(0)}_{MN}-\frac{g^{(0)}_{MN}}{2}\left(R^{(0)}-2\Lambda\right)\right]=0\Rightarrow R^{(0)}=\frac{2D}{D-2}\Lambda=-\frac{20}{L^2}. \tag{8.21}$$

The second useful relation comes from substituting (8.21) into the xx-component of the Einstein's equations for the background metric

$$R^{(0)}_{xx}-\frac{g_{xx}}{2}\left(-\frac{8}{L^2}\right)=0\Rightarrow\frac{4}{L^2}=-\frac{1}{g_{xx}}\left[-\frac{\nabla^2_{(0)}g_{xx}}{2}+\frac{g^{MN}_{(0)}\partial_M g_{xx}\partial_N g_{xx}}{2g_{xx}}\right]. \tag{8.22}$$

Substituting Eq. (8.21) into Eq. (8.20), plugging the result into the EH action and integrating by parts the term proportional to $\phi\nabla^2_{(0)}\phi$, we obtain, up to $\mathcal{O}(\phi^2)$

$$\begin{aligned}S_{\text{EH}} \approx &-\frac{1}{2\pi L^2G_5}V_4\int_\epsilon^{u_H}du\sqrt{-g^{(0)}}+\frac{1}{16\pi G_5}\int_{\mathcal{M}_5}d^5x\sqrt{-g^{(0)}}\left[-\frac{1}{2}g^{MN}_{(0)}\partial_M\phi\partial_N\phi+\mathcal{I}\right]+\\&+\frac{1}{8\pi G_5}\int_{\partial\mathcal{M}_5}d^4x\sqrt{-\gamma^{(0)}g^{uu}}\phi\phi'\Big|_\epsilon^{u_H},\end{aligned} \tag{8.23}$$

where $V_4=\int_{\partial\mathcal{M}_5}d^4x$ is the 4-volume of the boundary, $u=u_H$ is the position of the background black hole horizon in the radial coordinate[17] and

$$\begin{aligned}\int_{\mathcal{M}_5}d^5x\sqrt{-g^{(0)}}\mathcal{I}&=\int_{\mathcal{M}_5}d^5x\sqrt{-g^{(0)}}\left[\frac{g'_{xx}}{g_{uu}g_{xx}}\phi\phi'+\frac{4}{L^2}\phi^2\right]\\&=\int_{\mathcal{M}_5}d^5x\sqrt{-g^{(0)}}\left[\frac{g^{MN}_{(0)}\partial_M g_{xx}\partial_N(\phi^2)}{2g_{xx}}+\frac{\nabla^2_{(0)}g_{xx}}{2g_{xx}}\phi^2-\frac{g^{MN}_{(0)}\partial_M g_{xx}\partial_N g_{xx}}{2g^2_{xx}}\phi^2\right]\\&=\int_{\partial\mathcal{M}_5}d^4x\sqrt{-\gamma^{(0)}g^{uu}}\frac{g'_{xx}}{2g_{xx}}\phi^2\Big|_\epsilon^{u_H},\end{aligned} \tag{8.24}$$

where we used relation (8.22). Substituting Eq. (8.24) into Eq. (8.23), we obtain, up to

[16]The author thanks R. Critelli for discussions concerning this derivation.

[17]If the background has no event horizon (or some kind of infrared wall), then one must take $u_H\to\infty$.

$\mathcal{O}(\phi^2)$

$$S_{\rm EH} \approx -\frac{1}{2\pi L^2 G_5} V_4 \int_\epsilon^{u_H} du\sqrt{-g^{(0)}} - \frac{1}{32\pi G_5}\int_{\mathcal{M}_5} d^5x\sqrt{-g^{(0)}}\, g^{MN}_{(0)}\partial_M\phi\partial_N\phi + \\ + \frac{1}{8\pi G_5}\int_{\partial\mathcal{M}_5} d^4x\sqrt{-\gamma^{(0)}g^{uu}}\left[\phi\phi' + \frac{g'_{xx}}{4g_{xx}}\phi^2\right]\Bigg|_\epsilon^{u_H}. \tag{8.25}$$

From Eq. (8.25) we see that, as stated before, the bulk term of the disturbed EH action up to second order in the metric perturbation ϕ corresponds to the action for a massless scalar field in the undisturbed background $g^{(0)}_{MN}$, as is well-known. Hence, the linearized equation of motion for the mixed metric perturbation ϕ is just the massless Klein-Gordon equation in a curved background

$$\nabla^2_{(0)}\phi = \frac{1}{\sqrt{-g^{(0)}}}\partial_M\left(\sqrt{-g^{(0)}}g^{MN}_{(0)}\partial_N\phi\right) = 0\,. \tag{8.26}$$

Defining the Fourier transform as

$$\phi(u,t,z) = \int_{-\infty}^{\infty}\frac{d\omega dq}{(2\pi)^2}e^{-i\omega t+iqz}\phi(u,\omega,q), \tag{8.27}$$

one finds in momentum space

$$\partial_u\left(\sqrt{-g^{(0)}}g^{uu}\phi'(u,\omega,q)\right) = \sqrt{-g^{(0)}}\left(-g^{tt}\omega^2 + g^{xx}q^2\right)\phi(u,\omega,q)\,. \tag{8.28}$$

Integrating by parts the bulk piece of Eq. (8.25) and making use of Eq. (8.26), we put the EH action on-shell up to $\mathcal{O}(\phi^2)$

$$S^{\text{on-shell}}_{\rm EH,bdy} \approx \frac{1}{2\pi L^2 G_5}V_4\lim_{u\to\epsilon}\int du\sqrt{-g^{(0)}} - \frac{1}{32\pi G_5}\int_{\partial\mathcal{M}_5} d^4x\lim_{u\to\epsilon}\sqrt{-\gamma^{(0)}g^{uu}}\left[3\phi\phi' + \frac{g'_{xx}}{g_{xx}}\phi^2\right]^{\text{(on-shell)}}, \tag{8.29}$$

where, by following the prescription proposed in [127] for calculating the retarded propagator of the metric perturbation, we discarded the horizon contribution coming from the radial integration and took into account only the boundary contribution for the on-shell EH action.

Now we add Eq. (8.29) to the contributions coming from the disturbed GHY and counterterm actions evaluated up to $\mathcal{O}(\phi^2)$ to find the following expression for the total

regularized on-shell boundary action in momentum space[18] up to $\mathcal{O}(\phi^2, \omega^2, q^2)$

$$S_{\rm reg}(\epsilon) \approx \frac{1}{16\pi G_5} \lim_{u\to\epsilon} \left\{ \frac{V_4}{L^2} \left[-6L\sqrt{-\gamma^{(0)}} + 8\int du \sqrt{-g^{(0)}} - \frac{L^2 g_{xx}(g_{xx}g'_{tt} + 3g_{tt}g'_{xx})}{\sqrt{g_{uu}g_{tt}g_{xx}}} \right] + \right.$$
$$+ \int_{-\infty}^{\infty} \frac{d\omega dq}{(2\pi)^2} \frac{\phi(u,-k)}{2L^2} \left[\phi(u,k) \left(6L\sqrt{-\gamma^{(0)}} + \frac{L^2 g_{xx}(g_{xx}g'_{tt} + 2g_{tt}g'_{xx})}{\sqrt{g_{uu}g_{tt}g_{xx}}} + \right. \right.$$
$$\left. \left. + \frac{L^3 q^2 \sqrt{g_{tt}g_{xx}}}{2} - \frac{L^3\omega^2}{2}\sqrt{\frac{g_{xx}^3}{g_{tt}}} \right) + L^2\sqrt{-\gamma^{(0)}}g^{uu}\phi'(u,k) \right] \Bigg\}. \tag{8.30}$$

One can formally solve Eq. (8.28) in terms of the components of the undisturbed background metric, $g^{(0)}_{MN}(u)$, and the boundary value of the metric perturbation, $\varphi(\omega, q)$, by employing a perturbative expansion in $\omega \ll T$ and $q \ll T$. Such a solution up to $\mathcal{O}(\omega^2, q^2)$ is derived in details in Appendix G.1 and the results near the boundary read

$$\phi(\epsilon, k) \approx \varphi(k), \tag{8.31}$$

$$\phi'(\epsilon, k) \approx \varphi(k) \left[\frac{i\omega}{4\pi T(u_H - \epsilon)} + f'(\epsilon, k) \right]$$
$$\approx \frac{\varphi(k) g_{xx}^{3/2}(u_H)}{\sqrt{-g^{(0)}(\epsilon)}g^{uu}(\epsilon)} \left[i\omega + \omega^2 \int_{u_H}^{\epsilon} du \left(\frac{g_{xx}^{3/2}(u_H)}{\sqrt{-g^{(0)}}g^{uu}} - \frac{\sqrt{-g^{(0)}}g^{tt}}{g_{xx}^{3/2}(u_H)} \right) + q^2 \int_{u_H}^{\epsilon} du \frac{\sqrt{-g^{(0)}}g^{xx}}{g_{xx}^{3/2}(u_H)} \right]. \tag{8.32}$$

Substituting Eq. (8.31) and Eqs. (8.32) into (8.30) one obtains an expression for the total regularized on-shell boundary action up to $\mathcal{O}(\phi^2, \omega^2, q^2)$ written solely in terms of the components of the undisturbed background metric and the boundary value of the metric perturbation $\varphi(k)$.

The renormalized on-shell boundary gravity action is defined by

$$S_{\rm ren} \equiv \lim_{\epsilon\to 0} S_{\rm reg}(\epsilon). \tag{8.33}$$

For completeness, let us also review some useful formulas for calculating the pressure, the entropy density, and the shear viscosity of the boundary plasma using the gauge/gravity duality. From Eq. (8.11), we see that once we have extracted the retarded propagator from the renormalized on-shell boundary action by following the prescription proposed

[18] This is a rather lengthy calculation but it can be straightforwardly done with the help of a symbolic mathematical software such as Wolfram's Mathematica [371]. We used the EDCRGTC code [372] written for Mathematica in order to deal with the lengthy tensor manipulations involved in the course of these calculations.

in [127]

$$S_{\rm ren} = \lim_{\epsilon\to 0} S_{\rm reg}(\epsilon) = -\frac{1}{2}\lim_{\epsilon\to 0}\int_{-\infty}^{\infty}\frac{d\omega dq}{(2\pi)^2}\varphi(-\omega,-q)\mathcal{F}(\omega,q;\epsilon)\varphi(\omega,q) + (\varphi\text{-independent terms});$$
$$G_R^{xy,xy}(\omega,q) \equiv \lim_{\epsilon\to 0}\mathcal{F}(\omega,q;\epsilon) \tag{8.34}$$

one can obtain the pressure as follows

$$P = \lim_{k\to 0} G_R^{xy,xy}(k). \tag{8.35}$$

Since the perturbation-independent part of the on-shell boundary action gives $-PV_4$ [326], we can also calculate the pressure by using the following alternative formula

$$P = -\lim_{\varphi\to 0}\frac{S_{\rm ren}}{V_4}. \tag{8.36}$$

One can evaluate the entropy of the plasma by using the Bekenstein-Hawking's relation Eq. (3.45), that is,

$$S = \frac{A_H}{4G_5}, \tag{8.37}$$

where the "area" of the horizon is given by, in this coordinate system,

$$A_H = \int_{\rm horizon} d^3x\sqrt{g}\Big|_{u=u_H \text{ and } t \text{ fixed}} = \sqrt{g_{xx}^3(u_H)}V_3, \tag{8.38}$$

and the entropy density thus reads

$$s = \frac{S}{V_3} = \frac{\sqrt{g_{xx}^3(u_H)}}{4G_5}. \tag{8.39}$$

Application: Thermal $\mathcal{N}=4$ Supersymmetric Yang-Mills (SYM)

In this subsection we review the calculations for SYM at finite temperature [326] whose gravity dual is defined over an AdS_5-Schwarzschild background with metric components

$$g_{uu}(u) = \frac{L^2}{u^2 h(u)},\quad g_{tt}(u) = \frac{L^2 h(u)}{u^2},\quad g_{xx}(u) = \frac{L^2}{u^2};\quad h(u) = 1 - \frac{u^4}{u_H^4}. \tag{8.40}$$

The relation between G_5 and the number of colors of the strongly coupled SYM plasma reads (recall Eq. (3.20))

$$G_5 = \frac{G_{10}}{\pi^3 L^5} = \frac{\pi L^3}{2N_c^2}\,. \tag{8.41}$$

Recall that for $\mathcal{N}=4$ at strongly coupling, from Eqs. (3.44) and (3.49),

$$T = \frac{1}{\pi u_H}, \quad s = \frac{N_c^2}{2\pi L^3}\frac{L^3}{{u_H}^3} = \frac{\pi^2 T^3 N_c^2}{2}. \tag{8.42}$$

Now we use Eqs. (8.40), (8.41), and (8.42) to calculate Eq. (8.32) and, by substituting the result into Eq. (8.30) and then evaluating Eq. (8.33), we obtain the renormalized on-shell boundary action up to $\mathcal{O}(\phi^2, \omega^2, q^2)$ for SYM

$$S_{\rm ren} \approx -\frac{\pi^2 T^4 N_c^2}{8} V_4 + \int_{-\infty}^{\infty} \frac{d\omega dq}{(2\pi)^2} \varphi(-k)\varphi(k) \frac{T^2 N_c^2}{32} \left[q^2 - 2\pi^2 T^2 + 2i\omega\pi T - \omega^2(1-\ln 2)\right]\,. \tag{8.43}$$

Substituting Eq. (8.43) into Eq. (8.34), we obtain the graviton propagator up to $\mathcal{O}(\phi^2, \omega^2, q^2)$

$$G_R^{xy,xy}(\omega, q) \approx -\frac{T^2 N_c^2}{16}\left[q^2 - 2\pi^2 T^2 + 2i\omega\pi T - \omega^2(1-\ln 2)\right], \tag{8.44}$$

and by using Eq. (8.35) (or also Eq. (8.36)), we obtain, in an alternative way, the pressure of the conformal strongly-coupled SYM plasma, already given in Eq. (3.52) from the entropy density (3.49),

$$P = \frac{\pi^2 T^4 N_c^2}{8}. \tag{8.45}$$

The first order hydrodynamic transport coefficient η for the SYM plasma is found by substituting (8.44) into the Kubo formula (3.128)

$$\eta = \frac{\pi T^3 N_c^2}{8}. \tag{8.46}$$

From Eqs. (8.42) and (8.46), one re-obtains (3.156),

$$\frac{\eta}{s} = \frac{1}{4\pi}, \tag{8.47}$$

first computed in Section 3.8 by means of the membrane paradigm. The second order hydrodynamic transport coefficients κ and τ_π for the SYM plasma are found by substituting

Eq. (8.44) into Eqs. (8.13) and (8.14), respectively

$$\kappa = \frac{T^2 N_c^2}{8}, \tag{8.48}$$

$$\tau_\pi = \frac{2 - \ln 2}{2\pi T}. \tag{8.49}$$

These results for the conformal SYM plasma were originally obtained in Ref. [326].

8.3.2 General holographic formulas for κ and τ_π in Einstein+Scalar gravity duals

In this section we derive general formulas for κ and τ_π which are valid also for systems where the metric couples to matter fields in the bulk (we shall focus here on the case where there is a scalar field in the bulk).

For geometries corresponding to solutions of the field equations which take into account the backreaction of matter fields in the bulk, the pure gravity regularized action (8.30) shall feature, in general, temperature-independent divergences as one takes the limit $\epsilon \to 0$. For instance, this happens in Einstein+Scalar models [15–17, 252, 373]. For this kind of system, the general procedure of holographic renormalization is discussed in [369]. Here, since we are only interested in evaluating hydrodynamic transport coefficients[19], instead of dealing with a more complicated regularized action, we are going to apply a physical prescription which will allow us to obtain quite general formulas for κ and τ_π through a simple procedure. This prescription is based on three main facts:

1. The equation of motion for the xy-component of the metric perturbation depends only on the background metric [154, 326] and, therefore, the solution (8.32) remains valid also for Einstein+Scalar actions.

2. Ultraviolet divergences are temperature-independent and, consequently, one can remove these divergences by subtracting contributions evaluated at different temperatures.

3. The coefficients κ and $\tau_\pi \eta$, which appear in the gradient expansion, must vanish at sufficiently low temperatures (as one approaches the vacuum).

Let us first discuss the coefficient κ in Eq. (8.13). We begin by defining the following

[19] Notice that the Kubo's formulas for transport coefficients are defined in terms of momentum derivatives of retarded correlators and, therefore, momentum-independent terms in the on-shell action do not contribute in such calculations.

regularized quantity (see Eqs. (8.30) and (8.34))

$$\kappa_\epsilon := -\lim_{q\to 0}\lim_{\omega\to 0}\frac{\partial^2}{\partial q^2}\mathcal{F}(\omega,q;\epsilon) = \frac{1}{8\pi G_5}\left[\frac{L^3}{2\epsilon^2}+\int_{u_H}^{\epsilon} du\sqrt{-g^{(0)}}g^{xx}\right], \tag{8.50}$$

and then we take the following expression, which is free of ultraviolet divergences

$$\begin{aligned}\kappa(T) =& \lim_{\epsilon\to 0}\left(\kappa_\epsilon(T)-\kappa_\epsilon(T_{\rm high})\right)+\kappa_{\rm SYM}(T_{\rm high})-\kappa_0\\ \approx& \frac{1}{8\pi G_5}\left[\int_{u_H(T)}^{\epsilon} du\,\sqrt{-g^{(0)}}g^{xx}\Big|_{u_H(T)} - \int_{u_{\rm high}}^{\epsilon} du\,\sqrt{-g^{(0)}}g^{xx}\Big|_{u_{\rm high}}\right]\Bigg|_{\epsilon\ll 1}\\ &+\kappa_{\rm SYM}(T_{\rm high})-\kappa_0\,,\end{aligned} \tag{8.51}$$

where $T_{\rm high}$ is a temperature that is sufficiently large so that we are near the ultraviolet fixed point and the temperature-dependent part[20] of $\kappa_\epsilon(T_{\rm high})$ approaches $\kappa_{\rm SYM}(T_{\rm high})$, $u_{\rm high}=u_H(T_{\rm high})$, and κ_0 is a constant to be subtracted (generally by numerical inspection) in order to ensure that $\kappa(T_{\rm min})=0$ where $T_{\rm min}$ is the lowest temperature considered in our numerical calculations ($T_{\rm min}\sim 10$ MeV). From Eqs. (8.41) and (8.48), one finds

$$\kappa_{\rm SYM} = \frac{T^2N_c^2}{8} = \frac{\pi T^2L^3}{16G_5}\,. \tag{8.52}$$

Analogously, for τ_π in Eq. (8.14) we begin by defining

$$\tau_\pi = \frac{1}{2\eta}\left(\Omega-\kappa+T\frac{d\kappa}{dT}\right), \tag{8.53}$$

$$\begin{aligned}\Omega_\epsilon :=& \lim_{q\to 0}\lim_{\omega\to 0}\frac{\partial^2}{\partial\omega^2}\mathcal{F}(\omega,q;\epsilon) =\\ =& \frac{1}{8\pi G_5}\left[\frac{L^3}{2\epsilon^2}+g_{xx}^{3/2}(u_H)\int_{\epsilon}^{u_H} du\left(\frac{g_{xx}^{3/2}(u_H)}{\sqrt{-g^{(0)}}g^{uu}}-\frac{\sqrt{-g^{(0)}}g^{tt}}{g_{xx}^{3/2}(u_H)}\right)\right],\end{aligned} \tag{8.54}$$

and then we evaluate the UV finite expression

$$\begin{aligned}\Omega(T) =& \lim_{\epsilon\to 0}\left(\Omega_\epsilon(T)-\Omega_\epsilon(T_{\rm high})\right)+\Omega_{\rm SYM}(T_{\rm high})-\Omega_0\\ \approx& \frac{1}{8\pi G_5}\left(g_{xx}^{3/2}(u_H)\int_{\epsilon}^{u_H(T)} du\left[\frac{g_{xx}^{3/2}(u_H)}{\sqrt{-g^{(0)}}g^{uu}}-\frac{\sqrt{-g^{(0)}}g^{tt}}{g_{xx}^{3/2}(u_H)}\right]\Bigg|_{u_H(T)}+\right.\\ &\left.-g_{xx}^{3/2}(u_{\rm high})\int_{\epsilon}^{u_{\rm high}} du\left[\frac{g_{xx}^{3/2}(u_{\rm high})}{\sqrt{-g^{(0)}}g^{uu}}-\frac{\sqrt{-g^{(0)}}g^{tt}}{g_{xx}^{3/2}(u_{\rm high})}\right]\Bigg|_{u_{\rm high}}\right)\Bigg|_{\epsilon\ll 1}+\Omega_{\rm SYM}(T_{\rm high})-\Omega_0,\end{aligned} \tag{8.55}$$

[20] Which is independent of the ultraviolet cutoff ϵ as mentioned before.

where

$$\Omega_{\rm SYM} = \frac{T^2 N_c^2}{8}[1-\ln 2] = \frac{\pi T^2 L^3}{16 G_5}[1-\ln 2]\,, \tag{8.56}$$

and Ω_0 is a constant that is subtracted to ensure that $\tau_\pi(T_{\rm min})\eta(T_{\rm min}) = 0$.

Eqs. (8.51), (8.53), and (8.55) can be used to compute the transport coefficients κ and τ_π for Einstein+Scalar actions. In the next section we employ them to numerically evaluate κ and τ_π in the scalar + Einstein model B2, which reproduces the thermodynamics of (2+1) QCD.

8.4 Thermodynamics of the updated Einstein+Scalar holographic model B2

We shall now use model B2 to compute, using the formalism of the previous section, the transport coefficients of the second order hydrodynamical theory defined by Eq. (8.8), near the deconfinement transition.

The potential $V(\phi)$ used is still given by Eq. (6.125), by in this Chapter we use rhe following updated parametrization for Model B2, which yields a closer match to more recent lattice data [374][21]: $\gamma = 0.606$, $b_2 = 0.703$, $b_4 = -0.1$, $b_6 = 0.0034$ (and the asymptotic AdS_5 radius still fixed as $L = 1$, as before). As before, the temperature scale is chosen in order to match the minimum of the speed of sound c_s^2 computed holographically with that found on the lattice (we take this minimum now to be at 143.8 MeV, as in the recent data [374]). Also, by comparing the holographic result for the pressure with lattice data, we fix $G_5 = 0.5013$. In Figs. 8.1 and 8.2 we compare the lattice results for c_s^2 and P/T^4 of with the results of Ref. [374] with the updated Model B2, as a function of the temperature T. We also compare the trace anomaly θ in Fig. 8.3.

The model is able to describe quantitatively lattice data for the temperature region near the minimum of the speed of sound but the agreement does not persist at very high temperatures, which is expected since the model remains strongly interacting in this case while QCD is asymptotically free (as discussed at length in Section 6.5)[22]. Moreover, even though this model does not have the correct (hadronic) degrees of freedom at low temperatures, the temperature dependence of the thermodynamical quantities do follow lattice

[21] The data set from Ref. [374] is from 2012. The most recent lattice data for the thermodynamics of (2+1) QCD sfrom the Budapest-Wuppertal collaboration is from 2013 [76]. However, both data sets are similar, and are also similar to the 2010 data set used in Ref. [78].

[22] The agreement for the trace anomaly is not as good as for the pressure and the sound speed c_s^2. This is due to the fact that, in lattice, the trace anomaly is computed considering derivatives of the pressure. This procedure may introduce large errors, which can be responsible for the difference between the holographic model and lattice data.

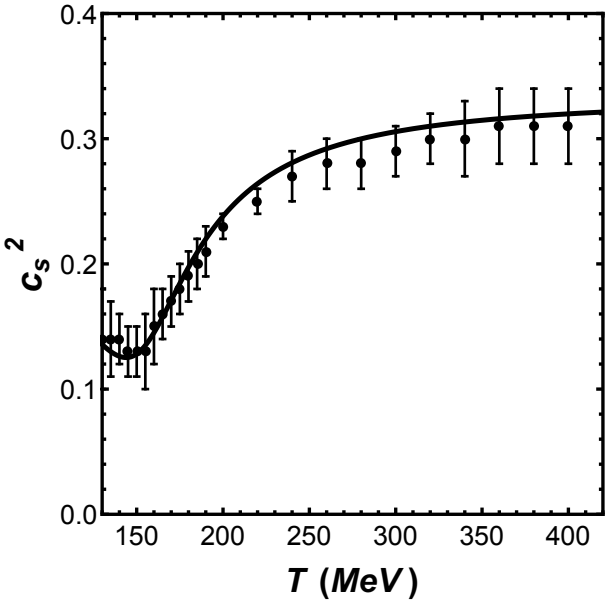

Figure 8.1: *c_s^2 as a function of the temperature T for the updated Model B2 (solid curve) and the corresponding lattice results for $(2+1)$-flavor QCD from [374].*

data even for $T \sim 130$ MeV. The model may then be useful precisely in the temperature region $T \sim 130 - 450$ MeV where a purely hadronic description is not adequate and the temperature may not be high enough to warrant a simple description using perturbative QCD[23].

8.5 Holographic calculation of the transport coefficients

Coefficient κ

The transport coefficients that we will compute in this section appear in the second-order gradient expansion equations in Eqs. (8.8) and (8.9). We first compute the coefficient κ using Eq. (8.51). The first step is to fix a $u_{\rm high}$ at which the geometry computed by solving the equations of motion has already reached its AdS_5 asymptotics. For numerical integration, it is necessary to keep the cutoff ϵ in Eq. (8.51). A value for the cutoff that is too small leads to truncation errors due to the subtraction of two small numbers in Eq. (8.51), which gives an artificial numerical divergence. Thus, to rule out errors introduced due to truncation, one should compute the integral in Eq. (8.51) with a range of choices

[23]We note, however, that *non-perturbative* weak coupling approaches such as the one pursued in [309, 375] do a fairly good job at describing the thermodynamic properties of QCD found on the lattice at high temperatures. The motivation for finding a holographic description of the strongly-coupled QGP relies on the fact that holography is not only able to describe the thermodynamics near the phase transition but it also allows for the direct calculation of non-equilibrium properties, such as transport coefficients, within the same setup.

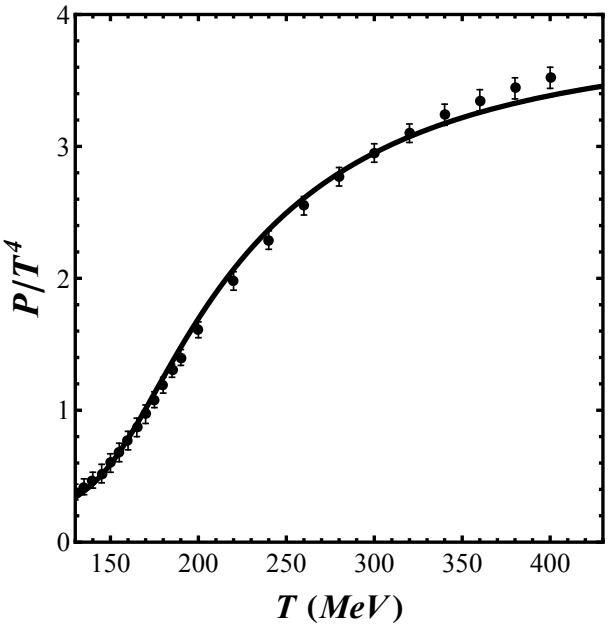

Figure 8.2: *P/T^4 as a function of the temperature T for the updated Model B2 (solid curve) (solid curve) and the corresponding lattice results for $(2+1)$-flavor QCD from [374].*

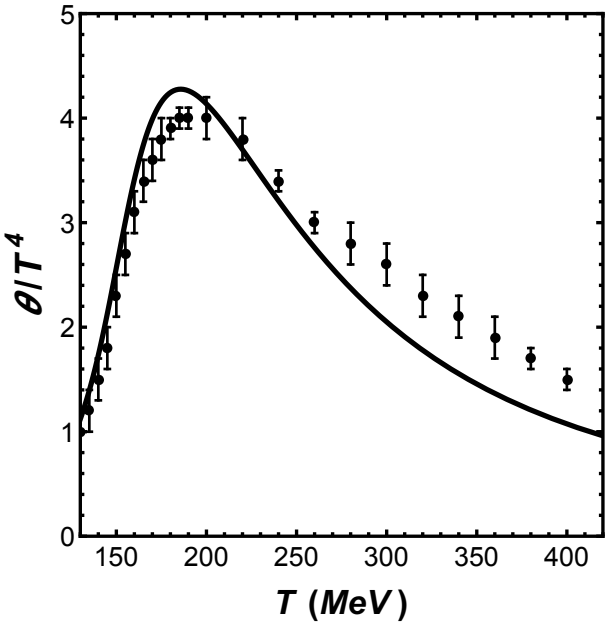

Figure 8.3: *θ/T^4 as a function of the temperature T for the updated Model B2 (solid curve) (solid curve) and the corresponding lattice results for $(2+1)$-flavour QCD from [374].*

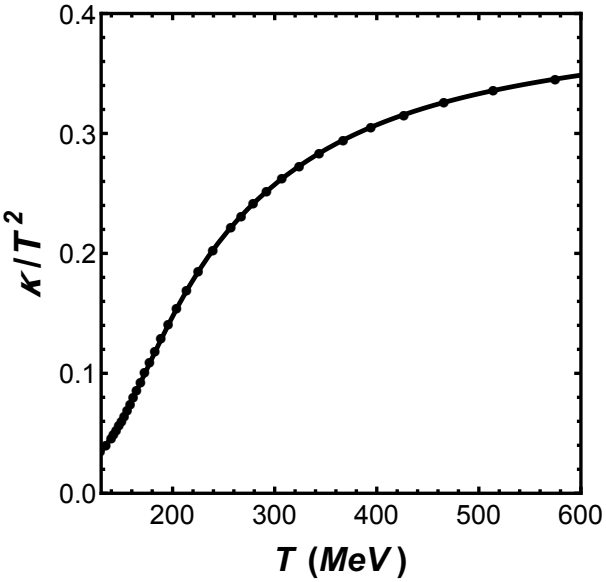

Figure 8.4: *κ/T^2 as a function of the temperature T for the bottom-up holographic model. The black points correspond to the numerical results from the model while the solid black line corresponds to the fit in Eq. (8.57) with the parameters in Table 8.1.*

for ϵ and search for a reasonable range that does not introduce numerical divergences in the integral (which gives a lower bound for ϵ) and also satisfies $\epsilon < u_{\rm high}$ (which gives an upper bound for ϵ). We found that the optimal region for numerical calculations is $10^{-3} < \epsilon < 10^{-1}$ and we have chosen in this work $\epsilon = 10^{-2}$ for the calculation of κ. We have chosen $u_{\rm high} = 0.201$, which corresponds to $T_{\rm high} = 7.813\, T_c$ (where $T_c = 143.8\,\text{MeV}$). We have checked that at this high temperature both the thermodynamics as well as the transport coefficients have matched their conformal plasma limits.

Proceeding as discussed in the previous paragraph, we determine κ as a function of $u_H(T)$ for the chosen $u_{\rm high}$. Using the conformal result at strongly coupling (8.52) and the value of G_5 determined in the previous section, we can determine the dimensionless ratio κ/T^2. In Fig. 8.4 we show the numerical results for κ/T^2 as a function of T. Moreover, we see that κ/T^2 approaches the conformal limit from below rising monotonically with T. Our results are consistent with the lattice results in Ref. [376] where the authors obtained $\kappa/T^2 \sim 0.36(15)$ for $T = 2 - 10\, T_c$ for a pure glue $SU(3)$ plasma (in this case T_c is the critical temperature for the first-order deconfinement phase transition). However, in our model we are able to obtain an estimate for the behavior of κ near the crossover transition of (2+1)-flavor QCD.

For further use, we also present a fit to our calculated points. We use as a fitting function the seven-parameter fit

$$\frac{\kappa}{T^2}\left(x = \frac{T}{T_c}\right) = \frac{a}{1 + e^{b(c-x)} + e^{d(e-x)} + e^{f(g-x)}}, \tag{8.57}$$

where a to g are dimensionless fit parameters and $T_c = 143.8$ MeV, as remarked before. A five parameter fit using parameters from a to e already yields good results - the two extra parameters f, g are used to provide a closer match to the points. This function corresponds to a modified Fermi-Dirac distribution. In Table 8.1 we present the parameters for the fit. These fit parameters provide a good description of our numerical data as shown in Fig. 8.4.

Table 8.1: *Parameters for the fit of κ/T^2 using Eq. (8.57).*

a	b	c	d	e	f	g
0.3817	2.047	1.274	6.0545	1.231	0.5438	-0.2076

Coefficient τ_π

With the same remarks as in the preceding section one can evaluate τ_π using Eqs. (8.53) and (8.55). The procedure is similar to the evaluation of κ. The same $u_{\rm high}$ was chosen while in the present case $\epsilon = 2\times10^{-2}$ - the integrals in (8.55) are more complicated than the integrals in Eq. (8.51) and also more sensitive to the choice of the cutoff.

In Fig. 8.5 we show the numerical results for $\tau_\pi\eta/T^2$ (this is a convenient choice since, by combining the conformal results (8.46) and (8.49), we see that $\tau_\pi\eta \sim T^2$ for a conformal plasma) as a function of T. We see the same general behavior as seen for κ/T^2 or P/T^4, with a marked increase near the crossover region. The transport quantity $\tau_\pi\eta/T^2$ approaches its conformal limit (~ 0.255) from below. We were able to fit these data points using the same parametrization as used for κ/T^2 in Eq. (8.57) - the fit parameters are shown in Table 8.2.

Table 8.2: *Parameters for the fit of $\tau_\pi\eta/T^2$ using Eq. (8.57).*

a	b	c	d	e	f	g
0.2664	2.029	0.7413	0.1717	-10.76	9.763	1.074

For convenience, we show in Fig. 8.6 the quantity $\tau_\pi T$. One can see that this quantity approaches its conformal value, $(2-\ln 2)/(2\pi)$, for $T > 300$ MeV while it displays a peak near the transition.

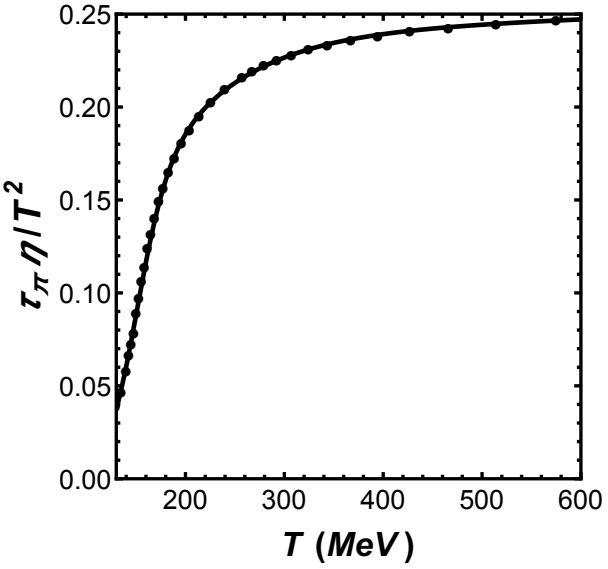

Figure 8.5: *$\tau_\pi \eta / T^2$ as a function of the temperature T for the bottom-up holographic model. The black points correspond to the numerical results from the model while the solid black line corresponds to the fit in Eq. (8.57) with the parameters from Table 8.2.*

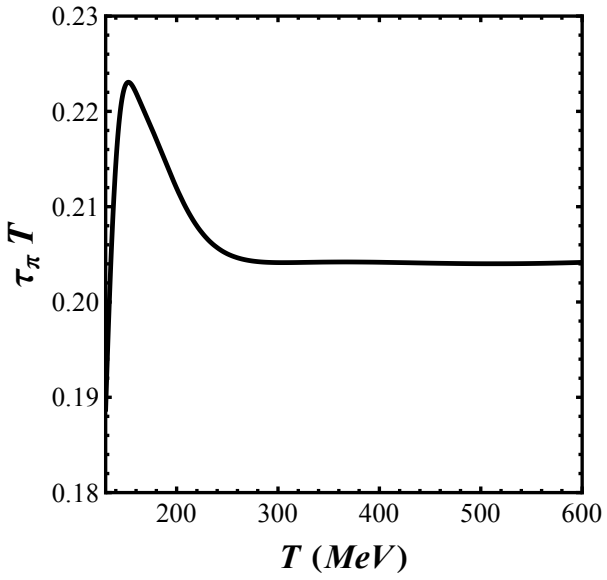

Figure 8.6: *$\tau_\pi T$ as a function of the temperature T for the bottom-up holographic model.*

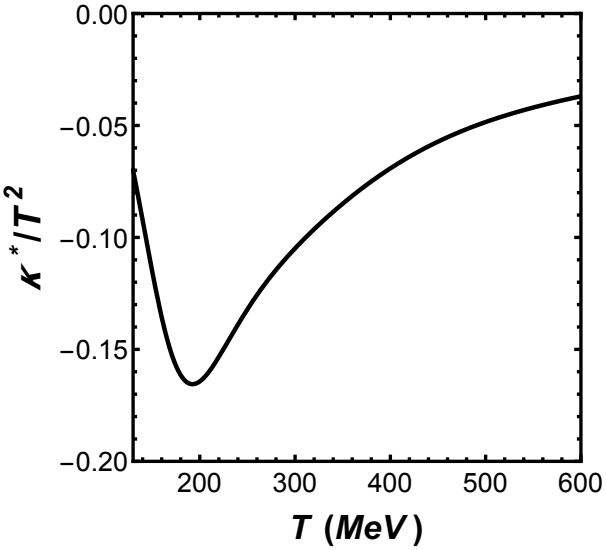

Figure 8.7: *κ^*/T^2 as a function of the temperature T for the bottom-up holographic model.*

Coefficient κ^*

We can now use our results for κ to evaluate several other transport coefficients of second order non-conformal hydrodynamics. Since these coefficients involve derivatives of κ with respect to the temperature, up to third order (in the case of the coefficient ξ_4 in Eq. (8.70), see below), to avoid discretization errors in the computation of the numerical derivatives we will use the parametrization given by Eq. (8.57) with the parameters displayed in Table 8.1. The numerical results for the coefficient κ^*, defined by Eq. (8.12) and computed this way, are shown in Fig. 8.7. One can see that $\kappa^*/T^2 \to 0$ as $T \to \infty$ - this can also be checked directly from the expression used for the fit, Eq. (8.57). We note that this is in agreement with the fact that this coefficient vanishes for a conformal plasma. Also, this coefficient has a very sharp dependence with the temperature near the phase transition (following the behavior displayed by c_s^2) and $\kappa^* < 0$ for all the temperatures used here.

Coefficient ξ_5

Another second order transport coefficient that we can directly evaluate is ξ_5, which is determined by the following constraint equation [360–363]

$$\xi_5 = \frac{1}{2}\left(c_s^2 T \frac{d\kappa}{dT} - c_s^2 \kappa - \frac{\kappa}{3}\right) . \tag{8.58}$$

In conformal hydrodynamics one finds that $\xi_5 = 0$. We evaluated ξ_5/T^2 as a function of the temperature using the equation above and the result can be found in Fig. 8.8. One can see that ξ_5/T^2 has a broad peak in the phase transition around $T \sim 150 - 250\,\mathrm{MeV}$

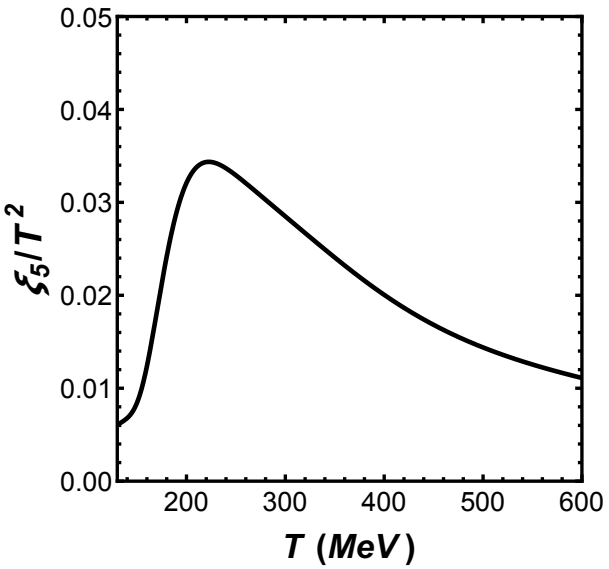

Figure 8.8: ξ_5/T^2 *as a function of the temperature* T *for the bottom-up holographic model.*

and decreases at high temperatures.

Shear and bulk viscosities

For any isotropic holographic model with an effective gravitational action with at most two derivatives, the shear viscosity satisfies the ratio $\eta/s = 1/(4\pi)$ [90] and this is the case of our model.

We can now compute the bulk viscosity ζ using the results of Ref. [254]. This transport coefficient has attracted some attention recently due to its interplay with shear viscosity effects in event-by-event hydrodynamic simulations [377–380]. The bulk viscosity is given by the Kubo formula

$$\zeta = -\frac{4}{9}\lim_{\omega\to 0}\frac{1}{\omega}\,\mathrm{Im}\left[G_R(\omega,\vec{q}=\vec{0})\right], \tag{8.59}$$

which is defined in terms of the retarded propagator of the spatial trace of the boundary stress-energy tensor

$$G_R(\omega,\vec{q}) \equiv -i\int_{\mathbb{R}^{1,3}} d^4x\, e^{i(\omega t-\vec{q}\cdot\vec{x})}\theta(t)\left\langle\left[\frac{1}{2}T^a_a(t,\vec{x}),\frac{1}{2}T^b_b(0,\vec{0})\right]\right\rangle . \tag{8.60}$$

Holographically, this coefficient is computed considering fluctuations of the xx-component of the metric[24], h_{xx}. The equation of motion for the perturbation $\psi \equiv h^x_x = e^{-2A(\phi)}h_{xx}$ is

[24]In Ref. [254] the authors have shown that in the Gubser $\phi = r$ gauge the h_{xx} fluctuation decouples from the other fluctuations, which means that we can examine this channel in separate in order to compute the bulk viscosity.

given by

$$\psi'' + \left(\frac{1}{3A'} + 4A' - 3B' + \frac{h'}{h}\right)\psi' + \left(\frac{e^{-2A+2B}}{h^2}\omega^2 - \frac{h'}{6hA'} + \frac{h'B'}{h}\right)\psi = 0, \tag{8.61}$$

where the prime denotes a ϕ-derivative.

As usual, in order to apply the real time prescription for the holographic computation of retarded correlators, we consider the infalling wave condition at the horizon $\phi = \phi_H$

$$\psi(\phi \to \phi_H) \approx C e^{i\omega t}|\phi - \phi_H|^{-\frac{i\omega}{4\pi T}}, \tag{8.62}$$

with the normalization condition $\psi(\phi \to 0) = 1$ at the boundary. The real time prescription implies that the imaginary part of the retarded correlator is given by

$$\mathrm{Im}\left[G_R(\omega)\right] = -\frac{\mathcal{F}(\omega,\phi)}{16\pi G_5}, \tag{8.63}$$

where $\mathcal{F}(\omega,\phi)$ is a conserved flux in the radial direction

$$\mathcal{F}(\omega,\phi) = \frac{e^{4A-B}h}{4A'^2}|\mathrm{Im}\left[\psi^*\psi'\right]|, \tag{8.64}$$

which can then be conveniently evaluated at the horizon[25]

$$\begin{aligned}\mathcal{F}(\omega,\phi\to\phi_H) &\approx \frac{e^{3A(\phi_H)}}{4A'(\phi_H)^2}\,\frac{e^{A(\phi_H)-B(\phi_H)}}{4\pi T}\,h'(\phi_H)\,\omega|C|^2 \\ &\approx \frac{\omega e^{3A(\phi_H)}|C|^2}{4A'(\phi_H)^2}.\end{aligned} \tag{8.65}$$

Substituting Eq. (8.65) into Eq. (8.63) and then into Eq. (8.59), one finds

$$\frac{\zeta}{s} = \frac{\eta}{s}\,|C|^2\frac{V'(\phi_H)^2}{V(\phi_H)^2}\,, \tag{8.66}$$

where we used Eq. (8.47) and also the relation $A'(\phi_H) = -V(\phi_H)/3V'(\phi_H)$, which can be derived using Einstein's equations for the background metric. Therefore, in order to compute ζ/s from (8.66), one only needs to evaluate (8.62) in the limit of zero frequency $C = \lim_{\omega\to 0}\psi(\phi\to\phi_H)$. We show the numerical results[26] for ζ/s in Fig. 8.9. The bulk viscosity displays a peak near the phase transition but its magnitude is still smaller than η/s.

[25] We expand $h(\phi)$ around $\phi = \phi_H$ to obtain $h(\phi\to\phi_H) \approx h'(\phi_H)(\phi - \phi_H)$.

[26] In order to solve Eq. (8.61) for the perturbation ψ we used a part of numerical code created by the authors of Ref. [137], which is available at https://www.princeton.edu/physics/research/high-energy-theory/gubser-group/code-repository/.

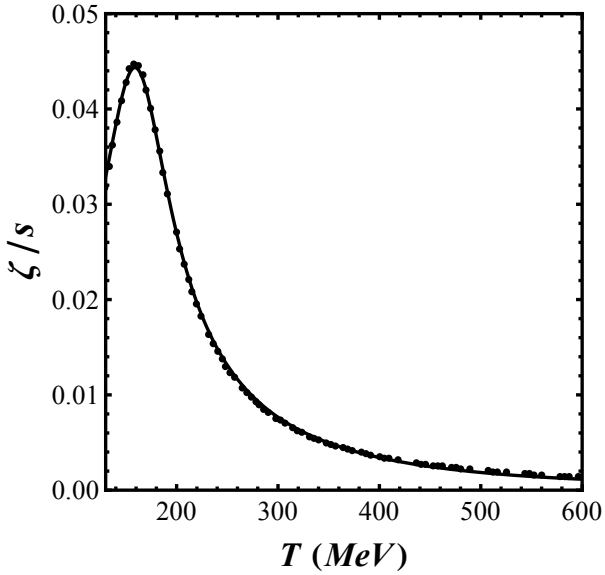

Figure 8.9: *ζ/s as a function of the temperature T for the bottom-up holographic model. The black points correspond to our numerical results while the black curve is the fit in Eq. (8.67) with the parameters in Table 8.3.*

For completeness, we also provide a fit to the numerical results of Fig. 8.9. The form of the function suggests a resonance-like fitting function. With this in mind we used a five-parameter trial function

$$\frac{\zeta}{s}\left(x=\frac{T}{T_c}\right)=\frac{a}{\sqrt{(x-b)^2+c^2}}+\frac{d}{x^2+e^2}, \tag{8.67}$$

where a to e are fit parameters (and $T_c = 143.8$ MeV). The first term of Eq. (8.67) describes the resonance-like peak of Fig. 8.9 while the second term describes a smooth background away from the peak. Using the parameters in Table 8.3, we obtain the fit shown in Fig. 8.9, which gives a good description of our numerical results.

Table 8.3: *Parameters for the fit of ζ/s using Eq. (8.67).*

a	b	c	d	e
0.01162	1.104	0.2387	-0.1081	4.870

At this point we have then directly computed 6 transport coefficients (besides matching lattice QCD thermodynamics): η/s, ζ/s, τ_π, κ, κ^*, and ξ_5. Among these coefficients, only η/s was found to be a constant with T - all the other coefficients displayed some nontrivial behavior near the crossover phase transition.

Next, we use these results to give our best estimate for the temperature dependence

of 6 other coefficients: λ_3, λ_4, ξ_3, ξ_4, ξ_6, and τ_Π.

Estimates for the coefficients ξ_3, ξ_4, ξ_6, λ_3, and λ_4

Let us now examine three other second order transport coefficients of non-conformal hydrodynamics, ξ_3, ξ_4, and ξ_6, which satisfy the following constraints [360]

$$\xi_6 = c_s^2\left(3T\frac{d\kappa}{dT} - 2T\frac{d\kappa^*}{dT} + 2\kappa^* - 3\kappa\right) - \kappa + \frac{4\kappa^*}{3} + \frac{\lambda_4}{c_s^2}, \tag{8.68}$$

$$\xi_3 = \frac{3c_s^2}{2}T\left(\frac{d\kappa^*}{dT} - \frac{d\kappa}{dT}\right) + \frac{3}{2}(c_s^2 - 1)\,(\kappa^* - \kappa) - \frac{\lambda_4}{c_s^2} + \frac{1}{4}\left(c_s^2 T\frac{d\lambda_3}{dT} - 3c_s^2\lambda_3 + \frac{\lambda_3}{3}\right), \tag{8.69}$$

$$\xi_4 = -\frac{\lambda_4}{6} - \frac{c_s^2}{2}\left(\lambda_4 + T\frac{d\lambda_4}{dT}\right) + c_s^4(1 - 3c_s^2)\left(T\frac{d\kappa}{dT} - T\frac{d\kappa^*}{dT} + \kappa^* - \kappa\right) + \\ - c_s^6 T^3\frac{d^2}{dT^2}\left(\frac{\kappa - \kappa^*}{T}\right), \tag{8.70}$$

where the second order coefficients λ_3 and λ_4 are given by the following Kubo's formulas involving Euclidean 3-point functions [360, 381]

$$\lambda_3 = 2\kappa^* - 4\lim_{p_z,q_z\to 0}\frac{\partial^2}{\partial p_z \partial q_z}G_E^{xt,yt,xy}(p_t = 0, \vec{p}, q_t = 0, \vec{q}), \tag{8.71}$$

$$\lambda_4 = -2\kappa^* + \kappa - \frac{c_s^4}{2}\lim_{p_x,q_y\to 0}\frac{\partial^2}{\partial p_x \partial q_y}G_E^{tt,tt,xy}(p_t = 0, \vec{p}, q_t = 0, \vec{q})\,. \tag{8.72}$$

In order to compute ξ_3, ξ_4, and ξ_6 using the constraints (8.68) to (8.70) it is necessary to evaluate λ_3 and λ_4. However, the holographic computation of 3-point functions is far more involved than the computation of 2-point functions. In fact, for the strongly coupled SYM plasma λ_3 has been evaluated explicitly by computing the Euclidean 3-point function $G_E^{xt,yt,xy}(p,q)$, yielding $\lambda_3 = 0$ [382]. Since $\kappa^* = 0$ in a conformal theory, from Eq. (8.71) we obtain that for a strongly coupled SYM

$$\lim_{p_z,q_z\to 0}\frac{\partial^2}{\partial p_z \partial q_z}G_E^{xt,yt,xy}(p_t = 0, \vec{p}, q_t = 0, \vec{q}) = 0. \tag{8.73}$$

In order to evaluate λ_4 one should in principle compute the Euclidean 3-point function $G_E^{tt,tt,xy}(p,q)$. However, there is a shortcut which makes use of the constraint (8.68). In a 4-dimensional CFT, we know that $c_s^2 = 1/3$ and we also know that $\kappa^* = 0$ and that $\xi_{3,4,5,6} = 0$, since these are coefficients of non-conformal hydrodynamics. Then, from Eq. (8.68) we deduce that in a CFT $\lambda_4 = 0$, which agrees with [358]. Then, from Eq. (8.72),

we conclude that in a strongly coupled CFT

$$\lim_{p_x,q_y\to 0}\frac{\partial^2}{\partial p_x\partial q_y}G_E^{tt,tt,xy}(p_t=0,\vec{p},q_t=0,\vec{q})=\frac{2\kappa}{c_s^4}. \tag{8.74}$$

The evaluation of the full 3-point functions required to compute the coefficients λ_3 and λ_4 in the effective model of Einstein+Scalar gravity where the metric is only known numerically is far beyond the scope of this work. In order to fully determine them it is necessary to compute the full bulk-to-boundary and bulk-to-bulk propagators - and it is very difficult to compute these functions in terms of a numerical metric such as the one used in this work.

Thus, in this Chapter we will resort to a sort of "hybrid CFT/non-CFT" approximation. For the evaluation of the second order coefficients λ_3 and λ_4 from Eqs. (8.71) and (8.72) we shall mix the CFT 3-point functions (8.73) and (8.74) with the full non-conformal results for κ and κ^*. In this case, the resulting approximations for λ_3 and λ_4 give

$$\lambda_3=-\lambda_4=2\kappa^*\,. \tag{8.75}$$

With these approximations, and the full non-conformal results for κ, κ^*, and c_s^2, we can approximately evaluate ξ_3, ξ_4, and ξ_6 from Eqs. (8.68) to (8.70). This sort of approximation provides our best estimate for these coefficients given the current lack of knowledge about 3-point functions in non-conformal holographic plasmas that display a crossover phase transition. In Figs. 8.10 to 8.12 we show the results for ξ_6/T^2, ξ_3/T^2, and ξ_4/T^2 as functions of T - all of these coefficients vary rapidly near the phase transition. We note that the approximations done here for these coefficients constitute the first deviations from the ultraviolet conformal regime and, therefore, they are much more reliable at high temperatures.

A lower bound estimate for τ_Π

Ref. [383] derived, using the asymptotic causality condition, a relation among the transport coefficients τ_π, τ_Π, η, and ζ

$$\frac{\zeta}{s\tau_\Pi T}+\frac{\eta}{s\tau_\pi T}\leq 1-c_s^2\,. \tag{8.76}$$

The computation of the transport coefficient τ_Π directly from its retarded Green's function, as was done for the shear coefficient τ_π, is beyond the scope of this Chapter. However, we note that one can use the relation (8.76) to obtain a lower bound for the coefficient

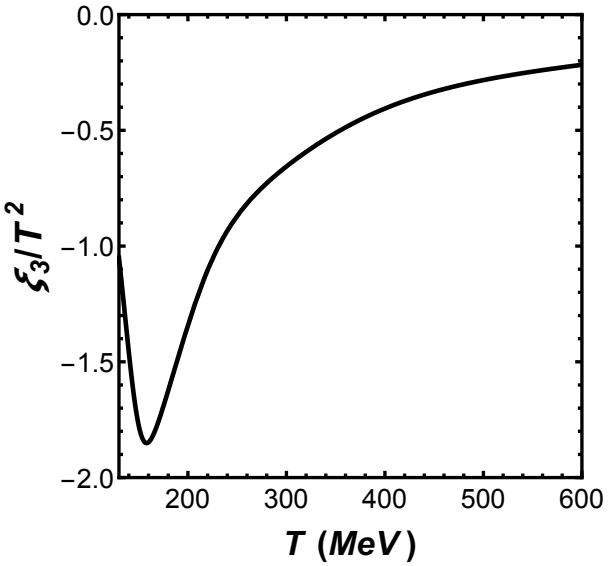

Figure 8.10: ξ_3/T^2 *as a function of the temperature* T *for the bottom-up holographic model.*

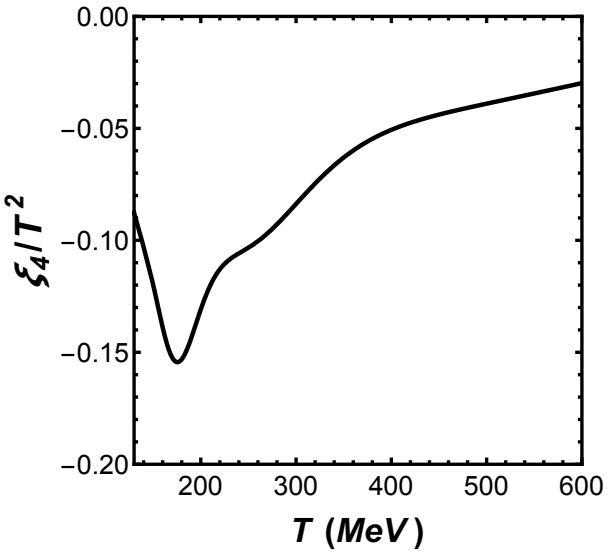

Figure 8.11: ξ_4/T^2 *as a function of the temperature* T *for the bottom-up holographic model.*

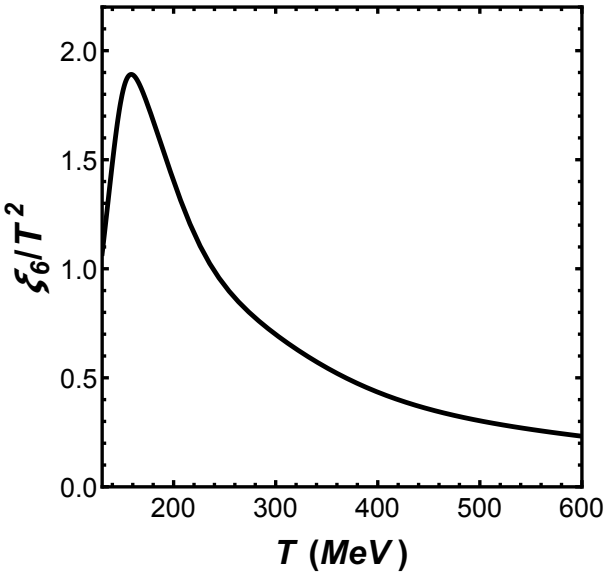

Figure 8.12: *ξ_6/T^2 as a function of the temperature T for the bottom-up holographic model.*

τ_Π that can still be useful for hydrodynamic modeling of the QGP [27]. The result for this lower bound in our holographic model is shown in Fig. 8.13 (this was computed using directly the fitting functions and Eq. (8.76)). This is the smallest value of $\tau_\Pi T$ in our model that is still consistent with causality and linear stability [383]. One can see that this coefficient displays a peak near the phase transition, as was the case for $\tau_\pi T$, but it becomes very small at high temperatures, as expected due to conformal invariance. The results in Fig. 8.13 also admit a fit using the following parametrization,

$$\tau_\Pi T\left(x=\frac{T}{T_c}\right)=\frac{a}{\sqrt{(x-b)^2+c^2}}+\frac{d}{x}, \tag{8.77}$$

with the corresponding fit parameters a to d being given in Tab. 8.4.

Table 8.4: *Parameters for the fit of $\tau_\Pi T$ using Eq. (8.77).*

a	b	c	d
0.05298	1.131	0.3958	-0.05060

Therefore, in this section we presented results (computed within different levels of approximations) for 12 transport coefficients that appear at second order in the gradient expansion of a non-conformal plasma that has thermodynamic properties similar to those found for the QGP on the lattice: η/s, ζ/s, τ_π, κ, κ^*, ξ_5 as well as ξ_3, ξ_4, ξ_6, λ_3, λ_4,

[27] A similar idea was used in Ref. [279] to estimate the coefficient τ_π in a hadronic gas with Hagedorn resonances given the result found in this case for η/s [280].

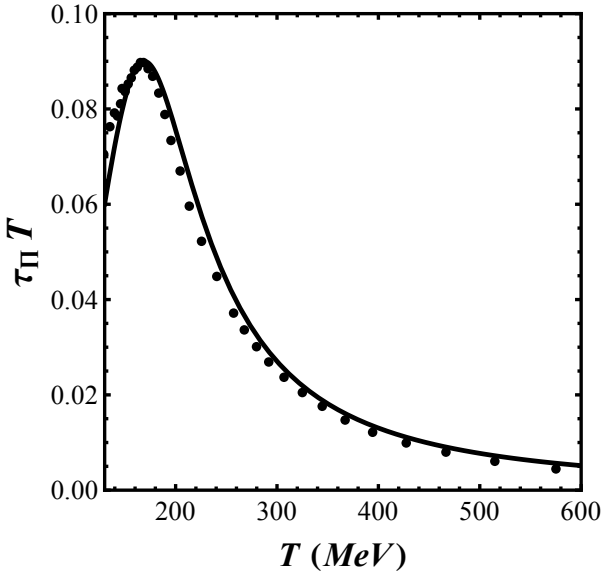

Figure 8.13: *A lower bound for $\tau_\Pi T$ as a function of the temperature T for the bottom-up holographic model. The black points correspond to our numerical results while the black curve is the fit in Eq. (8.77) with the parameters in Table 8.4.*

and τ_Π. However, the equations of motion obtained from Eqs. (8.8) and (8.9) are not in a form suitable for numerical implementation. In the next section we use the gradient expansion to find another 2nd order theory, similar to Israel-Stewart theory [384], that can be readily used in phenomenological studies of the QGP hydrodynamical evolution in heavy ion collisions.

8.6 Israel-Stewart-like 2nd order hydrodynamics for a non-conformal relativistic fluid

It is known that relativistic NS theory leads to acausal propagation of sound and shear linear disturbances around an equilibrium state at rest and that in the case of a moving background fluid these disturbances are unstable [385, 386]. It can be shown that the 2nd order theory in Eqs. (8.8) and (8.9) is linearly unstable above a certain critical wavenumber even for a fluid at rest, as demonstrated in Appendix G.3 (see also [387]). Note also that the inclusion of these spatial gradients cannot modify the theory at very large momenta k where the asymptotic causality conditions are defined [383]. However, it is not the purpose of hydrodynamics to accurately describe small wavelength phenomena - this is beyond the scope of this effective theory. Nevertheless, it is desirable that for a system that may be coupled to gravity causality (and stability!) are preserved.

In this section we use the 2nd order theory in Eqs. (8.8) and (8.9) to construct a relaxation-type theory (in curved spacetime) that is similar to that considered by Israel

and Stewart [384] and also to those that appear naturally within kinetic theory using the moments method [342]. The main idea, already pursued in [326] in the case of a conformal fluid, is to write a simple relaxation-type theory that reduces to the gradient expansion theory in Eqs. (8.8) and (8.9) in its asymptotic hydrodynamical limit. In this section we shall use the same procedure generalized to the case of a non-conformal fluid.

First, the terms involving comoving derivatives of $\sigma^{\mu\nu}$ and θ on the right-hand side of Eqs. (8.8) and (8.9) are transferred to the left-hand side of those equations using the lowest order substitutions $\sigma^{\mu\nu} \to -\pi^{\mu\nu}/\eta$ and $\theta \to -\Pi/\zeta$. Moreover, we use the leading order expression $Ds = -s\theta + \dots$ in Eq. (8.6) to simplify some of the terms (note that we are neglecting terms of third order in gradients that would appear in this general procedure). The same leading order substitution is done in the remaining 2nd order terms on the right-hand side of the equations with the exception of the term $\sim \tau_\pi \eta\, \theta\sigma^{\mu\nu}$ in Eq. (8.8) where only the substitution $\sigma^{\mu\nu} \to -\pi^{\mu\nu}/\eta$ is done. This choice is made to make it explicit that the combination $D\pi^{\langle\mu\nu\rangle} + 4\theta\pi^{\mu\nu}/3$ is the correct combination that survives in the conformal limit [326] (being, thus, homogeneous under Weyl transformations). One can then show that this leads to

$$\begin{aligned}
\tau_\pi \left(D\pi^{\langle\mu\nu\rangle} + \frac{4\theta}{3}\pi^{\mu\nu} \right) + \pi^{\mu\nu} &= -\eta\sigma^{\mu\nu} + \kappa \left(\mathcal{R}^{\langle\mu\nu\rangle} - 2u_\alpha u_\beta \mathcal{R}^{\alpha\langle\mu\nu\rangle\beta} \right) + \tau_\pi\, \pi^{\mu\nu}\; D\ln\left(\frac{\eta}{s}\right) \\
&+ \frac{\lambda_1}{\eta^2}\pi_\lambda^{\langle\mu}\pi^{\nu\rangle\lambda} - \frac{\lambda_2}{\eta}\pi_\lambda^{\langle\mu}\Omega^{\nu\rangle\lambda} - \lambda_3\Omega_\lambda^{\langle\mu}\Omega^{\nu\rangle\lambda} + 2\kappa^*\, u_\alpha u_\beta \mathcal{R}^{\alpha\langle\mu\nu\rangle\beta} \\
&+ \tau_\pi^* \pi^{\mu\nu}\, \frac{\Pi}{3\zeta} + \lambda_4 \nabla^{\langle\mu} \ln s\, \nabla^{\nu\rangle} \ln s
\end{aligned} \tag{8.78}$$

and

$$\begin{aligned}
\tau_\Pi \left(D\Pi + \Pi\theta \right) + \Pi &= -\zeta\theta + \frac{\xi_1}{\eta^2}\pi_{\mu\nu}\pi^{\mu\nu} + \frac{\xi_2}{\zeta^2}\Pi^2 + \tau_\Pi\, \Pi\; D\ln\left(\frac{\zeta}{s}\right) \\
&+ \xi_3\Omega_{\mu\nu}\Omega^{\mu\nu} + \xi_4 \nabla_\mu^\perp \ln s\, \nabla_\perp^\mu \ln s + \xi_5 \mathcal{R} + \xi_6 u^\mu u^\nu \mathcal{R}_{\mu\nu}\,.
\end{aligned} \tag{8.79}$$

These are nonlinear, coupled partial differential equations of relaxation-type for the new dynamical variables $\pi^{\mu\nu}$ and Π in curved spacetime that require (independent) initial conditions in order to solve Eqs. (8.78) and (8.79) together with the conservation equations (8.5)[28]. These equations are similar to those found in Israel-Stewart theory [384] and they possess most of the terms found in kinetic theory in flat spacetime [342][29]. Furthermore,

[28] This theory is qualitatively different than that in the gradient expansion - the dissipative parts of the energy-momentum tensor have their own differential equations and, thus, its initial conditions are not determined by the initial conditions for the hydrodynamic variables ε and u^μ.

[29] Ref. [342] used the Boltzmann equation and a completely distinct power-counting scheme to deal with the gradients in comparison to the one used to derived our equations for $\pi^{\mu\nu}$ and Π. For instance, according to the power-scheme of [342], the vast majority of their terms of order $\mathcal{O}(K_n^2)$ do not appear in our equations. Thus, perfect agreement among these approaches should not really be expected.

note that the asymptotic, leading order solution of these equations necessarily reduce to the gradient expansion in Eqs. (8.8) and (8.9) up to $\mathcal{O}(K_n^2)$.

However, for phenomenological applications in heavy ion collisions, the terms containing spacetime curvatures are negligible and can, thus, be dropped. Moreover, note that while in our holographic model η/s is a constant, in general one should keep the term involving $D\,\ln(\eta/s)$ to make sure that this theory reduces to the correct gradient expansion theory if the asymptotic limit $\pi^{\mu\nu} \to -\eta\sigma^{\mu\nu}$ is taken. For the same reason, one should keep $D\,\ln(\zeta/s)$ and, in fact, in our model since ζ/s is a not a constant its comoving derivative is not zero (note also that the conservation equations imply that, to lowest order, $D\,\ln(\eta/s)\,, D\,\ln(\zeta/s) \sim -\theta$).

This leads us to the following (reduced) set of equations that can be used in hydrodynamic simulations of the QGP

$$\begin{aligned}\tau_\pi\left(D\pi^{\langle\mu\nu\rangle}+\frac{4\theta}{3}\pi^{\mu\nu}\right)+\pi^{\mu\nu} &= -\eta\sigma^{\mu\nu}+\frac{\lambda_1}{\eta^2}\pi_\lambda^{\langle\mu}\pi^{\nu\rangle\lambda}-\frac{\lambda_2}{\eta}\pi_\lambda^{\langle\mu}\Omega^{\nu\rangle\lambda}-\lambda_3\Omega_\lambda^{\langle\mu}\Omega^{\nu\rangle\lambda}\\ &+ \tau_\pi\,\pi^{\mu\nu}\,D\,\ln\left(\frac{\eta}{s}\right)+\tau_\pi^*\pi^{\mu\nu}\,\frac{\Pi}{3\zeta}+\lambda_4\nabla^{\langle\mu}\ln s\,\nabla^{\nu\rangle}\ln s\end{aligned} \tag{8.80}$$

and

$$\begin{aligned}\tau_\Pi\left(D\Pi+\Pi\theta\right)+\Pi &= -\zeta\theta+\frac{\xi_1}{\eta^2}\pi_{\mu\nu}\pi^{\mu\nu}+\frac{\xi_2}{\zeta^2}\Pi^2+\xi_3\Omega_{\mu\nu}\Omega^{\mu\nu}\\ &+ \tau_\Pi\,\Pi\,D\,\ln\left(\frac{\zeta}{s}\right)+\xi_4\nabla_\mu^\perp\ln s\,\nabla_\perp^\mu\ln s\,.\end{aligned} \tag{8.81}$$

One can show that the hydrodynamic theory described above is linearly stable and causal according to the criteria of [383] and, thus, it should be suitable for implementation in modern numerical viscous hydrodynamic codes such as [377, 388–392]. We stress that the terms involving $D\ln(\eta/s)$ and $D\ln(\zeta/s)$ in the equations above are needed to recover the correct 2nd order gradient expansion and should not in principle be neglected in numerical simulations.

Among the 13 transport coefficients left in the equations above, results for 8 of them have already been presented in this Chapter while we have not yet discussed the coefficients λ_1, λ_2, ξ_1, ξ_2, and τ_π^*. The coefficients λ_1 and λ_2 have been studied at weak coupling in [393] and at strong coupling in [326, 346, 382]. The SYM values of these coefficients

computed at strong coupling via holography are[30]

$$\lambda_1 = 2\frac{\eta^2}{sT}\,, \qquad \lambda_2 = -\ln 2\frac{\eta}{\pi T}\,. \tag{8.82}$$

We are not aware of any calculation of these coefficients in a non-conformal strongly coupled plasma with a crossover transition. However, within the phenomenological "spirit" of this section and since we currently lack a better way to compute them, one may take the SYM expressions above for the non-conformal case at hand. This would imply that $\lambda_1/T^2 \sim s/T^3$ and $\lambda_2/T^2 \sim -s/T^3$. Thus, in this case these coefficients would display the same sharp rise observed by the entropy density near the phase transition.

Knowledge about the coefficients ξ_1 and ξ_2 is much more scarce. These coefficients only appear in non-conformal fluids and very little is known about them at strong coupling. An exception is the strongly coupled non-conformal plasma studied in Ref. [398] constructed via dimensional reduction of a higher dimensional pure gravity action. In this case, these coefficients can be extracted using the fluid/gravity correspondence and they read [358] [31]

$$\xi_1 = \lambda_1\left(\frac{1}{3} - c_s^2\right)\,, \qquad \xi_2 = 2\eta\tau_\pi c_s^2\left(\frac{1}{3} - c_s^2\right)\,. \tag{8.83}$$

Also, in this theory one finds [358]

$$\tau_\pi^* = -3\tau_\pi\left(\frac{1}{3} - c_s^2\right)\,. \tag{8.84}$$

In the absence of a better estimate for these three coefficients above in the non-conformal plasma proposed in this Chapter, it may be useful in hydrodynamic simulations of the QGP to use the expressions in Eqs. (8.83) and (8.84) hoping that they get at least part of the non-conformal dynamics near the phase transition. Notice, however, that these expressions contain $(\frac{1}{3} - c_s^2)$ and that this is an ubiquitous factor in non-conformal transport coefficients - for instance, the bulk viscosity of our model is proportional to this factor [254, 287]. Thus, it is reasonable to assume that these expressions may describe the temperature behavior of these coefficients in our model as well. Moreover, we would like to remark that our calculation for the transport coefficients are qualitatively consistent with

[30] For CFT's with a holographic description involving two derivatives in the bulk it was found in Refs. [394, 395] that $4\lambda_1 + \lambda_2 = 2\eta\tau_\pi$ (see also [396]). Moreover, Ref. [397] has recently found that this relation remains valid in a SYM plasma even when the leading order finite t'Hooft coupling corrections are taken into account.

[31] The transport coefficients in the theory [398] are known analytically and, even though their numerical values are different than the ones found in this Chapter (their theory is different than ours), qualitatively they possess the same features found here - ξ_5, ξ_6 have the same signal as ours and would also display a peak where c_s^2 has a minimum. However, their $\tau_\pi T$ is a constant while ours has a peak near the phase transition.

the results found in [399] for the large T expansion of the 2nd order transport coefficients for the non-conformal plasma dual to the Chamblin-Reall background [269].

Therefore, after this long discussion, the hydrodynamic theory described by Eqs. (8.80) and (8.81) together with the corresponding conservation equations (8.5) may be a good starting point for phenomenological applications of relativistic non-conformal hydrodynamics for the strongly-coupled QGP formed in heavy ion collisions[32]. To facilitate the use of our results in hydrodynamic simulations, we have provided a guide for all the relevant formulas for the 13 transport coefficients of this second order theory in Appendix G.2.

8.7 Conclusions and outlook for this chapter

In this Chapter we used the gauge/gravity duality to determine the transport coefficients of a non-conformal, strongly interacting non-Abelian plasma that displays a crossover transition similar to that found for the QGP determined via lattice calculations. The 5-dimensional gravity dual model involves the metric coupled with a dynamical scalar field and its simplicity and capability of describing several nontrivial features of the QGP have motivated us to pursue the calculations of the several transport coefficients shown in this Chapter.

We first obtained holographic formulas for the transport coefficients κ and τ_π present in the second-order gradient expansion of relativistic hydrodynamics in curved spacetime. Our method to compute these coefficients could also be applied in the case where the gravity dual possesses other fields besides the scalar field, such as the case of an Einstein+Scalar+Maxwell model with at most two derivatives in the action. Also, besides the well-known result for η/s, we were also able to directly compute five other coefficients that appear at second-order in the derivative expansion: τ_π, ζ/s, κ, κ^*, and ξ_5. Apart from η/s, all of these coefficients displayed nontrivial behavior near the crossover transition. In particular, $\tau_\pi T$, ζ/s, and ξ_5/T^2 display a peak near the transition while κ^*/T^2 is similar to c_s^2 (though it is negative) in that it displays a minimum at the crossover transition. On the other hand, κ/T^2 rises monotonically with T until it reaches its conformal limit (i.e., its value in SYM). Our values for $\tau_\pi T$ only deviates from the SYM result $(2-\ln 2)/(2\pi)$ at low temperatures. The coefficients κ, κ^*, and ξ_5 only contribute directly to the equations of motion in a curved spacetime.

Our ζ/s is in general smaller than that found in other works [400, 401] as it is clear

[32]Note that the thermodynamics of the model is very similar to lattice data and, thus, in hydrodynamic simulations one may as well just use directly the lattice data for the thermodynamical quantities such as c_s^2 or s.

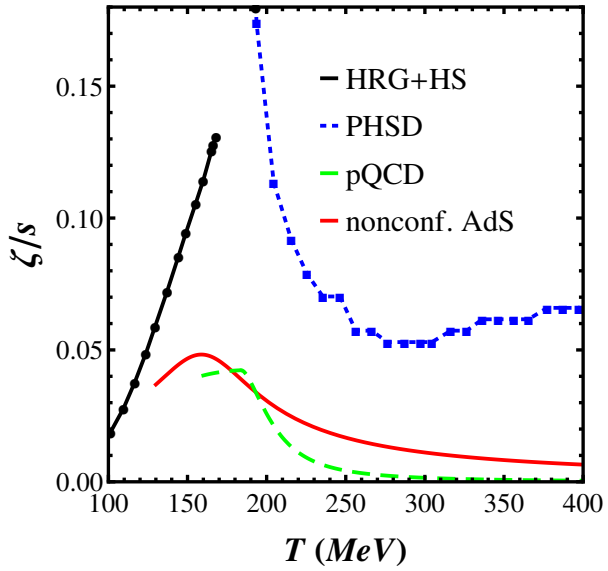

Figure 8.14: *Comparison between different calculations of ζ/s. The solid red curve shows the holographic calculation of this Chapter (cut at $T = 130$ MeV), the dashed green curve shows an extrapolation of the pQCD results of Ref. [353] towards low temperatures, the blue squares shows the calculation using the PHSD model [400], while the black points shows the hadronic calculation from Ref. [401].*

in[33] Fig. 8.14, though it is similar in magnitude to the pQCD calculation in Ref. [353]. Thus, at least according to our calculations, cavitation [402–404] induced by a large ζ/s in the phase transition is not likely to occur in the QGP (a similar conclusion was reached in Ref. [405] using a kinetic theory-derived bulk relaxation time in a Bjorken expanding fluid). However, it could be that the other coefficients that appear in the bulk equation, together with the shear-bulk coupling terms such as the $\pi^{\mu\nu}\Pi$ term in Eq. (8.80), may in the end take the evolving plasma towards cavitation. This is an interesting possibility that can be checked in numerical simulations.

We used these calculations to provide estimates for the other coefficients ξ_3, ξ_4, ξ_6, λ_3, λ_4, and τ_Π. We found that ξ_3/T^2 and ξ_4/T^2 are negative and have a minimum near the transition while ξ_6/T^2 is positive and displays a peak. Note that ξ_6 is only relevant in curved spacetime while ξ_3, λ_3, ξ_4, λ_4 do affect the motion of the fluid in flat spacetime. In fact, ξ_3 and λ_3 are related to the vorticity tensor $\Omega_{\mu\nu}$ whose role in hydrodynamic simulations has not yet been investigated in detail[34]. Moreover, ξ_4 and λ_4 also have not been investigated in hydrodynamic calculations and, thus, we hope the results of this Chapter may serve as motivation for a detailed investigation of their effects. In this Chapter we have used the asymptotic causality condition [383] to obtain the lowest possible value of the coefficient τ_Π associated with bulk viscosity relaxation. In this case, this lower bound

[33] We thank J. Noronha-Hostler for making this plot available to us.

[34] Note that for (0+1) purely Bjorken hydrodynamics this term disappears even in a non-conformal plasma.

for $\tau_\Pi T$ displays a peak near the transition (though its value at the peak is relatively small, in agreement with the small value of ζ/s found here)[35].

We have used the 2nd-order gradient expansion equations to construct an Israel-Stewart-like theory in flat spacetime, shown in Eqs. (8.80) and (8.81), which gives equations of motion that preserve causality and are linearly stable around thermal equilibrium[36]. These equations are similar to those used in current viscous hydrodynamic codes but they include additional 2nd order terms that are usually not taken into account.

This simplified theory still contains 13 transport coefficients and we have presented in this Chapter either direct calculations or leading estimates for all of them. In the case of the transport coefficients τ_π^*, λ_1, λ_2, ξ_1, and ξ_2 much more work needs to be done to obtain their exact temperature dependence in our holographic non-conformal model with a crossover phase transition. At the moment, our best estimate for their temperature behavior consisted in using the known expressions for λ_1 and λ_2 from SYM and the expressions for τ_π^*, ξ_1, and ξ_2 from the (related) non-conformal model of Ref. [398]. This (admittedly uncontrolled) approximation must be taken with care, as emphasized in the main text. However, given our current ignorance regarding these coefficients, we believe that it still may be of phenomenological interest to heavy ion collisions to use these expressions and investigate their consequences. In particular, the direct shear-bulk coupling term τ_π^* may be very relevant in hydrodynamic simulations, as emphasized in Refs. [407] and [408, 409].

Also, regarding the complete evaluation of the 2nd order transport coefficients that appear in the gradient expansion of non-conformal strongly-coupled hydrodynamics, the fluid/gravity correspondence [346] provides a way to compute all the coefficients. However, when the background metric is only known numerically, as it is in our case with a crossover phase transition, the actual implementation of the fluid/gravity approach becomes much

[35] We remark that the coefficients τ_π and τ_Π, as defined via the gradient expansion, do not necessarily correspond to relaxation time coefficients. Clearly, relaxation time coefficients require at least relaxation equations for $\pi_{\mu\nu}$ and Π, such as those in Israel-Stewart theory. In fact, according to their definitions in the gradient expansion, these coefficients do not even need to be positive. For instance, Ref. [406] has found an example of a gravity dual in which $\tau_\pi < 0$ as defined via the gradient expansion. This, however, was shown to not generate instabilities as it would have been the case if that coefficient were indeed a measure of shear relaxation. As discussed in Ref. [356], only the coefficients extracted from the poles of retarded correlators do have the meaning of shear or bulk relaxation time coefficients, which is not generally the case for the coefficients defined via derivatives of retarded Green's functions (such as in the gradient expansion).

[36] It is important to remark that the procedure used here to find relaxation equations using the gradient expansion has some ambiguities. Clearly, the set of relaxation equations obtained this way is not unique - it only corresponds to one of the possible sets of equations that have the 2nd order gradient expansion as their asymptotic solution. At this level, this can be viewed as a type of UV completion procedure of the gradient expansion equations that is consistent with the asymptotic causality condition. Alternatively, this general procedure can be illustrated via a simple classical mechanics example. The differential equations $\ddot{x} + \gamma\dot{x} + x = f(t)$ and $\gamma\dot{x} + x = f(t)$ have the same asymptotic solution $x_{asymp}(t) \sim f(t)$ for large times $t\gamma \gg 1$ though their transient (short time $t\gamma \sim 1$) behavior can be very different.

more challenging. In this context, it may be useful to consider a simpler analytical model that still possesses a phase transition. For instance, one may consider the finite temperature holographic model of Ref. [253] where the background metric and scalar field are known analytically and the system displays a 1st-order deconfinement phase transition. In this case, it should be possible to carry out the fluid/gravity procedure and find expressions for all the 2nd order transport coefficients. This would allow for a complete study of entropy production in 2nd order non-conformal hydrodynamics [358] for a theory that displays a phase transition.

We remark that very similar equations of motion for a non-conformal plasma have been derived from the Boltzmann equation in Ref. [407] and, in that Chapter, the authors also gave explicit formulas for several 2nd order transport coefficients. It would be interesting to compare the results of hydrodynamic simulations computed using the strongly coupled transport coefficients of this Chapter with those obtained using the kinetic theory-derived coefficients of Ref. [407][37]. We have gathered in Appendix G.2 the fitting functions that describe the temperature dependence of all the transport coefficients in this 2nd order Israel-Stewart theory to facilitate their use in current hydrodynamic codes.

This brings us to an important point concerning the equations of motion of strongly-coupled relativistic hydrodynamics in the light of the gauge/gravity duality. As discussed in Refs. [356, 410], the fact that the non-hydrodynamic modes of the $xy - xy$ energy-momentum tensor retarded correlator possess comparable real and imaginary parts at zero momentum [152] implies that, strictly speaking, the effective theory that should be able to describe the hydrodynamical sound and shear modes as well as the lowest set of non-hydrodynamic modes is not of relaxation-type such as in Israel-Stewart theory (as obtained from the Boltzmann equation). Ref. [411] has recently proposed a way to describe the approach towards hydrodynamics in strongly-coupled SYM that involves equations of motion that are qualitatively different than those in Eqs. (8.80) and (8.81) since they involve a second order, homogeneous differential equation for the part of the shear stress tensor associated with the two lowest quasinormal modes $\pi^{\mu\nu}_{QNM}$ (also, in their effective approach nonlinear terms in $\pi^{\mu\nu}_{QNM}$ are not taken into account). It would be interesting to investigate whether their effective theory is also applicable in the case of the non-conformal plasma studied in this Chapter.

The results of this Chapter were accepted for publication in JHEP [22].

[37] The transport coefficients in Ref. [407] were computed using the 14-moment approximation for the relativistic Boltzmann equation. Thus, their results are not valid for a strongly coupled fluid with a crossover phase transition. On the other hand, one should also keep in mind that the holographic approach pursued here is certainly not applicable at low temperatures (where a Boltzmann description of hadron dynamics should be applicable) or at sufficiently high temperatures (where asymptotic freedom is dominant).

Chapter 9

Conclusions

This thesis dealt with some applications of the gauge/gravity correspondence to study phenomena in strongly coupled non-Abelian plasma, using simple dual theories of gravity. After a general discussion of the physics of Yang-Mills theories, QCD and ultrarelativistic heavy-ion collision physics (Chapter 2), we presented a brief review of the gauge/gravity duality (Chapter 3). Then, we proceeded to the applications: a general formalism to compute the imaginary part of the heavy quark-antiquark potential in strongly coupled plasmas (Chapter 4), which was extended to deal with quark-antiquark dipoles moving through the plasma (Chapter 5); a holographic analysis of the Debye screening mass in non-perturbative non-Abelian gauge theories (Chapter 6); and the calculation of the electric conductivity in holographic bottom-up models that describe the thermodynamics of (2+1) QCD (Chapter 7). The same class of bottom-up models was used to compute several transport coefficients of a theory of second order hydrodynamics (Chapter 8). In this Chapter, we present some general considerations on the results of the preceding Chapters.

The general formalism for holographic Wilson loops presented in Chapters 4 and 5 allowed the evaluation of the imaginary part of heavy quark-antiquark potential. However, due to the limitations imposed by to the restriction to classical string configurations described by Nambu-Goto action [184], only relatively small lengths between the quark-antiquark pair can be probed; however, for small lengths, temperature induced effects are suppressed, being dominated by the conformal Coulomb part of the potential. Even with this limitation, we find qualitative behavior which indicates the emergence of a thermal width for heavy quarkonia. In fact, the lower bounds for the thermal width estimated, taking into account the limitations imposed by the consistency requirements described in Chapter 4, are compatible with recent estimates using phenomenological models for heavy-quarkonia suppression in the QGP [212,213]. This formalism was also extended to moving dipoles, in Chapter 5. Even though the use of the method is restricted to large rapidities

due to the absence of higher order corrections on the string worldsheet, the prediction of the onset of the imaginary part is more robust. In the case of moving dipoles, we see that increasing the velocity of the pair results in the onset of the imaginary part for smaller dipoles, which suggests that moving quarkonia may be less stable in the plasma. Also, the onset occurs for smaller dipoles in the case of dipoles moving with parallel orientation with respect to the plasma, which shows the the role of velocity induced anisotropy on the stability of the quarkonia in the plasma. It should be interesting to extend these calculations to other non-conformal gravity backgrounds - as done, for example, for the soft-wall model in Ref. [412].

In Chapter 6 we saw the shortcomings of the traditional prescriptions of Debye screening mass m_D in terms of the poles of the finite temperature gluon propagator or in terms of the correlator of Wilson loops, and then, based on the prescription involving the screening lengths of correlation functions of CT-odd operators [232], we presented the holographic prescription for the evaluation of Debye screening mass. For $\mathcal{N} = 4$ SYM, we saw that this holographic method presented similar results to the extraction done in Chapter 4. This prescription was then applied to some bottom-up Einstein + scalar models which model the thermodynamics of pure SU(3) Yang-Mills theory and of QCD near the crossover phase transition [15]. For the former, we saw that at the critical temperature T_c, a discontinuity of m_D as a function of T, characterized by a jump which is not N_c suppressed - the existence of this jump could be checked by lattice calculations, and present a robust feature of the models used. For the former, a minimum of m_D/T as a function of T, near T_c, was found. Recent lattice calculations which extract m_D in (2+1) QCD by analyzing the screening of the correlators of Polyakov loops [413], however, do not currently indicate the existence of a minimum of m_D.

The bottom-up model for the thermodynamics of (2+1) QCD was also used to estimate the electric conductivity of the plasma (Chapter 7), by adjoining to it a bulk Maxwell action in the probe limit (as $\mu_B = 0$). A functional form and the parameters for the Maxwell action were fixed by computing the charge susceptibility and comparing it to lattice data [318]. The estimates for the DC conductivity and the diffusion constant furnish good descriptions of the available lattice results.

Chapter 8 was dedicated to the computation of transport coefficients in a theory of non-conformal second order hydrodynamics [326, 358]. The shear viscosity η can be extracted from the membrane paradigm, as discussed at length on Chapter 3, while the bulk viscosity ζ follows from a computation, similar in spirit, to the membrane paradigm [137, 254], since both η and ζ both depend upon the imaginary part of a retarted Green's function of the energy-momentum tensor. However, the second order transport coefficients κ and τ_π, depend upon the real part of the retarted Green's function of the energy-

momentum tensor. This means that a direct extraction of these coefficients from the real-time gauge/gravity prescription was necessary, following the holographic prescription of Ref. [127], including dealing with the renormalization of the on-shell bulk action. After obtaining general formulas for κ and τ_π, we applied then in the same class of bottom-up models (Model B2) which match the thermodynamics of (2+1) QCD as seen in the lattice used in Chapters 6 and 7. By the use of Kubo formulas which relate the transport coefficients [360, 381], we also computed the transport coefficients κ^*, and ξ_5. Using more Kubo formulas and a hybrid conformal-non-conformal approximation, we also computed ξ_3, ξ_4, ξ_6, λ_3, and λ_4. We also extracted a lower bound for τ_Π considering the asymptotic causality condition. Finally, another set of approximations yielded the coefficients τ_π^*, λ_1, λ_2, ξ_1, and ξ_2. Altogether, considering the various degrees of approximation, we have computed from holography all 17 transport coefficients associated with the theory of second order hydrodynamics defined in Refs. [326, 358]. These transport coefficients can then be used in numerical simulations of hydrodynamics in order to study the effect of higher order corrections on the Knudsen number. For this last purpose, we have presented a causal and (linearly) stable theory of hydrodynamics which is an extension of the theory of Refs. [326, 358].

A next step in these holographic bottom-up setups for modeling (2+1) QCD is to consider non-zero baryonic chemical potential, $\mu_B \neq 0$. The extension of the models of Ref. [15] to non-zero μ_B was built on Refs. [311, 414], where the authors were interested in finding estimates of the critical point of QCD from holography. However, one could also study the thermodynamics and the movement of heavy probes in these holographic setups, which could also be checked against lattice results (for instance, the results for the thermodynamics at $\mu_B \neq 0$ from Ref. [415]). These goal is already being pursued [416]. Extending the results of Chapter 8 to non-zero μ_B are also interesting: in this, one is considering real-time phenomena at non-zero μ_B, a region of great challenges for lattice computations but approachable in the gauge/gravity framework.

Appendix A

Conformal Invariance and Tracelessness of Energy Momentum Tensor

In this Appendix, we show that that a sufficient condition for a classical field theory to be conformal is that the trace of its energy momentum tensor vanishes. This exposition is based on Refs. [34] and [359].

The argument requires two preliminary results.

The first one is the relation between the metric and the energy momentum tensor. Recall that the symmetric energy momentum tensor of a field theory described by an action S can be computed considering the theory recast in curved space with metric $g_{\mu\nu}$ and then evaluating[1]

$$T_{\mu\nu} = -2\frac{1}{\sqrt{-g}}\frac{\delta \mathcal{S}}{\delta g^{\mu\nu}}. \tag{A.1}$$

The energy momentum tensor in Minkowski space is obtained by setting $g_{\mu\nu} = \eta_{\mu\nu}$. This means that the metric $g_{\mu\nu}$ sources the energy-momentum tensor. That is, a transformation which modifies the metric as $g_{\mu\nu} \to g_{\mu\nu} + h_{\mu\nu}$ also modifies the action by

$$\delta S = -\frac{1}{2}\int d^d x \sqrt{-g} T^{\mu\nu} h_{\mu\nu}. \tag{A.2}$$

The second preliminary result comes from the definition of a conformal transformation. Consider a coordinate transformation of the form $x^\mu \to x^\mu + \epsilon^\mu$, where $\epsilon^\mu(x)$ is the transformation parameter. An infinitesimal transformation is given by

$$x^\mu \to x'^\mu = x^\mu + \epsilon^\mu(x). \tag{A.3}$$

[1] For a textbook on physics on curved space-times and general relativity, see, for example Ref. [359]

Under this infinitesimal transformation, the metric changes as

$$g_{\mu\nu} \to g'_{\mu\nu} = \frac{\partial x'_\mu}{\partial x_\rho}\frac{\partial x'_\nu}{\partial x_\sigma} g_{\rho\sigma} = g_{\mu\nu} - (\partial_\mu \epsilon_\nu + \partial_\nu \epsilon_\mu) + O(\epsilon^2). \tag{A.4}$$

To be a conformal transformation, $\epsilon(x)$ must satisfy

$$\partial_\mu \epsilon_\nu + \partial_\nu \epsilon_\mu = f(x) g_{\mu\nu}. \tag{A.5}$$

The function $f(x)$ is found by taking the trace of Eq. (A.5),

$$f(x) = \frac{2}{d}\partial_\rho \epsilon^\rho. \tag{A.6}$$

Then, the metric fluctuation for a infinitesimal conformal transformation is given by

$$h_{\mu\nu} = -\frac{2}{d}\partial_\rho \epsilon^\rho \tag{A.7}$$

Thus, under a conformal transformation, using Eqs. (A.2) and (A.7), the action changes by the term

$$\delta S = \frac{1}{d}\int d^d x \sqrt{-g}\; T^\mu_\mu \partial_\nu \epsilon^\nu. \tag{A.8}$$

Then, if the energy-tensor is traceless, $T^\mu_\mu = 0$, then $\delta S = 0$ and the action is invariant under a conformal transformation - the invariance of the theory under conformal transformations thus follows.

We remark that this proof is only valid at the classical level. Indeed, at the quantum level scale symmetry may be broken due to dimensional transmutation (as discussed in Chapter 2).

Appendix B

Infalling boundary conditions and Eddington-Finkelstein coordinates

In this Appendix, we present an argument that shows that the imposition of the black hole regularity, implemented by requiring infalling boundary conditions, is equivalent to requiring that the bulk fields depend only upon the Eddington-Finkelstein coordinate v near the horizon. This Appendix complements the discussion of the membrane paradigm in Chapter 3. We will largely follow the discussion in Ref. [138].

Consider a $(d+1)$-dimensional background of the isotropic form discussed in Chapter 3, that is, with a metric of the form

$$ds^2 = e^{2A(z)}\left(-h(z)dt^2 + dx_1^2 + \ldots + dx_{d-1}^2 + \frac{1}{h(z)}dz^2\right). \tag{B.1}$$

At $z = z_h$, we assume that the geometry has a black hole horizon. We will assume that the blackening factor $h(z)$ has a simple zero at z_h, so that the near horizon form of the metric will be

$$ds^2 \sim e^{2A(z_h)}\left(-h'(z_h)(z-z_h)dt^2 + dx_1^2 + \ldots + dx_{d-1}^2 + \frac{1}{h'(z_h)}\frac{dz^2}{z-z_h}\right). \tag{B.2}$$

Now, let be $\phi(x,z)$ be a massless scalar field in this background, with action

$$S = -\frac{1}{2}\int d^{d+1}x\sqrt{-g}\ (\partial\phi)^2. \tag{B.3}$$

The equation of motion for ϕ is the wave equation on the background (B.1)

$$\partial_\mu\left(\sqrt{-g}g^{\mu\nu}\partial_\nu\phi\right) = 0. \tag{B.4}$$

Take a plane wave ansatz with zero momentum, that is, take an ansatz of the form

$$\phi(x,z) = e^{-i\omega t}\tilde{\phi}(z). \tag{B.5}$$

The equation of motion becomes

$$\partial_z\left(\sqrt{-g}g^{zz}\partial_z\tilde{\phi}\right) + \sqrt{-g}g^{tt}\omega^2\tilde{\phi} = 0. \tag{B.6}$$

Let's analyze the equation of motion near the black hole horizon, $z \sim z_h$. As $\sqrt{-g} = e^{dA}$ is regular at the horiton (assuming a diagonal metric), the near horizon equation of motion is

$$g_{tt}\partial_z\left(\frac{1}{g_{zz}}\partial_z\tilde{\phi}\right) + \omega^2\tilde{\phi} = 0. \tag{B.7}$$

In the specific coordinate choice of the metric (B.2),

$$h'(z_h)^2(z-z_h)\partial_z\left((z-z_0)\partial_z\tilde{\phi}\right) + \omega^2\tilde{\phi} = 0. \tag{B.8}$$

We are now ready to proceed to the main argument. First introduce the rescaled z coordinate ξ by

$$d\xi = \sqrt{\frac{g_{zz}}{g_{tt}}}dr, \tag{B.9}$$

which near the horizon can be written as

$$d\xi \approx h'(z_h)\frac{dz}{z-z_h}. \tag{B.10}$$

Integrating Eq. (B.10) by choosing an integration constant such that $\xi(r_h) = 0$,

$$\xi = h'(z_h)\ln(z-z_h). \tag{B.11}$$

The equation of motion (B.8) then becomes simply

$$\frac{d^2}{d\xi^2}\tilde{\phi} + \omega^2\tilde{\phi} = 0, \tag{B.12}$$

whose solutions are

$$\tilde{\phi}(\xi) \propto e^{\pm i\omega\xi}. \tag{B.13}$$

Therefore, going back to the time domain, the full solution is

$$\phi(\xi,t) \propto e^{-i\omega(t\pm\xi)}. \tag{B.14}$$

An infalling (outgoing) solution is chosen by taking the plus (minus, respectively) sign in Eq. (B.14). Let's consider the infalling solution. Then Eq. (B.14) implies that ϕ depends on (ξ, t) on the combination $v = \xi + t$. That is, it only depends on the Eddington-Finkelstein v coordinate defined by (see Eq. (B.9))

$$dv = dt + \sqrt{\frac{g_{zz}}{g_{tt}}} dz. \tag{B.15}$$

This shows the equivalence of the imposition of infalling boundary conditions, horizon regularity and the requirement that bulk fields depend only upon the Eddington-Finkelstein coordinate v.

Let us finish this Appendix by writing the usual form used in the literature for the infalling boundary solution (B.14), using the (t, z) set of coordinates. Employing the general expression for the temperature, Eq. (3.55) of the main text, and comparing with Eq. (B.11) we see that

$$v = t + \frac{\beta}{4\pi} \ln(z - z_h) \tag{B.16}$$

Then, inserting this into Eq. (B.14), we obtain the standard form for the infalling boundary condition,

$$\phi(t, z) \propto (z - z_h)^{-\frac{i\omega\beta}{4\pi}} e^{-i\omega t}. \tag{B.17}$$

Appendix C

Wilson Loops and the Potential Energy of a Quark-Antiquark Pair

In this Appendix we will explore with more details, for the sake of completeness and for keeping the thesis self-contained, the relation between Wilson loops and the heavy quark-antiquark ($Q\bar{Q}$) interaction energy. In this exploration, we will uncover more details of the physical significance of the Wilson loop which are important for the discussion in Chapters 4 and 5.

C.1 Wilson loops and potential energy of a heavy $Q\bar{Q}$ pair

Consider the definition of the Wilson line operator in a SU(N_c) gauge theory,

$$\tilde{W}(l) = \frac{1}{N_c} P \exp\left[ig \int_C \hat{A}_\mu dx^\mu\right], \tag{C.1}$$

where P indicates path ordering and l is a given (smooth by parts) path in space-time. In the main text, we have considered only the fundamental representation, but the argument below applies to any given representation R of the gauge group. The Wilson line is a gauge covariant object - by considering the composition of infinitesimal paths, it is straightforward to show that under a gauge transformation implemented by $g(x)$ in SU(N_c), $\tilde{W}(l)$ transforms as

$$\tilde{W}(l) \to g(x_1)\tilde{W}(l)g^\dagger(x_0), \tag{C.2}$$

where x_0 (x_1) is the starting point (ending point, respectively) of the path l. However, from the Wilson line $\tilde{W}(l)$ a gauge invariant object can be built, the Wilson loop $W(C)$,

which was already defined in Chapter 4,

$$W(C) = \mathrm{Tr}_R \tilde{W}(C) = \frac{1}{N_c} \mathrm{tr}_R \left\{ P \exp \left[ig \int_C \hat{A}_\mu dx^\mu \right] \right\}, \tag{C.3}$$

where C is now a closed loop in space-time and where the trace is over the representation R of the gauge group. The gauge invariance of $W(C)$ follow directly from the definition, from Eq. (C.2) and from the cyclicity of the trace.

The main point is that the Wilson line tell us how to parallel transport gauge fields along a curve C. The Wilson loop (which is this sense is called the holonomy of the gauge group) gives us a measure of the failure of the parallel transport of elements of the gauge group along a closed loop. This means that when we consider external probes in our theory, to carry them around space-time we need to apply the Wilson line operator in order to transport the gauge fields correctly.

For instance, let $\phi(x) = \phi(t, \vec{x})$ be a complex scalar operator defined in the representation R of the gauge group that creates and annihilates a given scalar particle [1]. In this Appendix, we will work throughout with Euclidean signature. Let us suppose that the action of the theory is given by

$$S = \frac{1}{2} \int d^4x (D_\mu \phi^\dagger D^\mu \phi + m^2 \phi^\dagger \phi) - \frac{1}{4} \int d^4x \, \mathrm{tr}_A \, (F_{\mu\nu} F^{\mu\nu}), \tag{C.4}$$

where m is the mass of the ϕ particle, the trace is over the adjoint representation and the field strength $F_{\mu\nu}$ and covariant derivative are defined in Eqs. (2.3) and (2.6). A particle-antiparticle state along the axis x_1, with a spatial separation L, at a fixed time τ is created by the operator $Q(t)$ defined by

$$Q(\tau) = \phi^\dagger \left(\tau, -\frac{L}{2} \hat{x_1} \right) \tilde{W}(C_\tau) \phi \left(\tau, \frac{L}{2} \hat{x_1} \right), \tag{C.5}$$

where $\hat{x_1}$ is an unit vector in the x_1 direction and C_τ is an oriented line segment joining the point $(\tau, -L/2\,\hat{x_1})$ to the point $(\tau, L/2\,\hat{x_1})$. The Wilson line in Eq. (C.5) parallel transports the gauge field of the particle at $(\tau, -L/2\,\hat{x_1})$ to anti-particle at $(\tau, L/2\,\hat{x_1})$; the physical interpretation is the the creation of thin flux tube connecting particle and anti-particle.

The object of interest is a propagator of $Q(\tau)$, describing the propagation of a singlet particle-antiparticle pair from $\tau = 0$ (where the pair is created) to $\tau = \mathcal{T}$ (where it is annihilated),

$$\mathcal{C}(\mathcal{T}) = \langle \Omega | \mathrm{Tr}_R [Q^\dagger(\mathcal{T}) Q(0)] | \Omega \rangle = \frac{\int [DA_\mu] D\phi^\dagger D\phi \, \mathrm{tr}_R [Q^\dagger(\mathcal{T}) Q(0)] e^{-S}}{\int [DA_\mu][D\phi^\dagger][D\phi] \, e^{-S}}, \tag{C.6}$$

[1] As we will take the mass of the particle $m \to \infty$, the statistics of the particle is irrelevant.

where $|\Omega\rangle$ is the vacuum state. The trace makes the pair a colorless singlet. Consider the limit where $m \to \infty$. Then, the scalar field decouples from the theory, and can be integrated out. The result is that

$$\mathcal{C}(\mathcal{T}) \sim \text{const} \times \frac{\int [DA_\mu]\, W(C) e^{-S}}{\int [DA_\mu]\, e^{-S}} \sim \langle W(C) \rangle, \tag{C.7}$$

where the path C is the rectangle with vertices $(0, -L/2\,\hat{x_1})$, $(0, L/2\,\hat{x_1})$, $(\mathcal{T}, L/2\,\hat{x_1})$ and $(\mathcal{T}, -L/2\,\hat{x_1})$, as shown in Fig. 4.1, and the action S now includes only the kinetic contribution of the gauge fields, given by the second term in Eq. (C.4). The constant in Eq. (C.7) is irrelevant to this discussion. To see that the combination of Wilson lines in Eq. (C.6), $\text{Tr}_R[Q^\dagger(\mathcal{T})Q(0)]$, results in the Wilson loop $W(C)$, it is best to fix the temporal gauge, wherein $A_0 = 0$ and thus the parallel transport of the gauge fields along a temporal line is trivial. Since the Wilson loop is gauge invariant, this result is not restricted to the temporal gauge.

Now, let us look at the correlation function $\mathcal{C}(\mathcal{T})$ in an alternative form. First, note that, in Heisenberg's picture, the time evolution of $Q(t)$ is given by $Q(\tau) = e^{-\hat{H}\tau} Q(0)$, where $\hat{H}$ is the Hamiltonian of the system with a particle-antiparticle pair at the specified positions. Then,

$$\mathcal{C}(\mathcal{T}) = \langle \Omega | Q(0) e^{-\hat{H}\mathcal{T}} Q(0) | \Omega \rangle. \tag{C.8}$$

Now, consider a complete set of eigenvectors of the Hamiltonian $|n\rangle$, with $n = 0, 1, \ldots$, with eigenvalues E_n, ordered in sequence of increasing energies: $E_0 < E_1 \leq E_2 < \ldots$. By definition, $|0\rangle$ is the lowest energy state of the system with a particle-antiparticle pair present, whereas $|n\rangle$, with $n > 0$ gives the excited states of this configuration . Inserting two completeness relations into $\mathcal{C}(\mathcal{T})$, we obtain

$$\mathcal{C}(\mathcal{T}) = \sum_{m,n=0}^{\infty} \langle \Omega | Q(0) | m \rangle \langle m | e^{-\hat{H}\mathcal{T}} | n \rangle \langle n | Q(0) | \Omega \rangle = \sum_{n=0}^{\infty} \left| \langle \Omega | Q(0)^2 | n \rangle \right|^2 e^{-E_n \mathcal{T}}. \tag{C.9}$$

In the limit $T \gg L$, the contributions from the excited states are exponentially suppressed. Only E_0 remains and

$$\mathcal{C}(\mathcal{T} \gg L) \sim e^{-E_0 \mathcal{T}}. \tag{C.10}$$

Comparing Eqs. (C.7) and (C.10), we see that, in the limit $\mathcal{T} \gg L$, identifying E_0 with the potential energy $\mathcal{V}$ of the particle-antiquark pair relative to the vacuum of the system,

$$\langle W(C) \rangle \sim e^{-\mathcal{V}\mathcal{T}}, \tag{C.11}$$

for the rectangular contour C described above and in Fig. 4.1.

C.2 Polyakov loop, heavy quark free energy and confinement

So far, we have not assumed anything on the imaginary time axis. The argument above could be reproduced at real-time and there would be no difference apart from the change $T \to -iT$ in Eq. (C.14); this would lead directly to Eq. (4.2) in the main text. However, in the context of the imaginary time formalism, the imaginary time axis is compactified in a circle, with period $\beta = 1/T$. We could then consider a temporal Wilson line whose loop C wraps the imaginary-time axis - C is given by the line segment joining $(0, \vec{x})$ to $(\beta, \vec{x})$. This defines the Polyakov loop $\mathbf{L}(\vec{x})$ of Eq. (C.12) [160–162], namely

$$\mathbf{L}(\vec{x}) = \frac{1}{N_c} P\, e^{i\, g \int_0^{1/T} \hat{A}_0(\vec{x},\tau) d\tau}\,. \tag{C.12}$$

The the trace of $\mathbf{L}(\vec{x})$ is gauge invariant, as already remarked. One of the importances of the Polyakov loop operator $\mathbf{L}(\vec{x})$ is that it measures the spontaneous breaking of center symmetry group Z^{N_c} of $\mathrm{SU}(N_c)$ gauge theories in the absence of dynamical fermions (see Ref. [44] for more details); if the center symmetry is unbroken, as $\mathrm{tr}_F \mathbf{L}(\vec{x})$ transforms non-trivially under Z^{N_c}, one must have $\langle \mathrm{tr}\mathbf{L}(\vec{x})\rangle = 0$. If $\langle \mathrm{tr}\mathbf{L}(\vec{x})\rangle \neq 0$, then the center symmetry is broken.

We now consider the correlator

$$\bar{C}(\beta) = \langle \Omega | \phi\,(\beta, \vec{x})\, \mathbf{L}(\vec{x}) \phi^\dagger\,(0, \vec{x})\, |\Omega\rangle \tag{C.13}$$

which describes the propagation of static particle in the thermal bath. The same analysis pursued above can be applied in this case to yield

$$\langle |\mathbf{L}(\vec{x})| \rangle \sim e^{-\beta F_R}, \tag{C.14}$$

where F_R is the Helmholtz free-energy difference of the free-energy of the thermal bath with a particle ϕ and thermal bath alone; the Helmholtz free-energy comes about since we are in the canonical ensemble (see Section 2.4).

In a confining gauge theory, one the energy necessary to create an isolated particle (i.e., a quark or the particle ϕ) must be infinite, so that no excitation of the vacuum can excite a colored particle state - the least energetic configuration is a singlet state of two or more colored particles. This means that in a confining gauge theory $F_R \to \infty$. Coupled with the analysis of the center symmetry, this means that in a pure gauge theory, center symmetry is linked with confinement. This analysis breaks down when we have dynamical fermions in the theory, since they explicitly break center symmetry [44].

Appendix D

Some Auxiliary Results For Static Wilson Loops

In this Chapter we present a series of auxiliary results and technical details relative to the computation of holographic Wilson loops, complementing the results in Chapters 4 and 5. In Section D.1 we present a covariant calculation of the real and imaginary parts of the Wilson loop in strongly coupled N = 4 SYM using an explicitly covariant method, which supports the coordinate dependent calculation performed in the main text. Section D.2 shows some formulas and results necessary for evaluating the integrals one finds when computing holographic Wilson loops. Analytic formulas for the real and imaginary part of heavy quark-antiquark potential for a variety of Dp-branes constructions of dual theories of gravity are presented in Section D.3. A sign of the failure of the classical string calculation for a maximum length can appear on the curvature scalar for the string worldsheet - we address this possibility in Section D.4.

D.1 Covariant expansion of the Nambu-Goto action around the classical solution

Expansions of the string action around a given classical solution of the equations of motion, $X_0^\mu(\tau,\sigma)$, are somewhat nontrivial since the worldsheet fluctuations $\delta X^\mu(\tau,\sigma)$ do not transform simply under reparametrization [417]. Thus, the way the fluctuations around the classical solution were included in Section 4.4, though correct, are not manifestly covariant. In this section we perform a covariant expansion of the determinant of the worldsheet metric around a generic solution of the classical string equations of motion.

A fluctuation of the string worldsheet can be written as [417]

$$X_0^\mu + \delta X^\mu = X_0^\mu + \xi^\mu - \frac{1}{2}\Gamma^\mu_{\rho\lambda}(X_0)\xi^\rho\xi^\lambda + O(\xi^3) \tag{D.1}$$

where $\xi^\mu(\tau,\sigma)$ transforms as a vector under reparametrization (which plays the role of Riemann normal coordinates [418]). Derivatives with respect to the worldsheet variables τ and σ are given by

$$\partial_a(X_0^\mu + \delta X^\mu) = \partial_a X_0^\mu + D_a\xi^\mu + \frac{1}{3}\mathcal{R}^\mu_{\nu\rho\lambda}(X_0)\xi^\nu\xi^\rho\partial_a X_0^\lambda + O(\xi^3), \tag{D.2}$$

where $\mathcal{R}^\mu_{\nu\rho\lambda}$ is the Riemann curvature tensor and D_a is defined as

$$D_a\xi^\mu \equiv \partial_a\xi^\mu + \Gamma^\mu_{\nu\rho}(\partial_a X_0^\mu)\xi^\rho\,. \tag{D.3}$$

Note that using the chain rule one obtains $D_a\xi^\nu = D_\mu\xi^\nu\partial_a X_0^\mu$, where D_μ is the usual space time covariant derivative with an affine connection. This motivates the definition (D.3) as the covariant derivative of ξ on the worldsheet. The expansion for the background metric becomes

$$G_{\mu\nu}(X_0+\xi) = G_{\mu\nu}(X_0) - \frac{1}{3}\mathcal{R}_{\mu\nu\rho\lambda}(X_0)\xi^\rho\xi^\lambda + O(\xi^3)\,. \tag{D.4}$$

Using Eqs. (D.2) and (D.4) we obtain for the induced metric on the worldsheet $h_{ab} = G_{\mu\nu}\partial_a X^\mu\partial_b X^\nu$, up to second order in ξ,

$$h_{ab} = h^{(0)}_{ab} + h^{(1)}_{ab} + h^{(2)}_{ab} + O(\xi^3) \tag{D.5}$$

where

$$h^{(0)}_{ab} = \partial_a X_0\cdot\partial_b X_0, \tag{D.6}$$

$$h^{(1)}_{ab} = \partial_a X_0\cdot D_b\xi + \partial_b X_0\cdot D_a\xi \qquad \text{and} \tag{D.7}$$

$$h^{(2)}_{ab} = D_a\xi\cdot D_b\xi + \partial_a X_0^\mu\partial_b X_0^\nu\mathcal{R}_{\mu\nu\rho\lambda}\xi^\rho\xi^\lambda. \tag{D.8}$$

where the inner product here is defined with respect to the background metric, i.e, $A\cdot B = G_{\mu\nu}A^\mu B^\nu$. Eq. (D.5) takes into account the effect of worldsheet fluctuations on the induced worldsheet metric in an explicitly reparametrization invariant manner.

To show that this procedure yields the same results as the non-covariant approach developed in the main text, we use the AdS_5-Schwarzschild metric (4.42) in the formulas above. We also use the static gauge for the worldsheet embedding functions and, thus, $\tau = t$ and $\sigma = x$ and the classical solution is $X_0^\mu = (t, x, 0, 0, U_c(x))$. As before, the

fluctuations are $\delta X^\mu = (0,0,0,0,\delta U(x))$. Then, using the inverse of Eq. (D.1) into Eq. (D.5) and evaluating the induced metric determinant $h = det\, h_{ab}$ we obtain in the end

$$-h = \left(\frac{dU_c(x)}{dx}\right)^2 + \frac{1}{R^2}(U^4 - U_h^4) + \frac{4U^3}{R^4}\delta U + \frac{6U^2}{R^4}\delta U^2 + O(\delta U^3)\,. \tag{D.9}$$

The saddle point approximation for $e^{-S_{NB}}$ can also be obtained by taking the extremum of h with respect to δU. The extremum of Eq. (D.56) occurs at $\delta\bar{U} = -U/3$, which yields

$$-\bar{h} = \left(\frac{dU_c(x)}{dx}\right)^2 + \frac{U^4 - 3U_h^4}{3R^4}. \tag{D.10}$$

Now, dU_c/dx is given by the classical solution (4.11) and, thus, we obtain the following expression for the (regularized) effective action after integrating over τ and defining the dimensionless variables $y = U/U_h$ and $y_h = U_h/U_*$

$$S = \frac{\mathcal{T}}{\pi\alpha'}U_* \int_1^\infty dy \left\{ \sqrt{\left(\frac{y^4 - y_h^4}{y^4 - 1}\right) - \frac{2}{3}\frac{y^4(1-y_h^4)}{(y^4-1)(y^4-y_h^4)}} - 1 \right\} - \frac{\mathcal{T}}{\pi\alpha'}U_*. \tag{D.11}$$

Eq. (D.11) gives both the real and imaginary parts of $V_{Q\bar{Q}}$. Note that second term inside the square root above represents the contribution from worldsheet fluctuations and this term only becomes relevant close to the bottom of the classical string solution at U_* (also, see that this term is well behaved in the UV, $y \to \infty$, which is expected since it comes solely from thermal effects). The shift in $\mathrm{Re}V_{Q\bar{Q}}$ due to fluctuations is easier to obtain in the covariant approach and it can be determined from Eq. (D.11). For $T = 0$ (i.e., $y_h = 0$), Eq. (D.11) can be evaluated in terms of hypergeometric functions as explained in Appendix D.2. The result is

$$V_{Q\bar{Q}} = -\frac{4\pi^2}{\Gamma(1/4)^4}\frac{R^2}{\alpha'}\,{}_2F_1\left[-\frac{1}{2}, -\frac{1}{4}; \frac{1}{4}; \frac{2}{3}\right]\frac{1}{L}\,. \tag{D.12}$$

Since ${}_2F_1[-1/2, -1/4; 1/4; 2/3] = 1.38$, we see that long wavelength worldsheet fluctuations change the vacuum result for $\mathcal{N} = 4$ SYM by $\sim 40\%$ (which can be accommodated, for instance, by rescaling the t'Hooft coupling).

In Figure D.1 we show the effect of fluctuations on the real part of the potential while in Figure D.2 we compare the results for the imaginary part of the potential computed using the covariant method and the non-covariant method developed in the main text. The real part of the part of the potential changes slightly due to fluctuations while the imaginary part is almost unaffected by the choice of method. This is expected since in the non-covariant approach we focus mainly on fluctuations near the bottom of the string while in the covariant approach long-wavelength fluctuations along the whole worldsheet

are taken into account. Since the imaginary part is generated by the fluctuations near the bottom of the string both approaches are equivalent to determine $\mathrm{Im}\, V_{Q\bar{Q}}$.

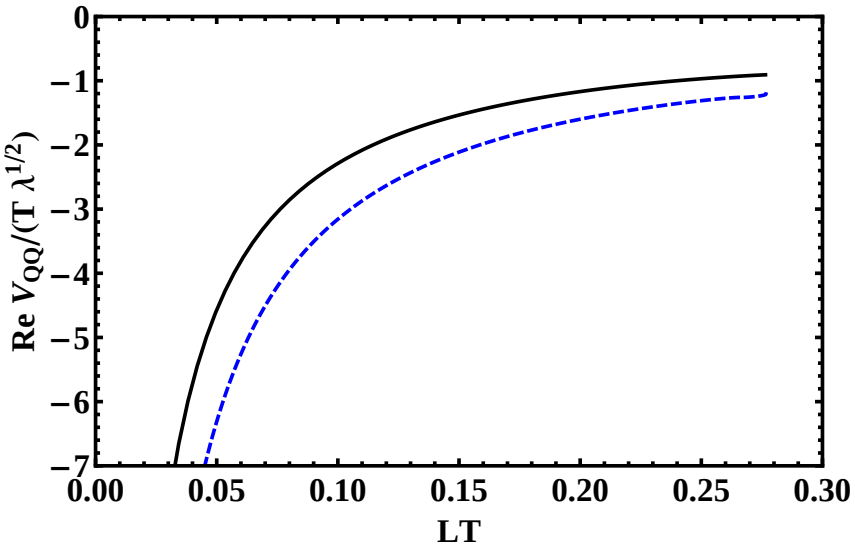

Figure D.1: $\mathrm{Re}\, V_{Q\bar{Q}}/(T\sqrt{\lambda})$ *as a function of LT for the strongly coupled* $\mathcal{N} = 4$ *SYM plasma. The solid line is the real part calculated without considering thermal fluctuations on the string worldsheet while the dashed line is the real part of the potential including the fluctuations.*

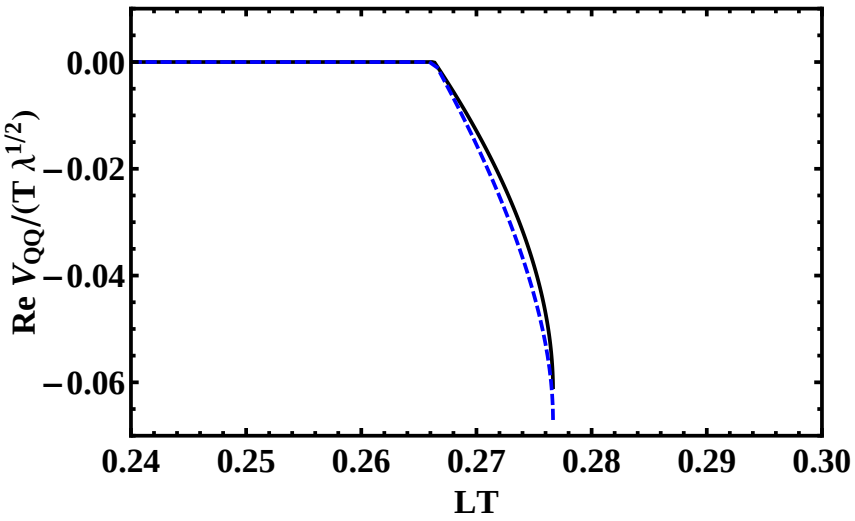

Figure D.2: $\mathrm{Im}\, V_{Q\bar{Q}}/(T\sqrt{\lambda})$ *as a function of LT for the strongly coupled* $\mathcal{N} = 4$ *SYM plasma. The solid (dashed) line is the result from the non-covariant (covariant) method, respectively.*

D.2 Some useful formulas for the evaluation of Wilson loops

In this Section we present some useful techniques to evaluate the integrals found in the calculation of Wilson loops via the gauge/gravity correspondence. All the integrals and properties studied in this section can be found, for example, in Ref. [193]. The main idea is to use integral representations of the beta and the (Gaussian) hypergeometric functions to perform the integrals that appear in the study of holographically computed Wilson loops.

D.2.1 Beta function

A recurring integral found in these calculations is the beta function

$$\mathrm{B}(a,b) \equiv \int_0^1 t^{a-1}(1-t)^{b-1}dt \tag{D.13}$$

with $\mathrm{Re}(a)$, $\mathrm{Re}(b) > 0$. This function satisfies the reflection property

$$\mathrm{B}(a,b) = \mathrm{B}(b,a) \tag{D.14}$$

and is related to the gamma function by

$$\mathrm{B}(a,b) = \frac{\Gamma(a)\Gamma(b)}{\Gamma(a+b)}\,. \tag{D.15}$$

For example, for $\mathcal{N}=4$ SYM at strong 't Hooft coupling (and $T=0$) one finds that the relation between U_* and L is given by Eq. (4.44)

$$\frac{L}{2} = \frac{R^2}{U_*}\int_1^\infty dy\,\frac{1}{y^2\sqrt{y^4-1}}. \tag{D.16}$$

Therefore, changing variables to $t = 1/y^4$ and using Eq. (D.13) one finds

$$\frac{L}{2} = \frac{R^2}{U_*}\frac{1}{4}\mathrm{B}(3/4,1/2) = \frac{R^2}{U_*}\frac{\Gamma(1/2)\Gamma(3/4)}{\Gamma(5/4)}. \tag{D.17}$$

To simplify Eq. (D.17) a bit further it is useful to remember that the gamma function satisfies

$$\Gamma(z+1) = z\Gamma(z) \quad \text{and} \tag{D.18}$$

$$\Gamma(1-z)\Gamma(z) = \frac{\pi}{\sin(\pi z)}. \tag{D.19}$$

Therefore, $\Gamma(1/2) = \sqrt{\pi}$. Moreover, we have that $\Gamma(3/4) = \sqrt{2}\pi/\Gamma(1/4)$ and $\Gamma(5/4) = \Gamma(1/4)/4$. We finally obtain Eq. (4.47)

$$\frac{L}{2} = \frac{R^2}{U_*}\frac{\sqrt{2}\pi^{3/2}}{\Gamma(1/4)^2}. \tag{D.20}$$

The same procedure can be applied to $V_{Q\bar{Q}}$ in Eq. (4.46). To avoid having a or b with a negative real part, one introduces a factor y^γ in the integrand, performs the integration, and then takes $\gamma \to 0$. This gives the expression in Eq. (4.48).

D.2.2 Gaussian hypergeometric function

The Gaussian hypergeometric function ${}_2F_1$ can be defined by the power series

$$\begin{aligned} {}_2F_1(a,b;c;z) \equiv & 1 + \frac{ab}{1!\,c}z + \frac{a(a+1)b(b+1)}{2!\,c(c+1)}z^2 + \\ & + \cdots + \frac{a(a+1)\cdots(a+n)b(b+1)\cdots(b+n)}{n!\,c(c+1)\cdots(c+n)}z^n + \cdots , \end{aligned} \tag{D.21}$$

where a, b, c, z are real numbers, with $c \neq -1, -2, \cdots$. The series converges for $|z| < 1$ while for the rest of the complex plane ${}_2F_1$ is obtained by analytic continuation.

We are mainly interested in the following integral representation of ${}_2F_1$

$${}_2F_1(a,b;c;z) = \frac{1}{\mathrm{B(b-c,b)}}\int_0^1 t^{b-1}(1-t)^{c-b-1}(1-zt)^{-a}dt\,. \tag{D.22}$$

This representation is valid for $|z| < 1$ and for $\mathrm{Re}(c) > \mathrm{Re}(b) > 0$. This relation follows immediately from the binomial theorem and Eq. (D.13).

Eq. (D.22) was used in Eq. (4.52) for thermal $\mathcal{N} = 4$ SYM at strong 't Hooft coupling to find

$$LT(y_h) = \frac{2}{\pi}y_h\sqrt{1-y_h^4}\int_1^\infty \frac{dy}{\sqrt{(y^4-y_h^4)(y^4-1)}}. \tag{D.23}$$

Applying the change of variables $t = 1/y^4$ we find that

$$LT(y_h) = \frac{2\sqrt{2\pi}}{\Gamma(1/4)^2}y_h\sqrt{1-y_h^4}\,{}_2F_1\left[\frac{1}{2},\frac{3}{4};\frac{5}{4};y_h^4\right]. \tag{D.24}$$

The same procedure can be applied to determine $\mathrm{Re}\,V_{Q\bar{Q}}/T$ in Eq. (4.53), which leads to

(4.55)

$$\frac{\mathrm{Re}\, V_{Q\bar{Q}}}{T} = -\frac{R^2}{\alpha'}\frac{\sqrt{2\pi^3}}{\Gamma(1/4)^2}\frac{1}{y_h}\,{}_2F_1\left[-\frac{1}{2},-\frac{1}{4};\frac{1}{4};y_h^4\right]. \tag{D.25}$$

The series definition of ${}_2F_1$ (D.21) also simplifies the derivation of the series expansion in Eq. (4.56). For example, for $LT < 1$ we find, up to linear terms on y_h^4,

$$\frac{LT}{2}\frac{\Gamma(1/4)^2}{\sqrt{2\pi}y_h} = 1 - \frac{1}{5}y_h^4. \tag{D.26}$$

For $\mathrm{Re}\, V_{Q\bar{Q}}/T$ in Eq. (D.25) we obtain

$$-\frac{\mathrm{Re}\, V_{Q\bar{Q}}}{T}\frac{\alpha'}{R^2}\frac{\Gamma(1/4)^2}{\sqrt{2}\pi^{3/2}}y_h = 1 + \frac{1}{2}y_h^4. \tag{D.27}$$

Therefore, after multiplying Eqs. (D.26) and (D.27) and using Eq. (D.26) to zeroth order in y_h^4 we obtain the following expression valid to order $(LT)^4$ (4.56)

$$\frac{\mathrm{Re}\, V_{Q\bar{Q}}}{T} = -\frac{4\pi^2\sqrt{\lambda}}{\Gamma(1/4)^4 LT}(1 + c(LT)^4), \tag{D.28}$$

with $c = 3\Gamma(1/8)^8/(5\cdot 2^7\pi^2)$. The same reasoning also shows that the series expansion of $\mathrm{Re}\, V_{Q\bar{Q}}/T$ is of the form $[1 + a_4(LT)^4 + a_8(LT)^8 + \cdots]/(LT)$.

As a last remark, note that the derivative of ${}_2F_1$ with respect to z is

$$\frac{d}{dz}{}_2F_1(a,b;c;z) = \frac{ab}{c}{}_2F_1(a+1,b+1;c+1;z)\,. \tag{D.29}$$

If the real part of the potential has the general form $\mathcal{V} \propto e^{-m_D/T(LT)}/(LT)^\delta$ then

$$\frac{d}{d(LT)}\left[(LT)^\delta\frac{\mathcal{V}}{T}\right] = -\frac{m_D}{T}(LT)^\delta\frac{\mathcal{V}}{T}\,. \tag{D.30}$$

However, by Eq. (D.29), the holographically computed potential given by Eqs. (D.24) and (D.25) does not satisfy this condition because

$$\frac{d}{d(LT)}\left[(LT)^\delta\frac{\mathrm{Re}\, V_{Q\bar{Q}}}{T}\right] = \frac{d\left[(LT)^\delta\frac{\mathrm{Re}\, V_{Q\bar{Q}}}{T}\right]/dy_h^4}{d(LT)/dy_h^4} \neq -\frac{m_D}{T}(LT)^\delta\frac{\mathrm{Re}\, V_{Q\bar{Q}}}{T}\,. \tag{D.31}$$

D.3 Some other results involving Wilson loops

In this Section we apply the formalism developed in the main text to calculate the real and imaginary part of heavy quark-antiquark potentials in a slightly more general class of gravity duals which include, as an interesting subset, the low energy theories of

coincident stacks of Type II Dp-branes. While some of these results were initially discussed in Ref. [419], as far as we know, a complete evaluation of $V_{Q\bar{Q}}$ and of its imaginary part has not been presented before.

This Section is organized as follows. First we present the class of metrics we use. We then calculate the Polyakov loop and $\mathrm{Re}\, V_{Q\bar{Q}}$. An approximation for small L is discussed. Finally, we show the results for the imaginary part of $V_{Q\bar{Q}}$ in these theories.

D.3.1 Gravity duals considered

We consider the gravity duals described by the following metric (in the string frame)[1]

$$ds^2 = \left(\frac{U}{R}\right)^{\alpha}\left\{-\left[1-\left(\frac{U_h}{U}\right)^{2\alpha}\right]dt^2 + dx_i dx^i\right\} + \left(\frac{R}{U}\right)^{\beta}\left[1-\left(\frac{U_h}{U}\right)^{2\alpha}\right]^{-1} dU^2 \quad \text{(D.32)}$$

where R is a constant, i runs from 1 to $D-1$ and D is the total number of dimensions of the corresponding gauge theory. From the confinement criteria [188], we see that as long as $\alpha \geq \beta$ the theory does not confine (in the sense of an area law for the rectangular Wilson loop).

The black brane temperature is

$$T = \frac{\alpha}{2\pi R}\left(\frac{U_h}{R}\right)^{\frac{\alpha+\beta-2}{2}} \quad \text{(D.33)}$$

and the entropy density is

$$s = \frac{1}{4G_5}\left(\frac{U_h}{R}\right)^{\frac{3\alpha}{2}}. \quad \text{(D.34)}$$

D.3.2 Polyakov loop

We start by calculating the Polyakov loop in this class of theories. The unregularized expression for the heavy quark free energy is given by

$$F_Q^{nreg} = \frac{1}{2\pi\alpha'} R^{\frac{\beta-\alpha}{2}} U_*^{\frac{2+\alpha-\beta}{2}} \int_{y_h}^{\infty} y^{\frac{\alpha-\beta}{2}} dy. \quad \text{(D.35)}$$

[1] In principle, we could generalize this metric a bit further by making the change $2\alpha \to \gamma$ in the exponent of the terms inside the square brackets. However, the expressions obtained cannot be integrated using the method discussed in Section D.2. Moreover, the analysis of the UV divergence gets more involved since in this case the metric is not asymptotic AdS. For these reasons, we keep the form of the metric shown in (D.32).

We have three possibilities. If $\alpha - \beta < -2$, then there is no UV divergence. If $\alpha - \beta = -2$, the integral diverges logarithmically. If $\alpha - \beta > -2$ the UV divergence is worse than logarithmic. If $\alpha - \beta \geq -2$ we use the temperature independent regularization $\int_0^\infty dy\, y^{(\alpha-\beta)/2}$ and, with this choice, the final regularized expression for F_Q is the same regardless of the sign of $\alpha - \beta$

$$F_Q = -\frac{1}{\pi\alpha'}\frac{R^{\frac{\beta-\alpha}{2}}U_*^{\frac{\alpha-\beta+2}{2}}}{2+\alpha-\beta}y_h^{\frac{\alpha-\beta+2}{2}} \quad \text{if} \quad \alpha-\beta \geq -2 \tag{D.36}$$

and the Polyakov loop is simply $|\langle \mathrm{tr}\, \mathbf{L}(T)\rangle| = e^{-F_Q/T}$.

D.3.3 Real part of the heavy quark potential

We can now proceed to the calculation of the real part of the heavy quark potential. Using Eq. (4.14) and adopting the regularization used for F_Q, we have

$$\frac{L}{2} = \frac{R^{\frac{\alpha+\beta}{2}}}{U_*^{\frac{\alpha+\beta-2}{2}}}\sqrt{1-y_h^{2\alpha}}\int_1^\infty dy\, \frac{y^{\frac{\alpha-\beta}{2}}}{\sqrt{(y^{2\alpha}-y_h^{2\alpha})(y^{2\alpha}-1)}} \tag{D.37}$$

and

$$\mathrm{Re}\, V_{Q\bar{Q}} = \frac{R^{\frac{\beta-\alpha}{2}}U_*^{\frac{2+\alpha-\beta}{2}}}{\pi\alpha'}\left\{\left[\int_1^\infty dy\, y^{\frac{\alpha-\beta}{2}}\left(\sqrt{\frac{y^{2\alpha}-y_h^{2\alpha}}{y^{2\alpha}-1}}-1\right)\right]-\frac{2}{\alpha-\beta+2}\right\}. \tag{D.38}$$

The evaluation of the integrals in both Eq. (D.37) and Eq. (D.38) proceed as discussed before. The results are

$$\frac{L}{2} = \frac{R^{\frac{\alpha+\beta}{2}}}{U_*^{\frac{\alpha+\beta-2}{2}}}\sqrt{1-y_h^{2\alpha}}\frac{1}{2\alpha}\mathrm{B}\left(\frac{5\alpha-\beta-2}{4\alpha},\frac{1}{2}\right){}_2F_1\left[\frac{1}{2},\frac{5\alpha-\beta-2}{4\alpha};\frac{7\alpha-\beta-2}{4\alpha};y_h^{2\alpha}\right] \tag{D.39}$$

and

$$\mathrm{Re}\, V_{Q\bar{Q}} = \frac{R^{\frac{\beta-\alpha}{2}}U_*^{\frac{2+\alpha-\beta}{2}}}{\pi\alpha'}\frac{1}{2\alpha}\mathrm{B}\left(\frac{\beta-\alpha-2}{4\alpha},\frac{1}{2}\right){}_2F_1\left[-\frac{1}{2},\frac{\beta-\alpha-2}{4\alpha};\frac{\alpha+\beta-2}{4\alpha};y_h^{2\alpha}\right]. \tag{D.40}$$

D.3.4 Imaginary part of the heavy quark potential

We can also calculate $\mathrm{Im}\, V_{Q\bar{Q}}$ via Eq. (4.36) and obtain

$$\mathrm{Im}\, V_{Q\bar{Q}} = -\frac{1}{4\sqrt{2}\alpha'}\frac{1}{\alpha}\left(\frac{U_h}{R}\right)^{\frac{\alpha-\beta}{2}} \frac{U_h}{y_h^{\frac{\alpha-\beta+2}{2}}}\frac{1}{4\alpha-2}\left[(4\alpha-2)y_h^{2\alpha}-2\alpha+2\right]. \tag{D.41}$$

The condition $\mathrm{Im}\, V_{Q\bar{Q}} < 0$ implies that

$$y_h > \left(\frac{\alpha-1}{2\alpha-1}\right)^{\frac{1}{2\alpha}}. \tag{D.42}$$

Note that one must require that $\alpha > 1/2$ for Eq. (D.42) to be well defined. One can check that the formulas above give the correct AdS_5 limit given by $\alpha = \beta = 2$.

D.3.5 Expansion for small y_h

The expressions for L and $\mathrm{Re}\, V_{Q\bar{Q}}$ in Eqs. (D.39) and (D.40) can be expanded for small $LU_h^{\frac{\alpha+\beta-2}{2}} \sim LT$. This amounts to an expansion in small y_h. By the same procedure applied before we obtain in this approximation

$$\mathrm{Re}\, V_{Q\bar{Q}} \propto \frac{1}{L^{\frac{\alpha-\beta+2}{\alpha+\beta-2}}}\left(1 + c\, U_h^{2\alpha} L^{\frac{4\alpha}{\alpha+\beta-2}}\right), \tag{D.43}$$

where c is a positive constant. The gauge theory has conformal behavior (i.e., $V_{Q\bar{Q}} \propto (1/L)(1+c(LT)^{\delta})$ only when $\alpha = \beta = 2$, which corresponds to the gravity dual in AdS_5.

D.3.6 Limit for $T \to \infty$

Suppose now that we take $T \to \infty$ in the dual thermal field theory. Then the Euclidean time radius $\beta \to 0$. This means that the gauge theory in this limit "loses" a dimension, becoming a (D-2)+1 field-theory at $T = 0$ (we can choose any of the remaining spatial directions assume the role of the Euclidean time dimension). By the same arguments presented for $\mathcal{N} = 4$ SYM in (3+1) dimensions going to pure $SU(N)$ gauge theory in (2+1) dimensions, we expect that whatever fermionic or scalar degrees of freedom the dual field theory had decouple in the $\beta \to 0$ limit, along with all remaining supersymmetries. Then, we expect to have pure $SU(N)$ in $(D-2)+1$ dimensions at $T = 0$.

We may easily check, from (D.32), that the field theory confines. The string tension is simply

$$\sigma = \frac{U_h^{\alpha}}{2\pi\alpha' R^{\alpha}}. \tag{D.44}$$

The calculation of the Wilson loop proceeds as before and we omit the details. We only remark that L is given by

$$\frac{L}{2} = \frac{R^{\frac{\alpha+\beta}{2}}}{U_*^{\frac{\alpha+\beta-2}{2}}} \frac{1}{2\alpha} \mathrm{B}\left(\frac{5\alpha-\beta-2}{4\alpha}, \frac{1}{2}\right) {}_2F_1\left[\frac{1}{2}, \frac{5\alpha-\beta-2}{4\alpha}; \frac{7\alpha-\beta-2}{4\alpha}; y_h^{2\alpha}\right] \tag{D.45}$$

The only difference between this and (D.39) is the absence of the factor $\sqrt{1-y^{2\alpha}}$. As discussed in the main text, this factor changes the qualitative behavior of L as a function of y_h. Without this factor, L diverges for $y_h \to 1$, as expected for a confining theory. This factor is, then, responsible for the deconfined behavior of the original theory.

D.3.7 Results for Dp-branes

The results of the previous sections can be applied to a special class of metrics corresponding to the (near horizon) supergravity solutions of stacks of Dp-branes in type II superstring theories. We start by writing the supergravity metric (in the string frame) for N coincident near-extremal black Dp-branes in the near-horizon limit [420],

$$\begin{aligned} ds^2 = \left(\frac{U}{R}\right)^{\left(\frac{7-p}{2}\right)} \left[-f(U)dt^2 + dx_i dx^i\right] + \left(\frac{R}{U}\right)^{\left(\frac{7-p}{2}\right)} \frac{dU^2}{f(U)} + \\ + g_{YM}\sqrt{d_p N} U^{\frac{p-3}{2}} d\Omega_{8-p}^2 \end{aligned} \tag{D.46}$$

where i runs from 1 to p,

$$R^{\frac{7-p}{2}} = g_{YM}\sqrt{d_p N}, \tag{D.47}$$

$$d_p = \Gamma\left(\frac{9-p}{2}\right) \frac{2^{11-2p}\pi^{\frac{13-2p}{2}}}{9-p} \quad \text{and} \tag{D.48}$$

$$f(U) = 1 - \left(\frac{U_h}{U}\right)^{7-p}. \tag{D.49}$$

The dilaton field ϕ is given by

$$e^{\phi} = (2\pi)^{2-p} g_{YM}^2 \left(\frac{R}{U}\right)^{\frac{(7-p)(3-p)}{4}}. \tag{D.50}$$

Note that taking $p = 3$ in Eq. (D.46) corresponds to the AdS_5 case. Only in this case the geometry separates in a product of a $p+2$ dimensional spacetime and an $8-p$ dimensional sphere. In the following we assume a fixed configuration for the compact coordinates. Also, note that if $p \neq 3$ the dilaton runs and, thus, the dual gauge theory is

not conformal even in the vacuum.

The metric is now of the form (D.32) with $\alpha = \beta = (7-p)/2$. The results of the previous sections then apply and the (regularized) heavy quark free energy is

$$F_Q = -\frac{1}{2\pi\alpha'} U_h \tag{D.51}$$

while

$$\frac{L}{2} = \frac{R^{7-p}}{U_*^{\frac{5-p}{2}}} \sqrt{1-y_h^{7-p}}\, \frac{1}{7-p} \mathrm{B}\left(\frac{6-p}{7-p}, \frac{1}{2}\right) {}_2F_1\left[\frac{1}{2}, \frac{6-p}{7-p}; \frac{19-3p}{14-2p}; y_h^{7-p}\right] \tag{D.52}$$

and the real part of the potential is

$$\mathrm{Re}\, V_{Q\bar{Q}} = \frac{U_*}{\pi\alpha'} \frac{1}{7-p} \mathrm{B}\left(-\frac{1}{7-p}, \frac{1}{2}\right) {}_2F_1\left[-\frac{1}{2}, -\frac{1}{7-p}; \frac{5-p}{14-2p}; y_h^{7-p}\right] . \tag{D.53}$$

Moreover, one can use Eq. (4.36) to find

$$\mathrm{Im}\, V_{Q\bar{Q}} = -\frac{1}{4\sqrt{2}\alpha'} \frac{1}{(6-p)(7-p)} \frac{U_h}{y_h} \left[(12-2p) y_h^{7-p} - 5 + p\right] . \tag{D.54}$$

For the last equation to be valid the following condition must be satisfied

$$y_h > \left(\frac{5-p}{12-2p}\right)^{\frac{1}{7-p}} . \tag{D.55}$$

D.4 Curvature scalar on the string worldsheet

In this Section we study the curvature scalar $\mathcal{R}$ associated with the induced metric on the string worldsheet. As a specific example, we will focus on the Schwarzschild/AdS_5 metric (4.42). Our main aim is to evaluate the curvature scalar at the bottom of the string at finite LT, $\mathcal{R}(LT)$, and compare it with the corresponding $T = 0$ result, $\mathcal{R}(0)$. If $\mathcal{R}(LT_{max}) \gg \mathcal{R}(0)$, this signals that near the maximum of LT, LT_{max}, highly curved string worldsheet configurations start to become relevant. This, in particular, means that one should be cautious in interpreting LT_{max} as a screening length of the quark-antiquark pair.

For the metric (4.42), the induced metric $h_{ab} = G_{\mu\nu}\partial_a X^\mu \partial_b X^\nu$ on the string worldsheet

configuration for the rectangular Wilson loop (in the static gauge) is given by

$$\begin{aligned} h_{\tau\tau} &= \frac{1}{4R^2}\left(\frac{U_h^4}{U(x)^2} - U(x)^2\right), \\ h_{\sigma\sigma} &= \frac{1}{4R^2}\left(U(x)^2 + \frac{4R^2U(x)^2U'(x)^2}{U(x)^4 - U_h^4}\right) \text{ and} \\ h_{\tau\sigma} &= h_{\sigma\tau} = 0. \end{aligned} \tag{D.56}$$

Computing the curvature scalar $\mathcal{R}$ using this metric and using the equation of motion (4.11) to remove $U'(x)$ and $U''(x)$ from the resulting expressions, one finds

$$\mathcal{R} = \frac{2R^6\left(\frac{R^8\left(3U_h^4-U(x)^4\right)\left(U_*^4-U(x)^4\right)^2}{\left(U_h^4-U_*^4\right)^2} + 2U(x)^4\left(U_h^8 - U(x)^8\right) + \frac{\left(U_h^4-U(x)^4\right)\left(6U_h^4U(x)^4+U(x)^8-3U_h^8\right)\left(U(x)^4-U_*^4\right)}{U_h^4-U_*^4}\right)}{U(x)^4\left(U_h^4 - U(x)^4\right)^2\left(\frac{R^8(U(x)^4-U_*^4)}{\left(U_h^4-U_*^4\right)\left(U_h^4-U(x)^4\right)} + U(x)^4 - U_h^4\right)^2}. \tag{D.57}$$

At the bottom of the string, $U(0) = U_*$. Then, Eq. (D.57) reduces to ($y_h = U_h/U_*$),

$$\mathcal{R}(y_h) = -\frac{4R^6\left(y_h^4+1\right)}{U_*^8\left(1-y_h^4\right)^3}. \tag{D.58}$$

The $T = 0$ curvature scalar is found by fixing $y_h = 0$ in the equation above. In this case, we may use Eq. (4.47) to obtain $\mathcal{R}$ explicitly as a function of L and obtain

$$\mathcal{R}(T=0) = -\frac{\Gamma\left(\frac{1}{4}\right)^{16}}{1024\pi^{12}}\frac{L^8}{R^{10}}. \tag{D.59}$$

One can see that the curvature scalar is well behaved for any finite L when $T = 0$.

The ratio between the curvature scalars for $T \neq 0$ and $T = 0$ at the bottom of the string is given by

$$\frac{\mathcal{R}(y_h)}{\mathcal{R}(0)} = \frac{1+y_h^4}{(1-y_h^4)^3}. \tag{D.60}$$

Note that this ratio diverges for $y_h \to 1$. This means that a string worldsheet that stretches up to the horizon is highly curved and must receive quantum corrections. In other words, the classical configurations with $y_h > y_{h,max} = 0.85$ are highly curved and must be dealt with care. Already for $y_h = y_{h,max}$, we have $\mathcal{R}(y_{h,max}) \sim 15\mathcal{R}(0)$. In Figure D.3 we present a plot of the ratio $\mathcal{R}(y_h)/\mathcal{R}(0)$ as a function of y_h.

Now we can use Eq. (4.54) to solve for y_h as a function of LT in the branch $0 < y < y_h$ and evaluate $\mathcal{R}$ as a function of LT, up to LT_{max}, as in Figure D.4. We see that for

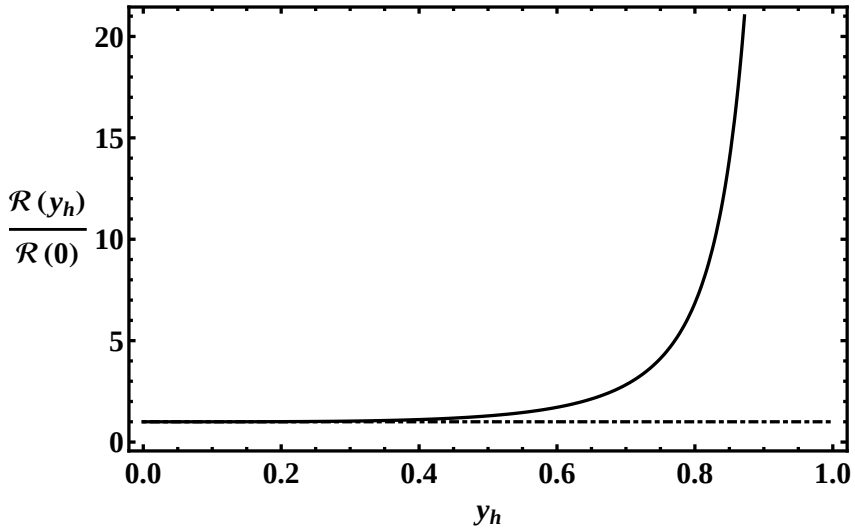

Figure D.3: *The ratio of curvature scalars $\mathcal{R}(y_h)/\mathcal{R}(0)$ as a function of y_h associated with the worldsheet metric for the strongly coupled $\mathcal{N} = 4$ SYM plasma. The ratio diverges when the bottom of the string reaches the horizon (where $y_h = 1$).*

$LT \sim LT_{max}$, $\mathcal{R}(LT) \sim 10\,\mathcal{R}(0)$, which corresponds to a situation of high curvature on the string worldsheet.

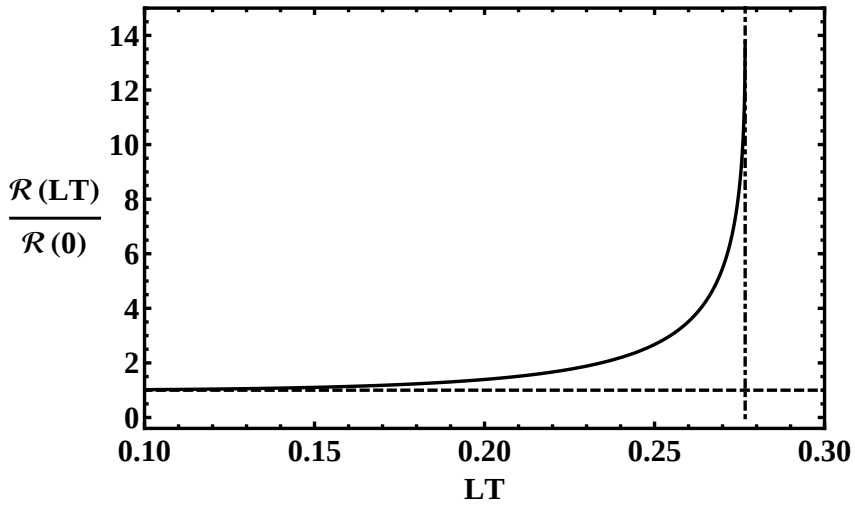

Figure D.4: *The ratio of curvature scalars $\mathcal{R}(LT)\mathcal{R}(0)$ as a function of LT, up LT_{max}, associated with the worldsheet metric for the strongly coupled $\mathcal{N} = 4$ SYM plasma. The vertical line denotes $LT = LT_{max}$ where $\mathcal{R}(LT_{max}) \sim 10\,\mathcal{R}(0)$.*

Appendix E

Debye screening mass at one loop in perturbation theory

In this Appendix we will compute the perturbative result of Eq. (6.8) for the Debye screening mass for a SU(N_c) Yang-Mills plasma with N_f fermions in the fundamental representation (first done in Ref. [227]). This calculation will serve as a contrasting example of the usual perturbative methods with the geometric, non-perturbative approach offered by the gauge/gravity duality. I will largely follow the notation and procedure of Ref. [421].

E.1 Generalities

At zero temperature, in an Euclidean formalism[1], the photon/gluon polarization tensor $\Pi_{\mu\nu}$ (see Fig.E.1) can be decomposed, by Euclidean and gauge invariance, as

$$\Pi_{\mu\nu}(Q) = \left(\delta_{\mu\nu} - \frac{Q_\mu Q_\nu}{Q^2}\right) F_0(Q^2), \tag{E.1}$$

where Q is the external 4-momentum of the photon, and F_0 is a scalar function which depends only upon $Q^2 = Q_\mu Q^\mu$. In components, the four-momentum Q is given by $Q_\mu = (q_4, \vec{q}) = (-i\omega, \vec{q})$. For convenience, we also defined a normalized 3-momentum by $\hat{q} = \vec{q}/q$. At finite temperature, Euclidean covariance is explicitly broken since we have a preferred frame of the plasma - namely, its rest frame. Thus, the decomposition of Eq. (E.1) is not valid anymore, and must substituted by a decomposition which respect rotation symmetry in the x_1, x_2, x_3 subspace, but not rotations about the imaginary time $x_0 = \tau$ axis. A

[1] We are already working with a Euclidean metric with signature $(+,+,+,+)$ foreshadowing the use of Matsubara formalism at finite temperature

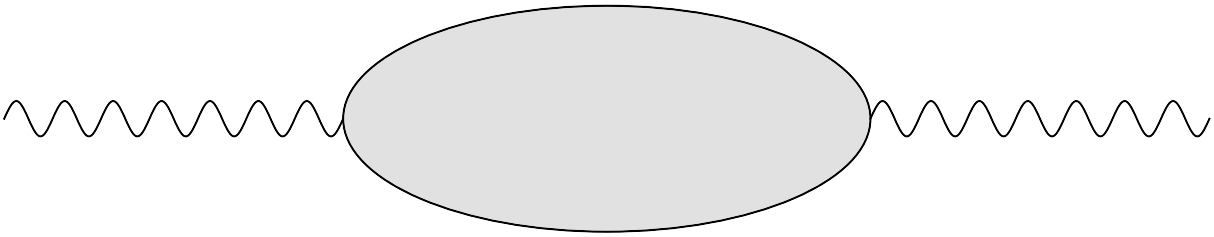

Figure E.1: *Diagrammatic representation of the photon polarization tensor.*

decomposition that respects these properties is given by

$$\Pi_{\mu\nu}(Q) = F(Q^2)P^L_{\mu\nu} + G(Q^2)P^T_{\mu\nu}, \tag{E.2}$$

where the projectors P^L and P^T are defined by

$$\begin{aligned} P^T_{00} &= P^T_{0i} = 0, \\ P^T_{ij} &= \delta_{ij} - \hat{q}_i\hat{q}_j, \\ P^L_{\mu\nu} &= \delta_{\mu\nu} - \frac{Q_\mu Q_\nu}{Q^2} - P^T_{\mu\nu}. \end{aligned} \tag{E.3}$$

It is easy to see that P^L and P^T satisfy

$$\begin{aligned} (P^T)^2 &= P^T, \\ (P^L)^2 &= P^L, \\ P^T P^L &= P^L P^T = 0. \end{aligned} \tag{E.4}$$

Also, note that directly from the definition,

$$P^L_{\mu\nu} + P^T_{\mu\nu} = \delta_{\mu\nu} - \frac{Q_\mu Q_\nu}{Q^2}. \tag{E.5}$$

Before proceeding, we notice that the full Euclidean propagator $G_{\mu\nu}$ for the photon/gluon can be written as

$$G_{\mu\nu} = \frac{1}{Q^2 + F(Q^2)}P^L_{\mu\nu} + \frac{1}{Q^2 + G(Q^2)}P^T_{\mu\nu} + \frac{\xi}{Q^2}\frac{Q_\mu Q_\nu}{Q^2}, \tag{E.6}$$

where we included a gauge fixing contribution in the last term; ξ is the gauge fixing parameter. Here in this Appendix, we will work in Feynman gauge, with $\xi = 1$.

To compute the Debye screening mass m_D perturbatively, we have to compute the pole of the electric-electric propagator G_{00} at zero frequency, as discussed in Chapter 6. That is, following Eq. (6.7), we search for the roots of $Q^2 + \Pi_{00}(Q) = 0$ at zero external

frequency and $\vec{q}^{\,2} = m_D^2$, that is,

$$\Pi_{00}(0, \vec{q}^{\,2} = -m_D^2) + m_D^2 = 0. \tag{E.7}$$

Using the definition of the projectors, Eq. (E.3), and the decomposition (E.2), we see that we have to search for the roots of $F(m_D^2) + m_D^2 = 0$. Latter in this Appendix we will justify more carefully this prescription in the context of perturbation theory.

The above definition captures the physics of the electric screening. A analogous definition for a magnetic screening mass m_{mag} would involve looking at the roots of $Q^2 + \Pi_{ij}(Q) = 0$ at zero external frequency:

$$\Pi_{ij}(0, \vec{q}^{\,2} = -m_{mag}^2) + m_{mag}^2 = 0. \tag{E.8}$$

However, as we will argue below, $m_{mag} = 0$ in perturbation theory, so magnetic fields are not screened (but only in the context perturbation theory).

E.2 Debye screening mass in perturbation theory - One loop

Thus, we need to investigate the function $F(Q)$ in perturbation theory. Let us proceed to compute the polarization tensor $\Pi_{\mu\nu}$ and the F and G functions in perturbation at one loop. We will make the assumption that the temperature is the largest scale of the system; that is, $T \gg m_f$, where m_f is the mass of any fermion field in the system, and that $T \gg Q$ - T is larger than the external momenta. This defines the called Hard Thermal Loop (HTL) approximation.

At one loop, in QED coupled to a massless fermion, the polarization tensor $\Pi_{\mu\nu}$ at one loop is given by the fermion loop diagram of Fig. E.4, where k is the internal loop momentum.

E.2.1 Fermion loop diagram

Evaluating the diagram

The first diagram, the fermion loop, yields, in Matsubara's formalism,

$$\Pi_{\mu\nu}(Q) = e^2 \frac{1}{\beta} \sum_n \int \frac{d^3k}{(2\pi)^3} \mathrm{Tr}\, [\gamma_\mu \not{k} \gamma_\nu (\not{k} - \not{Q})]\, \Delta(k)\Delta(k-Q), \tag{E.9}$$

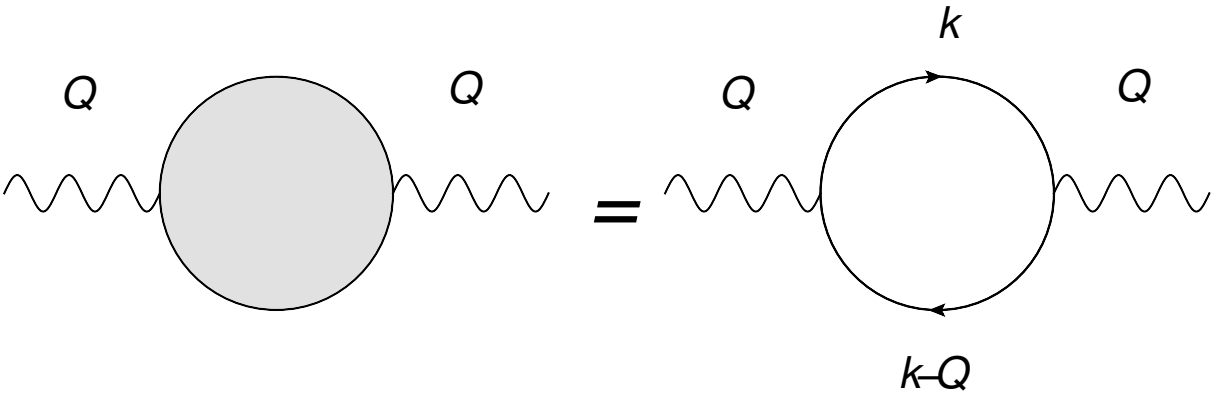

Figure E.2: *Feynman diagram for the polarization tensor in QED at one loop.*

where e is the QED coupling constant, γ_μ the Dirac matrices in four dimensions, $\not{a} \equiv a_\mu \gamma^\mu$ and the trace is over the Dirac matrices. The function $\Delta(k)$ is a shorthand for the free Euclidean propagator. Explicitly,

$$\Delta(i\omega_n, \vec{p}) = \frac{1}{\omega_n^2 + E_p^2}, \tag{E.10}$$

where $E_p^2 = m_f^2 + \vec{k}^2$ is the dispersion relation for the on-shell fermion and ω_n are the Matsubara frequencies for a fermion, $\omega_n = (2n+1)\pi T$.

By usual power counting arguments, we see that the integral is quadratically divergent in the UV and should be regularized. For the purposes of this calculation, we will not need to consider a full renormalization procedure, since thermal effects do not contribute to the UV divergence. Instead, we will use the fact the T is our largest scale, and use impose a momentum cutoff at the scale T.

To compute $\Pi_{\mu\nu}$, we have first to unpack the trace in Eq. (E.9), before computing the integrals. The trace unpacking follow the usual trace tricks and techniques for such calculations (see, for instance, Ref. [25]). In this case, we have only to use the trace identity

$$\text{Tr}\left[\gamma_\mu \not{a} \gamma_\nu \not{b}\right] = 4(a_\mu b_\nu + a_\nu b_\mu - \delta_{\mu\nu} a_\rho b^\rho), \tag{E.11}$$

which yields

$$\Pi_{\mu\nu} = 8e^2 I^a_{\mu\nu} - 4\delta_{\mu\nu} e^2 I^b, \tag{E.12}$$

where we defined

$$I^a_{\mu\nu} = \frac{1}{\beta}\sum_n \int \frac{d^3k}{(2\pi)^3} k_\mu k_\nu \Delta(k)\Delta(k-Q), \tag{E.13}$$

and

$$I^b = \frac{1}{\beta}\sum_n \int \frac{d^3k}{(2\pi)^3} k^2 \Delta(k)\Delta(k-Q). \tag{E.14}$$

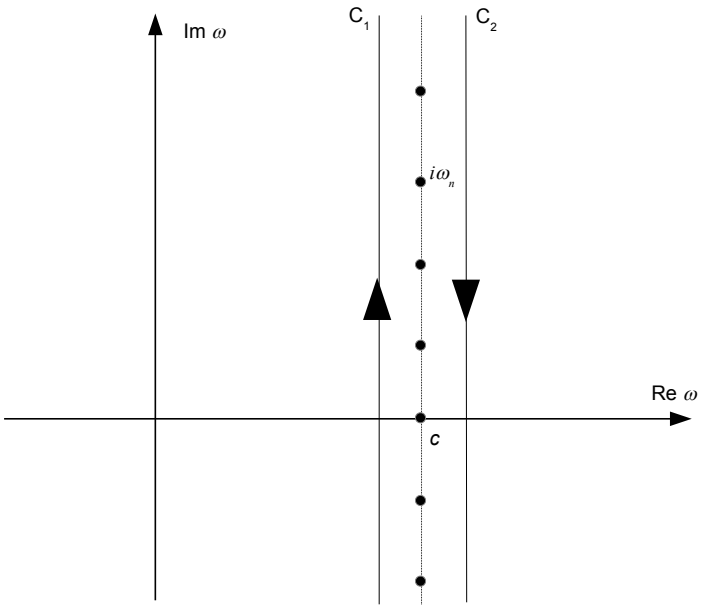

Figure E.3: *Contour integration for frequency sums.*

Evaluating frequency sums via contour integration

The next step is to compute the Matsubara frequency sums in the integrals I^a and I^b. Such sums are usually perfomed using complex integration methods. Let us discuss the basic method here.

Let $h(\omega)$ be a meromorphic function on the complex plane ω. Assume that $h(\omega)$ decreases faster than $1/|\omega|$ and that h is analytic along the line $\mathrm{Re}\,\omega = c$, where c is a real constant. Our objective is to compute the following sum over the Matsubara frequencies

$$S = \sum_{n=-\infty}^{\infty} h(c + i\omega_n). \tag{E.15}$$

To compute this, we first prove that

$$S = \frac{1}{\beta} \int_{C_1 \cup C_2} \frac{d\omega}{4i\pi} h(\omega) \coth\left[\frac{1}{2}\beta(\omega - c)\right], \tag{E.16}$$

where C_1 and C_2 are parallel paths to the imaginary ω axis, with opposite orientations, located (infinitesimally) to the left and to the right of the $\mathrm{Re}\,\omega = c$ line, respectively, as shown in Fig. E.3. To see this, first note that the function $g(z) = \coth z$ has all its (single) poles along the $\mathrm{Im}\,z$ axis, at $z = 2\pi n i$, with unit residue. By closing the contour $C_1 \cup C_2$ at infinity, Eq. (E.16) follows, by the residue theorem, since $g(\omega)$ is analytic.

Next, we consider once again the integral in Eq. (E.16), but now close off the path C_1 by a large semi-circle which closes the path to the left, and C_2 by a large semi-circle which

closes the path to the right, both with clockwise orientation. By hypothesis, $|h(\omega)| < 1/|\omega|$ as $|\omega| \to \infty$, so that the contribution of the semi-circles is negligible as we take their radii to infinity. Then, by the residue theorem, the integral in Eq. (E.16) is the sum of residues to the left of C_1 and to the right of C_2. As $g(z) = \coth z$ is analytic out of the imaginary axis, this means that

$$S = \sum_{n=-\infty}^{\infty} h(c + i\omega_n) = -\frac{1}{2} \sum \mathrm{Res}\, h(\omega) \coth \left[\frac{1}{2}\beta(\omega - c)\right], \tag{E.17}$$

where the sum in the right is over all residues of $h(\omega)$. Equation (E.17) is the central piece for evaluating Matsubara equations.

Examples of frequency sum and momentum integrals

Let us use this result to evaluate a typical frequency sum. Consider the integral

$$J = \frac{1}{\beta} \sum_{n=-\infty}^{\infty} \int \frac{d^3k}{(2\pi)^3} \vec{k}^2 \Delta(k)\Delta(k - Q). \tag{E.18}$$

The frequency sum is evaluted using Eq. (E.17), using the analytic forms of the free propagators (E.10). The result is

$$J = -\frac{1}{8\pi^2} \int \frac{\vec{k}^2 dk d\Omega}{4\pi} \frac{\vec{k}^2}{E_1 E_2} \left[(1 - \tilde{n}(E_1) - \tilde{n}(E_2) \left(\frac{1}{i\omega - E_1 - E_2} - \frac{1}{i\omega + E_1 + E_2} \right) + \right.$$
$$\left. -(\tilde{n}(E_1) - \tilde{n}(E_2)) \left(\frac{1}{i\omega + E_1 - E_2} - \frac{1}{i\omega - E_1 + E_2} \right) \right] \tag{E.19}$$

where $E_1 = |\vec{k}|$ and $E_2 = |\vec{q} - \vec{k}|$ are the off-shell energies of the fermions in the loop (where we already dropped the fermion masses, since we are working in the HTL approximation), $d\Omega = d(cos\theta)d\phi$ is the angle integration element and $\tilde{n}(E)$ is the Fermi-Dirac distribution:

$$\tilde{n}(E) = \frac{1}{e^{\beta E} + 1}. \tag{E.20}$$

Another frequency sum that will be needed is

$$J_l = \frac{1}{\beta} \sum_{n=-\infty}^{\infty} \int \frac{d^3k}{(2\pi)^3} \vec{k}^2 \omega_n k_l \Delta(k)\Delta(k - Q). \tag{E.21}$$

After a short calculation, similar to the one above, one can see that

$$J = \frac{1}{8\pi^2}\int \frac{\vec{k}^2 dk d\Omega}{4\pi}\vec{k}^2\frac{ik_l}{E_2}\left[(1-\tilde{n}(E_1)-\tilde{n}(E_2)\left(\frac{1}{i\omega - E_1 - E_2}+\frac{1}{i\omega + E_1 + E_2}\right)+\right.$$
$$\left.-(\tilde{n}(E_1)-\tilde{n}(E_2))\left(\frac{1}{i\omega + E_1 - E_2}+\frac{1}{i\omega - E_1 + E_2}\right)\right] \tag{E.22}$$

Let us analyze the leading order dependence on T of these integrals. In the HTL approximation, the external momentum is negligible when compared to the temperature of the thermal bath, $q \ll T$. Also, the integral is dominated by the cutoff contribution, so we may assume $q \ll k$. Then, we have that, in HTL, that

$$E_2 \approx k - q\cos\theta \tag{E.23}$$

and thus

$$\tilde{n}(E_2) = \tilde{n}(k - q\cos\theta) \approx \tilde{n}(k) - q\cos\theta\frac{d\tilde{n}}{dk}. \tag{E.24}$$

Now, for large k, $d\tilde{n}/dk \sim 0$. Thus,

$$1 - \tilde{n}_1 - \tilde{n}_2 \approx 1 - \tilde{n}(k), \tag{E.25}$$

Thus, we have that the typical momentum integral in the first term in brackets in Eq. (E.19) is of the form

$$\int_0^\infty dk\, k\,(1-\tilde{n}(E_1)-\tilde{n}(E_2) \approx \int_0^\infty dk\, k\,(1-2\tilde{n}(k)). \tag{E.26}$$

This term will lead to a leading dependence of T of T^2, as

$$\int_0^\infty dk\, k\,\tilde{n}(k) = \frac{\pi^2 T^2}{2}. \tag{E.27}$$

Another source of a leading T^2 dependence will come from the second term in the brackets in Eq. (E.19). There, the denominators are of the form

$$\frac{1}{i\omega \mp E_1 \pm E_2} \approx \frac{1}{i\omega \pm q\cos\theta}. \tag{E.28}$$

The numerator is

$$\tilde{n}(E_1) - \tilde{n}(E_2) \approx q\cos\theta\frac{d\tilde{n}}{dk}. \tag{E.29}$$

Thus, in the second term in brackets the angular integration and k integration decouple.

The remaining k integration is

$$\int dk k^2 \sim T^2, \tag{E.30}$$

where we used the HTL cutoff.

Integral I^b

Let us start by integral I^b. Inserting $\Delta(k) = 1/k^2$ and computing the frequency sum, we arrive at

$$I^b = \int \frac{d\Omega}{(2\pi)^2} \int_0^\infty dk \, \frac{1}{4\pi} k(1 - 2\tilde{n}(k)). \tag{E.31}$$

Integrating on k, only keeping the leading T contribution (as discussed in the preceding paragraph), then integrating over Ω, we arrive at the leading T result

$$I^b \approx -\frac{T^2}{24}. \tag{E.32}$$

Integral $I^a_{\mu\nu}$

The other integral necessary to compute $\Pi_{\mu\nu}$ is $I^a_{\mu\nu}$. In this case, we have to take bit more care in order to deal with the vector indices. The first step is to perform the Matsubara sum, which leads to

$$I^a_{\mu\nu} = -\frac{1}{8\pi^2} \int \frac{d\Omega dk}{4\pi} k_\mu k_\nu \frac{k^2}{E_1 E_2} \left[(1 - \tilde{n}(E_1) - \tilde{n}(E_2) \left(\frac{1}{i\omega - E_1 - E_2} - \frac{1}{i\omega + E_1 + E_2} \right) + \right.$$
$$\left. -(\tilde{n}(E_1) - \tilde{n}(E_2)) \left(\frac{1}{i\omega + E_1 - E_2} - \frac{1}{i\omega - E_1 + E_2} \right) \right]. \tag{E.33}$$

As $q \ll k$, following the arguments above, we have that the denominators in I^a can be written as

$$i\omega + E_1 - E_2 \approx i\omega + \vec{q} \cdot \hat{k} = Q \cdot \hat{K}, \tag{E.34}$$

$$i\omega - E_1 + E_2 \approx Q \cdot \hat{K}', \tag{E.35}$$

$$i\omega \pm (E_1 + E_2) \approx \pm k, \tag{E.36}$$

where we defined the normalized four-vectors

$$\hat{K} = (-i, \hat{k}), \tag{E.37}$$

$$\hat{K}' = (-i, -\hat{k}). \tag{E.38}$$

We remark again that $Q = (-i\omega, \vec{q})$. With these definitions, we then have that

$$\vec{q} \cdot \vec{k} = Q \cdot \hat{K}' - i\omega. \tag{E.39}$$

Using the approximations and definitions above, the spatial-spatial part of $I^a_{\mu\nu}$ becomes

$$I^a_{ij} = -\frac{1}{4\pi^2} \int \frac{d\Omega dk}{4\pi} k^2 \, \hat{k}_i \hat{k}_j \left[\frac{\tilde{n}(k)}{k} - \frac{d\tilde{n}}{dk} + \frac{d\tilde{n}}{dk} \frac{i\omega}{Q \cdot \hat{K}} \right]. \tag{E.40}$$

We then proceed to perform the integration in k. First, due to rotation invariance, one can see that for a given function of k^2, $f(k^2)$,

$$\int_0^\infty \hat{k}_i \hat{k}_j f(k^2) = \frac{1}{3} \delta_{ij} \int_0^\infty dk \, k^2 f(k^2). \tag{E.41}$$

Also, using that for the Fermi-Dirac distribution $\tilde{n}(k)$ we have that

$$\int_0^\infty dk \, k^2 \frac{\tilde{n}(k)}{k} = \frac{\pi^2}{12} T^2, \tag{E.42}$$

$$\int_0^\infty dk \, k^2 \frac{d\tilde{n}}{dk} = -\frac{\pi^2}{6} T^2. \tag{E.43}$$

With these results, also using the fact that the integrals in Ω and k decouple, we have that

$$I^a_{ij} = -\frac{T^2}{48} \delta_{ij} + \frac{T^2}{24} \int \frac{d\Omega}{4\pi} \hat{k}_i \hat{k}_j \frac{i\omega}{Q \cdot \hat{K}}. \tag{E.44}$$

The integrals I^a_{0j} and I^a_{00} can be evaluated in an analogous fashion.

The full correlator

From the preceding results for I^a_{ij} and I^b, we can write Π_{ij} in Eq. (E.12) as

$$\Pi_{ij} = \frac{e^2 T^2}{3} \int \frac{d\Omega}{4\pi} \frac{i\omega}{Q \cdot \hat{K}} \hat{k}_i \hat{k}_j. \tag{E.45}$$

For Π_{4j} and Π_{44} the computation is analogous. The final result is

$$\Pi_{0j} = \frac{e^2 T^2}{3} \int \frac{d\Omega}{4\pi} \frac{i\omega}{Q \cdot \hat{K}} \hat{k}_j, \tag{E.46}$$

$$\Pi_{00} = \frac{e^2 T^2}{3} \left(1 - \int \frac{d\Omega}{4\pi} \frac{i\omega}{Q \cdot \hat{K}} \right). \tag{E.47}$$

These results can be combined in a single expression for $\Pi_{\mu\nu}$:

$$\Pi_{\mu\nu} = 2m^2 \int \frac{d\Omega}{4\pi} \left(\frac{i\omega \hat{K}_\mu K_\nu}{Q \cdot \hat{K}} + \delta_{0\mu}\delta_{0\nu} \right), \tag{E.48}$$

where we defined a thermal mass m by

$$m^2 = \frac{e^2 T^2}{6}. \tag{E.49}$$

Extracting the functions F and G

From the result (E.48) for the one-loop correlator, we can extract the functions F and G in Eq. (E.2). Setting $\vec{q} = (0, 0, 0, q)$ (thus $\vec{q} = (0, 0, q)$, along the z axis), we have that

$$F(Q) = \frac{Q^2}{\omega q}\Pi_{03} = \frac{2m^2 Q^2}{\omega q} \int \frac{d\Omega}{4\pi} \frac{\omega \cos\theta}{i\omega + q\cos\theta}, \tag{E.50}$$

$$G(Q) = \Pi_{11} = 2m^2 \int \frac{d\Omega}{4\pi} \frac{i\omega \sin^2\theta \cos^2\phi}{i\omega + q\cos\theta}. \tag{E.51}$$

The angular integration is straightforward and leads to

$$F(Q) = \frac{2m^2 Q^2}{q^2} \left[1 - \frac{i\omega}{q} Q_0 \left(\frac{i\omega}{q} \right) \right], \tag{E.52}$$

$$G(Q) = \Pi_{11} = m^2 \left(\frac{i\omega}{q} \right) \left[\left(1 - \left(\frac{i\omega}{q} \right)^2 \right) Q_0 \left(\frac{i\omega}{q} \right) + \frac{i\omega}{q} \right], \tag{E.53}$$

where $Q_0(x)$ is a Legendre function of the second kind, defined by

$$Q_0(x) = \frac{1}{2} \ln \left(\frac{x+1}{x-1} \right). \tag{E.54}$$

The Debye screening mass in QED at one loop

We are now in position to extract the Debye screening mass for QED at one loop. Following the prescription (E.8), we have to look at Π_{00} and look at its form with $\omega = 0$:

$$\Pi_{00}(\omega = 0, \vec{q}) = F(\vec{q}^{\,2}) = 2m^2. \tag{E.55}$$

As $\Pi_{00}(\omega = 0, \vec{q})$ is independent of $\vec{q}$, it follows that the Debye screening mass m_D is given by

$$m_D^2 = 2m^2 = \frac{e^2 T^2}{3}. \tag{E.56}$$

On the other hand, one could look for the magnetic screening mass m_{mag}. Since $G(\omega =$

$0, \vec{q}) = 0$, it follows that

$$m_{mag} = 0. \tag{E.57}$$

Although we have seen this at one loop in perturbation theory, one can prove that Eq. (E.57) holds at all orders in perturbation theory [422].

E.3 The relation between static screening fields and the Debye screening mass in QED

Another viewpoint that enlightens the meaning of the Debye screening mass comes from linear response theory. Consider a weak external electromagnetic field $(\vec{E}_{cl}, \vec{B}_{cl})$, which couples with classical source $j^{\mu}_{cl} = (\rho_{cl}, \vec{j}_{cl})$ by the interaction term

$$V = \int d^3x \, j^{\mu}_{cl} \hat{A}_{\mu}, \tag{E.58}$$

where $\hat{A}_{\mu}$ is the quantum vector potential. The fluctuation of the quantized field $\langle \delta \hat{A}_{\mu} \rangle$ is given by the Kubo formula (see Section 3.8)

$$\langle \delta \hat{A}_{\mu} \rangle = A_{\mu} = -i \int d^4x' G^R_{\mu\nu}(x, x') j^{\nu}_{cl}(x'), \tag{E.59}$$

where $G^R_{\mu\nu}$ is retarted photon Green's function and A_{μ} is the expectation value of the vector potential under the influence of the external fields. We also assumed that the background fields have zero expectation value $\langle A_{\mu} \rangle = 0$, so that $\langle \delta \hat{A}_{\mu} \rangle = A_{\mu}$. In momentum space,

$$A_{\mu} = i G^R_{\mu\nu}(Q) j^{\nu}_{cl}(Q). \tag{E.60}$$

Our objective is to compute the linear response electric and magnetic fields $\vec{E}$ and $\vec{B}$ from the response vector potential A_{μ} which arise due to the response of the system due to the applied external fields $(\vec{E}_{cl}, \vec{B}_{cl})$.

So far, we have computed the Euclidean Green's function $G(Q)$. To obtain the retarted propagator G^R from the Euclidean propagator G, we need to perform the analytic continuation $i\omega \to q_0 + i\epsilon$, with $Q^2 \to -Q^2$. From Eq. (E.6),

$$G^R_{\mu\nu} = \frac{i}{Q^2 - \bar{F}(Q^2)} \hat{P}^L_{\mu\nu} + \frac{i}{Q^2 - \bar{G}(Q^2)} \hat{P}^T_{\mu\nu} - i \frac{\xi}{Q^2} \frac{Q_{\mu} Q_{\nu}}{Q^2}, \tag{E.61}$$

where the barred projectors now satisfy

$$\bar{P}^L_{\mu\nu} + \bar{P}^T_{\mu\nu} = -\eta_{\mu\nu} + \frac{Q_\mu Q_\nu}{Q^2}. \tag{E.62}$$

The barred $\bar{F}(Q)$ and $\bar{G}(Q)$ functions are obtained by analytic continuation from Eqs. (E.52) and (E.53):

$$\bar{F}(Q) = -\frac{2m^2Q^2}{q^2}\left[1 - \frac{q_0}{q}Q_0\left(\frac{q_0}{q}\right)\right], \tag{E.63}$$

$$\bar{G}(Q) = \frac{1}{2}[m_D^2 - \bar{F}(Q)]. \tag{E.64}$$

With the retarted propagator discussed, we now proceed to consider the components of A_μ from Eq. (E.60). We have that, from Eq. (E.61),

$$A^0 = -\frac{\rho_{cl}}{Q^2 - F}. \tag{E.65}$$

As for $\vec{A}$, we have that

$$\vec{A} = -\left(\frac{\vec{j}^L_{cl}}{Q^2 - F} + \frac{\vec{j}^T_{cl}}{Q^2 - G}\right), \tag{E.66}$$

where we splitted $\vec{j}_{cl}$ in two components, one parallel to $\vec{q}$, $\vec{j}^L_{cl}$, which satisfies $\vec{j}^L_{cl} \times \hat{q} = 0$, and one transverse to $\vec{q}$, $\vec{j}^T_{cl}$, which satisfies $\vec{j}^T_{cl} \cdot \hat{q} = 0$. The linear response electromagnetic fields $\vec{E}$ and $\vec{B}$ are given by

$$\vec{E} = -\partial_t \vec{A} - \nabla A_0, \tag{E.67}$$

$$\vec{B} = \nabla \times \vec{A}, \tag{E.68}$$

which in momentum space reads

$$\vec{E} = iq_0\vec{A} - i\vec{q}A_0, \tag{E.69}$$

$$\vec{B} = i\vec{q} \times \vec{A}. \tag{E.70}$$

Then, we have that, using also that $Q^2 = q_0^2 - q^2$,

$$\vec{E} = -i\left(\frac{\rho_{cl}}{Q^2 - F}\frac{Q^2}{q^2}\vec{q} + \frac{\vec{j}^T_{cl}}{Q^2 - G}q_0\right), \tag{E.71}$$

$$\vec{B} = -i\frac{\vec{q} \times \vec{j}^L_{cl}}{Q^2 - G}. \tag{E.72}$$

Now, the classical fields $(\vec{E}_{cl}, \vec{B}_{cl})$ satisfy Maxwell's equations, with the sources given by $j^{\mu}_{cl} = (\rho_{cl}, \vec{j}_{cl})$. We will need specifically the Gauss law and Ampère's law:

$$\nabla \cdot \vec{E}_{cl} = \rho_{cl}, \tag{E.73}$$

$$\nabla \times \vec{B}_{cl} = \vec{j}_{cl} + \partial_t \vec{E}_{cl}. \tag{E.74}$$

In momentum space, these read

$$i\vec{q} \cdot \vec{E}_{cl} = \rho_{cl}, \tag{E.75}$$

$$i\vec{q} \times \vec{B}_{cl} = \vec{j}_{cl} + iq_0 \vec{E}_{cl}. \tag{E.76}$$

Now, taking the cross product of Ampère's law with $i\vec{q}$,

$$\vec{j}^{T}_{cl} = -\vec{q} \times \vec{B}_{cl} - iq_0 \vec{E}^{T}_{cl}, \tag{E.77}$$

where the transverse electric field is $\vec{E}^{T}_{cl} = \vec{q} \times \vec{E}/q$. From Gauss' law, similarly,

$$\rho_{cl} = i\vec{q} \cdot \vec{E}^{L}_{cl}, \tag{E.78}$$

where $\vec{E}^{L}_{cl} = (\vec{q} \cdot \vec{E}_{cl}/q^2)\vec{q}$. We can then use Eqs. (E.77) and (E.78) to express the complete electric and magnetic fields $\vec{E}$ and $\vec{B}$ in Eqs. (E.71) and (E.72) in terms of the classical background fields $\vec{E}_{cl}$ and $\vec{B}_{cl}$,

$$\vec{E} = \frac{Q^2}{Q^2 - F}\vec{E}^{L}_{cl} + \frac{q_0}{Q^2 - G}\left(\vec{q} \times \vec{B}_{cl} + q_0 \vec{E}^{T}_{cl}\right), \tag{E.79}$$

$$\vec{B} = \frac{Q^2}{Q^2 - G}\vec{B}_{cl}. \tag{E.80}$$

Eqs. (E.79) and (E.80) make it clear that $\vec{E} = \vec{E}_{cl}$ and $\vec{B} = \vec{B}_{cl}$ in the limit that the plasma is non-interacting and $F = G = 1$.

With the linear response equations Eqs. (E.79) and (E.80) in hand, we may consider the limit of a static electric external field $\vec{E}_{cl}$. In this case, the external frequency is $q_0 = 0$. Also setting $\vec{B}_{cl} = 0$, we arrive at $\vec{B} = 0$ and

$$\vec{E} = \frac{Q^2}{Q^2 - F(q_0 = 0, \vec{q})}\vec{E}^{L}_{cl} = \frac{\vec{q} \cdot \vec{E}_{cl}}{q^2 + F(q_0 = 0, \vec{q})}\,\vec{q}. \tag{E.81}$$

From this, considering that in the static limit the potential $V(\vec{x})$ of unit charge at the origin is related to the static electric field by $\vec{E} = -\nabla \cdot \vec{V}$, or, in momentum space,

$\vec{E} = -i\vec{q}V$, we see that the potential $V(r)$ is given by

$$V(\vec{x}) = \int \frac{d^3q}{(2\pi)^3} \frac{e^{i\vec{q}\cdot\vec{x}}}{q^2 + F(q_0 = 0, \vec{q})}. \tag{E.82}$$

We now look at the long range behavior of $V(\vec{x})$, which is dominated by the lowest-lying pole of the denominator, which in turn corresponds to the Debye screening mass definition in Eq. (E.8). That is, the long range form of $V(\vec{x})$ is given by, after computing the integral in $\vec{q}$,

$$V(\vec{x}) = \frac{e^{-m_D r}}{r}, \tag{E.83}$$

where m_D is given exactly by Eq. (E.8). This clarifies the meaning of the Debye screening mass in QED as a static screening of charges by the plasma.

An analogous argument applies to screening by external static magnetic field. In this case, the screening is given by the poles of G. Since we have seen that the QED plasma does not develop a magnetic screening mass in perturbation theory, it follows that there is no static screening of currents in the plasma.

E.4 Debye screening mass in QCD at one loop order

Finally, to close this Appendix, we offer some comments on the one-loop evaluation of the Debye screening mass in QCD, with N_c colors and N_f massless quarks. Apart from the fermion loop discussed above, we also have the diagrams presented in Fig. E.4. We will not evaluate these diagrams here (the procedure is similar to the fermion loop), but we will offer some comments.

The fermion loop (a) is identical to the fermion loop in QED, with the result being exactly Eq. (E.12); the only two differences are a factor of N_f due to the N_f different quarks which can run in the loop, and the change of the coupling constant from e to g. The sum the gluon loop diagram (b), the ghost loop diagram (c), and the tadpole diagram (d) also lead to a modification of Eq. (E.12); one should take care of the different bosonic statistics for these diagrams when evaluating the Matsubara sums (see Ref. [421] for more details). In the end, the sum of diagrams (a) to (d) lead to

$$\Pi_{\mu\nu} = -2g^2 \left(N_c + \frac{1}{2} N_f \right) (2I^a_{\mu\nu} - \delta_{\mu\nu} I^b). \tag{E.84}$$

Thus, at one loop, the results from Eq. (E.48) for QED can be carried over to QCD with

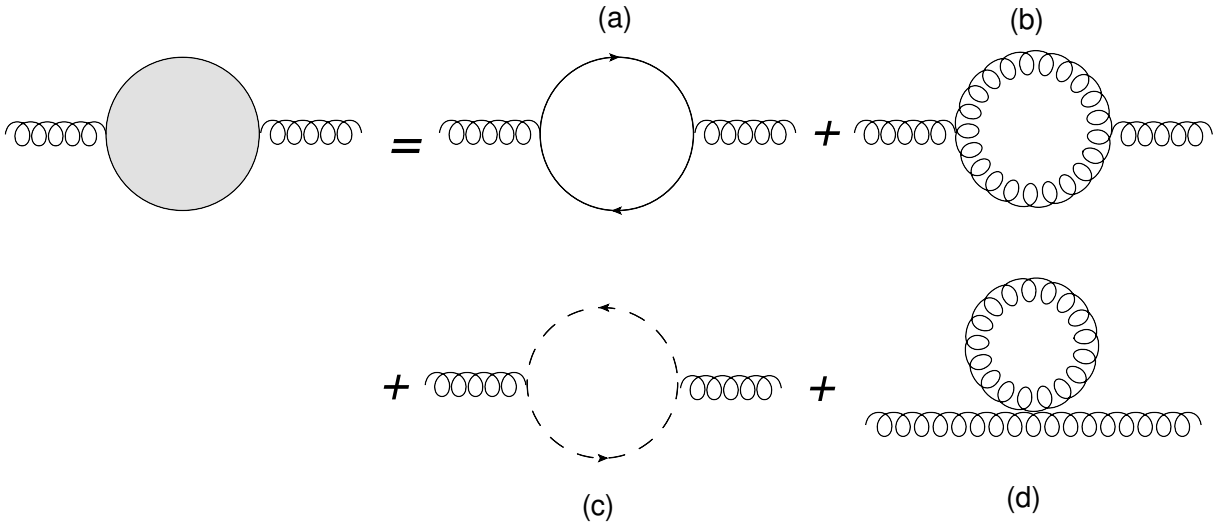

Figure E.4: *Feynman diagrams for the gluon polarization tensor in QCD at one loop. The fermion loop (a) is presented even in QED, while the other diagrams, the gluon loop diagram (b), the ghost diagram (c), and the tadpole diagram (d) are unique to QCD.*

the only modification being the change

$$e^2T^2 \to g^2T^2\left(N_c + \frac{1}{2}N_f\right). \tag{E.85}$$

In particular, the Debye screening mass in QCD, at one loop, is given by

$$m_D^2 = \left(N_c + \frac{1}{2}N_f\right)\frac{g^2T^2}{3}, \tag{E.86}$$

as given in Eq. (6.8). However, as remarked in the main text, the perturbative analysis of the Debye screening mass breaks down at higher orders.

Appendix F

Complementary Details about the Holographic Debye Screening Mass in Strongly Coupled Plasmas

In this Appendix we present some details relevant to the topics studied in Chapter 6. Section F.1 shows how to relate the string frame to the Einstein frame - this is necessary in order to correctly compute Polyakov loops on the Einstein + scalar models considered in Chapter 6. Section F.2 describes the coordinate system change from the Gubser gauge to the conformal gauge.

F.1 String and Einstein frames

The metric used in calculations of Wilson and Polyakov loops is the metric that the string "feels". From a string theory perspective, the metric used in this calculation is the one that arises from the low-energy limit of string theory and is referred to as the *string frame metric* [102]. However, this effective action that arises couples the dilaton field ϕ directly with the Ricci scalar $\mathcal{R}$; this means that this effective action does not correctly reduce to the Einstein-Hilbert action. To obtain an action that resembles Einstein's gravity, it is necessary to perform a redefinition of the fields of the theory - this is what means to go from the string frame to the *Einstein frame*. Let us review the details of this transformation. We will follow the discussion in Ref. [359], Appendix G.

F.1.1 Weyl rescaling

Let $g_{\mu\nu}$ be the metric of a d dimensional space-time, and consider the general conformal transformation (also called Weyl transformation or Weyl rescaling)

$$g_{\mu\nu}(x) \to \tilde{g}_{\mu\nu} = e^{2\omega(x)} g_{\mu\nu}(x), \tag{F.1}$$

where $\omega(x)$ is a smooth function. That is, we locally apply a scale transformation at each point of space-time. This transformation is *not*, for a general $\omega(x)$, a diffeomorphism - as we will show below, invariant quantities under coordinate transformations, such as the scalar curvature, transform non-trivially under a Weyl rescaling. One can interpret Eq. (F.1) as either a transformation of the space-time geometry or, for the purposes of this Section, as a redefinition of the dynamical fields of the spacetime, including the metric. Under a Weyl transformation it is a straightforward (if a little lenghty calculation - check Ref. [359] for further details) calculation to see that the curvature scalar $\mathcal{R}$ transform as

$$\mathcal{R} \to \tilde{\mathcal{R}} = e^{-2\omega} \left[\mathcal{R} - 2(d-1) g^{\alpha\beta} \nabla_\alpha \nabla_\beta \omega - (d-2)(d-1) g^{\alpha\beta} \nabla_\alpha \omega \nabla_\beta \omega \right]. \tag{F.2}$$

Now, the d'Alembertian of a scalar field ϕ, $\Box\phi$, transforms, under a Weyl rescaling, into $\tilde{\Box}\phi$, where

$$\tilde{\Box}\phi = e^{-2\omega} \left[\Box\phi + (d-2) g^{\alpha\beta} \nabla_\alpha \omega \nabla_\beta \omega \right]. \tag{F.3}$$

F.1.2 From the string frame to the Einstein frame

The effective action of the dilaton field ϕ coupled to gravity has the following general form in the string frame,

$$S_{\text{string}} = \int d^d x \sqrt{-g}\, e^{-2\phi} \left(\mathcal{R} + 4 g^{\mu\nu} \partial_\mu \phi \partial_\nu \phi \right). \tag{F.4}$$

The curvature scalar is directly coupled to the metric by the term $\mathcal{R} e^{-2\phi}$. To write this in the form of the Einstein-Hilbert action coupled to matter fields, we perform a Weyl rescaling of the form

$$g_{\mu\nu}(x) \to \tilde{g}_{\mu\nu} = e^{\alpha\phi} g_{\mu\nu}, \tag{F.5}$$

where α is a coefficient that will be determined below. Using the (inverse of the) transformation formulas (F.2) and (F.3) and identifying a boundary term of the form $\tilde{g}^{\alpha\beta} \tilde{\nabla}_\alpha \tilde{\nabla}_\beta \phi$ which vanishes assuming that $\tilde{\nabla}_\alpha \phi \to 0$ at the boundary of the space-time, we obtain

$$S = \int d^d x \sqrt{-\tilde{g}}\, e^{\frac{\alpha}{2}(d-2)-2} \left\{ \tilde{R} - \left[(d^2 - 3d - 2)\alpha^2 - 4 \right] \tilde{g}^{\alpha\beta} \tilde{\nabla}_\alpha \phi \tilde{\nabla}_\beta \phi \right\}. \tag{F.6}$$

To have a Einstein-Hilbert + matter action, we require that the exponential term in vanishes, that is,

$$\alpha = \frac{4}{d-2}. \tag{F.7}$$

Thus, the action in the so-called Einstein frame takes the form

$$S = \int d^d x \sqrt{-g} \left(\tilde{R} - \frac{4}{d-2} g^{\alpha\beta} \tilde{\nabla}_\alpha \phi \tilde{\nabla}_\beta \phi \right). \tag{F.8}$$

The metric then changes to

$$g_{\mu\nu}(x) \to \tilde{g}_{\mu\nu} = e^{\frac{4}{d-2}\phi} g_{\mu\nu}. \tag{F.9}$$

For $d = 10$, the case of dual theories of gravity derived from superstring theory, $\tilde{g}_{\mu\nu} = e^{\phi/2} g_{\mu\nu}$. In the case of some the IHQCD models used in Chapters 6 and 7, namely, those of Refs. [16, 17], it is assumed that the underlying string theory is a subcritical one with $d = 5$; in this case, $\tilde{g}_{\mu\nu} = e^{4/3\phi} g_{\mu\nu}$, which explains the Einstein to string frame metric transform factor used in Chapter 6.

F.2 Gauge choices for the B class of models

As mentioned in the main text, for the models B1 and B2, the Gubser gauge (6.63) while adequate for studying the thermodynamics is not convenient for evaluating Polyakov and Wilson loops or finding the glueball spectrum (as done in Appendix F.3). For these purposes, it is convenient to change to the conformal gauge given by

$$ds^2 = e^{2\tilde{A}(z)} \left(\tilde{h}(z) d\tau^2 + d\vec{x}^2 + \frac{dz^2}{\tilde{h}(z)} \right). \tag{F.10}$$

Comparing Eq. (F.10) with Eq. (6.63), we see that the following relation must hold among the metric functions

$$\frac{dz}{d\phi} = e^{B-A}. \tag{F.11}$$

We require that the asymptotic AdS_5 is located at $z = 0$ and that the horizon is at $z = z_h$. The solution of Eq. (F.11) that satisfies these requirements is

$$z(\phi) = \int_0^\phi d\tilde{\phi}\, e^{B(\tilde{\phi}) - A(\tilde{\phi})} \tag{F.12}$$

We can invert (numerically) Eq. (F.12) to get $\phi(z)$. Then, the functions $\tilde{\mathcal{A}}(z)$ and $\tilde{h}(z)$ are given by $\tilde{\mathcal{A}}(z) = A(\phi(z))$ and $\tilde{h}(z) = h(\phi(z))$.

F.3 Glueball spectra in B1 model

In this section we compute the glueball spectra for model B1, which displays confinement at $T = 0$. The parameters used in the scalar potential in this model are given in Table 6.2.

Let us briefly review the numerical procedure for finding the vacuum geometry and the glueball spectra. One first numerically integrates the equations of motion (6.77) subject to the boundary condition (6.78); then, we search, numerically, for the eigenvalues of the Schrödinger's equation (6.29), as described in the main text. To find the spectra, we change the metric from the $z = \phi$ gauge (6.63) to the conformal gauge, as described in Appendix F.2. The potential for the Schrödinger's equation is given by Eq. (6.30), where $\mathcal{B}$ depends on whether we are dealing with the scalar $J^{PC} = 0^{++}$ glueballs, tensor $J^{PC} = 2^{++}$ glueballs, or pseudo-scalar $J^{PC} = 0^{-+}$ glueballs [17, 423]

$$\begin{aligned} &(\text{scalar})\, 0^{++} \qquad \mathcal{B}(z) = \frac{3}{2}\mathcal{A}(z) + \frac{1}{2}\log X(z), \\ &(\text{tensor})\, 2^{++} \qquad \mathcal{B}(z) = \frac{3}{2}\mathcal{A}(z), \\ &(\text{axial})\, 0^{-+} \qquad \mathcal{B}(z) = \frac{3}{2}\mathcal{A}(z) + \frac{1}{2}\log \mathcal{Z}(\lambda(z)). \end{aligned} \tag{F.13}$$

In Eq. (F.13), $X(z)$ is defined by

$$X(z) \equiv \frac{d\Phi/dz}{3\mathcal{A}(z)}, \tag{F.14}$$

where $\Phi = \sqrt{3/8}\phi(z)$ while $\lambda(z) = e^{\phi(z)}$, with $Z(\lambda)$ still given by Eq. (6.59). For a comparison with lattice results, we normalize the spectrum by the fundamental 0^{++} glueball mass.

Our results are shown in Figs. F.1 and F.2. For comparison, we used lattice results for the glueball spectra in pure Yang-Mills with gauge groups $SU(3)$ [424, 425] and $SU(N_c)$ in the large-N_c limit [426, 427]. We see in Fig. F.1 that linear Regge trajectories are achieved for $n > 4$. Also, we note that the axial glueball has little sensitivity to the choice of c_4 - in the interval $c_4 = 0.1$ to $c_4 = 10$ the masses are almost degenerate. For this reason, in Fig. F.1 we show only the results for $c_4 = 1$. Comparing with lattice results (Fig. F.2), we see that reasonable agreement is found for the tensor glueball among all calculations. The axial glueball of the Model B1 and large-N_c $SU(N_c)$ Yang-Mills are both reasonably close; however, both axial glueball masses are off by a factor of 2 when compared with the SU(3) Yang-Mills fundamental axial glueball. This contrasts with the results found for the holographic Polyakov loop in Subsection 6.6.2, where the results where relatively insensitive to N_c.

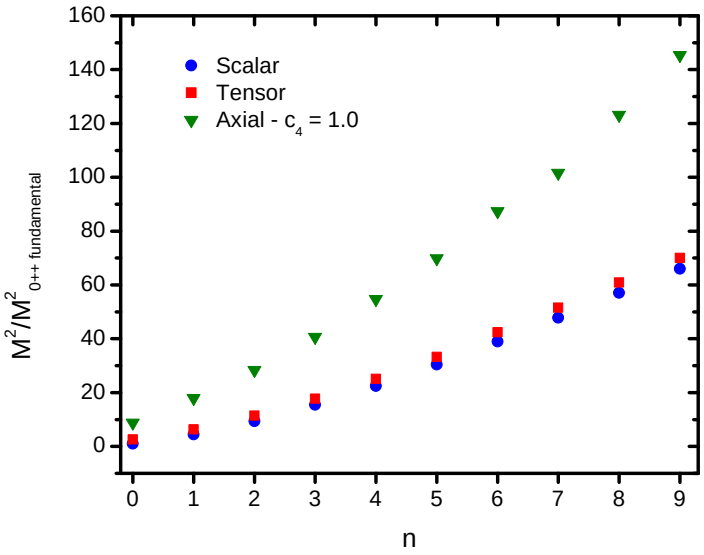

Figure F.1: *Glueball spectra in the Model B1. The glueball masses are normalized by the mass of the fundamental $J^{PC} = 0^{++}$ glueball. n indicates the order of the excited state; $n = 0$ is the fundamental state.*

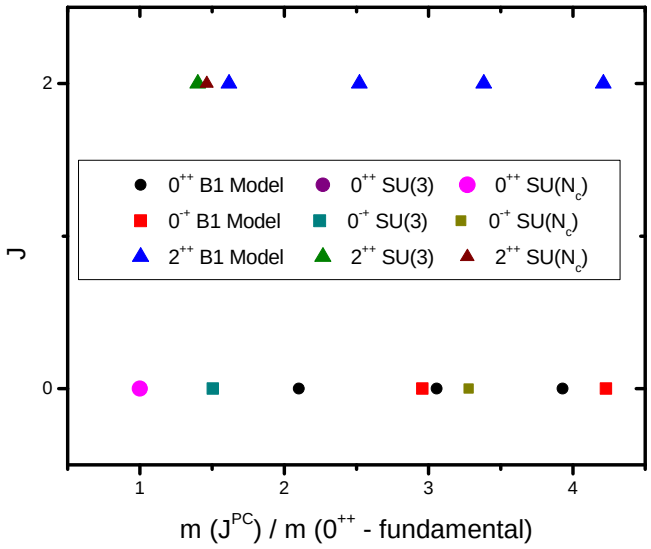

Figure F.2: *Chew-Frautschi plot of the glueball spectra, comparing results from Model B1 with lattice results for SU(3) [424, 425] and large-N_c $SU(N_c)$ [426, 427] Yang-Mills theory.*

Appendix G

Complementary Details About Second Order Transport Coefficient for Hydrodynamics

G.1 Solution for the metric perturbation up to $\mathcal{O}(\omega^2, q^2)$

In this Appendix we formally solve Eq. (8.28) in detail in terms of the coefficients of the undisturbed background metric, $g^{(0)}_{MN}(u)$, and the boundary value of the metric perturbation, $\varphi(\omega, q)$, up to $\mathcal{O}(\omega^2, q^2)$. In order to accomplish that one must specify the boundary conditions for the metric perturbation, $\phi(u, \omega, q)$, at the boundary and at the horizon.

We first consider the boundary. The asymptotic form of Eq. (8.28) near the boundary $u = \epsilon$ for any asymptotically AdS background reads[1]

$$\phi''_\epsilon - \frac{3}{u}\phi'_\epsilon - k^2\phi_\epsilon = 0 \Rightarrow \phi_\epsilon = C_1(k)\epsilon^2 K_2(k\epsilon) + C_2(k)\epsilon^2 I_2(k\epsilon), \tag{G.1}$$

where $k^2 = -\omega^2 + q^2$ and $I_n(\xi)$ and $K_n(\xi)$ are the modified Bessel functions of the first and second kinds, respectively. Now we take

$$\lim_{u\to 0}\phi(u,k) = \lim_{\epsilon\to 0}\phi_\epsilon(k) = \frac{2C_1(k)}{k^2}, \tag{G.2}$$

which is a constant in the radial direction. Therefore, in the case of a massless scalar field, one can safely impose the Dirichlet boundary condition as follows

$$\lim_{u\to 0}\phi(u,k) = \varphi(k)\,, \tag{G.3}$$

[1]For asymptotically AdS geometries one finds $g_{uu}(\epsilon) \sim g_{tt}(\epsilon) \sim g_{xx}(\epsilon) \sim L^2/\epsilon^2$.

where $\varphi(k)$ denotes the boundary value of the metric perturbation prescribed by the Dirichlet boundary condition.

Now that we have specified the boundary condition (G.3), let us discuss which kind of condition we must impose on the metric perturbation at the horizon. As discussed in [127, 128, 137, 364], in order to obtain the retarded propagator we must single out the solution of the equation of motion (8.28) which is regular at the horizon and corresponds to a wave being absorbed by the horizon. We begin by assuming that the g_{tt} component of the background metric has a simple zero at the horizon $u = u_H$ such that one can write

$$g_{uu}(u) = \frac{G(u)}{u_H - u}, \quad g_{tt}(u) = F(u)(u_H - u), \tag{G.4}$$

with $G(u_H)$ and $F(u_H)$ finite. Notice that the Hawking temperature of the black brane gives

$$T = \left.\frac{\sqrt{g'_{tt}g^{uu\,\prime}}}{4\pi}\right|_{u=u_H} = \frac{1}{4\pi}\sqrt{\frac{F(u_H)}{G(u_H)}} \Rightarrow \frac{F(u_H)}{G(u_H)} = (4\pi T)^2\,. \tag{G.5}$$

Using Eqs. (G.4) and (G.5), the asymptotic form of Eq. (8.28) near the horizon $u = u_H$ then reads[2]

$$\phi''_H - \frac{1}{u_H - u}\phi'_H + \frac{(\omega/4\pi T)^2}{(u_H - u)^2}\phi_H = 0 \Rightarrow \phi_H = C_1(\omega)(u_H - u)^{-i\omega/4\pi T} + C_2(\omega)(u_H - u)^{+i\omega/4\pi T}, \tag{G.6}$$

and the infalling wave mode at the horizon is obtained by setting $C_2(\omega) = 0$ in Eq. (G.6). Therefore, one is motivated to separate the infalling behavior of the solution and take the following Ansatz for the metric perturbation

$$\phi(u,k) = \varphi(k)u_H^{+i\omega/4\pi T}(u_H - u)^{-i\omega/4\pi T} f(u,k), \tag{G.7}$$

$$f(u,k) = f_0(u) + \omega f_1(\omega) + \frac{\omega^2}{2}f_2(u) + \frac{q^2}{2}f_3(u) + \mathcal{O}(\omega q^2, \omega^3)\,, \tag{G.8}$$

with $f(0,k) = 1$ and $f(u_H,k)$ being regular. We considered only even powers of q in the series expansion (G.8) due to spatial isotropy. Substituting Eq. (G.7) into Eq. (8.28) we obtain the differential equation for $f(u,k)$,

$$\partial_u\left[\sqrt{-g^{(0)}}g^{uu}\left(f' + \frac{i\omega f}{4\pi T(u_H - u)}\right)\right] + \sqrt{-g^{(0)}}g^{uu}\left(f' + \frac{i\omega f}{4\pi T(u_H - u)}\right)\frac{i\omega f}{4\pi T(u_H - u)} = \\ = \sqrt{-g^{(0)}}\left(-g^{tt}\omega^2 + g^{xx}q^2\right)f. \tag{G.9}$$

[2] We only keep the dominant terms in each order in radial derivatives of the metric perturbation.

Now we solve Eq. (G.9) order by order in the momentum expansion (G.8).

Zeroth order - f_0

At lowest order, one obtains the differential equation for $f_0(u)$,

$$\mathcal{O}(\omega^0, q^0): \quad \partial_u \left(\sqrt{-g^{(0)}} g^{uu} f_0' \right) = 0. \tag{G.10}$$

One can integrate Eq. (G.10) twice to obtain

$$f_0(u) = c_1 + c_2 \int_0^u \frac{d\xi}{\sqrt{-g^{(0)}(\xi)} g^{uu}(\xi)}, \tag{G.11}$$

where we just performed two indefinite integrations: the lower limit in the integral present in Eq. (G.11) has been conveniently chosen to lie at the boundary; however, we can choose any other value of the radial coordinate to be the lower limit of this integral and each possible different choice would just redefine the integration constants c_1 and c_2. We immediately fix these constants by using the boundary condition $f(0,k) = 1$ and the regularity condition for $f(u_H, k)$. The former fixes $c_1 = 1$ and the latter fixes $c_2 = 0$; therefore,

$$f_0(u) = 1\,. \tag{G.12}$$

First order - f_1

After using Eqs. (G.8), (G.9), and (G.12), the differential equation for $f_1(u)$ then reads

$$\mathcal{O}(\omega, q^0): \quad \partial_u \left[\sqrt{-g^{(0)}} g^{uu} \left(f_1' + \frac{i}{4\pi T (u_H - u)} \right) \right] = 0. \tag{G.13}$$

Integrating once, we obtain,

$$\sqrt{-g^{(0)}} g^{uu} \left(f_1' + \frac{i}{4\pi T (u_H - u)} \right) = c_2, \tag{G.14}$$

and, then, integrating again, we find

$$f_1(u) = c_1 + \int_0^u d\xi \left[\frac{c_2}{\sqrt{-g^{(0)}(\xi)} g^{uu}(\xi)} - \frac{i}{4\pi T (u_H - \xi)} \right]. \tag{G.15}$$

Applying the boundary condition $f(0,k) = 1$ we obtain $c_1 = 0$. The horizon regu-

larity condition implies

$$c_2 = \frac{i\sqrt{-g^{(0)}(u_H)}}{4\pi T G(u_H)} = i g_{xx}^{3/2}(u_H) \tag{G.16}$$

and, therefore,

$$f_1(u) = i\int_0^u d\xi \left[\frac{g_{xx}^{3/2}(u_H)}{\sqrt{-g^{(0)}(\xi)}g^{uu}(\xi)} - \frac{1}{4\pi T(u_H-\xi)}\right]. \tag{G.17}$$

Second order - f_2

Using Eqs. (G.8), (G.9), (G.12), (G.14), and (G.16) the differential equation for $f_2(u)$ reads

$$\mathcal{O}(\omega^2, q^0): \quad \partial_u\left[\sqrt{-g^{(0)}}g^{uu}\left(\frac{f_2'}{2} + \frac{i f_1}{4\pi T(u_H-u)}\right)\right] = \frac{g_{xx}^{3/2}(u_H)}{4\pi T(u_H-u)} - \sqrt{-g^{(0)}}g^{tt}. \tag{G.18}$$

Integrating Eq. (G.18) twice and using Eq. (G.17), we obtain

$$\begin{aligned} f_2(u) = c_1 + 2\int_0^u \frac{d\lambda}{4\pi T(u_H-\lambda)}\int_0^\lambda d\xi\left[\frac{g_{xx}^{3/2}(u_H)}{\sqrt{-g^{(0)}(\xi)}g^{uu}(\xi)} - \frac{1}{4\pi T(u_H-\xi)}\right] + \\ + 2\int_0^u \frac{d\lambda}{\sqrt{-g^{(0)}(\lambda)}g^{uu}(\lambda)}\left\{c_2 + \int_0^\lambda d\xi\left[\frac{g_{xx}^{3/2}(u_H)}{4\pi T(u_H-\xi)} - \sqrt{-g^{(0)}(\xi)}g^{tt}(\xi)\right]\right\}. \end{aligned} \tag{G.19}$$

In Eq. (G.19), the factors $(4\pi T(u_H-\lambda))^{-1}$ and $c_2/\sqrt{-g^{(0)}(\lambda)}g^{uu}(\lambda)$ diverge at the horizon while the factor $\sqrt{-g^{(0)}(\xi)}g^{tt}(\xi)$ diverges at the boundary; therefore, the boundary condition and horizon regularity fix $c_1 = 0$ and[3]

$$\begin{aligned} c_2 = -g_{xx}^{3/2}(u_H)\int_0^{u_H} d\xi\left[\frac{g_{xx}^{3/2}(u_H)}{\sqrt{-g^{(0)}(\xi)}g^{uu}(\xi)} - \frac{1}{4\pi T(u_H-\xi)}\right] + \\ - \int_0^{u_H} d\xi\left[\frac{g_{xx}^{3/2}(u_H)}{4\pi T(u_H-\xi)} - \sqrt{-g^{(0)}(\xi)}g^{tt}(\xi)\right]. \end{aligned} \tag{G.20}$$

[3]Notice that $\sqrt{-g^{(0)}(\lambda)}g^{uu}(\lambda)\Big|_{\lambda\to u_H} \sim g_{xx}^{3/2}(u_H)4\pi T(u_H-\lambda)$.

Thus,

$$f_2(u) = 2\left\{\int_0^u \frac{d\lambda}{4\pi T(u_H-\lambda)}\int_0^\lambda d\xi\left[\frac{g_{xx}^{3/2}(u_H)}{\sqrt{-g^{(0)}(\xi)}g^{uu}(\xi)}-\frac{1}{4\pi T(u_H-\xi)}\right]+\right.$$
$$+\int_0^u \frac{d\lambda}{\sqrt{-g^{(0)}(\lambda)}g^{uu}(\lambda)}\left(g_{xx}^{3/2}(u_H)\int_{u_H}^0 d\xi\left[\frac{g_{xx}^{3/2}(u_H)}{\sqrt{-g^{(0)}(\xi)}g^{uu}(\xi)}-\frac{1}{4\pi T(u_H-\xi)}\right]+\right.$$
$$\left.\left.+\int_{u_H}^\lambda d\xi\left[\frac{g_{xx}^{3/2}(u_H)}{4\pi T(u_H-\xi)}-\sqrt{-g^{(0)}(\xi)}g^{tt}(\xi)\right]\right)\right\}. \tag{G.21}$$

Second order - f_3

Using Eqs. (G.8)), (G.9)), and (G.12) the differential equation for $f_3(u)$ reads

$$\mathcal{O}(\omega^0,q^2): \quad \partial_u\left(\sqrt{-g^{(0)}}g^{uu}f_3'\right)=2\sqrt{-g^{(0)}}g^{xx}. \tag{G.22}$$

Integrating twice, we find

$$f_3(u)=c_1+c_2\int_0^u\frac{d\lambda}{\sqrt{-g^{(0)}(\lambda)}g^{uu}(\lambda)}+2\int_0^u\frac{d\lambda}{\sqrt{-g^{(0)}(\lambda)}g^{uu}(\lambda)}\int_0^\lambda d\xi\sqrt{-g^{(0)}(\xi)}g^{xx}(\xi). \tag{G.23}$$

The boundary condition fixes $c_1=0$ and the horizon regularity condition fixes

$$c_2=-2\int_0^{u_H}d\xi\sqrt{-g^{(0)}(\xi)}g^{xx}(\xi). \tag{G.24}$$

Consequently,

$$f_3(u)=2\int_0^u\frac{d\lambda}{\sqrt{-g^{(0)}(\lambda)}g^{uu}(\lambda)}\int_{u_H}^\lambda d\xi\sqrt{-g^{(0)}(\xi)}g^{xx}(\xi)\,. \tag{G.25}$$

G.2 Summary of the transport coefficients for hydrodynamic simulations

The equations of motion for the Israel-Stewart-like theory in flat spacetime are Eqs. (8.80) and (8.81) together with the conservation equations (8.5). The 13 transport coefficients in this theory, namely η/s, ζ/s, τ_π, τ_Π, τ_π^*, λ_1, λ_2, λ_3, λ_4, ξ_1, ξ_2, ξ_3, and ξ_4 were discussed already in the main text but here we gather the formulas that describe them in a single place with the intention to facilitate their use in hydrodynamic simulations.

Besides $\eta/s=1/(4\pi)$, the shear relaxation coefficient $\tau_\pi\eta/T^2$ is described by the function in Eq. (8.57) with parameters in Table 8.2. ζ/s is described by the fitting function

in Eq. (8.67) with the parameters in Table 8.3. The lower bound for the bulk relaxation coefficient $\tau_\Pi T$ is described by Eq. (8.77) with parameters in Table 8.4. The coefficients $\lambda_3 = -\lambda_4 = 2\kappa^*$, where κ^* in Eq. (8.12) is defined in terms of the coefficient κ. One can find a fit for κ/T^2 in Eq. (8.57) with parameters in Table 8.1. The coefficients λ_1 and λ_2 can be found in Eq. (8.82). Moreover, the coefficients ξ_1, ξ_2, and τ_π^* are found in Eqs. (8.83) and (8.84), respectively. The final coefficients ξ_3 and ξ_4 are given by Eqs. (8.69) and (8.70) and can be computed using the results for the previous coefficients discussed above. Furthermore, in all of these fitting functions and tables, the parameter T_c is equal to 143.8 MeV.

Given that the thermodynamic properties of the model are very similar to those found on the lattice [374] when $T \sim 130 - 450$ MeV, if one wants to use the transport coefficients computed in this thesis in hydrodynamic simulations of the QGP formed in heavy ion collisions one may just use directly an interpolation for the lattice data when computing c_s^2 and the entropy density s needed in the evaluation of the transport coefficients.

G.3 Linear instability of the gradient expansion at 2nd order

In this Section we investigate the *linear stability* properties of a fluid described by the 2nd order gradient expansion theory in (8.8) and (8.9) (in flat spacetime) around static equilibrium. In a linear analysis, the relevant linear terms involving the dissipative part of the energy-momentum tensor are

$$\begin{aligned} \pi^{\mu\nu} &= -\eta\sigma^{\mu\nu} + \eta\tau_\pi D\sigma^{<\mu\nu>} \ , \\ \Pi &= -\zeta\theta + \zeta\tau_\Pi D\theta \ . \end{aligned} \tag{G.26}$$

We follow Refs. [383,385,386,428] and consider linear perturbations around a static background. In order to investigate the stability of the sound channel, it is sufficient to study the effect of the perturbations

$$\begin{aligned} \varepsilon &= \varepsilon_0 + \delta\varepsilon(t,x) \ , \\ P &= P_0 + \delta P(t,x) \ , \\ u^\mu_{sound} &= (1,0,0,0) + (0,\delta u^x(t,x),0,0) \ , \\ \eta &= \eta_0 + \delta\eta(t,x) \ , \ \tau_\pi = \tau_{\pi,0} + \delta\tau_\pi(t,x) \ , \\ \zeta &= \zeta_0 + \delta\zeta(t,x) \ , \ \tau_\Pi = \tau_{\Pi,0} + \delta\tau_\Pi(t,x) \ . \end{aligned} \tag{G.27}$$

In this case, the relevant terms for linear perturbations are

$$\begin{aligned}\theta &= \partial_x \delta u^x \ , \\ \sigma^{xx} &= \frac{4}{3}\partial_x \delta u^x + \mathcal{O}(\delta^2) \ , \\ \pi^{xx} &= -\frac{4}{3}\eta_0 \partial_x \delta u^x + \frac{4}{3}\eta_0 \tau_{\pi,0} \partial_x \partial_t \delta u^x + \mathcal{O}(\delta^2) \ , \\ \Pi &= -\zeta_0 \partial_x \delta u^x + \zeta_0 \tau_{\Pi,0} \partial_t \partial_x \delta u^x + \mathcal{O}(\delta^2) \ . \end{aligned} \tag{G.28}$$

Using these results in the conservation equations (8.5), one obtains the following differential equation for the sound disturbance[4]

$$\left[\partial_t^2 - c_{s,0}^2 \partial_x^2 - \left(\frac{4}{3}\frac{\eta_0}{s_0} + \frac{\zeta_0}{s_0}\right)\partial_x^2 \partial_t + \left(\frac{4}{3}\frac{\eta_0}{s_0}\tau_{\pi,0} + \frac{\zeta_0}{s_0}\tau_{\Pi,0}\right)\partial_x^2 \partial_t^2\right] \delta u^x(t,x) = 0 \ , \tag{G.29}$$

where $s_0 T_0 = \varepsilon_0 + P_0$. In Fourier space, for $\delta u^x(t,x) = \delta u_0^x \, e^{i(kx-\omega t)}$, one finds the dispersion relation

$$\omega^2 - c_{s,0}^2 k^2 + \left(\frac{4}{3}\frac{\eta_0}{s_0} + \frac{\zeta_0}{s_0}\right) i\omega k^2 - \left(\frac{4}{3}\frac{\eta_0}{s_0}\tau_{\pi,0} + \frac{\zeta_0}{s_0}\tau_{\Pi,0}\right)\omega^2 k^2 = 0 \ . \tag{G.30}$$

While the equation above can be solved exactly, when it comes to the stability properties of these modes it is sufficient to look at the sum of the roots [387]. For the polynomial corresponding to sound disturbances, the sum of the two roots gives

$$\omega_1 + \omega_2 \ = \ \frac{i\left(\frac{4}{3}\frac{\eta_0}{s_0} + \frac{\zeta_0}{s_0}\right)}{\left(\frac{4}{3}\frac{\eta_0}{s_0}\tau_{\pi,0} + \frac{\zeta_0}{s_0}\tau_{\Pi,0}\right)k^2 - 1} \ . \tag{G.31}$$

Notice that for k larger than a critical wavenumber k_c^{sound} defined by

$$k_c^{sound} = \frac{1}{\sqrt{\frac{4}{3}\frac{\eta_0}{s_0}\tau_{\pi,0} + \frac{\zeta_0}{s_0}\tau_{\Pi,0}}} \ , \tag{G.32}$$

the sum of the roots adds up to a positive imaginary number. Therefore, for $k > k_c^{sound}$ one of the modes has a positive imaginary part and is, thus, unstable.

Note that in the limit when $\tau_{\pi,0}\,, \tau_{\Pi,0} \to 0$ one finds that k_c^{sound} diverges, which is in agreement with the fact that NS theory is stable against small perturbations in a fluid at rest [385]. Clearly, for a moving fluid the stability properties become more involved but it is possible to show that the same type of problems that appears in NS theory also appear

[4]Note that we use dimensionless variables $t \to t\,T_0$ and $x \to x T_0$ and, correspondingly, $\omega \to \omega/T_0$ and $k \to k/T_0$.

in this case [387]. However, we remark that hydrodynamics is only expected to be valid in the low frequency, large wavelength limit. Nevertheless, the instability found here at finite wavenumber motivates the search for a UV completion of this theory (for instance, the one discussed in Section 8.6) that is linearly stable and can, therefore, be safely used in numerical simulations.

A larger critical wavenumber, k_c^{shear}, appears in the shear channel. Linear stability of shear modes can be studied by choosing a flow disturbance of the kind $u^\mu_{shear} = (1,0,0,0) + (0,0,\delta u^y(t,x),0)$ while the other relations in Eq. (G.28) remain valid (see [428]). This leads to the following dispersion relation

$$\omega\left(1 - \frac{\eta_0}{s_0}\tau_{\pi_0}k^2\right) + i\frac{\eta_0}{s_0}k^2 = 0 \ , \tag{G.33}$$

which can be easily solved to give

$$\begin{aligned} \omega(k) &= \frac{i\,\frac{\eta_0}{s_0}k^2}{\frac{\eta_0}{s_0}\tau_{\pi,0}k^2 - 1} \ , \\ k_c^{shear} &= \frac{1}{\sqrt{\frac{\eta_0}{s_0}\tau_{\pi,0}}} > k_c^{sound} \ . \end{aligned} \tag{G.34}$$

For a recent study involving the first nonlinear corrections to the stability analysis and the propagation of waves in relativistic hydrodynamics see, for instance, [429].

Bibliography

[1] D. J. Gross and F. Wilczek, Phys. Rev. Lett. 30, 1343 (1973) 1, 5

[2] H. D. Politzer, Phys. Rev. Lett. 30, 1346 (1973) 1, 5

[3] D. J. Gross and F. Wilczek, Phys. Rev. D 8, 3633 (1973) 1, 5

[4] A. S. Kronfeld and C. Quigg, Am. J. Phys. **78**, 1081 (2010) [arXiv:1002.5032 [hep-ph]]. 1, 6

[5] E. V. Shuryak, Phys. Rept. **61**, 71 (1980). 2, 19, 22, 110, 135, 139

[6] M. Gyulassy and L. McLerran, Nucl. Phys. A **750**, 30 (2005) [nucl-th/0405013]. 2, 24, 180

[7] H. Satz, Phys. Rept. **403-404**, 33 (2004) [hep-ph/0405051]. 2

[8] J. Adams *et al.* [STAR Collaboration], Nucl. Phys. A **757**, 102 (2005) [nucl-ex/0501009]. 2, 24, 198

[9] K. Adcox *et al.* [PHENIX Collaboration], Nucl. Phys. A **757**, 184 (2005) [nucl-ex/0410003]. 2, 24, 198

[10] I. Arsene *et al.* [BRAHMS Collaboration], Nucl. Phys. A **757**, 1 (2005) [nucl-ex/0410020]. 2, 24, 198

[11] B. B. Back, M. D. Baker, M. Ballintijn, D. S. Barton, B. Becker, R. R. Betts, A. A. Bickley and R. Bindel *et al.*, Nucl. Phys. A **757**, 28 (2005) [nucl-ex/0410022]. 2, 24, 198

[12] K. G. Wilson, Phys. Rev. D **10**, 2445 (1974). 2, 75

[13] D. Marolf, Am. J. Phys. **72**, 730 (2004) [hep-th/0311044]. 3

[14] J. M. Maldacena, Adv. Theor. Math. Phys. **2**, 231 (1998) [hep-th/9711200]. 3, 16, 29, 35, 38, 77, 111, 135, 180, 198, 204

[15] S. S. Gubser and A. Nellore, Phys. Rev. D **78**, 086007 (2008) [arXiv:0804.0434 [hep-th]]. 3, 40, 109, 134, 136, 156, 157, 159, 181, 212, 237, 238

[16] U. Gursoy and E. Kiritsis, JHEP **0802**, 032 (2008) [arXiv:0707.1324 [hep-th]]. 3, 40, 134, 136, 144, 147, 148, 151, 152, 154, 212, 279

[17] U. Gursoy, E. Kiritsis and F. Nitti, JHEP **0802**, 019 (2008) [arXiv:0707.1349 [hep-th]]. 3, 40, 134, 136, 144, 147, 149, 150, 151, 152, 154, 212, 279, 280

[18] S. I. Finazzo and J. Noronha, JHEP **1311**, 042 (2013) [arXiv:1306.2613 [hep-ph]]. 4, 109, 110, 114, 116, 177, 179

[19] S. I. Finazzo and J. Noronha, JHEP **1501**, 051 (2015) [arXiv:1406.2683 [hep-th]]. 4, 134

[20] S. I. Finazzo and J. Noronha, Phys. Rev. D **90**, 115028 (2014) [arXiv:1411.4330 [hep-th]]. 4, 179

[21] S. I. Finazzo and J. Noronha, Phys. Rev. D **89**, 106008 (2014) [arXiv:1311.6675 [hep-th]]. 4, 197

[22] S. I. Finazzo, R. Rougemont, H. Marrochio and J. Noronha, JHEP **1502**, 051 (2015) [arXiv:1412.2968 [hep-ph]]. 4, 235

[23] C. S. Machado, S. I. Finazzo, R. D. Matheus and J. Noronha, Phys. Rev. D **89**, 074027 (2014) [arXiv:1307.1797 [hep-ph]]. 4

[24] R. Critelli, S. I. Finazzo, M. Zaniboni and J. Noronha, Phys. Rev. D **90**, 066006 (2014) [arXiv:1406.6019 [hep-th]]. 4, 57, 179

[25] M. E. Peskin and D. V. Schroeder, *Introduction to quantum field theory*. 1st Ed. Perseus Books, Reading, 1995. 6, 11, 42, 265

[26] T. Muta, *Foundations of Perturbative QCD*. World Scientific, 2010. 6, 11

[27] W. Greiner, S. Schramm, E. Stein, *Quantum Chromodynamics*. Springer, 3rd Ed., 2006. 6

[28] G. 't Hooft, Nucl. Phys. B33 (1971) 173 7

[29] G. 't Hooft, Nucl. Phys. B **72**, 461 (1974). 7

[30] E. Witten, Nucl. Phys. B **160**, 57 (1979). 7

[31] A. V. Manohar, hep-ph/9802419. 7

[32] R. P. Feynman, Acta Phys. Polon. **24**, 697 (1963). 8

[33] L. D. Faddeev and V. N. Popov, Phys. Lett. B **25**, 29 (1967). 8

[34] P. di Francesco, P. Mathieu and D. Senechal, *Conformal Field Theories*. Springer, 1999. 8, 239

[35] S. L. Adler, Phys. Rev. **177**, 2426 (1969). 10

[36] J. S. Bell and R. Jackiw, Nuovo Cim. A **60**, 47 (1969). 10

[37] M. Gell-Mann, R. J. Oakes and B. Renner, Phys. Rev. **175**, 2195 (1968). 11

[38] M. Gell-Mann and F. E. Low, Phys. Rev. **95**, 1300 (1954). 11, 31

[39] K. G. Wilson and J. B. Kogut, Phys. Rept. **12**, 75 (1974). 11, 31

[40] L. P. Kadanoff, Physics **2**, 263 (1966). 11, 31

[41] K. G. Wilson, Rev. Mod. Phys. **47**, 773 (1975). 11, 31

[42] T. van Ritbergen, J. A. M. Vermaseren and S. A. Larin, Phys. Lett. B **400**, 379 (1997) [hep-ph/9701390]. 11

[43] E. Eichten, K. Gottfried, T. Kinoshita, J. Kogut, K. D. Lane, T.-M. Yan. Phys. Rev. Lett., 34, 369372 (1975) 13

[44] J. Greensite, *An Introduction to the Confinement Problem*. Lecture Notes in Physics 821. Springer, 2011. 14, 83, 247

[45] K. G. Wilson. Phys. Rev. D 10, 2445(1974). 14

[46] L. D. McLerran and B. Svetisky, Phys. Lett. 98B, 195 (1981). 14

[47] L. D. McLerran and B. Svetisky, Phys. Rev. D 24, 450 (1981). 14

[48] S. Scherer, *A Primer for Chiral Perturbation Theory*. Springer, 2011. 14

[49] K. Ġ. Wilson, Phys. Rev. 179, 1499 (1969). 14

[50] M. Shifman, A. Vainshtein, and V. Zakharov. Nuclear Physics B 147, 385 (1979). 14

[51] P. Colangelo and A. Khodjamirian, In *Shifman, M. (ed.): At the frontier of particle physics, vol. 3* 1495-1576 [hep-ph/0010175]. 14

[52] P. Pascual and R. Tarrach, *QCD: Renormalization for the Practioner*. Lecture Notes In Physics 194. Springer, 1984. 14

[53] M. Creutz, *Quarks, Gluons And Lattices*, Cambridge, Uk: Univ. Pr. (1983) 169 P. (Cambridge Monographs On Mathematical Physics) 14

[54] C. Gattringer and C. B. Lang, *Quantum chromodynamics on the lattice*, Lect. Notes Phys. **788**, 1 (2010). 14

[55] S. Durr, Z. Fodor, J. Frison, C. Hoelbling, R. Hoffmann, S. D. Katz, S. Krieg and T. Kurth *et al.*, Science **322**, 1224 (2008) [arXiv:0906.3599 [hep-lat]]. 15

[56] Z. Fodor and C. Hoelbling, Rev. Mod. Phys. **84**, 449 (2012) [arXiv:1203.4789 [hep-lat]]. 15

[57] Y. Nakahara, M. Asakawa and T. Hatsuda, Phys. Rev. D **60**, 091503 (1999) [hep-lat/9905034]. 16

[58] H. B. Meyer, Eur. Phys. J. A **47**, 86 (2011) [arXiv:1104.3708 [hep-lat]]. 16, 70

[59] A. Adams, L. D. Carr, T. Schäfer, P. Steinberg and J. E. Thomas, New J. Phys. **14**, 115009 (2012) [arXiv:1205.5180 [hep-th]]. 16, 28, 30

[60] A. Das, *Finite Temperature Field Theory*. World Scientific Publishing, 2004. 16, 18, 55

[61] J. I. Kapusta and C. Gale, *Finite-temperature field theory: Principles and applications*, Cambridge, UK: Univ. Pr. (2006) 428 p 16, 18, 57, 75, 82, 135, 137, 139, 192

[62] J. P. Blaizot, arXiv:1108.3482 [hep-ph]. 18

[63] V. Skokov, A. Y. .Illarionov and V. Toneev, Int. J. Mod. Phys. A **24**, 5925 (2009) [arXiv:0907.1396 [nucl-th]]. 19, 180, 195

[64] K. Tuchin, Adv. High Energy Phys. **2013**, 490495 (2013) [arXiv:1301.0099 [hep-ph]]. 19, 180, 195

[65] J. C. Collins and M. J. Perry, Phys. Rev. Lett. **34**, 1353 (1975). 19, 22

[66] B. A. Freedman and L. D. McLerran, Phys. Rev. D **16**, 1169 (1977). 19, 22

[67] K. Szabo, arXiv:1401.4192 [hep-lat]. 19

[68] E. V. Shuryak, Sov. Phys. JETP **47**, 212 (1978) [Zh. Eksp. Teor. Fiz. **74**, 408 (1978)]. 19, 22

[69] J. I. Kapusta, Nucl. Phys. B **148**, 461 (1979). 19, 22

[70] S. P. Klevansky, Rev. Mod. Phys. **64**, 649 (1992). 19

[71] C. DeTar and U. M. Heller, Eur. Phys. J. A **41**, 405 (2009) [arXiv:0905.2949 [hep-lat]]. 19, 20

[72] O. Philipsen, Prog. Part. Nucl. Phys. **70**, 55 (2013) [arXiv:1207.5999 [hep-lat]]. 19, 20

[73] Y. Aoki, G. Endrodi, Z. Fodor, S. D. Katz and K. K. Szabo, Nature **443**, 675 (2006) [hep-lat/0611014]. 20, 74, 158, 198

[74] G. Boyd, J. Engels, F. Karsch, E. Laermann, C. Legeland, M. Lutgemeier and B. Petersson, Nucl. Phys. B **469**, 419 (1996) [hep-lat/9602007]. 20, 48, 136, 167, 169, 170

[75] R. D. Pisarski and F. Wilczek, Phys. Rev. D **29**, 338 (1984). 20

[76] S. Borsanyi, Z. Fodor, C. Hoelbling, S. D. Katz, S. Krieg and K. K. Szabo, Phys. Lett. B **730**, 99 (2014) [arXiv:1309.5258 [hep-lat]]. 20, 74, 181, 214

[77] A. Bazavov *et al.* [HotQCD Collaboration], arXiv:1407.6387 [hep-lat]. 20

[78] S. Borsanyi, G. Endrodi, Z. Fodor, A. Jakovac, S. D. Katz, S. Krieg, C. Ratti and K. K. Szabo, JHEP **1011**, 077 (2010) [arXiv:1007.2580 [hep-lat]]. ix, xi, 21, 22, 74, 136, 167, 171, 173, 174, 181, 182, 183, 195, 214

[79] M. G. Alford, Ann. Rev. Nucl. Part. Sci. **51**, 131 (2001) [hep-ph/0102047]. 21

[80] M. G. Alford, A. Schmitt, K. Rajagopal and T. Schäfer, Rev. Mod. Phys. **80**, 1455 (2008) [arXiv:0709.4635 [hep-ph]]. 21

[81] S. Borsanyi, Z. Fodor, S. D. Katz, S. Krieg, C. Ratti and K. K. Szabo, Phys. Rev. Lett. **113**, 052301 (2014) [arXiv:1403.4576 [hep-lat]]. 21

[82] U. Heinz and R. Snellings, Ann. Rev. Nucl. Part. Sci. **63**, 123 (2013) [arXiv:1301.2826 [nucl-th]]. 25, 198

[83] P. Romatschke and U. Romatschke, Phys. Rev. Lett. **99**, 172301 (2007) [arXiv:0706.1522 [nucl-th]]. 25, 27

[84] K. Huang, *Statistical Mechanics*. John Wiley & Sons. 2nd Edition, 1983. 25

[85] T. Schäfer and D. Teaney, Rept. Prog. Phys. **72**, 126001 (2009) [arXiv:0904.3107 [hep-ph]]. 25

[86] D. Teaney, Phys. Rev. D **74**, 045025 (2006) [hep-ph/0602044]. 25, 181, 192, 195

[87] P. Danielewicz and M. Gyulassy, Phys. Rev. D **31**, 53 (1985). 27

[88] P. B. Arnold, G. D. Moore and L. G. Yaffe, JHEP **0011**, 001 (2000) [hep-ph/0010177] 27, 181

[89] P. B. Arnold, G. D. Moore and L. G. Yaffe, JHEP **0305**, 051 (2003) [hep-ph/0302165]. 27, 181

[90] P. Kovtun, D. T. Son and A. O. Starinets, Phys. Rev. Lett. **94**, 111601 (2005) [hep-th/0405231]. 27, 28, 56, 67, 101, 136, 175, 180, 198, 221

[91] M. Brigante, H. Liu, R. C. Myers, S. Shenker and S. Yaida, Phys. Rev. D **77**, 126006 (2008) [arXiv:0712.0805 [hep-th]]. 28, 56, 102, 136, 177

[92] M. Brigante, H. Liu, R. C. Myers, S. Shenker and S. Yaida, Phys. Rev. Lett. **100**, 191601 (2008) [arXiv:0802.3318 [hep-th]]. 28, 56, 102, 136, 177

[93] S. S. Gubser, I. R. Klebanov and A. M. Polyakov, Phys. Lett. B **428**, 105 (1998) [hep-th/9802109]. 29, 41, 77, 135, 142, 180, 198, 204

[94] E. Witten, Adv. Theor. Math. Phys. **2**, 253 (1998) [hep-th/9802150]. 29, 39, 41, 77, 111, 135, 142, 180, 181, 198, 204

[95] G. 't Hooft, gr-qc/9310026. 29, 33

[96] L. Susskind, J. Math. Phys. **36**, 6377 (1995) [hep-th/9409089]. 29, 33

[97] O. Aharony, S. S. Gubser, J. M. Maldacena, H. Ooguri and Y. Oz, Phys. Rept. **323**, 183 (2000) [hep-th/9905111]. 29, 39

[98] E. D'Hoker and D. Z. Freedman, hep-th/0201253. 29

[99] H. Nastase, arXiv:0712.0689 [hep-th]. 29

[100] A. V. Ramallo, arXiv:1310.4319 [hep-th]. 29

[101] K. Becker, M. Becker, J. H. Schwarz, *String Theory and M-Theory: A Modern Introduction*. Cambridge University Press, 2007. 29

[102] E. Kiritsis, *String theory in a nutshell*, Princeton University Press, 2007 29, 80, 93, 277

[103] J. Casalderrey-Solana, H. Liu, D. Mateos, K. Rajagopal and U. A. Wiedemann, arXiv:1101.0618 [hep-th]. 30, 180, 181, 198

[104] K. S. Thorne, R. H. Price and D. A. Macdonald, *Black Holes: The Membrane Paradigm*, New Haven, USA: Yale Univ. Press (1986) 367p 30, 56

[105] S. Weinberg, Phys. Rev. **135**, B1049 (1964). 32

[106] S. Weinberg and E. Witten, Phys. Lett. B **96**, 59 (1980). 32

[107] A. Zee, *Einstein Gravity in a Nutshell*, Princeton University Press, 2013 34

[108] R. Bousso, Rev. Mod. Phys. **74**, 825 (2002) [hep-th/0203101]. 33

[109] C. V. Johnson, *D-branes*, Cambridge, USA: Univ. Pr. (2003) 548 p 35, 36

[110] D. Tong, arXiv:0908.0333 [hep-th]. 36

[111] M. F. Sohnius, Phys. Rept. **128**, 39 (1985). 36

[112] J. Polchinski, Cambridge, UK: Univ. Pr. (1998) 531 p 36

[113] G. T. Horowitz and A. Strominger, Nucl. Phys. B **360**, 197 (1991). 37

[114] H. J. Kim, L. J. Romans and P. van Nieuwenhuizen, Phys. Rev. D **32**, 389 (1985). 39

[115] I. R. Klebanov and M. J. Strassler, JHEP **0008**, 052 (2000) [hep-th/0007191]. 40

[116] T. Sakai and S. Sugimoto, Prog. Theor. Phys. **113**, 843 (2005) [hep-th/0412141]. 40

[117] J. Polchinski and M. J. Strassler, Phys. Rev. Lett. **88**, 031601 (2002) [hep-th/0109174]. 40

[118] J. Erlich, E. Katz, D. T. Son and M. A. Stephanov, Phys. Rev. Lett. **95**, 261602 (2005) [hep-ph/0501128]. 40

[119] L. Da Rold and A. Pomarol, Nucl. Phys. B **721**, 79 (2005) [hep-ph/0501218]. 40

[120] S. de Haro, S. N. Solodukhin and K. Skenderis, Commun. Math. Phys. **217**, 595 (2001) [hep-th/0002230]. 42, 205

[121] M. Bianchi, D. Z. Freedman and K. Skenderis, Nucl. Phys. B **631**, 159 (2002) [hep-th/0112119]. 42, 148

[122] K. Skenderis, Class. Quant. Grav. **19**, 5849 (2002) [hep-th/0209067]. 42, 148, 205

[123] J. de Boer, E. P. Verlinde and H. L. Verlinde, JHEP **0008**, 003 (2000) [hep-th/9912012]. 42

[124] P. Breitenlohner, D. Z. Freedman, Ann. Phys., 144, No. 2, 249 43

[125] I. R. Klebanov and E. Witten, Nucl. Phys. B **556**, 89 (1999) [hep-th/9905104]. 44

[126] E. Witten, Adv. Theor. Math. Phys. **2**, 505 (1998) [hep-th/9803131]. 45, 111, 135, 145

[127] D. T. Son and A. O. Starinets, JHEP **0209**, 042 (2002) [hep-th/0205051]. 45, 50, 53, 182, 205, 208, 210, 238, 283

[128] C. P. Herzog and D. T. Son, JHEP **0303**, 046 (2003) [hep-th/0212072]. 45, 46, 50, 205, 283

[129] S. W. Hawking, Nature **248**, 30 (1974). 45

[130] S. W. Hawking, Commun. Math. Phys. **43**, 199 (1975) [Erratum-ibid. **46**, 206 (1976)]. 45

[131] K. Hoffman, K. Kunze, *Linear Algebra*. 1971, 2nd Edition, Prentice-Hall. 46

[132] S. W. Hawking, Phys. Rev. D **18** (1978) 1747. 46

[133] J. D. Bekenstein, Phys. Rev. D **7**, 2333 (1973). 47

[134] S. W. Hawking, Phys. Rev. D **13**, 191 (1976). 47

[135] R. M. Wald, gr-qc/9702022. 49

[136] R. C. Myers, *Black holes in higher curvature gravity*, in Iyer, B.R. (ed.) et al.: Black holes, gravitational radiation and the universe 121-136 [gr-qc/9811042]. 49

[137] S. S. Gubser, S. S. Pufu and F. D. Rocha, JHEP **0808**, 085 (2008) [arXiv:0806.0407 [hep-th]]. 50, 55, 136, 142, 156, 180, 205, 222, 237, 283

[138] N. Iqbal and H. Liu, Phys. Rev. D **79**, 025023 (2009) [arXiv:0809.3808 [hep-th]]. 56, 62, 67, 71, 72, 182, 183, 191, 241

[139] L. Susskind, L. Thorlacius and J. Uglum, Phys. Rev. D **48**, 3743 (1993) [hep-th/9306069]. 56

[140] L. Susskind, J. Lindsay, *An Introduction to Black Holes, Information and the String Theory - The Holographic Universe*. World Scientific, Singapore, 2005. 56

[141] A. Almheiri, D. Marolf, J. Polchinski and J. Sully, JHEP **1302**, 062 (2013) [arXiv:1207.3123 [hep-th]]. 56

[142] J. Maldacena and L. Susskind, Fortsch. Phys. **61**, 781 (2013) [arXiv:1306.0533 [hep-th]]. 56

[143] G. Policastro, D. T. Son and A. O. Starinets, Phys. Rev. Lett. **87**, 081601 (2001) [hep-th/0104066]. 56, 136, 180

[144] P. Kovtun, D. T. Son and A. O. Starinets, JHEP **0310**, 064 (2003) [hep-th/0309213]. 56, 70, 188

[145] A. Buchel and J. T. Liu, Phys. Rev. Lett. **93**, 090602 (2004) [hep-th/0311175]. 56, 136, 180

[146] R. -G. Cai, Phys. Rev. D **65**, 084014 (2002) [hep-th/0109133]. 56, 102, 136

[147] Y. Kats and P. Petrov, JHEP **0901**, 044 (2009) [arXiv:0712.0743 [hep-th]]. 56, 102

[148] D. Mateos and D. Trancanelli, Phys. Rev. Lett. **107**, 101601 (2011) [arXiv:1105.3472 [hep-th]]. 57, 109, 179

[149] A. Rebhan and D. Steineder, Phys. Rev. Lett. **108**, 021601 (2012) [arXiv:1110.6825 [hep-th]]. 57, 179

[150] J. Erdmenger, P. Kerner and H. Zeller, Phys. Lett. B **699**, 301 (2011) [arXiv:1011.5912 [hep-th]]. 57

[151] J. Erdmenger, D. Fernandez and H. Zeller, JHEP **1304**, 049 (2013) [arXiv:1212.4838 [hep-th]]. 57

[152] P. K. Kovtun and A. O. Starinets, Phys. Rev. D **72**, 086009 (2005) [hep-th/0506184]. 57, 235

[153] L. D. Landau and E. M. Lifshitz, *Fluid mechanics*. Course of Theoretical Physics, Vol. 6. Second edition, revised. Pergamon Press, 1987. 61

[154] G. Policastro, D. T. Son and A. O. Starinets, JHEP **0209**, 043 (2002) [hep-th/0205052]. 70, 188, 205, 206, 212

[155] A. O. Starinets, Phys. Lett. B **670**, 442 (2009) [arXiv:0806.3797 [hep-th]]. 70, 188

[156] D. Forster, *Hydrodynamics, Fluctuations, Broken Symmetry, and Correlation Functions*, Cmabridge, Massachusetts: Perseus-Books (1990). 70, 188, 199

[157] P. Kovtun and A. Ritz, Phys. Rev. D **78**, 066009 (2008) [arXiv:0806.0110 [hep-th]]. 72, 181

[158] A. Bazavov, T. Bhattacharya, M. Cheng, N. H. Christ, C. DeTar, S. Ejiri, S. Gottlieb and R. Gupta *et al.*, Phys. Rev. D **80**, 014504 (2009) [arXiv:0903.4379 [hep-lat]]. 74

[159] J. -L. Gervais and A. Neveu, Nucl. Phys. B **163**, 189 (1980); A. M. Polyakov, Nucl. Phys. B **164**, 171 (1980). 75

[160] A. M. Polyakov, Phys. Lett. B **72**, 477 (1978). 76, 151, 247

[161] G. 't Hooft, Nucl. Phys. B **138**, 1 (1978); **153**, 141 (1979). 76, 151, 247

[162] B. Svetitsky and L. G. Yaffe, Nucl. Phys. B **210**, 423 (1982). 76, 151, 247

[163] L. D. McLerran and B. Svetitsky, Phys. Lett. B **98**, 195 (1981); Phys. Rev. D **24**, 450 (1981). 76, 151

[164] O. Kaczmarek, F. Karsch, P. Petreczky, F. Zantow, Phys. Lett. B **543**, 41 (2002) [hep-lat/0207002]. 76, 82

[165] O. Kaczmarek, F. Karsch, F. Zantow and P. Petreczky, Phys. Rev. D **70**, 074505 (2004) [Erratum-ibid. D **72**, 059903 (2005)] [hep-lat/0406036]. 76, 82

[166] O. Philipsen, arXiv:1009.4089 [hep-lat]. 76, 96

[167] M. Laine et al., JHEP **0703** (2007) 054. 77, 106, 108, 110, 120

[168] M. Laine et al., JHEP **0705**, (2007) 028. 77, 106, 108, 110

[169] A. Beraudo, J. P. Blaizot and C. Ratti, Nucl. Phys. A **806**, 312 (2008) 77, 106, 108

[170] N. Brambilla, J. Ghiglieri, A. Vairo, P. Petreczky, Phys. Rev. D **78**, 014017 (2008). 77

[171] C. Miao, A. Mocsy, and P. Petreczky, Nucl. Phys. A **855**, 125 (2011), arXiv:1012.4433 [hep-ph] 77

[172] N. Brambilla, M. A. Escobedo, J. Ghiglieri, J. Soto, and A. Vairo, JHEP **09**, 038 (2010), arXiv:1007.4156 [hep-ph]. 77

[173] Y. Burnier, M. Laine, and M. Vepsalainen, (2009), arXiv:0903.3467 [hep-ph] 77

[174] A. Dumitru, Y. Guo, and M. Strickland, Phys. Rev. D **79**, 114003 (2009), arXiv:0903.4703 [hep-ph] 77

[175] O. Philipsen and M. Tassler, arXiv:0908.1746 [hep-ph]. 77

[176] Y. Akamatsu and A. Rothkopf, Phys. Rev. D **85**, 105011 (2012) [arXiv:1110.1203 [hep-ph]]. 77, 110

[177] Y. Akamatsu, arXiv:1403.5783 [hep-ph]. 77, 110

[178] A. Rothkopf, T. Hatsuda, S. Sasaki, Phys. Rev. Lett. **108**, 162001 (2012) [arXiv:1108.1579 [hep-lat]]. 77, 110, 120

[179] J. Noronha and A. Dumitru, Phys. Rev. Lett. **103**, 152304 (2009) [arXiv:0907.3062 [hep-ph]]. 77, 84, 88, 91, 98, 106, 108, 110, 116, 120

[180] J. M. Maldacena, Phys. Rev. Lett. **80**, 4859 (1998) [hep-th/9803002]. 78, 82, 93, 111

[181] S. J. Rey and J. T. Yee, Eur. Phys. J. C **22**, 379 (2001) [hep-th/9803001]. 78, 111

[182] A. Brandhuber, N. Itzhaki, J. Sonnenschein and S. Yankielowicz, Phys. Lett. B **434**, 36 (1998) [hep-th/9803137]. 78, 93

[183] S. -J. Rey, S. Theisen and J. -T. Yee, Nucl. Phys. B **527**, 171 (1998) [hep-th/9803135]. 78, 93

[184] D. Bak, A. Karch and L. G. Yaffe, JHEP **0708**, 049 (2007) [arXiv:0705.0994 [hep-th]]. 78, 82, 94, 95, 96, 108, 118, 135, 136, 137, 138, 146, 178, 236

[185] J. Noronha, Phys. Rev. D **81**, 045011 (2010) [arXiv:0910.1261 [hep-th]]. 82, 134, 156, 181

[186] J. Noronha, Phys. Rev. D **82**, 065016 (2010) [arXiv:1003.0914 [hep-th]]. 82, 156

[187] H. R. Grigoryan and Y. V. Kovchegov, Nucl. Phys. B **852**, 1 (2011) [arXiv:1105.2300 [hep-th]]. 82

[188] Y. Kinar, E. Schreiber and J. Sonnenschein, Nucl. Phys. B **566**, 103 (2000) [hep-th/9811192]. 83, 255

[189] J. Sonnenschein, hep-th/0003032. 83

[190] J. L. Albacete, Y. V. Kovchegov and A. Taliotis, Phys. Rev. D **78**, 115007 (2008) [arXiv:0807.4747 [hep-th]]. 84, 93, 97, 108

[191] J. L. Albacete, Nucl. Phys. A **830**, 311C (2009) [arXiv:0908.2541 [hep-ph]]. 84, 97, 108, 110, 120, 134

[192] T. Hayata, K. Nawa and T. Hatsuda, arXiv:1211.4942 [hep-ph]. 84, 97, 108, 110, 134

[193] S. Gradshteyn and I. M. Ryzhik; A. Jeffrey, D. Zwillinger, editors. *Table of Integrals, Series, and Products*, seventh edition. Academic Press, 2007. 87, 118, 154, 252

[194] B. Zwiebach, Phys. Lett. B **156**, 315 (1985). 91, 102, 136, 175

[195] A. Buchel, R. C. Myers and A. Sinha, JHEP **0903**, 084 (2009) [arXiv:0812.2521 [hep-th]]. 91, 102, 176

[196] A. Buchel, J. Escobedo, R. C. Myers, M. F. Paulos, A. Sinha and M. Smolkin, JHEP **1003**, 111 (2010) [arXiv:0911.4257 [hep-th]]. 91, 102

[197] J. Noronha, M. Gyulassy and G. Torrieri, arXiv:0906.4099 [hep-ph] 93

[198] J. Noronha, M. Gyulassy and G. Torrieri, Phys. Rev. C **82**, 054903 (2010) [arXiv:1009.2286 [nucl-th]]. 93

[199] F. Karsch, M. T. Mehr and H. Satz, Z. Phys. C **37**, 617 (1988). 96, 110

[200] G. Aarts, C. Allton, S. Kim, M. P. Lombardo, M. B. Oktay, S. M. Ryan, D. K. Sinclair and J. I. Skullerud, JHEP **1111**, 103 (2011) [arXiv:1109.4496 [hep-lat]]. 99, 110

[201] J. Noronha and A. Dumitru, Phys. Rev. D **80**, 014007 (2009) [arXiv:0903.2804 [hep-ph]]. 102, 103, 176

[202] K. B. Fadafan, Eur. Phys. J. C **71**, 1799 (2011) [arXiv:1102.2289 [hep-th]]. 102

[203] M. Ali-Akbari and K. Bitaghsir Fadafan, Nucl. Phys. B **835**, 221 (2010) [arXiv:0908.3921 [hep-th]]. 102

[204] M. Strickland, Phys. Rev. Lett. **107**, 132301 (2011) [arXiv:1106.2571 [hep-ph]]. 108, 110, 236

[205] M. Strickland and D. Bazow, Nucl. Phys. A **879**, 25 (2012) [arXiv:1112.2761 [nucl-th]]. 108, 110, 236

[206] M. Margotta, K. McCarty, C. McGahan, M. Strickland, and D. Yager-Elorriaga, Phys. Rev. D **83**, 105019 (2011), arXiv:1101.4651 [hep-ph]. 108, 110

[207] T. Faulkner and H. Liu, Phys. Lett. B **673**, 161 (2009) [arXiv:0807.0063 [hep-th]]. 108, 111, 117, 134

[208] D. Mateos and D. Trancanelli, JHEP **1107**, 054 (2011) [arXiv:1106.1637 [hep-th]]. 109

[209] U. Gursoy, E. Kiritsis, L. Mazzanti and F. Nitti, Nucl. Phys. B **820**, 148 (2009) [arXiv:0903.2859 [hep-th]]. 109, 136, 144, 147, 151, 181

[210] D. Giataganas, arXiv:1306.1404 [hep-th]. 109

[211] K. B. Fadafan and S. K. Tabatabaei, Eur. Phys. J. C **74**, 2842 (2014) [arXiv:1308.3971 [hep-th]]. 109, 110

[212] M. Strickland, Phys. Rev. Lett. **107**, 132301 (2011) [arXiv:1106.2571 [hep-ph]]. 108, 110, 236

[213] M. Strickland and D. Bazow, Nucl. Phys. A **879**, 25 (2012) [arXiv:1112.2761 [nucl-th]]. 108, 110, 236

[214] M. Margotta, K. McCarty, C. McGahan, M. Strickland, and D. Yager-Elorriaga, Phys. Rev. D **83**, 105019 (2011), arXiv:1101.4651 [hep-ph]. 108, 110

[215] G. Aarts, C. Allton, S. Kim, M. P. Lombardo, M. B. Oktay, S. M. Ryan, D. K. Sinclair and J. -I. Skullerud, JHEP **1303**, 084 (2013) [arXiv:1210.2903 [hep-lat]]. 110

[216] G. Aarts, C. Allton, S. Kim, M. P. Lombardo, S. M. Ryan and J. -I. Skullerud, JHEP **1312**, 064 (2013) [arXiv:1310.5467 [hep-lat]]. 110

[217] K. B. Fadafan, D. Giataganas and H. Soltanpanahi, arXiv:1306.2929 [hep-th]. 110

[218] M. A. Escobedo, F. Giannuzzi, M. Mannarelli and J. Soto, Phys. Rev. D **87**, no. 11, 114005 (2013) [arXiv:1304.4087 [hep-ph]]. 110

[219] H. Liu, K. Rajagopal and U. A. Wiedemann, Phys. Rev. Lett. **98**, 182301 (2007) [hep-ph/0607062]. 111, 112, 118, 122, 123, 129, 134

[220] H. Liu, K. Rajagopal and U. A. Wiedemann, JHEP **0703**, 066 (2007) [hep-ph/0612168]. 111, 112, 118, 122, 123, 128, 129, 134

[221] E. Caceres, M. Natsuume and T. Okamura, JHEP **0610**, 011 (2006) [hep-th/0607233]. 111

[222] Q. J. Ejaz, T. Faulkner, H. Liu, K. Rajagopal and U. A. Wiedemann, JHEP **0804**, 089 (2008) [arXiv:0712.0590 [hep-th]]. 111, 134

[223] A. Karch and E. Katz, JHEP **0206**, 043 (2002) [hep-th/0205236]. 117, 178

[224] U. Gursoy, E. Kiritsis, L. Mazzanti and F. Nitti, Phys. Rev. Lett. **101**, 181601 (2008) [arXiv:0804.0899 [hep-th]]. 134, 136, 144, 147, 151, 181

[225] M. Ali-Akbari, D. Giataganas and Z. Rezaei, arXiv:1406.1994 [hep-th]. 134

[226] T. Matsui and H. Satz, Phys. Lett. B **178**, 416 (1986). 135

[227] D. J. Gross, R. D. Pisarski and L. G. Yaffe, Rev. Mod. Phys. **53**, 43 (1981). 135, 139, 262

[228] S. Nadkarni, Phys. Rev. D **33**, 3738 (1986). 135, 139

[229] A. K. Rebhan, Phys. Rev. D **48**, 3967 (1993) [hep-ph/9308232]. 135, 139

[230] E. Braaten and A. Nieto, Phys. Rev. Lett. **73**, 2402 (1994) [hep-ph/9408273]. 135, 139

[231] A. K. Rebhan, Nucl. Phys. B **430**, 319 (1994) [hep-ph/9408262]. 135, 139

[232] P. B. Arnold and L. G. Yaffe, Phys. Rev. D **52**, 7208 (1995) [hep-ph/9508280]. 135, 138, 140, 141, 178, 179, 237

[233] K. Kajantie, M. Laine, J. Peisa, A. Rajantie, K. Rummukainen and M. E. Shaposhnikov, Phys. Rev. Lett. **79**, 3130 (1997) [hep-ph/9708207]. 135

[234] S. Datta and S. Gupta, Phys. Lett. B **471**, 382 (2000) [hep-lat/9906023]. 135

[235] S. Datta and S. Gupta, Nucl. Phys. B **534**, 392 (1998) [hep-lat/9806034]. 135

[236] S. Datta and S. Gupta, Phys. Rev. D **67**, 054503 (2003) [hep-lat/0208001]. 135

[237] M. Laine and O. Philipsen, Phys. Lett. B **459**, 259 (1999) [hep-lat/9905004]. 135

[238] A. Hart, M. Laine and O. Philipsen, Nucl. Phys. B **586**, 443 (2000) [hep-ph/0004060]. 135

[239] A. Nakamura, T. Saito and S. Sakai, Phys. Rev. D **69**, 014506 (2004) [hep-lat/0311024]. 135, 178

[240] A. Cucchieri, F. Karsch and P. Petreczky, Phys. Lett. B **497**, 80 (2001) [hep-lat/0004027]. 135

[241] A. Cucchieri, D. Dudal, T. Mendes and N. Vandersickel, arXiv:1202.0639 [hep-lat]. 135

[242] R. Aouane, F. Burger, E.-M. Ilgenfritz, M. Müller-Preussker and A. Sternbeck, Phys. Rev. D **87**, no. 11, 114502 (2013) [arXiv:1212.1102 [hep-lat]]. 135

[243] P. J. Silva, O. Oliveira, P. Bicudo and N. Cardoso, Phys. Rev. D **89**, 074503 (2014) [arXiv:1310.5629 [hep-lat]]. 135

[244] M. Laine and M. Vepsalainen, JHEP **0909**, 023 (2009) [arXiv:0906.4450 [hep-ph]]. 135

[245] P. Chakraborty, M. G. Mustafa and M. H. Thoma, Phys. Rev. D **85**, 056002 (2012) [arXiv:1109.1971 [hep-ph]]. 135

[246] C. Hoyos, S. Paik and L. G. Yaffe, JHEP **1110**, 062 (2011) [arXiv:1108.2053 [hep-th]]. 135, 155

[247] A. Singh and A. Sinha, Nucl. Phys. B **864**, 167 (2012) [arXiv:1204.1817 [hep-th]]. 135

[248] O. Philipsen, hep-ph/0010327.

[249] C. Csaki, H. Ooguri, Y. Oz and J. Terning, JHEP **9901**, 017 (1999) [hep-th/9806021]. 136, 137, 142, 146

[250] R. de Mello Koch, A. Jevicki, M. Mihailescu and J. P. Nunes, Phys. Rev. D **58**, 105009 (1998) [hep-th/9806125]. 136, 137

[251] J. L. Petersen, Int. J. Mod. Phys. A **14**, 3597 (1999) [hep-th/9902131].

[252] U. Gursoy, E. Kiritsis, L. Mazzanti and F. Nitti, JHEP **0905**, 033 (2009) [arXiv:0812.0792 [hep-th]]. 136, 144, 147, 151, 181, 212

[253] K. Kajantie, M. Krssak, M. Vepsalainen and A. Vuorinen, Phys. Rev. D **84**, 086004 (2011) [arXiv:1104.5352 [hep-ph]]. 136, 147, 149, 150, 152, 154, 235

[254] S. S. Gubser, A. Nellore, S. S. Pufu and F. D. Rocha, Phys. Rev. Lett. **101**, 131601 (2008) [arXiv:0804.1950 [hep-th]]. 136, 156, 164, 166, 181, 221, 231, 237

[255] M. Panero, Phys. Rev. Lett. **103**, 232001 (2009) [arXiv:0907.3719 [hep-lat]]. 136, 151, 152, 167

[256] S. Borsanyi, G. Endrodi, Z. Fodor, S. D. Katz and K. K. Szabo, JHEP **1207**, 056 (2012) [arXiv:1204.6184 [hep-lat]]. 136

[257] A. Mykkanen, M. Panero and K. Rummukainen, JHEP **1205**, 069 (2012) [arXiv:1202.2762 [hep-lat]]. xi, 137, 152, 153, 170, 171, 178

[258] U. Gürsoy, I. Iatrakis, E. Kiritsis, F. Nitti and A. O'Bannon, JHEP **1302**, 119 (2013) [arXiv:1212.3894 [hep-th]]. 144, 154

[259] K. Pilch and N. P. Warner, Nucl. Phys. B **594**, 209 (2001) [hep-th/0004063]. 155

[260] A. Buchel and J. T. Liu, JHEP **0311**, 031 (2003) [hep-th/0305064]. 155

[261] A. Buchel, S. Deakin, P. Kerner and J. T. Liu, Nucl. Phys. B **784**, 72 (2007) [hep-th/0701142]. 155

[262] A. Amato, G. Aarts, C. Allton, P. Giudice, S. Hands and J. -I. Skullerud, Phys. Rev. Lett. **111**, 172001 (2013) [arXiv:1307.6763 [hep-lat]]. 156, 180, 187

[263] A. Ficnar, J. Noronha and M. Gyulassy, Nucl. Phys. A **855**, 372 (2011) [arXiv:1012.0116 [hep-ph]]. 156, 167, 172

[264] A. Ficnar, J. Noronha and M. Gyulassy, J. Phys. G **38**, 124176 (2011) [arXiv:1106.6303 [hep-ph]]. 156, 167

[265] A. Ficnar, J. Noronha and M. Gyulassy, Nucl. Phys. A **910-911**, 252 (2013) [arXiv:1208.0305 [hep-ph]]. 156, 167

[266] D. Li and M. Huang, JHEP **1311**, 088 (2013) [arXiv:1303.6929 [hep-ph]]. 156

[267] D. Li, S. He and M. Huang, arXiv:1411.5332 [hep-ph]. 156

[268] A. Karch, E. Katz, D. T. Son and M. A. Stephanov, Phys. Rev. D **74**, 015005 (2006) [hep-ph/0602229]. 156, 197

[269] H. A. Chamblin and H. S. Reall, Nucl. Phys. B **562**, 133 (1999) [hep-th/9903225]. 157, 232

[270] J. Beringer et al. (Particle Data Group), Phys. Rev. D86, 010001 (2012) and 2013 partial update for the 2014 edition. 166

[271] S. S. Gubser, Adv. Theor. Math. Phys. **4**, 679 (2000) [hep-th/0002160]. 166

[272] F. Zuo, JHEP **1406**, 143 (2014) [arXiv:1404.4512 [hep-ph]]. 170

[273] M. Kruczenski, D. Mateos, R. C. Myers and D. J. Winters, JHEP **0307**, 049 (2003) [hep-th/0304032]. 178

[274] J. Erdmenger, N. Evans, I. Kirsch and E. Threlfall, Eur. Phys. J. A **35**, 81 (2008) [arXiv:0711.4467 [hep-th]]. 178

[275] T. Alho, M. Jarvinen, K. Kajantie, E. Kiritsis, C. Rosen and K. Tuominen, arXiv:1312.5199 [hep-ph]. 178, 181

[276] A. Dumitru and R. D. Pisarski, Phys. Lett. B **525**, 95 (2002) [hep-ph/0106176]. 179

[277] T. Hirano and M. Gyulassy, Nucl. Phys. A **769**, 71 (2006) [nucl-th/0506049]. 179

[278] L. P. Csernai, J. I. Kapusta and L. D. McLerran, Phys. Rev. Lett. **97**, 152303 (2006) [nucl-th/0604032]. 179

[279] J. Noronha-Hostler, J. Noronha and C. Greiner, Phys. Rev. C **86**, 024913 (2012) [arXiv:1206.5138 [nucl-th]]. 179, 181, 227

[280] J. Noronha-Hostler, J. Noronha and C. Greiner, Phys. Rev. Lett. **103**, 172302 (2009) [arXiv:0811.1571 [nucl-th]]. 179, 181, 227

[281] R. D. Pisarski, Phys. Rev. D **62**, 111501 (2000) [hep-ph/0006205]. 179

[282] Y. Hidaka and R. D. Pisarski, Phys. Rev. D **80**, 036004 (2009) [arXiv:0906.1751 [hep-ph]]. 179

[283] Y. Hidaka and R. D. Pisarski, Phys. Rev. D **78**, 071501 (2008) [arXiv:0803.0453 [hep-ph]]. 179

[284] Y. Hidaka and R. D. Pisarski, Phys. Rev. D **81**, 076002 (2010) [arXiv:0912.0940 [hep-ph]]. 179

[285] E. D'Hoker and P. Kraus, JHEP **0910**, 088 (2009) [arXiv:0908.3875 [hep-th]]. 179

[286] E. D'Hoker and P. Kraus, JHEP **1003**, 095 (2010) [arXiv:0911.4518 [hep-th]]. 179

[287] A. Buchel, Phys. Lett. B **663**, 286 (2008) [arXiv:0708.3459 [hep-th]]. 180, 231

[288] L. McLerran and V. Skokov, arXiv:1305.0774 [hep-ph]. 180, 195

[289] Y. Hirono, M. Hongo and T. Hirano, arXiv:1211.1114 [nucl-th]. 180, 195

[290] S. Caron-Huot, P. Kovtun, G. D. Moore, A. Starinets and L. G. Yaffe, JHEP **0612**, 015 (2006) [hep-th/0607237]. 181, 185, 187, 197

[291] J. -W. Chen, Y. -F. Liu, S. Pu, Y. -K. Song and Q. Wang, Phys. Rev. D **88**, 085039 (2013) [arXiv:1308.2945 [hep-ph]]. 181

[292] W. Cassing, O. Linnyk, T. Steinert and V. Ozvenchuk, Phys. Rev. Lett. **110**, 182301 (2013) [arXiv:1302.0906 [hep-ph]]. 181

[293] S. -x. Qin, arXiv:1307.4587 [nucl-th]. 181

[294] C. P. Herzog, P. Kovtun, S. Sachdev and D. T. Son, Phys. Rev. D **75**, 085020 (2007) [hep-th/0701036]. 181

[295] A. Karch and A. O'Bannon, JHEP **0709**, 024 (2007) [arXiv:0705.3870 [hep-th]]. 181

[296] R. C. Myers, A. O. Starinets and R. M. Thomson, JHEP **0711**, 091 (2007) [arXiv:0706.0162 [hep-th]]. 181, 189

[297] D. Mateos and L. Patino, JHEP **0711**, 025 (2007) [arXiv:0709.2168 [hep-th]]. 181

[298] A. Cherman and A. Nellore, Phys. Rev. D **80**, 066006 (2009) [arXiv:0905.2969 [hep-th]]. 181

[299] B. Hassanain and M. Schvellinger, JHEP **1010**, 068 (2010) [arXiv:1006.5480 [hep-th]]. 181

[300] B. Hassanain and M. Schvellinger, JHEP **1201**, 114 (2012) [arXiv:1108.6306 [hep-th]]. 181

[301] L. Patino and D. Trancanelli, JHEP **1302**, 154 (2013) [arXiv:1211.2199 [hep-th]]. 181

[302] S. -Y. Wu and D. -L. Yang, JHEP **1308**, 032 (2013) [arXiv:1305.5509 [hep-th]]. 181

[303] V. Jahnke, A. Luna, L. Patino and D. Trancanelli, arXiv:1311.5513 [hep-th]. 181

[304] J. Noronha, J. Phys. G **37**, 094018 (2010) [arXiv:1001.3155 [hep-th]]. 181

[305] F. Karsch, K. Redlich and A. Tawfik, Eur. Phys. J. C **29**, 549 (2003) [hep-ph/0303108]. 181

[306] P. Huovinen and P. Petreczky, Nucl. Phys. A **837**, 26 (2010) [arXiv:0912.2541 [hep-ph]]. 181

[307] J. O. Andersen, L. E. Leganger, M. Strickland and N. Su, JHEP **1108**, 053 (2011) [arXiv:1103.2528 [hep-ph]]. 181

[308] N. Haque, M. G. Mustafa and M. Strickland, JHEP **1307**, 184 (2013) [arXiv:1302.3228 [hep-ph]]. 181

[309] S. Mogliacci, J. O. Andersen, M. Strickland, N. Su and A. Vuorinen, arXiv:1307.8098 [hep-ph]. 181, 215

[310] N. Haque, J. O. Andersen, M. G. Mustafa, M. Strickland and N. Su, arXiv:1309.3968 [hep-ph]. 181

[311] O. DeWolfe, S. S. Gubser and C. Rosen, Phys. Rev. D **83**, 086005 (2011) [arXiv:1012.1864 [hep-th]]. 181, 238

[312] M. Jarvinen and E. Kiritsis, JHEP **1203**, 002 (2012) [arXiv:1112.1261 [hep-ph]]. 181

[313] T. Alho, M. Jarvinen, K. Kajantie, E. Kiritsis and K. Tuominen, JHEP **1301**, 093 (2013) [arXiv:1210.4516 [hep-ph]]. 181

[314] S. A. Hartnoll, Class. Quant. Grav. **26**, 224002 (2009) [arXiv:0903.3246 [hep-th]]. 182

[315] C. Charmousis, B. Gouteraux, B. S. Kim, E. Kiritsis and R. Meyer, JHEP **1011**, 151 (2010) [arXiv:1005.4690 [hep-th]]. 182

[316] R. -G. Cai, S. He and D. Li, JHEP **1203**, 033 (2012) [arXiv:1201.0820 [hep-th]]. 182

[317] S. He, S. -Y. Wu, Y. Yang and P. -H. Yuan, JHEP **1304**, 093 (2013) [arXiv:1301.0385 [hep-th]]. 182

[318] S. Borsanyi, Z. Fodor, S. D. Katz, S. Krieg, C. Ratti and K. Szabo, JHEP **1201**, 138 (2012) [arXiv:1112.4416 [hep-lat]]. 182, 185, 186, 195, 237

[319] A. Bazavov *et al.* [HotQCD Collaboration], Phys. Rev. D **86**, 034509 (2012) [arXiv:1203.0784 [hep-lat]]. 185

[320] G. Aarts, C. Allton, A. Amato, P. Giudice, S. Hands and J. I. Skullerud, arXiv:1412.6411 [hep-lat]. 189, 190

[321] M. Greif, I. Bouras, Z. Xu and C. Greiner, arXiv:1408.7049 [nucl-th]. xii, 189

[322] M. Greif, Private communcation. xii, 189

[323] A. Amato, G. Aarts, C. Allton, P. Giudice, S. Hands and J. -I. Skullerud, arXiv:1310.7466 [hep-lat]. 195

[324] G. Aarts and J. M. Martinez Resco, JHEP **0204**, 053 (2002) [hep-ph/0203177]. 195

[325] A. Nata Atmaja and K. Schalm, JHEP **1008**, 124 (2010) [arXiv:0802.1460 [hep-th]]. 197

[326] R. Baier, P. Romatschke, D. T. Son, A. O. Starinets and M. A. Stephanov, JHEP **0804**, 100 (2008) [arXiv:0712.2451 [hep-th]]. 199, 202, 203, 204, 205, 210, 212, 229, 230, 237, 238

[327] M. Martinez and M. Strickland, Nucl. Phys. A **848**, 183 (2010) [arXiv:1007.0889 [nucl-th]]. 199

[328] W. Florkowski and R. Ryblewski, Phys. Rev. C **83**, 034907 (2011) [arXiv:1007.0130 [nucl-th]]. 199

[329] R. Ryblewski and W. Florkowski, Phys. Rev. C **85**, 064901 (2012) [arXiv:1204.2624 [nucl-th]]. 199

[330] M. Martinez, R. Ryblewski and M. Strickland, Phys. Rev. C **85**, 064913 (2012) [arXiv:1204.1473 [nucl-th]]. 199

[331] W. Florkowski, R. Ryblewski and M. Strickland, Nucl. Phys. A **916**, 249 (2013) [arXiv:1304.0665 [nucl-th]]. 199

[332] W. Florkowski, R. Ryblewski and M. Strickland, Phys. Rev. C **88**, 024903 (2013) [arXiv:1305.7234 [nucl-th]]. 199

[333] M. Strickland, arXiv:1410.5786 [nucl-th]. 199

[334] X. G. Huang, A. Sedrakian and D. H. Rischke, Annals Phys. **326**, 3075 (2011) [arXiv:1108.0602 [astro-ph.HE]]. 199

[335] L. D. Landau and E. M. Lifshitz, *Course of Theoretical Physics, Volume 6, Fluid Mechanics*, 2nd ed., Pergamon Press, 1987. 199, 200, 201

[336] D. K. Forster, *Hydrodynamic Fluctuations, Broken Symmetry, and Correlation Functions*, Advanced Book Classics, West-view Press, 1995. 70, 188, 199

[337] S. Chapman and T. G. Cowling, *The Mathematical Theory of Non-Uniform Gases*, Cambridge University Press, 1970. 199

[338] L. D. Landau and E. M. Lifshitz, *Course of Theoretical Physics, Volume 10, Physical Kinetics* Pergamon Press, 1981. 199

[339] H. Grad, *On the kinetic theory of rarefied gas*, Commun. Pure Appl. Math. **2** (1949) 331. 199

[340] D. Burnett, *The distribution of molecular velocities and the mean motion in a non-uniform gas*, Proc. London Math. Soc. **40** (1936) 382. 199

[341] S. R. de Groot, W. A. van Leeuwen and Ch. G. van Weert, *Relativistic Kinetic Theory - Principles and Applications*, North-Holland 1980. 199

[342] G. S. Denicol, H. Niemi, E. Molnar and D. H. Rischke, Phys. Rev. D **85**, 114047 (2012) [arXiv:1202.4551 [nucl-th]]. 199, 202, 229

[343] C. Cercignani and G. M. Kremer, *The Relativistic Boltzmann Equation: Theory and Applications* (Boston; Basel; Berlin: Birkhauser, 2002). 199

[344] S. Jeon, Phys. Rev. D **52**, 3591 (1995) [hep-ph/9409250]. 199

[345] S. Jeon and L. G. Yaffe, Phys. Rev. D **53**, 5799 (1996) [hep-ph/9512263]. 199

[346] S. Bhattacharyya, V. E. Hubeny, S. Minwalla and M. Rangamani, JHEP **0802**, 045 (2008) [arXiv:0712.2456 [hep-th]]. 200, 230, 234

[347] G. Torrieri, Phys. Rev. D **85**, 065006 (2012). 200

[348] S. Dubovsky, L. Hui, A. Nicolis and D. T. Son, Phys. Rev. D **85**, 085029 (2012). 200

[349] P. Kovtun, G. D. Moore and P. Romatschke, JHEP **1407**, 123 (2014). 200

[350] P. Arnold, P. Romatschke and W. van der Schee, JHEP **1410**, 110 (2014) [arXiv:1408.2518 [hep-th]]. 200

[351] Y. Hatta, J. Noronha and B. W. Xiao, Phys. Rev. D **89**, 051702 (R) (2014) [arXiv:1401.6248 [hep-th]]. 201

[352] Y. Hatta, J. Noronha and B. W. Xiao, Phys. Rev. D **89**, 114011 (2014) [arXiv:1403.7693 [hep-th]]. 201

[353] P. B. Arnold, C. Dogan and G. D. Moore, Phys. Rev. D **74**, 085021 (2006) [hep-ph/0608012]. 201, 233

[354] H. Niemi and G. S. Denicol, arXiv:1404.7327 [nucl-th]. 201, 202

[355] M. P. Heller, R. A. Janik and P. Witaszczyk, Phys. Rev. Lett. **110**, no. 21, 211602 (2013) [arXiv:1302.0697 [hep-th]]. 201

[356] G. S. Denicol, J. Noronha, H. Niemi and D. H. Rischke, Phys. Rev. D **83**, 074019 (2011) [arXiv:1102.4780 [hep-th]]. 201, 234, 235

[357] B. Schenke, P. Tribedy and R. Venugopalan, Phys. Rev. Lett. **108**, 252301 (2012) [arXiv:1202.6646 [nucl-th]]. 202, 203

[358] P. Romatschke, Class. Quant. Grav. **27**, 025006 (2010) [arXiv:0906.4787 [hep-th]]. 202, 203, 204, 224, 231, 235, 237, 238

[359] S. M. Carroll, *Spacetime and geometry: An introduction to general relativity*, San Francisco, USA: Addison-Wesley (2004) 513 p 202, 239, 277, 278

[360] G. D. Moore and K. A. Sohrabi, JHEP **11** (2012) 148, [arXiv:1210.3340 [hep-ph]]. 202, 203, 204, 220, 224, 238

[361] S. Bhattacharyya, JHEP **07** (2012) 104, [arXiv:1201.4654 [hep-th]]. 203, 204, 220

[362] K. Jensen, M. Kaminski, P. Kovtun, R. Meyer, A. Ritz and A. Yarom, Phys. Rev. Lett. **109**, 101601 (2012), [arXiv:1203.3556 [hep-th]]. 203, 204, 220

[363] N. Banerjee, J. Bhattacharya, S. Bhattacharyya, S. Jain, S. Minwalla and T. Sharma, JHEP **09** (2012) 046, [arXiv:1203.3544 [hep-th]]. 203, 204, 220

[364] K. Skenderis and B. C. van Rees, JHEP **05** (2009) 085, [arXiv:0812.2909 [hep-th]]. 205, 283

[365] J. W. York Jr., Phys. Rev. Lett. **28**, 1082 (1972). 205

[366] G. W. Gibbons and S. W. Hawking, Phys. Rev. D **15**, 2752 (1977). 205

[367] J. McGreevy, Adv. High Energy Phys. **2010** (2010) 723105, [arXiv:0909.0518 [hep-th]]. 206

[368] I. Papadimitriou and K. Skenderis, [arXiv:hep-th/0404176]. 205, 206

[369] I. Papadimitriou, JHEP **08** (2011) 119, [arXiv:1106.4826 [hep-th]]. 205, 212

[370] M. Henningson and K. Skenderis, JHEP **07** (1998) 023, [arXiv:hep-th/9806087]. 205

[371] Wolfram Research, Inc., Mathematica, Version 9.0, Champaign, IL (2012). 209

[372] S. Bonanos (2013), *Riemannian Geometry and Tensor Calculus at Mathematica*. Retrieved March 4, 2014, from http://www.inp.demokritos.gr/~sbonano/RGTC/. 209

[373] D. Li, S. He, M. Huang and Q. S. Yan, JHEP **1109**, 041 (2011) [arXiv:1103.5389 [hep-th]]. 212

[374] Sz. Borsanyi, G. Endrodi, Z. Fodor, S. D. Katz, S. Krieg, C. Ratti and K. K. Szabo, JHEP **08** (2012) 053, [arXiv:1204.6710 [hep-lat]]. xii, xiii, 214, 215, 216, 287

[375] N. Haque, A. Bandyopadhyay, J. O. Andersen, M. G. Mustafa, M. Strickland and N. Su, JHEP **1405**, 027 (2014) [arXiv:1402.6907 [hep-ph]]. 215

[376] O. Philipsen and C. Schafer, JHEP **02** (2014) 003, [arXiv:1311.6618 [hep-lat]]. 217

[377] J. Noronha-Hostler, G. S. Denicol, J. Noronha, R. P. G. Andrade and F. Grassi, Phys. Rev. C **88**, 044916 (2013) [arXiv:1305.1981 [nucl-th]]. 221, 230

[378] J. Noronha-Hostler, J. Noronha and F. Grassi, Phys. Rev. C **90**, 034907 (2014) [arXiv:1406.3333 [nucl-th]]. 221

[379] J. B. Rose, J. F. Paquet, G. S. Denicol, M. Luzum, B. Schenke, S. Jeon and C. Gale, arXiv:1408.0024 [nucl-th]. 221

[380] F. G. Gardim, J. Noronha-Hostler, M. Luzum and F. Grassi, arXiv:1411.2574 [nucl-th]. 221

[381] G. D. Moore and K. A. Sohrabi, Phys. Rev. Lett. **106**, 122302 (2011) [arXiv:1007.5333 [hep-ph]]. 224, 238

[382] P. Arnold, D. Vaman, C. Wu and W. Xiao, JHEP **1110**, 033 (2011) [arXiv:1105.4645 [hep-th]]. 224, 230

[383] S. Pu, T. Koide and D. H. Rischke, Phys. Rev. D **81**, 114039 (2010), [arXiv:0907.3906 [hep-ph]]. 225, 227, 228, 230, 233, 287

[384] W. Israel, Annals Phys. **100**, 310 (1976); W. Israel and J. M. Stewart, Annals Phys. **118**, 341 (1979). 228, 229

[385] W. A. Hiscock and L. Lindblom, Ann. Phys. (N.Y.) **151**, 466 (1983); Phys. Rev. D **31**, 725 (1985); Phys. Rev. D **35**, 3723 (1987); Phys. Lett. A **131**, 509 (1988). 228, 287, 288

[386] G. S. Denicol, T. Kodama, T. Koide and P. Mota, J. Phys. G **35**, 115102 (2008). 228, 287

[387] H. Marrochio, D. A. Fogaça, J. Noronha, and G. S. Denicol, to appear. 228, 288, 289

[388] B. Schenke, S. Jeon and C. Gale, Phys. Rev. Lett. **106**, 042301 (2011) [arXiv:1009.3244 [hep-ph]]. 230

[389] P. Bozek, Phys. Rev. C **85**, 034901 (2012) [arXiv:1110.6742 [nucl-th]]. 230

[390] L. Del Zanna, V. Chandra, G. Inghirami, V. Rolando, A. Beraudo, A. De Pace, G. Pagliara and A. Drago *et al.*, Eur. Phys. J. C **73**, 2524 (2013) [arXiv:1305.7052 [nucl-th]]. 230

[391] I. Karpenko, P. Huovinen and M. Bleicher, Comput. Phys. Commun. **185**, 3016 (2014) [arXiv:1312.4160 [nucl-th]]. 230

[392] C. Shen, Z. Qiu, H. Song, J. Bernhard, S. Bass and U. Heinz, arXiv:1409.8164 [nucl-th]. 230

[393] M. A. York and G. D. Moore, Phys. Rev. D **79**, 054011 (2009) [arXiv:0811.0729 [hep-ph]]. 230

[394] J. Erdmenger, M. Haack, M. Kaminski and A. Yarom, JHEP **0901**, 055 (2009) [arXiv:0809.2488 [hep-th]]. 231

[395] M. Haack and A. Yarom, Nucl. Phys. B **813**, 140 (2009) [arXiv:0811.1794 [hep-th]]. 231

[396] F. M. Haehl, R. Loganayagam and M. Rangamani, arXiv:1412.1090 [hep-th]. 231

[397] S. Grozdanov and A. O. Starinets, arXiv:1412.5685 [hep-th]. 231

[398] I. Kanitscheider and K. Skenderis, JHEP **0904**, 062 (2009) [arXiv:0901.1487 [hep-th]]. 231, 234

[399] F. Bigazzi and A. L. Cotrone, JHEP **1008**, 128 (2010) [arXiv:1006.4634 [hep-ph]]. 232

[400] V. Ozvenchuk, O. Linnyk, M. I. Gorenstein, E. L. Bratkovskaya and W. Cassing, Phys. Rev. C **87**, no. 6, 064903 (2013) [arXiv:1212.5393]. 232, 233

[401] G. P. Kadam and H. Mishra, arXiv:1408.6329 [hep-ph]. 232, 233

[402] G. Torrieri, B. Tomasik and I. Mishustin, Phys. Rev. C **77**, 034903 (2008) [arXiv:0707.4405 [nucl-th]]. 233

[403] G. Torrieri and I. Mishustin, Phys. Rev. C **78**, 021901 (2008) [arXiv:0805.0442 [hep-ph]]. 233

[404] K. Rajagopal and N. Tripuraneni, JHEP **1003**, 018 (2010) [arXiv:0908.1785 [hep-ph]]. 233

[405] A. Jaiswal, R. S. Bhalerao and S. Pal, Phys. Rev. C **87**, 021901 (2013) [arXiv:1302.0666 [nucl-th]]. 233

[406] T. Schaefer, arXiv:1408.4503 [hep-th]. 234

[407] G. S. Denicol, S. Jeon and C. Gale, arXiv:1403.0962 [nucl-th]. 234, 235

[408] G. S. Denicol, W. Florkowski, R. Ryblewski and M. Strickland, Phys. Rev. C **90**, 044905 (2014) [arXiv:1407.4767 [hep-ph]]. 234

[409] A. Jaiswal, R. Ryblewski and M. Strickland, Phys. Rev. C **90**, no. 4, 044908 (2014) [arXiv:1407.7231 [hep-ph]]. 234

[410] J. Noronha and G. S. Denicol, arXiv:1104.2415 [hep-th]. 235

[411] M. P. Heller, R. A. Janik, M. Spalinski and P. Witaszczyk, arXiv:1409.5087 [hep-th]. 235

[412] J. Sadeghi and S. Tahery, arXiv:1412.8332 [hep-th]. 237

[413] S. Borsányi, Z. Fodor, S. D. Katz, A. Pásztor, K. K. Szabó and C. Török, arXiv:1501.02173 [hep-lat]. 237

[414] O. DeWolfe, S. S. Gubser and C. Rosen, Phys. Rev. D **84**, 126014 (2011) [arXiv:1108.2029 [hep-th]]. 238

[415] S. Borsanyi, G. Endrodi, Z. Fodor, S. D. Katz, S. Krieg, C. Ratti and K. K. Szabo, JHEP **1208**, 053 (2012) [arXiv:1204.6710 [hep-lat]]. 238

[416] R. Rougemont, S. I. Finazzo, A. Ficnar and J. Noronha, *Holographic QCD thermodynamics and energy loss phenomena at finite temperature and baryon chemical potential*. In preparation. 238

[417] L. Alvarez-Gaume, D. Z. Freedman and S. Mukhi, Annals Phys. **134**, 85 (1981). 248, 249

[418] C. W. Misner, K. S. Thorne and J. A. Wheeler, *Gravitation*. W. H. Freeman, 1973. 249

[419] A. Brandhuber, N. Itzhaki, J. Sonnenschein and S. Yankielowicz, JHEP **9806**, 001 (1998) [hep-th/9803263]. 255

[420] N. Itzhaki, J. M. Maldacena, J. Sonnenschein and S. Yankielowicz, Phys. Rev. D **58**, 046004 (1998) [hep-th/9802042]. 258

[421] M. le Bellac, *Thermal Field Theory*. Cambridge University Press, 2000 262, 275

[422] J. P. Blaizot, E. Iancu and R. R. Parwani, Phys. Rev. D **52**, 2543 (1995) [hep-ph/9504408]. 272

[423] E. Kiritsis and F. Nitti, Nucl. Phys. B **772**, 67 (2007) [hep-th/0611344]. 280

[424] C. J. Morningstar and M. J. Peardon, Phys. Rev. D **60**, 034509 (1999) [hep-lat/9901004]. xiv, 280, 281

[425] Y. Chen, A. Alexandru, S. J. Dong, T. Draper, I. Horvath, F. X. Lee, K. F. Liu and N. Mathur *et al.*, Phys. Rev. D **73**, 014516 (2006) [hep-lat/0510074]. xiv, 280, 281

[426] B. Lucini and M. Teper, JHEP **0106**, 050 (2001) [hep-lat/0103027]. xiv, 280, 281

[427] B. Lucini, A. Rago and E. Rinaldi, JHEP **1008**, 119 (2010) [arXiv:1007.3879 [hep-lat]]. xiv, 280, 281

[428] P. Romatschke, Int. J. Mod. Phys. E **19**, 1 (2010) [arXiv:0902.3663 [hep-ph]]. 287, 289

[429] D. A. Fogaça, H. Marrochio, F. S. Navarra and J. Noronha, arXiv:1402.5548 [nucl-th], to appear in Nuclear Physics A. 289